Vol. 66 November, 1962 No. 11

THE JOURNAL OF PHYSICAL CHEMISTRY

(Registered in U. S. Patent Office)

CONTENTS

Contents continued on page 1A

THE JOURNAL OF PHYSICAL CHEMISTRY

(Registered in U. S. Patent Office)

Published monthly by the American Chemical Society at 20th and Northampton Sts., Easton, Pa. Second-class postage paid at Easton, Pa.

The *Journal of Physical Chemistry* is devoted to the publication of selected symposia in the broad field of physical chemistry and to other contributed papers.

Manuscripts originating in the British Isles, Europe, and Africa should be sent to F. C. Tompkins, The Faraday Society, 6 Gray's Inn Square, London W. C. 1, England.

Manuscripts originating elsewhere should be sent to W. Albert Noyes, Jr., Department of Chemistry, University of Rochester, Rochester 20, N. Y.

Correspondence regarding accepted copy, proofs, and reprints should be directed to Senior Production Editor, Allen D. Bliss, ACS Office, Mack Printing Company, 20th and Northampton Sts., Easton, Pa.

Advertising Office: Reinhold Publishing Corporation, 430 Park Avenue, New York 22, N. Y.

Articles must be submitted in duplicate, typed, and double spaced. They should have at the beginning a brief Abstract, in no case exceeding 300 words. Original drawings should accompany the manuscript. Lettering at the sides of graphs (black on white or blue) may be pencilled in and will be typeset. Figures and tables should be held to a minimum consistent with adequate presentation of information. Photographs will not be printed on glossy paper except by special arrangement. All footnotes and references to the literature should be numbered consecutively and placed in the manuscript at the proper places. Initials of authors referred to in citations should be given. Nomenclature should conform to that used in *Chemical Abstracts*, mathematical characters be marked for italic, Greek letters carefully made or annotated, and subscripts and superscripts clearly shown. Articles should be written as briefly as possible consistent with clarity and should avoid historical background unnecessary for specialists.

Notes describe fragmentary or incomplete studies but do not otherwise differ fundamentally from articles and are subjected to the same editorial appraisal as are articles. In their preparation particular attention should be paid to brevity and conciseness. Material included in Notes must be definitive and may not be republished subsequently.

Communications to the Editor are designed to afford prompt preliminary publication of observations or discoveries whose value to science is so great that immediate publication is imperative. The appearance of related work from other laboratories is in itself not considered sufficient justification for the publication of a Communication, which must in addition meet special requirements of timeliness and significance. Their total length may in no case exceed 1000 words or their equivalent. They differ from Articles and Notes in that their subject matter may be republished.

Symposium papers should be sent in all cases to Secretaries of Divisions sponsoring the symposium, who will be responsible for their transmittal to the Editor. The Secretary of the Division by agreement with the Editor will specify a time after which symposium papers cannot be accepted. The Editor reserves the right to refuse to publish symposium articles, for valid scientific reasons. Each symposium paper may not exceed four printed pages (about sixteen double spaced typewritten pages) in length except by prior arrangement with the Editor.

Remittances and orders for subscriptions and for single copies, notices of changes of address and new professional connections, and claims for missing numbers should be sent to the Subscription Service Department, American Chemical Society, 1155 Sixteenth St., N. W., Washington 6, D. C. Changes of address for the *Journal of Physical Chemistry* must be received on or before the 30th of the preceding month. Please include an old address label with the notification.

Claims for missing numbers will not be allowed (1) if received more than sixty days from date of issue (because of delivery hazards, no claims can be honored from subscribers in Central Europe, Asia, or Pacific Islands other than Hawaii), (2) if loss was due to failure of notice of change of address to be received before the date specified in the preceding paragraph, or (3) if the reason for the claim is "missing from files."

Subscription rates (1962): members of American Chemical Society, $12.00 for 1 year; to non-members, $24.00 for 1 year. Postage to countries in the Pan-American Union $0.80; Canada, $0.40; all other countries, $1.20. Single copies, current volume, $2.50; foreign postage, $0.15; Canadian postage $0.10; Pan-American Union, $0.10. Back volumes (Vol. 56–65) $30.00 per volume; foreign postage, per volume $1.20, Canadian, $0.40; Pan-American Union, $0.80. Single copies: back issues, $3.00; for current year, $2.50; postage, single copies: foreign, $0.15; Canadian, $0.10; Pan-American Union, $0.10.

Contents continued

AUTHOR INDEX

Special Notice to Authors

Beginning with the January issue, 1963, a page charge for publication will go into effect. The ACS position is described in detail *via* a series of questions and answers in "The Case for Page Charges," *Chem. Eng. News*, March 19, 1962, p. 92. The editors of the *Journal of Physical Chemistry* wish to emphasize the following points.

1. The page charge is a publication service charge designed to aid in covering the costs of publishing an article in a journal. The page charge covers only costs of setting the article in type and preparing it for the presses. As administered by the ACS, it will also include 100 reprints supplied to the author.

2. Manuscripts received after August 15, 1962, or accepted for publication after September 15, may be published in January, 1963, and subsequent issues, and therefore be subject to the page charge.

3. Payment is expected from sponsored funds supporting the research reported. Page charge payment is not a condition for publication.

4. The editor's decision to publish is made before assessment of page charges and the editor's office will not be advised on charges or payment.

5. With the institution of page charges, subscription rates to ACS journals should be stabilized at current levels for an indefinite period of time.

THE JOURNAL OF PHYSICAL CHEMISTRY

(Registered in U. S. Patent Office)

VOLUME 66 NOVEMBER 15, 1962 NUMBER 11

A STUDY OF THE CONDUCTANCE BEHAVIOR OF LITHIUM AND AMMONIUM IODIDES IN *n*-BUTANOL[1-3]

BY H. V. VENKATASETTY AND GLENN H. BROWN[4]

Department of Chemistry, University of Cincinnati, Cincinnati, Ohio

Received September 6, 1961

The conductances of lithium iodide and ammonium iodide have been measured in *n*-butanol at 0, 25, and 50°. The values of the dissociation constants for the ion-pairs and the limiting equivalent conductances are obtained by the method of Shedlovsky. The ion-size parameters are calculated by Bjerrum's method as well as by the Denison–Ramsey method. Both of the salts are found to behave as weak electrolytes. The observed differences in the dissociation constants and the mobilities are explained in terms of the specific types of ion–ion and ion–solvent interactions.

Introduction

The investigation of the properties of solutions of ionophores[5] in non-aqueous systems has received considerable attention in recent years with a view to understanding the nature of ion–ion and ion–solvent interactions in these systems under a wide variety of conditions. A large number of 1:1 electrolytes have been investigated in a wide variety of solvents.[6] A literature survey of non-aqueous systems reveals the absence of conductance data for solutions of ionophores in *n*-butanol over a range of temperature. Seward[7] measured the conductances and viscosities of the solutions of tetra-*n*-butylammonium picrate in *n*-butanol over the entire concentration range from dilute solution to fused salt at 91°. *n*-Butanol, being an associated solvent with low vapor pressure and moderate value of dielectric constant of 17.1 at 25°, offers an interesting solvent to study specific ion–ion and ion–solvent interactions.

(1) Presented at the 139th National Meeting of the American Chemical Society, St. Louis, Missouri, March 21–30, 1961.

(2) This paper is abstracted in part from a dissertation submitted by H. V. Venkatasetty to the Graduate School of the University of Cincinnati in partial fulfillment of the requirements for the Degree of the Doctor of Philosophy, 1961.

(3) The conductance equipment used in this research was made available through a grant from the Research Corporation.

(4) Department of Chemistry, Kent State University, Kent, Ohio.

(5) R. N. Fuoss, *J. Chem. Educ.*, **32**, 527 (1955).

(6) H. S. Harned and B. B. Owen, "The Physical Chemistry of Electrolyte Solutions," 3rd Ed., Reinhold Publ. Corp., New York, N. Y., 1958, Chapter 6.

(7) R. P. Seward, *J. Am. Chem. Soc.*, **73**, 515 (1951).

Experimental

Apparatus.—The conductance measurements were made using a conventional alternating current Wheatstone bridge equipped with a Wagner earthing device. The power source for the bridge was a Leeds and Northrup oscillator with a frequency of 1000 c.p.s. The balance detection device consisted of a crystal headphone. The ratio arms of the bridge consisted of a Kohlrausch slide wire purchased from Leeds and Northrup and in almost all the measurements great care was taken in measuring resistances to balance the bridge at the center of the slide wire to eliminate errors due to inductance.[8] The conductance cell used was designed according to the recommendations of Jones and Bollinger[9] and had a graded seal between the Pyrex and the platinum. The electrodes were slightly platinized using a standard procedure.[10] The cell constant was determined using 0.01 *D* KCl solution according to the procedure of Jones and Bradshaw.[10] The cell constant was 0.15000 cm.$^{-1}$ at 0.0° and the cell constants at the other temperatures were calculated[11] using the 0.0° value. The cell constant calculated for 25.0° was checked experimentally using the procedure of Ives and Sames,[12] with benzoic acid solutions prepared from a National Bureau of Standards sample. The cell was maintained at 25.00 ± 0.02° and 50.00 ± 0.02° in an oil bath and the measurements at 0.0° were made in an oil trough placed in a well insulated ice chest.[13] The temperature of the bath was measured with a Beckmann thermometer which had been calibrated against a thermometer certified by the National Bureau of Standards.

Materials.—A saturated solution of lithium iodide trihydrate of "National Formulary" quality, purchased from

(8) G. Jones and R. C. Josephs, *ibid.*, **50**, 1049 (1928).

(9) G. Jones and G. M. Bollinger, *ibid.*, **53**, 411 (1931).

(10) G. Jones and B. C. Bradshaw, *ibid.*, **55**, 1780 (1933).

(11) E. W. Washburn, *ibid.*, **38**, 2455 (1916).

(12) D. J. G. Ives and K. Sames, *J. Chem. Soc.*, 511 (1943).

(13) G. Jones and M. J. Prendergast, *J. Am. Chem. Soc.*, **59**, 731 (1937).

the Mallinckrodt Chemical Works, was prepared in conductivity water and freed from anionic impurities by passing it through the anion-exchange resin Amberlite IRA-400. After evaporating the solvent from this solution under vacuum, and cooling, lithium iodide crystallized. These crystals were dried in a vacuum oven at about 120° and stored over P_2O_5 in a vacuum desiccator for several weeks. The solid lithium iodide was placed in a specially designed steel bomb and heated under vacuum in a furnace at about 650° for about 2 hr. and then the temperature was raised to about 850° for 1.5 hr. to completely dehydrate the salt. The salt showed no alkalinity and analysis of the sample by Fajans' method showed it to be better than 99.96% pure.

The ammonium iodide was Baker analyzed "Reagent Grade" and a saturated solution was made in de-ionized water freed from dissolved oxygen by boiling. This solution was passed through a column containing the cation-exchange resin Dower 50-X, equilibrated with 2 *M* ammonium nitrate solution, and then washed free of nitrate; the cation-exchanger was followed by an anion exchange resin IRA-400 which had been equilibrated with 2 *M* potassium iodide solution and then washed free of iodide ion. The effluent was collected in a colored bottle to protect the ammonium iodide from photochemical action. The solution of ammonium iodide was evaporated under reduced pressure, the salt recrystallized from an ethanol–ether mixture, and dried to constant weight *in vacuo* at 60–65°. Analysis by Fajans' method showed a purity of 99.98%.

Reagent grade *n*-butanol was refluxed for several hours with lime and distilled three times. In the final distillation the fraction boiling between 117.3 and 117.5° under atmospheric pressure was collected. The refractive index of the purified solvent was 1.3992 compared to the literature value of 1.3991.[14] The specific conductance of the solvent reported in the literature[15] is 9.12×10^{-9} mho at 25°. The dielectric constant of *n*-butanol calculated according to Circular No. 514 of National Bureau of Standards[16] is 20.44 at 0°, 17.1 at 25°, and 14.10 at 50°. The viscosities of *n*-butanol at different temperatures reported in the literature are 0.05186 poise at 0°,[17] 0.0246 poise at 25°,[18] and 0.01411 poise at 50°[17]; these values check well with the extrapolated values of viscosity temperature functions of liquids found in the literature.[19] The densities of *n*-butanol determined in this work are 0.8246 g./cm.^{3} at 0°, 0.8057 g./cm.^{3} at 25°, and 0.7875 g./cm.^{3} at 50°; these values are in agreement with the values reported in the literature.[20] The purified solvent was stored in sealed bottles and any transfer of the solvent was made in a drybox under a positive pressure of dry nitrogen.

Preparation of Solutions.—All solutions were prepared in a drybox by transferring to a container a known weight of the salt and dissolving it in an exact volume of the solvent. Dilute solutions were prepared by further dilutions, using calibrated pipets and burets. Concentrations were established by analysis. These solutions were preserved in bottles which had been coated on the outside with black paint and were sealed with serum caps. *n*-Butanol is found to have no effect on these serum caps. Transfers of solutions always were made using the proper sized hypodermic syringe. All weighings were corrected for the buoyancy effect of air.

Procedure for Making Measurements.—The cell was first cleaned with potassium dichromate–sulfuric acid cleaning solution, washed several times with distilled water, and finally with de-ionized water. It then was rinsed well with "chemically pure" acetone, dried, and stored in a drybox. From this point on, all handling of solutions was carried out in a drybox. Before each filling of the cell, it was rinsed well a number of times with the solution under study. The transfer of the solution from the bottle to the cell was conveniently accomplished by the use of a syringe fitted with a suitable hypodermic needle that was inserted through the stopcock into the filling tube of the cell. The conductance cell was placed in the appropriate bath and allowed to come to temperature. Readings were taken every 20 min. until the resistance was constant. Since the specific conductance of *n*-butanol is 9.12×10^{-9} mho at 25°, solvent correction is not necessary even for the most dilute solutions.

(14) "International Critical Tables," Vol. 7, McGraw-Hill Book Co., Inc., New York, N. Y., 1930, p. 36.

(15) L. Scheflan and M. B. Jacobs, "The Handbook of Solvents," D. Van Nostrand Co., Inc., New York, N. Y., 1953, p. 159.

(16) National Bureau of Standards Circular No. 514, 1951.

(17) "Handbook of Chemistry and Physics," 40th edition, Chemical Rubber Publishing Co., Cleveland, Ohio, 1958, p. 2158.

(18) Reference 14, p. 41.

(19) A. N. Nissan, *Phil. Mag.*, **32**, 441 (1941).

(20) J. Timmermann, "Physico-Chemical Constants of Pure Organic Compounds," Elsevier Publishing Co., New York, N. Y., 1950, p. 319.

Results and Discussion

The data for the equivalent conductance of lithium iodide and ammonium iodide corresponding to different concentrations at 0, 25, and 50° are recorded in Table I. The maximum experimental error inherent in these data is 0.1%.

TABLE I

EQUIVALENT CONDUCTANCE OF LiI IN *n*-BUTANOL

Temp. 0.0°		Temp. 25 ± 0.02°		Temp. 50 ± 0.02°	
$c \times 10^4$ *N*	Λ_{obsd}	$c \times 10^4$ *N*	Λ_{obsd}	$c \times 10^4$ *N*	Λ_{obsd}
8.21	6.37	8.02	12.13	7.84	19.39
16.42	5.74	16.04	10.69	15.68	16.57
20.50	5.44	20.05	10.17	19.60	15.64
24.62	5.27	24.06	9.75	23.52	15.02
41.00	4.66	40.10	8.69	39.20	13.02
61.50	4.32	60.10	7.79	58.70	11.64
82.10	3.87	80.20	7.02	78.40	10.71
102.60	3.66	100.20	6.73	97.90	10.06
123.10	3.59	120.30	6.30	117.60	9.53
143.70	3.28	140.40	5.98	137.20	9.15
164.20	3.05	160.40	5.91	156.80	8.81

EQUIVALENT CONDUCTANCE OF NH_4I IN *n*-BUTANOL

Temp. 0.0°		Temp. 25 ± 0.02°		Temp. 50 ± 0.02°	
$c \times 10^4$ *N*	Λ_{obsd}	$c \times 10^4$ *N*	Λ_{obsd}	$c \times 10^4$ *N*	Λ_{obsd}
6.79	6.86	6.60	12.23	6.50	19.25
13.57	6.07	13.26	10.99	12.96	16.53
16.90	5.84	16.57	10.59	16.20	15.84
23.74	5.43	23.20	9.84	22.68	14.43
33.90	4.97	33.15	8.98	32.40	13.04
50.90	4.42	49.70	7.97	48.60	11.67
67.80	4.07	66.30	7.28	64.80	10.77
84.80	3.94	82.90	7.10	81.00	10.08
101.80	3.78	99.40	6.77	97.20	9.51
118.70	3.57	116.00	6.33	113.40	9.07
135.70	3.49	132.60	6.32	129.60	8.55

The plots of equivalent conductance *vs.* the square root of concentration for both LiI and NH_4I at the three temperatures studied show marked deviation from linearity. This indicates that these salts behave as weak electrolytes in *n*-butanol with definite ion-pair formation. The limiting equivalent conductance (Λ_0) and the ion-pair dissociation constant (K) for the different solutions were evaluated by the Shedlovsky method.[21,22] Figure 1 shows the Shedlovsky plot for ammonium iodide. Comparable curves are obtained for lithium iodide solutions. The values of Λ_0 and K are summarized in Table II.

The conductance of ions to a large measure depends on the size of the ions and also on the viscosity of the medium through which they move.

(21) T. Shedlovsky, *J. Franklin Inst.*, **225**, 739 (1938).

(22) R. M. Fuoss and T. Shedlovsky, *J. Am. Chem. Soc.*, **71**, 1496 (1949).

TABLE II

SUMMARY OF DATA FOR SOLUTIONS OF LiI AND NH_4I IN n-BUTANOL

Electrolyte	Temp., °C.	Λ_0 Exp.	K × 10^4	a_{Bj},[a] cm. × 10^8	a_{DR},[b] cm. × 10^8	$\Lambda_0\eta_0$
LiI	0.0	8.58	20.94	3.54	4.81	0.444
LiI	25.0	17.42	13.74	3.71	4.94	.429
LiI	50.0	30.30	7.41	3.83	5.05	.427
NH_4I	0.0	9.09	17.39	3.34	4.67	.471
NH_4I	25.0	16.00	19.53	4.15	5.21	.394
NH_4I	50.0	29.85	6.73	3.76	4.98	.421

[a] a_{Bj} is the ion-size parameter from Bjerrum's theory. [b] a_{DR} is the ion-size parameter from the Denison-Ramsey equation.

The interaction between two oppositely charged ions depends on the charge, size, structure, and polarizability of the ions as well as the interaction of the ions with the solvent molecules. n-Butanol being an electron donor solvent with the dipole moment of 1.67 Debye units is expected to solvate the cations much more strongly than the anions.

The values of Λ_0 and K for LiI and NH_4I at 0, 25, and 50° are comparable to each other. Therefore, the cations Li^+ and NH_4^+ are either of comparable size or there must exist specific interactions between these cations and the polar solvent molecules which affect the motion of these ions through the solvent medium.

The model proposed to explain the small values of Λ_0 for LiI solutions assumes that the Li^+ ions, because of their small size and high charge density, can exert a strong attractive force on the polar solvent molecules and thus create a tight solvent atmosphere in the first solvent shell around the cation. This model is supported by experimental evidence from other measurements[23] of Λ_0 and from X-ray data on the structure of solutions.[24,25] The ion-size parameter calculated using Bjerrum's theory[26] of ion-pair formation and the Denison-Ramsey method (Table II) is larger than the crystallographic radius of 2.76 Å. (Pauling) for LiI. These results, together with the nearly constant Walden product (Table II) at all the temperatures studied, indicate that the Li^+ ions are surrounded by a single layer of solvent molecules and that there is little change in the size of the solvodynamic unit over the entire temperature range. The large values of the dissociation constant (K) can be explained by realizing that strongly coördinated solvent molecules around the Li^+ ions hinder the close approach of iodide ions to form stable ion-pairs. The values of Λ_0 and K obtained for LiI in this study compare favorably with the values obtained by Ogston[27] for $LiI \cdot 3H_2O$ in ethanol.

(23) Reference 6, pp. 698-704.

(24) G. W. Brady, *J. Chem. Phys.*, **27**, 304 (1957).

(25) M. Strauss, Doctoral Dissertation, University of Cincinnati, 1960.

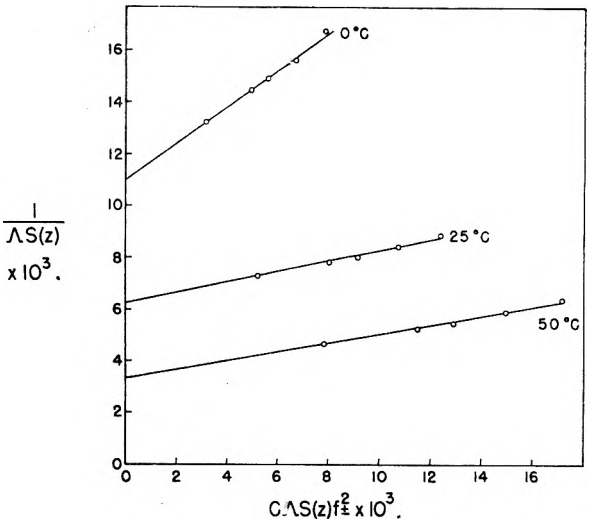

Fig. 1.—Shedlovsky plot for ammonium iodide at 0, 25, and 50°.

Since the ammonium ion, with a tetrahedral configuration, is large relative to the Li^+ ion and since it has a lower charge density than the Li^+ ion, it cannot exert as strong an attractive force on the solvent dipoles to solvate itself as is the case with the Li^+ ion. However, the experimentally observed low values of Λ_0 (Table II) may be explained, in part, as due to the electrostatic attraction between the charge on the NH_4^+ ion and the solvent dipoles. This interaction can produce a distortion of the quasi-crystalline structure of the solvent and thus interfere with the motion of the ions. This coulombic ion–dipole interaction may be reinforced by hydrogen bonding between the nitrogen of the ammonium ion and the oxygen of n-butanol, possibly at all the corners of the tetrahedron. Even though these interactions do not give a tightly held solvent atmosphere around the ammonium ion, they can account for the low values of Λ_0 and the large values of K. This model of the ammonium ion in n-butanol is supported by the reasonable agreement between the calculated Bjerrum ion-size parameter (Table II) and the crystallographic interionic distance of 3.63 Å. (Goldschmidt). Burgess and Kraus[28] evaluated Λ_0 and K for NH_4I in pyridine at 25°. Their values of $\Lambda_0 = 95.2$ and $K = 2.4 \times 10^{-4}$ compared to the present values of $\Lambda_0 = 16.00$ and $K = 19.53 \times 10^{-4}$ suggest that there are specific ion–solvent interactions in n-butanol and a very small amount of such interactions, if any at all, in pyridine.

(26) N. Bjerrum, *Kgl. Danske Videnskab*, **7**, No. 9 (1926).

(27) A. G. Ogston, *Trans. Faraday Soc.*, **32**, 1679 (1936).

(28) D. S. Burgess and C. A. Kraus, *J. Am. Chem. Soc.*, **70**, 706 (1948).

THE DECOMPOSITION OF CHLOROACETIC ACID IN AQUEOUS SOLUTIONS BY ATOMIC HYDROGEN. I. COMPARISON WITH RADIATION CHEMICAL DATA

BY JOSHUA JORTNER AND JOSEPH RABANI

Department of Physical Chemistry, Hebrew University, Jerusalem, Israel

Received December 21, 1961

The decomposition of aqueous solutions of chloroacetic acid in acid and neutral solutions by H atoms was investigated. The rate constants for hydrogen and chloride abstraction from the chloroacetic acid and from the chloroacetic anion by H atoms were derived. It was found that H atoms as such react with chloroacetic acid mainly by hydrogen abstraction. The comparison of these results with radiation chemical data yields evidence for the nature of the reducing radicals produced in the radiolysis of water. The acid form of these reducing radicals involves the H atom as such.

Introduction

Recent experimental studies indicate that the reducing radicals formed in the radiolysis of water can exist in two forms, exhibiting widely different reactivity with specific scavengers, *e.g.*, H_2O_2,[1,2] N_2O,[3] organic alcohols, and ketones[4] and chloroacetic acid.[5,6] It was shown[2] that the form of H atom equivalent produced by irradiation of neutral aqueous solutions differs from the species produced by the oxidation of H_2 by OH radicals, and from those produced by radiolysis of acid aqueous solutions.[1,7] The possible pairs of the reducing species considered were e_{aq} and H, or alternately H atom and H_2^+ ion. Radiation chemical data do not make it possible so far to discriminate unambiguously between these possibilities.[1,2,6]

Comparative studies of the reactivity of H atoms generated as such and introduced into the solution[8] and of the reducing species produced in the radiolysis of water may yield information concerning the nature of the reducing radicals produced in irradiated solutions under various experimental conditions. Recent studies[8f] of the decomposition of aqueous solutions of H_2O_2 by H atoms showed that the acid form of the reducing radical involves a hydrogen atom as such. In order to provide further evidence for the nature of these species, the decomposition of aqueous solutions of chloroacetic acid by atomic hydrogen was investigated. Radiation-chemical studies of this system were recently carried out.[5,6] In the present work the radiation chemical data are compared with experimental results for the decomposition of acid and neutral chloroacetic solutions by atomic hydrogen.

Experimental

Production of H-Atoms.—Atomic hydrogen was generated by a method previously described,[8] by an electrodeless discharge in H_2 gas at 30 mm. pressure. The pumping velocity was 150 l. min.$^{-1}$. Atomic hydrogen was passed for 15 min. through 25 cc. of the evacuated solution kept at 4°.

Determination of dose of H atoms was carried out by reduction of 10^{-3} *M* ferricyanide solution.[8c] During the runs the dose rate of H atoms was checked. The mean dose in this series of experiments was 1×10^{-6} mole l.$^{-1}$ sec.$^{-1}$ (2.5×10^{-8} mole sec.$^{-1}$). After using the ferricyanide dosimeter, it was found necessary to pass atomic hydrogen through pure water in order to obtain reproducible results.

Analysis.—Chloride was determined by a turbidometric method. The reagent solution consisted of 0.01*N* $AgNO_3$ in 2 *N* HNO_3. Equal volumes of the reagent solution with the analyzed solution were mixed at room temperature, 25°. The turbidity was measured at 400 mμ with a Beckman DU spectrophotometer. The optical density increases with time, reaching a maximum value after 20–30 min. depending on Cl^- and chloroacetic acid concentration. The maximum reading was taken. The measured optical density is linear with Cl^- concentration up to o.d. 0.8, for a 1-cm. light path.

The method is adequate for microdetermination of inorganic chloride in the concentration region 5×10^{-5}–10^{-3} *M*. The results were found to depend on chloroacetic concentration higher than 0.5 *M*, and were duly corrected. The accuracy of the method is ±3%. At chloroacetic acid concentrations above 3 *M*, the chloride production during the analysis was very fast and no experiments were carried out in this region.

Materials and Solution.—A.R. grade chloroacetic acid (Hopkin & Williams), sulfuric acid, and KOH were used. The pH usually was adjusted by H_2SO_4 and KOH. In some cases 10^{-3} *M* phosphate buffer was employed. Solutions were freshly prepared and kept in ice until used. The initial chloride concentration of solutions up to 0.5 *M* did not exceed 2.5×10^{-5} *M* chloride. Solutions in the concentration region 1–3 *M* did not contain more than 2×10^{-4} *M* chloride.

Results

The decomposition of chloroacetic acid by atomic hydrogen was followed by measuring the formation of inorganic chloride. It was found convenient to define the *reaction yield R* for the product in terms of

$$R(Cl^-) = \frac{[Cl^-]V}{At} \qquad (I)$$

where *A* is the dose rate of H atoms expressed in mole sec.$^{-1}$, *V* the volume of the solution expressed in l., and *t* the duration of the run. The values of $R(Cl^-)$ were obtained as mean values of at least three runs, and were reproducible within ±20% or better.

Reaction Yields in Acid Solutions.—The experimental results for $R(Cl^-)$ obtained in acid solutions from pH 0.4 to pH 2 are presented in Table I. In acid solutions $R(Cl^-)$ is dependent on chloroacetic acid concentration leveling off at high concentration. The limiting value observed is

(1) A. O. Allen and H. Schwarz, *Proc. Intern. Conf. Peaceful Uses At. Energy, Geneva*, **29**, 30 (1958).
(2) N. F. Barr and A. O. Allen, *J. Phys. Chem.*, **63**, 928 (1959).
(3) F. S. Dainton and D. B. Peterson, *Nature*, **186**, 878 (1960).
(4) J. T. Allan and G. Scholes, *ibid.*, **187**, 218 (1960).
(5) E. Hayon and J. Weiss, *Proc. Intern. Conf. Peaceful Uses At. Energy, Geneva*, **29**, 80 (1958).
(6) E. Hayon and A. O. Allen, *J. Phys. Chem.*, **65**, 2181 (1961).
(7) J. T. Sworski, *J. Am. Chem. Soc.*, **76**, 4687 (1954).
(8) (a) G. Czapski and G. Stein, *J. Phys. Chem.*, **63**, 850 (1959); (b) G. Czapski, J. Jortner, and G. Stein, *ibid.*, **63**, 1769 (1959); (c) G. Czapski and G. Stein, *ibid.*, **64**, 219 (1960); (d) G. Czapski, J. Jortner, and G. Stein, *ibid.*, **65**, 956 (1961); (e) **65**, 960 (1961); (f) **65**, 964 (1961).

$R^0(Cl^-) = 0.33$. At constant chloroacetic acid concentration, the chloride yield is independent of pH in the region 0.4–2.0.

Reaction Mechanism in Acid Solutions.—The limiting chloride reaction yield reaches the value of 0.33 at high scavenger concentrations. Thus the experimental results are interpreted by assuming competition between two first-order scavenging reactions, which involve hydrogen and chloride abstraction from chloroacetic acid.

TABLE I

CHLORIDE YIELDS FROM AQUEOUS SOLUTIONS OF CHLOROACETIC ACID AT 4°

Dose of H atoms/10^{-6} mole $l.^{-1}$ $sec.^{-1}$; duration of run 900 sec.

pH	$[CH_2ClCOOH]$, mole $l.^{-1}$	$R(Cl^-)$
0.4	0.5	0.18
.4	.05	.032
.4	.005	.02
1.0	3.5	(.33)
1.0	3.3	(.33)
1.0	2.5	.33
1.0	1.0	.21
1.0	0.5	.15
1.0	.2	.08
1.0	.1	.07
1.0	.05	.02
1.2	.5	.18
1.9	3.5	(.28)
1.9	0.5	.16
1.9	.05	.02
3.3	.4	.07
3.3	.05	.06
4.2	.87	.08
4.2	.44	.07
4.2	.01	.03
4.4	.5	.08
4.4	.05	.07
7.4	.01	.04

$$H + CH_2ClCOOH \longrightarrow H_2 + CHClCOOH \quad (1)$$

$$H + CH_2ClCOOH \longrightarrow Cl^- + CH_2COOH + H^+ \quad (2)$$

The present data were obtained at a relatively high dose rate of H atoms, thus second-order radical recombination reactions have to be included. The concentration dependence of $R(Cl^-)$ is attributed to the recombination reaction

$$2H \longrightarrow H_2 \quad (3)$$

Evaluation of the Experimental Results.—In a previous work[8d] approximate kinetic expressions were derived for the reactivity of H atoms introduced from the gaseous phase into the solution. By application of the diffusion model[8d] the sum of the reaction yields for H_2 and Cl^- production is

$$R(Cl^-) + R(H_2) = \frac{\Delta}{W} \quad (II)$$

where Δ is obtained from the cubic equation

$$2\Delta^3 + 3\Delta^2 + \Delta = W \quad (III)$$

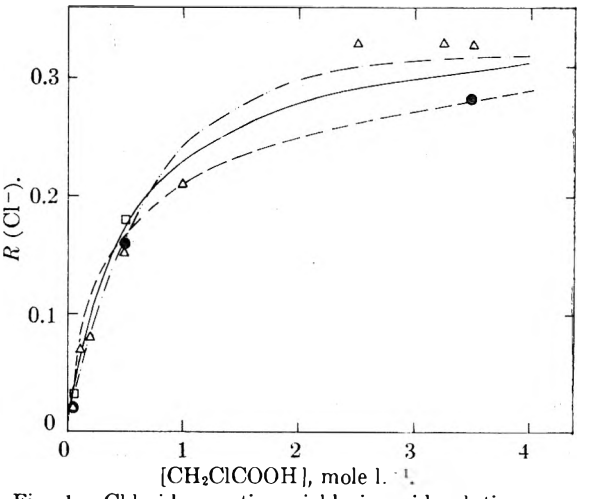

Fig. 1.—Chloride reaction yields in acid solutions: □, pH 0.4; △, pH 1; ●, pH 1.9. Calculated curves: — ·· —, homogeneous kinetics; ———, diffusion treatment; — — —, forced convection treatment.

The parameter W is expressed using the same notation as in previous work[8d]

$$W = \frac{k_3 A}{6\{(k_1 + k_2)[CH_2ClCOOH]\}^{3/2} D^{1/2} \varphi} \quad (IV)$$

where A is the dose rate of H atoms, D their diffusion coefficient, and φ the mean surface area for mass transport.

The chloride yield can be expressed in terms of the limiting yield $R^0(Cl^-)$

$$R(Cl^-) = R^0(Cl^-)(\Delta/W) \quad (V)$$

Setting the experimental value for the dose rate $A = 2.5 \times 10^{-8}$ mole $sec.^{-1}$ and using the constants[8d,8e] $D = 4 \times 10^{-5}$ $cm.^2/sec.$ and $k_3 = 10^{13}$ $mole^{-1}$ $cm.^3$ $sec.^{-1}$, we obtain

$$W = \frac{6.6 \times 10^6}{\{(k_1 + k_2)\varphi^{2/3}\}^{3/2}[CH_2ClCOOH]^{3/2}} \quad (VI)$$

Best agreement with experimental data was obtained setting $(k_1 + k_2)\varphi^{2/3} = 1.3 \times 10^5$ $mole^{-1}$ l. $sec.^{-1}$ $cm.^{4/3}$ Analysis of the results according to the forced convection mechanism[8c] leads to

$$R(Cl^-) = R^0(Cl^-) \frac{(k_1 + k_2)\varphi\mu[CH_2ClCOOH]}{k_3 A} \times \ln\left\{1 + \frac{k_3 A}{(k_1 + k_2)\varphi\mu[CH_2ClCOOH]}\right\} \quad (VII)$$

where μ is the velocity of the liquid. Reasonable agreement was obtained setting $(k_1 + k_2)\varphi\mu = 2.5 \times 10^5$ l. $mole^{-1}$ $sec.^{-1}$ $cm.^3$ $sec.^{-1}$. Finally, the homogeneous kinetic treatment was employed

$$R(Cl^-) = R^0(Cl^-) \frac{V\tau[CH_2ClCOOH]^2}{A} \times \left\{\left(1 + \frac{2A}{V\tau[CH_2ClCOOH]^2}\right)^{1/2} - 1\right\} \quad (VIII)$$

where $\tau = (k_1 + k_2)^2/2k_3$ and V is the volume of the solution. The experimental results were fitted by setting $\tau = 10^{-6}$ $l.^{-1}$ mole $sec.^{-1}$. The comparison of the experimental results and calculated data is presented in Fig. 1.

Derivation of "Absolute Rate Constants."—In a previous analysis[8c] it was shown that the homogeneous kinetic treatment yields the lower limit for the rate constants. The scavenging rate constants were estimated from the result of the diffusion model. The effective surface area for introduction of H atoms was estimated as 10–20 cm.^{2}.[8d,8e] Setting $\varphi^{2/3} = 10$ cm.$^{4/3}$ we obtain $k_1 + k_2 = 1.3 \times 10^4$ l. mole^{-1} sec.$^{-1}$. This estimation is based on the values of k_3[8,9] and of φ.

Alternatively, similar conclusions can be derived by comparing the present results with the kinetic data previously obtained[8e] under similar experimental conditions for the oxidation of Fe^{+2} ion by H atoms. We have calculated the ratio $k_1 + k_2/k_{H+Fe^{+2}}$ using the three kinetic models. The calculation of the rate constants ratio $k_1 + k_2/k_{H+Fe^{+2}}$ yielded 1.42×10^{-2} using homogeneous kinetics, 1.74×10^{-2} using the diffusion model, and 1.67×10^{-2} applying the forced convection model.

These rate constants ratios are independent of the value chosen for k_3. The rate constants ratio for H atom scavenging in these two different systems is not changed by the kinetic treatment employed. This conclusion yields further support to the validity of the kinetic data obtained[8] by using this experimental method. Using the rate constant $k_{H+Fe^{+2}} = 6.7 \times 10^5$ mole l.$^{-1}$ sec.$^{-1}$ obtained[10] from comparison of radiation chemical results with gaseous phase data,[10] we obtain $k_1 + k_2 = 10^4$ l. mole^{-1} sec.$^{-1}$. Thus the two independent methods lead to similar results.

In the present treatment only the recombination reaction 3 was considered. The recombination of H atoms with the radicals CH_2COOH and $CHClCOOH$ was not included. The nature of this approximation will be considered briefly. Assuming equal reaction rates of H atoms with these radicals and equal rates for the recombination of these radicals, the kinetic scheme should include the reactions

$$H + B \longrightarrow HB \qquad (4)$$

$$2B \longrightarrow B_2 \qquad (5)$$

where B represents both $CHClCOOH$ and CH_2COOH.

At relatively high chloroacetic acid concentrations, the steady state concentration of H atoms is determined by the first-order scavenging reactions 1 and 2, and thus the effect of reaction 4 is negligible. The greatest effect of the recombination reactions 4 and 5 is manifested in the low concentration region of the scavenger. It can be shown that the sum of the rate constants $k_1 + k_2$ may then be altered by a factor of 2 only. This will not affect the general conclusions of the present kinetic analysis.

The rate constants ratio k_2/k_1 was obtained from the limiting value $R^0(Cl^-) = 0.33$ at pH < 2. Thus we calculated

$$\frac{k_2}{k_1} = \frac{R^0(Cl^-)}{1 - R^0(Cl^-)} = 0.5 \pm 0.1$$

(9) H. L. Friedman and A. H. Zeltman, *J. Chem. Phys.*, **28**, 878 (1959).

(10) P. Riesz and E. J. Hart, *J. Phys. Chem.*, **63**, 859 (1959).

Decomposition by H Atoms at Neutral pH.—Low chloride yields were obtained at the neutral pH region 3–8. The experimental results are presented in Table I. The analytical accuracy is somewhat less satisfactory in this region, and only semiquantitative conclusions can be derived. $R(Cl^-)$ was found to be independent of pH over this whole region. The reaction yield was found to be independent of chloroacetate concentration in the region 0.05–1 M. The limiting yield in this region was found to be $R^0(Cl^-) = 0.08 \pm 0.02$.

As the dissociation constant of monochloroacetic acid is pK = 2.8, the change of the reactivity when passing from acid to neutral solutions is attributed to the change of the reacting species from the undissociated acid $CH_2ClCOOH$ to the anion CH_2ClCOO^-. The reaction mechanism in the neutral pH region is presented in the form

$$CH_2ClCOO^- + H \longrightarrow H_2 + CHClCOO^- \qquad (1')$$

$$CH_2ClCOO^- + H \longrightarrow Cl^- + CH_2COO^- + H^+ \qquad (2')$$

Application of eq. XI and the experimental value of $R^0(Cl^-)$ leads to $k_2'/k_1' = 0.09$.

The levelling-off of $R(Cl^-)$ at lower concentrations at the neutral pH region than in the acid region indicates that the sum of the scavenging rate constants $k_1' + k_2'$ is higher for the anion than the corresponding sum for the acid. Using the approximate value $R(Cl^-)/R^0(Cl^-) = 0.5$ at 0.02 M, then by application of the diffusion model we estimate $(k_1' + k_2')\varphi^{3/2} = 1.5 \times 10^6$ l. mole^{-1} sec.$^{-1}$ cm.$^{4/3}$; hence $k_1' + k_2' = 1.5 \times 10^5$ l. mole^{-1} sec.$^{-1}$.

Discussion

The rate constants for the decomposition of chloroacetic acid by atomic hydrogen are presented in Table II.

These results indicate the enhanced reactivity of the anion compared to the acid in the dehydrogenation and chloride abstraction reaction by H atoms. Recent data indicate that the relative efficiency of the dehydrogenation of the anion compared with the acid may be general for the case of aliphatic acids. The most extreme case is that of formic acid where $k_{H+HCOO^-}/k_{H+HCOOH} > 100$.[11] The increased reactivity of the formic acid anion compared with the conjugated acid was demonstrated in some other radical reactions.[12,13]

TABLE II

RATE CONSTANTS FOR SCAVENGING OF H ATOMS BY CHLOROACETIC ACID

Reacting species	k_1, l. mole^{-1} sec.$^{-1}$	k_2, l. mole^{-1} sec.$^{-1}$
$CH_2ClCOOH$	9×10^3	4×10^3
CH_2ClCOO^-	1.3×10^5	1.3×10^4

In the case of the reactivity of acetic acid with H atoms it was found that $k_{H+CH_3COO^-}/k_{H+CH_3COOH} = 3$.[13] Until recently, the different reactivity of H atoms with acids and their conjugated anions was not taken into account in radiation chemical studies of such systems.

(11) J. Rabani, *ibid.*, **66**, 361 (1962).

(12) E. J. Hart, *J. Am. Chem. Soc.*, **83**, 567 (1961).

(13) J. Rabani and G. Stein, to be published.

The rate constants ratios k_2/k_1 and k_2'/k_1' indicate that H atoms as such react with chloroacetic acid mainly by hydrogen abstraction. These results should be compared with recent radiation chemical studies of this system.[5,6] Radiation chemical investigations of aqueous chloroacetic acid solutions were interpreted by Hayon and Weiss[5] by assuming that transient negative ions formed as primary products in the radiolysis of water react with monochloroacetic acid with the formation of chloride ion. These species are the precursors of H atoms which react by dehydrogenation. The quantitative study of this system by Hayon and Allen[6] indicates that the reducing radical formed from the radiolysis of water yields Cl^- ion. H^+ and chloroacetic acid compete for this radical. The product of the reaction with H^+ ion is another radical which reacts with the acid to form either Cl^- or H_2. These studies cannot determine unambiguously the nature of the two reducing radicals.[6]

The experimental results obtained in the present work in the acid region indicate no pH dependence of the chloride yield in the pH region 0.4–2. This result rules out the formation of H_2^+ under our experimental conditions, and the participation of this radical in dehydrogenation reactions. The concentration dependence of $R(Cl^-)$ at pH 1.9 and 3.3 (Table I) cannot be adequately interpreted in terms of H atoms reacting at pH > 3 and of H_2^+ reacting at pH < 2. It thus appears that the H_2^+ molecule ion is of no kinetic importance in this system. This conclusion is consistent with the low rate of formation of this species in acid solution.[8b] The rate constants ratio $k_2/k_1 = 0.5$ obtained in our experiments using H atoms as such is in good agreement with the rate constants ratio 0.55 derived by Hayon and Allen[6] for the reactivity of the acid form of H atoms (denoted as H′ by Allen)[1,2] in irradiated solutions of chloroacetic acid. This agreement indicates that the acid form of the reducing radical formed in the radiolysis of water involves an H atom as such.

Our experimental results obtained in the neutral pH region indicate that about 90% of the H atoms scavenged by chloroacetic acid lead to dehydrogenation. On the other hand, radiation chemical studies[6] indicate that at pH 5.5 the chloride yield is $G(Cl^-) = 2.8$ at 0.01 M chloroacetic acid.[6] This value is near to the standard yield of the reducing radicals in neutral solutions, obtained from the hydrogen–oxygen[14] and ethanol–oxygen[15] systems. Thus the reducing radical formed as the *main* product by radiolysis in the neutral pH region exhibits reactivity different from the H atoms. This H atom precursor is presumably the solvated electron e_{aq}. The reaction mechanism in irradiated aqueous solutions of chloroacetic acid involves the reactions

$$e_{aq} + CH_2ClCOOH \longrightarrow Cl^- + CH_2COOH \quad (6)$$

$$e_{aq} + CH_2ClCOO^- \longrightarrow Cl^- + CH_2COO^- \quad (6')$$

$$e_{aq} + H^+ \longrightarrow H \quad (7)$$

and H atoms reacting by reactions 1 and 2.

These conclusions are consistent with the results of a previous work[8f] where the reactivity of H atoms in H_2O_2 solutions was compared with the reactivity of the reducing species formed from the radiolysis of water.[1,2] The results of the present and the previous study[8f] of the reactivity of H atoms in aqueous solutions make possible an unambiguous identification of the acid form of the reducing radical produced in the radiolysis of water. These conclusions are consistent with recent tentative identifications of the pair of the reducing radicals.[4,5] The primary reducing species e_{aq} has a sufficiently long lifetime to react with active scavengers. The conversion of e_{aq} to H atoms proceeds by reaction 7 rather than by reaction with a water molecule.

NOTE ADDED IN PROOF.—Recently, kinetic salt effects were utilized (G. Czapski and H. A. Schwarz, *J. Phys. Chem.*, **66**, 471 (1962)) as an evidence that the reducing radical produced in the radiolysis of neutral aqueous solutions may be identified as the solvated electron. This conclusion is in complete agreement with the results of the present work.

(14) C. J. Hochanadel, *J. Phys. Chem.*, **56**, 587 (1952).

(15) G. G. Jayson, G. Scholes, and J. Weiss, *J. Chem. Soc.*, 1358 (1957).

THE DECOMPOSITION OF CHLOROACETIC ACID IN AQUEOUS SOLUTIONS BY ATOMIC HYDROGEN. II. REACTION MECHANISM IN ALKALINE SOLUTIONS

BY JOSHUA JORTNER AND JOSEPH RABANI

Department of Physical Chemistry, Hebrew University, Jerusalem, Israel

Received December 21, 1961

The reactivity of atomic hydrogen in alkaline solutions of chloroacetic acid was investigated. The pH and concentration dependence yield kinetic evidence for the formation of H_2O^- in alkaline solutions: $H + OH^- \rightarrow H_2O^-$ with $k_{H+OH^-} = 6 \times 10^6$ l. mole^{-1} sec.$^{-1}$. These results are correlated with radiation chemical data, and the nature of the H_2O^- radical is discussed.

Introduction

In the preceding work[1] it was shown that H atoms generated in an electrodeless discharge and the reducing radicals produced by radiolysis of aqueous solutions at neutral pH[2,3] differ in their reactivity with chloroacetic acid. Aqueous solutions of

(1) J. Jortner and J. Rabani, *J. Phys. Chem.*, **66**, 2078 (1962).

(2) E. Hayon and J. Weiss, *Proc. Intern. Conf. Peaceful Uses At. Energy, Geneva*, **29**, 80 (1958).

(3) E. Hayon and A. O. Allen, *J. Phys. Chem.*, **65**, 2181 (1961).

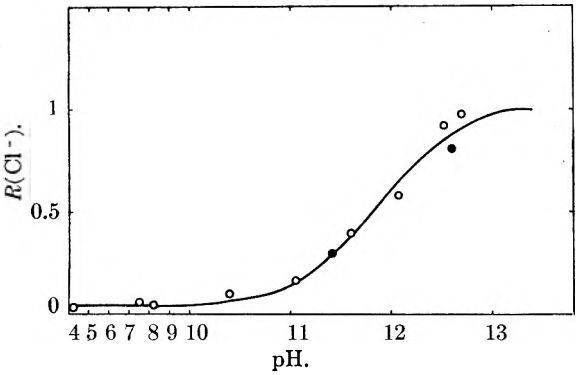

Fig. 1.—The pH dependence of $R(Cl^-)$: $[CH_2ClCOO^-]$ = 0.01 M; temperature 4°; dose rate of H atom 10^{-6} mole $l.^{-1}$ $sec.^{-1}$; volume of solution 25 cc.; duration of run 15 min.; open circles, pH adjusted with KOH; full circles, 0.25 M Na_2CO_3 added; curve calculated from eq. VI.

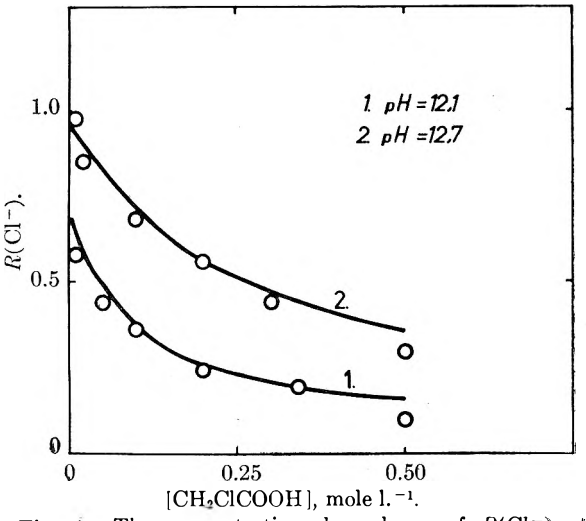

Fig. 2.—The concentration dependence of $R(Cl^-)$ at alkaline pH: experimental condition is stated in Fig. 1; curves calculated from eq. VI.

chloroacetic acid manifest different reactivity with the two forms of H atom equivalent[1-3] and are convenient for the study of H atoms in solutions. We have recently investigated the decomposition of chloroacetic acid in alkaline solutions. A preliminary report of this work was given.[4] In alkaline solutions an enhancement of chloride abstraction was observed. These results were interpreted in terms of a mechanism involving an interaction of the H atom and the OH^- ion. The species thus formed reacts with chloroacetic acid by chloride abstraction. In the present work, we present our detailed results of the reactivity of H atoms in alkaline solutions of chloroacetic acid.

Experimental

The experimental technique was the same as described in the previous work.[1] Freshly prepared solutions were always used. Solutions of chloroacetic acid in the pH region 8–13 were prepared by adjusting the pH with KOH while the solution was kept at 0°. The solutions were kept at this temperature before and after passing H atoms, which was carried out at about 4°. Blank experiments were run parallel with the analysis of irradiated solutions and corrections for hydrolysis were introduced. Chloroacetic acid solutions in the concentration region 0.01–0.05 M were found to be stable under these conditions, the amount of Cl^- did not exceed 2×10^{-5} M. In the concentration region 0.1–0.5 M the chloride content of the blank solutions did not exceed 2×10^{-4} M. Chloroacetic acid, KOH, $NaHCO_3$, Na_2CO_3, and formic acid used were of Analar grade. Water was triply distilled. Solutions were prepared in freshly boiled water. As only a negligible effect of added Na_2CO_3 on the experimental results was observed, no further precautions were necessary. pH measurements were carried out with a Metrohm pH meter equipped with an "alkaline" electrode.

Results

Chloride Yields at Alkaline pH.—The decomposition of chloroacetic acid by atomic hydrogen was investigated over the pH region 8–13 varying the chloroacetic concentration in the region 2×10^{-3}–0.5 M. From the amount of chloride produced and the dose of H atoms, the reaction yields[1] $R(Cl^-)$ for Cl^- production were obtained. The experimental results are presented in Fig. 1 and 2. These results indicate that at constant chloroacetic acid concentration, the reaction yield for Cl^- production increases with increasing pH in the pH region above 11. In this region the reaction yield for Cl^- production decreases with increasing chloroacetic acid concentration at constant pH.

We attempted to ascertain that the increase of the chloride yield at pH > 11 is not due to the hydrolysis of the reaction products, which as indicated by previous results[1,3,4] are presumably chloro derivatives of carboxylic acids. A 0.01 M chloroacetic acid solution was decomposed by H atoms at pH 7 and the pH of the solution was then adjusted to 12.6 by addition of KOH. No increase of the Cl^- concentration was observed after 1 hr. This conclusion also is consistent with the observed concentration dependence at high pH. In the previous work[1] it was shown that in the neutral pH region the chloride yield is independent of chloroacetic acid concentration in the concentration region 0.05–0.5 M. Thus in this concentration region at neutral pH, the yield of the chlorodicarboxylic acids is constant. However, in the alkaline region the concentration dependence is entirely different. These considerations rule out the above mentioned trivial mechanism of chloride production in alkaline pH.

Effects of Some Added Solutes.—In order to establish the reaction mechanism, the effect of carbonate and bicarbonate ions on the chloride yields was investigated. Experiments were carried out in the presence of $NaHCO_3$ and Na_2CO_3 (Table I). No enhanced decomposition in the presence of carbonate and bicarbonate ions was observed. On the contrary, $R(Cl^-)$ in the presence of 0.25 M Na_2CO_3 at pH 12.6 is about 15% lower than obtained at this pH in its absence.

Recent radiation chemical studies[5] indicate that H atom precursors (*i.e.*, solvated electrons) react with the HCO_3^- ion with the formation of the CO_2^- ion. It may be argued that the CO_2^- radical ion is formed in alkaline solutions by decomposition of HCO_3^- or CO_3^{-2} ion by H atoms, and that this species reacts with chloroacetic acid with Cl^- formation. This argument is not consistent with the fact that $R(Cl^-)$ is not increased by added $NaHCO_3$ and Na_2CO_3. Besides, a decrease in the chloride yield was observed in the presence of

(4) J. Jortner and J. Rabani, *J. Am. Chem. Soc.*, **83**, 4868 (1961).
(5) G. Scholes, M. Simic, and J. Weiss, *Nature*, **188**, 1019 (1960).

formate ion (Table I). This result indicates that the formate ion, $HCOO^-$, competes with the decomposition of chloroacetic acid. As dehydrogenation of the $HCOO^-$ anion leads to the formation of CO_2^-, these results indicate that this radical ion probably does not react with chloroacetic acid.

TABLE I

EFFECTS OF ADDED SOLUTES ON Cl^- YIELD IN ALKALINE SOLUTIONS OF CHLOROACETIC ACID DECOMPOSED BY ATOMIC HYDROGEN AT 4°

Dose rate of H atoms 10^{-6} mole $l.^{-1}$ $sec.^{-1}$; volume of solution 25 cc.; duration of run 15 min.

pH	$CH_2ClCOOH$, mole $l.^{-1}$	Added solutes	$R(Cl^-)$
7.5	0.010	10^{-3} *M* sodium phosphate	(0.01)
		0.25 *M* formic acid	
7.5	.010	10^{-3} *M* sodium phosphate	.04
8.15	.010	10^{-3} *M* sodium phosphate	.05
		0.25 *M* sodium bicarbonate	.05
8.10	.010	10^{-3} *M* sodium phosphate	
11.43	.010	0.25 *M* sodium carbonate	.30
11.4	.010	KOH	.30
12.66	.010	0.25 *M* sodium carbonate	.80
12.7	.010	KOH	.95

Reaction Mechanism in Alkaline pH.—The increased chloride yields at alkaline pH are attributed to the interaction of H atom and OH^- ion with the formation of a species which will be denoted H_2O^-.

$$H + OH^- \longrightarrow H_2O \qquad (1)$$

This "alkaline" form of H atoms will react with chloroacetic acid anion by chloride formation:

$$H_2O^- + CH_2ClCOO^- \longrightarrow Cl^- + CH_2COO^- + H_2O \qquad (2)$$

Reaction 1 competes with the first-order scavenging reactions of H atoms by chloroacetic acid

$$CH_2ClCOO^- + H \longrightarrow H_2 + CHClCOO^- \qquad (3)$$

$$CH_2ClCOO^- + H \longrightarrow Cl^- + H^+ + CH_2COO^- \qquad (4)$$

At low chloroacetic acid and OH^- ion concentrations, H atom recombination should be considered

$$2H \longrightarrow H_2 \qquad (5)$$

This mechanism accounts properly for the pH and concentration dependence of $R(Cl^-)$.

Evaluation of Experimental Data.—The experimental results were treated by application of the diffusion model,[6] which is probably most adequate for semiquantitative evaluation of rate constants from such experiments. Neglecting the diffusion of the active intermediate H_2O^-,[6] the concentration of H atoms is given by the expression

$$D\frac{\partial^2[H]}{\partial X^2} = k_5[H]^2 + P[H] \qquad (I)$$

where

$$P = k_3\left\{\left(1+\frac{k_4}{k_3}\right)[CH_2ClCOO^-] + \frac{k_1}{k_3}[OH^-]\right\} \qquad (II)$$

In the present treatment the concentration of OH^- ion will be defined by $[OH^-] = 10^{-14+pH}$.

Following the notation used in previous work,[1,6] the total reaction yield for H_2 and Cl^- production is given by

$$R(Cl^-) + R(H_2) = \Delta/W \qquad (III)$$

where

$$2\Delta^3 + 3\Delta^2 + \Delta = W = \frac{k_5 A}{6P^{3/2}D^{1/2}\varphi} \qquad (IV)$$

Setting the experimental value $A = 2.5 \times 10^{-8}$ mole $sec.^{-1}$, $D = 4 \times 10^{-5}$ $cm.^2$ $sec.^{-1}$, and using the rate constants ratio[1] $k_4/k_3 = 0.09$ we get

$$W = \frac{6.6 \times 10^6}{\left\{1.09[CH_2ClCO_2^-] + \frac{k_1}{k_3}[OH^-]\right\}^{3/2}(k_3\varphi^{2/3})^{3/2}} \qquad (V)$$

The reaction yield for chloride production is given by

$$R(Cl^-) = \frac{0.09[CH_2ClCO_2^-] + \frac{k_1}{k_3}[OH^-]}{1.09[CH_2ClCO_2^-] + \frac{k_1}{k_3}[OH^-]}\frac{\Delta}{W} \qquad (VI)$$

An estimation of the rate constants ratio k_1/k_3 was carried out by using the experimental results at pH 12.7. At high OH^- concentration, H atom recombination can be neglected and then $\Delta/W = 1$. Applying this simplifying assumption, eq. VI can be written in the form

$$\frac{k_1}{k_3}[OH^-](1 - R(Cl^-)) = [CH_2ClCOO^-](1.09\,R(Cl^-) - 0.09) \qquad (VII)$$

A plot of the experimental results at pH 12.7 according to eq. VII (Fig. 3) yields a straight line with an intercept of zero, as required by eq. VI. From the slope we obtain $k_1/k_3 = 4.5 \pm 1$.

The pH dependence and the concentration dependence of $R(Cl^-)$ in alkaline solution could be adequately fitted by eq. VI setting $k_1/k_3 = 4.5$; $(k_3\varphi^{2/3})^{3/2} = 3 \times 10^9$ $l.^{3/2}$ $mole^{-3/2}$ $sec.^{-3/2}$ $cm.^2$. The value of $k_3 = 1.4 \times 10^5$ l. $mole^{-1}$ $sec.^{-1}$ obtained by setting $\varphi^{2/3} = 10$ $cm.^{4/3}$ is consistent with the value estimated from the experimental results at neutral pH.[1]

Discussion

The comparison between the experimental results and the calculated data according to eq. VI is presented in Fig. 1 and 2. It thus appears that the experimental results are satisfactorily accounted for by the proposed mechanism involv-

(6) G. Czapski, J. Jortner, and G. Stein, *J. Phys. Chem.*, **65**, 956 (1961).

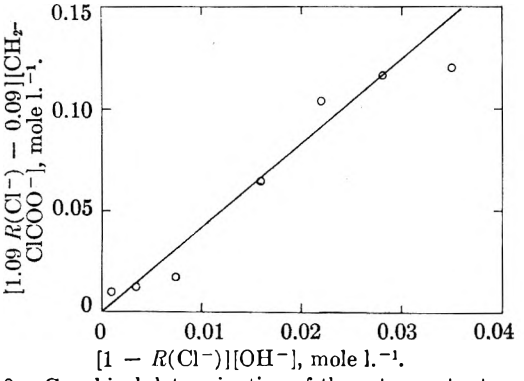

Fig. 3.—Graphical determination of the rate constants ratio k_1/k_3 according to eq. VII.

ing H_2O^- formation. The rate constant for the formation of this species is 6×10^5 l. mole^{-1} sec.$^{-1}$.

These results yield kinetic evidence for the interaction of H atom with OH^- ion in alkaline solutions. The nature of the species thus formed, which we denote H_2O^-, should be briefly considered. The product of the reaction with chloroacetic acid of the species produced under our experimental conditions is identical with that of the reducing species produced by the radiolysis of neutral aqueous solutions.[1-3] The latter species is identified as the solvated electron. The problem of electron binding in water[7-9] and in non-aqueous solutions[10,11] was treated by the application of a continuous dielectric model for the system.

The most plausible picture is an electron bound by the polarization of the dielectric medium. The electron solvated according to this model is delocalized and its charge distribution is distributed over few solvent molecules. This picture was applied for electrons produced in irradiated neutral solutions.[7-9] On the other hand, the species H_2O^- where the unpaired electron is localized on a single water molecule (presumably in a $3s\sigma$ orbital) is not stable in the gaseous phase. Experimental[12] and theoretical[13] evidence indicates that a single water molecule in the gaseous phase does not exhibit a positive electron affinity. However, in a polar medium the species H_2O^- may be stabilized by solvation. It is not clear at present whether the species produced by reaction 1 does lead to electron delocalization. We can only conclude at present that the similar reactivity of the alkaline form of H atoms produced under our experimental conditions, and of H atom precursors in radiation chemistry, may indicate their identity.

In the concentration region of chloroacetic acid below 10^{-2} *M* at constant high pH, a decrease of the chloride yield was observed. At pH 12.1 at 0.01 *M* CH_2ClOO^-, we get $R(Cl^-) = 0.58$, decreasing to $R(Cl^-) = 0.47$ at 0.005 *M* CH_2ClCOO^-. At pH 12.7, $R(Cl^-)$ decreased from 0.98 at 0.01 *M* CH_2ClCOO^- to $R(Cl^-) = 0.66$ at 0.002 *M* CH_2ClCOO^-. The decrease is outside of the experimental uncertainty and should be considered as significant. The reaction scheme proposed above postulates that the species H_2O^- once produced reacts with the acid with Cl^- production. However, when the chloroacetic acid concentration is reduced, alternative mechanisms for the disappearance of H_2O^- have to be considered.

The decomposition reactions of H_2O^- without chloride production may proceed by the recombination reactions $2H_2O^- \rightarrow H_2 + 2OH^-$ and $H + H_2O^- \rightarrow H_2 + OH^-$, which were not considered in the kinetic scheme. Besides, at low scavenger concentrations, the reaction products may compete for the H_2O^- without chloride production.

The present results yield the first evidence for the enhanced reactivity of H atoms in alkaline solution. Reaction 1 was previously postulated in radiation chemical studies.[2,14] However, these experimental results can be accounted for adequately by the formation of e_{aq} (or H_2O^-) as a *primary* product in irradiated solutions.

In a previous work from this Laboratory[15] no enhanced decomposition of H_2O_2 at pH 13 relative to pH 7 was observed. However, the dissociation constant of H_2O_2 is pK = 11.8 at 20°.[16,17] Thus under these experimental conditions the decomposition of the HO_2^- ion was investigated. Therefore the interpretation of those experimental results would require the consideration of two possible superimposed pH effects.

Acknowledgment.—This research was sponsored by the Israel Atomic Energy Commission. We wish to thank Professor G. Stein for his interest and valuable comments.

(7) G. Stein, *Discussions Faraday Soc.*, **12**, 227, 289 (1950).
(8) R. L. Platzman and H. Frohlich, *Phys. Rev.*, **92**, 1152 (1953).
(9) J. Weiss, *Nature*, **186**, 751 (1960).
(10) S. Pekar, *J. Phys. (USSR)*, **10**, 341, 347 (1946).
(11) J. Jortner, *J. Chem. Phys.*, **29**, 823 (1959).
(12) N. E. Bradbury and H. E. Tatel, *ibid.*, **2**, 839 (1934).
(13) F. O. Ellison and H. Schull, *ibid.*, **23**, 2348 (1955).
(14) J. H. Baxendale and G. Hughes, *Z. physik. Chem.* (Frankfurt), **14**, 323 (1958).
(15) J. Jortner, G. Czapski, and G. Stein, *J. Phys. Chem.*, **65**, 564 (1961).
(16) M. G. Evans and N. Uri, *Trans. Faraday Soc.*, **45**, 224 (1949).
(17) J. Jortner and G. Stein, *Bull. Res. Council Israel*, **A6**, 239 (1957).

SYNTHESIS AND CHARACTERIZATION OF SOME HIGHLY CONJUGATED SEMICONDUCTING POLYMERS

BY H. A. POHL* AND E. H. ENGELHARDT

School of Engineering, Princeton University, Princeton, New Jersey

Received December 21, 1961

Conductivity, energy interval (corresponding to the energy gap in single crystal semiconductors), thermoelectric power, Hall coefficient, Ohmic behavior, spin concentration, photoconductivity, and photo-voltage were studied, using a series of synthetic organic polymer semiconductors. These included the polyacene quinone radical polymers, polyquinazones, a polyacene, and aniline black. Conduction was shown to be electronic, not ionic, and, in a homologous series, to depend upon the chemical structure. The conductivity–thermoelectric power data are best fitted by a two-carrier model. A slight field dependence of conductivity is observable. A common feature of high conjugation appears in these semiconductors. High spin concentration (e.s.r.) parallels high conductivity, but spin concentrations greatly exceed the apparent carrier concentrations.

Introduction

Semiconductors, as presently regarded, are materials which have electrical conductivity characteristics somewhere between those of insulators and metals. They are broadly characterized by a conductivity at room temperature in the range 10^3 mho/cm. down to about 10^{-12} or 10^{-14} mho/cm. Additional criteria which are useful in differentiating semiconductors from metals may include a positive temperature-conductivity coefficient, a high sensitivity to certain impurities or to morphology, and a high Seebeck or Hall coefficient.

In recent years the literature on organic semiconductors has increased considerably. Comprehensive reviews have been made by Akamatsu,[1,2] Eley,[3] Garrett,[4] and Pohl.[5-7] The organic semiconductors developed to date, all of which are based on a high degree of conjugation, may be considered conveniently almost without exception in two broad categories, (a) crystals of monomeric solids or (b) polymeric bodies. The latter may be bonded datively (as in the donor–acceptor complexes), covalently (as in conventional organic polymers), or ionically (as in the salts of organic ions). The smaller organic monomers, such as naphthalene and anthracene, are insulators.[1,8,9] Some of the larger[3,9] (*e.g.*, violanthrone[2] B or the phthalocyanines)[8,10] show appreciable semiconduction.

The datively bonded charge transfer complexes may show considerable conduction,[1,3,11-16] some as high as 10^{-1} mho/cm., but they are generally of low thermal stability.

Polymers with extensive conjugation and highly enhanced electronic properties are formed, for example, by the destructive cyclization[17-19] of organic materials. The heat-induced dehydrochlorination of polyvinyl chloride and polyvinylidene chloride copolymers, the dehydration of sugar,[20] and the pyrolysis of many organic compounds at temperatures above 400–600° all are examples of this technique.

Work in the field of pyrolyzed polymers and polymer carbons has been reported, for example, by Baker,[18] Mrozowski,[21,22] Oster,[23] Pohl,[5-7,24-28] and Turkevich.[20]

Directly synthesized semiconducting polymers, as opposed to pyrolytic polymers, have only recently been reported.

In 1959, Pohl and Itoh[7,29] prepared a large number of semiconducting phenolphthalein-type polymers, made by treating various phenols with acid anhydrides. McNeill and Weiss[30] reported on the preparation of xanthene-type polymers related to fluorescein. Conductivities as low as 1.4×10^{-4} mho/cm. were observed.

A polymeric copper phthalocyanine with semiconducting properties has been prepared by replacing phthalic anhydride with pyromellitic di-

* Department of Chemistry, Polytechnic Institute of Brooklyn, Brocklyn, N.Y.

(1) H. Akamatsu and H. Inokuchi, "Solid State Physics," Vol. 12, ed. by F. Seitz and D. Turnbull, Academic Press, New York, N. Y., 1955.

(2) H. Akamatsu, *Kagaku to Kogyo* (Tokyo), **11**, 607 (1958).

(3) D. D. Eley, *Research*, **12**, 293 (1959).

(4) C. G. B. Garrett, Chapter on "Organic Semiconductors," in "Semiconductors," ed. by N. B. Hannay, Reinhold Publ. Corp., New York, N. Y., 1959.

(5) H. A. Pohl, *Chem. Eng.*, **68**, 104 (1961).

(6) H. A. Pohl, *Electro-Technol.*, **67**, 85 (1961).

(7) H. A. Pohl, "Semiconduction in Polymers," Plastics Lab. Tech. Report 61D, Princeton Univ., 1961; also, chapter in "Modern Aspects of the Vitreous State," ed. by J. D. Mackenzie, Butterworths, New York, N. Y., 1962.

(8) A. Terenin, *Proc. Chem. Soc.*, 321 (1961).

(9) M. Wilk, *Z. Elektrochem.*, **64**, 930 (1960).

(10) A. T. Vartanyan, *Acta Physicochim. URSS*, **22**, 201 (1947).

(11) H. Akamatsu, H. Inokuchi, and Y. Matsunaga, *Bull. Chem. Soc. Japan*, **29**, 213 (1956).

(12) J. Kommandeur and F. R. Hall, *J. Chem. Phys.*, **34**, 129 (1961).

(13) J. Kommandeur and L. S. Singer, *ibid.*, **34**, 133 (1961).

(14) M. M. Labes, R. Sehr, and M. Bose, *ibid.*, **32**, 1570 (1960).

(15) M. M. Labes, R. Sehr, and M. Bose, "Semiconduction in Molecular Solids," Proc. of the Princeton Conf., Ed. by H. A. Pohl, Ivy-Curtis Press, 1960.

(16) O. H. Leblanc and C. M. Huggins, *Nature*, **186**, 552 (1960).

(17) J. J. Bohrer, *Trans. N. Y. Acad. Sci.*, **20**, 367 (1958).

(18) F. H. Winslow, W. O. Baker, and N. R. Pape, *J. Polymer Sci.*, **16**, 101 (1955).

(19) F. H. Winslow, W. Matreyek, and W. A. Yager, *Ind. Carbon & Graphite*, 190 (1958).

(20) J. Turkevich, ref. 15, p. 85.

(21) S. Mrozowski, *Phys. Rev.*, **85**, 609 (1952); *errata*, **86**, 1056 (1952); **92**, 1320 (1953).

(22) S. Mrozowski, *J. Chem. Phys.*, **21**, 492 (1953).

(23) G. Oster, G. Oster, and M. Kyszewski, *Nature*, **191**, 164 (1961).

(24) J. P. Laherrere and H. A. Pohl, ref. 15, pp. 93–123.

(25) H. A. Pohl, "Proc. Fourth Conf. on Carbon," Pergamon Press, 1960, pp. 241–257.

(26) H. A. Pohl and J. P. Laherrere, ref. 25, pp. 259–265.

(27) H. A. Pohl, ref. 15, pp. 9–24.

(28) H. A. Pohl and S. A. Rosen, "Proc. Fifth Conf. on Carbon," Pergamon Press, London, 1960, in press.

(29) J. A. Bornmann and H. A. Pohl, "Further Studies on Some Semiconducting Polymers," Plastics Laboratory Technical Report 63A, Sept., 1961, Princeton Univ., 1961.

(30) (a) R. McNeill and D. E. Weiss, *Australian J. Chem.*, **12**, 643 (1959); (b) R. McNeill and D. E. Weiss, ref. 25, pp. 281–290.

anhydride in the phthalocyanine dye synthesis.[31,32] Eley[33] reported on dehydrated proteins, which showed very low conductivities for the most part.

Berlin[34] recently has written an excellent review of Russian work on highly conjugated polymers. Several directly synthesized semiconducting polymers including polyphenyleneazo-compounds and a polymer of diethylnybenzene were discussed.

Experimental

It seems probable that a prerequisite for enhanced electronic behavior in organic polymers is that they contain a set of highly conjugated systems. Until recently, polymers which might meet this criterion generally have been avoided purposefully. This necessitated our development of new classes of polymers, only several of which had been described previously. The materials synthesized in this study include condensation polymers of acenes with aromatic acid anhydrides, condensation polymers of 1,2,4,5-tetrabromobenzene, condensation polymers of diisocyanates and quinones, and aniline black polymers. Studies were made using various useful physical parameters such as e.s.r., Seebeck coefficient (thermoelectric power), Hall effect, nonohmic character, specific conductivity and its temperature coefficient, and the electronic (*vis-a-vis* ionic) nature of the conduction.

Syntheses. Polyacene Quinone Radical Polymers (P-AQR-Polymers).—The relative ease of synthesis and the interesting electronic nature of the quinone and lactone structures evoked the investigation of a polymer class based on various acene nuclei linked by both quinone and lactone groups, *e.g.*

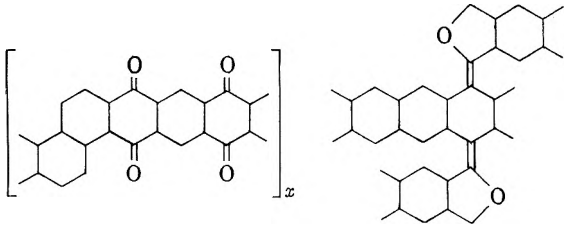

A synthesis analogous to that commonly employed for making simple quinones was used to condense pyromellitic dianhydride with analogs of naphthalene.

The Freidel–Crafts type of reaction on an acid anhydride or acid chloride is one of the most useful methods for affecting inter- and intramolecular acylations. A wide variety of conditions for acylations, using Lewis acids, is available from the literature.[35-38]

In this study, two methods were used for condensing derivatives of pyromellitic acid, etc., with a number of acenes.

PAQR-I, Polymers.—The first procedure involved reaction of pyromellitic dianhydride or phthalic anhydride with several aromatics to produce a homologous series of polymers.

The desired molar ratio of anhydride and acene was mixed by grinding in a mortar. Generally 2 moles of zinc chloride catalyst was added per mole of acid anhydride. After the components were mixed thoroughly, they were placed in a 150 × 20-mm. test tube and heated for the desired time in a constant temperature bath. Since it was determined that the presence of air during reaction had rather little effect on conductivity of the polymers, the reaction tubes were merely stoppered. The majority of polymerizations were carried out at 256 or 306° for 24 hr.

At the completion of polymerization, the polymers were ground to fine powders. The materials were leached with dilute hydrochloric acid for 12 hr. to aid in removing the zinc chloride catalyst. Subsequent to the leaching, the powders were extracted with water for 12 hr., ethanol for 24 hr., and benzene for 12 hr., in a Soxhlet apparatus. The polymers then were dried at 50° for 12 hr. After drying, the materials again were finely ground and stored in a desiccator until evaluations were to begin.

The zinc chloride-catalyzed PAQR polymers were, in all cases, black, insoluble, infusible materials containing from 1 to 5 p.p.m. of Zn. Yields expressed as the ratio of polymer-to-dianhydride plus acene ranged from approximately 5 to 50%, depending on the reactivity of the hydrocarbons.

Examination of the polymer structure by infrared and X-ray analyses was unsuccessful, necessitating conclusions based on elemental analysis and on analogy with model syntheses reported in the literature.

Two general possibilities for reaction mechanism during acylation are encountered. One mechanism leads to the formation of a keto or a quinone linkage; the alternate produces a lactone structure.

Several workers, including Marschalk,[39] have published papers concerning the synthesis of quinones under conditions roughly similar to those employed in this study. Marschalk reported synthesis and positive identification of linear quinones, up to 11 rings, from reaction of pyromellitic dianhydride and naphthalene at 200°.

The formation of lactones also is known to occur under the conditions employed in our zinc chloride-catalyzed system. A review of the literature indicates that this reaction seems to be predominant only when electron donating substituents are present on the acene. Such examples, however, are based only on observations with benzene and its derivatives. The higher resonance stability of the larger acenes might well influence the ratio of quinone formation to lactone formation.

On the basis of analogy to past investigations, it therefore was inferred that a majority of the linkages would be keto or quinone, as opposed to lactone. In addition to the directly formed links, a number of secondary linkages and groupings could have been formed. At the reaction conditions employed, semiquinones, hydroquinones, etc., could have resulted from a partial reduction, rearrangement, acylation, and other reactions of quinone groups, giving rise to a number of coexistent structures, many of which are known to be free radical.[40]

Carbon, hydrogen, oxygen analyses for several polymers, made with equimolar quantities of acene and dianhydride, indicate that the polymers contain approximately 2 moles of acene per mole of pyromellitic dianhydride, with a loss of 2 moles of water. Polymers made with a higher ratio of dianhydride to monomer contained an increased percentage of oxygen.

Sample 26	C	O	H	(Mole %)
Actual	64.2	4.6	31.2	(Av. of duplicates)
Theoretical (assumes 2 acene per PMA)	63.3	6.67	30.0	
Sample 39				
Actual	63.4	6.0	30.6	(Av. of duplicates)
Theoretical (assumes 2 acene per PMA)	65.6	6.25	28.1	

Sample no.	Moles PMA	Moles pyrene	% C	% O	% H
39	1	1	83.90	10.57	3.33
40	3	1	77.24	15.30	2.72

(31) A. Epstein and B. S. Wildi, *J. Chem. Phys.*, **32**, 324 (1960).

(32) W. Felmayer and I. Wolf, *J. Electrochem. Soc.*, **105**, 141 (1958).

(33) D. D. Eley, H. Inokuchi, and M. R. Willis, *Discussions Faraday Soc.*, **28**, 54 (1960).

(34) A. A. Berlin, *Khim. Teknol. Polymeriv.*, **7-8**, 139 (1960), translation in English by H. N. Friedlander, Standard Oil Information Division, Translation TR 60-122.

(35) J. W. Cook and C. L. Hewett, *J. Chem. Soc.*, 398 (1933).

(36) E. A. Speight, A. Stevenson, and J. F. Thorpe, *ibid.*, **125**, 2185 (1924).

(37) J. Thiele and A. Wanscheidt, *Ann. Chem.*, **376**, 269 (1910).

(38) A. Winterstein, H. Vetter, and K. Schoen, *Ber.*, **68**, 1079 (1953).

(39) C. M. Marschalk, *Bull. Soc. Chem.*, **9**, 400 (1942).

(40) G. W. Wheland, "Resonance in Organic Chemistry," John [illegible] N. Y., 1955.

PAQR-II, Polymers.—Polymers also were prepared by the Freidel–Crafts synthesis, employing $AlCl_3$ as a catalyst and nitrobenzene as a solvent. The purification procedure was the same as that previously described for the zinc chloride catalyzed polymers.

Polyacenes.—An attempt was made at preparation of polyacenes, using a procedure similar to that previously outlined by Edwards and Goldfinger.[41] The reaction involved the condensation of 1,2,4,5-tetrabromobenzene by a Wurtz–Fittig type reaction using Na–K alloy.

The yellow-red, polymeric material was separated from the solvents and washed with ethanol to remove safely all traces of the metals. After washing with hexane and drying, the polymer was ground and extracted with water, ethanol, and benzene. The fractions soluble in hot ethanol and benzene were recovered by evaporation.

Quinazone Polymers (Schiff's Base Type).—A polymer with a potentially highly conjugated structure was made by reacting di- and triisocyanates with quinones. The reaction, which was reported by Lieser and Nischk,[42] is

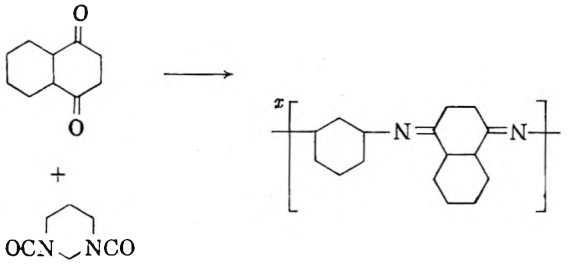

Polymerizations were done by heating equimolar quantities of quinones and polyfunctional isocyanates, in the absence of air, to temperatures as high as 300°. A reaction was immediately apparent from formation of a deep brown color. Depending on temperature, the mass remained liquid for a certain period of time and then rapidly solidified. Deep brown, insoluble, infusible materials were produced. The polymers were ground and extracted in the manner previously described for the polyacene quinones.

Aniline Black Polymer.—A number of references in the literature describe resistivity measurements on various commercial aniline dyes.[10,43] We synthesized a polymeric material by oxidizing aqueous aniline hydrochloride with $NaClO_3$. This material, which is soluble in ethyl ether, was extracted thoroughly with water and ethanol. A suggested structure for this polymer was given by Packer[44] as

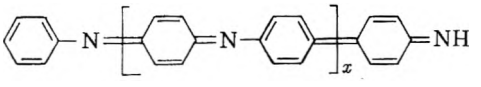

Characterization Methods.—Generally, all of the polymers evaluated in this program were insoluble, infusible materials, and consequently were powdered and examined as molded pellets.

The resistivity of the polymers was measured by a d.c. technique, using field strengths below 150 v./cm.

The powdered polymers were contained in an electrically heated steel cell, with platinum contacts, capable of being loaded to pressures in excess of 10,000 kg./cm.^{2}. Tetrafluoroethylene and Nylatron (nylon polymer containing *ca.* 30% MoS_2) were used as electrical insulators.

An inherent cell resistance well in excess of 10^{13} ohms was determined by measurements with mica spacers. This cell limitation was several orders of magnitude higher than the maximum values of interest in this study. The polymer resistivity samples were in the form of fine powders, which were stored in a desiccator over silica gel until used.

The Seebeck coefficient and related parameters of several polymers were studied as a function of average sample temperature, temperature gradient across the sample, and compaction pressure.

A cylindrical cell with a Pt sample contact surface area of approximately 4.3 cm.^{2} was used for the measurements.

The Seebeck coefficient was calculated as

$$Q = \Delta V/\Delta T, \ \mu v./°C.$$

where V is the thermal e.m.f. across the platinum-polymer–platinum junctions, and T the thermal gradient between platinum electrodes.

Values of thermoelectric power presented in this paper have been corrected for the effect of platinum, and therefore are absolute. Values for the absolute thermoelectric power of platinum were obtained from the work of Wilson.[45]

A magnetic field of approximately 17 kgauss was used for Hall voltage determinations.

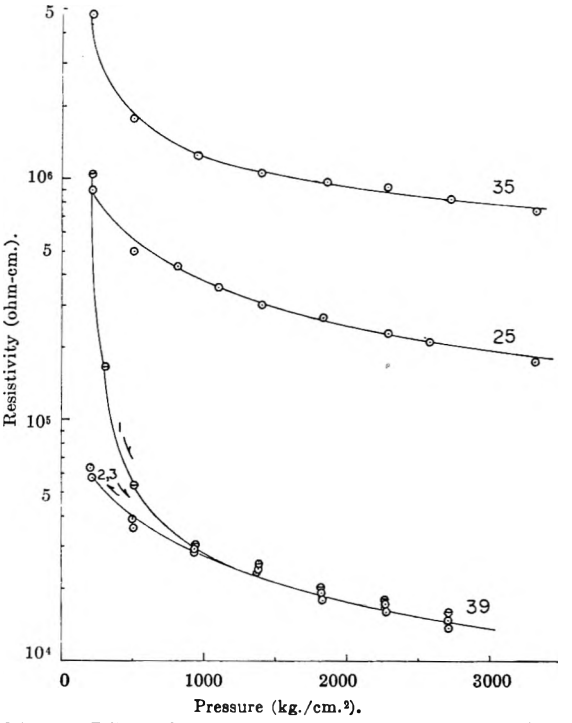

Fig. 1.—Effect of measurement pressure on the resistivity of PAQR polymers. Curve numbers correspond to polymers described in Tables V and VI.

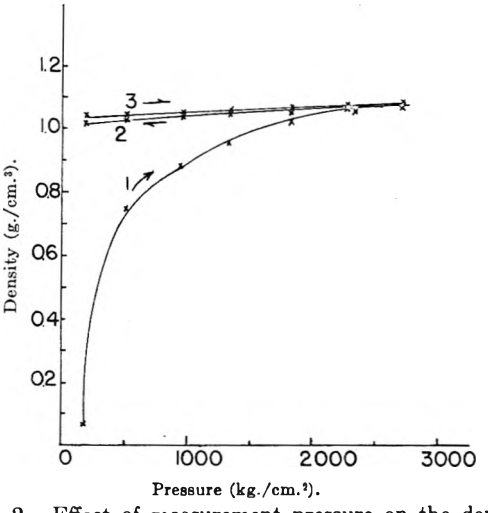

Fig. 2.—Effect of measurement pressure on the density of PAQR polymers: curve 1, taken on initial compression; curves 2 and 3 followed.

(41) G. A. Edwards and G. Goldfinger, *J. Polymer Sci.*, **16**, 589 (1955).

(42) T. Lieser and G. Nischk, *Ann. Chem.*, **569**, 66 (1950).

(43) G. P. Brown and S. Aftergut, "Investigation of Organic Semiconductors," WADC Tech. Report 59-469, Sept., 1960.

(44) J. Packer and J. Vaughan, "Organic Chemistry," Clarendon Press, London, 1958.

(45) A. H. Wilson, "Theory of Metals," 2nd Ed., Cambridge Univ. Press, 1953, p. 207.

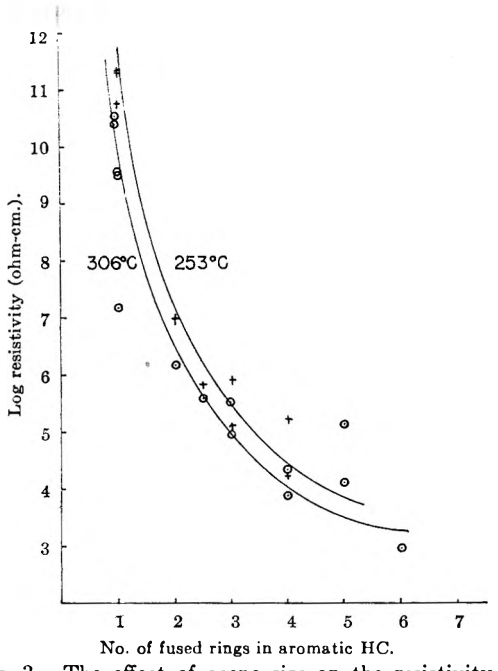

Fig. 3.—The effect of acene size on the resistivity$_{25°}$ of PAQR polymers: +, polymerization at 253°; ⊙, polymerization at 306°.

Polymer samples were compacted into briquettes, 1 × $^1/_4$ × $^1/_{16}$ in., and placed into a special yoke for insertion between the magnet poles. The yoke contained the customary end contacts for carrier supply as well as the Hall contacts for measuring transverse potential gradient.

The transverse potential gradient of samples in a magnetic field was measured with a Leeds–Northrup model K-3 potentiometer. Magnetic field strength and direction, as well as current through the sample, were recorded.

The transverse e.m.f. gradient, induced by the magnetic field, was obtained by reversing the field several times and recording the potential with each field direction. Average values for each field direction then were used to obtain the Hall voltage.

$$\text{E.m.f.} = \frac{(A + \Delta\text{e.m.f.} - (A - \Delta\text{e.m.f.})}{2}$$

where

A = asymmetric potential of the sample
Δe.m.f. = Hall voltage, v.

$$R_H = \frac{10^8 t(\Delta\text{e.m.f.})}{IH}$$

where

I = longitudinal current (amp.)
H = field strength (gauss)
t = thickness of sample (cm.)
R_H = Hall coefficient (cm.^{3}/coul.)

The concentration of unpaired electrons in polymer samples was determined by the electron spin resonance method with a conventional spectrometer operating at 8550 megacycles. Spin concentrations in a number of polymers were measured in the equipment of Dr. R. Pressley, with his considerable assistance, at the Palmer Physical Laboratory using a carefully purified (by ether crystallization) polycrystalline sample of diphenyl picryl hydrazyl (DPPH) as a standard.

Pressure Resistivity.—In order to select an appropriate sample-compaction pressure for the bulk of the resistivity determinations, in this work the relationship between resistivity and pressure was studied for three representative polymers. The results are shown in Fig. 1 and 2.

Below approximately 1000 kg./cm.^{2}, large incremental changes in resistivity were observed, probably due to the presence of voids in the sample. At higher pressures, the elimination of voids probably becomes subordinate to the normal decrease in resistivity due to orbital overlap, etc.

Curve 3 shows the effect of repeated pressure cycling on the resistivity–pressure characteristics. After one compaction cycle above 1500 kg./cm.^{2}, the materials exhibit essentially reversible behavior.

Based on the observed characteristics, a compaction pressure in excess of 1500 kg./cm.^{2} was deemed necessary to ensure reliability of measurements. In order to compare conveniently the results of this investigation with concurrent work[29,46,47] in this Laboratory on the other directly synthesized semiconductors, a compaction pressure of 1800 ± 70 kg./cm.^{2} was used in the resistivity determinations, except where noted. The polymer compositions, except where noted, are reported as based on initial composition of the monomer mixture.

Results

In an attempt to gain some insight as to the conduction mechanism in PAQR Polymers, a "homologous" series was prepared. Fourteen aromatic neuclei were incorporated into the zinc chloride-catalyzed pyromellitic dianhydride–acene polymer. The results are summarized in Table I. A decrease in resistivity was observed as the size of fused aromatic nuclear portion of the acene component of the polymer increased. The correlation between acene size and polymer resistivity is presented in Fig. 3.

TABLE I

EFFECT OF THE AROMATIC CO-MONOMER ON THE ROOM TEMPERATURE RESISTIVITY OF PAQR POLYMERS

ACENE/PMA/$ZnCl_2$ = 1/1/2; polymerization time = 24 hr.

Sample no.	Acene	Polymerization temp. 253°	Polymerization temp. 306°
50	Biphenyl		3.4×10^{10}
31, 51	Terphenyl	5.6×10^{10}	1.4×10^{7}
33, 52	Naphthalene	9.7×10^{6}	1.4×10^{6}
35, 53	Anthracene	8.3×10^{5}	3.2×10^{5}
37, 54	Phenanthrene	1.0×10^{5}	9.2×10^{4}
39, 55	Pyrene	1.6×10^{4}	7.6×10^{3}
41, 56	Chrysene	1.6×10^{5}	2.1×10^{4}
46, 58	Triphenylchloromethane	4.6×10^{11}	3.7×10^{9}
66, 67	Triphenylmethane	5.8×10^{11}	3.1×10^{9}
48, 59	Fluoranthrene	4.4×10^{5}	3.5×10^{5}
85	Perylene		1.8×10^{5}
86	Dibenzpyrene		9.5×10^{2}
87	Picene		1.6×10^{4}
68	Ferrocene	1.7×10^{9}	

Polymers formed by the condensation of acenes with phthalic anhydride generally exhibitied somewhat higher resistivities than the acene–pyromellitic dianhydride series. The results of condensations with six aromatic hydrocarbons are presented in Table II.

Heteroatoms seem to increase the conductivity of the PAQR polymers.

A polymer made with acridine exhibited similar

(46) H. A. Pohl, J. A. Bornmann, and W. Itoh, "Semiconducting Polymers," Plastics Lab. Tech. Report 60C, Princeton Univ., 1961; *cf. J. Electrochem. Soc.*, in press.

(47) H. A. Pohl and D. A. Opp. Abstracts of papers presented at Chicago, Ill., Sept., 1961, Div. Phys. Chem., American Chemical Society, pp. 32–33.

TABLE II

EFFECT OF THE ACID ANHYDRIDE ON RESISTIVITY OF PAQR POLYMERS

Constant polymerization condition: temperature = 253°; time = 24 hr., 2 moles $ZnCl_2$ per mole anhydride

Samples	Hydrocarbon	Resistivity (ohm-cm.) 1 mole phthalic anhydride / 1 mole hydrocarbon	Resistivity (ohm-cm.) 1 mole PMA / 1 mole hydrocarbon
60, 33	Naphthalene	3.2×10^5	9.7×10^6
61, 35	Anthracene	6.1×10^6	8.4×10^5
62, 37	Phenanthrene	8.4×10^6	1.0×10^6
63, 39	Pyrene	5.9×10^4	1.6×10^4
64, 46	Triphenylchloromethane	2.0×10^{12}	4.6×10^{11}
65, 41	Chrysene	8.6×10^5	1.6×10^5

resistivity to anthracene, while an anthraquinone PAQR polymer exhibited a markedly lower value. Values are presented in Table III.

TABLE III

EFFECT OF HETEROATOMS IN THE ACENE

Acene	Polymerization—Temp. (°C.)	Polymerization—Time (hr.)	Room temp. Resistivity (ohm-cm.)
Anthracene	306	24	1.8×10^5
Acridine	306	24	6.8×10^6
Anthraquinone	306	24	1.2×10^4

The introduction of a nitrogen in place of the gamma carbon would not be expected to affect radically the intramolecular conjugation, hence resistivity. Presence of the quinone groups on the acene could lead to a higher number of electrically unstable linkages in the polymer or possibly to a side reaction consisting of fusion of quinones to give large ring systems for incorporation into the polymer. Alternatively, increased internal polarity introduced by the heteroatoms would be expected to increase chain–chain transfer of carriers.

Thermal Activation Energy.—The relationships between measurement temperature and resistivity were obtained at compaction pressures of 650 and 1820 kg./cm.^{2}. The temperature range extended from approximately 25 to 100°.

It was determined that the logarithm of resistivity for the polymers is a linear function of reciprocal temperature in the range under study.

Both thermal activation energy (E_a), and "energy interval," (E_g), values were obtained for the series. The quantities are described by

$$\rho = \rho_0 \exp(E_a/KT)$$

and

$$E_g = 2E_a$$

where

ρ_0 = constant
ρ = resistivity at T
K = Boltzmann constant

It should be noted that although the quantity E_g might be used here to describe the thermal activation behavior, adherence to the simple band theory is not implied.[29] The activation energy, or "energy gap," in organic semiconductors probably is a function of both intra- and intermolecular barriers, and therefore is a composite of both. For the present it seems preferable to refer to $E_g = 2E_a$ as the "energy interval" rather than energy gap or forbidden band gap in the case of the organic semiconductors until it is shown that the particular sample meets the theoretical requirements implied in the use of the term energy gap. At present, justification for the use of E_g in describing polymeric organic semiconductors lies only in the facilitation of comparison with other semiconductor systems.

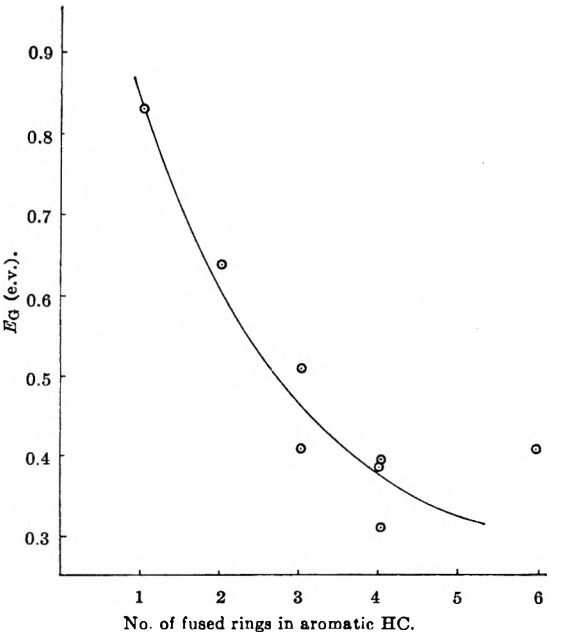

Fig. 4.—"Energy gap," (2 × activation energy), as a function of monomeric acene size in PAQR polymers.

Values of activation energy and ρ_0 for representative PAQR polymers are summarized in Table IV.

For the series of polymers measured, E_g values ranged from approximately 0.3 to 0.8 e.v. Both E_g and ρ_0 generally increased with increasing room temperature resistivity.

The relationship between E_g and the number of fused rings in the acene monomer is shown in Fig. 4. A notable deviation from the general order was encountered with the dibenzpyrene polymer.

Although no distinguishable effect of compaction pressure on E_g was noticed here, as can be seen in Table IV, concurrent work with a similar polymer at pressures to 106,000 kg./cm.^{2} indicates that a decrease of 1.7×10^{-6} e.v. cm.^{2}/kg. might be expected.[47] This contribution (0.002 e.v.) would be indistinguishable in the limited pressure range studied here.

Thermoelectric Effects.—The Seebeck coefficient and related parameters were evaluated for seven PAQR polymers. Samples with room temperature resistivities ranging from approximately 10^3 to 10^6 ohm cm. were measured; the maximum resistivity value was set by equipment limitations. Accuracy of the determinations was largely a function of the temperature differential at each measurement, and varied from approximately 2 to 15% as the temperature differential decreased from approximately 20 to 2°.

TABLE IV

ACTIVATION ENERGY (E_a) VALUES FOR PAQR POLYMERS

Sample	Acene[a]	Resistivity (ohm-cm.) 25°	E_a (e.v.) 1820 kg./cm.²	E_a (e.v.) 650 kg./cm.²	ρ_0
26g	Pyrolyzed, 26a	3.05×10^{-2}	−0.001	...	...
86	Dibenzpyrene	9.5×10^{2}	+ .206	0.202	0.31
55	Pyrene (306°)	7.6×10^{3}	.155	.165	18
39	Pyrene (253°)	1.6×10^{4}	.198	.197	7.1
26a	Phenanthrene	6.7×10^{4}	.198	.191	30
37	Phenanthrene	1.0×10^{5}	.205	.205	34
35	Anthracene	8.3×10^{5}	.257	.259	38
33	Naphthalene	9.7×10^{6}	.322	.324	34
66	Triphenylmethane	5.8×10^{11}	.420	...	4.6×10^{4}

[a] For polymerization conditions see Tables I and II.

All of the polymers exhibited essentially linear relationships between the thermal gradient (ΔT) and the induced potential (ΔV). This permitted the development of a single-valued relationship between the Seebeck coefficient (Q) and the median sample temperature. The absolute Seebeck coefficients, Peltier coefficients, and $\Delta V/\Delta T$ relationships for a representative PAQR polymer are shown in Fig. 5.

Seebeck coefficients, ranging from −19.0 to 345.5 μv. per °C., were obtained with the measured PAQR series. The Seebeck values at 25° are summarized in Table V.

TABLE V

SEEBECK COEFFICIENTS OF SEVERAL PAQR POLYMERS

Polymer no.	Acene[a]	Resistivity at 25°, (ohm-cm.)	Q at 25° (μv./°C.)	dQ/dt (μv./°C./°C.)
86	Dibenzpyrene	9.5×10^{2}	−19.0	+0.55
55	Pyrene	7.6×10^{3}	+69.6	− .90
39	Pyrene	1.6×10^{4}	+21.8	−1.76
37	Phenanthrene	1.0×10^{5}	+155.9	−0.50
41	Chrysene	1.6×10^{5}	+122.5	−6.87
35	Anthracene	8.3×10^{5}	+345.5	−1.80
43	Chrysene	1.2×10^{6}	+123.0	−6.85

[a] For polymerization conditions see Tables I and II.

All samples exhibited p-type conduction, with the exception of the dibenzpyrene PAQR polymer. This material exhibited the lowest resistivity of the PAQR polymer series.

The Seebeck coefficient of the p-type materials declined slightly with temperature in all observed cases, whereas the n-type polymer exhibited an increase. One therefore may conclude that the polymers all became more "negative" in carrier type as temperature increased. The temperature coefficient of Q was generally on the order of −1 μv./°C.[2].

A trend toward higher Seebeck coefficient with increasing room-temperature resistivity is noted (Fig. 6). A similar trend is noted in the results of Loebner in his studies concerning the effect of pyrolysis temperatures (above 700°) on the thermoelectric power of baked carbons.[48]

The Seebeck coefficients observed in these PAQR polymers (−19 to +350 μv./°C.) fall in the range observed on other organic materials, *i.e.*, poly copper phthalocyanine[31] (+15 to +35); molecular complexes[14,15] (up to +1100); phenolphthalein-type polymers[47] (+50 to +500); xanthane polymers[29,30] (+500); metal-free phthalocyanine[49] (+50); crystal violet[50] (−300).

Hall Coefficient.—The apparatus and technique employed for determination of the Hall coefficient was found to be generally inadequate for measurements on samples with resistivities encountered in the PAQR polymer series. Large asymmetry potentials, resulting from the high potentials required to pass sufficient carriers through the samples and from the difficulty in placing electrodes symmetrically, prevented detection of the Hall voltage in most samples.

A reliable value was, however, obtained for sample 55, the PAQR polymer of pyrene and pyromellitic dianhydride (306°). The Hall determination corroborated the results of thermoelectric power measurements in that p-type conductivity was observed. The magnitude of the Hall coefficient at room temperature was 288 cm.³/coul.

This provides, in itself, almost certain proof that conduction in this polymer is electronic and not ionic, for ionically conducting materials do not exhibit a detectable Hall voltage.

A rough estimate of the effective carrier density may be obtained by use of the relationship

$$N_h = (R_H e V)^{-1}$$

where

N_h = the number of effective p-type carriers
R_H = the Hall coefficient
e = electron charge
V = the velocity of light

From this equation, the effective number of carriers is estimated as 2×10^{16}/cm.³.

The mobility was estimated by the relationship

$$\mu_H = R_H \sigma$$

where

μ_H = Hall mobility
σ = conductivity = 7.6×10^{3} mho cm.$^{-1}$

A value of 0.04 cm.²/v. sec. was obtained.

(48) E. E. Loebner, *Phys. Rev.*, **84**, 153 (1951); *errata*, **86**, 1056 (1952).

(49) P. E. Fielding and F. Gutman, *J. Chem. Phys.*, **26**, 411 (1957).

(50) C. Schroeder, Masters's Thesis, Ohio State Univ., 1952.

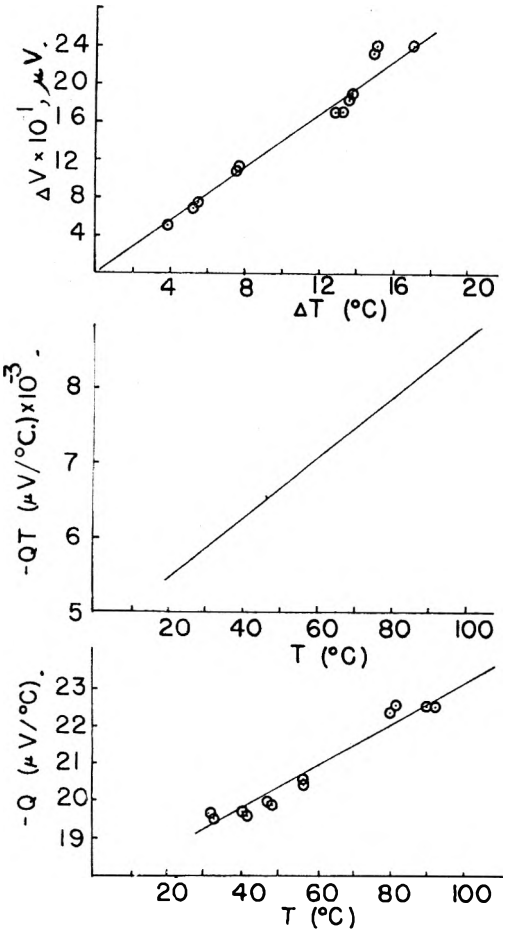

Fig. 5.—Thermoelectric properties of polymer 86, 1:1:2, dibenzpyrene:pyromellitic dianhydride:$ZnCl_2$; Q = Seebeck coeff.; QT = Peltier coeff.

Somewhat higher carrier concentrations were found in poly copper phthalocyanine in Hall coefficient determinations by Epstein and Wildi.[31] They estimated N_h at approximately 10^{18}/cm.^{3}.

Electron Spin Resonance.—A significant correlation between conductivity and unpaired electrons in PAQR polymer samples was observed. Figure 7 contains a plot of electron spin density at room temperature *vs.* the room temperature sample resistivity.

The general level of unpaired spins in PAQR polymer samples ranged from approximately 10^{17} to 10^{20} spins/g. (see Table VI.) As previously discussed, a minimum positive carrier concentration of approximately 3×10^{16} was estimated from our Hall determination. Epstein and Wildi[31] estimated a minimum of 10^{16} to 10^{18} carriers/cc.[26] on poly Cu phthalocyanine.

Current-Carrying Characteristics.—The conduction mechanism in PAQR polymers was found to be electronic. Using the measurement procedure outlined in the Experimental section, a cumulative current of 4.5×10^5 coulombs per gram was passed through polymer sample No. 25. There was no significant change in resistivity during the passage of 4.7 g. equivalents/g. of polymer.

Scatter in the resistivity data (*i.e.*, $\pm 1\%$) was primarily due to slight compaction and temperature differences between the sample and the control polymer. On the basis of polymer structure, approximately 1.1 g. equivalent should have been sufficient to electrolyze all of the O and H atoms. On this basis, if ionic conduction were significant, it easily would have been detected by this experiment.

In addition to the above evidence for the electronic nature of the polymers, no polarization was

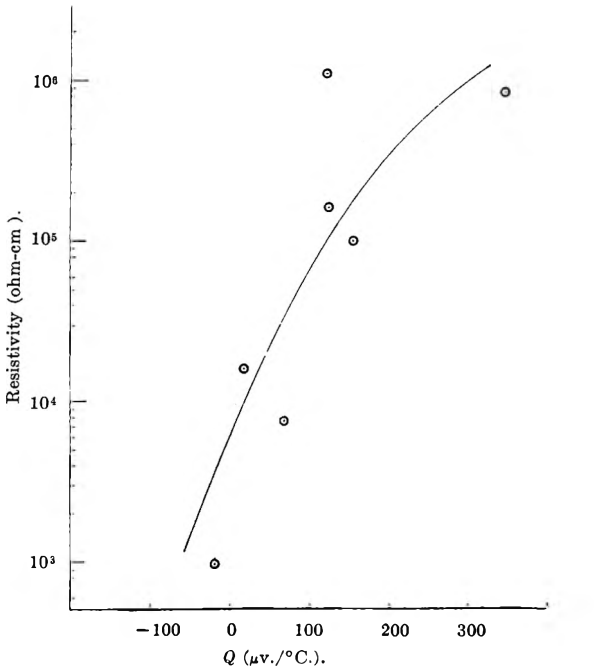

Fig. 6.—Seebeck coefficient as a function of resistivity$_{25°}$ in PAQR polymers.

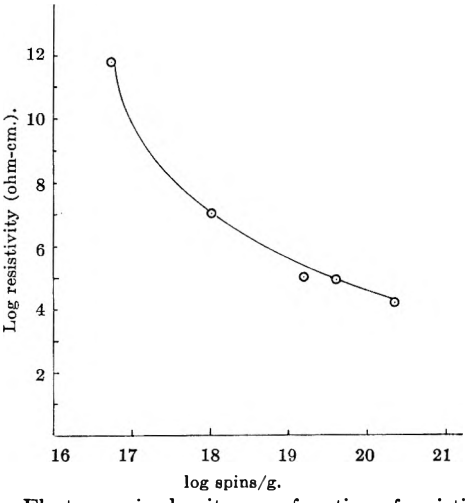

Fig. 7.—Electron spin density as a function of resistivity$_{25°}$ in PAQR polymers.

TABLE VI

ELECTRON SPIN DENSITY IN PAQR POLYMERS

Sample[a]	Room temp. resistivity (ohm-cm.)	Spins per g.	Approx. spins, av. polymer unit	Peak half-width, (gauss)
66	5.8×10^{11}	5.0×10^{16}	6.6×10^{-5}	8
33	9.7×10^{6}	1.5×10^{18}	1.1×10^{-3}	5.75
37	1.0×10^{5}	1.5×10^{19}	1.3×10^{-2}	5
39	1.6×10^{4}	1.9×10^{20}	1.9×10^{-1}	3.5
26	6.6×10^{4}	6.5×10^{19}	5.8×10^{-2}	4.25

[a] Polymerization conditions in Tables I and II.

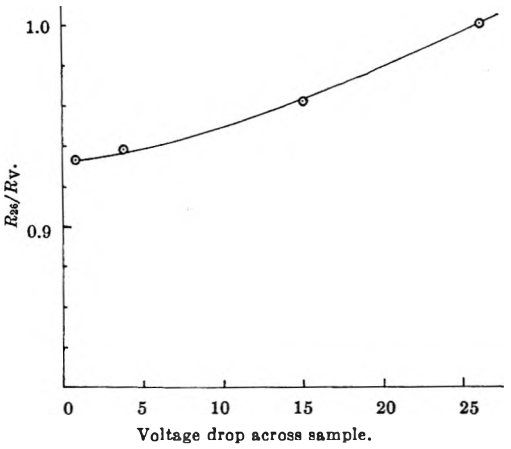

Fig. 8.—Effect of applied potential on the resistance of a PAQR polymer (polymer 39).

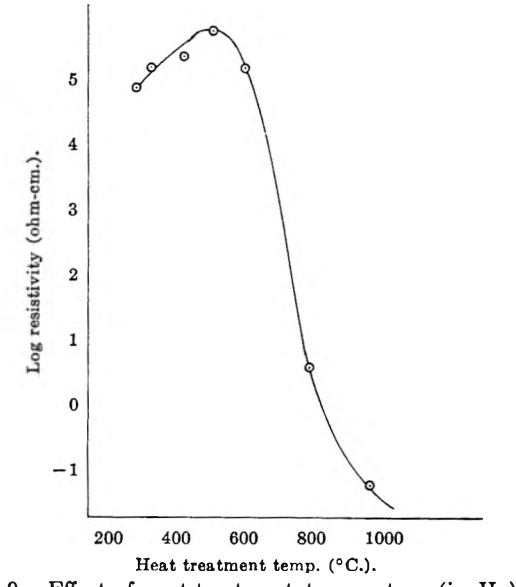

Fig. 9.—Effect of post-treatment temperature (in He) on the resistivity$_{25°}$ of a PAQR polymer (polymer 26).

evident from visual observations of current increase or decrease on applying or removing a potential. The measurements were, however, limited by the response of the meters, and more refined techniques such as high frequency a.c. measurements were not employed.

The above coulombic evidence, together with that obtained on determination of a large Hall coefficient, prove quite conclusively that electronic and not ionic conduction takes place in these PAQR polymers.

The resistance of a representative PAQR polymer was found to vary non-linearly with the applied field strength. High relative precision was achieved by comparison of the polymer sample with metallic (ohmic) resistors in a Wheatstone bridge. Potentials applied across the bridge ranged from 1.55 to 52 v., corresponding to a potential range of 0.78 to 26 v. across the polymer sample. The resistivities from three independent determinations are presented in Fig. 8. A reduced expression for resistance was employed, for convenience of comparison between samples

$$\frac{R_{26}}{R_V} = \frac{\text{Resistance at a potential drop of 26 v.}}{\text{Resistance at a potential drop of } x \text{ v.}}$$

PAQR Polymer Stability.—The thermal stability of a PAQR polymer was studied by heating in a helium atmosphere to temperatures up to 1200° for 0.5 hr. The relationship between heat treatment temperature and resistivity (measured at room temperature) is shown in Fig. 9. The conductivity was found to go through a minimum at approximately 500°, showing that the original synthetic structure of the PAQR polymers is unique and thermally sensitive and is not that of a pyropolymer.

At temperatures in excess of 600°, it is probable that extensive changes in the polymer structure occur, due to the volatilization of H, CO, and CO_2, etc.

The e.s.r. characteristics of the 1000° treated polymer were quite different from those of the PAQR materials. A very faint resonance was observed with a peak half-width of approximately 1200 gauss, as opposed to the rather sharp resonances of the original PAQR corresponding in a peak half-width field variation of only 3 to 5 gauss. This is indicative of gross changes in conduction mechanism, since the interaction of free carriers, and perhaps spins, has increased markedly.

Obvious changes in polymer composition also are reflected by the analysis of the 1000° heat treated polymer.

	C	O	H
Sample 26	84.48	7.21	3.52
Sample 26 (heated to 1000°)	96.45	1.32	1.37

The heat treated sample had a negative temperature conductivity coefficient (Table IV) and was a degenerate semi-metal.

Photoelectric Properties.—The PAQR polymers exhibit photoconductivity and a photo-e.m.f. When a sample of polymer number 55 was illuminated with white light passed through a heat filter through the transparent conducting tin oxide (NESA) window, a steady increase in voltage, to approximately 9 mv., was observed. The time required to reach a maximum was approximately 0.8 min.

After maintaining illumination for 1.2 min. at the equilibrium photo-e.m.f., the source was turned off and the voltage was observed to decay to a minimum within 0.8 min. The photo-e.m.f. curve for polymer 55 is shown in Fig. 10.

Measurement of the photo current showed no corresponding maximization after 0.8 min. The photo current steadily increased over a period of approximately 2 min. to a maximum of 0.5 mμa., after which the illumination was terminated. When irradiation was terminated, an exponential decrease in current was observed, over a period of approximately 0.8 min.

Considering the sample resistance (3×10^6 ohms), and the steady state photo-e.m.f. (9×10^{-3} v.), a maximum photo current of approximately 2 mμa. was anticipated.

The change in sample resistivity was determined by applying a potential of 1.5 v. and measuring the

change incurrent upon illumination. When the light source was turned on, a steady increase in current was observed, over a period of *ca.* 0.9 min. The steady-state current corresponded to a resistivity decrease (assuming approximately ohmic behavior) of approximately 6%. A decay time of approximately 1.1 min. was observed subsequent to removal of the illumination. Assuming that the arrival of the 3×10^{17} photons/cm.^{2} sec. with energies of 1.1 e.v. produces carriers at that rate in a depth of 10^{-4} cm. in the 0.4 cm. thick sample, with a time of transit through the sample of 1 to 5 sec., this corresponds to a mean free time of the carrier (*i.e.*, "lifetime") of 0.2 to 1 sec.

Aluminum Chloride Catalyzed PAQR Polymers.—The polymers were synthesized at relatively low temperatures using aluminum chloride as a catalyst, and pyromellitoyl chloride as the acylating agent, all exhibited resistivities several orders of magnitude higher than the zinc chloride catalyzed materials.

At the temperatures employed, the lactone formation reaction should have been relatively minor.

The acid chloride can exist as either 1,2,4,5-benzenetetracarboxyl chloride or as isomeric 3,3′-dichloroisobenzobisfuranones, lower temperatures generally favoring the former, which leads to quinone formation.

Resistivities of the polymers were determined on samples as synthesized, and also subsequent to heating in the presence of $SOCl_2$. Results are summarized in Table VII. The ethanol and benzene soluble fractions exhibited higher resistivities than the insoluble polymeric material.

Polymerization of pyromellitoly chloride with bi- and terphenyl produced yellow-tan, insoluble, infusible materials. The fused-nuclei acenes generally yielded deeply purple-black polymers, indicating a lower molecular weight and/or lower level of conjugation than experienced with the zinc chloride catalyzed polymers. This is reflected in the higher resistivities encountered with the aluminum chloride catalyzed materials.

Quinazone Polymers (Schiff's Base Type).—The materials were deep brown to black, solid, insoluble, infusible materials. Resistivities generally were above 10^{11} ohm-cm. Carbon, hydrogen, oxygen analysis of a polymer sample indicated that the desired highly conjugated structure was not attained, since oxygen did remain in the sample: C = 77.33%; H = 4.01%; N = 4.43%; O = 11.05%. Results are summarized in Table VIII.

TABLE VII

	Acene	Resistivity (ohm-cm.)	Resistivity after $SOCl_2$ treatment (ohm-cm.)	Resistivity of $ZnCl_2$ catalyzed PAQR (ohm-cm.)
I & J	Biphenyl	9.1×10^{11}	(Dec. to tar) 10^4	3.4×10^{10}
C & D	Terphenyl	6.2×10^{11}	2.8×10^{11}	1.4×10^{7}
G & H	Naphthalene	1.6×10^{12}	6.7×10^{11}	1.4×10^{6}
A & B	Anthracene	1.5×10^{8}	2×10^{9}	3.2×10^{5}
E & F	Phenanthracene	7.8×10^{11}	4.9×10^{11}	1.0×10^{5}

Polyacenes.—The polymeric materials obtained after separation of the ethanol soluble, benzene soluble, and insoluble fractions were not highly conductive.

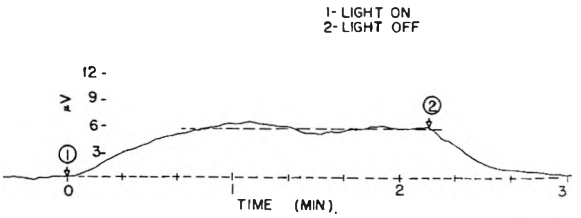

Fig. 10.—Photovoltaic curve for a PAQR polymer (polymer 55).

Fraction	Description	Room temp. resistivity (ohm-cm.)
ethanol souble	thermoplastic	1.2×10^{12}
benzene souble	thermoplastic	6.0×10^{11}
insoluble	infusible	2.6×10^{11}

Aniline Black Polymer.—The resistivity of the aniline black polymer was found to be 3×10^{10} ohm-cm. at 25°. The deep violet-black color indicates appreciable loosening of the frontier electrons over that met with in compounds not so highly conjugated. That eka-conjugation is not attained probably is due to flexibility about single bonds limiting pi–pi orbital overlap to relatively short regions.

Discussion

As has been discussed previously, the organic semiconductors do not always meet the criteria for the rigorous application of simple band theory for interpreting their enhanced electronic behavior. It was nevertheless of interest to determine the electronic parameters in several PAQR polymers, on the assumption that the models did apply.

The theoretical development of the band theory and pertinent equations are described by Cusack.[51] Equations relating the thermoelectric power to the carrier parameters such as number and mobility have been derived by V. A. Johnson and K. Lark-Horovitz.[52,53]

Parameters have been derived, assuming intrinsic behavior (concentration of positive carriers = concentration of negative carriers) and extrinsic, or impurity, behavior (one carrier type predominates).

In intrinsic non-degenerate semiconductors, the Seebeck coefficient can be described by

$$Q = \frac{K}{e}\frac{(C-1)}{(C+1)}\left[\frac{E_g}{2kT}+2\right]$$

where

Q = Seebeck coefficient
K = Boltzmann constant
e = charge on an electron
E_g = energy gap
T = absolute temperature
$C = \mu'_e/\mu'_h$ = ratio of mobilities, electrons to holes

(51) N. Cusack, "The Electrical and Magnetic Properties of Solids," Longmans Green and Co., Ltd., 1958.

(52) V. A. Johnson and K. Lark-Horovitz, *Phys. Rev.*, **92**, 226 (1953).

(53) V. A. Johnson, "Progress in Semiconductors," Vol. I, Heywood and Co., 1956.

TABLE VIII

POLYMERS OF QUINONES AND DIISOCYANATES[a]

	Monomers	Temp., °C.	Solidification time (min.)	Total polymerization time (hr.)	Resistivity $\times 10^{-11}$
101	1,4-Naphthaquinone + TODI	100	No polymer		
102	1,4-Naphthaquinone + TODI	100	No polymer		
103	1,4-Naphthaquinone + TODI	250	15	18.25	4.6
104	1,4-Naphthaquinone + TODI	250	15	1.25	2.5
105	1,4-Naphthaquinone + TODI	250	15	0.25	2.5
106	1,4-Naphthaquinone + TODI	306	4	18	5.9
110	1,4-Naphthaquinone + TODI	306	4	4 (min.)	6.7
113	Anthraquinone + TODI	306	50	1	6.5
114	Anthraquinone + TODI	306	50	19	6.2
115	Paraquinone + TODI	256	23	18	5.6
116	Paraquinone + TODI	306	8	18	4.7

[a] TODI = *p*-toluenediisocyanate.

This can be rearranged to give

$$C = \frac{-QT + E_g/2 + 2KT}{QT + E_g/2 + 2KT}$$

The mobilities can be calculated by

$$\mu'_h = \frac{\sigma}{en'(C + 1)}$$

$$\mu'_e = C\mu'_h$$

where

σ = conductivity
μ'_h = mobility of positive carriers
μ'_e = mobility of negative carriers
η' = number of positive carriers
$= (2M_h'kT)^{3/2}/h^2 \times \exp(-E_g/2kT)$

where

h = Planck's constant
M_h' = effective mass of carrier

Since the carrier mass could not be determined, the mass of an electron at rest was assumed.

Carrier parameters based on the intrinsic model are presented in Table IX.

TABLE IX

CARRIER PARAMETERS BASED ON THE INTRINSIC MODEL (BAND THEORY)—FROM THERMOELECTRIC DATA

Polymer	Room temp. resistivity (ohm-cm.)	$C = \mu_e/\mu_h$	$N_h' \times 10^{-15}$ (cm.$^{-3}$)	$\mu'_h \times 10^3$ (cm.^{2})/(v. sec.)	$\mu'_e \times 10^3$ (cm.^{2})/(v. sec.)
86	9.5×10^2	1.04	8.3	390	4.1×10^{-1}
55	7.6×10^3	0.82	60.0	7.5	6.2×10^{-3}
39	1.6×10^4	.95	11.0	18.0	1.7×10^{-2}
37	1.0×10^5	.69	8.3	4.5	3.1×10^{-3}
35	8.3×10^5	.47	1.2	4.3	2.1×10^{-3}

Compared with the electron spin density and chemical treatment results, the carrier concentration values are several orders of magnitude lower.

Assuming extrinsic non-degenerate behavior, the Seebeck coefficient may be represented by

$$Q = \frac{\pm K}{e}\left\{2 - \ln\left[\frac{n_h h^3}{2(2\pi M_h^* KT)^{3/2}}\right]\right\}$$

This can be rearranged to give

$$n_h = \frac{2(2\pi M_h^* KT)^{3/2}}{h^3} \exp(2 + Qe/K)$$

Mobility can be calculated by

$$\sigma = n_h e \mu$$

Carrier parameters based on the extrinsic model are presented in Table X. If we calculate the number of impurities, on the basis of this model, a value in excess of 10^{24} cm.$^{-3}$ is obtained; hence, the extrinsic model certainly is inapplicable.

TABLE X

CARRIER PARAMETERS BASED ON THE IMPURITY MODEL (BAND THEORY)—FROM THERMOELECTRIC DATA

Polymer	$N_h' \times 10^{-20}$ (cm.$^{-3}$)	$\mu'_h \times 10^{-4}$ (cm.^{2})/(v. sec.)
86	2.3	270
55	4.1	200
39	2.4	160
37	11	5.7
35	100	0.075

Eka-Conjugation and Enhanced Electronic Behavior.—As an alternative to the simple band model approach in considering the semiconducting polymers, we have used the following working hypothesis. There now is appreciable evidence that when the size of a set of conjugated double and single bonds is larger than some number (about 10 to 15 double–single bond pairs) then the molecule acquires unusual characteristics. It is to be expected that the formation of the biradical and exciton states then will become easy. For ease of reference, we have termed this required degree of conjugation as *eka-conjugation*. Eka-conjugation may be said to exist when the degree of conjugation becomes such that the population of electronically excited states in thermal equilibrium becomes appreciable at room temperature. The energetics of the transition may be semiquantitatively considered by the "electron-in-a-box" model. Representing the biradical as ·R·, and its eka-conjugated precursor as R, we may write

$$R \rightleftarrows \cdot R \cdot;\ \Delta F_1 \cong {}^3E \text{ and} \quad (1)$$

$$(\cdot R \cdot)/(R) = K_1 = \exp(-\Delta F_1/kT) \quad (2)$$

$$\Delta F_1 = \Delta H_1 - T\Delta S_1 \cong {}^3E \quad (3)$$

where ^3E is the energy of conversion to the triplet state biradical. We may estimate ^3E by the "metallic model" of linearly conjugated molecules containing Z atoms each contributing a π-electron in the same nodal plane.

$$E = h^2n^2/8ml^2 \qquad (4)$$

$n = 1,2,3, \ldots\ldots$; $L = Zl$ (includes $^1/_2$ bond length overlap at ends); h is Planck's constant; l is the C–C bond distance; m is the rest mass of the electron; and E is the energy of the particular state. The molecule will contain two π-electrons per orbital filled up to $Z = 2n$ in the ground state. The energy to excite a frontier electron up to the first unfilled orbital, $n \rightarrow n + 1$, is

$$\Delta E = h^2(2n + 1)/8ml^2Z^2 = h^2(Z + 1)/8ml^2Z^2 = {}^1E \cong {}^3E \qquad (5)$$

$$= 19.2(Z + 1)/Z^2 \text{ (in e.v.)}$$

The estimate for a "ring model" molecule containing a largest *closed loop* path for the π-electrons of Z atoms in the same nodal plane is

$$E = h^2(2q)^2/8mL^2 \qquad (6)$$

$$q = 0,1,2,3, \ldots\ldots$$

The molecule will contain filled orbitals up to $Z = 4q + 2$. The desired transition is for $q \rightarrow q + 1$, hence

$$\Delta E = h^2/4ml^2Z = {}^1E \cong {}^3E = 38.4/Z \text{ (in e.v.)} \qquad (7)$$

The ion-pair forming reaction from which the carriers result may be written

$$\cdot\mathrm{R}\cdot + \mathrm{R} \rightleftarrows \underset{\text{roving electron}}{\cdot\mathrm{R}:^-} + \underset{\text{roving hole}}{\cdot\mathrm{R}^+} \qquad (8)$$

$$(\cdot\mathrm{R}:^-)(\cdot\mathrm{R}^+)/(\cdot\mathrm{R}\cdot)(\mathrm{R}) = K_2 = \exp(-\Delta F_2/kT) \qquad (9)$$

By this argument, we will expect to have an "intrinsic-type" semiconductor where

$$(\cdot\mathrm{R}:^-) = (\cdot\mathrm{R}^+) = n_e = n_h = n_i \qquad (10)$$

and we may set $(\cdot\mathrm{R}\cdot) = s/2 = {}^1/_2$ the concentration of observable spins per cm.^{3}.

Combining we get

$$2n_i^2/(\mathrm{R})S = K_2 \qquad (11)$$

$$n_i = (s/2)\exp\left[\frac{-\Delta F_2 + \Delta F_1}{2kT}\right] \simeq (s/2)\exp\left[\frac{-\Delta F_2 + {}^3E}{2kT}\right] \qquad (12)$$

$$= (\mathrm{R})\exp\left[\frac{-\Delta F_2 - \Delta F_1}{2kT}\right] \simeq (\mathrm{R})\exp\left[\frac{-\Delta F_2 - {}^3E}{2kT}\right]$$

where n_i is the number of either mobile electrons or mobile holes acting as carriers.

As discussed elsewhere at greater length,[7] there is reason to expect the mobility to occur by way of hopping processes, where E_s is the saddle height energy for the hopping process, and

$$u = (\text{const.})T^2\exp(-E_s/kT) \qquad (13)$$

In the event that there is a cooperative process between the carriers and excitons, a factor of $(n_{ix}/n_i + n_{ix})$ must be included, and the new $E_S' < E_s$. Recalling that the eka-conjugated structures are large and asymmetrical as well as highly polarizable, it will be expected that some field dependence of the conductivity will result. The eka-conjugation model appears to account qualitatively and occasionally semiquantitatively for the various attributes previously mentioned for the PAQR polymers.

As a partial check on the eka-conjugation hypothesis, we observed that in one sample (39) the uptake of O_2 at 250° to the extent of 4×10^{20} molecules/g. was just sufficient to destroy the e.s.r. signal originally of 1.9×10^{20}/g. From this, by eq. 2 we estimate ΔF_1 as 0.019 e.v. This is comparable to the observed temperature dependence of spin concentration by e.s.r., where a value of 0.016 e.v. was obtained for this semiconductor.

Acknowledgment.—We wish to thank Dr. D. A. Ross and Mr. R. F. Bailey of the Industrial Reactor Laboratories for assistance in making radioisotopic analyses for zinc, and Dr. Robert Pressley of the Physics Dept., Princeton University, and Mr. Emil Bretz of Elion Corporation for assistance in e.s.r. determinations. The work here was supported jointly by the Army, Navy, and Air Force under Signal Corps Contract DA-36-039sc-78105; DA Project 3A99-15-001; ONR Project NR 356-375. E. H. Englehardt wishes to express thanks to the California Research Corporation for a Fellowship during the period.

POLYMORPHISM IN FIBROUS POLYPEPTIDES: $\alpha \rightleftharpoons \beta$ TRANSFORMATION IN NATURALLY OCCURRING KERATIN[1]

BY A. F. DIORIO, L. MANDELKERN, AND E. R. LIPPINCOTT

Polymer Structure Section, National Bureau of Standards, Washington, D. C., and Department of Chemistry, University of Maryland, College Park, Md.

Received January 20, 1962

The crystallization of completely molten keratin (Lincoln wool) was investigated in order to delineate the conditions under which the α and β crystalline phases are formed. The nature of the crystalline phase developed depends on the deformation imposed on the amorphous system prior to crystallization and on the crystallization temperature. Elongation favors the formation of the β-form, and the axial deformation required decreases markedly as the crystallization temperature is increased. It is concluded that no simple relation based solely on molecular structure exists between the crystal form observed and the per cent fiber extension. The melting temperatures of β-keratin prepared from α-keratin and of α-keratin itself are compared when the fibers are immersed in 11.6 M LiBr. The melting temperatures are virtually identical, indicating that the two crystalline forms have similar thermodynamic stabilities.

Introduction

In a series of classical experiments, Astbury and collaborators[2,3] have demonstrated that by axially deforming a native α-keratin fiber in an appropriate medium, transformation to the β-keratin form can be accomplished. The major evidence was the accompanying change that occurred in the wide-angle X-ray diffraction patterns from that characteristic of the native α-form to a pattern containing the predominant reflections of the naturally occurring β-structure. On stretching a wool fiber, the native α-pattern remains virtually unchanged up to about 20% extension. On further stretching, which must be accomplished in a liquid medium such as water, the X-ray pattern begins to show changes. Characteristics of the β-pattern are observed, and at about 35% extension a mixed α- and β-pattern becomes prominent. The mixed pattern is completely replaced by a well defined β-pattern at about 70% extension. These observations were formally interpreted in terms of a crystal–crystal transformation, with a 1:1 correspondence being postulated between the disappearance of the α-form and the development of the β-structure.[4]

However, more quantitative and refined X-ray diffraction studies do not support the postulate of the direct correspondence between the appearance of the β-structure and the disappearance of the α-form.[5–7] In particular, Bendit[5,6] found that the X-ray diagram of Lincoln wool starts changing at low extensions (5% or less). Moreover, with further extension the decrease in the intensity of the predominant α-reflection at 5.1 Å. is not accompanied by a related increase in the corresponding β-reflection at 4.65 Å., and there is no evidence of a rapid change between 30 and 50% extension. Consequently, the molecular nature of the transformation was brought into question.

Considerations of this polymorphic transition heretofore have been concerned solely with the two crystalline or ordered phases involved. The possible role of an amorphous or non-crystalline phase has been tacitly ignored. Polymorphic transitions can be classified either as crystal–crystal transitions or crystal–liquid–crystal transitions. The appropriate category for the transition in keratin has not as yet been elucidated. In order to accomplish this, an appropriate reference state, preferably a single phase, must be established in order to measure or calculate the appropriate thermodynamic quantities pertinent to the respective crystalline phases.

In the present work, advantage is taken of the fact that completely amorphous keratin can be prepared under relatively mild conditions.[8] In particular, Lincoln wool can be rendered amorphous by immersion in appropriate aqueous LiBr solutions at temperatures as low as 10°. In the absence of any external deformation, the native α-structure is regenerated by transfer of the system to pure water.[8] In an effort to establish a basis for a thermodynamic analysis of polymorphism in the fibrous proteins, the premise that stable oriented β-structures can be developed from the pure molten state has been examined.

Experimental

Materials.—The α-keratin fiber selected for study was Lincoln wool. Fibers were Soxhlet-extracted with benzene and ethyl alcohol, and after being washed in distilled water, they were dried at room temperature and humidity. The LiBr used was of reagent grade, and the solutions of desired molarity were prepared by diluting a saturated solution whose concentration was determined by the Mohr analysis for bromide ion.

X-Ray Diffraction.—A Norelco X-ray diffraction unit was operated at 30 kv. and 20 ma., and nickel-filtered copper radiation was employed. X-Ray photographs were taken with a Norelco microcamera, which enabled the diffraction effects of single wool fibers to be studied. The fiber to be examined was mounted on a holder directly behind the collimator; a microscope was used to align the specimen with the collimator bore. A collimator of 0.004-in. bore, a sample-to-film distance of 15 mm., and an exposure time of approximately 20 hr. were used. The camera was filled with helium gas during the exposure to eliminate air scattering of the X-ray beams.

The Deformation Process.—A simple stretching frame was constructed out of a glass rod, Nichrome wire of 0.20-in. diameter, and ordinary paper-binder clips. Small Nichrome wire rings of minimum weight, 15–20 mg., required to keep

(1) Taken in part from a Thesis submitted by A. F. D. in partial fulfillment of the requirements for the degree of Master of Science in the Graduate School of the University of Maryland.

(2) (a) W. T. Astbury and A. Street, *Phil. Trans. Roy. Soc.*, **A230**, 75 (1931); (b) W. T. Astbury and H. J. Woods, *ibid.*, **A232**, 333 (1933).

(3) W. T. Astbury and W. A. Sisson, *Proc. Roy. Soc.* (London), **150A**, 533 (1935).

(4) W. T. Astbury and F. O. Bell, *Nature*, **147**, 696 (1941).

(5) E. G. Bendit, *ibid.*, **179**, 535 (1957).

(6) E. G. Bendit, *Textile Res. J.*, **30**, 547 (1960).

(7) A. R. B. Skertchly, *Nature*, **181**, 638 (1958).

(8) L. Mandelkern, J. C. Halpin, A. F. Diorio, and A. S. Posner, *J. Am. Chem. Soc.*, **84**, 1383 (1962).

the specimen uncrimped, were attached to each end of a fiber by leading the fiber through the wire loop and tying it. The fibers thus mounted were 3–4 cm. in length. Each fiber was rendered molten by suspending it at room temperature for 5 hr. in a closed tube containing a large excess of 7.2 *M* aqueous LiBr solution. The melting temperature of Lincoln wool in this medium had been determined previously to be 8 ± 2°.[8] Concomitantly with melting, a contraction in length of 8–12% was observed. The amorphous fiber then was mounted in the stretching frame between a fixed and a movable jaw and extended the desired amount. During this process the whole assembly was immersed in the 7.2 *M* LiBr solution. The extensions imposed, ranging up to 81%, were based on the length of the amorphous undeformed fiber in the LiBr medium. Lengths were measured by means of a cathetometer which had a range of 100 mm. and could be read directly to 0.001 mm.

Crystallization Procedure.—The crystallization of the deformed amorphous fiber was achieved by immersing the stretching frame containing the mounted fiber into distilled water held constant at a predetermined temperature. The times allowed for crystallization ranged from 1 min. to 22 days for specific experiments. For crystallization temperatures in the range 10–100°, about 400 ml. of distilled water was contained in a test tube of 62-mm. diameter and the tube was immersed in a thermostatic bath controlled to ±0.1°. The distilled water was stirred by a stream of compressed air during the course of the experiment. For the crystallization of samples at 100°, the stretching frame and contents were immersed in boiling water for times ranging from 1 min. to 3 hr.

For the crystallization in water at temperatures above 100°, a modification of a commercial vulcanizer was utilized. The autoclave, made of forged steel, was 11.5 cm. in diameter. The cover, also made of steel, was fitted with a neoprene rubber gasket and clamped to the cylindrical vessel. Two insulated copper wires were led through the gasket and connected to the top of the inside casing. The copper leads were connected to a piece of thin Nichrome wire 0.004 in. in diameter, from which the sample holder with the mounted fiber was suspended. The sample holder was constructed of brass and had two immovable jaws. The molten fiber was stretched the desired amount, following the procedures previously described, and mounted in the sample holder with the length held constant. The sample holder then was wrapped with glass wool and suspended on the Nichrome wire inside the autoclave.

About 500 ml. of distilled water then was introduced into the autoclave, and the apparatus was sealed, and then heated by means of a gas burner. After the desired crystallization temperature was reached, in approximately 10–15 min., voltage was applied across the copper wires, causing the thin Nichrome wire to disintegrate and allowing the fiber sample to plunge into the water. By controlling the heating rate manually it was possible to maintain the temperature constant within ±2°. The procedure outlined was utilized for crystallizations at 110, 120, and 130°. The times allowed for crystallization ranged from 1–10 min.

Results and Discussion

The Formation of α- and β-Structures from Molten Fibers.—Preliminary experiments established the feasibility of producing the crystalline β-form from the amorphous state. Though occasionally it was possible to extend a fiber 100%, extensions of 80% could be obtained repeatedly and this figure was set as an upper limit for subsequent investigation. An X-ray diffraction pattern of a fiber deformed to this limit showed the same characteristic broad amorphous halo at a Bragg spacing of approximately 3.9 Å. that was obtained prior to the stretching process.[8] Thus, the deformation process, when conducted in aqueous LiBr solution, does not in itself induce crystallization. Crystallization occurs with the transfer of the specimen to pure water.

As an example, an amorphous fiber stretched 81% and immersed in distilled water for 2 hr. at room temperature yielded a β-pattern when the fiber was removed from the stretching frame and dried. Similar results also could be attained at this extension ratio by crystallization at elevated temperatures. However, a significant difference in the kinetics of crystallization was observed, depending on the temperature. Fibers crystallized at 100° gave relatively intense, sharp, oriented crystalline patterns even when the time allowed for crystallization was reduced to 1 min. However, the X-ray patterns of specimens crystallized at 10° were relatively weak, even when the crystallization time was 1 hr. The reflections became more intense and less diffuse when the crystallization period was extended to 12–24 hr. at this temperature. When the deformation in the amorphous state was decreased, the oriented β-form still could be developed at 10°, but crystallization times of the order of 10–14 days were required. Thus the liquid–crystal phase transition for keratin is accompanied by time–temperature relations typical of such processes in general and widely observed in the simpler macromolecular systems.[9]

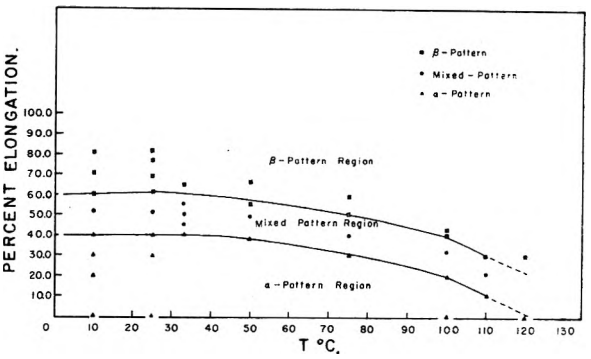

Fig. 1.—Diagrammatic representation of the crystalline polymorph observed as a function of the amount of axial deformation applied in the amorphous state and the isothermal crystallization temperature.

The results of a more systematic study, which specifies the conditions of temperature and deformation under which either the α- or β-forms are developed, are represented schematically in Fig. 1. After crystallization, the X-ray diffraction patterns of the unstressed dried fibers were examined. Restricting present considerations to crystallization temperatures of 110° or less, one of three different types of X-ray patterns was observed. Only an oriented α-structure, or an oriented β-structure, or a mixed pattern containing both oriented α- and β-structures was noted. The solid lines in the figure delineate the regions where one of the forms is observed distinctly. In general, at all temperatures, the α-form is produced at the lower elongations, a mixture of the α- and β-form is produced at intermediate elongations, and the β-form is produced at still higher elongations. The deformation required for the formation of the β-form decreases significantly as the crystallization temperature is raised. The increasing magnitude of the slope of the lines in Fig. 1 over the temperature range 50–110° indicates the possibility that at the higher crystallization temperatures the β-structure

(9) L. Mandelkern, in "Growth and Perfection of Crystals," edited by R. H. Doremus, B. W. Roberts, and D. Turnbull, John Wiley and Sons, New York, N. Y., 1958, p. 457.

might be formed with a substantial decrease in the applied deformation.

To investigate this possibility, isothermal crystallization experiments in water were conducted at 110, 120, and 130°. At 110° the minimum extension required to produce an oriented β-form was reduced to 30% as compared to 43% for crystallization at 100°. However, because of the well known degradative processes that occur when α-keratin fibers are immersed in water at temperatures above 100°,[10-12] the time allowed for crystallization had to be reduced substantially. At 120° the oriented α-form is developed by the crystallization of the undeformed fiber when the time allowed for crystallization is 2 min. When the crystallization time is extended to 5 min., the resulting X-ray pattern is quite different from that previously obtained. Though the Bragg spacings observed are still characteristic of the α-structure, the reflections have become more diffuse and have become arced, indicating partial randomization in the orientation of the crystalline regions with respect to the fiber axis. When the total crystallization time (at 120°) was extended to 10 min., a completely disoriented β-pattern was obtained. The Bragg spacings were found at 4.6 and 9.8 Å., respectively, characteristic of a β-structure, and the X-ray pattern displayed two crystalline rings. Undeformed amorphous fibers crystallized at 130° for 1 min. gave a similar pattern.

The crystallization of disoriented structures is indicative of the restriction in the number of intermolecular cross links. This conclusion is based on the results obtained for the structurally simpler polymers, polyethylene[13] and natural rubber,[14] wherein the imposition of intermolecular cross links in the axially oriented state results in preferred oriented crystallization on subsequent melting and recrystallization. The high concentration of cystine residues in native α-keratin suggests a high level of intermolecular cross links, which is consistent with the development of axially oriented crystallization from the molten state at the lower crystallization temperatures. Consequently, from purely physical-chemical evidence, it is deduced that the fission of disulfide bonds has occurred at the higher temperatures. This conclusion is supported by direct chemical evidence, since it has been shown[10] that the action of boiling water on wool leads to the severance of the disulfide bond with the formation of a thiol and a –SOH group. Although the rate of breakdown of cystine is relatively slow at 100°, only 20% being lost in 24 hr., the degradation rate becomes much more rapid at higher temperatures.[11,12]

Owing to the rapid degradation rate of the fibers at elevated temperatures, the minimum extension required to form an oriented β-structure could not be established. However, the results obtained for crystallization up to 120° indicate that the amount of deformation required for the formation of an oriented β-form decreases markedly with increasing crystallization temperature. Since a disoriented β-pattern is observed after crystallization at 130°, the hypothetical possibility is suggested of the formation of an oriented β-structure in the absence of any deformation at a sufficiently high crystallization temperature. It thus is possible to interpret the α–β transformation observed on stretching a native fiber immersed in water as the development of oriented β-crystallites from the amorphous portions of the fiber under the influence of the applied stress with the concurrent melting of the α-form. It is not *a priori* necessary to postulate a crystal–crystal transformation in explaining the formation of a β-structure during the deformation of a partially crystalline native α-keratin fiber.[2,3] The postulation of a geometric-molecular conformational relationship between the extent of the α–β transformation and the percentage fiber extension is not required and in effect ignores completely the presence of the amorphous polymer phase. This premise, moveover, is not substantiated by quantitative X-ray diffraction analyses.[5-7]

Although the investigations involving the elongation of the native fiber have not been conducted under conditions of thermodynamic equilibrium, it is instructive to consider the consequences of such a hypothetical experiment. According to the phase rule, this two-component system is invariant at constant pressure when the four phases under consideration coexist. Equilibrium therefore can be established only at a unique force and temperature. A change in either of the intensive variables must result in the disappearance of one of the phases if equilibrium is to be maintained. Since the β-crystalline phase has been formed during the course of the experiment and the supernatant aqueous phase will always be present, one of the two remaining polymer phases, either the amorphous phase or the α-crystalline phase, must vanish. Thus the interpretation proferred above is consistent with any tendency of the system to approach equilibrium.

The results summarized in Fig. 1 must reflect in a rigorous sense the kinetic processes involved in the crystallization of either the α- or the β-forms. The polymorph that is less impeded by kinetic barriers will be the one observed. It can be expected from general considerations that the kinetics will be governed to a large extent by the relation between the crystallization temperature and the melting temperature. The latter temperature for each polymorph will be altered by the deformation imposed. Thus the favoring of the crystallization of one form over the other can be expected because of different relative changes in the melting temperatures caused by the deformation.

The Stability of the β-Crystalline Form.—Since the oriented β-form can be formed under a variety of conditions, its thermodynamic stability in pure water in the absence of an external force was investigated. Particular attention was given to the effects of the crystallization temperature, the time allowed for crystallization, and the amount of deformation imposed during the transformation.

(10) A. Schoberl, *Angew. Chem.*, **53**, 227 (1940).

(11) E. Elod, H. Nowotug, and H. Zahn, *Melliand Textilber.*, **25**, 773 (1944).

(12) E. Elod, H. Nowotug, and H. Zahn, *ibid.*, **31**, 481 (1950).

(13) L. Mandelkern, D. E. Roberts, A. F. Diorio, and A. S. Posner, *J. Am. Chem. Soc.*, **81**, 4148 (1959).

(14) J. F. M. Oth and P. J. Flory, *ibid.*, **80**, 1297 (1958).

The results obtained for crystallization conducted at 100° for various periods of time at fixed deformation are summarized in Table I.

TABLE I

THE DIMENSIONAL AND THERMODYNAMIC STABILITY OF β-FIBERS, FORMED AT 100° IN WATER, TO SUBSEQUENT TREATMENT IN THE SAME MEDIUM AT 100° IN THE ABSENCE OF AN EXTERNAL FORCE

Sample	% Deformation	Crystn. time, min.	%[a] Shrinkage	Resulting X-ray pattern
52	70.2	1	38.8	Oriented α
53	69.8	5	47.2	Oriented β
54	70.7	10	38.7	Oriented β
73	70.1	60	34.3	Oriented β

[a] After heating for 2 hr. in boiling water with no force.

In all instances an oriented β-pattern was observed after the initial crystallization from the melt. Significant shrinkage occurred during subsequent treatment of the unstressed fiber at 100° in boiling water. However, as is indicated in the last column of the table, the oriented β-structure persists except for the specimen crystallized for only 1 min. In the latter case, melting can be presumed to have occurred followed by recrystallization of the α-form. The redevelopment of an oriented α-structure indicates that the integrity of the native intermolecular cross links is maintained during the initial crystallization and the subsequent fusion and recrystallization. The shrinkage observed in the other cases cannot be attributed to melting, but must result from the relaxation of the strained amorphous chains. Thus, though the melting of oriented structures invariably is accompanied by an axial contraction,[8,13-16] it does not follow that all shrinkages that are observed necessarily involve a crystal–liquid phase transition.[11] The fact that the thermodynamic stability of the β-form depends on the crystallization time implies that the crystallization mechanisms play a significant role in determining the resulting texture and perfection of the crystalline state. When adequate time is allowed for the crystallization process, the β-structure formed at 100° with a 70% deformation is thermodynamically stable at 100° without an external force. Similar results are obtained at all deformations wherein the β-form develops from the molten state at this temperature.

The temperature of crystallization, at a fixed deformation, also affects the stability of the resulting unstressed β-structures. The experimental observations in this connection are summarized in Table II. For β-structures crystallized at temperatures below 75°, melting of the unstressed fibers and conversion to oriented α-structures occur at temperatures equal to or less than the crystallization temperature (under deformation).[17] For crystallization conducted at 75°, melting of the unstressed fiber in water occurs at 75° but does not occur at 25°. Heating of this latter fiber in water results in the melting at 50° with subsequent regeneration of the oriented α-structure.

TABLE II

THE DIMENSIONAL AND THERMODYNAMIC STABILITY OF UNSTRESSED β-FIBERS FORMED AT VARIOUS TEMPERATURES

Sample	% Deformation	Crystn. condition	Post-treatment of unstressed fiber	% Shrinkage	Resulting X-ray pattern
112	70.9	75°, 4 hr.	75°, 2 hr.	33.8	Oriented α
113	69.9	75°, 4 hr.	25°, 2 days	20.4	Oriented β
116	70.0	50°, 5 hr.	50°, 2 hr.	39.4	Oriented α
125	69.8	50°, 17 hr.	50°, 7 hr.	35.0	Oriented α
115	71.3	50°, 5 hr.	25°, 2 days	40.4	Oriented α
117	70.7	50°, 5 hr.	10°, 3 days	30.3	Oriented α
109	70.4	25°, 17 hr.	25°, 3 days	30.7	Oriented α
107	72.6	10°, 10 days	10°, 2 days	30.7	Oriented α

The data in Tables I and II bear close resemblance to the early work of Astbury and Woods,[2b] who showed that a wool fiber stretched when moist and allowed to dry under tension will remain elongated with the β-form being produced. When treated with water, the fiber contracts and concomitantly the α-structure redevelops. However, unstressed fibers which initially had been held stretched and exposed to steam for at least 30 min. do not contract during subsequent treatment with boiling water. The β-structure developed during the deformation and heat processing remains intact.

These observations indicate a strong dependence of the melting temperature on the crystallization conditions, particularly the crystallization temperature and time of crystallization. Similar effects commonly are observed in regard to the thermodynamic stability of the crystalline phase in simpler macromolecules.[18] In this latter case these effects have been shown to be due to kinetic limitations imposed on the crystallization process so that the perfection of the crystalline state is governed, to a large extent, by the crystallization temperature and the time allowed for the transformation. It is possible, therefore, to offer the same explanation for the stability of β-keratin crystallized from the molten state. A more detailed investigation of the crystallization kinetics and mechanisms of this system would be required to substantiate the explanation offered.

An alternative explanation of the stability of the β-structure formed by these methods has been offered by Speakman.[19,20] It is suggested that in water, at the temperatures involved, scission of the native intermolecular cross links occurs through hydrolysis of the cystine linkages followed by the formation of new types of cross links. One type postulated would result from reaction between sulfenic acid residues and free amino side chains. It is supposed that when formed, the new cross links stabilize the β-structure. If the chemical reactions postulated actually occurred, an extremely high activation energy would be required to explain the stability imparted to fibers formed at 100° in

(15) P. J. Flory, *Science*, **124**, 53 (1956).

(16) P. J. Flory, *J. Am. Chem. Soc.*, **78**, 5222 (1956).

(17) The apparent ambiguity of melting occurring below the crystallization temperature can be clarified by the realization that the melting of the unstressed fiber is being considered while the crystallization was conducted with the fiber being subject to a uniaxial deformation. In general, the melting temperature under stress will be increased substantially over that of the undeformed fiber.

(18) L. Mandelkern, *J. Polymer Sci.*, **47**, 494 (1960).

(19) J. B. Speakman, *J. Soc. Dyers and Colourists*, **52**, 335 (1936).

(20) R. S. Asguith and J. B. Speakman, *Proc. Intern. Wool Textile Res. Conf. Australia*, **C**, 303, 492 (1955).

comparison to those formed at 75°. Moreover, analytical studies have failed to substantiate the existence of the new bonds postulated. It is clear, however, that *a priori* changes in the chemical constitution are not required to explain the resulting stability of the β-crystalline phase. Resort to this more complex explanation would appear warranted only when the nature of the crystalline phase is shown to be independent of crystallization conditions.

Comparison of the Melting of α- and β-Keratin.—Previous studies have shown that naturally occurring fibrous β-keratin (from white turkey calamus) melts at considerably higher temperatures than α-keratin from Lincoln wool or horse hair when fibers are immersed in a large excess of aqueous LiBr solutions.[8,21] In particular, for an 11.6 *M* supernatant phase, Lincoln wool melts at 34 ± 2°, while the corresponding temperature for the turkey feather is 60 ± 2°. Since the amino acid composition, including the disulfide content, is different in these two cases, the differences in melting temperature cannot be attributed solely to the structural differences in the crystalline phase, since the chemical constitution and composition of the molten phase also influences melting. However, since a β-keratin can be prepared from a naturally occurring α-keratin, a comparison of the melting of the latter two types of fibers would be instructive.

For these experiments, amorphous fibers were stretched 70% and crystallized in boiling water for 2 and 3 hr., respectively. The unstressed fibers then were relaxed in boiling water for 1 hr. X-Ray diffraction analyses indicated the existence of well developed, oriented β-structures. The fibers then were immersed in a large excess of 11.6 *M* aqueous LiBr solutions at 20° and the lengths were determined as a function of temperature. As a control experiment, a native Lincoln wool fiber was immersed in a similar solution and subjected to the same measurements. The melting of the α-keratin specimen was reconfirmed to occur at 34 ± 2° in this medium and concomitantly a 6.5% contraction was observed. Melting of the β-fibers occurs at the same temperature as the native α-fiber. The X-ray diffraction pattern of the fibers obtained after contraction and removal from the LiBr solution is amorphous and supports the conclusion that melting has occurred. After immersion in pure water, the oriented α-structure is regenerated, thus completing the cycle. The fiber crystallized for 2 hr. displays a 3.6% contraction, while that crystallized for 3 hr. shortens by 8.2%. In the latter instance, the development of more oriented crystallinity or the severance of cross links with the longer time of crystallization is indicated.

The most stable β-structure that presently can be prepared has a melting temperature, in concentrated LiBr solution, virtually identical with that of the native α-structure from which it can be formed. Since the constitution and composition of the molten phase now is the same in both cases, this is strong indication of a similarity in thermodynamic stability of the two different crystallographic forms.

Conclusion.—The results reported indicate that stable β-structures can be formed from molten keratin. A more complete and formal thermodynamic analysis of the polymorphism would involve the determination of the free energy of fusion of the two crystalline structures (relative to the same liquid state). Although this type of analysis has been accomplished for the simpler polymer gutta-percha, which is capable of crystallizing in more than one modification,[22] the necessary experiments are more complex for the keratins. However, the principles involved would be the same in the two cases.

(21) L. Mandelkern, J. C. Halpin, and A. F. Diorio, *J. Polymer Sci.*, in press.

(22) L. Mandelkern, F. A. Quinn, Jr., and D. E. Roberts, *J. Am. Chem. Soc.*, **78**, 926 (1956).

CORRESPONDING STATE TREATMENT OF CHEMICAL KINETIC DATA—SOLVENT EFFECTS

BY H. L. FRISCH,

Bell Telephone Laboratories, Inc., Murray Hill, New Jersey

THOR A. BAK,

Institute for Physical Chemistry, University of Copenhagen, Denmark

AND ELEANOR R. WEBSTER

Department of Chemistry, Wellesley College, Wellesley 81, Massachusetts

Received January 26, 1962

We discuss briefly three general procedures for applying a corresponding state treatment of kinetic data. We apply one of these procedures to obtain a corresponding state theory for inert, non-polar solvent effects. A detailed statistical mechanical modification of the "equilibrium rate" of a gas reaction to take account of the presence of weak interactions between the reactant(s) and the inert, spherical, non-polar solvent leads to the rate constant expression of the corresponding state treatment. This asserts that if the rate of a reaction in a solvent is k and the corresponding rate in a reference solvent is k_0, then the ratio of log (k/k_0) divided by the difference in critical volume (or pressure) between the solvent and the reference solvent is a linear function of the ratio of the differences in critical temperature to critical volume (or pressure). We have applied this simple relation to selected sets of kinetic data in various solvents and have obtained in most cases a fair correlation. This is astonishing in certain instances, since the reaction system and/or solvents were polar. Extensions of the theory to take account of somewhat non-inert, non-polar solvents or inert, somewhat polar solvents are stated.

1. Introduction to Corresponding State Theories of Chemical Reactions

The principle of corresponding states provides a practical, if rough, method of making use of the properties of one or more substances to predict the properties of other substances or mixtures. This method is particularly useful if no data are available or no other satisfactory theoretical treatment can be applied. It has been used, with some success, in predicting equilibrium properties of sufficiently simple substances or mixtures[1] and in correlating certain transport properties[2] such as viscosity, thermal conductivity, and self-diffusivity. It has not been applied in any systematic fashion to the prediction and study of chemical reaction rate constants.

We are interested here in pursuing the question of the extent to which the principle of corresponding states can serve as a qualitative, if not quantitative, guide for the empirical classification of a sequence of chemical reactions possessing some common mechanistic features.[3] We will carry out the derivations of this paper as if they applied only to first-order reactions. Actually, the theory can be extended to comparisons of rate constants of higher order reactions so long as the activities of the reactants in such a comparison are held constant.

A great variety of corresponding state treatments of chemical kinetic data are possible. We present in this section three possible procedures. In the next section we present the statistical mechanical "equilibrium rate" theory of solvent effects and the last section is devoted to comparison of our inert solvent effect rate expression with experimental data.

(1) See, *e.g.*, J. S. Rowlinson, "Liquids and Liquid Mixtures," Academic Press, New York, N. Y., 1959.

(2) See, *e.g.*, J. O. Hirschfelder, C. F. Curtiss, and R. B. Bird, "Molecular Theory of Gases and Liquids," John Wiley and Sons, Inc., New York, N. Y., 1954.

(3) These common features include the nature of the chemical entities, reaction paths, external constraints, or combinations of these.

The first procedure, which is simplest from the viewpoint of theory, is *direct dimensional scaling* of the rate constants in a given, suitably homologous sequence of reactions. One applies dimensional analysis (*i.e.*, Buckingham's pi theorem) to the rate constant by first choosing a *dimensional model* and then obtains the functional form of the rate constant in terms of dimensionless combinations of the parameters characterizing the chosen model by comparison with experimental data. Choosing the dimensional model consists of finding or guessing the minimal number of physical parameters, *e.g.*, energies, bond distances, masses, dielectric constants, temperature, etc., which suffice to describe the variations in chemical entities and reaction paths involved in the sequence of reactions under consideration. To illustrate the procedure, consider one of a suitable sequence of bimolecular, homogeneous reactions whose rate constant is Γ_2.[4] An oversimplified model for the sequence, chosen for purposes of illustration only, involving a single characteristic energy ϵ, effective distance σ, effective mass m, and kT, where T is the absolute temperature, leads to the functional form

$$\Gamma_2 = \sigma^2 \left(\frac{kT}{m}\right)^{1/2} f\left(\frac{\epsilon}{kT}\right) \qquad (1.1)$$

with f an as yet arbitrary function of the indicated variable, a special case of which is the usual classical kinetic theory formula.[5] This procedure, while exact, is applicable only if the correct dimensional model is used and in practice, is useful only if the number of parameters needed is small and the values of the parameters are available in the literature.

A second procedure for applying a corresponding state treatment to a restricted sequence of reac-

(4) We employ Γ as a symbol for a rate constant in the first two sections of this paper to avoid confusion with Boltzmann's constant k.

(5) S. Glasstone, K. J. Laidler, and H. Eyring, "Theory of Rate Processes," McGraw-Hill Book Co., New York N. Y., 1941.

tions, possessing a homologous transition state whose chemical structure is known sufficiently well, *involves dimensional scaling of a simplified theoretical rate constant expression* such as that given, for example, by the absolute rate theory.[5] This reduces to dimensional analysis of the ratios of partition functions of reactants and the activated complex which can be carried out in the same manner as the scaling of a partition function in predicting the thermodynamic properties of a fluid in equilibrium.[1,2] The simplified theory is used primarily to specify which physical parameters suffice for the dimensional scaling and not to provide a complete, explicit expression for the rate constant.

In this paper we will not follow the above ambitious procedures. Rather we restrict ourselves at the outset to dealing with corresponding state correlations in a sequence of reactions possessing the common features that in all instances the reactant molecule(s) and product molecule(s) remain the same from reaction-to-reaction and in which only one constraint or entity is varied within the sequence. Two examples are furnished by the variation in rate of unimolecular reactions with changing pressure, and the effect of different inert solvents on reactions, preferably those where the gas phase reaction also has been studied. The change of inert solvent is to represent a relatively minor perturbation in the mechanism of the gas reaction. A corresponding state treatment is most easily achieved in these cases by using a third and different procedure which is essentially *an expansion method in small differences of the parameters* characterizing the varied constraint or entity.

For the inert solvent effect we consider two solvents, one of which is the reference solvent (subscript zero), in which a given reaction is carried out. The intermolecular potential energy of the reference solvent composed of roughly spherical, non-polar molecules requires the specification of at least two parameters, a characteristic energy ϵ_0 and a characteristic molecular diameter σ_0. Similarly, the second solvent possesses a characteristic energy, $\epsilon = \epsilon_0 + \delta\epsilon$, and characteristic molecular diameter, $\sigma = \sigma_0 + \delta\sigma$, and can be thought to arise from the reference solvent by changing ϵ_0 and σ_0 by the addition of the small variations in the parameters $\delta\epsilon$, $\delta\sigma$. Let the measured rate constants in these two solvents be Γ and Γ_0; then by the definition of the usual activation free energy per molecule ΔF^*,

$$-kT \ln \Gamma/\Gamma_0 = \delta\Delta F^* \qquad (1.2)$$

If the solvent is inert, the indicated variation in ΔF^* is due solely to the smooth variation with the parameters ϵ and σ and not one in the form of the function ΔF^*. Thus to first order

$$\delta\Delta F^* = \left(\frac{\partial\Delta F^*}{\partial\epsilon}\right)_{\sigma_0,\epsilon_0}\delta\epsilon + \left(\frac{\partial\Delta F^*}{\partial\sigma}\right)_{\sigma_0,\epsilon_0}\delta\sigma \qquad (1.3)$$

and where to the same order of approximation $\delta\epsilon$ is proportional to the difference of critical temperatures of the solvents, $T_c - T_c^0 = \Delta T_c$ and $\delta\sigma$ is proportional to the difference in critical volumes of the solvents, $V_c - V_c^0 = \Delta V_c$ (*cf.* p. 278 of ref. 2). At fixed temperature and pressure (1.2) becomes, by virtue of (1.3)

$$\ln \Gamma/\Gamma_0 = A\Delta T_c + B\Delta V_c$$

or

$$\frac{\ln \Gamma/\Gamma_0}{\Delta V_c} = A\frac{\Delta T_c}{\Delta V_c} + B \qquad (1.4)$$

where A and B are characteristic constants for the reaction and the chosen reference solvent (*cf.* 1.3). If the pure solvents satisfy a corresponding state relation, P_cV_c/kT_c = constant, then (1.4) can be expressed in terms of the critical pressure difference ΔP_c

$$\frac{\ln \Gamma/\Gamma_0}{\Delta P_c} = a\frac{\Delta T_c}{\Delta P_c} + b \qquad (1.5)$$

with a and b replacing A and B. For non-spherical or somewhat non-polar solvent molecules, other parameters than ϵ, σ are needed; *e.g.*, an acentric factor ω or Riedel parameter α_k may suffice (see section 8.4 of ref. 2) and (1.4) is replaced to the same order of approximation by

$$\ln \Gamma/\Gamma_0 = A\Delta T_c + B\Delta V_c + C\Delta\omega \qquad (1.6)$$

which is difficult to fit to experimental data even if the required data for $\Delta\omega$ were available for the solvents used.

In, general, if the varied constraint is determined by variations in parameters $\vec{\alpha}$, $\delta\vec{\alpha}$ then

$$\ln\frac{\Gamma(\vec{\alpha}_0 + \delta\vec{\alpha})}{\Gamma_0(\vec{\alpha}_0)} = -\frac{1}{kT}\frac{\partial\Delta F^*}{\partial\vec{\alpha}}\cdot\delta\vec{\alpha};\quad \frac{|\delta\vec{\alpha}|}{|\vec{\alpha}_0|} \ll 1 \qquad (1.7)$$

In particular (1.7) leads directly to the usual treatment of pressure effects of unimolecular reactions since with given reference pressure $P_0 = \alpha_0$ ($P = \alpha$) we obtain (Γ in appropriate activity units)

$$\ln\frac{\Gamma(P_0 + \delta P)}{\Gamma_0(P_0)} = -\frac{\overline{\Delta V}^*}{RT}\delta P \qquad (1.8)$$

with R the gas constant and $\overline{\Delta V}^*$ the difference of partial molar volumes of activation.

The justification of the choice of parameters used in (1.4) or (1.7) and the form of the variation taken in (1.3) or (1.7) results from an intermediate dimensional scaling of ratios of rate constants with arguments corresponding to small variation in parameters derived from a general microscopic statistical mechanical theory. The rate constant being an averaged integrated cross section, mechanics, whether quantum or classical, asserts that this is a suitable surface integral (or trace) of an appropriately defined particle current divided by a suitable volume integral (or trace) of the particle density (or density matrix). The integrations are carried out over the configuration space of the mechanical system representing the chemical reac-

tion in its environment. The geometry of the volume and surface integrals is uniquely determined by the potential energy of this system. The formulation of the appropriate current and density functions is particularly simple when we can assume that the thermostated reaction system is effectively in equilibrium, so that these functions are derivable from the Gibbsian canonical distribution in the phase space of the system. This limiting form of the general theory disregarding departures from the equilibrium distribution as well as multiple recrossings of the surface in configuration space separating the "reacted" from the "unreacted" states presumably is satisfactory if the activation energy per molecule is sufficiently high, *i.e.*, exceeds 10 kT.[6-11] In the next section we shall carry out an explicit calculation of the solvent effect based on this "equilibrium theory."[6,7,11]

2. The Equilibrium Rate Theory Formulation of the Solvent Effect

We follow in formulating the equilibrium rate theory for the gas reaction the development and notation of Vineyard's[10] elegant formulation of frequency factors in solid state processes. The configuration space of the reacting entity (or reacting entities) in its gaseous environment is spanned by the vector y. The potential energy $\varphi = \varphi(y)$ of the reacting system possesses a minimum at a point A in this space, corresponding to the "unreacted" entity and the environment in an equilibrium position. Similarly, φ possesses another minimum at point B which corresponds to the "reacted" entity in the again relaxed environment. Assuming only a single saddle point P somewhere between A and B we construct the "reaction surface" $S(y)$, a unique hypersurface determined by φ of dimension one less than that of the configuration space, in the manner indicated by Vineyard.[10] $S(y)$ thus separates the configuration space into a region $A(y)$ centered about A of the "unreacted entity" and a region $B(y)$ enclosing B of the "reacted entity." The rate, Γ_G, of the gas phase reaction is the integrated current through $S(y)$ divided by the integrated density, proportional to $e^{-\beta\varphi}$, $\beta = 1/kT$, over the region $A(y)$ and is given exactly (see eq. 2–10 of ref. 10) by

$$\Gamma_G = \sqrt{\frac{kT}{2\pi}} \frac{\int_{S(y)} e^{-\beta\varphi(y)}\, dS}{\int_{A(y)} e^{-\beta\varphi(y)}\, dy} \qquad (2.1)$$

If q_i, ν_i ($i = 1, \ldots, N$; N the number of components of y) are the normal modes and frequencies about A and q_i', ν_i' ($i = 1, \ldots, N-1$) those about P within the constraining surface S; *i.e.*,

$$\varphi \cong \varphi(A) + \frac{1}{2}\sum_{j=1}^{N} (2\pi\nu_i)^2 q_i^2$$

$$\varphi \cong \varphi(P) + \frac{1}{2}\sum_{i=1}^{N} (2\pi\nu_i')^2 q_i'^2 \qquad (2.2)$$

then on introducing (2.2) into (2.1) and carrying out the indicated integrations one finds[10]

$$\Gamma_G = \left(\prod_{i=1}^{N} \nu_i\right) \Big/ \left(\prod_{i=1}^{N-1} \nu_i'\right) \exp \{-\beta[\varphi(P) - \varphi(A)]\} \qquad (2.3)$$

In the condensed, liquid phase in the presence of the solvent, the configurational space of our reaction system is a direct product of the space spanned by y and the configurational space of the solvent molecules spanned by the vector x, possessing M components. The potential energy $\Psi(y,x)$ is now given by

$$\Psi(y,x) = \varphi(y) + V(y,x) + U(x) \qquad (2.4)$$

with $V(y,x)$ the interaction energy between the reacting species and solvent and $U(x)$ the sum over pairs of the intermolecular potential of the solvent molecules. Thus only U and V are functions of the ϵ and σ, etc., which appear as the natural parameters of the intermolecular potential. The rate in the presence of solvent $\tilde{\Gamma}$ is

$$\tilde{\Gamma} = \sqrt{\frac{kT}{2\pi}} \frac{\int_V \int_{\tilde{S}(y,x)} e^{-\beta\Psi(y,x)}\, dS\, dx}{\int_V \int_{\tilde{A}(y,x)} e^{-\beta\Psi(y,x)}\, dy\, dx} \qquad (2.5)$$

cf. (2.1), where $\tilde{S}(y,x)$ is, in general, a shifted hypersurface through a new saddle point $\tilde{P}$ (determined by Ψ and not φ) and $\tilde{A}(y,x)$ the new region of configurational space (x,y) of the "solvented" reactant(s). Only if the solvent is *inert*, *i.e.*, strictly does not affect the gas phase reaction path, can we simplify (2.5) to the rate for an *inert* solvent Γ

$$\Gamma = \sqrt{\frac{kT}{2\pi}} \frac{\int_V \int_{S(y)} e^{-\beta\Psi(y,x)}\, dS\, dx}{\int_V \int_{A(y)} e^{-\beta\Psi(y,x)}\, dy\, dx} \qquad (2.6)$$

As can be seen clearly from (2.5) the molecular parameters α which can appear in (1.7) are identified as those only arising from $\Psi - \varphi$, at least in this limiting "equilibrium rate" theory.

For an explicit evaluation of Γ we must specify $V(y,x)$. In a condensed medium, the collisions between the inert solvent and "reactant entity" are multiple ("solvent cage effect"), rather uncorrelated collisions, each transferring only small amounts of energy or momentum (*i.e.*, we have a "Brownian motion"). This justifies a "weak coupling" approximation, in which the interaction potential V can be expanded in the neighborhood of A and P on S as

$$V(y,x) \cong \sum_{i=1}^{N} q_i V_i(x,\nu_i;\ \epsilon,\sigma)$$

$$V(y,x) = \sum_{i=1}^{N-1} q_i' V_i'(x,\nu_i';\ \epsilon,\sigma) \qquad (2.7)$$

(6) N. B. Slater, "Theory of Unimolecular Reactions," Cornell University Press, Ithaca, N. Y., 1959.

(7) R. Landauer and J. A. Swanson, *Phys. Rev.*, **121**, 1668 (1961).

(8) T. A. Bak, "Contributions to the Theory of Chemical Kinetics," Munksguard, Copenhagen, 1959.

(9) S. Rice and H. L. Frisch, *J. Chem. Phys.*, **32**, 1026 (1960).

(10) G. H. Vineyard, *J. Phys. Chem. Solids*, **3**, 121 (1957).

(11) E. W. Montroll and K. E. Shuler, *Advan. Chem. Phys.*, **1**, 361 (1958).

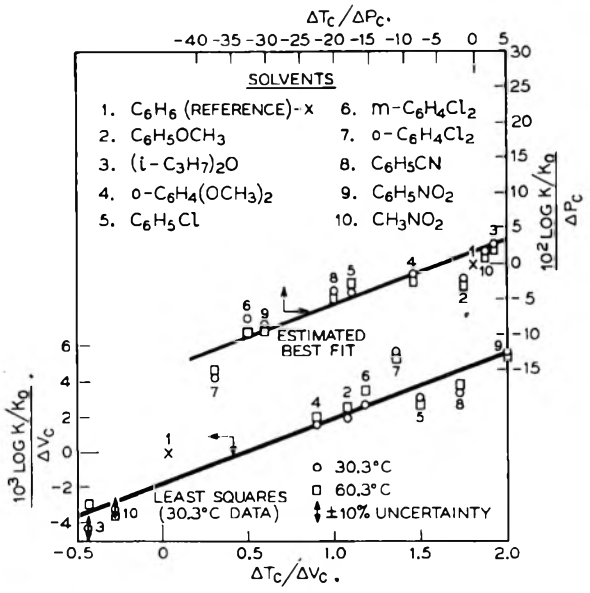

Fig. 1.—Corresponding state plot for the Diels–Alder condensation of 2-methylbutadiene with maleic anhydride at 30.3 and 60.3°. The upper straight line is a visually estimated best fit of (1.5) while the lower straight line is a least squares fit of the data to (1.4). Note the arrows identifying the appropriate coördinate scales. Plots of k, log k and the activation energy against various first-order functions of the dielectric constant gave in all cases much more scatter than shown in this plot.

relations similar to that used by Peierls[12] to treat phonon interactions in solids. We shall assume for the frequency dependence

$$|V_i|^2/\nu_i^2 = |V_i'|^2/\nu_i'^2 = c_i(x;\ \epsilon,\sigma) + O(\nu_i^2) \geq 0 \quad (2.8)$$

which is equivalent to an approximation originally suggested by Peierls (ref. 12, p. 130) for similar interaction energies in solids, which is known to be exact for Debye solids and which applies sufficiently well for any short range, non-polar interaction. The coefficients $c_i(x)$ are expected to vary very slowly with x around the most probable configurations of the solvent molecules x_0 and $c_i(x_0)$ should, in principle, be furnished by solution spectroscopy. Introducing (2.2), (2.4), (2.7), and (2.8) into (2.6) and using (2.3), we find on integrating first over the y and subsequently asymptotically approximating the integration over x

$$\frac{\Gamma}{\Gamma_G} = \frac{\int_V dx \exp\left\{-\beta\left[U(x) + \sum_{i=1}^{N-1} V_i'^2(x)/8\pi^2\nu_i'^2\right]\right\}}{\int_V dx \exp\left\{-\beta\left[U(x) + \sum_{i=1}^{N} V_i^2(x)/8\pi^2\nu_i^2\right]\right\}} = \frac{I_{N-1}}{I_N} \cong \exp\{\beta c_N(x_c,\ \epsilon,\sigma)/8^2\} \geq 1 \quad (2.9)$$

since[13]

$$I_N = \exp\left[\beta \sum_{i=1}^{N} c_i(x_0)/8\pi^2\right] \exp\left[-\beta U(x_0)\right] \sqrt{\pi^M/|(\partial^2 U/\partial x_i \partial x_k)_{x=x_0}|} \quad (2.10)$$

Equation 2.9 is our principal result. It gives explicitly Γ/Γ_G in terms of the single c_N which corresponds to the normal mode normal to $S(y)$ at P. The inequality is experimentally verified in all cases cited by Laidler.[14]

Thus for two solvents, one of which is the reference solvent with ϵ_0 and σ_0, application of (2.9) yields (1.4), since

$$\ln \Gamma/\Gamma_0 = \frac{\beta}{8\pi^2}\left[c_N(x_0;\ \epsilon_0 + \delta\epsilon, \delta_0 + \delta\sigma) - c_N(x_0;\ \epsilon_0,\sigma_0)\right] \cong \frac{\beta}{8\pi^2}\left(\frac{\partial c_N(x_0)}{\partial \epsilon}\right)_{\epsilon_0,\sigma_0} \delta\epsilon + \frac{\beta}{8\pi^2}\left(\frac{\partial c_N(x_0)}{\partial \sigma}\right)_{\epsilon_0,\sigma_0} \delta\sigma = \frac{\beta^2}{8\pi^2}\left[\frac{k}{1.25}\left(\frac{\partial c_N(x_0)}{\partial \epsilon}\right)_{\epsilon_0,\sigma_0} \Delta T_c + (9.42 N \sigma_c^2)^{-1}\left(\frac{\partial c_N(x_0)}{\partial \sigma}\right)_{\epsilon_0,\sigma_0} \Delta V_c\right]$$

$$\frac{\Delta T_c}{T_c^{(0)}},\ \frac{\Delta V_c}{V_c^{(0)}} < 1 \quad (2.11)$$

which gives A and B explicitly for a Lennard-Jones (6,12) solvent intermolecular potential.[2]

For a non-inert solvent for which the new reaction surface $\bar{S}(y,x)$ is obtained by small local vector displacements of the old surface $S(y)$, $\xi(y,x)$, one can show that (2.5) reduces to

$$\frac{\bar{\Gamma}}{\Gamma} = 1 - \langle \mathrm{div}_q \xi \rangle_\Psi - \langle |\xi| \rangle_\Psi^{\sim} \Gamma + 0(|\xi|)^2 \quad (2.12)$$

with

$$\langle f(\xi) \rangle_\Psi = \frac{\int_V \int_{S(y)} e^{-\beta\Psi} f(\xi) dS\, dx}{\int_V \int_{S(y)} e^{\beta\Psi}\, dS\, dx}$$

If ΔF_{solv} represents the change in free energy of activation due to "solvation" (*i.e.*, non-inertness of the solvent) and this quantity is small compared to β^{-1}, then $\Delta F_{solv} = \beta^{-1} < \mathrm{div}_q' \xi >_\Psi$. This detailed treatment of the solvent effect serves as a sufficient model of how in other instances (1.7) may be justified within the indicated limitations and approximations.

3. Analysis of Solvent Effect Kinetic Data

We tested (1.4) and (1.5) on experimental data on solvent effects at fixed temperature on reactions tabulated in the NBS compilation of kinetic data[15] and those discussed in standard works on chemical

(12) R. E. Peierls, "Quantum Theory of Solids," Oxford at the Clarendon Press, New York, N. Y., 1955.

(13) See, *e.g.*, N. G. de Bruijn, "Asymptotic Methods in Analysis," North Holland Publishing Co., Amsterdam, 1958.

(14) K. J. Laidler, "Chemical Kinetics," McGraw-Hill Book Co., New York, N. Y., 1950, Chapter 5.

(15) National Bureau of Standards, Circular 510, "Tables of Chemical Kinetics, Homogeneous Reactions," 1950–1953.

TABLE I

REACTION SEQUENCES USED TO TEST CORRESPONDING STATES TREATMENT

(1) Reactions	(2) Temp., °C.	(3) No. of solvents	(4) Ref. solvent	(5) Range of k/k_0	(6) Plot	(7) Quality	(8) Refs.
First order							
A. Decomposition of nitrogen pentoxide	20	10	CCl_4	0.08–1.46	ΔV_c	Fair	
					ΔP_c	Fair	*a, b, c*
B. Beckmann rearrangement of picryl ethers							
1. of acetophenone oxime	60	5	CCl_4	1.0–575	ΔV_c	Fair	*d, e*
					ΔP_c	Fair	
2. of benzophenone oxime	50	4	CCl_4	1.0–202	ΔV_c	Fair	*d, e, f*
					ΔP_c	Fair	
C. *cis–trans* isomerization of azobenzene	59.5	16	n-C_7H_{16}	0.17–1.0	ΔV_c	Fair	*f'*
	25	11	CCl_4	.15–1.0	ΔV_c	Fair	*g*
D. Dimerization of cyclopentadiene	50	7	CCl_4	.5–1.5	ΔV_c	Fair	*h*
					ΔP_c		
E. Decarboxylation of 2,4,6-trinitrobenzoic acid	70	5	$C_6H_5CH_3$	.002–1.0	ΔV_c	Poor	*i*
F. Decomposition of triethylsulfonium bromide	70	8	$CHCl_3$	.004–1.0	ΔV_c	Poor	*j*
G. Racemization of optically active biphenyls							
1. (−)-2-nitro-2'-propoxy-diphenyl-6-carboxylic acid	25	7	$CH_3CO_2C_2H_5$	.8–1.3	ΔP_c	Poor	*k*
2. (−)-2-nitro-2'-ethoxy-diphenyl-6-carboxylic acid	25	7	$CH_3CO_2C_2H_5$	.8–1.2	ΔP_c	Poor	*l*
H. Tautomerism of enol to keto form of ethyl ester of 1-phenyl-5-hydroxytriazolecarboxylic acid	10	8	$CHCl_3$	.02–2.6	ΔV_c	Fair	*m*
Second order							
G. Menschutkin reaction forming quaternary salts							
1. Ethyl iodide + triethylamine	100	22	n-C_6H_{12}	1.0–742	ΔV_c	Good	*n*
	100	22	C_6H_6	0.03–22	ΔV_c	Good	*n*
2. Methyl iodide + pyridine	100	12	CCl_4	.3–82	ΔV_c	Good	*o*
					ΔP_c	Good	
3. Ethyl iodide + pyridine	25	10	C_6H_6	.9–25	ΔV_c	Poor	*p*
					ΔP_c	Poor	
H. Benzoylation reaction							
1. Benzoyl chloride + ethanol	25	7	n-C_6H_{12}	.19–2.8	ΔV_c	Fair	*q*
	25	7	C_6H_6	.3–4.6	ΔV_c	Fair	
2. Benzoyl chloride + m-nitroaniline	100	8	CCl_4	1.0–1000	ΔV_c	Fair	*r*
I. Diels–Alder condensation of 2-methylbutadiene with maleic anhydride	30 3	10	C_6H_6	0.3–3.8	ΔV_c	Good	*s*
					ΔP_c	Good	

[a] NBS, ref. 15, Table 542.560.1. [b] R. H. Lueck, *J. Am. Chem. Soc.*, **44**, 757 (1922). [c] H. Eyring and F. Daniels, *ibid.*, **52**, 1473 (1930). [d] Reference 15, Table 162.455. [e] A. W. Chapman and C. C. Howis, *J. Chem. Soc.*, 806 (1933). [f] A. W. Chapman, *ibid.*, 1550 (1934). [f'] J. Halpern, G. W. Brady, and C. A. Winkler, *Can. J. Res.*, **B28**, 140 (1950). [g] NBS, Ref. 15, Table 122.550.1. Data from G. S. Hartley, *J. Chem. Soc.*, 633 (1938); R. J. W. Le Fevre and J. Northcutt, *ibid.*, 944 (1949); 867 (1953). [h] Data from A. Wasserman, *Monatsh.*, **83**, 543 (1952). [i] E. A. Moelwyn-Hughes and C. N. Hinshelwood, *Proc. Roy. Soc.* (London), **A131**, 186 (1931). [j] von Halban, *Z. physik. Chem.*, **67**, 129 (1909). [k] NBS, ref. 15, Table 112.443.10. [l] NBS, ref. 15, Table 112.443.8. [m] Data from O. Dimroth and J. Mason, *Ann.*, **399**, 91 (1913). [n] N. Menschutkin, *Z. physik. Chem.*, **6**, 41 (1890). [o] NBS, ref. 15, Table 652.477. Data from J. F. Norris and S. W. Prentiss, *J. Am. Chem. Soc.*, **50**, 3042 (1928). [p] NBS, ref. 15, Table 652.477. [q] NBS, ref. 15, Table 242.472.55. Data from J. F. Norris and E. C. Haines, *J. Am. Chem. Soc.*, **57**, 1425 (1935); G. E. K. Branch and A. C. Nixon, *ibid.*, **58**, 2499 (1936). [r] N. J. T. Pickles and C. N. Hinshelwood, *J. Chem. Soc.*, 1353 (1936). [s] M. J. S. Dewar, private communications.

kinetics as well as a few other cases brought to our attention. In addition to the 16 reaction sequences (representing 11 different reaction types) listed in Table I,[16] for which complete calculations have been made, another dozen or so were examined, but were eliminated for various reasons: (1) the limited number (fewer than 4) of solvents used; (2) the limited range of measured rates; and (3) the use of obviously non-inert solvents.

(16) We now revert to the standard notation for rate constants designating them by the letter k rather than Γ.

Discrepancies in fitting (1.4) or (1.5) to these data are expected theoretically for at least three reasons: (a) the solvent molecules in many instances are far from roughly spherical; (b) the solvents are sometimes far from non-polar; and (c) the assumption that $\Delta T_c < T_c$, $\Delta V_c < V_c$, $\Delta P_c < P_c$ is sometimes unjustified, so that the strict equality in (2.11) is more relevant than the first-order expansion formulas (1.4) or (1.5). Most of the pure solvents employed in the kinetic studies possess equilibrium properties which at best could only

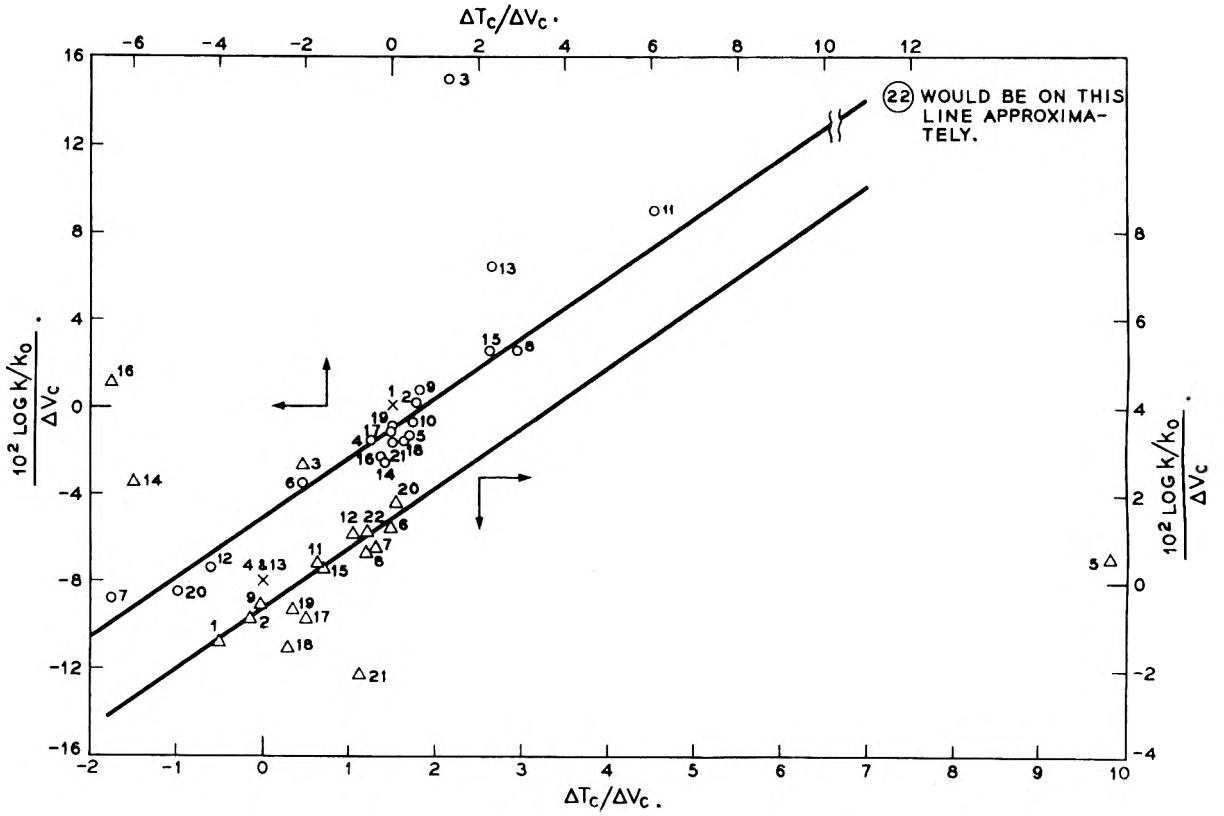

Fig. 2.—Corresponding state plot for quaternary salt formation $C_2H_5I + (C_2H_5)_3N \rightarrow (C_2H_5)_4N^+I^-$ at 100° according to (1.4).[a] Illustrated is the effect of changing the reference solvent at fixed temperature. The reference solvent for the upper straight line is *n*-hexane while the reference solvent for the lower straight line is benzene (×). Solvents: (1) *n*-C_6H_{14}; (2) *n*-C_7H_{16}; (3) *p*-$C_6H_4(CH_3)_2$; (4) C_6H_6; (5) *n*-C_3H_7Cl; (6) C_6H_5Cl; (7) C_6H_5Br; (8) α-$BrC_{10}H_7$; (9) *i*-$C_5H_{11}OC_2H_5$; (10) $(C_2H_5)_2O$; (11) $C_6H_5OC_2H_5$; (12) $C_6H_5OCH_3$; (13) $CH_3COOC_4H_9$-*i*; (14) $CH_3COOC_2H_5$; (15) $C_6H_5COOC_2H_5$; (16) *i*-C_4H_9OH; (17) C_2H_5OH; (18) $CH_2{=}CHCH_2OH$; (19) CH_3OH; (20) $C_6H_5CH_2OH$; (21) CH_3COCH_3; (22) $C_6H_5COCH_3$.

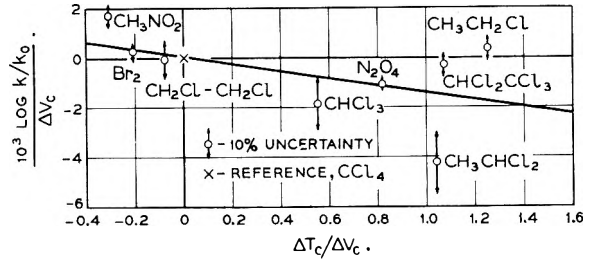

Fig. 3.—Corresponding state plot for the decomposition of N_2O_5 ($2N_2O_5 \rightarrow 2N_2O_4 + O_2$) at 20° according to (1.4).[a,b,c]

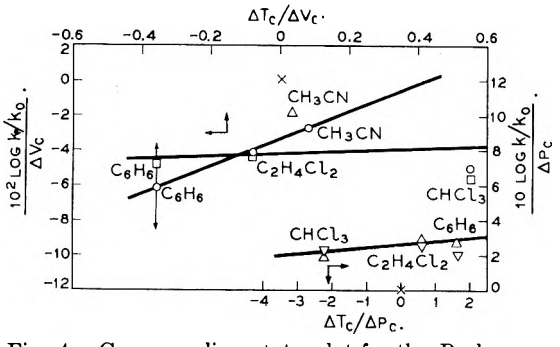

Fig. 4.—Corresponding state plot for the Beckmann rearrangement of two picryl ethers of $C_6H_5C(R) = NOH$.[d,e,f] The reference solvent (×) is CCl_4. Points according to (1.4) are ○ for R = CH_3 at 60° and □ for R = C_6H_5 at 50°. Points according to (1.5) are △ for R = CH_3 at 60° and ▽ for R = C_6H_5 at 50°. The data for R = C_6H_5 correlate with the dipole moment of the solvent.[f]

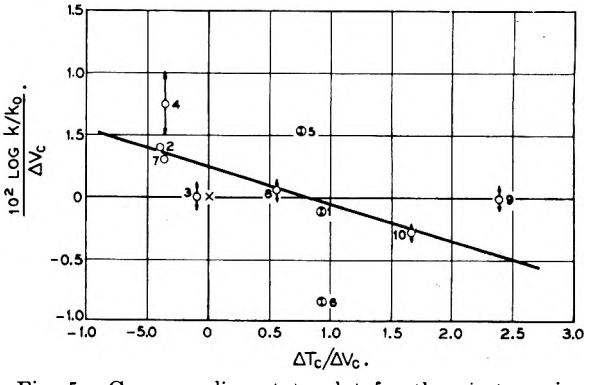

Fig. 5.—Corresponding state plot for the *cis–trans* isomerization of azobenzene at 25°.[g] Solvents: (1) pure azobenzene; (2) H_2O; (3) *cyclo*-C_6H_{12}; (4) C_6H_6; (5) CH_3COCH_3; (6) *cyclo*-$C_6H_{10}O$; (7) CH_3COOH; (8) $CHCl_3$; (9) C_6H_5Cl; (10) *o*-$C_6H_4Cl_2$; (11) CCl_4, the reference solvent (×).

very crudely be correlated by a two-parameter corresponding state treatment.[2] Two principal sources of uncertainty in the handling of the published kinetic data are: (1) the reliability and comparability of reported rate constants; *e.g.*, traces of water (or other impurities) change observed rate constants by factors of 50–10^6 (see reference *i* of Table I) and even with apparently identical materials and techniques different investigators report rate constants differing by 15–50% (see ref. 14, p. 113); and (2) shifts in solvents

sometimes involved changes in reaction temperature which introduced considerable uncertainty in calculating comparable rate constants from activation energies determined from Arrhenius plots consisting of just two points. Thus in typical plots of (1.4) or (1.5) against experimental data, Fig. 1–6, we have indicated in some instances graphically a region corresponding to a 10% uncertainty in our knowledge of k/k_0 although in some cases this figure may be an order of magnitude too small. Finally, another uncertainty in testing the linear relations (1.4) and (1.5) arises because many critical constants of the 61 solvents used in the 20-odd kinetic studies which we have considered do not appear in compilations and had to be estimated by Lydersen's empirical methods.[17]

Column (7) of Table I gives a qualitative evaluation of the observed correlation as indicated by the scatter of points in our plots, typical examples of which are shown (Fig. 1–6). Tables II and III compare observed values for $10^3 \log k/k_0$ (which is more sensitive than k/k_0) with those calculated using the constants A and B of (1.4) determined by least squares fit of the probably reliable data for two reactions which give a "fair" and a "good" estimate of correlation, respectively. Clearly, the theory of the previous sections is inadequate in accounting for the fortuitous cancellation of departures expected in applying (1.4) to the data summarized in Table I (*cf.* Fig. 2 and 6). We have no explanation of this cancellation.

TABLE II

COMPARISON OF CALCULATED AND OBSERVED 10^3 LOG k/k_0 FOR THE DECOMPOSITION OF N_2O_5

	—10^3 log k/k_0—			—10^3 log k/k_0—	
Solvent	Calcd.	Obsd.	Solvent	Calcd.	Obsd.
N_2O_4	168.2	165.2	CH_3CH_2Cl	132.2	− 28.9
CH_2CHCl_2	45.5	136.7	Br_2	− 51.7	− 38.6
$CHCl_3$	25.6	66.7	Cl_2CHCCl_3	−147.4	− 28.9
$ClCH_2CH_2Cl$	−5.49	5.2	CH_3NO_2	− 54.9	−175.2
[CCl_4	0	0]			

In part, the usefulness of this simple empirical correlation of inert solvent effects stems from the fact that the departure of a solvent or class of solvents in a sequence from the behavior of known inert ones in the series (*cf.* Fig. 6) gives a relative measure of its tendency to participate directly in a given reaction (*i.e.*, a desirable measure of "non-inertness"). While Table I suggests some promise of a fair empirical correlation of inert solvent effects through (1.4) or (1.5), further careful experimental studies are clearly indicated which should be designed to test the applicability of our simple relationships. We suggest the following reactions as possible candidates for such a study: (1) further studies of the N_2O_5 decomposition, (2) *cis–trans* isomerizations like that of azobenzene in non-polar solvents, (3) the spontaneous rearrangement of oxime picryl ethers, (4) thermal decomposition of *o*-nitrophenyl azides,[18] and (5) the so-called Cornforth rearrangement of oxazoles, particularly in symmetrical non-polar solvents.[19]

(17) A more detailed report of the derivations and treatment of experimental data is available on request.

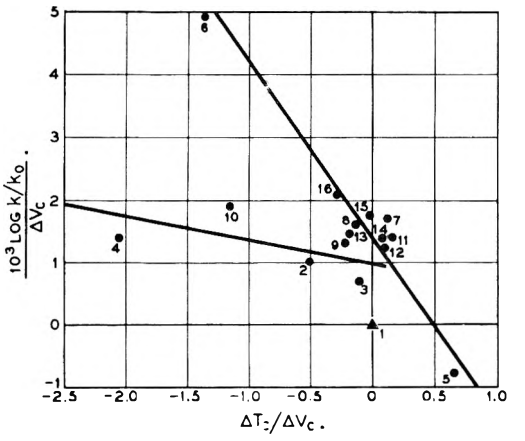

Fig. 6.—Corresponding state plot for the *cis–trans* isomerization of azobenzene at 59.5° including a considerable number of polar and hydroxylic solvents.[17] The hydroxylic solvents appear to fall on the straight line with the more negative slope. Solvents: (1) "heptane" (reference solvent, Δ); (2) $C_6H_5CH_3$; (3) C_6H_6; (4) $C_6H_5NO_2$; (5) "decanol"; (6) "hexanol"; (7) $CH_3CO_2C_2H_5$; (8) "butanol"; (9) dioxane; (10) $C_6H_5NH_2$; (11) CH_3COCH_3; (12) C_2H_5OH; (13) CH_3NO_2; (14) CH_3OH; (15) CH_3CN; (16) N_2O. No apparent correlation was found of the observed rates with dielectric constant or the square root of the internal pressure of the solvents.[17]

TABLE III

COMPARISON OF CALCULATED AND OBSERVED 10^3 LOG k/k_0 FOR THE DIELS-ALDER CONDENSATION OF 2-METHYLBUTADIENE WITH MALEIC ANHYDRIDE [LEAST SQUARES TREATMENT OF 30.3° DATA GIVES A = 0.387 (°K.)$^{-1}$ and B = − 1.62 (cc.)$^{-1}$.]

		—10^3 log k/k_0—				—10^3 log k/k_0—	
	Solvent	Calcd.	Obsd.		Solvent	Calcd.	Obsd.
1.	C_6H_6	0	0	6.	*m*-$C_6H_4Cl_2$	278	276
2.	$C_6H_5OCH_3$	185	158	7.	*o*-$C_6H_4Cl_2$	345	581
3.	$(i\text{-}C_3H_7)_2O$	−415	−544	8.	C_6H_5CN	400	292
4.	*o*-$C_6H_4(OCH_3)_2$	259	248	9.	$C_6H_5NO_2$	480	480
5.	C_6H_5Cl	194	158	10.	CH_3NO_2	242	279

(18) E. Andersen, E. A. Birkhmer, and T. A. Bak, *Acta Chem. Scand.*, **14**, 1899 (1960).

(19) We are indebted to Prof. M. J. S. Dewar for this suggestion.

γ-IRRADIATION OF AQUEOUS SOLUTIONS OF Fe(II)–HYDRAZINE[1]

BY R. W. AHRENS

Savannah River Laboratory, E. I. du Pont de Nemours & Co., Aiken, South Carolina

Received February 3, 1962

γ-Induced oxidation of Fe^{2+} in 0.4 *M* H_2SO_4 in the presence of oxygen is inhibited by hydrazine. The decrease in Fe^{3+} yield due to hydrazine is greatest at the highest dose rates. The results are explained quantitatively by the assumption that hydrazine reacts with OH radicals to form hydrazyl radicals, which either oxidize Fe^{2+} or combine to form ammonia. At a dose rate of 2×10^6 rad/hr. about 90% of the hydrazyl radicals react to form ammonia.

Introduction

Interference with the aqueous processing of irradiated reactor fuel is often encountered from chemical reactions originating in the radiolysis of the solutions. A possible method of minimizing the interfering reactions is the addition of a radical scavenger to the solution. For initial studies, the effect of hydrazine on the γ-oxidation of ferrous ion was selected, since many studies relating to this system have been made. The oxidation of ferrous ion in sulfuric acid solutions has been the object of many investigations and the reactions involved are well understood.[2] The radiolysis of hydrazine in aqueous solutions has been investigated previously,[3] and the reduction of ferric ion by hydrazine also has been studied by several investigators.[4–7] The present investigation was designed to determine the mechanism of the protection of Fe^{2+} by hydrazine during radiolysis; the results of this work also provide supporting evidence for some of the reactions proposed in the reduction of ferric ion by hydrazine.

Experimental

Water was purified according to the process developed by the L. I. Biological Laboratory[8]: distilled water was successively distilled from alkaline permanganate and acid dichromate through columns packed with Pyrex helices. The vapor, mixed with washed oxygen, was passed through a quartz tube packed with quartz fragments that had been heated to about 900° in a tube furnace. The vapor then was condensed and redistilled into glass-stoppered bottles for storage. Ferrous sulfate dosimeter solutions prepared with and without 10^{-3} *M* chloride showed that organic impurities in this water were below the detectable concentration.[9,10]

The solutions were prepared with Mallinckrodt "Reagent Grade" sulfuric acid. "Baker Analyzed" Reagent Grade ferrous sulfate, $FeSO_4 \cdot 7H_2O$, was recrystallized from 0.4 *M* H_2SO_4 in some of the final experiments. The hydrazine was obtained from a 35% stock solution of "Hyzeen," manufactured by Betz Laboratories, Inc., and was used without further purification. The sodium chloride used in some of the experiments was "Fisher Certified Reagent" grade. The concentration of Fe^{3+} in irradiated solutions was determined spectrophotometrically with a Beckman DU spectrophotometer. Measurements were made at 304 mμ. The absorbancy index[11] used in calculating the Fe^{3+} concentration was corrected to the temperature of the sample (room temperature).

The procedure of Dewhurst and Burton[3] was modified to give an improved analysis for NH_3 at the concentrations encountered in this work. Hydrazine in the irradiated samples was destroyed by adding an excess of KIO_4 in the presence of about 3 *M* H_2SO_4 and heating (without boiling) until the iodine color disappeared. The solution was diluted with water immediately after this treatment to prevent formation of I_2 by decomposition of the concentrated KIO_4. Mossy zinc was added, and the solution was made alkaline with NaOH (the mossy zinc provided stirring by the liberation of H_2). The ammonia was distilled from the alkaline solution and was absorbed in a solution of HCl. The latter solution was diluted to 100 ml. in a volumetric flask, and the NH_3 in an aliquot of this solution was determined spectrophotometrically with Nessler's reagent.[12] The calibration curve used in this determination was prepared by analyses of known concentrations of ammonia in solutions which had the same composition as the samples. The calibration curve was linear for the amounts of NH_3 investigated (0 to 5.0×10^{-3} meq.).

The radiation source consisted of five slugs 11-5/8 in. long, each containing 2200 c. of Co^{60}, surrounding the bottom portion of a 3-3/16-in. i.d. aluminum sample tube which was 13 ft. long. The slugs and the major portion of the sample tube were immersed in a water pit containing water to a depth of about 12 ft. for shielding. The 11,000 c. of Co^{60} provided a maximum dose rate of 2.2×10^6 rad/hr. Samples were placed in a sample carrier that was grooved to fit four ribs extending down the inside wall of the sample tube. With this arrangement it was possible to position the samples reproducibly inside the sample tube. Lower dose rates were obtained by attaching spacers to the bottom of the sample carrier to position the samples at various distances from the cobalt slugs. The duration of irradiations could be timed to within 1 sec.

Results

Hydrazine reduces the yield of Fe^{3+} in the radiolytic oxidation of Fe^{2+} in 0.4 *M* H_2SO_4. Typical data for the radiolytic yield of Fe^{3+} as a function of N_2H_4 concentration are shown in Fig. 1. The yield of Fe^{3+} approaches a constant value at N_2H_4 concentrations above about 0.04 *M* ($N_2H_4/Fe^{2+} \doteq 30$). The difference between the yield of Fe^{3+} at this constant value and the yield in the absence of N_2H_4 increases with increasing dose rate (Fig. 2). The data in Fig. 2 show the fractional decrease in yield due to N_2H_4, $(-\Delta Fe^{3+}/Fe_0^{3+})$, as a function of dose rate. The quantity $(-\Delta Fe^{3+}/Fe_0^{3+})$ approaches a value between 0.46 and 0.49 at high dose rates. In some of the experiments 10^{-3} *M* Cl^- was present for the purpose of suppressing the effect of minute amounts of organic impurities.[9,10] The difference found be-

(1) The information contained in this article was developed during the course of work under contract AT(07-2)-1 with the U. S. Atomic Energy Commission.

(2) (a) H. Fricke and S. Morse, *Phil. Mag.*, **7**, 129 (1929); (b) A. O. Allen, "The Radiation Chemistry of Water and Aqueous Solutions," D. Van Nostrand Co., Inc., Princeton, N. J., 1961.

(3) H. A. Dewhurst and M. Burton, *J. Am. Chem. Soc.*, **77**, 5781 (1955).

(4) F. H. Pollard and G. Nickless, *J. Chromatog.*, **4**, 196 (1960).

(5) J. W. Cahn and R. E. Powell, *J. Am. Chem. Soc.*, **76**, 2568 (1954).

(6) W. C. E. Higginson and P. Wright, *J. Chem. Soc.*, 1551 (1955).

(7) D. R. Rosseinsky, *ibid.*, 4685 (1957).

(8) H. Fricke, E. J. Hart, and H. P. Smith, *J. Chem. Phys.*, **6**, 229 (1938).

(9) H. A. Dewhurst, *ibid.*, **19**, 1329 (1951).

(10) D. M. Donaldson and N. Miller, *J. chim. phys.*, **52**, 578 (1955).

(11) C. M. Henderson and N. Miller, *Radiation Res.*, **13**, 641 (1960).

(12) N. H. Furman, Ed., "Scott's Standard Methods of Chemical Analysis," Vol. I, 5th ed., D. Van Nostrand Co., New York, N. Y., 1939, p. 630.

tween the results of experiments with and without Cl^- was small. However, the data in Fig. 2 show consistently higher values of $(-\Delta Fe^{3+}/Fe_0^{3+})$ in the presence of Cl^- so that separate curves could be drawn through the two sets of points. The reaction between Fe^{3+} and N_2H_4 was neglected since most of the irradiations lasted between 30 sec. and 20 min., and solutions were analyzed for Fe^{3+} immediately after irradiation. The calculated[4] decrease in Fe^{3+} concentration due to this reaction was less than 2%/hr. On standing overnight, a decrease of about 10% was observed for a 0.1 *M* N_2H_4 sample.

Dewhurst and Burton[3] observed the radiolytic production of NH_3 in the irradiation of air-free aqueous solutions of hydrazine. The *G*-values for NH_3 increased with increasing initial hydrazine concentration and reached a constant value of 5.2 above $2 \times 10^{-2} M$ hydrazine.

G_{NH_3} as a function of initial N_2H_4 concentration also was measured in the present work. However, in this case the solutions were saturated with either air or oxygen. The yield, G_{NH_3}, for a constant total dose increased with increasing initial hydrazine concentration up to about 4×10^{-2} *M*; thereafter, the yield of ammonia was nearly constant with increasing hydrazine concentration (Fig. 3). In the solutions that were initially saturated with oxygen, the constant value attained for G_{NH_3} was 6.2. In the solutions that were initially saturated with air, the constant value attained was 4.6. In both of these experiments the total dose received by each sample was 1.33×10^5 rad. All the dissolved oxygen was consumed in the air-saturated solution after a dose of about 5×10^4 rad[13]; the oxygen-saturated solution contained some dissolved oxygen throughout the entire irradiation.

Discussion

Radiolytic oxidation of Fe^{2+} in acidic aqueous solution (0.4 *M* H_2SO_4) containing dissolved oxygen occurs as a result of reaction of the Fe^{2+} with OH radicals, HO_2 radicals, and H_2O_2 molecules according to the scheme[14]

$$H_2O \rightsquigarrow H, OH, H_2, H_2O_2 \quad (1)$$

$$OH + Fe^{2+} \longrightarrow Fe^{3+} + OH^- \quad (2)$$

$$H + O_2 \longrightarrow HO_2 \quad (3)$$

$$H^+ + HO_2 + Fe^{2+} \longrightarrow Fe^{3+} + H_2O_2 \quad (4)$$

$$H_2O_2 + Fe^{2+} \longrightarrow Fe(OH)^{2+} + OH \quad (5)$$

The OH formed in (5) reacts with another Fe^{2+} as in (2).

The part played by hydrazine in reducing the radiolytic yield of Fe^{3+} can be explained by the scheme

$$OH + N_2H_4 \longrightarrow H_2O + N_2H_3 \quad (6)$$

(13) J. Weiss, A. O. Allen, and H. A. Schwarz, "Use of the Fricke Ferrous Sulfate Dosimeter for Gamma-Ray Doses in the Range 4 to 40 kr." *Proc. Intern. Conf. Peaceful Uses At. Energy, Geneva*, **14**, 179 (1955).

(14) E. J. Hart, *J. Chem. Educ.*, **36**, 266 (1959).

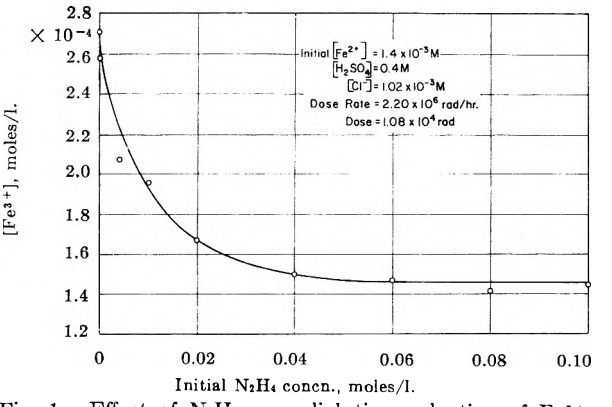

Fig. 1.—Effect of N_2H_4 on radiolytic production of Fe^{3+}.

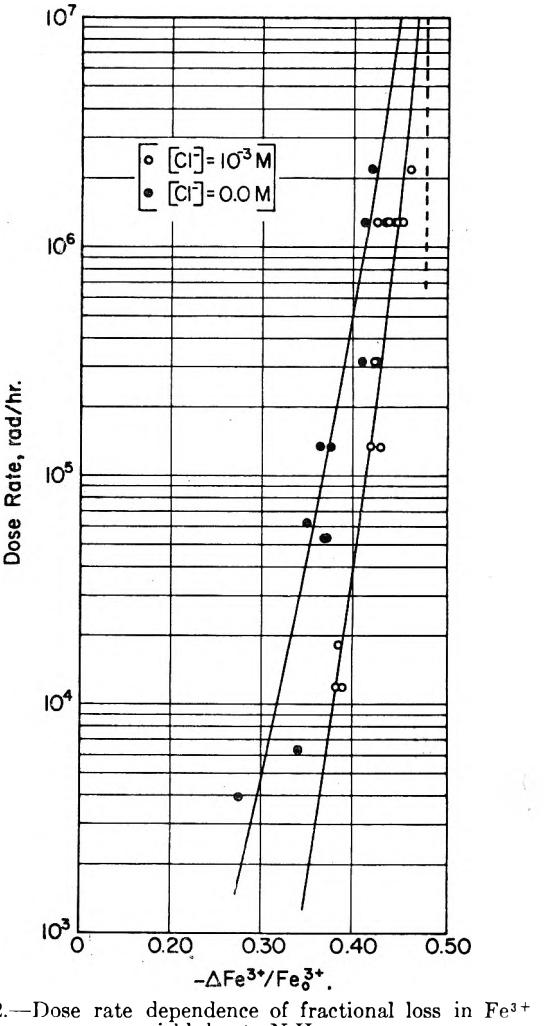

Fig. 2.—Dose rate dependence of fractional loss in Fe^{3+} yield due to N_2H_4.

$$H^+ + N_2H_3 + Fe^{2+} \longrightarrow Fe^{3+} + N_2H_4 \quad (7)$$

$$\left.\begin{aligned} 2N_2H_3 &\longrightarrow N_4H_6 \\ N_4H_6 &\longrightarrow 2NH_3 + N_2 \end{aligned}\right\} \quad (8)$$

$$H + N_2H_4 \longrightarrow H_2 + N_2H_3 \quad (9)$$

For simplicity, the formulas used here are designed to represent the oxidation state of the nitrogen atoms rather than the actual structure of the radicals. Reaction 9 would compete with (3) since the

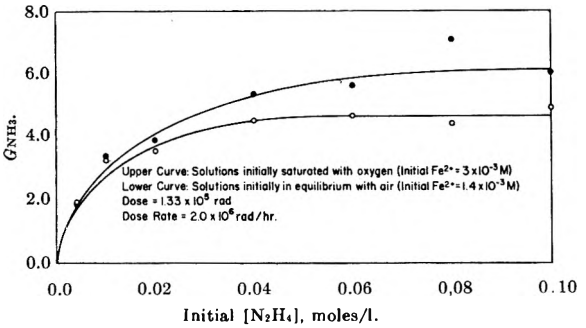

Fig. 3.—Variation of G_{NH_3} with initial hydrazine concentration.

solutions always were initially saturated with air or O_2. Reactions 6 and 9 were postulated by Dewhurst and Burton[3] to occur in deaerated solutions. Since O_2 is an efficient scavenger for the H atom it is likely that reaction 9 is negligible in the present system. Reaction 7 has been proposed by Pollard and Nickless[4] and by Higginson and Wright[6] as part of the reaction scheme for the slow reaction between Fe^{3+} and hydrazine.

A steady-state treatment of the rate equations for reactions 2, 6, 7, and 8 results in the expression

$$\frac{k_6(N_2H_4)k_RI}{k_2(Fe^{2+}) + k_6(N_2H_4)} = k_8(N_2H_3)^2 + k_7(Fe^{2+})(N_2H_3) \quad (I)$$

The quantity, k_RI, is defined as the rate of formation of OH radicals from the decomposition of water and includes OH radicals formed by reaction 5; I is the radiation intensity. At high concentrations of hydrazine (N_2H_4/Fe^{2+} > about 30), reaction 2 is assumed to be negligible compared to reaction 6, and $k_2(Fe^{2+}) << k_6(N_2H_4)$. This condition corresponds to the plateau in Fig. 1. Then

$$k_8(N_2H_3)^2 + k_7(Fe^{2+})(N_2H_3) - k_RI = 0 \quad (II)$$

The above reaction scheme provides for the loss of hydrazyl radicals through reactions 7 and 8. The ratio of the rates of these two reactions is given by

$$\frac{R_8}{R_7} = \frac{k_8(N_2H_3)^2}{k_7(Fe^{2+})(N_2H_3)} = \frac{k_8(N_2H_3)}{k_7(Fe^{2+})} \quad (III)$$

The quadratic equation II can be solved for (N_2H_3) and this expression substituted in (III)

$$\frac{R_8}{R_7} = -\frac{1}{2} + \frac{1}{2}\left[1 + \frac{4k_8k_RI}{[k_7(Fe^{2+})]^2}\right]^{1/2} \quad (IV)$$

This expression shows that the relative number of hydrazyl radicals used up through the formation of ammonia will increase with increasing radiation intensity (dose rate). Thus reaction 7 should become less important at higher dose rates. This relationship explains the variation of the fractional loss in Fe^{3+} yield with dose rate as shown in Fig. 2. The maximum fractional loss in Fe^{3+} yield (assuming reaction 6 to be solely responsible for the loss) can be calculated from the G-values for the production of H atoms, OH radicals, H_2 molecules, and H_2O_2 molecules in 0.4 M H_2SO_4. Allen describes the decomposition of water by radiation with three stoichiometric modes

$$2H_2O = H_2 + H_2O_2 \quad (F)$$

$$2H_2O = 2H + H_2O_2 \quad (E)$$

$$H_2O = H + OH \quad (R)$$

where $G_{H_2} = F$, $G_{OH} = R$, $G_{H_2O_2} = F + E$, and $G_H = R + 2E$. From the results of various irradiations of 0.4 M H_2SO_4 solutions in the presence of oxygen the best values[15] are $F = 0.45$, $E = 0.36$, and $R = 2.96$ for very dilute solutions of the solutes studied. The oxidation of Fe^{2+} according to the mechanism of reactions 2 through 5 results in a yield ($G_{Fe^{3+}} = 15.6$) given by $2F + 8E + 4R$. If all OH radicals disappear *via* reaction 6 and all N_2H_3 radicals *via* reaction 8, the fractional loss in Fe^{3+} yield is given by $(G_H + G_{OH} + G_{H_2O_2})/15.6$. The value of $(-\Delta Fe^{3+}/Fe_0^{3+})$ thus can be calculated from the equivalent expression $(2R + 3E + F)/15.6$. The value obtained, 0.48, is approached at high dose rates by both curves shown in Fig. 2. A graph of R_8/R_7, calculated for each point in Fig. 2, as a function of the square root of the dose rate allows an estimate for $k_8^{1/2}/k_7$ of 0.05.

Chloride ion present in some of the experiments at a concentration of 10^{-3} M had a small but measurable effect on the kinetics. Chloride ion participates in the oxidation of Fe^{2+} through a radical transfer mechanism.[9]

$$OH + Cl^- + H^+ \rightarrow Cl + H_2O \quad (10)$$

The Cl atoms formed in reaction 10 oxidize Fe^{2+} quantitatively. Most organic impurities that are encountered in nature cause abnormally high yields of Fe^{3+} in the presence of O_2 due to the reactions[9]

$$R{-}CH_2{-}R' + OH \longrightarrow R{-}\underset{|}{CH}{-}R' + H_2O \quad (11)$$

$$R{-}\underset{|}{CH}{-}R' + O_2 \longrightarrow R{-}\underset{|}{\overset{|}{CH}}{-}R' \quad (12)$$
$$\qquad\qquad\qquad\qquad\qquad\qquad\quad O_2$$

The organic peroxide formed in reaction 12 leads to the oxidation of two or more ferrous ions. Chlorine atoms from reaction 10 oxidize ferrous ions in preference to undergoing reactions similar to reaction 11 and the effect of the organic impurity is effectively suppressed. In those experiments in the present work in which chloride ion was present, the observed effect of hydrazine was probably due to the competition between the reactions

$$Cl + Fe^{2+} \longrightarrow Fe^{3+} + Cl^- \quad (13)$$

$$Cl + N_2H_4 \longrightarrow N_2H_3 + HCl \quad (14)$$

These reactions are analogous to reactions 2 and 6. The Cl atoms are formed from the very rapid

(15) H. A. Mahlman and J. W. Boyle, *J. Am. Chem. Soc.*, **80**, 773 (1958).

reaction 10. The somewhat larger values of $(-\Delta Fe^{3+}/Fe_0^{3+})$ obtained in the presence of 10^{-3} M chloride ion can be explained by assuming that the rate of production of N_2H_3 radicals by reaction 10 followed by reaction 14 is faster than the rate of production of N_2H_3 radicals by reaction 6. Thus the steady-state concentration of N_2H_3 radicals is higher in the presence of Cl^-. Equation III shows that more hydrazyl radicals would react to form NH_3 in this case, resulting in a larger value of $(-\Delta Fe^{3+}/Fe_0^{3+})$. It was not possible to determine the relative magnitudes of the rates of reactions 10 and 2 from the data; both reactions are considerably faster than reaction 6. The ratio of rate constants, k_2/k_6, in the absence of chloride is estimated from the Fe^{3+} *vs.* N_2H_4 curves, Fig. 1, to be about 11.

The yield of NH_3 from reaction 8 should be equivalent to the net loss in Fe^{3+} yield when all OH radicals are scavenged by reaction 6 if reactions 7 and 8 are the only paths by which hydrazyl radicals are consumed. Cahn and Powell[5] proposed that the reaction

$$2N_2H_3 \longrightarrow N_2H_4 + N_2H_2 \qquad (15)$$
$$2Fe^{3+} + N_2H_2 \longrightarrow N_2 + 2Fe^{2+} + 2H^+$$

competes with reaction 8. Since reaction 15 results in the reduction of two Fe^{3+} for each OH radical originally scavenged, $(-\Delta Fe^{3+}/Fe_0^{3+})$ would exceed the limiting value of 0.48 at high dose rates if reaction 15 were important. Work by Higginson and Wright[6] and Pollard and Nickless[4] indicates that $k_{15}/k_8 = 0.015 \pm 0.015$. The balance between $(-\Delta Fe^{3+}/Fe_0^{3+})$ and G_{NH_3} in this work indicates that G_{N_2} [reaction 15] is less than 0.35.

The yield of ammonia, G_{NH_3}, (Fig. 3) approaches a value of about 6.2 in the oxygen-saturated system for a dose rate of 2.0×10^6 rad/hr. In this experiment the initial Fe^{2+} concentration (3.0×10^{-3} M) was larger than in any of the other experiments because it was necessary to have Fe^{2+} ion present in solution throughout the entire irradiation. The dose was over 10 times as great as in the other experiments because the ammonia analysis was less sensitive than the Fe^{3+} analysis. The fractional loss in Fe^{3+} yield at this dose rate (obtained from Fig. 2) with a small correction for the larger initial (Fe^{2+}) is about 0.43. The G_{NH_3} at this dose rate then should be 0.43×15.6, or 6.7. The air-saturated solution results in a lower yield of NH_3 in Fig. 3 because all the oxygen is consumed after about 5.0×10^4 rad[13] and the yields during the latter part of the irradiation, 8.3×10^4 rad, are characteristic of a deaerated solution (*i.e.*, $G_{Fe^{3+}} = 8.3$). Here the calculated G_{NH_3} is approximately 5.0, a figure close to the experimental value, 4.6. This agreement in both air-saturated and oxygen-saturated solutions constitutes an acceptable material balance between the Fe^{3+} and NH_3 analyses and indicates that reactions 7 and 8 are the only important means by which hydrazyl radicals are consumed in this system.

THE DISSOCIATION OF DIATOMIC MOLECULES AND THE RECOMBINATION OF ATOMS

By H. O. Pritchard

Chemistry Department, University of Manchester, Manchester 13, England

Received March 3, 1962

In a recent paper, O. K. Rice shows that the forward and reverse rate constants of a reaction are likely to be related by the equilibrium constant of the reaction, even if the processes are taking place irreversibly. While this conclusion sometimes may be correct, it is not so in the special case of the dissociation of a diatomic molecule.

The present experimental situation in regard to atom recombination reactions is unsatisfactory because there is a large change in the slope of Arrhenius plots between the results obtained at low temperature by flash photolysis and those obtained at high temperature from shock waves.[1] There is as yet no good theoretical reason why this should happen, and the author has suggested[2] that it is not permissible to calculate the high-temperature recombination rate constants from the observed shock-wave dissociation rates *via* the equilibrium constant, because such dissociations take place irreversibly; the same point has been made independently by other authors.[3] However, it has been pointed out by Rice[4] and by Davidson[5] that if a steady state is set up in both the forward and reverse reactions, the over-all forward and reverse rate constants must necessarily be related by the true equilibrium constant, irrespective of the fact that the Boltzmann distributions are disturbed during the reaction. The author believes this conclusion is incorrect when applied to *the special case* of the dissociation-recombination kinetics of a *diatomic molecule*. In order to demonstrate this, it is necessary to describe, individually and in detail, the dissociation and recombination processes.

Dissociation.—Dissociation of a diatomic molecule takes place, to all intents and purposes, by a series of single-step activation processes, and no loss of generality will occur if we confine our attention to such a model. The number of molecules per second making the transition from state $v = i$ to $v = j = (i + 1)$ can be represented by

(1) H. O. Pritchard, *Quart. Rev.*, **14**, 46 (1960).
(2) H. O. Pritchard, *J. Phys. Chem.*, **65**, 504 (1961).
(3) See footnote 2 of ref. 4.
(4) O. K. Rice, *J. Phys. Chem.*, **65**, 1972 (1961).
(5) Norman Davidson personal communication.

$N_{ij} = zN_iP_{ij}$ where P_{ij} is the probability (averaged over the Maxwell distribution of approach velocities) per collision, of a transition from $v = i \rightarrow j$; N_i is the number of molecules in the state $v = i$, and z is the number of collisions suffered per second by each molecule, ignoring for the present any possible variation of z with i. It was shown previously[2] that P_{ij} depends on Δ_{ij} (the energy separation between states $v = i$ and $v = j$) and on the temperature T roughly as $e^{-\Delta_{ij}/RT}$. Considering for the moment the equilibrium situation, N_i falls off as i increases in accordance with the Boltzmann law, but, for an anharmonic oscillator, P_{ij} increases because the energy levels get closer together. Thus, the product N_{ij} can, under certain circumstances, go through a minimum, implying that there is a rate-determining step in the middle of the activation ladder; this has been shown to be the case by numerical calculation,[2] and also can be demonstrated analytically for a Morse oscillator.[6]

We now consider a hypothetical experiment [A] (analogous to Rice's case I) in which we have X_2 and X + X in equilibrium with each other, and we suddenly remove all the X atoms. There are two kinds of depopulation of the molecular vibrational energy levels which may now occur.

(i) We may have the situation where $N_{j-1,j}$ is always greater than $N_{j,j+1}$ (*i.e.*, x_{ij} is small[6]). In such a case we can in principle set up a series of quasi-steady state equations for each of the vibrational energy levels[8] and solve them by relaxation methods. Since the topmost bound level is now denied its repopulation by recombining pairs, its population will fall, and so gradually the effect will work its way down the levels. However, since there are always *more* molecules coming *up to* a given level than are going *up from* it, the system soon reaches a quasi-steady state in which the populations do not conform to the Boltzmann law, but are not very far from it. This is the sort of disequilibrium that usually is envisaged in discussions of this problem.

(ii) We also may have, as we apparently do in diatomic molecules,[2] the situation where

$$\ldots N_{j-3,\,j-2} > N_{j-2,\,j-1} > N_{j-1,j} < N_{j,j+1} < N_{j+1,\,j+2} < N_{j+2,\,j+3} \ldots\ldots \quad (1)$$

Below the level $v = j$, the situation is as in (i) above, but above $v = j$, because there are now *less* molecules coming *up to* a given state than are going *up from* it, there must be a catastrophic reduction in the populations of all these upper levels. *This phenomenon occurs in diatomic molecules only because they are anharmonic oscillators;* however, we would not expect it in a polyatomic molecule like ethane, because although the reaction coördinate may be regarded as an anharmonic oscillator, it derives increments of energy not only by collision, but by transfer of energy from other oscillators within the molecule. The fact that the observed Arrhenius temperature dependence (*i.e.*, "activation energy") is less than the heat of the reaction is readily accounted for because the transition from type (i) behavior to type (ii) behavior moves to lower and lower values of j as the temperature increases; thus, the depopulation becomes more severe as the temperature goes up, and therefore the rate of dissociation fails to rise as fast as it would if measured under equilibrium conditions.[2]

Finally, we must ask ourselves what we actually measure in the shock-wave experiment. Since it is the practice to measure the extinction coefficient of the gas at the operating temperature, the observations refer to the rate of disappearance of molecules, irrespective of vibrational state. The procedure then is to follow the rate of disappearance of molecules *via* the optical density. In principle, the rate constant could be obtained in two ways: (a) by doing a first-order plot on the optical density curve, or (b) by extrapolating the optical density plot back to zero time to get an initial rate; the former is impracticable, and it remains to decide how the observed initial rate constant (${}^{obs}k_{diss}$) is related to the theoretical equilibrium rate constant (${}^{eq}k_{diss}$). If we can label our diatomic molecules, we can define ${}^{eq}k_{diss}$ from the rate at which molecules are transferred from the topmost bound levels to the continuum (this rate being exactly counterbalanced by the reverse recombination process having a rate constant ${}^{eq}k_{recomb}$). Figure 1 shows schematically the variation of the true first-order rate constant with the progress of the reaction. To begin with, while we are waiting for the upper vibrational levels to become populated, there is no dissociation. We then reach a condition where the upper levels are populated and dissociation proceeds, the true rate constant increasing all the time because of the increasing repopulation of the upper states by recombination. Extrapolation of the optical density plot corresponds roughly to extrapolation of the true first-order rate constant back to zero time, yielding ${}^{obs}k_{diss}$ as shown. In our hypothetical experiment [A] we start at time $t = 0$ with the true $k = {}^{eq}k_{diss}$, but then there is a catastrophic fall because of the depopulation of the upper levels, as shown in the dotted curve, until again we reach a quasi-stable operating condition.

Recombination.—Recombination occurs when a pair of atoms in fairly close proximity to each other suffer an encounter with a third particle which removes sufficient of the atoms' relative kinetic energy to yield a stable (although highly excited) molecule. The total number of encounters is very insensitive to temperature,[2] but the number of effective encounters decreases slowly as the tempera-

(6) The Morse oscillator is defined by the two constants D [depth of the well] and k [where the number of bound levels is the integral part of $(k + 1/2)$, *i.e.*, $0 \leq i \leq (k - 1/2)$], so that the energy of any level $v = i$ is $E_i = -D(k - i - 1/2)^2/k^2$. If the form of P_{ij} is taken to be $e^{-x_{ij}\Delta_{ij}/RT}$, one can write the expression N_{ij} by substituting for E_0, E_i and E_j in N_i and P_{ij}; it can then be shown that $N_{j,j+1} > N_{j-1,j}$ if $1/2(x_{j,j+1} + x_{j-1,j}) > k - j - 1$, or $j > k - 1 - 1/2(x_{j,j+1} + x_{j-1,j})$. A value of x_{ij} of about unity appears to be appropriate for the $v = 0 \rightarrow 1$ transition,[7] but there is no data available on its behavior for transitions between higher energy levels; the previous calculation[2] suggests that x_{ij} increases as i increases, and that it also increases slightly with T.

(7) T. L. Cottrell and J. C. McCoubrey, "Molecular Energy Transfer in Gases," Butterworths, London, 1961, p. 165.

(8) E. V. Stupochenko and A. I. Osipov, *Russ. J. Phys. Chem.*, **33**, 30 (1959).

ture rises. There are two opposing effects here, one that the probability goes down because the higher the temperature, the larger the average amount of energy to be removed, whereas, on the other hand, the higher the temperature, the easier it is to remove larger amounts of energy; the balance between these is such as to give a roughly linear Arrhenius plot corresponding to a small negative "activation energy." On succeeding collisions, this newly formed molecule either may be further stabilized or redissociate.

At equilibrium, we have, because of microscopic reversibility, an analogous relation to (1) for the rate of deactivation, *i.e.*

$$\ldots . N_{j-2,j-3} > N_{j-1,j-2} > N_{j,j-1} < N_{j+1,j} < N_{j+2,j+1} < N_{j+3,j+2} \ldots \ldots \ldots \quad (2)$$

Corresponding to our hypothetical experiment [A] we now consider a situation [B] in which we suddenly remove all the ground-state X_2 molecules. Because of the relationship (2) between the rates, the ground state will be repopulated by serious depletion of the populations of the states $v = 1$ to $v = (j-1)$, and the states above $v = j$ will be in a quasi-steady state—precisely the reverse kind of situation to what we had in the dissociation. Thus the variation of the true bimolecular rate constant for recombination, defined from the rate of appearance of ground-state molecules, will behave as the dotted curve in Fig. 1. On the other hand, if we start with a gas containing no diatomic molecules, having completely dissociated them by a shock or a flash, the solid curve in Fig. 1 would be appropriate. In a real experiment, a population distribution of atoms and molecules which is not appropriate to the ambient temperature is generated, and relaxation occurs until we fall back to the situation depicted in Fig. 1.

To define the recombination rate constant from the rate of formation of ground-state molecules is correct, since this is essentially what is measured in the optical density curves obtained in flash photolysis. However, we do not extrapolate the rate back to zero time, as in the dissociation case, because we can do a second-order plot on the optical density curve, and derive a rate constant which is essentially an average over the period of observation, *i.e.*, ${}^{obs}k_{recomb}$.

Comparison of Dissociation and Recombination Rate Constants.—In the first place, ${}^{obs}k_{diss}$ and ${}^{obs}k_{recomb}$ will not (shall we say for want of a better word) "commute" because we are not measuring

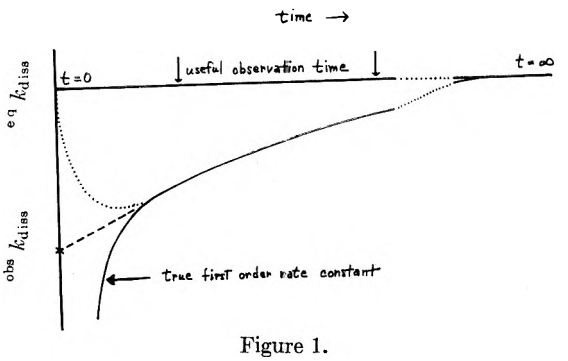

Figure 1.

precisely complementary rate constants; however, the effect of this probably will be small, and we will go on to consider the situation assuming that we could perform ideal experiments. Let us compare dissociation and recombination, in both cases, not very far away from equilibrium. In the dissociation, we will have a quasi-steady state in which the populations of all the levels below $v = j$ have essentially their Boltzmann distribution, but all the levels above $v = j$ will have populations significantly different from their equilibrium values. The observed rate of dissociation will be determined by the "rate determining step," *i.e.*, by $N_{j-1,j}$, modified by a parameter which depends on the extent to which the Boltzmann populations of the *upper* levels are disturbed. Similarly, in recombination, we will have essentially an equilibrium distribution for the continuum and all levels above $v = j$, and a disturbed distribution for all levels below $v = j$. The observed rate will then be determined by $N_{j,j-1}$, again modified by a parameter which depends on the extent to which the populations of the *lower* levels are disturbed. Now, if the energy levels were symmetrically[9] disposed about the level where the minimum rate of activation occurs, these two modifying parameters would be the same, and our rates would "commute." However, our molecule is an anharmonic oscillator, with all levels unequally spaced, and therefore this cannot be so. As a simple analogy, we may construct two hour glasses. The first has both limbs symmetrical about the waist, and the sand will fall through in the same time whichever limb is at the top. The second has limbs which are both different in shape and diameter, in which case the time constant will depend on which way the sand falls.

(9) In the sense that, at equilibrium, $N_{j-n-1,j-n} = N_{j+n-1,j+n}$: such a system does not exist.

THE CATALYTIC DECOMPOSITION OF BROMATE IN FUSED ALKALI NITRATES[1]

BY FREDERICK R. DUKE AND ELIZABETH A. SHUTE

Institute for Atomic Research and Department of Chemistry, Iowa State University, Ames, Iowa

Received March 5, 1962

The catalytic decomposition reaction: $BrO_3^- + Br^- \rightarrow Br^- + O_2$ proceeds at a measurable rate in fused $NaNO_3$, KNO_3, or $NaNO_3$–KNO_3 mixtures in the temperature range 340 to 370°. A kinetic study of the reaction shows that the decomposition proceeds by a slow rate-controlling step: $BrO_3^- + Br^- \rightarrow BrO_2^- + BrO^-$ followed by rapid reactions of the intermediates to give the final products. The activation energy for the reaction in molten $NaNO_3$ is determined and the effect of the alkali cation on the reaction rate is demonstrated. This effect is interpreted on the basis of the polarizing power of the cation.

Introduction

Solutions of bromate in fused alkali nitrates are quite stable for several days; then over a period of a few hours, the bromate completely decomposes to bromide and oxygen. This observation led to the addition of bromide as catalyst for the decomposition of bromate and a study of the kinetics of the reaction.

Experimental

Materials and Apparatus.—ACS reagent grade chemicals were used throughout the study, except when pure KNO_3 was used as the solvent. For this determination, $KBrO_3$ was prepared by precipitation from an aqueous solution of KNO_3 and $NaBrO_3$. All of the determinations were carried out in test tube-shaped Vycor vessels immersed in a constant temperature bath of a type previously described.[2]

The reaction vessel used was constructed from 31 mm. i.d. Vycor tubing. A 34/45 standard taper Vycor joint at the top was fitted with a gas inlet tube extending to within 1/2 in. of the bottom of the reaction vessel, and an outlet tube extending from the cap. This arrangement allowed easy access to the reacting solution and for the agitation of the solution by a metered stream of inert gas.

Procedure.—The rate of decomposition of bromate was obtained by following the decrease in bromate concentration with time. Weighed amounts of pure alkali nitrate or mixtures of varying mole per cent of $NaNO_3$ and KNO_3 were placed in the reaction vessel which was immersed in the constant temperature bath. When the salt had melted, weighed amounts of solutions of the corresponding alkali bromide and bromate in the fused nitrate were added. The concentration of bromide was always in large excess of the bromate and was varied from run to run. However, in the study of the solvent effect, the same approximate amount of bromide was used in each run to facilitate comparison of the rates.

Samples were withdrawn at periodic intervals with a preheated elongated medicine dropper, allowed to solidify on a cool porcelain plate, and weighed. These were analyzed for bromate by an aqueous iodometric titration. The concentration of bromide was determined at the beginning and end of a run by an aqueous silver nitrate titration using an eosin indicator. Zero time of the reaction was taken as the time of withdrawal of the first sample.

Results and Discussion

Rate Law and Mechanism.—The reaction was found to be first order in both bromate and bromide. A plot of the experimental data $[BrO_3^-]$ *vs.* time for a run in $NaNO_3$ at 370° yielded an S-shaped logarithmic curve which is typical of a second-order autocatalytic reaction. This indicates that the reaction takes place by the simple mechanism: $BrO_3^- + Br^- \xrightarrow{k}$ products, with bromide catalyzing the reaction. The rate expression for the disappearance of bromate by such a mechanism is

$$-\frac{d[BrO_3^-]}{dt} = k[BrO_3^-][Br^-] \qquad (1)$$

which reduces to a pseudo-first-order equation at high bromide concentration

$$-\frac{d[BrO_3^-]}{dt} = k'[BrO_3^-] \qquad (2)$$

where $k' = k[Br^-]$ or

$$\log k' = \log k + \log [Br^-] \qquad (3)$$

TABLE I

KINETIC DATA FOR BROMATE DECOMPOSITION IN MOLTEN $NaNO_3$ SOLVENT

t, °C.	$[BrO_3^-]$, m(initial)	$k' \times 10^2$, min.$^{-1}$	$[Br^-]$, m	k, mole^{-1} min.$^{-1}$
350	0.0268	0.472	0.2947	0.016
	.0153	.509	.3536	.014
	.0256	.495	.3401	.015
	.0206	.435	.4138	.011
	.0125	.855	.5874	.015
	.0443	.698	.5189	.014
	.0478	.955	.7856	.012
355	.0372	.430	.2692	.016
	.0277	.652	.3588	.018
	.0306	.572	.3629	.016
	.0303	.836	.4873	.017
	.0618	.645	.4895	.013
	.0452	.698	.4359	.016
	.0277	.665	.4481	.015
	.0391	.618	.4439	.014
	.0207	.802	.4467	.018
	.0302	.782	.6429	.012
	.0511	.985	.6403	.015
360	.0276	.549	.2262	.024
	.0308	.692	.2552	.027
	.0283	.806	.3591	.022
	.0232	1.268	.5135	.025
	.0216	1.505	.5235	.029
	.0227	1.452	.5901	.025
	.0217	1.640	.5915	.028
370	.0312	1.020	.2466	.041
	.0259	1.887	.4309	.044
	.0227	2.084	.5445	.038
	.0287	2.170	.6083	.036
	.0172	2.980	.7593	.039
	.0255	3.560	1.0249	.035

(1) Contribution no. 1120. Work was performed in the Ames Laboratory of the U. S. Atomic Energy Commission.

(2) F. R. Duke and H. M. Garfinkel, *J. Phys. Chem.*, **65**, 461 (1961).

TABLE II

SUMMARY OF THE KINETIC DATA FOR THE REACTION IN $NaNO_3$ SOLVENT OVER THE TEMPERATURE RANGE 340 TO 370°

t, °C.	$[BrO_3^-]$, m(initial)	$[Br^-]$, m	$k' \times 10^2$, min.$^{-1}$	k, mole^{-1} min.$^{-1}$
340	0.0173–0.0300	0.5178–0.8382	0.359–0.663	0.0076 ± 0.0008
350	.0125– .0478	.2947– .7856	.435– .955	.012 ± .004
355	.0207– .0618	.2692– .6429	.430– .985	.014 ± .005
360	.0216– .0308	.2262– .5919	.549–1.640	.027 ± .005
370	.0172– .0312	.2466–1.0249	1.020–3.560	.035 ± .004

The pseudo-constant, k', for the reaction at a particular bromide concentration, can be evaluated from the slope of a plot of log $[BrO_3^-]$ *vs.* time. Division of k' by $[Br^-]$ then gives the specific rate constant, k, for that run. Variation of the bromide concentration from run to run at a given temperature resulted in a series of k values from which an average value and the standard deviation of the mean were calculated. Alternatively, the rate constant at a given temperature can be determined graphically by a least squares analysis of the variation of the pseudo-constant with bromide concentration. A plot of k' *vs.* $[Br^-]$ results in a straight line, the slope of which is k. A plot of log k' *vs.* log $[Br^-]$ also yields a straight line, the intercept of which is log k. Treatment of the data by the method of least squares gave values of k and confidence limits at a confidence level of 95%.

The data obtained for the reaction in molten $NaNO_3$ over the temperature range 350 to 370° shown in Table I were analyzed by these three methods. The average of the three values of k so obtained ± the mean of the deviations is recorded in Table II. The value of k reported for the reaction at 340° is the average ± the mean deviation of two determinations. Only two runs were made at 340° as the reaction is extremely slow at this temperature.

The Arrhenius activation energy for the reaction in molten $NaNO_3$ over the temperature range 340 to 370° was determined from a plot of log k *vs.* $1/T$ to be 43 ± 6 kcal./mole at a confidence level of 60%. A frequency factor of $1.7 \times 10^{13} \pm 0.1 \times 10^{13}$ S.D. min.$^{-1}$ was calculated. It should be noted that the temperature range of the investigation was limited by the decomposition temperature of $NaNO_3$ and the extreme slowness of the reaction below 340°.

The catalysis of the decomposition reaction by bromide presumably is the result of an initial acceptance of an oxide ion from the bromate to form the intermediates $BrO_2^- + BrO^-$

$$BrO_3^- + Br^- \longrightarrow BrO_2^- + BrO^-$$

These intermediates then could decompose by the more rapid reactions

$$BrO_2^- \longrightarrow Br^- + O_2$$

$$BrO_3^- + BrO^- \longrightarrow 2BrO_2^-$$

to give the final products.

Solvent Effect.—Variation of the cation of the fused nitrate solvent had a large effect upon the rate of decomposition of bromate. It was observed that the rate increased with decreasing size or increasing polarizing power of the cation. This is interpreted as indicating that one or more of the cations become involved in the activated complex. Probably, the cation polarizes one or both of the reactants so as to reduce the electrostatic repulsion between the two like-charged ions, thereby lowering the free energy of activation. The reaction then would be expected to proceed faster in the solvent containing the smaller cation, as is evident in the results recorded in Table III. Figure 1 shows the free energy relationship of the specific rate constant and solvent composition.

Attempts to run the reaction in the presence of

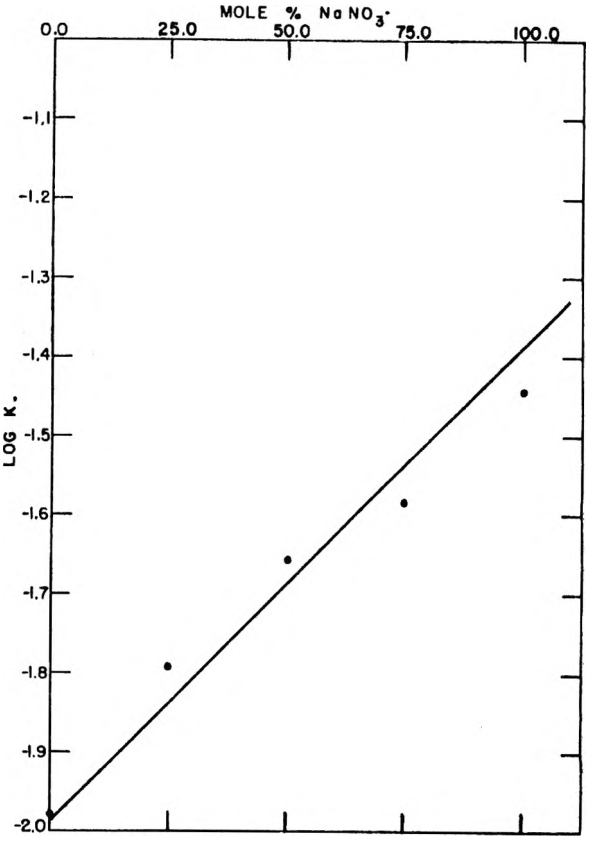

Fig. 1.—Variation of specific rate constant with solvent composition.

TABLE III

VARIATION OF REACTION RATE WITH SOLVENT COMPOSITION

370°, $[BrO_3^-]_{initial}$ = 0.0148–0.0371 m, $[Br^-]$ = 0.5831–0.6247 m

Solvent comp., mole %	k, mole^{-1} min.$^{-1}$
100% KNO_3– 0% $NaNO_3$	0.0105 ± 0.001
75% KNO_3– 25% $NaNO_3$	.0162
50% KNO_3– 50% $NaNO_3$	.0220 ± .001
25% KNO_3– 75% $NaNO_3$	.0260 ± .001
0% KNO_3–100% $NaNO_3$	.0360 ± .004

lithium ion resulted in the production of bromine and lithium oxide. Presumably, lithium reacts with the bromate ion to form a complex $Li_2BrO_3^+$ which then reacts with bromide and decomposes in a manner analogous to that reported in a previous study.[3]

Acknowledgment.—We are indebted to Dr. Walter Lawrence for demonstrating the feasibility of this study and for the initial observations on the reaction.

(3) F. R. Duke and W. W. Lawrence, *J. Am. Chem. Soc.*, **83**, 1271 (1961).

SOME EFFECTS OF IONIZING RADIATION ON FLUOROCARBON LIQUIDS[1]

BY RICHARD F. HEINE

Chemical Division, Minnesota Mining and Manufacturing Company, St. Paul, Minn.

Received March 14, 1962

The effects of γ-radiation on three perfluorinated liquids, C_8F_{18}, c-$C_8F_{16}O$, and $(C_4F_9)_3N$ were studied. Radiation-induced changes in physical properties and in structure were determined. The results show the stability of the fluorocarbons toward radiation to be greater than that of the analogous hydrocarbons.

Fluorocarbons are known to have extraordinary chemical and thermal stability. The very vigorous thermal and chemical attack which these materials can withstand has caused this class of compounds to be called "inert liquids."[2] Early irradiations of fluorocarbon polymers, however, suggest that they might be more susceptible to radiation than their hydrocarbon counterparts.[3] More recent publications have shown that, with pure fluorocarbons in the absence of air, this may not be true.[4,5] The findings of our work tend to substantiate these latter results.

The perfluoroöctane used was believed to be mostly the normal isomer. The cyclic ether was primarily a mixture of perfluoro-(2-butyltetrahydrofuran) and perfluoro-(2-propyltetrahydropyran). A summary of the effect of γ-radiation on these materials plus perfluorotributylamine is shown in Table I.

Prior to irradiation, the fluorocarbons showed neither unsaturation nor hydrolyzable fluoride. As is shown in Table I, the amine was the most affected as determined by these two tests. The greater amounts of unsaturation and hydrolyzable fluoride in the irradiated amine and ether as compared to C_8F_{18} probably arise from the influence of the nitrogen and oxygen atoms, respectively. Infrared analysis showed acyl fluoride in the ether radiation products and imine type products in irradiated $(C_4F_9)_3N$. Olefin absorption was found in the infrared spectra of all three liquids. The permanganate analysis is an approximate measure of all types of carbon–carbon and carbon–nitrogen unsaturation.

Changes in viscosity reflect the increased average molecular weight of the total irradiated sample.

TABLE I

COMPARISON OF γ-RADIATION EFFECTS ON THREE LIQUID PERFLUOROCARBONS

Dose is 5×10^8 rads

		C_8F_{18}	c-$C_8F_{16}O$	$(C_4F_9)_3N$
1.	Hydrolyzable fluoride, mg./g.	0.97	2.62	4.2
2.	Unsaturation (C_8F_{18} = 1)[a]	1	2.5	250
3.	Viscosity (25°)			
	starting materials	0.731	0.79	3.14
	after 5×10^8 rads	2.133	2.11	4.21
4.	Rate constant for disappearance of starting material	1.9×10^{-3} mr.$^{-1}$	2.6×10^{-3}	4.3×10^{-3}
5.	Starting material remaining	37 wt. %[b]	22[b]	1[
6.	Wt. % converted to gas	1.8[b]	2.3[b]	
7.	G_{gas}	0.5 ± 0.15	1.0 ± 0.15	
8.	Wt. % products having b.p. higher than st. mat.	55 wt. %[b]	57[b]	

[a] 1×10^8 rads. C_8F_{18} consumed 2.8 meq. of 0.01 *M* $KMnO_4$/ml. of irradiated liquid. [b] These do not total to 100% since some radiation products were liquids with about the same or lower b.p. than the starting material.

Perfluorotributylamine, though exhibiting greater change because of the radiation than the others, showed a smaller viscosity increase than C_8F_{18} and c-$C_8F_{16}O$. This is because a large percentage of $(C_4F_9)_3N$ was broken down into low boiling liquids, whereas for C_8F_{18} and c-$C_8F_{16}O$ more higher boiling products were formed.

The first-order rate equation was found to describe quite accurately the disappearance of C_8F_{18} and c-$C_8F_{16}O$. First-order rate constants were calculated and are shown in Table I. For a γ-source whose output would be constant over the period of irradiation, megarad^{-1} would be equivalent to time^{-1}.

From these results, it appears that the fluorocarbon which contains only carbon and fluorine is the most stable toward radiation.

Gaseous products found included CF_4, C_2F_6, C_3F_8, C_4F_{10}, CO_2, and traces of several unknowns. Perfluoromethane predominated, though the ether gave a much greater percentage of CO_2 than did the other samples.

(1) Presented in part at the 138th National Meeting of the American Chemical Society, New York, N. Y., September, 1960.

(2) R. R. Burford, *et al.*, paper presented before the 136th National Meeting of the American Chemical Society, Atlantic City, New Jersey, September, 1959.

(3) (a) C. G. Collins and V. P. Calkins, "Radiation Damage to Elastomers, Plastics and Organic Liquids," USAF Contract AF-33 (038)-21102, September, 1959; (b) O. Sisman and C. D. Bopp, "Physical Properties of Irradiated Plastics," USAEC, ORNL-928 June, 1951.

(4) (a) J. H. Simons and E. A. Taylor, *J. Phys. Chem.*, **63**, 636 (1959); (b) R. E. Florin, L. A. Wall, and D. W. Brown, *J. Res. Natl. Bur. Std.*, **64A**, 269 (1960).

(5) L. A. Wall and R. E. Florin, *J. Appl. Pol. Sci.*, **2**, 251 (1959).

The major products from the radiation experiments were higher boiling than the starting materials. These products ranged all the way from liquids boiling just above starting material up to what could best be described as polymer. Pot residues from the distillation of irradiated C_8F_{18} and c-$C_8F_{16}O$ set to hard glasses on cooling. As an example, after 5×10^8 rads, C_8F_{18} was 55% converted to products having a boiling point higher than C_8F_{18}. Half of this 55% had an average molecular weight over 2000. The remainder had molecular weights of from 438 to 2000. No predominance of any "*n*-mer" could be found either by g.l.c. or distillation analyses. If the C–F bonds were predominantly broken and the fluorocarbon radicals combined, one would expect a detectable amount of $C_{16}F_{34}$, $C_{24}F_{50}$, etc., from C_8F_{16}. Since this was not the case, C–C bond rupture followed by random recombination of the radicals may represent a major share of the irradiation-caused reactions. The reactions causing the formation of higher boiling products may be similar to that which crosslinks irradiated poly TFE.[5]

The products smaller than starting material were about equally distributed among 5 to 7 carbon fragments for C_8F_{18} and c-$C_8F_{16}O$, *i.e.*, 1–2% of each based on the total weight. For $(C_4F_9)_3N$, however, two products accounted for most of the degradation fragments: $CF_3N(C_4F_9)_2$ and $C_3F_7{=}NC_4F_9$. The relatively large amount of these accounts for the smaller viscosity increase observed in irradiated $(C_4F_9)_3N$.

A comparison of γ-radiation on liquids exposed in air and to an inert gas, or vacuum, was made. These results are shown in Table II. A comparison of gamma and electron irradiation for c-$C_8F_{16}O$ also is included.

TABLE II

COMPARISON OF C_8F_{18} AND c-$C_8F_{16}O$ IRRADIATED IN THE PRESENCE OF AIR AND UNDER VACUUM

1×10^8 rads

	C_8F_{18}		c-$C_8F_{16}O$		
	Air	Vac.	Air	Vac.	Air[a]
Viscosity (initial)	0.73	0.73	0.79	0.79	0.79
after 1×10^8 rads	0.81	0.866	0.87	0.943	0.87
Hydrolyzable fluoride, mg./g.	0.6	15	0.7	0.65	0.74

[a] Electron irradiated sample.

The net effect of the presence of air seems to be as a free radical inhibitor. The lower viscosity of the samples irradiated under air shows that less high molecular weight material was produced than in absence of air. Also, no difference exists between the effects obtained from γ- and electron irradiation.

When the results are compared with similar results in the hydrocarbon series, the fluorocarbons appear to have somewhat greater resistance to radiation. At 0.5×10^8 rads, hexane (C_6H_{14}) has $G_{gas} = 3.8$ and $-G_m = 9.9$. For C_8F_{18} at the same dose, $G_{gas} = 0.5$ and $-G_m = 4.8$. Thus the fluorocarbon seems to be the more radiation resistant. The comparison of G_{gas} values is not entirely valid, however, since G_{gas} values reported for the hydrocarbons included a part due to hydrogen formation G_{H_2}, whereas G_{gas} C_8F_{18} has no part due to F_2 formation. If we compare C_8H_{18}, we find that G_{gas} $C_8H_{18} = 0.31$, which is the part due to carbon-containing gases.[6]

This result can be compared with our value of G_{gas} $C_8F_{18} = 0.5$. The foregoing is not meant to imply that fluorine is not formed, but only that because of its reactivity, it was not found as such. Also, the fate of any fluorine formed during the radiation cannot be determined with certainty.

The conclusion is that gaseous products formed as a result of C–C bond breaking are about the same from both fluorocarbons and hydrocarbons. The point of difference then between fluorocarbons and the analogous hydrocarbons is in $-G_m$ and, therefore, a greater percentage of hydrocarbon than fluorocarbon must be converted to higher molecular weight or to non-gaseous lower molecular weight products.

Experimental

Materials.—The three liquids all are products of the electrochemical fluorination cell. The crude materials were stabilized with aqueous and then fused 85% potassium hydroxide. Both C_8F_{18} and c-$C_8F_{16}O$ were greater than 98% as described. The $(C_4F_9)_3N$ was 95% one component. Usually no special precautions to ensure dryness were used. Water is soluble in the fluorocarbons to less than 25 p.p.m. On one occasion, the liquid was passed through P_2O_5 into a sealed can which had been dried at 100°. The results of this experiment were no different from others in which the liquid was not specially dried. Normally, the cans were rinsed with aqueous hydrofluoric acid, then dried for a day or two at 100°.

γ-Irradiation.—Aluminum bottles of 250 and 500-ml. capacity were used. They were about half filled with liquid, the air space flushed out with nitrogen or helium, and the caps were tightened.

When gas samples were desired, a $^3/_{16}$-in. i.d. aluminum tube was welded into a hole in the cap and the cap was welded to the bottle. After filling the cans about one-third full, the contents were frozen in liquid air and the can was evacuated. The tube was crimped shut and the end was welded shut with the can under vacuum.

Irradiation was carried out in a spent fuel element facility. The water of the facility kept the samples at 25°. The average energy of the radiations was 0.69 mev.

Electron Irradiation.—Samples for electron irradiation were placed in a shallow aluminum cup, fitted with a gas-tight cover with a 0.0035-in. thick aluminum window. These samples were irradiated in the presence of air; that is, the container was not swept out with an inert gas after filling. The irradiation, however, was done with the samples cooled in Dry Ice and the radiation was given in passes under the window of about 10-sec. duration each.

The source of the electrons was a G. E. 1 mev. transformer type beam generator operated at 0.9 ma. and 1000 kvp.

Analysis.—All gas–liquid chromatographic analyses were done with a 12-ft. "Kel-F" 200 wax on firebrick column at 130°. Chromatographic analysis of gases was done on a 6-ft. silica gel column at 100°.

Liquid samples were taken directly from the irradiated sample containers. Gas samples were taken by venting the cans fitted with tubes in the caps into an evacuated system and measuring the pressure. This was done by fastening a tight "T" tube connected to the evacuated system down over the aluminum nozzle and drilling a hole in the tube through a rubber stopper in the stem of the T.

Since the higher-boiling "polymer" did not chromatograph well, the liquids usually were distilled and the fraction was taken from room temperature up to about 10–15° over the boiling point of the starting materials. Chromatographic analysis of this distillate, plus knowledge of the distillate as a per cent of the total sample, gave accurate analysis for liquid products boiling at or below the boiling point of the starting materials. Attempts to resolve individual

(6) E. M. Kinderman, WADC Tech. Rept. 57-465, Stanford Research Institute, July, 1957.

components of the higher boiling products at higher column temperatures were not successful.

Hydrolyzable fluoride was determined by refluxing equal weights of fluorocarbon and 1% sodium bicarbonate and titrating the aqueous layer for fluoride ion.

The permanganate test for unsaturation was done with a freshly prepared 0.01 *M* $KMnO_4$–acetone solution. Decreasing quantities of this reagent were mixed with 1 ml. of sample in acetone until a quantity was found which retained its characteristic permanganate color after 1 min. of shaking.

Acknowledgment.—The help of W. E. Rowe and R. J. Kunz is greatly appreciated in carrying out the γ-radiation experiments. Jun Tomita was very helpful with the electron irradiation.

PHOTOCHEMICAL INTERCHANGE OF HALOGENS IN AROMATIC COMPOUNDS. II. TEMPERATURE DEPENDENCE OF SOME SUBSTITUENT EFFECTS

BY BARTON MILLIGAN AND RONALD L. BRADOW

Department of Chemistry, The University of Mississippi, University, Mississippi

Received March 14, 1962

The changes with temperature of several substituent effects in photochemical aromatic halogen interchange have been determined. The enthalpy and entropy differences obtained from these data suggest the intervention of π complex formation prior to the substitution step.

Introduction

In a previous report[1] we described some general features of photochemical interchange of halogens in aromatic compounds, reactions represented by

$$ArX + X' \longrightarrow ArX' + X$$

and reported some room temperature substituent effects in a number of these reactions. The mechanism of displacement was seen to be most probably a direct displacement on carbon by halogen atoms and one in which the bond from carbon to the halogen atom displaced is but little broken in the transition state.

The substituent effects we report are generally small but readily measurable. These effects, determined by competitive experiments, fail to fit conventional linear free energy relationships and do not even form a consistent qualitative pattern. We suggested that the reason for these inconsistencies is the kinetic significance of π complexes as postulated by Miller and Walling[2] for one case. In this paper we wish to report data which lend great weight to this contention. Though often discussed, the formation of π complexes prior to the substitution step has never before received concrete experimental support for any aromatic displacement reaction.

Experimental

The materials and methods employed were those described previously.[1] Briefly, a solution of appropriate halogen in CCl_4 was added to a solution of a substituted and an unsubstituted aryl halide in CCl_4. With two exceptions, aromatic concentrations were 0.10 *M* and halogen concentrations ranged from 0.01 to 0.1 *M*. When *p*-bromoanisole and *m*-fluorobromobenzene were compared to bromobenzene, 0.1: 0.5 and 0.5 : 0.1 molar ratios, respectively, were used. Aliquots of the solutions were placed in a thermostat bath regulated to 0.05° and irradiated by mercury arc lamps provided with filters to remove ultraviolet radiation. The products were analyzed by gas chromatography.

Results

The effects of several substituents on the rates of three halogen interchange reactions, each at three or four temperatures, are given in Table I. When the reagent supplying the displacing halogen was ICl or Br_2, reaction was carried only to low conversion (5% or less), and the reactivity ratio given in Table I is the ratio of substituted to unsubstituted product. When chlorine was the reagent, conversion of the aromatics was approximately 20%, and the usual integrated expression was used.

$$W = \frac{\log (A - x)/A}{\log (B - x)/B}$$

The quantities in this equation were obtained by solution of simultaneous equations employing the ratio of products, from gas chromatography, and the total chlorine used, as determined by iodometric titration after reaction. Such a treatment is valid if chlorine is completely and quantitatively converted to bromine.[1]

We also have measured, at different temperatures, the relative reactivities of iodo- and bromobenzenes toward chlorine from ICl by means of the indirect method described earlier.[1] If iodo- and bromobenzenes were compared directly in a competitive experiment, only one product, chlorobenzene, would be formed. However, in order to minimize the possibility that the bromine displaced might react with iodobenzene to generate new bromobenzene, one would have to carry the reaction to very low conversion of ICl and would thereby be faced with the difficulty of measuring the small difference between two large numbers. Therefore, we tagged first one and then the other of the compounds with a *p*-fluoro substituent and corrected the result for the substituent effect. The results obtained in this study as well as the previously reported value at 27.3° are given in Table II.

Plots of log W *vs.* $1/T$ are linear. The apparent enthalpy and entropy of activation differences

(1) B. Milligan, R. L. Bradow, J. E. Rose, H. E. Hubbert, and A. Roe, *J. Am. Chem. Soc.*, **84**, 158 (1962).

(2) B. Miller and C. Walling, *ibid.*, **79**, 4187 (1957).

TABLE I

SUBSTITUENT EFFECTS ON PHOTOCHEMICAL HALOGEN DISPLACEMENT

Substnt.	Atom leaving (X)	Atom entering (X′)	Reagt.	Reactivity ratio (W)[a] (substd./unsubstd.) Temp., °C. 11.0	15.2	22.5	27.3	37.5
4-F	Br	Cl	Cl_2		1.30	1.28[b]	1.23	
	Br	Cl	ICl	2.50		2.20	2.08	
	I	Br	Br_2	1.04	1.05	1.09	1.11	
	I	Cl	ICl	7.59		4.03	3.10	
3-F	Br	Cl	Cl_2		0.204	0.153[b]		0.120
	I	Br	Br_2	0.248	0.238[c]		0.225	.214
2-F	Br	Cl	Cl_2	.781		.809[d]		.849
4-CH_3O	Br	Cl	Cl_2		34.9[f]		13.7[e]	8.45

[a] See text. [b] 25.8°. [c] 17.5°. [d] 23.0°. [e] 28.0°. [f] 14.0°.

TABLE II

RELATIVE REACTIVITIES OF IODOBENZENE AND BROMOBENZENE TOWARD CHLORINE FROM IODINE CHLORIDE

Temp., °C.	27.3	22.8	11.0
W (Iodo)/(Bromo)	2.26	1.97	1.43

derived from the slopes and intercepts, respectively, of these plots are given in Table III. The limits of error quoted reflect the variations between individual measurements. Immediately apparent from Table III is the fact that the enthalpies and entropies are always of opposite sign and more or

TABLE III

APPARENT DIFFERENTIAL ACTIVATION PARAMETERS IN PHOTOCHEMICAL HALOGEN INTERCHANGE

Substnt.	Atom leaving	Atom entering	Reagt.	$\Delta\Delta H^*$ Unsubstd. − substd. (kcal./mole)	$\Delta\Delta S^*$ Unsubstd. − substd. (e.u./mole)
4-F	Br	Cl	Cl_2	+ 0.61 ± 0.2	− 1.6 ± 2
	Br	Cl	ICl	+ 1.8 ± .3	− 4.8 ± 3
	I	Cl	ICl	+ 9.8 ± .4	−28 ± 5
	I	Br	Br_2	− 0.70 ± .05	+ 2.0 ± 1
3-F	Br	Cl	Cl_2	+ 3.5 ± .1	−15 ± 2
	I	Br	Br_2	+ 0.98 ± .05	− 5.5 ± 1
2-F	Br	Cl	Cl_2	− 0.55 ± .05	+ 1.4 ± 0.5
4-CH_3O	Br	Cl	Cl_2	+10.7 ± .4	−30 ± 3
None[a]	Br/I	Cl	ICl	− 4.7 ± .1	+17 ± 4

[a] From Table II.

less parallel one another in magnitude. A plot of $\Delta\Delta H$ *vs.* $\Delta\Delta S$ gives a reasonable fit to a straight line passing through the origin. From the least squares treatment of all points

$$\Delta\Delta H \text{ (cal.)} = -330\Delta\Delta S + 158$$

The correlation coefficient, r, is 0.98. In view of the great diversity of the reactions on which this plot is based, the correlation is remarkably good and may be fortuitous.

Petersen, Markgraf, and Ross[3] have pointed out that random errors of measurement can lead to a linear plot of ΔH^* *vs.* ΔS^* with slope T if the range of ΔH^* is not large. Their treatment can be applied to our relative rate data with minor modifications. Accordingly, any correlation between $\Delta\Delta H$ and $\Delta\Delta S$ for about half of our data is open to suspicion, but the correlation of the larger values may have some significance. One should note that a plot of our data has negative slope, which might lead to difficulty in application of the isokinetic relationship discussed by Leffler.[4]

(3) R. C. Petersen, J. H. Markgraf, and S. D. Ross, *J. Am. Chem. Soc.* **83**, 3819 (1961).

Discussion

If photochemical halogen interchange were a simple direct displacement

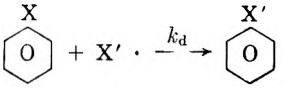

the reactivity ratio obtained from a competitive experiment should be the ratio of the rate constants for the displacement step.

$$W = k/k_0$$

Therefore

$$\ln W = \frac{\Delta H_0^* - \Delta H^*}{RT} - \frac{\Delta S_0^* - \Delta S^*}{R}$$

The results presented in the previous section deal, saving two exceptions, with *meta*- and *para*-substituted benzene derivatives. The exceptions are *o*-fluorobromobenzene and the comparison of iodo- and bromobenzenes. Very little or no differential steric interaction is expected in the latter case, since it could arise only from the larger bulk of the iodine atom over the bromine atom. In the former case the small size of fluorine should lead to a minimal steric effect. Since the absence of steric effects in *meta*- and *para*-substituted benzenes is widely accepted, one can fairly state that for a simple displacement mechanism the entropy term in the equation above should be zero or negligibly small in all cases studied. Therefore, plots of log W *vs.* $1/T$ should be linear and pass through or near the origin. Furthermore, the slope of the line should have the same sign as log W. Examination of Table III reveals that these predictions fail. The photochemical reaction of bromobenzene with chlorine is a chain reaction[2] ($\Phi \approx 50$).[5] Since none of the bromoaromatics considered here is vastly different from bromobenzene in its reactivity toward chlorine, the assumption of chain kinetics in all of these cases is reasonable. On the other hand, the reactions of iodine chloride with bromides and iodides and of bromine with

(4) J. E. Leffler, *J. Org. Chem.*, **20**, 1202 (1955).

(5) J. E. Rose, unpublished results, University of Mississppi.

iodides are non-chain processes ($\Phi < 10^{-2}$).[5,6] One should note that examples of both chain and non-chain reactions exhibit the inverse temperature dependence.

Another argument against such a simple mechanism lies in the slope of the log W *vs.* $1/T$ plot for the competition of *p*-bromoanisole and bromobenzene. According to the principles of chain reaction kinetics,[7] all propagation steps must have activation energies of no more than a few kcal. Therefore, for the reaction of bromobenzene to have nearly 11 kcal. *more* activation energy than that of *p*-bromoanisole, as indicated by our data, is inconsistent with a simple chain mechanism. An alternate explanation must be sought.

A plausible explanation of our data is provided by the intervention of π complexes prior to the substitution step. Although a complete kinetic analysis is complicated, one can show that under certain limiting conditions, the measured reactivity ratio includes the ratio of the equilibrium constants for π complex formation, as well as the ratio of rate constants for substitution. Whether the proper equilibrium constant is that for the aromatic–halogen atom complex[8]

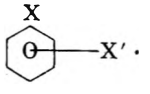

or the aromatic–halogen molecule complex

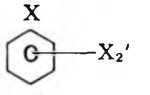

depends on a number of factors which cannot be assessed at present. In any event, the apparent differential enthalpy of activation obtained from the slope of a log W *vs.* $1/T$ plot is determined not only by the effect of the substituent on the enthalpy of activation but also on the enthalpy of π complex formation. These effects need not (but may) be in the same direction.

The inverse temperature effects we have observed can be accounted for by a π complex mechanism by postulating that the effect of the substituent on complex formation outweighs its activating or deactivating influence on the substitution process. Furthermore, the abnormally large (nearly 11 kcal.) apparent enthalpy difference measured for the comparison of *p*-bromoanisole and bromobenzene can be reconciled with chain kinetics by arguing that the *p*-methoxy substituent not only lowers the enthalpy of activation for substitution but also causes complex formation to become exothermic. Anisole is known to be a highly effective donor.[9]

If the measured reactivity ratio contains equilibrium constants for π complex formation, the intercept of the log W *vs.* $1/T$ plot is composed of the substituent effect on both entropy of activation and complex formation. In the cases of *m*- and *p*-substituents, the former is expected to be small, but because of symmetry differences, the latter is expected to have a substantial value.

The flash photolysis studies of Strong, Rand, and Britt[8c] of aromatic iodine atom complexes reveal that they disappear by second-order kinetics with rate constants on the order of 10^9 l. mole^{-1} sec.$^{-1}$. It is worth noting that if similar considerations applied in the cases we have studied, half-order kinetics should be observed. However, we find that product ratios are proportional to the first power of reactant ratios in both chain and non-chain reactions, effectively ruling out control of the steady state concentration of an aromatic–halogen atom complex by bimolecular recombination reactions.

Acknowledgment.—This work was supported in part by a grant from the Petroleum Research Fund administered by the American Chemical Society, and grateful acknowledgment to donors of the fund is hereby given. Earlier parts of the work were supported by a grant from Research Corporation.

(6) That this should be so is reasonable because in these cases, propagation steps are endothermic by 8 kcal. or more.

(7) C. Walling, "Free Radicals in Solution," John Wiley and Sons, Inc., New York, N. Y., 1957, p. 240.

(8) The existence of such complexes has been amply demonstrated by a number of workers: (a) G. A. Russell, *Tetrahedron*, **8**, 101 (1960); (b) C. Walling and M. F. Mayahi, *J. Am. Chem. Soc.*, **81**, 1485 (1959); and (c) R. L. Strong, S. J. Rand, and J. A. Britt, *ibid.*, **82**, 5053 (1960).

(9) L. J. Andrews and R. M. Keefer, *ibid.*, **75**, 3776 (1953); P. A. D. de Maine, *J. Chem. Phys.*, **26**, 1189 (1957).

THE NATURE OF SEMICONDUCTION IN SOME ACENE QUINONE RADICAL POLYMERS

BY HERBERT A. POHL AND DAVID A. OPP

School of Engineering, Princeton University, Princeton, N. J.

Received March 15, 1962

Semiconduction ranges from 10^{-5} to 10^{-12} mho/cm. in 51 examples of organic polymers prepared by condensing aromatic hydrocarbon derivatives with acids. Conduction is electronic, not ionic or electrolytic. It depends strongly on the chemical nature of the monomeric units, mildly on the field strength. The concentration of unpaired spins (*ca.* 10^{19} cm.$^{-3}$) is roughly 100-fold larger than the apparent carrier concentration. Certain of these substances are highly piezo-conductive, reflecting sensitivity of orbital overlap to intermolecular distance in these eka-conjugated structures.

This work is a continuation of studies on the polymers obtained earlier from the reaction of various substituted aromatic hydrocarbons with aromatic acid anhydrides as reported by Pohl, Bornmann, and Itoh.[1] The present studies were made to assist in the interpretation of conduction events in those polymers.

The polymers (designated as PAQR polymers for brevity) as described earlier, were prepared by the reaction of the chosen substituted hydrocarbon and acid anhydride pair in the presence of $ZnCl_2$ as a catalyst. They were purified by exhaustive solvent extractions with a series of solvents, followed by prolonged drying. Measurements on molded disks were made to determine the resistivity as a function of temperature, pressure, and field strength, the Seebeck coefficient (thermoelectric power), and the electron spin concentration.

The conductivity in these polymers is electronic and not ionic in character, as evidenced by (a) constancy of resistivity with long time current passage, (b) absence of polarization effects upon passage of many times the amount of current required to deposit out electrolytically all atoms present, and (c) the presence of an observable Hall effect.

Experimental

Determinations of the resistivity in this work were made with somewhat more care than those described earlier.[1] The molded sample was measured between circular electrodes 0.95 cm. in diameter, faced with platinum. Several materials were used for the surrounding insulator ring, including nylon, Nylatron, hard rubber, Teflon, and filled phenolics. In each case the resistance value of the cell was checked using several layers of mica in the cell in place of the sample to ascertain that the cell insulator and supports had a resistivity at least 100 times greater than the sample measured. The resistance was obtained using d.c. methods with a field strength of 150 v./cm. or less. Thickness measurements were made using a dial micrometer. The resistivity measurements were made at a reference pressure of 1800 kg./cm.^{2}. $\pm$ 3% except where noted.

High pressure measurements of the resistivity and its temperature coefficient were made using Bridgeman anvils made of stainless steel.

Electron spin resonance determinations were made at 25°, at 3000 gauss, and at about 9350 Mc., using direct comparison with prepared standards of diphenylpicryl hydrazyl. The polymer samples were cylindrical pellets of $^1/_4$-in. diam. and $^1/_8$ in. thick, molded at 1840 kg./cm.^{2} at 125°.

Measurements of the Seebeck coefficient (thermoelectric power) were made on pressed pellets.

Determinations by radio-activation analysis showed the purified polymers to contain only several p.p.m. of zinc.

Results

Despite the results of others who had reported little or no observable pressure effects on the resistivity of organic materials at pressures above 80 kg./cm.^{2},[2-5] it was evident from our measurements that the PAQR polymers exhibit marked changes in resistivity with pressure. Typical results obtained in the moderate pressure range of 200 to 2800 kg./cm.^{2} are shown in Fig. 1. Results on the same material for the higher range of 2000 to 68,000 kg./cm.^{2} (*i.e.*, to about 60,000 atm.) are shown in Fig. 2. The resistivities given are uncorrected for the unknown change in sample thickness with pressure (compressibility). However, the resistance changes, at least in the high pressure range, are large and quite reversible. The reversible drop in resistivity of 120-fold during the pressure cycle of 2000 to 68,000 to 2000 kg./cm.^{2} greatly exceeds that which might be expected from gross dimensional changes (about a factor of 1.2 is expected). One is forced to conclude that the pressure–resistance effect involves more than mere foreshortening of the sample dimension.

The effect of pressure on the thermal activation energy is shown in Fig. 3.

Using the reference pressure of 1840 kg./cm.^{2} $\pm$ 3%, the room temperature resistance values were obtained and are shown in Table I for various PAQR polymers. Room temperature was 23 $\pm$ 2° and values shown are the result of triplicate measurements.

Temperature coefficients of resistivity were obtained by first molding the polymers at 125° and 1850–2000 kg./cm.^{2} for 1 hr. in the resistivity cell. Table I shows the values of the "activation energies" for the various polymers examined. The activation energies were calculated from the observed straight-line Arrhenius plots and calculated from the relation

$$\sigma/\sigma_0 = \exp(-E_g/2kT)$$

where σ is the specific conductivity.

Note should be taken that these are given in terms of the energy interval, E_g, where

(1) H. A. Pohl, J. A. Bornmann, and W. Itoh, "Semiconducting Polymers," Princeton University Plastics Lab. Tech. Rpt. 60C, January, 1961; "Papers Presented at the St. Louis Meeting," March, 1961 Am. Chem. Soc., Div. Polymer Chemistry, Vol. 1, No. 2, p. 211.

(2) H. A. Pohl, A. Rembaum, and A. W. Henry, *J. Am. Chem., Soc.*, **84**, 2699 (1962).

(3) D. D. Eley, G. D. Parfitt, G. D. Perry, and D. H. Taysum, *Trans. Faraday Soc.*, **49**, 79 (1953).

(4) H. Akamatsu and H. Inokuchi, *J. Chem. Phys.*, **18**, 810 (1950).

(5) H. Inokuchi, *Bull. Chem. Soc. Japan*, **28**, 570 (1955).

TABLE I

THE RESISTIVITIES AND ACTIVATION ENERGIES FOR SOME POLYACENE QUINONE RADICAL POLYMERS

Polymer precursor components Hydrocarbon derivative	Acidic derivative	Sample no.	Specific resistivity, ohm-cm.	Activation energy, as E_g, e.v.
Resistivity at 25° and 1840 kg./cm.²; polymerization temp., 256°.				
1,5-Dihydroxyanthraquinone	N.A.[a]	135	3.6×10^5	0.63
1,8-Dihydroxyanthraquinone	N.A.	134	2.8×10^5	.52
1,8-Dihydroxyanthraquinone	P.M.A.[a]	A	9.2×10^7	.67
1,4-Dihydroxyanthraquinone	N.A.	136	1.8×10^7	.50
1,4-Dihydroxyanthraquinone	P.M.A.	D	7.0×10^9	..
1,2-Dihydroxyanthraquinone	N.A.	137	2.1×10^7	.68
1-Hydroxyanthraquinone	N.A.	138	1.34×10^8	.62
1-Hydroxyanthraquinone	P.A.[a]	124	6.0×10^6	.58
1,4,9,10-Tetrahydroxyanthracene	N.A.	133	2.4×10^6	.63
1,4,9,10-Tetrahydroxyanthracene	P.A.	123	1.39×10^7	..
1,4-Dihydroxynaphthalene	N.A.	139	10^{12}	1.11
1,4-Dihydroxynaphthalene	P.M.A.	F	5.6×10^{11}	1.00
1,4-Dihydroxynaphthalene	P.A.	H	1.01×10^8	0.56
2,7-Dihydroxynaphthalene	P.M.A.	I	3.3×10^{10}	1.83
2,3-Dihydroxynaphthalene	N.A.	4	9.4×10^7	0.58
6-Bromo-2-naphthol	N.A.	130	9.6×10^6	.58
6-Bromo-2-naphthol	P.M.A.	108	5.9×10^6	.66
6-Bromo-2-naphthol	P.A.	112	7.2×10^6	.58
1-Bromo-2-naphthol	N.A.	129	6.8×10^6	.53
1-Bromo-2-naphthol	P.M.A.	105	1.13×10^7	.68
1-Bromo-2-naphthol	P.A.	110	4.6×10^6	.62
7-Acenaphthol	N.A.	125	1.37×10^8	.60
7-Acenaphtho	P.M.A.	106	4.9×10^7	.71
7-Acenaphthol	P.A.	119	4.2×10^7	.58
9-Bromophenanthrene	N.A.	131	5.6×10^6	.34
Carbazole	N.A.	126	2.1×10^8	.59
Carbazole	P.A.	120	1.9×10^8	.54
Phenolphthalein	N.A.	132	6.4×10^6	.77
Phenolphthalein	P.M.A.	J	5.3×10^9	.65
Phenolphthalein	P.A.	K	6.0×10^8	.60
p-Naphtholbenzein	N.A.	127	1.0×10^{11}	.68
p-Naphtholbenzein	P.A.	121	1.3×10^8	(.13)
2-Bromo-4-phenylphenol	N.A.	128	1.0×10^{11}	1.20
2-Bromo-4-phenylphenol	P.A.	116	2.3×10^8	.62
Dibenzanthrone(violanthrone)	P.M.A.	5	1.9×10^8	0.43
p,p'-Diphenol	P.A.	114	1.0×10^{12}	..
1,4-Diphenylpiperazein	P.A.	118	2.0×10^{12}	..
1,8-Dihydroxyanthraquinone	T.D.A.	103	2.9×10^5	0.52
1,5-Dihydroxyanthraquinone	N.A.	115	5.2×10^6	.703
1,5-Dihydroxyanthraquinone	P.M.A.	101	5.8×10^8	.845
1,8-Dihydroxyanthraquinone	N.A.	109	2.2×10^7	.766
1,8-Dihydroxyanthraquinone	P.M.A.	B	2.3×10^8	.563
1,4-Dihydroxyanthraquinone	P.M.A.	E	5.5×10^8	.570
1,2-Dihydroxyanthraquinone	N.A.	113	7.9×10^7	.690
1-Hydroxyanthraquinone	N.A.	107	5.0×10^5	.503
1-Hydroxyanthraquinone	P.M.A.	104	7.0×10^5	..
1,4,9,10-Tetrahydroxyanthracene	N.A.	117	8.7×10^5	.516
1,4-Bisanthraquinonylaminoanthraquinone	N.A.	1	2.7×10^6	.472
1,4-Bisanthraquinonylaminoanthraquinone	P.M.A.	2	1.5×10^7	.515
1,4-Dihydroxynaphthalene	P.M.A.	G	1.4×10^9	..
1-Bromo-2-naphthol	N.A.	111	2.9×10^6	.571

[a] N.A.: 1,8-naphthalic anhydride; P.A.: phthalic anhydride; P.M.A.: pyromellitic dianhydride; T.D.A.: tetraphenyl-1,2-dihydrophthalic anhydride.

$$E_g = 2E_a$$

where E_a is the usual Arrhenius activation energy of a process obeying Boltzmann statistics.

The variation of the thermoelectric power, Q, with temperature was determined for six semiconducting polymers. The potentiometer and its balancing circuit was such that the cell had to contain samples showing a resistivity of about 10^7 ohms/cm. or less. The plots of temperature gradient *vs.* resultant voltage gradient were quite linear. This permitted evaluating Q at various mean tem-

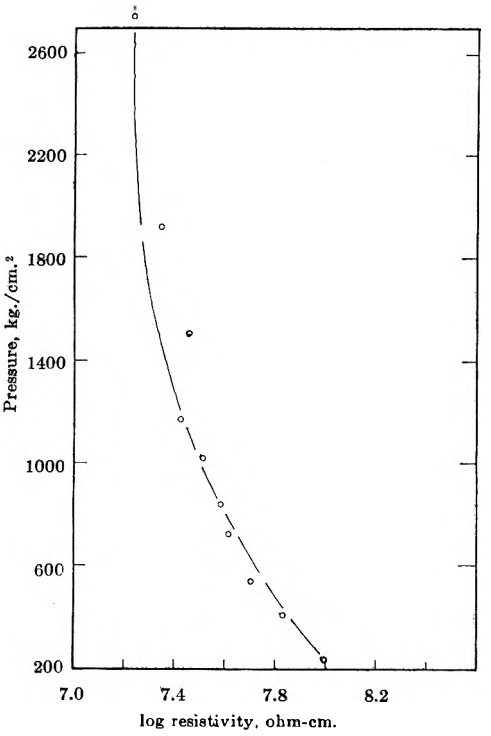

Fig. 1.—The piezo-resistive response at low pressures and at 25° of a PAQR polymer made with 1,8-dihydroxyanthraquinone and naphthalic anhydride, polymer no. 109.

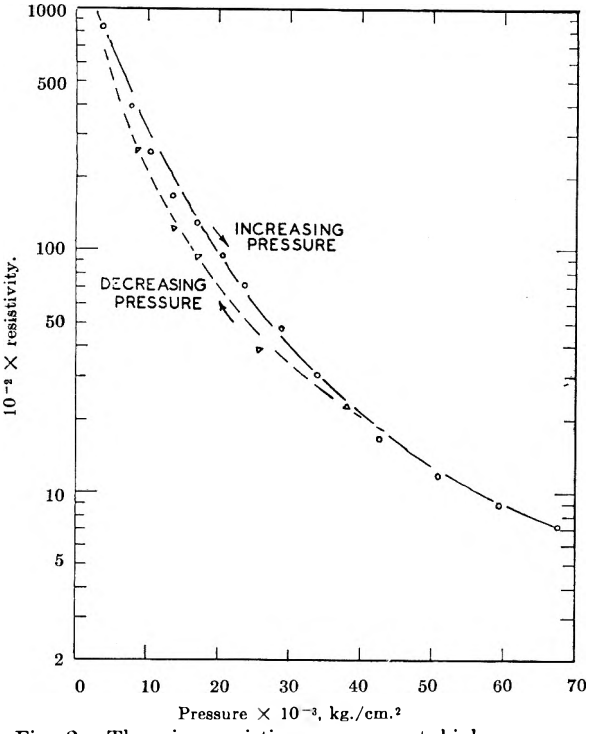

Fig. 2.—The piezo-resistive response at high pressures and at 25° of a PAQR polymer, no. 109. The apparent hysteresis is that later shown inherent in the pressuring apparatus. The curve obtained on increasing pressure is that closest to the actual behavior of the material as pressure changes.

peratures, as shown in Fig. 4. The changes of Q with temperature, as may be noted, are not large; Q is positive over the range studied, indicating a

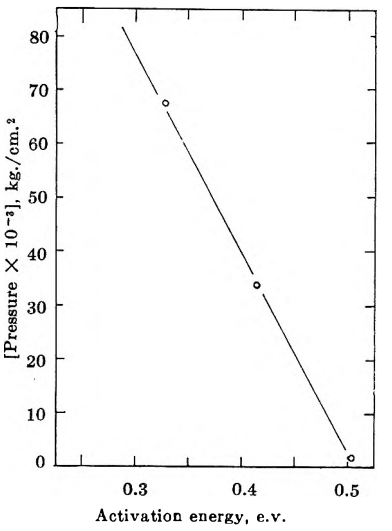

Fig. 3.—Pressure effects on the activation energy of a PAQR polymer no. 107, made from 1-hydroxyanthraquinone and naphthalic anhydride.

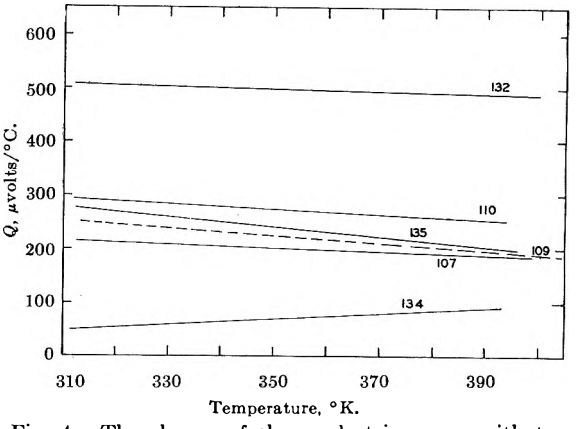

Fig. 4.—The change of thermoelectric power with temperature for several PAQR polymers at a pressure of about 100 atm. To identify, see Table I.

dominance of hole-type current mechanisms over free electron-type current mechanisms.

The concentrations of unpaired electrons as measured by e.s.r. are quite large, ranging from 2.7 to 7 × 10^{18} spins/g. As will be noted, they outnumber the indicated current carrier concentrations by about 100 to 1 and therefore are not to be identified in a 1:1 manner with carriers. The integral curve half widths at 3000 gauss ranged from 6 to 7.5 gauss.

An examination of the ohmic behavior of these materials was made because it was thought that the long length of the polarizable highly-conjugated polymer molecules might either permit some carriers to be formed or made more easily mobile by electric field energy. Eley[3] observed non-ohmic behavior in one instance. Wilk[6] also observed the non-ohmic character of conduction in several aromatic hydrocarbons. The polymer sample served as one arm of a Wheatstone bridge made of resistance wire components. The results are shown in Fig. 5, on sample no. 39, a PAQR polymer prepared from one mole of pyrene with one mole of pyromellitic dianhydride with $ZnCl_2$ catalyst at 283°.

(6) M. Wilk, *Z. Elektrochem.*, **64**, 930 (1960).

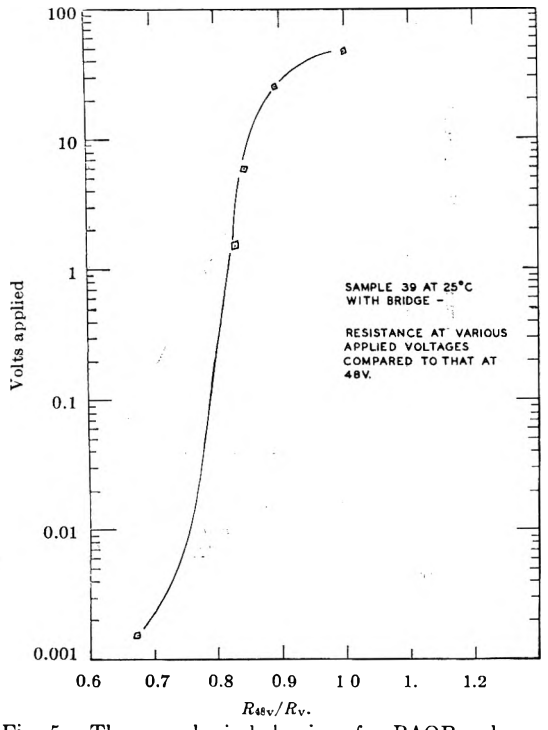

Fig. 5.—The non-ohmic behavior of a PAQR polymer is shown here by comparing the resistivities at various applied field strengths with that at a reference field strength.

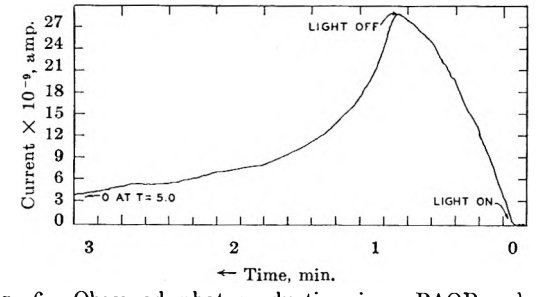

Fig. 6.—Observed photoconduction in a PAQR polymer (no. 109).

The resistivity of this material varies in a manner fairly well representable by the equation

$$\rho = \rho_0 \mathcal{E}^{-\alpha}$$

where $\alpha \cong 0.02$, ρ_0 is the specific resistivity at zero field strength, and $\mathcal{E}$ is the field strength in volts/cm. over the range 0.0015 to 48 applied volts.

This sample also showed p-type character in that a Hall coefficient of 288 cm.^{3}/coul. was observed[7] in a field of 17 kgauss.

As expected, the PAQR polymers show photoconduction. For example, sample No. 109, compressed at 1840 kg./cm.^{2} and irradiated on one face of the pellet through a conductive tin oxide-coated glass, produced a current of 1 ma., shunted. The cell area was approximately 0.5 cm.^{2}.

The sample, with a 1.5-v. cell in series, increased its conductivity by 14% upon being illuminated. This was shown to be much larger than the 1° observed temperature rise would produce in the sample. The results for the sample with 22.5 v. applied are shown in Fig. 6.

(7) E. H. Engelhardt and H. A. Pohl, "Synthesis and Characterization of Some Highly Conjugated Semiconducting Polymers," Princeton Univ. Plastics Lab. Tech. Rpt. 64A, January, 1962.

Discussion

In view of the demonstrated electronic nature (as opposed to ionic or electrolytic) of conduction in the PAQR polymers, provisional calculations were made in terms of the conventional band theoretical model for "intrinsic" and "impurity" crystalline semiconductors. There is some considerable doubt that such a theoretical model should apply in this instance. The band theory model equations used here were those conventionally employed,[8,9] making the common simplifying assumptions that (a) the effective masses of the carriers were identical with the real mass of the electron, and (b) that the mobility varied as for lattice scattering, proportional to $T^{-3/2}$. Typical results for these calculations are shown in Table II.

TABLE II

RESULTS OF SIMPLE BAND MODEL CALCULATIONS (300°K.)

Sample no.	Activation energy, E_g, e.v.	Mobility ratio, C	Intrinsic carrier concn., n'_i (cm.$^{-3}$)	Electron mobility, μ_e, cm.^{2}/v. sec.
107	0.503	0.643	1.87×10^{17}	2.61×10^{-5}
109	.766	.730	1.47×10^{16}	8.15×10^{-6}
110	.615	.620	6.39×10^{16}	8.12×10^{-6}
132	.445	.294	3.32×10^{17}	6.70×10^{-7}
134	.519	.980	1.61×10^{17}	6.70×10^{-5}
135	.620	.684	3.95×10^{17}	1.77×10^{-5}

Sample no.	Hole mobility, μ, cm.^{2}/v. sec.	Impurity hole concn., h' (cm.$^{-3}$)	Impurity concn. for $E_a = E_g N_a$ (cm.$^{-3}$)
107	4.06×10^{-5}	1.43×10^{19}	1.25×10^{24}
109	1.12×10^{-5}	1.36×10^{19}	1.87×10^{24}
110	1.31×10^{-5}	7.20×10^{18}	3.73×10^{23}
132	2.28×10^{-6}	5.60×10^{17}	1.29×10^{21}
134	6.86×10^{-6}	1.04×10^{23}	7.56×10^{25}
135	2.59×10^{-5}	6.38×10^{13}	2.96×10^{23}

It is clear that the "intrinsic" model can be made to fit the observed data, but that the "impurity" model cannot, as it gives unreasonable values for the impurity concentration (*i.e.*, 10^{24} impurity atoms/cc.).

As discussed elsewhere at greater length, there is considerable reservation to be made in applying conventional band theoretical considerations to materials of low mobility. In materials of low mobility it is probable that carrier motion proceeds by hopping processes and is not describable by the grand scale drifting of wave packets in terms of a Bloch model. This conclusion can be reached by either of several arguments.

The electron mean-free-path, l_L, in an atomic lattice for electrons scattered only by phonons, using the Lorentz-type modification of the Boltzmann thermal distribution of electron momenta as is customary in calculating the electron velocity distribution,[10] gives

(8) J. S. Blakemore, *Elec. Commun.*, **29**, 131 (1952).

(9) V. A. Johnson and K. Lark-Horovitz, *Phys. Rev.*, **92**, 226 (1953).

(10) A. H. Wilson, "Theory of Metals," Univ. Press, Cambridge, 1953, p. 265

$$l_L = 3(2\pi m^* kT)^{1/2} \mu_L /4|e| \cong \sqrt{\frac{m^*}{m}} \times 10^{-8} \mu_L; \text{ [cm.]}$$

where μ_L = mobility in cm.^{2}/v. sec.; m^* and m are the effective (crystal momentum) mass and real mass of the electron. It can be seen from this relation that the mean free path in high mobility materials (μ_L over 1000 cm.^{2}/v. sec.) is rather longer than the dimension of an electron wave length, while for mobilities of 5 or less the indicated electron mean free path is as small as or smaller than a lattice spacing. The scattering time is then no longer small with respect to the time of motion between collisions, and the precise classical notion of a mean velocity of a distribution of velocities no longer exists. One concludes that the application of such theory with its implied distribution of velocities of the free charges can only be made safely to materials having high carrier mobilities.

The same conclusion can be reached by another line of argument. The conductivity, σ, varies as

$$\sigma = b \cdot Le$$

where b is the specific birth rate of carriers, L is the mean path length of the carrier in unit field strength, and e is the electronic charge. The number of carriers born in one second per unit volume can be written as

$$b = NA \exp(E_a/kT)$$

where N is the number of all molecules per unit volume, A is the "frequency factor," E_a is the activation energy for the process, k is Boltzmann's constant, and T is the absolute temperature. A generally is of the order 10^{13} to 10^{15} sec.$^{-1}$ for monomolecular or bimolecular reactions. Inserting typical values for organic semiconductors, such as $\sigma = 10^{-4}$ mho cm.$^{-1}$, $E_g = 2E_a = 0.4$ e.v., or $\sigma = 10^{-10}$ mho cm.$^{-1}$, $E = 1.9$ e.v., one finds values of L as 10^{-2} to 10^{-11} Å. Such values of the mean path in unit field strength are many times smaller than the lattice distances (about 10 Å.) and cast doubt that thermalization of the carriers can occur in such short path lengths. It seems preferable in such cases to consider activated hopping processes rather than drifting of wave packets.

It can be shown that the drift mobility for a hopping process[11] is

$$\mu = (\text{const.})T^2 \exp(-E_s/kT)$$

where E_s s the saddle height energy for the hopping. In the event that there is a cooperative process between the ions and the biradical (or exciton), the mobility for the ion–exciton process will be[12]

$$\mu = (\text{const.})T^2 \left[n_{ix}/n_i + n_{ix}\right] \exp(-E'_s/kT); \; E_s' < E_s$$

(11) F. Seitz, "Modern Theory of Solids," McGraw-Hill Book Co., New York, N. Y., 1940, p. 548.

(12) H. A. Pohl, chapter in "Modern Aspects of the Vitreous State," Vol. II, ed. by J. D Mackenzie, Butterworths, 1962; also H. A. Pohl, "Semiconduction in Polymers. A Review," Princeton Univ. Plastics Lab. Tech. Rpt. 61D. March 1961.

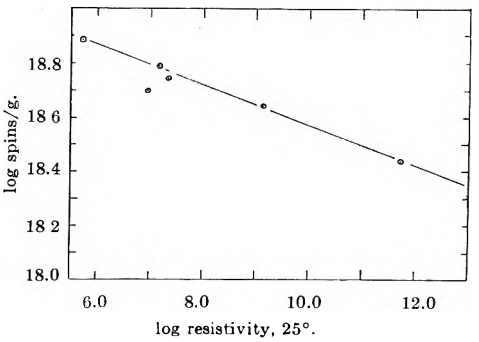

Fig. 7.—The interdependence of observed unpaired spin concentration and electronic conductivity in a series of PAQR polymers.

where n_{ix} is the concentration of the ion-exciton pairs, and n_i is the concentration of the ions. This latter process may become important where the concentration of excitons becomes comparable with the number of carriers, for there can be an appreciable energy of association of ions with the excitons. The formation of ion–exciton complexes might then be appreciable, increasing the likelihood of free carrier formation and aiding the hopping process by offering a lowered E_s for the process. Field dependence of the conductivity might be expected in such instances. The observance of field dependence of the conductivity in the PAQR polymers therefore is suggestive of an ion–exciton model for the hopping process. As will be shown in a later paper, a large Hall coefficient was observed in one PAQR polymer. This not only implies electronic conduction, but also suggests that the hopping type of carrier motion, if present, must be one of very low E_s. This is not unreasonable to expect in an ion–exciton type cooperative process.

There is by now appreciable evidence that when the size of a set of conjugated bonds is greater than some number (in the order of 10 to 15 double–single bond pairs) then the molecule acquires unusual characteristics. The degree of electron delocalization becomes high, and the production of excited states occurs at lower and lower energies. Among these excited states will be quasi-ionic ones, regardable as excitons, and also the formation of biradical states. For ease of reference, let us refer to this required degree of conjugation as "eka-conjugation." Eka-conjugation[7] may be said to exist when the degree of conjugation and electron delocalization becomes such that the content of electronically excited states such as excitons or biradicals, etc., becomes appreciable at room temperature. In view of this, one should expect a parallelism in the fractions of excited states visible on examination by various experiments. One should see, for example, a parallelism between the (a) population of exciton states demonstrable by non-ohmic effects during conduction measurements, or during dielectric loss experiments, (b) population of unpaired spins detectable by e.s.r., (c) population of carriers detectable by conductance measurements, and (d) mobilities following a hopping or tunneling process. It is not necessary that there be a one-to-one population ratio between observable spins and carrier populations.

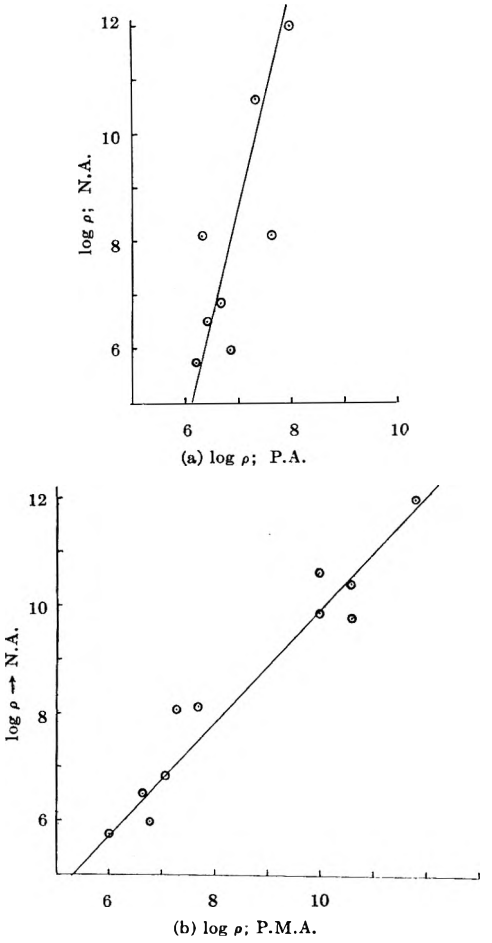

Fig. 8.—Structure *vs.* electronic conductivity. Here the conductivity of a PAQR polymer prepared from a given substituted hydrocarbon, but prepared with either naphthalic anhydride or phthalic anhydride (Fig. 8a) with either naphthalic anhydride or pyromellitic anhydride (Fig. 8b) is compared. From inspection of Fig. 8a, one sees that exchange of phthalic anhydride for naphthalic anhydride yields more highly conducting polymers among the smaller hydrocarbon derivatives, whereas exchange for naphthalic anhydride by pyromellitic anhydride causes little change.

Briefly, one may expect the following behavior in homogeneous polymeric organic semiconductors.

(1) The number of carriers (and therefore the conductivity) and the number of unpaired electrons present will be proportional to the amount of eka-conjugated material present.

(2) Conductivity will be affected by impurity only to the degree that the impurity consumes or contributes eka-conjugated structure, or to the degree that it affects the mobility as in the hopping processes. Certain types of impurity, then, can be present in rather substantial amounts before the conductivity will be greatly affected. Only a limited number of other types will be important.

(3) Conductivity in reasonably pure polymeric materials having native eka-conjugation will be dependent upon the monomeric structure of the polymer.

(4) Increased orbital interaction and hence carrier formation and mobility will result from an increase of pressure.

(5) Conductivity can be expected to be somewhat frequency and field dependent in such substances in view of the considerable geometrical extent and resultant field concentration effects on the eka-conjugated structures.

All of these expectations from the eka-conjugation model are borne out experimentally. As can be seen from Fig. 7, the conductivity is proportional to the spin concentration in the various polymers examined. Furthermore, the conductivity bears some relation to the monomeric structure of the polymer, which would not be the case necessarily if impurity effects were random and dominant. For example, those PAQR polymers having single aromatic rings in the hydrocarbon part of the monomer (as opposed to the acidic part) have higher resistances and higher activation energies than those with double rings, etc. The results are summarized in the following table.

No. of aromatic rings fused in hydrocarbon portion of polymer	Log of specific resistivity (av.)	"Forbidden energy gap" (av.)	No. of samples
1	9.8	0.70	7
2	8.1	.64	16
3	7.3	.59	25
9	..	.43	1

Further, as shown in Fig. 8a,b, the logarithm of the resistivities of various polymers made with naphthalic anhydride when compared with those made with pyromellitic anhydride shows a rather different correlation from that obtained in the case of the naphthalic *vs.* phthalic anhydrides. The slopes of the lines are 1 and 5, respectively.

Pressure decreases the resistivity and activation energy, as shown in Fig. 1, 2, and 3, in accord with expectation.

Examination of the field dependence of the resistivity showed (see Fig. 8) that over the range of 0.01 to 200 v./cm. the resistivity varied slightly, changing about 30% and in the direction expected from the eka-conjugation model.

Finally, a large Hall coefficient was observable on the one PAQR polymer so examined. This not only implies electronic (as opposed to ionic) conduction, but also suggests that the hopping type of carrier motion, if present, must be one of very low activation energy. This is not unreasonable to expect in an ion–exciton coöperative process.

Acknowledgment.—The authors express their appreciation to the American Cyanamid Corporation, the Signal Corps, U. S. Army, and the Office of Naval Research, for support.

THE MEASUREMENT OF HEATS OF ADSORPTION OF n-PENTANE AND ETHER BY ZEOLITE TYPE 5A BY MEANS OF AN ISOTHERMAL CONSTANT HEAT EXCHANGE CALORIMETER

BY O. M. DZHIGIT, A. V. KISELEV, AND G. G. MUTTIK

Laboratory of Adsorption and Gas-Chromatography, Department of Chemistry, M. V. Lomonosov University of Moscow, Moscow, U.S.S.R.

Received March 19, 1962

An isothermal calorimeter with constant heat exchange between the calorimeter cell and its jacket was constructed for the measurement of heat effects that are different in value and duration. It is possible to obtain the isothermal work of the calorimeter by compensating the measured positive (or negative) heat effects by switching off (or on) the calorimeter heater at constant power. It is necessary to know the heater power and the total heating time with a precision of $\pm 0.2\%$. This is easily realized by a potentiometer and chronograph with a quartz frequency stabilizer. The chronograph has a device for automatic heating time summation. The heat effect studied is fully compensated by the measured change of the heater energy. This calorimeter is used in heat of absorption measurements. The differential heats of adsorption of geometrically similar molecules of n-pentane and diethyl ether, as functions of the filling of the channels of zeolite type 5A, were measured. The heat of adsorption of n-pentane initially is about 14 kcal./mole and increases with the pore filling. The heat of adsorption of ether initially is about 27 kcal./mole and diminishes with the pore filling. The difference between the heats of adsorption of ether and n-pentane is close to the possible energy of Coulomb interaction of the ether dipole with the zeolite cations. The entropy of adsorption drops sharply as a result of adsorption in zeolite channels, especially for ether.

Introduction

The study of the potential energy of the adsorption forces and of the thermodynamics of adsorption by porous crystals is of great interest. The fixed space arrangement of the force centers of these adsorbents, in principle, permits the calculation of the potential energy of the adsorbed molecules just in the same way as for adsorption on the surface of non-porous crystals[1-5] and thence allows one to calculate the thermodynamic properties of the adsorption system from the geometrical and electronic structure of adsorbent and adsorbate taken separately.[6]

In Barrer and Wasilewski's paper[7] an attempt was made to calculate the potential energy of dispersion interactions of iodine molecules with zeolite oxygen atoms. For compound molecules such a calculation encounters great difficulties. However, in the case of such molecules, it is possible, purely experimentally, to derive the contributions of the energy of dispersion and electrostatic forces by comparing the heats of adsorption of the molecules of close geometrical but of a different local electronic structure—for example, such molecules as n-pentane and diethyl ether.[8]

The heats of adsorption of these substances on the surface of a non-polar adsorbent, namely, graphitized carbon black,[9] as well as the theoretically calculated potential energy of their adsorption on graphite,[6,9] are as close to each other as are their condensation heats. But in the presence of dipoles on the surface, for example in the adsorption on a hydrated surface of silica, the heat of adsorption of ether greatly exceeds that of n-pentane (approximately by the energy of two hydrogen bonds).[8] One would expect for adsorption in the channels of porous crystals, first an increase of the heat of adsorption of n-pentane due to increased dispersion energy, and second that the heat of adsorption of ether would increase especially, on account of additional electrostatic interactions of its dipole with the cations on the wall surface of the silica–alumina skeleton of the zeolite. An analogous increase of the heat of adsorption of nitrogen molecules of large quadrupole moment above the heat of adsorption of argon was observed in zeolite channels,[10] although these heats are close to each other when the adsorption occurs on graphitized carbon black surfaces.[11]

The same effect was noticed for adsorption on the surfaces of non-porous ionic crystals and on rutile.[2,12,13] This contribution of electrostatic forces can be roughly estimated theoretically. However, one would expect a different dependence of the adsorption energy of these substances on the channel filling of porous crystals of zeolite. The surface of these channels in regard to the adsorption of non-polar n-pentane should be much more homogeneous. The adsorbate–adsorbate interactions in such cases should be manifested in the rise of the heat of adsorption with filling.[4,14] But in the case of the adsorption of polar molecules of ether the zeolite surface, for example, the surface of zeolite type 5A, is more inhomogeneous since in various

(1) R. M. Barrer, *Proc. Roy. Soc.* (London), **A161**, 476 (1937).

(2) W. Orr, *ibid.*, **A173**, 349 (1939); T. Hayakowa, *Bull. Chem. Soc. Japan*, **30**, 236 (1957).

(3) N. N. Avgul, A. A. Isirikyan, A. V. Kiselev, I. A. Lygina, and D. P Poskys, *Izv. Akad. Nauk SSSR, Otd. Khim. Nauk*, 1314 (1957); N. N. Avgul, A. V. Kiselev, I. A. Lygina, and D. P. Poskys, *ibid.*, 1196 (1959); A. V. Kiselev and D. P. Poskys, *Zh. Fiz. Khim.*, **32**, 2824 (1958).

(4) A. V. Kiselev, *ibid.*, **35**, 233 (1961).

(5) A. D. Crowell and R. B. Steele, *J. Chem. Phys.*, **26**, 1407, (1957); A. D. Crowell and R. B. Steele, *ibid.*, **34**, 1347 (1961); E. L. Pace and A. R. Siebert, *J. Phys. Chem.*, **64**, 961 (1960).

(6) A. V. Kiselev and D. P. Poskys, *Trans. Faraday Soc.*, in press.

(7) R. M. Barrer and S. Wasilewski, *ibid.*, **57**, 1140, 1153 (1961).

(8) O. M. Dzhigit, A. V. Kiselev, and G. G. Muttik, *Kolloidn. Zh.*, **23**, 504 (1961).

(9) N. N. Avgul, A. V. Kiselev, and I. A. Lygina, *Izv. Akad. Nauk SSSR, Otd. Khim. Nauk*, 2116 (1961).

(10) G. L. Kington, "The Structure and Properties of Porous Materials," ed. by D. H. Everett and F. S. Stone, Butterworths, London, 1958 p. 59.

(11) S. Ross and W. J. Winkler, *J. Colloid. Sci.*, **10**, 319 (1955); S. Ross and W. W. Pultz, *ibid.*, **13**, 397 (1958).

(12) L. D. Belyakova and A. V. Kiselev, *Izv Akad. Nauk SSSR, Otd. Khim. Nauk*, 969, 1185 (1962).

(13) L. E. Drain and J. A. Morrison, *Trans. Faraday Soc.*, **49**, 654 (1953); L. E. Drain, *ibid.*, **49**, 650 (1953).

(14) A. V. Kiselev, *Vestm. Mosk. Univ., Ser. Khim.*, **1**, 3 (1962); *Kolloidn. Zh.*, **24**, 185 (1962).

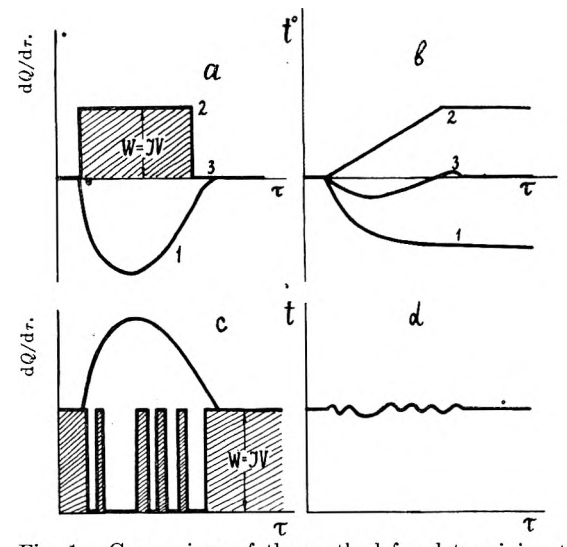

Fig. 1.—Comparison of the method for determining the thermal effects by the change in the calorimeter temperature (a,b) and by the compensation method of measurement (c,d).

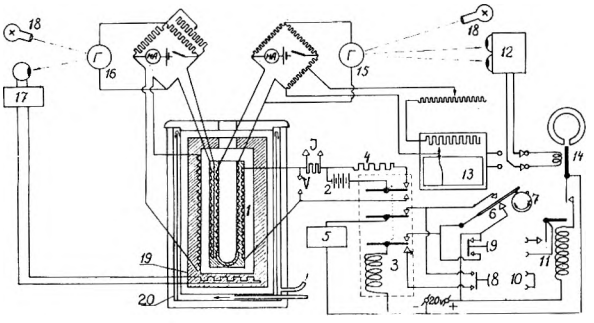

Fig. 2.—Circuit of the isothermal calorimeter: the designations 1–15 are given in the text; 16, adjusting galvanometer; 17, thyratron relay; 18, illuminators, 19, metal jacket of the calorimeter, and 20, water jacket–thermostat.

places there are bivalent calcium ions of differing accessibility and probably monovalent sodium ions (on aluminum–oxygen tetrahedra[15]).[16]

All this makes the direct determination of heats of adsorption of *n*-pentane and ether in zeolite channels very interesting. Due to very high adsorption energy, the zeolite channels are filled up by these substances at vapor pressures which are so low that the determination of heat of adsorption from isosteres in those cases is not very reliable or may even be impossible. Therefore, direct calorimetric measurements are necessary.

Experimental

The Isothermal Calorimeter with Constant Heat Exchange.[18]—The thermal effects of various processes, and particularly the adsorption heats of gases and vapors, usually are determined by the change in temperature of the calorimeter. In these cases the heat capacity of the calorimeter intended for precision measurements should be found experimentally.

From the point of view of the accuracy and convenience of work (possibility of applying the compensation method), it is very important to use the isothermal method in carrying out the calorimetric experiment. Isothermal conditions are obtained in calorimeters which utilize first-order phase transitions, as for example the ice calorimeter (see survey[19]). However, such calorimeters can operate only at the temperature of the corresponding phase transition, they are not sensitive enough, and they are inconvenient to handle. The principle of compensation for approximation to the isothermal conditions has been utilized by Calvet[20] by means of adsorbing most of the heat in the investigated process through the Peltier effect.

When we employed heat-liberating resistance thermometers in a number of our calorimeters,[21] we quite naturally did not strive to eliminate heat exchange between the calorimeter and the jacket, but tried to ensure its *constancy* with the aim of compensating the joule heat of the resistance thermometers by heat exchange between the calorimeter and the jacket as a result of the change of the temperature of the former. Constant heat exchange between the calorimeter and the jacket made possible a rational use of the advantages offered by resistance thermometers, *i.e.*, their sensitivity, stability, and simplicity of design.

At first[21] we made measurements during rising temperature (during adsorption) or decreasing temperature (for desorption). In ref. 22, thermal effects already were compensated partly by switching the calorimeter heater on or off, which brought the calorimeter nearer to isothermal conditions. In the present work, improvement in the operation of our calorimeter with constant heat exchange was effected by automatic compensation of the measured thermal effect, which fully ensured *isothermal* conditions.

Let us first examine an experiment in which heat is absorbed in a calorimeter. It can be represented by curve 1 in Fig. 1a. In the case of a calorimeter with an adiabatic jacket, there will occur a change of temperature as shown by curve 1 in Fig. 1b. If a heater of power W is switched on in the calorimeter (Fig. 1a, curve 2) the temperature will change as shown by curve 2 in Fig. 1b.

If this heater with an appropriate power is switched on during the absorption of heat at the expense of the measured thermal effect, the temperature of the calorimeter will change according to curve 3, Fig. 1b. Practically the same result also should be assured when the investigated process results in the liberation of heat in the calorimeter. The only difference is that during the heat liberation, the calorimeter heater should be switched on before the experiment begins and the temperature of its jacket should be such that all heat given off by this heater and the resistance thermometers is transmitted to the jacket. However, with this method of compensating the measured thermal effect, the current intensity in the heater should change continuously. To obviate this difficulty, we made use of intermittent switching on of a constant power heater in the calorimeter (Fig. 1c). As can be seen from Fig. 1d, in this case the temperature of the calorimeter during the experiment shows only very small deviations from constancy and the computation of the quantity of heat is reduced to determining the power of the heater and its off-time in heat liberation or on-time in heat absorption.

Figure 2 shows the electric circuit of a calorimeter. The compensating heater of the calorimeter (1) is fed from the storage battery (2). The heater is switched on by a group of contacts of the electromagnetic relay (3). When the heater is switched off, the storage batteries carry the ballast resistance (4). The on-time of the heater is summed up by the counter (5) actuated by the contacts (6). The disk (7) is rotated at 1 r.p.s. by the synchronous motor of a printing chronograph operated by an electron generator with a piezoelectric frequency stabilizer. This system makes it possible to account for the on- or off-time of the heater with an ac-

(15) The heat of adsorption of molecules having dipole, quadrupole, and π-bonds on dehydrated surfaces of silica is not great.[4,14]

(16) The energetic heterogeneity of surface of zeolites, especially Ca zeolites, was described in ref. 7, 10, and 17.

(17) R. M. Barrer and W. I. Stuart, *Proc. Roy. Soc.* (London), **A249**, 464 (1959).

(18) This part of the paper was presented at the first U.S.S.R. calorimetry conference in January, 1961, and at the 9th International Calorimetry Conference in Canada, August, 1961.

(19) M. M. Popov, Ed., "Termometrie and Calorimetrie," Moscow University Press, Moscow, 1954.

(20) E. Calvet and H. Prat, "Récents progrès en microcalorimétrie," Paris, 1958.

(21) A. A. Isirikyan, A. V. Kiselev, and G. G. Muttik, *Proc. Intern. Congr. Surface Activity, 2, London, 1957*, p. 214; N. N. Avgul, G. I. Berezin, A. V. Kiselev, I. A. Lygina, and G. G. Muttik, *Zh. Fiz. Khim.*, **31**, 1111 (1957).

(22) A. A. Isirikyan and A. V. Kiselev, *Zh. Fiz. Khim.*, **31**, 2127 (1957).

curacy not below 0.01 sec. A signal for switching on heater 1 can be sent manually by push-button 8 (for switching off, by push-button 9), but the heater is switched on (or off) only after the contacts (6) controlled by the chronograph have operated. In automatic operation, push-button 8 is closed by jumper 10, auxiliary relay 11 being switched on instead of push-button 9. During the main part of the experiment, the recording of the calorimeter drift is interrupted; the output of the differential relay (12) is switched over from the recorder (13) onto the polarized relay (14), which actuates relay 11.

As was noted above, in our former calorimeters[21] the thermal effect was determined by the rise in the temperature of the calorimeter, the heat capacity of which was measured by a special experiment. Control of the temperature of the calorimeter jacket was effected in such a way as to maintain a constant difference of temperature between the calorimeter and the jacket during the entire experiment, *i.e.*, to ensure conditions for a constant heat exchange. This was achieved by means of a regulator comprising a differential bridge, a thyratron photoelectric relay, and the heater of the calorimeter *jacket*. With the new isothermal method the temperatures of the calorimeter and the jacket selected before the experiment do not change essentially during an experiment. In this way the temperature difference between the calorimeter and the jacket which ensures a constant heat exchange is likewise maintained the same during an experiment. The constant temperature of the calorimeter is ensured by adjusting the work of the heater in the *calorimeter itself* by means of a control resistance thermometer *via* the galvanometer (15) and the differential photoelectric relay (12), which controls the mechanical relay switching the heater (1) on or off.

As in the former designs of calorimeters with metal jackets,[21] the main parts of the electric circuit are arranged in the calorimeter jacket. Since in the present calorimeter the temperature of the jacket does not change at all, these sections of the circuit are in exceptionally good isothermal condition, which further improves the stability of the calorimeter operation.

As can be seen from Fig. 2, the adjusting circuit of the calorimeter jacket in this device is the same as in the former designs of calorimeters with constant heat exchange.[21] In principle, it can be replaced by sufficiently accurate thermostating of only one jacket.

A certain disadvantage of this method lies in the fact that it is difficult to follow the rate of heat liberation in the calorimeter when the thermal effect is accounted for with the help of the heater on- and off-time counter (sometimes the kinetics of heat liberation can supply additional information on the process under investigation). Besides, during several tenths of a second after the calorimeter heater has been switched on, the resistance of the heater differs somewhat from its steady state value. However, despite the fact that during an experiment the heater is switched on 50 to 200 times, the resultant error with this design of the heater,[21] which ensures an effective heat transfer to the calorimeter, does not exceed 0.01–0.02%.

In the described method of measurement, the calorimeter heat capacity does not affect practically the value of the measured heat though the sensitivity certainly rises with the diminishing of the heat capacity. As 98–99% of the measured heat effect is compensated by the heater, the precision of heat measurement by this method is almost fully determined by the sum of the heater power and the time inaccuracies, which do not exceed 0.1%. Graphic calculation of the non-compensated part of the heat effect (which is less than 1–2% out of the total heat effect) is made with precision by 2–3%. Such a precision of 0.1% is obtained easily as the negligible change of the calorimeter temperature during the experiment usually does not disturb the linearity of calorimeter drift even during many hours of measurements.

The study of differential heats of adsorption of different substances by silica gel in the calorimeter described[8,23] showed good reproducibility of the results and the precision which was shown above.

Adsorption Measurement.—The measurement of adsorption was made in a vacuum microburet[24] by the change of liquid level in a calibrated glass capillary. The calorimetric vessel with the adsorbent, liquid microburet, and other parts of the vacuum unit were separated from each other by metallic electromagnetic valves with Teflon linings.[23]

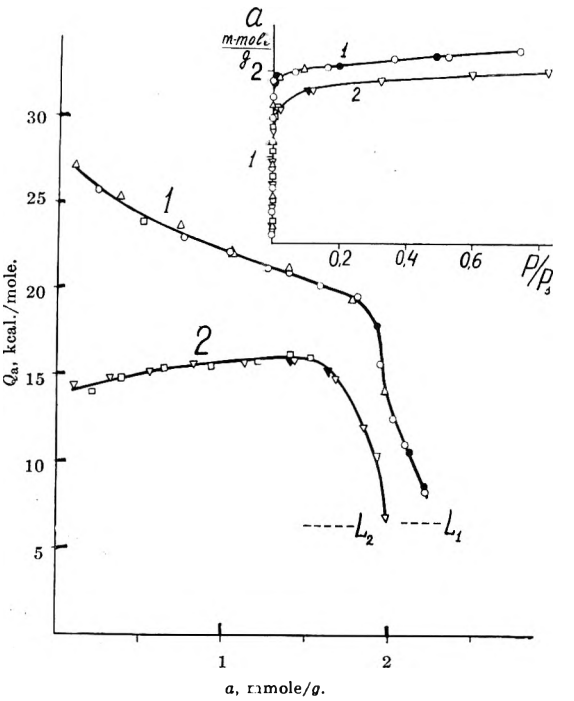

Fig. 3.—(a) The dependence of the differential heat of adsorption of diethyl ether (1) and *n*-pentane (2) vapors on the amount of adsorption a by type 5A porous crystals. The various designations of the points correspond to the different series of measurements after the evacuation. (b) the corresponding isotherm of adsorption a (p/p_s is the relative vapor pressure); black points signify desorption.

The Adsorbent.—For this study a zeolite similar to Linde Molecular Sieve 5A was used, the channels of which are accessible both for the molecules of *n*-pentane and ether. To avoid the possible complications and inhomogeneities brought about by the bond material in the production of the molecular sieve tablets, we used pure porous crystals without any bond material. These crystals, having the composition $0.216Na_2O \cdot 0.764CaO \cdot Al_2O_3 \cdot 1.92SiO_2 \cdot xH_2O$, were prepared in Dr. Zhdanov's laboratory.[25] The porous crystals were evacuated before the calorimetric measurements at 450° during 100–150 hr.

Results and Discussion

The experimental isotherms of adsorption and the dependences of differential heats of adsorption Q_a on the quantity adsorbed are presented in Fig. 3. The equilibrium vapor pressure of ether, as well as of *n*-pentane, in the mean region of channel filling amounted to less than 0.2 mm., so from the isotherm of adsorption it was impossible to draw conclusions as to the difference in the adsorption properties of these systems. On the other hand, this difference is obvious from the heat of adsorption curves. The heat of adsorption of *n*-pentane in the porous crystal channels of zeolite type 5A is very great in comparison with the adsorption on silica gel[26] and even on carbon black.[3,4] For low adsorp-

(23) O. M. Dzhigit, A. V. Kiselev, and G. G. Muttik, *Kolloidn. Zh.*, **23**, 553 (1961); **24**, 15 (1962).

(24) V. P. Dreving, A. V. Kiselev, and Y. A. Eltekov, *Dokl. Akad. Nauk SSSR*, **86**, 349 (1952).

(25) O. M. Dzhigit, S. P. Zhdanov, A. V. Kiselev, and G. G. Muttik, *Zh. Fiz. Khim.*, **36**, 919 (1962).

(26) A. A. Isirikyan, A. V. Kiselev, and B. A. Frolov, *Zh. Fiz. Khim.*, **33**, 389 (1959); A. V. Kiselev and B. A. Frolov, *Kinetika i Kataliz*, **3**, No. 5 (1962).

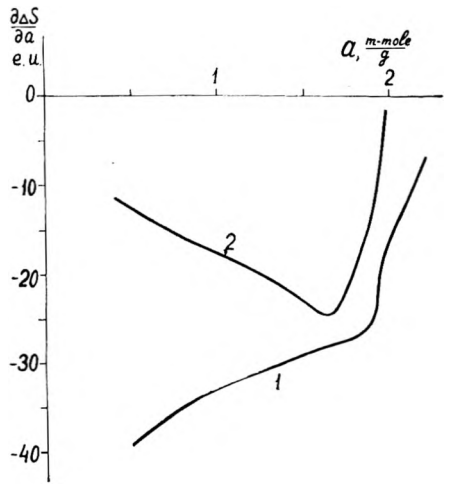

Fig. 4.—The change of differential molar entropy of the adsorption of ether (1) and *n*-pentane (2) by zeolite type 5A with the increase of the adsorbed quantity *a*.

tion it is about 14 kcal./mole. We did not notice any initial drop of the heat of adsorption. This points out the great homogeneity of porous crystals produced in Dr. Zhdanov's laboratory. With the increase of filling, the heat of adsorption of *n*-pentane rises approximately by 2.0 kcal./mole and reaches the maximum value of 16.0 kcal./mole at $a = 1.5$ mmoles/g.[27] This value of *a* corresponds to the sharp turn of the isotherm of adsorption to the right (the beginning of rapid rise of equilibrium vapor pressure). After this maximum the heat of adsorption quickly falls to a value which is close to the heat of condensation. Such form of the heat of adsorption isotherm is characteristic for sufficiently homogeneous surfaces.[14] The existing geometrical and chemical inhomogeneity of a solid surface cannot now hide the adsorbate–adsorbate attractions, which appear as the increase of heat of adsorption with the filling of the adsorption space.

The heat of ether adsorption at the small fillings is about 27 kcal./mole. This is a very high value for physical adsorption. It is at least 10–11 kcal./mole larger than the initial heat of ether adsorption on the hydrated silica surface,[8] with the hydroxyl groups of which the ether molecules form hydrogen bonds.[14] The initial heat of ether adsorption on the walls of the zeolite channels which contain Na^+ and Ca^{++} cations is larger by 12 kcal./mole than the heat of *n*-pentane adsorption at the same filling. With increasing filling, the heat of ether adsorption diminishes gradually,[29] remaining, however, larger than the heat of *n*-pentane adsorption. Close to complete filling of the porous crystal channels, it quickly falls to the value which is close to the heat of condensation.

In recent papers[30,31] of our Laboratory, it was noted that there is some further sorption, and hence greater density of the adsorbate molecules in porous crystal channels with the rise of vapor pressure (or gas-phase concentration).

It follows from the adsorption isotherms that at the relative vapor pressure $p/p_s = 0.5$, one large cavity of type 5A zeolite contains only about 3.5 molecules of ether or *n*-pentane. Thus, the state of the adsorbate in the porous crystal channels differs sharply from the normal liquid state.[10]

In Fig. 4 are represented the curves of differential molar entropies of ether and *n*-pentane adsorption by this zeolite (the standard state is the ordinary liquid sorbate). Naturally, such large values of heats of adsorption lead to sharp loss of mobility of molecules in the channels of porous crystals. This loss for the polar molecules of ether is much more pronounced than for their adsorption on the hydrated surface of silica gel.[8]

As was noted in the Introduction, the difference between the heats of adsorption of ether and *n*-pentane (which diminishes with the filling up of zeolite channels, as can be seen from Fig. 3) might be attributed in the main to the contribution to the energy of adsorption of electrostatic interaction of the dipoles of the ether molecules mainly with the Ca^{+2} and perhaps Na^+ cations of the porous crystal skeleton. It is natural to expect that at the beginning of sorption the ether molecules must be fixed on the more favorably located bivalent Ca^{+2} ions and then on less favorably located Ca^{+2} ions and probably on monovalent Na^+ ions. Though there is no precise information about the arrangement of these cations on the silica–alumina skeleton, it is possible in any case to assume that the accessible cations for the adsorbing molecules are arranged above the AlO_4^- ions and are directed into the zeolite cavities. As the AlO_4^- ions are bound only through the SiO_4 tetrahedra, for the rough evaluation of electrostatic energy it is possible to assume the model of interaction of ether dipole with the isolated cations.[32] For such a model of dipole–isolated ion interaction de Boer[33] and Iliin[34] had given the approximate formula for the Coulomb attraction energy in the most favorable orientation

$$\Phi_c = -\frac{\mu\nu l}{z_0^2} \qquad (1)$$

in which μ is the dipole moment, l is the electron charge, ν is the ion valence, and z_0 is the equilibrium distance between the dipole and ion centers. The value of z_0 is not known precisely. However, for a crude evaluation, it might be assumed as the sum of van der Waals radii of an oxygen atom in ether ($r_{oi} = 1.6$ Å.[35]) and that of a cation, r_{oj}. As the selection of the r_{oj} value is difficult, we made the evaluation of Φ_c for two choices of r_{oj}—first, from

(27) Barrer and co-workers also found the maxima of the heats of adsorption for iodine,[7] oxygen,[16] carbon dioxide,[16] and fluorocarbons[28] by zeolites.

(28) R. M. Barrer and P. J. Reucroft, *Proc. Roy. Soc.* (London), **A258**, 449 (1960).

(29) The diminishing of the heat of adsorption, especially in the case of Ca zeolites, was obtained in ref. 7, 10, and 17.

(30) A. V. Kiselev and L. F. Pavlova, *Kinetika i Kataliz*, **2**, 599 (1961); S. P. Zhdanov, A. V. Kiselev, and L. F. Pavlova, *ibid.*, **3**, 445 (1962).

(31) A. V. Kiselev, V. N. Semenova, and Y. A. Eltekov, *ibid.*, **3**, 421 (1962).

(32) The contribution of induction energy in this case is not large and for the ether and *n*-pentane is approximately the same.

(33) J. H. de Boer, "Electron Emission and Adsorption Phenomena," Cambridge University Press, New York, N. Y., 1935.

(34) B. V. Iliin, A. A. Leontjeva, and S. V. Bragin, *ZhETF*, **6**, 1155 (1936); *Phil. Mag.*, [7] **23**, 294 (1937).

(35) Landolt-Börnstein, "Tabellen," 6 Auflage, 1Bd, 3 teil, 1951, pp. 532–538.

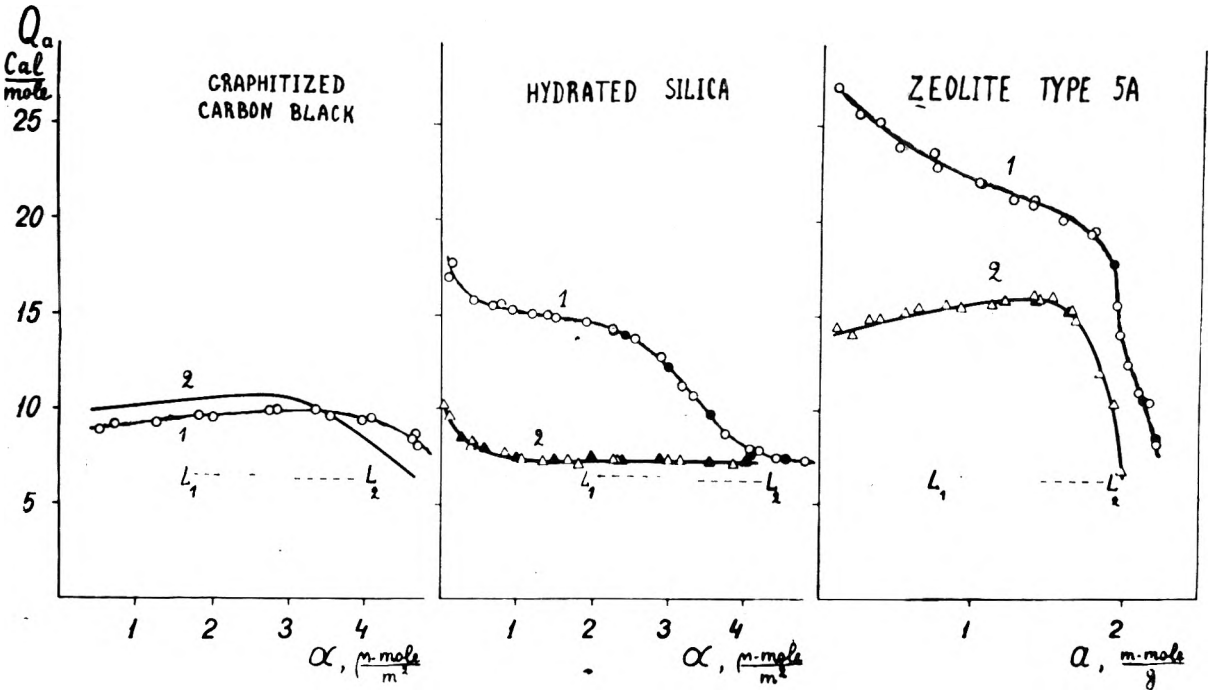

Fig. 5.—A comparison of the differential heat of adsorption of diethyl ether (1) and *n*-pentane (2) vapors on the amount of adsorption α (per unit surface) or a (per gram) by graphitized thermal carbon black (a), hydrated silica (b), and type 5A porous crystals (c).

the lattice of the corresponding metal (as it is possible that this value is closer to the van der Waals radius; in the case of calcium it agrees with the van der Waals radius of the atom of the neighboring noble gas, namely, argon; in the case of sodium it exceeds r_{oj} for neon only by about 15%). Second, we took the r_{oj} value from the lattice of the ionic crystal (ionic radii). In Table I, the results of these approximate evaluations of Φ_c are given and also the Φ_c values for mean values of r_{oj}, as well as corresponding values of $0.65\Phi_c$ (*i.e.*, with 35% deducted for the energy of repulsion).[3] The less favorable orientation of a dipole should decrease these values to some extent. The data given in the last two columns of this table show that the observed difference between the heats of adsorption of ether and *n*-pentane in the channels of the zeolite type 5A and the diminishing of this difference with the increase of the pore filling (see Fig. 3) can be explained mainly by the energy of the Coulomb interaction of the ether dipoles with the Ca^{+2} in different orientation and probably with the Na^+ of the zeolite. For more precise evaluation, it is of course necessary to take into consideration the interaction of the ether dipole with all the neighboring cations and with the complex AlO_4^- ions, and also the arrangement of ether molecules in the most favorable places, of minimum total potential energy, both electrostatic and dispersion, with the porous crystal skeleton as a whole. For the solution of these problems, experimental work on the heat of adsorption by zeolites of different types is necessary (for example zeolites of types A and X with different cations and different Al_2O_3:SiO_2 ratios), as well as the calculations of the potential of dispersion and electrostatic forces in zeolite channels.

The data necessary for such calculations have not been obtained as yet, but it is interesting to compare the experimentally determined energy of adsorption of ether and *n*-pentane on the surface of the adsorbents of different nature: non-polar, carrying dipoles, and ions. In Fig. 5 there are compared the dependence curves of differential heats of adsorption on the adsorption values for ether and *n*-pentane on the graphitized carbon black,[3,9,36] hydroxylated surface of silica,[8,26] and in the channels of the zeolite type 5A crystals. It is clear from this figure that on graphitized carbon black, on which adsorption is mainly determined by dispersion forces, the heats of adsorption of these two substances are close to each other (as their heats of condensation L), the heat of adsorption of ether even being 0.7–0.8 kcal./mole lower than the heat of adsorption of *n*-pentane. On the adsorbents

TABLE I

The results of the approximate evaluation of the energy of coulomb interaction Φ_c of the ether dipole $\mu = 1.18D$ (r_{oj} = 1.6 Å.) with the isolated ions Ca^{+2} and Na^+ at the different values of their radii, r_{oj}.

Choice of ion radius value	r_{oj}, Å.		$-\Phi_c$, kcal./mole		$-0.65\Phi_c$, kcal./mole	
	Ca^{+2}	Na^+	Ca^{+2}	Na^+	Ca^{+2}	Na^+
As in the metal lattice	2.0	1.9	13	7	9	5
As in the ion lattice	1.0	1.0	24	12	16	8
Mean values	1.5	1.4	17	9	11	6

(36) In ref. 3 the heat of adsorption of *n*-pentane on the Spheron-6 carbon black, heated to 1700°, was studied. In Fig. 5 these data are corrected for the small difference between the heats of adsorption at the transfer to the Thermal carbon black, graphitized at 3000°. This correction was made on the basis of related measurements of heat of adsorption of *n*-hexane on Channel and Thermal blacks graphitized at about 3000°.[37]

(37) A. A. Isirikyan and A. V. Kiselev, *J. Phys. Chem.*, **65**, 601 (1961); **66**, 205 (1962).

carrying dipoles (hydroxylated silica surface) or exchanging ions (porous crystals of zeolite) the heat of ether adsorption exceeds greatly the heat of *n*-pentane adsorption: namely, this excess for the hydroxylated silica is about 7.5 kcal./mole and for type 5A zeolite is even larger, about 10–13 kcal./mole.

The excess of the heat of ether adsorption above the heat of *n*-pentane adsorption on the hydroxylated silica surface was explained by us by the forming of hydrogen bonds between the oxygen of the ether molecule and the silanol hydroxyl groups of the surface. However, in the case of type 5A zeolite, the heat of ether adsorption exceeds the heat of *n*-pentane adsorption by a still greater quantity than in the case of hydroxylated silica surface, though in the case of zeolite, the hydrogen bonds are not formed (the infrared spectrum does not show the hydroxyl groups in the zeolite 5A evacuated at the high temperature). The difference between the heats of adsorption of ether and *n*-pentane appears to be greatest not in the case of adsorption on the hydroxylated surface when there is the possibility of hydrogen bond forming, but in the case of the adsorption on ionic surfaces when this bond is impossible. As was mentioned before, in the case of ether adsorption by type 5A zeolite, the sharp increase of the heat of adsorption at the transfer from *n*-pentane to ether apparently is due to the additional electrostatic interaction of the dipole of an ether molecule with the cations, which exist on the walls of zeolite channels. This leads to the assumption that in the cases shown in Fig. 5 b and c we have a quantitative difference, rather than a qualitative one; the heat of ether adsorption rises with the increase of the contribution of the electrostatic forces in the total energy of the adsorption interaction. This comparison shows that the experimental and theoretical investigations of the adsorption on the possibly more homogeneous solid non-polar surfaces as well as surfaces carrying different dipoles and also different ions would help us to understand the nature of intermolecular interactions and particularly the interactions which usually are named hydrogen bonds. At the adsorption on both hydroxylated and cationic surfaces the quantum-mechanical effects probably are also important.[38]

Acknowledgment.—The authors are indebted to Dr. S. P. Zhdanov for the presentation of zeolite type 5A crystal sample and to K. N. Mikos and T. A. Melnikova for their assistance in the measurements. The authors are thankful also to Professor J. M. Holmes and Dr. C. H. Amberg (who kindly took upon themselves the trouble of presenting this paper to the 9th International Calorimetry Conference and to the *Journal of Physical Chemistry*) and to Professor R. M. Barrer for his valuable discussion and comments.

(38) A. V. Kiselev, Ya. Koutetski, and J. Chizhek, *Dokl. Akad. Nauk SSSR*, **137**, 638 (1961); Ya. Koutetski and J. Chizhek, *Zh. Fiz. Khim.*, **36**, 1508 (1962).

CHARGE TRANSFER IN THE RADIOLYSIS OF ORGANIC LIQUIDS. I. EVIDENCE FROM HYDROGEN GAS YIELDS

BY T. J. HARDWICK

Gulf Research & Development Company, Pittsburgh 30, Pennsylvania

Received March 26, 1962

Hydrogen gas yields from the radiolysis of mixtures of saturated hydrocarbons do not necessarily follow a "law of averages" ($G_{H_2} = \Sigma$ electron fraction $\times G_{H_2(0)}$), but may be greater or smaller than the predicted value. This effect is believed to result from a charge exchange occurring on collision between the parent positive ion and a neighboring molecule of lower ionization potential. Subsequent charge neutralization results in the decomposition of a different molecule than that which absorbed energy. Not all molecules which can decompose can transfer energy in this fashion; those which cannot transfer energy are considered to be electronically excited. On the assumption that charge transfer occurs during the interval between ionization and charge neutralization, it can be determined that the lifetime of the charge pair is about 4×10^{-13} sec. in alkane solvents.

Introduction

In radiation chemistry, the term "protective effect" has two general meanings. In one case, a particular solute is "protected" from decomposition by the presence of a second solute which is much more reactive toward the intermediates (free radicals, ions, etc.) produced by the decomposition of the solvent. Usually, this can be considered a simple case of competing reactions. The extent of solvent decomposition is unchanged.

In the second case, the solute in some manner decreases the decomposition of the solvent molecules. The mechanisms suggested have included energy transfer from solvent to solute molecule, negative ion formation, and charge transfer. An excellent description of these mechanisms has been made by Burton and Lipsky.[1] It is this second case, where the solvent molecules are protected from decomposition, that will be considered exclusively in this paper.

Magee and Burton[2,3] suggested on theoretical grounds that energy transfer would take place by a charge transfer mechanism. In the radiolysis of a mixture of A and B molecules, if the ionization potential of B is greater than that of A, a charge transfer from B^+ to A will occur, giving a system increasingly rich in A^+. The radiolysis products, formed subsequent to charge neutralization, will

(1) M. Burton and S. Lipsky, *J. Phys. Chem.*, **61**, 1461 (1957).

(2) J. L. Magee and M. Burton, *J. Am. Chem. Soc.*, **72**, 1965 (1950).

(3) J. L. Magee and M. Burton, *ibid.*, **73**, 523 (1951).

be more characteristic of A than would be expected from the gross composition of the system.

In addition to charge transfer, it has been shown in certain cases that energy may be transferred between electronically excited states in multicomponent systems. Dreeskamp and Burton[4] have reviewed the possible consequences in radiation chemistry. It should be noted, however, that in all systems giving evidence of this type of energy transfer, at least one component has been aromatic in nature.

Many experimental studies to determine the extent of such solvent protection by energy transfer have been made. It is not practical, however, to measure directly the change in the amount of solvent decomposed. Accordingly, one must select a measurable product, and relate a change in its radiolytic yield to the degree of protection. Such a step presupposes an unambiguous explanation of the mechanism of reaction, and it is on the validity of this assumption that most objections arise.

A case in point is the radiolytic hydrogen gas yield from alkane–aromatic mixtures, particularly the system cyclohexane–benzene, which has been studied extensively.[5-12] In this case the hydrogen gas yield from cyclohexane is decreased markedly by small amounts of benzene. The decrease may be due entirely to energy transfer from cyclohexane to benzene. On the other hand, hydrogen atoms, which are known to be intermediates in alkane radiolysis, may add preferentially to the benzene ring. Accordingly, the decrease in hydrogen gas yield may result from scavenging action of the "protecting" molecule.

It is perhaps unfortunate that in most systems studied there are few cases where one can positively say that the fate of intermediate free radicals is not affected to some extent by the presence of the "protecting" material. Such cases where radical scavenging appears not to affect the product yield are: C_2 gases from cyclohexane–cyclohexene; ethylene from cyclohexane–benzene; acetylene from benzene–cyclohexene, and from benzene–toluene.[5] In these systems there is good qualitative evidence for energy transfer, but the accuracy of the data is not sufficient to give quantitative results. Too, in all these systems the details of the reactions to form the measured product are only speculative.

There is, however, one type of system where the presence of protective effects can be determined unambiguously. The hydrogen gas yield from mixtures of pure saturated hydrocarbons at low conversion should give unambiguous results.

(4) H. Dreeskamp and M. Burton, *Discussions Faraday Soc.*, **27**, 64 (1959).

(5) J. P. Manion and M. Burton, *J. Phys. Chem.*, **56**, 560 (1952).

(6) M. Burton and W. N. Patrick, *ibid.*, **58**, 421 (1954).

(7) R. H. Schuler and A. O. Allen, *J. Am. Chem. Soc.*, **77**, 507 (1955).

(8) H. A. Dewhurst, *J. Chem. Phys.*, **24**, 1254 (1956).

(9) M. Burton, J. Chang, S. Lipsky, and M. P. Reddy, *ibid.*, **26**, 1337 (1957).

(10) G. R. Freeman, *ibid.*, **33**, 71 (1960).

(11) J. Lamborn and A. J. Swallow, *J. Phys. Chem.*, **65**, 920 (1961).

(12) P. J. Dyne and W. M. Jenkinson, *Can. J. Chem.*, **39**, 2163 (1961).

In alkane radiolysis, hydrogen gas is produced by two mechanisms[5,6,13,14]

$$\mathrm{RH} \xrightarrow{G_1} \mathrm{H_2} + \text{products} \qquad (1)$$

$$\mathrm{RH} \xrightarrow{G_2} \mathrm{H} + \mathrm{R} \qquad (2)$$

$$\mathrm{H} + \mathrm{RH} \xrightarrow{k_3} \mathrm{H_2} + \mathrm{R} \qquad (3)$$

In the first, hydrogen gas is produced directly, in yield G_1, unaffected by the presence of free radical scavengers. Whether the mechanism be extraction of hydrogen from a nearest neighbor by a hot hydrogen atom, or whether a molecular detachment process takes place, is immaterial to the present argument. In the second, hydrogen atoms are produced in yield G_2 and degrade to thermal energies. In the absence of scavengers, all such hydrogen atoms react by reaction 3 to produce hydrogen gas. The total hydrogen gas yield $G_{\mathrm{H_2(0)}}$ is the sum of G_1 and G_2.

In any binary mixture of alkanes B and A, the hydrogen gas yield from reaction 1 will be $x \times G_{1\mathrm{B}} + (1 - x) \times G_{1\mathrm{A}}$, where x and $1 - x$ are the electron fractions of B and A (representing the fraction of energy absorbed by each) and $G_{1\mathrm{B}}$, $G_{1\mathrm{A}}$ are the respective values of G_1 for B and A. Similarly, the hydrogen gas yield from reactions 2 and 3 will be $x \times G_{2\mathrm{B}} + (1 - x) \times G_{2\mathrm{A}}$, for it does not matter whether the thermal hydrogen atoms produced in reaction 2 react with A or B.

The total hydrogen yield ($G_{\mathrm{H_2(0)}}$) expected from such a mixture therefore is $x \times G_{\mathrm{H_2(0)}}\mathrm{B} + (1 - x) \times G_{\mathrm{H_2(0)}}\mathrm{A}$. In other words, a plot of the total hydrogen gas yield *vs.* electron fraction of one component should give a straight line (law of averages[5]). We have found experimentally that a considerable deviation from a straight line normally is found, and in this paper a program of experiments to exploit this difference is reported. A model has been developed from the results, incorporating features of energy transfer which have been suggested previously. If the model is correct, certain values with respect to the lifetime of the excited species can be calculated.

As indicated previously, apparently incontrovertible evidence for energy transfer is available in the evolution of light hydrocarbons from the radiolysis of certain hydrocarbon mixtures. This will be discussed further in a second paper in which concurring experimental data will be presented. The present paper is limited to measurement of hydrogen yields and their interpretation.

Experimental

Materials.—Saturated hydrocarbons were Phillips Pure Grade, and were further purified by stirring with sulfuric acid. The extent of unsaturation of the purified material, as measured by bromination, was less than 0.1 mM, except for 2,3-dimethylbutane, where the unsaturation content was 0.23 mM. Fisher Reagent isopropyl alcohol was further purified with 2,4-diphenylhydrazine and distilled. Isopropyl ether (Eastman White Label) was refluxed with lithium alu-

(13) T. J. Hardwick, *J. Phys. Chem.*, **64**, 1623 (1960).

(14) T. J. Hardwick, *ibid.*, **65**, 101 (1961).

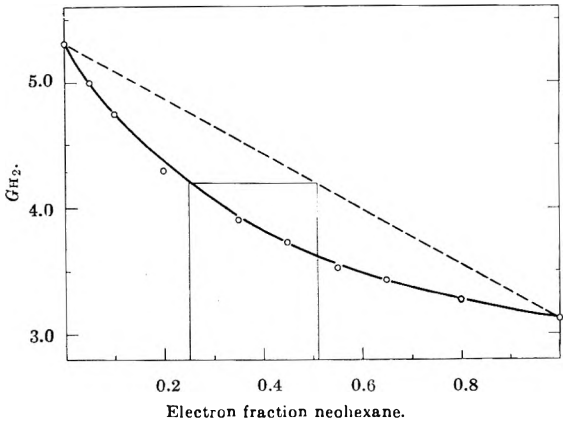

Fig. 1.—Hydrogen yields from the system *n*-hexane–neohexane.

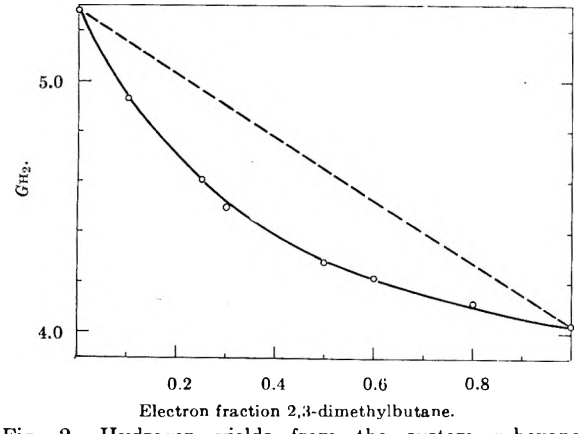

Fig. 2.—Hydrogen yields from the system *n*-hexane–2,3-dimethylbutane.

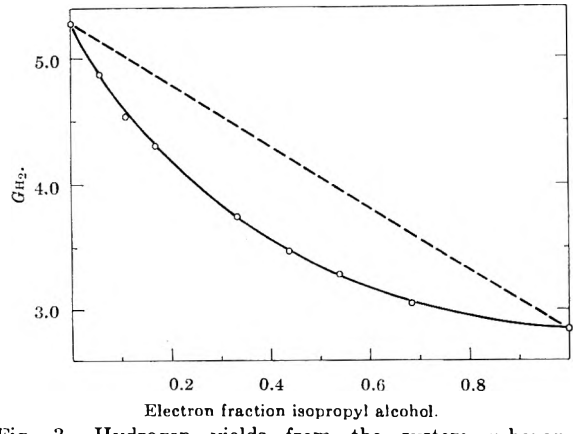

Fig. 3.—Hydrogen yields from the system *n*-hexane–isopropyl alcohol.

minum hydride, distilled, and stored under nitrogen before use. Methyl methacrylate was obtained from Rohm & Haas.

Solutions.—Mixtures of the various components were made up by volume at 23°, and the densities were measured. With the exception of isopropyl alcohol solutions at high alcohol concentrations, ideal behavior on mixing was observed. Where desirable, viscosities were measured at 23°; mole fractions and electron fractions were calculated for the mixture.

Irradiations.—Irradiations were carried out at 23° in a manner described previously.[13,14] Briefly, a 100-ml. sample of solution was degassed and irradiated to 20–50 krad, using X-rays from a 3 Mev. Van de Graaff accelerator. The energy absorbed was monitored concurrently by the Fricke dosimeter. Appropriate corrections were made by taking into account the relative electron densities of the solutions.

Hydrogen Gas Analysis.—After radiolysis, hydrogen was pumped off the solution through a trap at −196°. The gas then was isolated from other contaminants (air, methane) and the amount was measured on a McLeod gage. Reproducibility of the hydrogen yield was better than ±1%.

Systems Studied.—Hydrogen gas yields were measured for the following mixtures: (a) neohexane–*n*-hexane, (b) 2,3-dimethylbutane–*n*-hexane, (c) isopropyl alcohol–*n*-hexane, (d) isopropyl ether–*n*-hexane, (e) cyclopentane–2,3-dimethylbutane, and (f) 2-methylpentane–*n*-octane. In addition, hydrogen yields were measured for the system 75% *n*-hexane–25% neohexane (by volume) containing varying amounts of methyl methacrylate.

Results

Throughout this paper we have assumed that energy is absorbed in proportion to the relative electron density of the components. This postulate is considered to hold true, although a suggestion to the contrary has been made in cases where π electrons are present.[11] In any case, however, Σ bonding only is present in the alkanes, alcohols, and ethers studied.

Hydrogen Gas Yields.—In Fig. 1–4 the radiolytic hydrogen gas yields have been plotted as a function of electron fraction for various two-component systems. In no case does this yield correspond to that expected from the electron fraction of the individual components. In the systems studied, the yields are lower than expected, but the direction of change is not necessarily always to lower yields. The direction of change in six binary systems is listed in Table I.

TABLE I

DIRECTION OF OBSERVED ENERGY TRANSFER

Ionization potentials in e.v. are in parentheses[20]

Donor		Acceptor	
n-Hexane	(10.17)	Neohexane	(10.04)
n-Hexane	(10.17)	2,3-Dimethylbutane	(10.00)
n-Hexane	(10.17)	Isopropyl alcohol	(10.15)[a]
n-Hexane	(10.17)	Diisopropyl ether	(9.3)[b]
Cyclopentane	(10.51)	2,3-Dimethylbutane	(10.00)
2-Methylpentane	(10.09)	*n*-Octane	(9.99)[c]

[a] Value uncertain to ±0.05 e.v. [b] Estimated from values for dimethyl ether and diethyl ether. [c] Estimated as per method (a), Table III.

We shall consider that a transfer of energy has occurred from, for example, *n*-hexane to neohexane (Fig. 1). For 0.25 electron fraction neohexane, the hydrogen gas yield is that expected from the decomposition of 0.51 electron fraction neohexane. It would appear that some 0.26 electron fraction *n*-hexane had transferred its energy to neohexane before chemical decomposition occurred.

This phenomenon may be generalized for a two-component system, A and B, where there is a net transfer of energy from B → A. Let x be the electron fraction of B as calculated from relative concentrations. Let y be the mole fraction of B. Let z be the apparent electron fraction of B as indicated by the measured value of G_{H_2}. In the example given above for *n*-hexane (B)–neohexane (A) (Fig. 1) $1 - x = 0.25$, $1 - z = 0.51$.

The amount of B which transfers energy is $(1 - z) - (1 - x) = x - z$. The fraction of B mole-

TABLE II

PARAMETERS CALCULATED FROM DATA IN FIGURES 1–5, FOR VARIOUS BINARY MIXTURES[a]

Direction of charge transfer % Acceptor by volume	*n*-Hexane → neohexane		*n*-Hexane → 2,3-dimethylbutane		*n*-Hexane → isopropanol		Cyclopentane → 2,3-dimethylbutane	
	F	*N*λ	*F*	*N*λ	*F*	*N*λ	*F*	*N*λ
5	0.125	2.52	0.145	2.98	0.169	2.13		
10	.223	2.28	.265	2.70	.290	1.97	0.175	2.38
15	.329	2.25	.375	2.58	.393	1.94	.257	2.33
20	.420	2.18	.462	2.40	.484	1.98	.341	2.30
25	.485	2.04	.541	2.26	.562	2.05	.418	2.25
30	.559	1.98	.611	2.16	.632	2.15	.481	2.15
35	.613	1.88	.657	2.02	.675	2.23	.561	2.13
40	.664	1.80	.713	1.92	.751	2.47	.616	2.04
50	.726	1.60	.754	1.66	.858	3.00	.729	1.89

[a] *F* is the fraction of eligible molecules which transfer energy. *N*λ is the total number of collisions by B* during its lifetime.

cules absorbing energy, and which subsequently transfer this energy, is $(x - z)/x$.

In Fig. 5 we have plotted the function $(x - z)/x$ against electron fraction of A, using data obtained from Fig. 1–3. In all cases the donor molecule is *n*-hexane, while the energy is accepted by neohexane, 2,3-dimethylbutane, and isopropyl alcohol. Two points are of interest: (a) the limiting value of $(x - z)/x$ for all three components (A) is identical within experimental error, indicating that the characteristics of the donor rather than acceptor molecule govern the process, and (b) even at high acceptor concentrations not all of the donor type molecules can transfer energy. For *n*-hexane only 70% of the molecules absorbing energy can transfer it to another molecule.

On making a similar plot for the system cyclopentane–2,3-dimethylbutane, one finds that 79% of the excited molecules of cyclopentane molecules can transfer energy. Likewise, it is found that 52% of the energy absorbed by 2-methylpentane is transferable to *n*-octane. This limiting number (L) of excited molecules "eligible" for energy transfer appears to vary with the nature of the donor molecule.

Knowing the limiting fraction of excited molecules which *can* transfer energy, the fraction (F) of these "eligible" molecules which *do* transfer their energy can be calculated ($F = (x - z)/Lx$). Values of F for several binary systems are given in Table II for various concentrations of acceptor A.

In order to transfer energy, we have assumed that collisions between excited donor molecule and acceptor molecule must occur, and in absence of evidence to the contrary, that such collisions are governed by the normal laws of diffusion in liquids. The collision frequency of an excited molecule B* with A will be proportional to the mole fraction of A. We also are assuming throughout the discussion that energy transfer occurs in unit probability on collision of B* with A.

It is easily seen from the values of F in Table II that the excited species B* exists during several collisions with other molecules of the system. The total number of collisions (N) which B* will undergo during its existence will be $F/(1 - y)$.

Collision frequency depends on collision diameter, molecular weight, viscosity, and temperature.

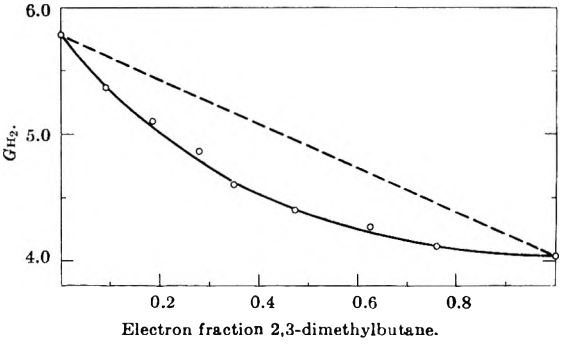

Fig. 4.—Hydrogen yields from the system cyclopentane–2,3-dimethylbutane.

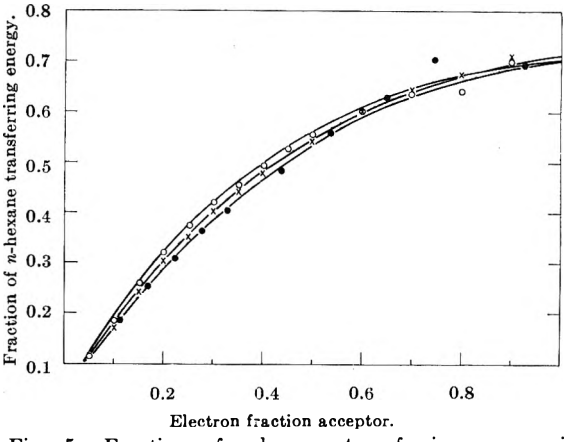

Fig. 5.—Fraction of *n*-hexane transferring energy in various systems $(x - z)/x$, ×, neohexane; ○, 2,3-dimethylbutane; ●, isopropyl alcohol.

The first two parameters are constant in a particular binary system, but the viscosity may vary. We are not entirely sure of the legitimacy of applying a viscosity correction to the total number of collisions of B* in the present instance, for can it be said that a molecule, and an excited one at that, recognizes the viscosity of the medium within several collisions? In addition, although the gross temperature of the system is constant during radiolysis, the local temperature, or kinetic energy, of molecules near the original column of ionization may be greater than normal. A local decrease in viscosity therefore would be expected. Nevertheless, we have applied a viscosity normalizing factor

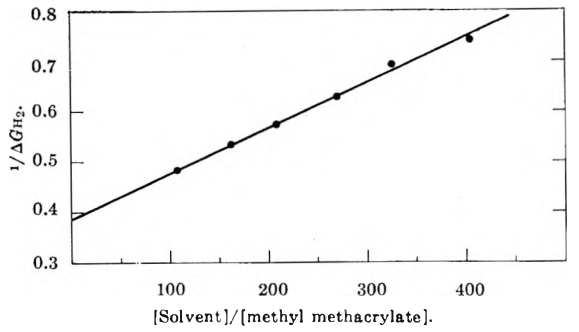

Fig. 6.—Kinetic plot for determining G_2 in the system 0.25 electron fraction neohexane–0.75 electron fraction *n*-hexane; H atom scavenger–methyl methacrylate.

to the systems containing *n*-hexane, consisting of a term λ, the ratio of the viscosity of the solution to that of the pure donor η/η_0 at 23°. Values of $N\lambda$ are given in Table II for various concentrations of acceptor.

As the concentration of acceptor molecules increases, the "lifetime" of B*, as measured by the total number of collisions, is somewhat reduced. It would appear that two processes are instrumental in removing B*, and that energy transfer is predominant at higher concentrations of acceptor molecules. The mechanisms of these processes will be discussed later.

Effect of Energy Transfer on G_1 and G_2.—In any binary system, factors affecting $G_{H_2(0)}$ naturally would be reflected in values of G_1 and/or G_2. Consider the case of neohexane (G_1 = 1.16, G_2 = 1.96)–*n*-hexane (G_1 = 2.12, G_2 = 3.16) mixtures. A solution 0.25 electron fraction neohexane radiolytically decomposes as 0.51 electron fraction neohexane (Fig. 1). As a result, for this mixture one would expect G_1 to be $0.51 \times 1.16 + 0.49 \times 2.12 = 1.62$; $G_2 = 0.51 \times 1.96 + 0.49 \times 3.16 = 2.55$.

This prediction has been checked experimentally by measuring the radiolytic hydrogen yield from the system 0.25 electron fraction neohexane–0.75 electron fraction *n*-hexane, with varying amounts of methyl methacrylate scavenger added. It has been shown previously[13,14] that a plot of the reciprocal of the decrease in hydrogen yield, $1/\Delta G_{H_2}$, due to the added scavenger, *vs.* the ratio [solvent]/[solute] gives a straight line, the ordinate intercept of which is $1/G_2$. In Fig. 6 we show such a plot, using experimentally determined values for the decrease in hydrogen gas yield due to methyl methacrylate. The ordinate intercept is 0.385, giving G_2 = 2.60. Since $G_{H_2(0)}$ for this system is 4.17, G_1 = 1.57. Within experimental error these values agree with those predicted in the previous paragraph. Such a result supports the contention that energy transfer occurs prior to any chemical decomposition.

Discussion

Nature of the "Eligible" Molecules.—One of the significant findings of these experiments is that not all molecules which decompose are capable of transferring energy. This limitation seems to be a property of the donor molecule, *e.g.*, 70% for *n*-hexane, 79% for cyclopentane, etc., and is unaffected by the nature of the acceptor molecule.

At this time we make the suggestion that those molecules which transfer energy do so while in the ionized state, that is, in the time between ionization and subsequent charge neutralization by an electron. This energy transfer is in reality a charge transfer, and we shall refer to it as such for the rest of the paper. The remaining molecules which are not "eligible" to transfer, but which decompose to give products, are considered to be electronically excited, and cannot transfer energy in the time available before unimolecular decomposition.

A criterion for charge transfer is that the acceptor molecule be at a lower ionization potential than the donor molecule. Pertinent ionization potential data for the compounds studied are given in Table I. We have used photoionization data as these should be more accurate when considering differences in ionization potential. In all cases the ionization potential of the donor is higher than that of the acceptor.

In the systems chosen for detailed study, it so happens that the donor molecule has both a higher ionization potential and a higher radiolytic hydrogen gas yield than the acceptor. This of course results in a lower hydrogen gas yield than expected from electron fraction data. However, in the system *n*-octane ($G_{H_2(0)}$ = 6.18)–2-methylpentane ($G_{H_2(0)}$ = 4.47), the ionization potential of *n*-octane is lower than that of 2-methylpentane. As a result, *n*-octane is an acceptor molecule, and higher yields of radiolytic hydrogen are observed than would be expected without charge transfer.

It is implicit in our arguments thus far that for *n*-hexane 70% of molecules which decompose were originally in the ionized state, while only 30% were in an electronically excited state (cross sections for absorption of energy by vibration and rotation alone are very small, and such energy absorption processes will not be considered further). From general considerations of energy absorption in the slowing down of ionizing electrons, one would expect more excitation events than ionization. It must be remembered, however, that not all excitation levels are repulsive, and accordingly only part of that energy absorbed by electronic excitation leads to decomposition. Since we are measuring the relative number of events that lead to decomposition, it is understandable that the ionization events are in the majority, for it is likely that all excited molecules formed on charge neutralization will decompose.

At the lower concentrations of acceptor, a large number of "eligible" molecules do not transfer energy. From our interpretation, under such conditions many ions are neutralized before charge transfer can take place. Once neutralized, energy transfer is "quenched."

Lifetime of the Charge Pair.—For a particular donor (*e.g.*, *n*-hexane) it would be expected that at low acceptor concentrations the number of collisions before charge neutralization would be about the same, regardless of the nature of the acceptor molecule. This does not appear to be so from the data in Table II.

A referee has suggested an explanation of this discrepancy. It is expected that, of the molecules

decomposing through intermediate charge pair formation, only a fraction will eventually produce hydrogen gas; furthermore this fraction will vary from one compound to another, in general being large for *n*- and cycloalkanes, and smaller with increasingly branched alkanes. In the transfer of charge from *n*-hexane to the other hexane isomers, ions which eventually would have produced hydrogen gas now have been replaced by those which form predominantly alkyl radical pairs. The resulting decrease in hydrogen gas yield is in accord with the observed decrease of $N\lambda$ with increasing acceptor concentration.

The proper values of $N\lambda$ are those obtained by extrapolation to zero concentration of acceptor. For *n*-hexane–isohexane systems $(N\lambda)_0 = 2.5$ and 2.9 collisions for acceptors neohexane and 2,3-dimethylbutane, respectively. In the case of such mixtures, the collision frequency of one molecule with its neighbors can be calculated with some accuracy (6.6×10^{12} collisions/sec.). The lifetime of a charge pair is therefore 2.5–2.9 collisions/6.6×10^{12} collisions/sec. = 4–5 $\times 10^{-13}$ sec.

Evidence for Charge Transfer in Previous Work.—For the cyclohexane–benzene system Freeman[10] concluded that the ratio of rate constants k_4/k_5

$$\text{c-}C_6H_{12}^* + C_6H_6 \xrightarrow{k_4} \text{c-}C_6H_{12} + C_6H_6^* \quad (4)$$

$$\text{c-}C_6H_{12}^* \xrightarrow{k_5} \text{c-}C_6H_{11} + H \quad (5)$$

was 0.78 l./mole, where c-C_6H_{12}* represents only a specific fraction of the cyclohexane molecules which absorb energy. Clearly k_4 must be very fast in order to compete with reaction 5. Very likely the c-C_6H_{12}* molecules of Freeman are similar to our positive ions, but as was remarked before, it is difficult to present unchallengeable explanations in the cyclohexane–benzene system. Ramaradhya and Freeman[15] found evidence for positive ion transfer in the vapor phase from cyclohexane to benzene and propylene, although it is not clear if such a mechanism can occur in liquid systems.

Dyne and Jenkinson[16] have shown that D_2 is produced in the radiolysis of cyclohexane containing cyclohexane-d_{12}. They further showed that at low concentration of C_6D_{12}, both atoms of the D_2 molecule come from the same parent molecule. Thus in any system containing small amounts of C_6D_{12}, the D_2 yield based on the energy absorbed by C_6D_{12} (G_1(D) in their terminology) is a measure of the amount of C_6D_{12} which decomposes. If no energy transfer occurred, G_1(D) should be invariant from one solvent to another.

Experimentally, however, Dyne[17] found that G_1(D) varies widely in various saturated hydrocarbons. Some have values of G_1(D) larger than that found with ordinary cyclohexane (0.32)[18]; others have lower values. In the first column of Table III are listed hydrocarbon solvents where $G_1(D) > 0.32$; in the second column, those solvents where $G_1(D) < 0.32$. Photoionization potentials for each hydrocarbon are given in parentheses. Significantly, all compounds in the first column, where $G_1(D) > 0.32$, have ionization potentials greater than that of cyclohexane, while those in the second column $\{G_1(D) < 0.32\}$ have ionization potentials less than that of cyclohexane.[19]

The explanation for the variation of G_1(D) follows from our postulate of charge transfer. All compounds in the first column are donor molecules with respect to cyclohexane; hence more C_6D_{12} will decompose, giving larger values of G_1(D). On the other hand, hydrocarbons in the second column are acceptor molecules with respect to C_6D_{12}, and, after charge transfer, fewer C_6D_{12} molecules will decompose, thus giving smaller values of G_1(D).

TABLE III

COMPARISON OF G_1(D) FOR SOME SATURATED HYDROCARBONS WITH G_1(D) FOR CYCLOHEXANE

Values of Dyne and Denhartog[17]

Photoionization potentials in e.v. are in parentheses[20]

Hydrocarbons where $G_1(D) < 0.32$		Hydrocarbons where $G_1(D) > 0.32$	
n-Pentane	(10.33)	Decahydronaphthalene	(<9.8)[b]
Isopentane	(10.30)	Ethylcyclohexane	(<9.86)[c]
n-Hexane	(10.17)	Methylcyclohexane	(9.86)
2-Methylpentane	(10.09)	2,2,4-Trimethylpentane	(9.84)
Neohexane	(10.04)		
2,4-Dimethylpentane	(~9.9)		
n-Octane	(9.99)[a]		
n-Nonane	(9.94)[a]		

Cyclohexane (9.88) $G_1(D) = 0.32$

[a] Estimated by extrapolation of the photoionization potentials of normal C_3–C_7 hydrocarbons, using a curve parallel to a similar plot of ionization potentials measured by electron impact. [b] Estimated by analogy of cyclohexane–decahydronaphthalene with benzene–naphthalene. [c] Estimated as less than methylcyclohexane.

It would appear, therefore, that many of the results indicating energy transfer in liquid systems can be considered as a positive charge transfer. In this we agree with the suggestions of Burton and Magee,[2,3] and have found the lifetime of the charge pair to be about 4×10^{-13} sec.

It probably is pertinent to conclude with a comparison of the decrease in hydrogen yields due to charge transfer and to the scavenging of hydrogen atoms. Reactions involving radiolytically induced hydrogen atoms normally are measured using solutes present in less than 0.01 mole fraction.[19] The extent of charge transfer at these low concentrations is negligible, for only an insignificant fraction of positive ions will charge exchange with solute molecules in the time available. The decrease in hydrogen yield therefore certainly is due to scavenging of hydrogen atoms by the solute.

At the same time it must be recognized that above solute concentrations of several per cent, one must be prepared for products more typical of the solute, for most solutes have ionization potentials lower than that of alkanes. In addition, on irradiating a pure material beyond several per cent conversion,

(15) J. M. Ramaradhya and G. R. Freeman, *Can. J. Chem.*, **39**, 1769 (1961).

(16) P. J. Dyne and W. M. Jenkinson, *ibid.*, **38**, 539 (1960).

(17) P. J. Dyne, private communication, 1962.

(18) T. J. Hardwick, *J. Phys. Chem.*, **66**, 117 (1962).

(19) It has been assumed that the ionization of C_6D_{12} is equal to that of C_6H_{12}, or at least not more than 0.05 e.v. higher.

(20) W. C. Price, R. Bralsford, P. V. Harris, and R. G. Ridley, *Spectrochem. Acta*, **14**, 45 (1959).

charge transfer to products of lower ionization potential must be considered.

A suggestion of two different effects in the radiolysis of mixtures already has been made. Forrestal and Hamill[21] have concluded that in the system cyclohexane–methyl iodide, entirely different mechanisms accounted for the decrease in G_{H_2} in the ranges 0–0.1% and 0.1–10% methyl iodide. We suggest that H atom scavenging only occurs in the lower concentration range, but that charge transfer plays a significant role in the higher range. Freeman[22] has interpreted the decrease in hydrogen yield in the system methylcyclohexane–benzene as arising from two distinct phenomena—one occurring below 5% benzene concentration, which he considers to be hydrogen atom scavenging, and one effective over the whole range, which he suggests is energy and/or charge transfer.

Acknowledgment.—The author is particularly grateful to Dr. P. J. Dyne for permission to use his unpublished results. He also wishes to thank Dr. G. J. Mains for helpful comment. The Van de Graaff accelerator was operated by personnel of the Nuclear Applications Section.

(21) L. J. Forrestal and W. H. Hamill, *J. Am. Chem. Soc.*, **83**, 1535 (1961).

(22) G. R. Freeman, *J. Chem. Phys.*, **36**, 1542 (1962).

THE LITHIUM–STRONTIUM EQUILIBRIUM SYSTEM

BY FREDERICK E. WANG, FRANK A. KANDA, AND ADEN J. KING

Chemistry Department, Syracuse University, Syracuse 10, N. Y.

Received March 29, 1962

The complete equilibrium diagram of the lithium–strontium system has been determined by the use of differential thermal analysis and X-ray diffraction methods at room and high temperatures. The system displays limited solubility at both ends. The degree of solubility of lithium in strontium varies with the allotropic modification of strontium. These modifications are: β-Sr (f.c.c.) up to 231°; γ-Sr (h.c.p.) between 231 and 623°; δ-Sr (b.c.c.) above 623°. Three compounds form by peritectic reactions: liquid + γ-Sr → Sr_8Li (h.c.p.)—496°; liquid + Sr_8Li → Sr_3Li_2—198°; and liquid + Sr_3Li_2 → Sr_6Li_{23}—152°. A congruent melting compound approximating the formula Sr_7Li (body-centered tet.) has a melting point of 584°. This compound forms a eutectic with δ-Sr solid solution at a composition of 88.5 atom % strontium with a melting point of 578°. Another eutectic forms between Sr_6Li_{23} and the lithium solid solution (α) at 12.5 atom. % strontium with a melting point of 134°. The compound, Sr_7Li, and the δ-Sr solid solution decompose by inverse peritectic reactions upon cooling: Sr_7Li → liquid + δ-Sr—530°; δ-Sr → liquid + γ-Sr—515°. The compound Sr_8Li exists in two modifications; the high temperature form (h.c.p.) transforms upon cooling into a low temperature form (tet.) within the temperature range 196–198°.

I. Introduction

The lithium–strontium system was investigated in order to continue the study of lithium equilibrium systems with the alkaline earth metals. Of interest to us are the effects produced in these systems by alloying lithium with metals of a constant valence but varying in atomic diameter, electronegativity, and allotropic modifications in the solid state. Similar studies are under way involving sodium metal and the alkaline earths. The lithium–barium system[1] was the first of these to be studied in our Laboratory. The calcium–lithium system is currently under investigation as are the systems involving sodium with strontium and barium. Although some of these systems have been reported by other investigators,[2] they are incomplete or there is some question regarding the validity of some of the phases reported. There has been no previous report published regarding the lithium–strontium system.

II. Experimental

Purity of the Metals and Sample Preparation.—Lithium metal of purity 99.86–99.89 wt. % Li was supplied by the Foote Mineral Co. Sodium was found to be the major impurity and was shown by spectrographic analysis to be present in the range of 0.09–0.10% by weight. The m.p. of the metal was observed to be 180 ± 1°, which is in good agreement with results reported previously.[1,3,4] Commercial grade strontium obtained from King Laboratories, Inc., in Syracuse, N. Y., was vacuum distilled at a temperature of 850° and a pressure of less than 1 μ. Spectrographic analysis showed the purified strontium to be free of barium and to contain only 0.1% calcium and no more than 0.01% each of other detectable impurities. The melting point of the purified strontium was found to be 773–774°. Both strontium and lithium gave ideal flat isothermal pauses in their cooling curves at the melting point. For the initial investigations, samples were prepared for every 2-atom % composition interval. Thin walled iron crucibles were used as the sample containers. Iron does not dissolve significantly in the metals of the system, nor does excessive intergranular penetration of the crucible walls occur under the conditions of the experiment.[1,5] Quantities of metals appropriate for the particular alloys investigated were weighed on an analytical balance prior to loading the crucibles. These operations were carried out in an argon atmosphere in a drybox provided with access through a vacuum type air lock chamber. The drybox argon was circulated continually through a purification train consisting of a column of zeolite 4A and a stainless steel tube containing barium chips and titanium turnings maintained at 400–500°. Sample size usually was of the order of 10 cm.^{3}.

Thermal Analysis.—In general, the thermal analysis was performed with the equipment and technique previously reported by Hirst, *et al.*[6] Controlled heating and cooling rates within the range 0.8–5.0 deg./min. were used in this investigation. The recording Chromel–Alumel thermocouple was calibrated and periodically checked against a standard Pt–Pt(Rh) (10%) thermocouple certified by the National

(1) D. V. Keller, F. A. Kanda, and A. J. King, *J. Phys. Chem.*, **62**, 732 (1958).

(2) H. Remy, G. Wolfrum, and H. W. Haase, *Schweiz. Arch.*, **26**, 5 (1960); M. R. Wolfson, *Trans. Am. Soc. Metals*, **49**, 44 (1956); M. I. Zamotorin, *Metallurgy*, **13**, 96 (1938).

(3) S. B. Kliner, *J. Am. Chem. Soc.*, **74**, 5221 (1952).

(4) T. B. Douglas, L. F. Epstein, J. L. Dever, and H. J. Howland, *ibid.*, **77**, 2144 (1955).

(5) J. C. Schottmiller, A. J. King, and F. A. Kanda, *J. Phys. Chem.*, **62**, 1446 (1958).

(6) R. G. Hirst, A. J. King, and F. A. Kanda, *ibid.*, **60**, 302 (1956).

Bureau of Standards. All temperatures recorded in this investigation therefore are considered to be accurate within ±1°. Cooling and heating curves were recorded on two Brown electronic recorders. One of these recorded a normal temperature *vs.* time curve and the other a temperature differential *vs.* time. Runs were repeated until reproducibility of inflections and isothermal pauses was obtained to within ±1°. As the nature of the system became evident, additional samples were made up for particular compositional ranges in order to establish definitely the curvature or termination of a phase boundary.

X-Ray Diffraction Studies.—All alloy compositions investigated in this system were subjected to X-ray powder diffraction studies at room temperature. High temperature X-ray powder diffraction studies also were made for most of these alloys with a specially constructed Debye–Scherrer type high temperature camera.[6] The reliability of the sample temperature measurement and control in this camera was ±1°.

A high temperature diffractometer[7] also was used to investigate strontium-rich alloys between 83 and 97 atom % strontium. This was necessitated by the fact that these alloys exhibited retrograde melting above 500° and the resulting high temperature liquid phase reacted with the Vycor capillaries used with the high temperature powder camera. An improved specimen furnace in the high temperature diffractometer resulted in low thermal gradients between the edge and center of the sample amounting to ±1° below 400° and ±2° above 400°. All solid state transitions and boundaries were determined by high temperature X-ray methods. Single crystal Weissenberg techniques were used to determine the crystal structures of Sr_6Li_{23} and Sr_3Li_2 described elsewhere.[8] The interplanar spacings of strontium (β, γ, δ) and all intermediate phases of this system as observed by the powder method are given in Table I. The method utilized for the indexing of all the powder patterns was that of Ito[9] and Cernohorsky.[10]

TABLE I

INTERPLANAR DISTANCES OBSERVED ON X-RAY POWDER DIFFRACTION PATTERNS OF THE PHASES WHICH APPEAR IN THE Li–Sr SYSTEM (WITH THE EXCEPTION OF Li (α) PHASE)

Sr_6Li_{23} — f.c.c. a_0 = 14.88 Å.

d	(hkl)	I_0
8.50	(111)	w.
7.50	(200)	w.
5.26	(220)	v.w.
4.31	(222)	s.
3.71	(400)	w.
3.41	(331)	s.
3.31	(420)	v.w.
3.03	(422)	w.
2.86	(511)	s.
2.62	(440)	s.
2.48	(600)	m.s.
2.35	(620)	v.w.
2.24	(533)	v.w.
2.15	(444)	v.v.w.

Sr_3Li_2 — tetragonal a_0 = 9.63 Å. c_0 = 8.55 Å.

d	(hkl)	I_0
6.75	(110)	m.s.
6.53	(011)	m.s.
4.31	(120)	m.s.
4.27	(002)	s.
3.62	(112)	v.s.
3.41	(220)	v.s.
3.16	(221)	w.
3.04	(122)	m.s.
2.86	(131)	w.
2.73	(013)	v.w.
2.55	(231)	v.v.w.
2.40	(040)	w.
2.34	(140)	m.s.
2.27	(330)	v.v.w.

Sr_8Li (room temp.–198°) — tetragonal a_0 = 6.16 Å. c_0 = 8.86 Å.

d	(hkl)	I_0
4.47	(110)	v.v.w.
3.86	(111)	v.v.w.
3.52	(102)	s.
3.27	(112)	v.w.
3.04	(200)	w.
2.93	(003)	w.
2.71	(210)	v.w.
2.38	(113)	v.w.
2.20	(004)	w.
2.15	(220)	m.s.
2.10	(104)	v.w.
2.05	(300)	v.w.
1.97	(310)	w.
1.83	(302)	s.

Sr_8Li (198–496°) — h.c.p. a_0 = 4.31 Å. c_0 = 13.85 Å.

d	($hk.l$)	I_0
3.74	(10.0)	w.
3.63	(10.1)	v.v.w.
3.50	(00.4)	s.
3.29	(10.2)	v.w.
2.90	(10.3)	w.
2.55	(10.4)	w.
2.20	(10.5)	v.v.w.
2.15	(11.0)	w.
2.03	(11.2)	v.v.w.
1.98	(10.6)	w.
1.83	(11.4)	w.
1.80	(20.2)	v.w.
1.45	(10.8)	v.v.w.
1.38	(12.2)	v.w.

Sr_7Li (530–584°) — body-centered tetragonal a_0 = 7.61 Å. c_0 = 6.50 Å.

d	(hkl)	I_0
3.25	(002)	m.s.
2.68	(220)	s.
2.12	(222)	m.s.
1.94	(132)	w.
1.65	(402)	v.w.
1.59	(332)	v.w.
1.54	(114)	v.w.
1.42	(143)	w.
1.34	(440)	v.v.w.

Sr(β) — f.c.c. a_0 = 6.08 Å.

d	(hkl)	I_0
3.52	(111)	v.s.
3.05	(200)	w.
2.15	(220)	m.s.
1.84	(311)	s.
1.76	(222)	w.
1.52	(400)	v.w.
1.39	(331)	w.
1.36	(420)	v.w.
1.24	(422)	v.w.
1.17	(511)	w.
1.08	(440)	v.w.

Sr(γ) — h.c.p. a_0 = 4.31 Å. c_0 = 7.05 Å.

d	($hk.l$)	I_0
3.75	(10.0)	w.
3.51	(00.2)	m.s.
3.30	(10.1)	s.
2.56	(10.2)	w.
2.16	(11.0)	v.w.
1.98	(10.3)	v.w.
1.84	(11.2)	m.s.
1.81	(20.1)	v.w.
1.76	(00.4)	v.v.w.
1.65	(20.2)	v.v.w.
1.59	(11.3)	v.w.
1.46	(20.3)	v.w.
1.41	(21.1)	v.w.

Sr(δ) — b.c.c. a_0 = 4.84 Å.

d	(hkl)	I_0
3.44	(110)	v.w.
2.43	(200)	s.
1.94	(211)	w.
1.74	(220)	v.w.
1.47	(310)	w.
1.40	(222)	v.w.
1.29	(321)	v.v.w.
1.21	(400)	w.
1.08	(411)	v.w.
0.99	(332)	v.w.
0.94	(422)	w.

III. The Sr–Li Phase System

The phase diagram for this system is shown in Fig. 1. Particular expanded sections also are shown in Fig. 2 and 3. The system displays a lithium-rich eutectic at 12.5 atom % strontium. The eutectic reaction forms the terminal lithium solid solution (α) which has a maximum solubility of 2 atom % strontium and the compound Sr_6Li_{23}. The eutectic temperature, 134°, is observed over the composition range 2–20.8 atom % strontium. The compound Sr_6Li_{23} is generated also by the peritectic reaction: liquid + $Sr_3Li_2 \rightleftarrows Sr_6Li_{23}$. This reaction occurs at 152° over the composition range 20–60 atom % strontium. A second peritectic reaction occurs at 198° over the composition range 40–89 atom % strontium in which the compound, Sr_3Li_2, is formed by the reaction: Sr_8Li + liquid $\rightleftarrows Sr_3Li_2$. A third peritectic reaction occurs at 496° over the composition range 81–97 atom % strontium to form the compound Sr_8Li: liquid + γ-Sr (h.c.p.) $\rightleftarrows Sr_8Li$ (h.c.p.). A congruent melting compound, m.p. 584°, approximating the formula Sr_7Li forms a eutectic with the b.c.c. solid solution δ-Sr at a composition of 88.5 atom % strontium. The eutectic isothermal is observed over the composition range 87–91 atom % strontium. One of the very interesting features of this system is the appearance of two inverse peritectic reactions in the strontium-rich alloys at 515 and 530°. Several cases involving retrograde melting processes have been reported in recent years.[11] The region of the diagram en-

(7) "Phase Equilibrium Studies of Systems Involving the Alkali and Alkaline Earth Metals," A.E.C. Report No. Chem. 1620.411P-6003R4, 1960, p. 54.

(8) F. E. Wang, A. J. King, and F. A. Kanda, *J. Phys. Chem.*, **66**, 2142 (1962).

(9) T. Ito, "X-ray Studies on Polymorphism," Maruzen Co. Ltd., Tokyo, 1950, pp. 187–228.

(10) M. Cernohorsky, *Acta Cryst.*, **14**, 108 (1961).

(11) W. D. Wilkinson, "Extractive and Physical Metallurgy of Plutonium and Its Alloys," Interscience Publ., New York, N. Y., 1960, pp. 149–167; A. S. Coffinberry and W. N. Miner, "The Metal Plutonium" (World Metallurgical Congress, 2nd) Chicago Univ. Press., 1961, pp. 252, 270–272; E. Grison, W. B. H. Lord, and R. D. Fowler, Eds., "Plutonium 1960. The Proceedings of the Second International Conference on Plutonium Metallurgy, Grenoble, France, 19–22 April 1960," London, Cleaver-Hume Press Ltd., 1961, pp. 276–280; K. A. Gschneidner, Jr., "Rare Earth Alloys," D. Van Nostrand Co., Inc., 1961, p. 145; A. E. Martin, I. Johnson, and H. M. Feder, *Trans. AIME*, **221**, (No. 4) 789 (1961).

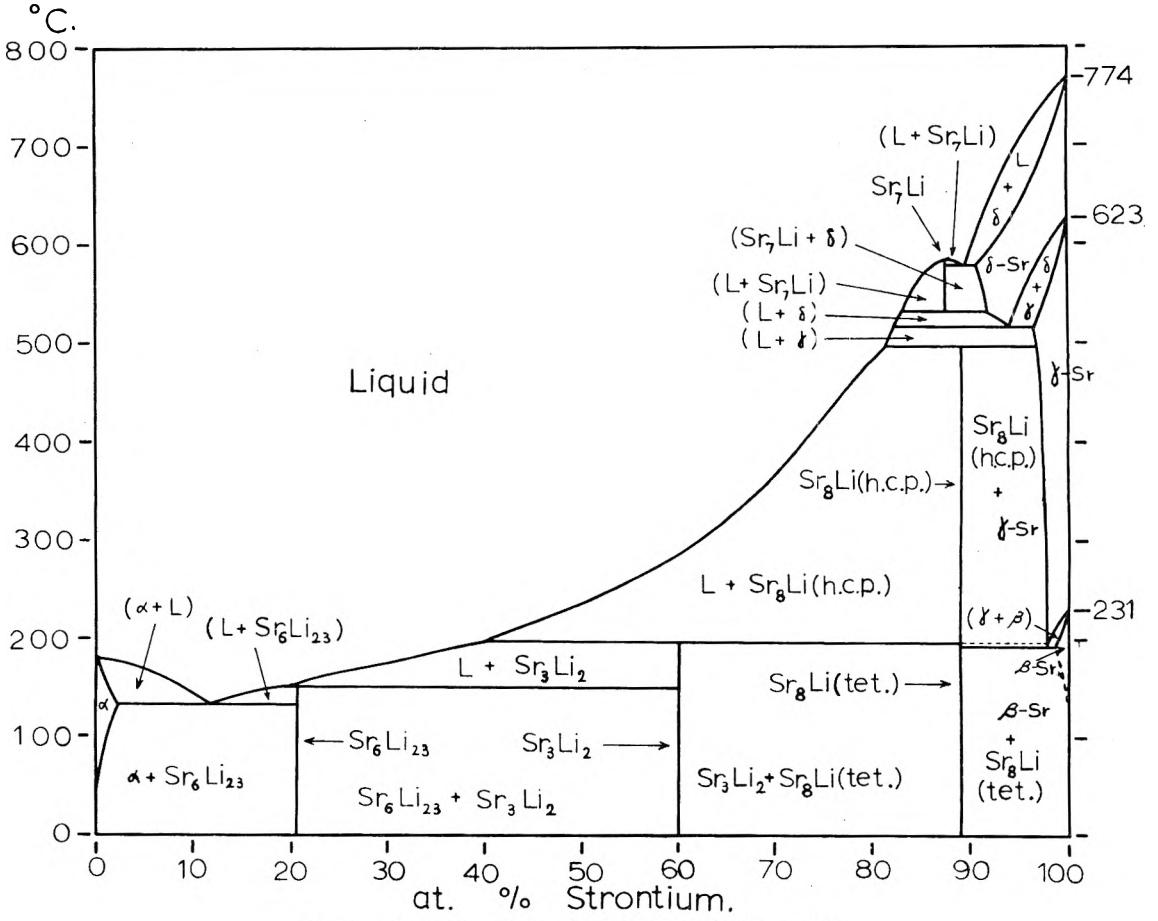

Fig. 1.—Complete phase diagram of the Li–Sr system.

compassing these reactions proved difficult to investigate and interpret.

Since X-ray evidence indicated only one compound, Sr_8Li (approximate composition of 89 atom % Sr), between 85 and 90 atom % strontium, the liquidus dome at 87 atom % strontium was at first considered to be a small immiscibility gap associated with a monotectic process. However, it was found that primary crystals formed in the metal the instant the liquidus was crossed, ruling out immiscibility. In order to identify the solid phase, high temperature X-ray studies were attempted using the high temperature powder camera, but all samples reacted with the Vycor capillaries when heated above 500°. This was contrary to the behavior of X-ray specimens above 97 atom % strontium, which could be heated safely in Vycor capillaries to temperatures exceeding 630°. Cooling and heating curves indicated isothermal processes occurring between 496 and 530°, but thermal pauses in the curves seemed erratic. Cooling curves gave the higher value and heating curves the lower value, but seldom did either curve give both. This seemed to indicate the possible occurrence of segregation accompanied by a lack of equilibration for solid–liquid reactions. In an effort to avoid this, specimens were stirred during the cooling process below the liquidus temperature. It then was found that samples above 87 atom % strontium could not be stirred below 578°, but at 530° they became quite mushy, more so between 496 and 515°, and finally solidified again at 496°. Since the thermal analyses were performed in closed iron crucibles, the system was modified in order to observe visually the sample while it cooled through this peculiar zone.

The sample was placed in a shallow iron thimble supported in a Pyrex container. Provision was made for admitting and maintaining an argon atmosphere, as well as suitable thermocouple attachments to the thimble. An iron rod was inserted and manipulated through an opening in the top of the unit so the sample could be probed during heating or cooling. Induction heating was utilized for these experiments. There was no doubt that the samples investigated solidified, remelted, and solidified again during a cooling cycle. The reverse processes occurred upon heating the sample. Since the retrograde melting seemed evident from these experiments, it was logical to suspect that the dome shaped liquidus defined a congruent melting compound, the composition of which approximated Sr_7Li. Since X-ray photographs taken below 496° displayed lines belonging only to Sr_8Li (h.c.p.) and/or γ-Sr solid solution, the disappearance of Sr_7Li by retrograde melting would account for the observed results. Two other isothermal processes must of necessity occur; δ-Sr solid solution (b.c.c.) must change to γ-Sr solid solution (h.c.p.) and Sr_8Li must form peritectically. The solid solution transformation could occur by a eutectoid reaction provided the eutectoid temperature was above the retrograde melting temperature of Sr_7Li, or by an

inverse peritectic reaction if the transition temperature was below. Since two isothermal reactions cannot occur concurrently without contradicting the phase rule, three consecutive horizontal isothermal boundaries must exist. It remained to locate these boundaries as well as to prove the nature of the reactions associated with them in addition to obtaining diffraction data for Sr_7Li. For this purpose the high temperature diffractometer[7] was constructed because the appearance or disappearance of characteristic diffraction peaks would delineate the melting point of Sr_8Li, the transition of δ-Sr solid solution to γ-Sr, and the lower melting point of Sr_7Li. Small iron boat-type sample holders designed for this camera allowed for investigating mushy specimens without fear of reaction with the container.

Samples in 1 atom % intervals were investigated over the range 80–100 atom % strontium. The appearance and growth of all solid phases in either cooling or heating cycles could be followed readily. It was found that Sr_7Li readily disappeared upon cooling below 530° but Sr_8Li formed slowly upon cooling below 496°. Upon heating, Sr_8Li readily melted at 496° but Sr_7Li formed slowly at 530°. This accounted for the variation of isothermal pauses observed in heating and cooling curves taken for these samples.

The boundaries of δ-Sr (b.c.c.) $\rightleftarrows$ γ-Sr(h.c.p.) and the eutectoid γ-Sr (h.c.p.) $\rightleftarrows$ β-Sr (f.c.c.) + Sr_8Li were readily determined using the high temperature X-ray camera for specimens above 97 atom % strontium, since none of these compositions undergoes the melting processes discussed above. Filed specimens usually suffer sufficient working so that room temperature samples display the γ-Sr structure. This results from the samples being transformed by the heat of filing into the γ-Sr form, which transforms very sluggishly into the room temperature β-Sr form. This has been observed consistently in all alkaline earth systems involving the (h.c.p.) $\rightleftarrows$ (f.c.c.) transition.[12,13]

The solid solubility limits of the β-Sr terminal solid solution at and near room temperature were too small to be determined by X-ray techniques.

The compound, Sr_8Li, undergoes a transition from the high temperature h.c.p. form to the low temperature tetragonal form somewhere in the vicinity of 196–198°. Figure 3 (A) and (B) illustrate two possibilities for this transition; in one case (A), it occurs above, and in (B) below the eutectoid temperature. Since both thermal analysis and high temperature X-ray data are certain to at best ±1°, the determination of three phase boundaries within a 2° interval is questionable. We know for certain that the h.c.p. form exists above 198° and the tetragonal form exists below 196°. It would be contradictory to the phase rule if the compound transition coincided with either one of these temperatures. However, coincidence of experimental temperature data is purely relative here since a difference of a fraction of a degree (experimentally indiscernible) between the two different transitions would be sufficient to allow for obeyance of the phase rule. It is for this reason that the transition is shown to be an extension of the 198° horizontal in Fig. 1 and 2. It could just as well be shown as an extension of the 196° horizontal.

(12) E. A. Sheldon, Ph.D. Dissertation, Syracuse University, 1949.
(13) J. C. Schottmiller, Ph.D. Dissertation, Syracuse University, 1958.

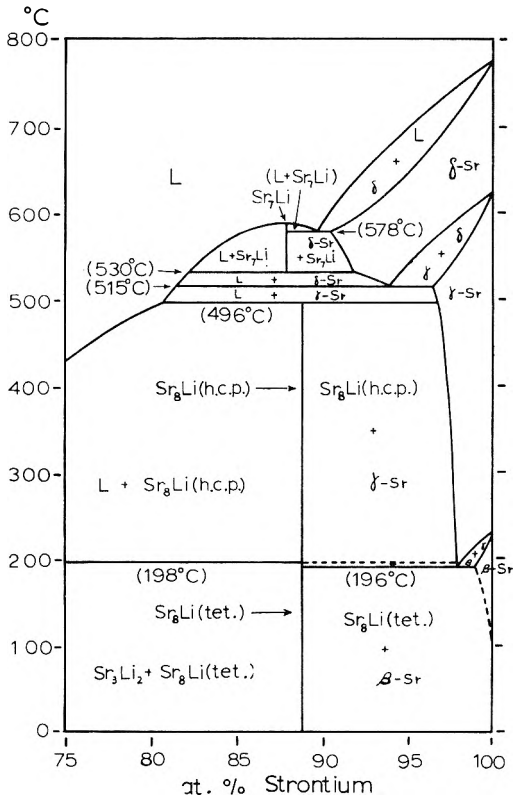

Fig. 2.—Detailed diagram of the Sr-rich portion of the Li–Sr system.

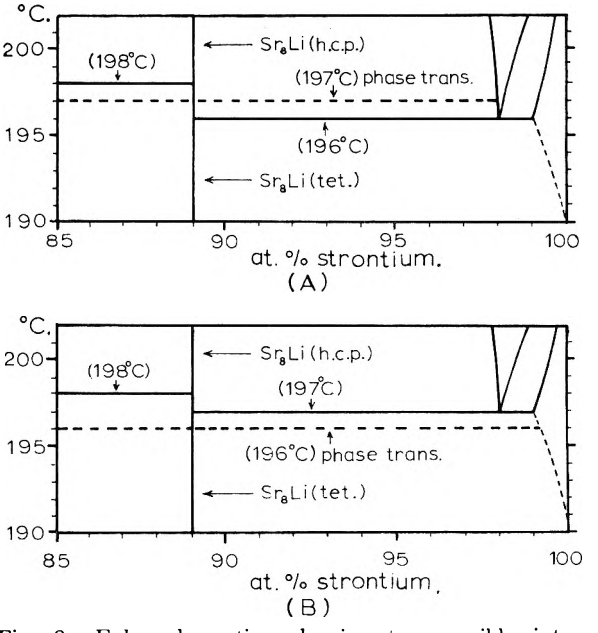

Fig. 3.—Enlarged portion showing two possible interpretations of the transitional temperature of Sr_8Li.

IV. Discussion

The extremely limited solid solubility at either end of the phase diagram must be due to the size factor,

which is unfavorable for interstitial[14] and substitutional[15] solid solution formation. The possibility that the observed retrograde melting band between 496 and 530° is the result of non-equilibrated reactions may be discarded for these reasons: (1) the reactions take place at fairly high temperature where reasonably fast reaction rates can be expected as evident by the fast γ-Sr ⇄ δ-Sr transitions observed in the solid state for alloys above 97 atom % Sr; (2) diffractometer studies showed that rapid melting occurred for Sr_7Li on cooling and Sr_8Li on heating and the subsequent reactions in either cycle, after the melting process and involving the liquid state, were the slow reactions; (3) prolonged soaking treatments above, below, and within this range of temperature had no effect on the nature of the reactions.

Sr_8Li in its high temperature form shows a number of X-ray diffraction lines which are common to the γ-Sr solid solution. A similar relationship exists between the low temperature form of the compound Sr_8Li and β-Sr solid solution. However, in each case the larger crystal lattice of the compound requires and displays extra diffraction values. Careful observation of the powder diffraction photographs and diffractometer readings with respect to d values and relative intensities for all compositions between 75 and 100 atom % Sr taken at various temperatures readily established the boundaries involving these phases as given in this paper.

In no case were there diffraction lines which could not be accounted for by the phases which should exist under these particular conditions. It also was found that as compositions approached 88 atom % Sr from either direction, not only did the characteristic diffraction patterns of the compound increase in intensity, but also the alloys became progressively more brittle.

Similarity of the diffraction patterns between the compound Sr_8Li (tet. and h.c.p.) and the Sr (β and γ) phase, respectively, suggests the majority of strontium atomic positions in the Sr_8Li lattices is essentially that of β-Sr and γ-Sr phases. Consequently, the lattice free energy in Sr_8Li probably is controlled by the strontium atoms and results in a transition similar to β-Sr ⇄ γ-Sr, and occurs at approximately the same temperature.

Acknowledgment.—This work was supported by the U. S. Atomic Energy Commission. The authors wish to acknowledge the assistance of Dr. D. V. Keller in the investigation and interpretation of the retrograde melting zone.

(14) G. Hagg, *Z. physik. Chem.*, **A12**, 33 (1931).

(15) W. Hume-Rothery, "Structure of Metals and Alloys," Institute of Metals, London, 1947.

THE CRYSTAL STRUCTURE OF Sr_6Li_{23} AND Sr_3Li_2

BY FREDERICK E. WANG, ADEN J. KING, AND FRANK A. KANDA

Chemistry Department, Syracuse University, Syracuse 10, N. Y.

Received March 29, 1962.

Two intermediate phases, Sr_6Li_{23} and Sr_3Li_2, of the strontium–lithium phase equilibrium system have been isolated in a single crystal form and their structures have been studied by single crystal X-ray methods. Sr_6Li_{23} was found to be cubic, $O_h^5 \simeq F_{m3m}$, with $a_0 = 14.88 \pm 0.05$ Å. Its density, 1.36 ± 0.05 g./cm.^{3}, corresponds to a cell content of four molecules. It appears to be isomorphous with Th_6Mn_{23}. The 24 strontium atoms lie on (e) with $x = 0.208$. The distribution of the 92 Li atoms is as follows: 4 on (b), 24 on (d), 32 on $(f)_1$, and 32 on $(f)_2$ with $x = 0.390$ and 0.150 for $(f)_1$, and $(f)_2$, respectively. Complete verification of the atomic positions of class (b) and (d) has been realized with the help of another compound, Sr_6Mg_{23}, isomorphous with Sr_6Li_{23} and Th_6Mn_{23}. Sr_3Li_2 crystallizes on a tetragonal lattice with $a_0 = 9.628 \pm 0.004$ Å., $c_0 = 8.550 \pm 0.003$ Å. Its diffraction effects are in accord with space group $D_{4h}^{14} \simeq F_{4_2/m,2_1/n,2/m}$. Its density of 2.15 ± 0.03 g./cm.^{3} requires a cell content of four molecules. The 12 strontium atoms are distributed as follows: 4 on (d), 4 on (f) with $x = 0.29$, and 4 on (g) with $x = 0.15$. Suitable space is available in the cell for the 8 lithium atoms on the equivalent positions (j) with $x = 0.11$ and $z = 0.37$.

I. Introduction

The two intermediate phases, Sr_6Li_{23} and Sr_3Li_2, were discovered in the investigation of the Li–Sr phase equilibrium system.[1] Both of these phases are formed by peritectic reactions and were found to melt incongruently at 152 and 198°, respectively. Single crystals were prepared and isolated by techniques described below. The X-ray data used in the structure determination of Sr_6Li_{23} were obtained from both powder and Weissenberg photographs and for Sr_3Li_2 Weissenberg photographs alone were used. The parameters of the Sr atoms in both phases were determined by Patterson–Harker and Fourier syntheses. Due to the low X-ray scattering coefficient of lithium relative to strontium, the parameters of the lithium are based largely upon space considerations. The positions selected for these atoms are in accord with their respective space groups and the calculated interatomic distances are within acceptable limits.

(1) F. E. Wang, F. A. Kanda, and A. J. King, *J. Phys. Chem.*, **66**, 2138 (1962).

II. Experimental

Growth of Single Crystals.—The composition of Sr_6Li_{23} is so close to that at which its peritectic isothermal boundary intersects the liquidus[1] that a melt corresponding in composition to Sr_6Li_{23} crystallizes almost as though it were a congruent melting phase. An alloy containing 79.2 atom % Li and 20.8 atom % Sr was prepared by melting and homogenizing at a temperature 100° above the peritectic temperature (152°) in the thermal analysis equipment described in the preceeding article.[1]

After cooling to room temperature, the brittle alloy was transferred to a glass tube containing dry mineral oil. Since the density of the alloy (1.3 g./cm.^{3}) was greater than that of the oil (0.8 g./cm.^{3}), melting it (m.p. 152°) under oil

(b.p. 230°) provided a convenient method for subsequent single crystal growth and pulling. Single crystals for use in the X-ray studies were prepared by drawing alternate layers of oil and molten alloy into thin walled Pyrex capillary tubes (0.5 mm. o.d.). The tubes then were withdrawn very slowly from the hot oil so that crystallization progressed down the capillary. Practically all of the single crystals obtained in this manner displayed [110] directions parallel to the axis of the capillary.

Single crystals of the Sr_3Li_2 phase could not be grown in this manner since its composition was too far removed from the junction of the peritectic isothermal and the liquidus line.[1] Sr_3Li_2 forms by reaction of liquid with solid Sr_8Li for alloys of higher strontium content than 40 atom %. It is difficult or even impossible to obtain homogeneous single crystals of suitable size in a diffusion process of this sort. However, primary crystals of Sr_3Li_2 form from cooled melts ranging in composition between 21 and 40 atom % Sr. These crystals and their liquid matrix alloy react at 152° to form Sr_6Li_{23} by a peritectic reaction. The crystals of Sr_3Li_2 used in this investigation were prepared in the following manner. A 40 atom % Sr alloy was melted and homogenized at 270° and cooled at a rate of 0.5 deg./min. to 160°. The alloy and container were held at this temperature for 2 hr., and finally quenched in ice water. The slow cool to 160° and subsequent soaking assured good crystal formation. The quench prevented the crystals from reacting with the remaining liquid to form Sr_6Li_{23}. Single crystals of Sr_3Li_2 trapped in the alloy could be separated readily from the matrix under oil. The crystals obtained this way then were sealed under oil in a capillary.

Structure Determination. Sr_6Li_{23}.—Weissenberg photographs of the zero, second, and fourth layers in the [110] direction were taken with filtered Cu $K\alpha$ radiation. Visual estimates of the intensities were made by use of the multiple film technique.[2] The usual Lorentz-polarization corrections were applied. The absorption correction was not made because the effect was computed to be negligible. The systematic absence in h,k,L, of mixed odd and even, and the symmetry for these h,k,L, indicated a f.c.c. cell with a parameter of $a_0 = 14.88 \pm 0.03$ Å. The density of the crystals was determined by the flotation method using xylene and carbon tetrachloride as the miscible liquids. The average of five determinations was 1.36 ± 0.05 g./cm.^{3}. On the basis of the thermal analysis, the compound composition was within the range 20–21 atom % strontium. Three possible formulas of the compound which fall within this range are $SrLi_4$, Sr_8Li_{31}, and Sr_6Li_{23}. On the basis of the cell parameters and the density, the number of molecules in the unit cell for these were calculated to be 23.4, 3.1, and 3.9, respectively. Since a f.c.c. structure should have a number of molecules which is a multiple of four, Sr_6Li_{23} seemed to be the most likely choice.

TABLE I

IDENTIFICATION OF THE PEAKS OBSERVED IN FIG. 1

Peak	Identification	Position (x)
A	Origin vector peak	0.00
B	24 lithium atoms in class (d)[a]	.116
C	32 lithium atoms in class $(f)_1$	.220
D	32 lithium atoms in class $(f)_2$	.300
E	24 strontium atoms in class (e)	.416

[a] See discussion concerning the assignment of class (d) to these 24 Li atoms.

TABLE II

PARAMETERS OF ATOMIC POSITIONS IN Sr_6Li_{23} AS DETERMINED FROM PATTERSON–HARKER PEAKS COMPARED WITH THOSE OF Th_6Mn_{23}, REPORTED BY FLORIO, *et al.*[3]

Atom class	Sr_6Li_{23}	Th_6Mn_{23}
(e)	$Sr(x) = 0.208$	$Th(x) = 0.203$
$(f)_1$	$Li(x) = .390$	$Mn(x) = .378$
$(f)_2$	$Li(x) = .150$	$Mn(x) = .178$
(d)	$Li(x)^a = .058$	$Mn(x) = .250$

[a] See discussion concerning the assignment of class (d) to these 24 Li atoms.

(2) J. Robertson, *J. Sci. Instr.*, **20**, 175 (1943).

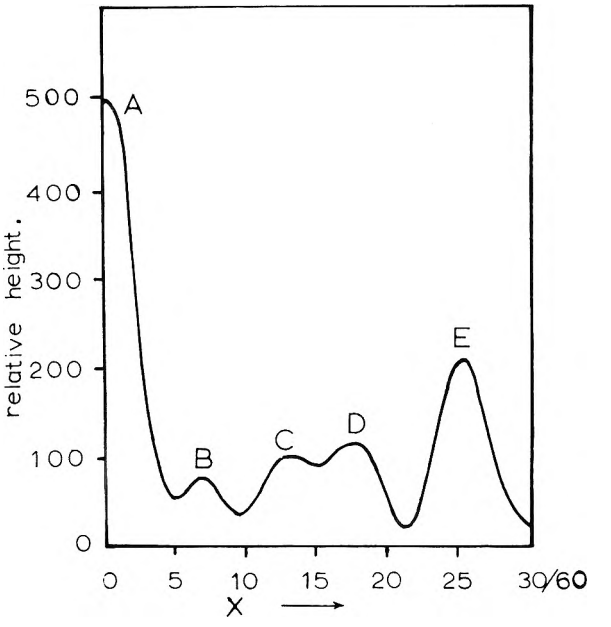

Fig. 1.—One-dimensional Patterson–Harker synthesis of Sr_6Li_{23}.

TABLE III

ATOMIC POSITIONS AND PARAMETERS OF Sr_6Li_{23}

Add ($1/2$, $1/2$, 0; $1/2$, 0, $1/2$; 0, $1/2$, $1/2$) to each set	
24 Sr (e);	x, 0, 0; 0, x, 0; 0, 0, x $\bar{x}$, 0, 0; 0, $\bar{x}$, 0; 0, 0, $\bar{x}$ with $x = 0.208$
4 Li (b);	$1/2$, $1/2$, $1/2$
24 Li (d);	0, $1/4$, $1/4$; $1/4$, 0, $1/4$; $1/4$, $1/4$, 0; 0, $1/4$, $3/4$; $3/4$, 0, $1/4$; $1/4$, $3/4$, 0
32 Li $(f)_1$;	x, x, x; $x, \bar{x}, \bar{x}$; $\bar{x}, x, \bar{x}$; $\bar{x}, \bar{x}, x$ $\bar{x}, \bar{x}, \bar{x}$; $\bar{x}, x, x$; $x, \bar{x}, x$; $x, x, \bar{x}$ with $x = 0.390$
32 Li $(f)_2$;	Same as (f), except $x = 0.150$

Additional support for this selection was obtained from the crystal structure data for Th_6Mn_{23} (formerly considered to be $ThMn_4$).[3]

The atomic radii ratio of Th/Mn considering an eight coördination number was 1.388. For similar coördination, the Sr/Li ratio is 1.381. On the basis of the similarities in formulas and radii ratio, the space group $O_h^5 \simeq F_{m3m}$ found for Th_6Mn_{23} seemed a logical choice for Sr_6Li_{23}.

Subsequently, a one-dimensional Patterson–Harker synthesis was performed using 65 symmetry-independent observed reflections; the result is given in Fig. 1.

The identification of each peak was made on the basis of their relative heights when compared to the origin peak and is given in Table I.

On this basis, peak B appeared to possess the right weight to be assigned to 24 Li atoms but this did not coincide with class (d) positions. The latter, being special positions, require a Patterson peak at $x = 30/60$ (0.50) which was missing from the vector plot. It can be seen from Table II that with the exception of these 24 Li atoms, the remainder of the parameters are in excellent agreement with those of Th_6Mn_{23} and present a strong argument for isomorphism existing between the compounds. Unfortunately, the low scattering ability of Li compared to Sr did not allow for resolution of the choice of parameters for these 24 Li atoms. Calculated structure factors using the Patterson derived parameter (0.058) and the Th_6Mn_{23} parameter (0.250) were equally good in comparison with the observed values. The proper choice of parameters for these Li atoms was finally settled by the determination of the crystal structure of Sr_6Mg_{23}.[4]

(3) J. V. Florio, *et al.*, *Acta Cryst.*, **5**, 451 (1952).

(4) C. F. Miskell, Ph.D. Thesis, in progress.

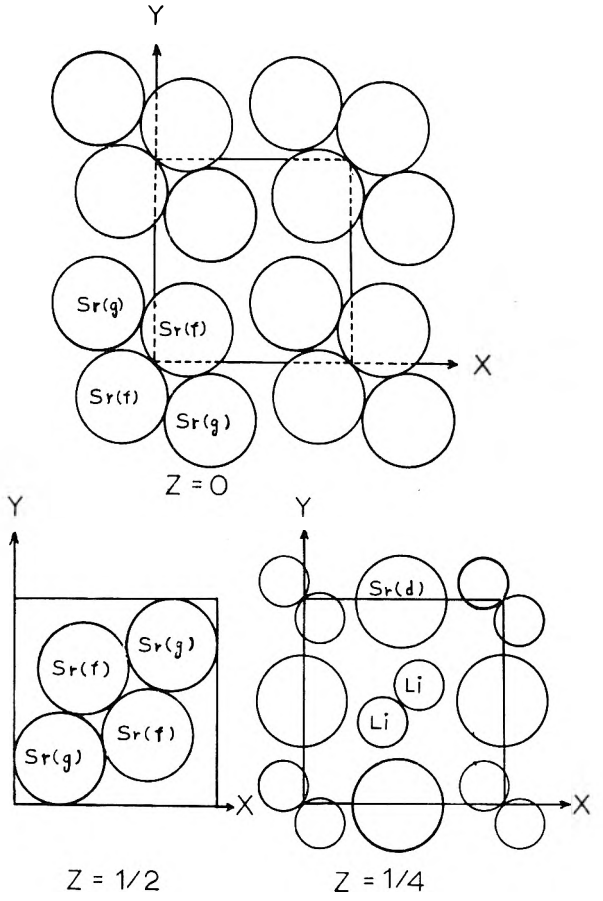

Fig. 2.—Distribution of strontium atoms in the x-y plane at $z = 0$, $z = 1/2$, and $z = 1/4$: lithium atoms shown in the $z = 1/4$ projection lie at $z = 0.37$.

Sr_6Mg_{23} was found to be isomorphous with Sr_6Li_{23}. This recently has been verified by Gladyshevskii, *et al.*[5] Sr_6Mg_{23} has a lattice constant of 14.90 Å., which is very close to the 14.88 Å. value of Sr_6Li_{23}. X-Ray powder photographs of both compounds, side by side, are virtually indistinguishable relative to d values and the pattern of intensities. Calculated structure factors were determined by assigning the parameters of Sr_6Li_{23} to the 24 Sr(e), 4 Mg(b), 32 Mg(f)$_1$, and 32 Mg(f)$_2$. The contributions of these atoms were subtracted from 206 symmetry independent properly adjusted observed structure factors and a complete 3-dimensional difference Fourier was synthesized in order to determine the positions of the remaining 24 Mg atoms. The result proved conclusively that the remaining 24 Mg atoms belong to class (d) for this space group. Thus, it can be concluded that the peak B in Fig. 1 is fortuitous and may be due to the short termination of the Fourier coefficients and not due to 24 Li atoms. The final parameters of Sr_6Li_{23} are given in Table III and verify that Sr_6Li_{23} and Th_6Mn_{23} are isomorphous.

The packing model of Sr_6Li_{23} is shown in Fig. 4. The 3-dimensional Fourier synthesis showed that no Mg atom exists in the center of the octahedral arrangement of Sr atoms, so it is assumed that the same restriction pertains to lithium.

Since, as previously described, the rotation axis of the single Sr_6Li_{23} crystal coincided with the [110] direction yielding few observed $F(h\ k\ l)$ values, the observed data were augmented by utilizing additional diffraction intensities from powder photographs.

This proved convenient in this case because the crystal belonged to the cubic system. When an observed intensity was due to diffraction from more than one plane, as frequently is the case in powder diffraction, the intensity contributions from individual planes were calculated separately and then added together. The final calculated values of intensities using the parameters listed in Table III are compared with observed intensities and given in Table IV.[6] The correctness of the structure is evident from the close agreement between calculated and observed intensities. The reliability factor, based on intensities, $R = (||I_o| - |Ic||)/|I_o|$ for 90 symmetry-independent diffractions is 0.26. The (111) was omitted from this calculation because of abnormal extinction.

(5) E. I. Gladyshevskii, P. I. Kripyakevich, Yu. B. Kuzma, and M. yu. Teslyuk, *J. Crystallography* (Soviet Physics), **6**, No. 5, 615 (1962).

TABLE V

PROPOSED AND CONFIRMED ATOMIC POSITIONS AND PARAMETERS FOR Sr_3Li_2

4 Sr (d)	$0, 1/2, 1/4;\ 1/2, 0, 1/4;\ 0, 1/2, \bar{1}/4;\ 1/2, 0, \bar{1}/4,$
4 Sr (g)	$x, \bar{x}, 0;\ \bar{x}, x, 0,$
	$1/2 + x, 1/2 + x, 1/2;\ 1/2 - x, 1/2 - x, 1/2,$
	with $x = 0.15$
4 Sr (f)	$x, x, 0;\ \bar{x}, \bar{x}, 0$
	$1/2 + x, 1/2 - x, 1/2;\ 1/2 - x, 1/2 + x, 1/2,$
	with $x = 0.26$
8 Li (j)	$x, x, z;\ \bar{x}, \bar{x}, z;\ x, x, \bar{z};\ \bar{x}, \bar{x}, \bar{z}$
	$1/2 + x, 1/2 - x, 1/2 + z;\ 1/2 - x, 1/2 + x, 1/2 + z$
	$1/2 + x, 1/2 - x, 1/2 - z;\ 1/2 - x, 1/2 + x, 1/2 - z$
	with $x = 0.11$ and $z = 0.37$

Sr_3Li_2.—Cu Kα radiation was employed to take Weissenberg photographs of single crystals about both the a- and c-axes. The tetragonal cell was found to have the lattice constants of: $a_0 = b_0 = 9.628 \pm 0.004$ Å. and $c_0 = 8.550 \pm 0.003$ Å. In this unit cell there are four moelcules of Sr_3Li_2 required by the density of 2.15 g./cm.^{3}. The diffraction characteristics of 228 observed and identified reflections showed $k + L = 2n$ for $(0\ k\ L)$, $L = 2n$ for $(0\ 0\ L)$ and $k = 2n$ for $(0\ k\ 0)$, where $(h\ k\ L)$ and $(h\ h\ 0)$ had no restrictions. These characteristic reflections lead to three possible space groups: $D_{4h}{}^{14} = P_{4_2/m,2_1/n,2/m}$, $C_{4v}{}^4 = P_{4_2,n,m}$, and $D^3{}_{2d} = P\bar{4}_1n_12$. $D_{4h}{}^{14}$ was the only one which was centrosymmetric. The choice of the centrosymmetric space group over the non-centrosymmetric ones as well as the strontium atomic positions was arrived at through a combination of trial and error methods alone. The atomic positions derived this way met the symmetry operations in the space group $D_{4h}{}^{14}$ and are given in Table V and pictorially given in Fig. 2.

TABLE VII

CALCULATED INTERATOMIC DISTANCES IN Sr_3Li_2

Sr (f)——Sr (f)	4.092 ± 0.010 Å.
Sr (g)——Sr (f)	4.457 ± .009 Å.
Sr (d)——Sr (f)	4.242 ± .008 Å.
Sr (d)——Sr (g)	4.057 ± .008 Å.
Li (j)——Li (j)	2.99 ± 0.04 Å.
Li (j)——Sr (d)	4.03 ± .03 Å.
Li (j)——Sr (f)	3.44 ± .02 Å.
Li (j)——Sr (g)	4.02 ± .03 Å.

The reliability factor, $R = (\Sigma||F_o| - |F_c||)/\Sigma|F_o|$ obtained from these parameters was 0.17 for 228 symmetry-independent diffractions. Following this a two-dimensional Fourier synthesis was performed. The result as shown in Fig. 3 substantiated the validity of the space group and the strontium atomic positions. The atomic positions of the lithium atoms could not be determined unequivocally through the reflection intensities because of their small X-ray scattering power relative to strontium. The only alternative was through spatial consideration, which in this particular case was rather straightforward. After the strontium atoms were placed throughout the cell, sufficient but restricted spaces remained to accommodate the lithium atoms. The param-

(6) Tables IV and VI of this paper have been deposited as Document Number 7183 with the ADI Auxiliary Publications Project, Photoduplication Service, Library of Congress, Washington 25, D. C. A copy may be secured by citing the Document Number and by remitting $1.25 for photoprints, or $1.25 for 35 mm. microfilm. Advance payment is required. Make check or money order payable to: Chief, Photoduplication Service, Library of Congress.

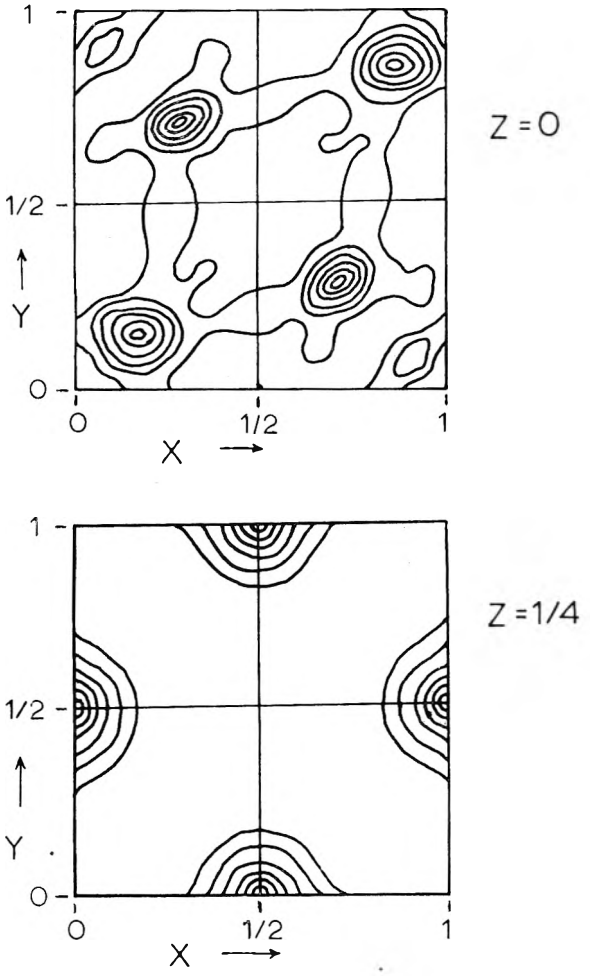

Fig. 3.—Electron density map of Sr_3Li_2 at $z = 0$ and $z = 1/4$, respectively (arbitrary units).

eters for these then were calculated by considering the lithium atoms to occupy a position equidistant between the strontium atoms surrounding the space. From this computation, which also met the space group D_{4h}^{14} symmetry requirements, the lithium atoms were assumed to be in the equivalent position of (j) as shown in Table V. The atomic positions of the strontium were refined by the least square refinement method using an IBM 704 computer and the program of W. R. Busing and H. A. Levy. After three cycles of least square refinements, the R value including all the lithium atoms was reduced to 0.15. The only parameter which shifted significantly (11%) belonged to the Sr(f) group and this gave a final parameter of 0.291 for this group.

The complete list of the observed and calculated structure factors is given in Table VI[6] and the interatomic distances are given in Table VII.

III. Discussion

The positions of Sr and Li atoms in Sr_3Li_2 are shown for three different layers of the cell in Fig. 2.

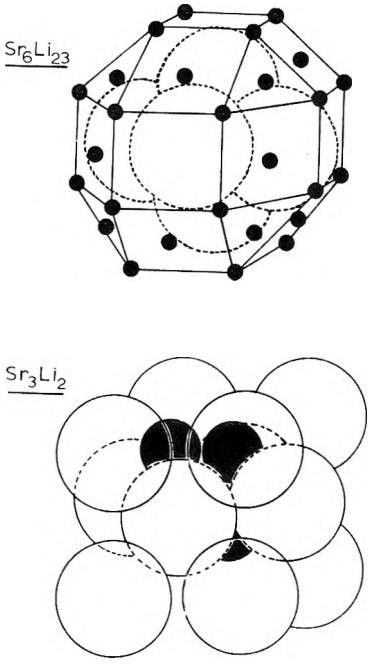

Fig. 4.—Packing models of Sr_6Li_{23} and Sr_3Li_2: Sr_6Li_{23}: small solid circle, Li (d), $(f)_2$, and $(f)_2$; large open circle, Sr (e); Sr_3Li_2: small solid circle, Li (j); large open circle, Sr (d), (f), and (g).

The packing model is shown in Fig. 4. In the planar diamond shaped arrangement of four Sr atoms at $z = 0$, the two Sr atoms which are closest to each other belong to the (f) class whereas the other two belong to the (g) class as shown in Fig. 2. The four Sr atoms and four Li atoms on the $z = 1/4$ plane belong to the (d) and (j) classes, respectively.

From the interatomic distances obtained (Table VII) the shortest radius of Sr atom was calculated to be 2.03 Å., which is about 2.9 % less than the 2.1 Å. radius given for metallic strontium by Pauling.[7] In the intermetallic compound, this much deviation of atomic radii is not considered unusual.[8] Analogous calculation showed the radius of the Li atom to be 1.48 Å., which deviates by only 1.1% from the radius given by Pauling.

Acknowledgment.—We wish to thank the U. S. Atomic Energy Commission for their financial support of this work. A word of appreciation is also due to Professor W. N. Lipscomb of Harvard University for giving us the computer time for the least square refinement of Sr_3Li_2, and to Richard A. Van Dyck of the General Electric Electronics Park Computer Laboratory, Syracuse, N. Y., for the use of the IBM-7090 computer.

(7) L. Pauling, *J. Am. Chem. Soc.*, **69**, 543 (1947).
(8) F. Laves, *Trans. Am. Soc. Metals*, **48A**, 124 (1956).

THE SORPTION OF ORGANIC VAPORS BY POLYOLEFINS

BY K. P. KWEI

Newark College of Engineering, Newark, New Jersey

AND T. K. KWEI

Interchemical Corporation, Central Research Laboratory, New York, N. Y.

Received April 2, 1962

The equilibrium sorption of aliphatic and aromatic hydrocarbons by isotactic and by completely amorphous polypropylene was studied. The contribution of the enthalpy change of network deformation is analyzed. In addition, the average molecular weight of polypropylene chain between crystalline regions is calculated.

Introduction

The sorption of organic vapors by polyethylene at room temperature is accompanied by a significant change in enthalpy.[1] Thus the isosteric enthalpy of sorption,[2] defined by eq. 1

$$\left(\frac{\partial \ln a_1}{\partial T}\right)_{v_1} = -\frac{(\Delta\bar{H}_1)_{sorp}}{RT^2} \qquad (1)$$

can be estimated from the data of Rogers and co-workers[1] to be in the neighborhood of 1 kcal./mole for the system hexane–polyethylene in the temperature range 0 to 30°. The enthalpy of sorption is composed of enthalpies of mixing, $(\Delta\bar{H}_1)_{mix}$, and of network deformation, $(\Delta\bar{H}_1)_{el}$. It is customary to neglect the latter quantity,[2] with the assumption that the elastic properties of the network structure do not deviate, to any significant extent, from ideal rubber elasticity. The enthalpy of vapor sorption then can be equated to the enthalpy of mixing, which conventionally is expressed in terms of the net interaction energies of solvent–polymer pair contacts.[2] It is difficult to understand, however, that the pair contact interaction energy of two chemically alike substances such as hexane and polyethylene can reach the magnitude of 1 kcal./mole. The sorption of toluene vapor by polystyrene,[3] and the sorption of various C_3 to C_5 aliphatic hydrocarbon vapors by polyisobutylene[4] show no temperature coefficient; hence $(\Delta\bar{H}_1)_{sorp}$ for the above systems must be negligible. The heat of mixing *n*-heptane with polyisobutylene (PIB) also has been measured calorimetrically by Watters and co-workers[5]; $(\Delta\bar{H}_1)_{mix}$ can be calculated from their data to be slightly negative, *i.e.*, about −60 cal./mole. Recently, Flory, Ciferri, and Chiang[6] measured the temperature coefficient of the swelling of the radiation-crosslinked PE by *n*-octacosane at 140–180° (above the melting point of PE crystallites) and concluded that the heat of mixing was almost negligible. The vapor sorption experiments by Rogers and co-workers were carried out near room temperature, at which the amorphous regions of the PE film were under severe strain as a result of the restriction imposed by the neighboring crystallites. It is possible that the deformation of such a network produces changes in chain conformation with a concomitant change in the potential energy of the network.[7] The above situation is unlikely to occur when amorphous polymers are used as absorbents. There is reason to suspect, therefore, that the difference between the $(\Delta\bar{H}_1)_{sorp}$ values for the sorption of aliphatic hydrocarbons by PE and by PIB originates, not from the difference in $(\Delta\bar{H}_1)_{mix}$, but rather from the contribution of the $(\Delta\bar{H}_1)_{el}$ term.

The present investigation was undertaken to elucidate the contribution of $(\Delta\bar{H}_1)_{el}$ to the sorption of organic vapors by polycrystalline materials. Isotactic polypropylene (PP) film was used because no change in the crystallinity of PP with temperature has been reported between 25 and 60°; the ambiguity arising from the phenomenon of crystallite "melt-out,"[8] such as in the case of low density PE, thus is minimized. The significance of energy and entropy changes in the swelling of a non-ideal network is discussed briefly. In addition, the length of the repeating units in the amorphous region of PP is estimated. For the purpose of comparison, experiments also were conducted with completely amorphous PP.

Theoretical Considerations

Enthalpy Change in Network Swelling.—According to the current viewpoint, the energy change in the deformation of a network structure may arise from the change in chain conformation from the low energy to the high energy state. It is assumed that

$$\Delta H_{el} = gw \qquad (2)$$

where g is the number of low energy-to-high energy conversions, each of which is characterized by an energy change w. In the swelling of a polymer by solvent molecules, the polymer chain segments, originally occupying a volume V, are redistributed in a volume $V + \Delta V$, where ΔV is the volume of the solvent imbibed by the polymer at equilibrium. Many segments of the polymer chain are displaced by the solvent molecules from their original posi-

(1) C. E. Rogers, V. Stannett, and M. Szwarc, *J. Polymer Sci.*, **45**, 61 (1960).

(2) P. J. Flory, "Principles of Polymer Chemistry," Cornell University Press, Ithaca, N. Y., 1953, chapters 11–13; *J. Am. Chem. Soc.*, **78**, 5222 (1956); P. J. Flory, C. A. J. Hoeve, and A. Ciferri, *J. Polymer Sci.*, **34**, 337 (1959).

(3) C. E. H. Bawn, R. F. J. Freeman, and A. R. Kammaliddin, *Trans. Faraday Soc.*, **46**, 677 (1950).

(4) S. Prager, E. Bagley, and F. A. Long, *J. Am. Chem. Soc.*, **75**, 2742 (1953).

(5) C. Watters, H. Daust, and M. Rinfret, *Can. J. Chem.*, **38**, 1087 (1960).

(6) P. J. Flory, A. Ciferri, and R. Chiang, *J. Am. Chem. Soc.*, **83**, 1023 (1961).

(7) A. Ciferri, C. A. J. Hoeve, and P. J. Flory, *ibid.*, **83**, 1015 (1961).

(8) A. S. Michaels and H. J. Bixler, *J. Polymer Sci.*, **50**, 393 (1961).

tions in the lattice to new positions. In the course of this process, some of the displaced segments or their neighbors will be forced to assume conformationally high energy states. As a first approximation, it is assumed that g is proportional to the number of such displacements, or the number of solvent–polymer contacts, p_{12}

$$g = qp_{12} \tag{3}$$

provided that the tendency for the solvent molecules to form clusters[9] is small. The factor q is the probability that each solvent–polymer contact is accompanied by a change in the chain conformation of the polymer.

According to the lattice theory of polymer solutions,[2]

$$p_{12} = zn_1v_2 \tag{4}$$

where n_1 is the number of solvent molecules, v_2 is the volume fraction of the polymer, and z is the lattice coördination number. Upon substitution in eq. 2, there is obtained

$$\Delta H_{el} = \epsilon_h n_1 v_2 \tag{5}$$

and

$$\epsilon_h = qzw \tag{6}$$

Differentiation of ΔH_{el} with respect to n_1 gives

$$(\Delta \bar{H}_1)_{el} = \left(\frac{\partial \Delta H_{el}}{\partial n_1}\right) = \epsilon_h v_2^2 \tag{7}$$

It readily can be seen that $(\Delta \bar{H}_1)_{el}$ is a function of ϵ_h, which is characteristic of the network, but is independent of the nature of the swelling solvent. Eq. 7 also demands that $(\Delta \bar{H}_1)_{el}$ is directly proportional to v_2^2.

Swelling Equilibrium.—The equation for swelling equilibrium now can be rewritten to include the energy contribution of network deformation. The elastic free energy ΔF_{el} involved in the expansion of a network structure is[2]

$$\Delta F_{el} = \Delta H_{el} - T\Delta S_{el}$$

and

$$N_{av}\left(\frac{\partial \Delta F_{el}}{\partial n_1}\right) = RT\left[\frac{\rho \bar{V}_1}{M_c}\left(\langle\alpha\rangle_0^2 v_2^{1/3} - \frac{2}{f}v_2\right) + \epsilon_h v_2^2\right]$$

At swelling equilibrium, the equation of state may be written as

$$\ln a_1 = \ln v_1 + v_2 + \chi' v_2^2 + \frac{\rho \bar{V}_1}{M_c}\left(\langle\alpha\rangle_0^2 v_2^{1/3} - \frac{2}{f}v_2\right) + \frac{\epsilon_h}{RT}v_2^2 \tag{8}$$

Equation 8 is of the same form as the conventional one except that $(\chi' + \epsilon_h/RT)v_2^2$ replaces $\chi_1{}^{1/2}$. The state of randomness of the chains of the amorphous fraction of a polycrystalline polymer may differ from that of completely amorphous polymer chains. The parameter χ' of our interest is not necessarily the same as χ_1. The quantities $d\chi'/dT$ and $d\chi_1/dT$, however, are identical because both represent pair contact interaction energies. An alternate form of eq. 8 is

$$\ln a_1 = \ln v_1 + v_2 + \left(\chi_1 + \lambda + \frac{\epsilon_h}{RT}\right)v_2^2 + \frac{\rho \bar{V}_1}{M_c}\left(\langle\alpha\rangle_0^2 v_2^{1/3} - \frac{2}{f}v_2\right) \tag{9}$$

where λ represents the difference between χ' for polycrystalline material and χ_1 for the completely amorphous polymer.

The evaluation of the various parameters ϵ_h, λ, and M_c from the vapor sorption data can be carried out as follows; the crystallites are considered as cross-link junctions with a functionality f equal to twice the number of chains in the cross-section of a crystallite.[10] The term $(2^1/_2)/f$ can be neglected because f is much greater than $2v_2$. The molecular weight of cross-linked chain M_c is the average molecular weight between crystallites. Upon simplification and rearrangement,[9] eq. 9 becomes

$$\left(\ln \frac{a_1}{v_1} - v_2\right)\Big/ v_2 = \left(\chi_1 + \lambda + \frac{\epsilon_h}{RT}\right) + \frac{\rho_1 \bar{V}}{M_c}\langle\alpha\rangle_0^2 v_2^{-5/3} \tag{10}$$

A plot of the left hand side *vs.* $\rho \bar{V}_1 v_2^{-5/3}$ will yield a straight line with $\langle\alpha\rangle_0^2/M_c$ as the slope and $(\chi_1 + \lambda + \epsilon_h/RT)$ as the intercept with the ordinate.

If a suitable solvent can be found so that the net pair contact energy of the polymer and the solvent is zero, the quantity $d\chi'/dT$ or $d\chi_1/dT$ is zero. A plot of $(\chi_1 + \lambda + \epsilon_h/RT)$ *vs.* $1/T$ then will result in a straight line with ϵ_h/R as its slope. The intercept of this straight line with its ordinate is $(\chi_1 + \lambda)$. The value of ϵ_h obtained by this procedure must agree with eq. 7, if the above analysis is self consistent.

In order to establish whether the net pair contact energy of a given solvent with the amorphous fraction of the isotactic polypropylene film is zero, the sorption of organic vapors by a completely amorphous polypropylene sample also was studied. (Many aliphatic hydrocarbons fulfill this requirement.) The parameter χ_1 can be obtained readily from the relationship[4]

$$\ln a_1 = \ln v_1 + v_1 + \chi_1 v_2^2 \tag{11}$$

Experimental

Materials.—Completely amorphous polypropylene (sample A) from Hercules Powder Co. has limited solubility in xylene at room temperature. Film was cast from xylene solution over mercury at 70°, followed by subsequent evacuation *in vacuo* to remove any residual solvent. The density of the resulting material is 0.854 g./cm.^{3} at 25° and 0.827 g./cm.^{3} at 50°.

Isotactic polypropylene film (sample B) from Avisun Co. was used. The density of the film is 0.908 g./cm.^{3} at 16° and

(9) B. H. Zimm and J. L. Lundberg, *J. Phys. Chem.*, **60**, 425 (1956).

(10) C. E. Rogers, V. Stannett, and M. Szwarc, *ibid.*, **63**, 1406 (1959).

TABLE I

SUMMARY OF THE SORPTION DATA

Polymer	Solvent	Temp., °C.	χ_1	$\frac{M_0}{\langle\alpha\rangle_0^2}\left(\chi_1+\lambda+\frac{e_h}{RT}\right)$	$(\chi_1+\lambda)$	$\frac{e_h}{RT}$	λ
Amorphous PP	Hexane	30–50	0.27				
Isotactic PP	Hexane	35		227	−0.005	−2.4	2.35	−2.7
		40		232	− .035			
		49.3		232	− .100			
	Heptane	40		250	− .11	−2.4	2.31	−2.7
		50		250	− .175			
		60		250	− .245			
		70		250	− .295			
	2,2,4-Trimethylpentane	60		232	− .49			
	Benzene	40		250	.394			
		50		250	.30			
		60		250	.206			

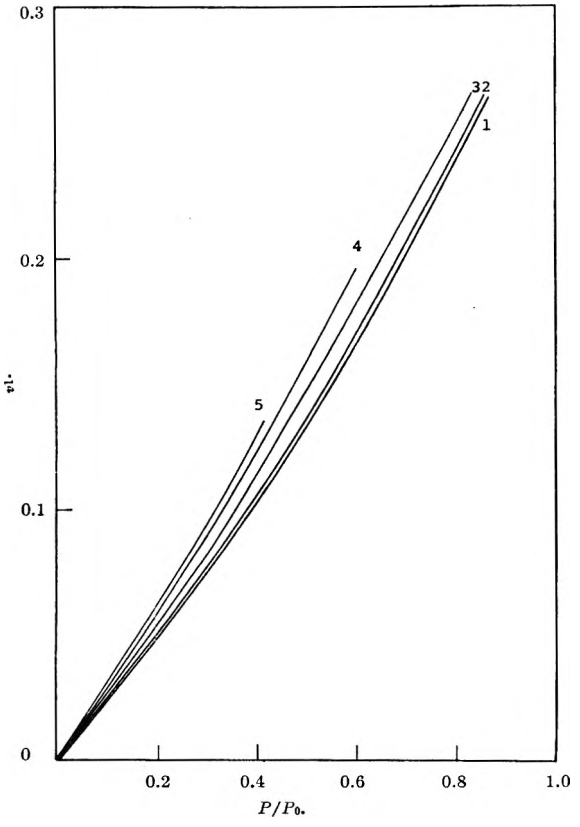

Fig. 1.—Sorption isotherms of aliphatic hydrocarbons by isotactic polypropylene: curve (1), hexane 35°; (2) hexane, heptane 40°; (3) hexane, heptane 50°; (4) heptane, 2,2,4-trimethylpentane 60°; (5) heptane 70°.

0.906 g./cm.³ at 21.7°. The percentage of crystallinity of the sample is estimated from Natta's formula[11] to be approximately 62%. In all our calculations, the weight of the polymer refers to the weight of the amorphous portion of the material.

The density of the amorphous fraction of isotactic polypropylene has been reported by various investigators[12] to be in the range 0.850 to 0.856 g./cm.³ at 25°. The latter value was preferred in view of the fact that the completely amorphous sample has a density of 0.854 g./cm.³ at the same temperature. The variation of the density of the amorphous fraction of isotactic PP with temperature is not known with certainty. Within the temperature range of the present investigation, it is assumed to be similar to that of the amorphous fraction of polyethylene,[13] namely, about 0.05%/°C. Any inaccuracy introduced by this approximation will not affect the results of our calculation seriously.

Spectrograde 2,2,4-trimethylpentane and reagent grade benzene were used without further purification. Hexane and heptane (purified grade from Eastman Chemicals Co.) were passed through a silica gel–alumina column several times. The activity of the vapor is taken as P/P_0, with no further correction made.

Equilibrium Vapor Sorption.—The procedure for measuring equilibrium vapor sorption was similar to that used by Prager and Long.[14] A film of polypropylene was suspended from a calibrated quartz spring microbalance in an atmosphere of the hydrocarbon vapor. After equilibrium had been reached, the weight of the sorbed vapor was calculated from the elongation of the spring as measured by a cathetometer. The volume fractions of the amorphous material v_2 and of the sorbed vapor v_1 at equilibrium were obtained from the densities of the pure components, assuming additivity of the volumes of the components.

Results and Discussion

The sorption isotherms of hexane by completely amorphous PP are identical at 30, 40, and 50°. The mixing of hexane with amorphous PP therefore is athermal. The experimental data can be represented accurately by eq. 11 with an χ_1 value of 0.27. The isotherms for heptane and 2,2,4-trimethylpentane are the same as those for hexane.

The equilibrium sorption of hexane, heptane, and 2,2,4,-trimethylpentane by the amorphous fraction of isotactic PP shows a definite increase with temperature. Figure 1 shows part of the experimental results. The isotherms for the three vapors are identical at the same temperature. For these three aliphatic hydrocarbons, $(\Delta\bar{H}_1)_{sorp}$ can be equated to $(\Delta\bar{H}_1)_{el}$. Within the limits of experimental error, the results of our experiments (Fig. 1), in accord with the predictions of eq. 7, obey the relationship

$$(\Delta\bar{H}_1)_{el} = 1450v_2^2 \text{ cal./mole} \qquad (12)$$

The magnitude of $(\Delta\bar{H}_1)_{el}$ also is in fair agreement with the $(\Delta\bar{H}_1)_{sorp}$ value of about 1 kcal./mole at $v_2 = 0.9$ for the hexane–PE system.[1]

The partial molar enthalpy of sorption of benzene by amorphous PP was determined to be $(610 \pm 100)v_2^2$ cal./mole within the range $v_2 = 0.85$ to $v_2 = 0.95$, and could be equated to $(\Delta\bar{H}_1)_{mix}$. The above quantity is to be compared with the heat absorbed during the mixing of benzene with excess

(11) W. Heinen, *J. Polymer Sci.*, **38**, 545 (1959).

(12) R. G. Quynn, J. L. Riley, D. A. Young, and H. D. Noether, *J. Appl. Polymer Sci.*, **2**, 166 (1959).

(13) P. R. Swan, *J. Polymer Sci.*, **42**, 525 (1960).

(14) S. Prager and F. A. Long, *J. Am. Chem. Soc.*, **73**, 407 (1951).

heptane or octane, reported in the literature[15] to be 690 cal./mole. The partial molar enthalpy of sorption of benzene by isotactic PP, containing both the elastic contribution $(\Delta\bar{H}_1)_{el}$ and the $(\Delta\bar{H}_1)_{mix}$ term, was found to be

$$(\Delta\bar{H}_1)_{sorp} = 2100v_2^2 \text{ cal./mole for benzene–isotactic PP} \quad (13)$$

Similar $(\Delta\bar{H}_1)_{sorp}$ value can be calculated for the benzene–PE system from Rogers' data. Subtraction of the $(\Delta\bar{H}_1)_{mix}$ term from $(\Delta\bar{H}_1)_{sorp}$ yields $(\Delta\bar{H}_1)_{el}$ of 1490 ± 100 cal./mole at $v_2 = 1.0$. The agreement of this value in eq. 12 is satisfying.

Typical plots of the vapor sorption data according to eq. 10 yield straight lines. The quantities $(\chi_1 + \lambda + \epsilon_h/RT)$ and $M_c/\langle\alpha\rangle_0^2$ obtained from these straight lines are listed in Table I.

The quantity $M_c/\langle\alpha\rangle_0^2$ remains constant within the temperature range of this study. Moreover, the value obtained with aliphatic hydrocarbon solvents is in excellent agreement with that obtained with benzene. The presumption that crystallite "melt-out" does not play a role in our experiments therefore is substantiated. The term $\langle\alpha\rangle_0^2$, not known with certainty, has a minimum value of 1.0 and probably does not exceed 1.4. The average molecular weight of polypropylene chain between crystallites therefore is about 250 to 350, or approximately 6 to 8 monomer units. M_c of similar magnitude was found for PE.[9]

With hexane and heptane as solvents, plots of $(\chi_1 + \lambda + \epsilon_h/RT)$ *vs.* $1/T$ give straight lines with slopes of 7.0 ± 0.2 × 10^2. The slopes of the straight lines correspond to ϵ_h/R, from which ϵ_h can be calculated to be 1400 cal./mole, in agreement with eq. 12. The intercepts of these straight lines with the ordinate gives $(\chi_1 + \lambda)$, from which λ can be calculated. Table I summarizes the results of these calculations.

The quantities ϵ_h/RT and λ are comparable in magnitude but opposite in sign. The deviation of both the energy and the entropy contributions from conventional expressions of polymer solutions and rubber elasticity appear to be important considerations in dealing with the sorption of vapors by polycrystalline materials. It is of interest to speculate that, at −5°, ϵ_h/RT and λ cancel each other and $(\chi_1 + \lambda + \epsilon_h/RT)$ is identical with χ_1. The sorption of hexane by the isotactic PP film at −5° may then become "pseudo-ideal."

(15) "International Critical Tables," McGraw-Hill Book Co., New York, N. Y., Vol. 5, p. 151.

HEATS OF NEUTRALIZATION AND RELATIVE STRENGTHS OF AMINES IN BENZENE

By Thomas E. Mead

Central Research Division, American Cyanamid Company, Stamford, Connecticut

Received April 5, 1962

Heats of neutralization of amines have been obtained in benzene at 28° from thermometric titrations with trichloroacetic acid. A plot of these ΔH values *vs.* base strength in water for aliphatic amines shows three parallel lines corresponding to 1, 2, and 3° amines. This splitting has been ascribed to differences in solvation by benzene and water of both amines and reference acid. Base strength order in benzene was 1° > 2° > 3°. This order is believed due to "F strain" between amine and undissociated acid and to solvation of the protonated amines by the benzene π-electrons. Primary and secondary aromatic amines showed a weakening of base strength in benzene relative to the aliphatic and tertiary aromatic amines. Heats of reaction were estimated for 1:2 and 1:3 molar amine:acid associations.

Introduction

The dissociation constants of amines in water are used commonly as a measure of base strength. It is well known that discrepancies occur in comparing base strength values (dissociation constants) with molecular structure of amines.[1-3] Solvation of an amine molecule or its conjugate acid with water molecules limits direct comparison of dissociation constants of primary, secondary, and tertiary amines.[4,5] A non-solvating solvent would appear the best choice for obtaining these base strength values. Forman and Hume[6] have correlated Taft $\Sigma\sigma^*$ values with heats of neutralization (ΔH_n) of aliphatic primary and straight chain secondary amines in acetonitrile. They found ΔH_n for *meta*- and *para*-substituted aromatic amines correlated with $pK_b(H_2O)$ values, but "no obvious correlation" of ΔH_n with $pK_b(H_2O)$ values for non-aromatic amines was obtained. Deviation of branched chain secondary and tertiary aliphatic amines was explained by the B strain hypothesis. Limited solvation of amines and ammonium ions in acetonitrile explained these results.

Preliminary thermometric titrations of amines in benzene with trichloroacetic acid by the author indicated a greater spread of ΔH_n values than those obtained by Forman and Hume in acetonitrile. Solvation of amine molecules and cations should be less in benzene. This study concerns the heats of neutralization of amines in benzene with a reference acid, and the correlation of these reaction heats with base strength values in various solvents.

(1) R. P. Bell and J. W. Bayles, *J. Chem. Soc.*, 1518 (1952).
(2) A. F. Trotman-Dickenson, *ibid.*, 1293 (1949).
(3) H. K. Hall, Jr., *J. Phys. Chem.*, **60**, 63 (1956).
(4) H. K. Hall, Jr., *J. Am. Chem. Soc.*, **79**, 5441 (1957).
(5) M. M. Davis and H. B. Hetzer, *J. Res. Natl. Bur. Std.*, **60**, 569 (1958), RP 2871.
(6) E. J. Forman and D. N. Hume, *J. Phys. Chem.*, **63**, 1949 (1959).

Experimental

Materials.—Reagent grade benzene and trichloroacetic acid from Baker and Adamson Co. were used throughout.

Both were employed without further purification. A Karl Fischer titration indicated 0.03% water in the benzene. Titrant solutions consisted of trichloroacetic acid in benzene of approximately 1.0 *M* with a water content of 0.06% by Karl Fischer titration. Titrant solutions were standardized daily by diluting an aliquot with acetone and titrating potentiometrically with 0.1 *N* aqueous sodium hydroxide. Solutions of amines in benzene were 0.02 *M*, and were placed in ground glass-stoppered Erlenmeyer flasks prior to thermometric titration. Most of the amines were Eastman Kodak White Label grade. Eastman Practical grade diallylamine was distilled and analyzed 99+% by gas–liquid chromatography. Mass spectroscopy found no apparent impurities. Eastman White Label grade N,N-diethylaniline was distilled and analyzed 99+% pure by gas–liquid chromatography. Triethylenediamine, tetramethylguanidine, and bis-(cyanomethyl)-amine were prepared and purified in our Laboratories. Anhydrous grade tetramethylethylenediamine was obtained from Rohm and Haas Co.

Apparatus.—The automatic thermometric titration apparatus consisted of the following. A Sargent Model C motor-driven 10-ml. capacity buret delivered titrant at a constant rate of 1 ml./min. to the adiabatic titration cell, a dewar flask of approximately 175-ml. capacity. Situated on top of the neck of the flask is a three-holed flat cork disk which admits the capillary buret delivery tube, a glass stirrer powered by a 500 r.p.m. synchronous motor (Bodine Electric Co.), and a temperature detector. A reservoir (approximately 7-ml. capacity) placed in the titrant delivery tube inside the dewar flask allowed for initial temperature equilibrium between total titrant to be delivered and solution to be titrated. The buret tip was fitted with thin-wall polyethylene tubing drawn out to a capillary to minimize heat transfer and decrease diffusion between titrant and titrated solution. A Veco No. 32A24 bead thermistor available from Victory Engineering Corp. and having a resistance of 2000 ohms ± 10% at 25° was the temperature detector. Thermistors were calibrated over an approximate temperature range of 4°. A maximum temperature sensitivity of approximately 10^{-4}° could be obtained on a 0–1 mv. Speedomax recording potentiometer with the thermistor connected as one leg of an a.c. rectified Wheatstone bridge. A constant temperature box enclosed all apparatus except the recorder. Temperature regulation to approximately 0.1° was obtained with a blower, 200-w. heater, and thermistor electronic controller (Model 63 from Yellow Springs Instrument Co.). A flexible hose connected at diagonal corners outside the box provided for continuous recycling of the temperature-controlled air. All thermometric titrations were performed in the constant temperature box at 28.0°.

All infrared studies were performed with a Beckman IR-4 infrared spectrophotometer.

Technique.—The initial slope method of Keily and Hume[7] was used to determine heats of reaction from the expression

$$\Delta H = -\frac{C_p}{M}\left(\frac{dT}{dV}\right) \qquad (1)$$

where C_p in cal./deg. is the total heat capacity of the dewar flask and its contents and of the liquid to be titrated. M is the concentration of titrant in moles/l., dT is the temperature change in °C., and dV is the corresponding volume change in ml. The dT/dV change is assumed equal to $\Delta T/\Delta V$.

The total heat capacity (C_p) for 50-ml. volumes was determined by performing a thermometric titration of known ΔH, and calculating C_p from eq. 1. Fifty-ml. volumes of aqueous 0.02 *M* hydrochloric acid were titrated thermometrically with 1.0 *M* sodium hydroxide ($\Delta H = -13.5$ kcal./mole). The total heat capacity consists of the heat capacity of the solution to be titrated ($C_{p\,soln}$), and the heat capacity of the dewar flask and contents (C_p'). Using specific heat data listed in the International Critical Tables,[8] $C_{p\,soln}$ for the known reaction was calculated as

$$C_{p\,soln} = (cd)V \qquad (2)$$

(7) H. J. Keily and D. N. Hume, *Anal. Chem.*, **28**, 1294 (1956).

(8) "International Critical Tables," Vol. 5, McGraw–Hill Book Co., Inc., New York, N. Y., 1929, p. 115.

where c, d, and V are the specific heat, density, and volume, respectively, of the solution. C_p' then was calculated from eq. 3

$$C_p' = C_p - C_{p\,soln} \qquad (3)$$

$C_{p\,soln}$ for benzene was calculated from eq. 2 using literature specific heat data.[8] The sum of C_p' (12.18 cal./deg.) and $C_{p\,soln}$ (17.89 cal./deg.) for benzene was the total heat capacity value for the amine solutions in benzene (30.07 cal./deg.), and was used for all calculations of ΔH. The specific heat of the 0.02 *M* amine in benzene solutions was assumed to be equal to the specific heat of pure benzene. The average C_p value obtained from aqueous sodium hydroxide–hydrochloric acid thermometric titrations agreed within experimental error with an average C_p value obtained by the method of Keily and Hume,[7] *i.e.*, addition of heat electrically to known amounts of water.

The general operating procedure consisted in adjusting the temperature of the solution to be titrated as close to the titrant temperature (28.0°) as possible. This was accomplished by placing the benzene solution of the amine in an Erlenmeyer flask and adjusting to the desired temperature by heating the flask under a stream of warm water. Next a 50-ml. aliquot was pipetted into the dewar flask (pipet and flask set at 28°) and the solution was titrated thermometrically.

The volume of titrant added to effect a 1:1 molar reaction was calculated by measuring the calibrated recorder chart length along the time (volume) axis from the start of the titration (point B on Fig. 1) to the projected end point F.

Figure 1 illustrates the calculation of the initial slope (dT/dV). The product of the length BC and the appropriate ΔT per chart deflection was dT. The corresponding differential volume change, dV, was the chart length (CD) times the appropriate calibration factor. Thus the heat change for the 1:1 molar reaction (ΔH_1) was determined by substituting the above calculated values in eq. 1.

The heat of reaction (ΔH_2) for the 1:2 amine:acid association was estimated by calculating slope EG (Fig. 1) and substituting this value in eq. 1 along with the values of C_p and M used in calculating ΔH_1. This calculated value of ΔH_2 was only approximate, for the initial temperature for the second association was greater than the titrant temperature. However, this should not introduce an error greater than about 2%.

The pooled standard deviation of all the thermometric titration determinations of 0.02 *M* amines in benzene (124 trials with 34 amines) was 0.37 kcal./mole.

Effect of Concentration on ΔH.—To determine the effects of concentration on ΔH values, benzyl-, isobutyl-, and tributylamine were treated with 0.5 and 1.5 *M* titrant concentrations. Amine concentrations were 0.004 and 0.04 *M* (or 0.02 *M*), respectively. No change in ΔH was noted at these concentrations.

Results

Experimental heats of neutralization obtained from thermometric titration of amines with trichloroacetic acid in benzene are listed in Table I along with corresponding base strength values in various solvents.

Aliphatic Amines.—Sharp 1:1 molar end point breaks were obtained for all aliphatic amines (containing no other heteroatoms) with the exception of sterically hindered tribenzylamine. Quantitative titrations are possible at 0.001 *M* amine concentration. The 1:2 and 1:3 amine:acid association end points were rounded and semiquantitative. A representative thermometric titration curve is presented in Fig. 1. Primary and secondary aliphatic amines had lower 1:2 and 1:3 molar heats of association than shown in Fig. 1. (See Table I.)

A plot of ΔH values obtained for aliphatic amines in benzene under the conditions described *vs.* $pK_b(H_2O)$ values obtained from the literature

TABLE I

CORRELATION[a] OF BASE STRENGTHS, $\Sigma\sigma^*$, AND HEATS OF REACTION OF AMINES

No.	Amines	$-\Delta H_1$, kcal./mole	Std. dev., kcal./mole	No. of detns.	$-\Delta H_2$, kcal./mole	pK_b (H_2O)	Lit. ref.	ΔHNP in nitromethane (mv.)	ΔHNP in ethyl acetate (mv.)	$\Sigma\sigma^*$	Lit. ref.
	1° Amines										
1	*n*-Butylamine	29.3	0.0	3	0.7	3.36	20	3	−33	0.79	4
2	*sec*-Butylamine	29.6	.6	8	.3	3.44	6	42	−35	.77	4
3	*t*-Butylamine	29.1	.3	4	.7	3.58	6	43	−21	.79	4
4	Allylamine	27.4	.2	4	.4	4.51	4	72	11	1.11	4
5	Benzylamine	26.6	.1	4	.6	4.66	4	105	21	1.20	4
6	*p*-Anisidine	18.8	.3	3	.0	8.71	6	375	267		
7	Aniline	16.4	.2	3		9.42	6	445[b]	338		
8	*m*-Nitroaniline	0.3		1		11.54	21	597[b]	503		
9	*m*-Bromoaniline	6.2	.2	2		10.49	3	529	443		
10	*p*-Chloroaniline	9.8	.3	3		10.00	6	487	416		
	2° Amines										
11	Di-*i*-propylamine	29.4	.1	4	1.2	2.95	6	−19	−33	0.11	4
12	Di-*n*-butylamine	33.3	.4	3	1.9	2.75	4	−24	−31	.23	4
13	Di-*sec*-butylamine	28.5	.3	8	1.3	2.99	6	−19	0	.08	4
14	Di-*i*-butylamine	27.2	.4	4	2.9	3.50	4	4	21	.23	4
15	Diallylamine	24.5	2	4	1.8	4.71	4	87	61	.75	4
16	Piperidine	28.3	.3	5	2.3	2.88	20	−47	−67	0.35	4
17	Morpholine	25.0	.5	4	2.3	5.64	4	79	23	1.16	4
18	Dibenzylamine	22.5	.2	4	2.6	5.57	9	154	108		
19	N-Methylaniline	13.8	.1	4		9.15	6	434			
20	1,3-Diphenylguanidine	23.8	.2	4	1.9	4.00	6	0 (std.)	0 (std.)		
21	Tetramethylguanidine	31.2	.2	4	3.3	−0.06	9	−297	−186		
22	N-Ethylaniline	16.5	.2	3		8.85	9	411	338		
23	Di-*n*-propylamine	29.8	.3	4	2.0	3.00	4	−19	−40	0.25	4
24	Isoquinoline	12.7	.4	4		8.70	22	299	289		
34	Bis-(cyanomethyl)-amine	0.8		1		13.8	23	386	597		
	3° Amines										
25	Tri-*n*-butylamine	23.0	.5	4	4.9	3.11	6	−36	42	−0.39	6
26	Tribenzylamine	13.5	.3	2		7.10	9	274	212		
27	Dimethylbenzylamine	19.8	.2	4	4.8	5.07	4	78	82	0.22	4
28	N,N-Dimethylaniline	11.3	.5	4		8.94	6	374	348	.6	24
29	N,N-Diethylaniline	15.3	.4	3		7.48	6	286	280	.41	24
30	Pyridine	13.6	.4	3		8.81	6	286	307		
31	Triethylenediamino	21.6	.2	3		5.32	9	−34			
32	Tetramethylethylene-diamine	22.2	.1	3		4.90	9	−65	1		
33	Triethanolamine	27.8	.8	2		6.24	20	49	11		
35	*p*-Chloro-N,N-diethylaniline	12.7	.6	3		8.25	9	343	333		

[a] $-\Delta H_1$ is the heat of reaction for a 1:1 trichloroacetic acid:amine reaction in benzene. $-\Delta H_2$ is the heat of association for a 2:1 trichloroacetic acid:amine association in benzene. [b] ΔHNP values in nitromethane and ethyl acetate were obtained from Dr. C. A. Streuli, with the following exceptions. ΔHNP values in nitromethane for aniline and *m*-nitroaniline were obtained from ref. 25.

gave three parallel lines corresponding to 1, 2, and 3° amines (Fig. 2). The lines shown in Fig. 2 represent least squares solutions of the appropriate data. To our knowledge, no such correlation has been noted in the literature for other non-aqueous solvents in which potentiometric data were obtained. If these same ΔH values were plotted *vs.* half-neutralization potential values (ΔHNP) obtained for these amines in ethyl acetate (Table II), a similar but less obvious splitting was observed. ΔHNP values were obtained from Streuli[9] and are a potentiometric measure of base strength in non-aqueous solvents.[3] The separation of a given group of compounds on the basis of 1, 2, and 3° amine as illustrated in the plot of ΔH in benzene *vs.* $pK_b(H_2O)$ appears to be due to differences in solvation of the amines in the two solvents. Less splitting was observed in the plot of ΔH in benzene *vs.* ΔHNP in ethyl acetate because of the greater similarity in solvating power of these two solvents. These results substantiate the importance of solute–solvent interaction in comparing relative base strengths.

Aniline and 1 and 2° aryl amines with alkyl substitution on the nitrogen were included with the respective 1 and 2° aliphatic amines in the calculation of the least squares line, as little change in slope or standard deviation of the lines was observed when these data were included or excluded (Table II). Di-*n*-butylamine was excluded from all least squares calculations, as the experimental value of ΔH exceeded the 99% confidence limits for line numbers 6 and 10, and exceeded the 95%

(9) C. A. Streuli, private communication.

TABLE II

Eq. no.	Type of amine	Least squares lines	Std. dev. of line (kcal./mole)
	LEAST SQUARES LINES FOR $-\Delta H$ IN BENZENE *vs.* pK_b (H_2O)		
4	1° Aliphatic	$-\Delta H = -2.05pK_b + 36.40$	0.26
5	1° Aliphatic and aniline	$-\Delta H = 2.17pK_b + 36.89$	.26
6	2° Aliphatic, N-methylaniline, and N-ethylaniline	$-\Delta H = -2.32pK_b + 35.84$	.79
7	3° Aliphatic and aromatic	$-\Delta H = -2.04pK_b + 29.52$	.96
8	1° and 2° Aromatic (including substituted)	$-\Delta H = -6.44pK_b + 74.42$	1.49
	LEAST SQUARES LINES FOR $-\Delta H$ IN BENZENE *vs.* ΔHNP (ETHYL ACETATE)		
9	1° Aliphatic and aniline	$-\Delta H = -0.0367\ \Delta HNP + 28.12$	0.57
10	2° Aliphatic, N-methylaniline, and N-ethylaniline	$-\Delta H = -0.0383\ \Delta HNP + 27.95$	0.96
11	3° Aliphatic and aromatic	$-\Delta H = -0.0331\ \Delta HNP + 23.09$	1.69
12	1° and 2° Aromatic (including substituted)	$-\Delta H = -0.0829\ \Delta HNP + 43.31$	1.53
	LEAST SQUARES LINES FOR $-\Delta H$ IN BENZENE *vs.* ΔHNP (NITROMETHANE)		
13	1° Aliphatic and aniline	$-\Delta H = -0.0306\ \Delta HNP + 30.00$	0.62
14	2° Aliphatic, N-methylaniline, and N-ethylaniline,	$-\Delta H = -0.0315\ \Delta HNP + 28.10$	1.00
15	3° Aliphatic and aromatic	$-\Delta H = -0.0282\ \Delta HNP + 22.12$	0.78
16	1° and 2° Aromatic (including substituted)	$-\Delta H = -0.0866\ \Delta HNP + 52.23$	1.37
	LEAST SQUARES LINE FOR $-\Delta H$ IN BENZENE *vs.* $\Sigma\sigma^*$		
17	1° Aliphatic	$-\Delta H = -6.39\ \Sigma\sigma^* + 34.36$	0.18

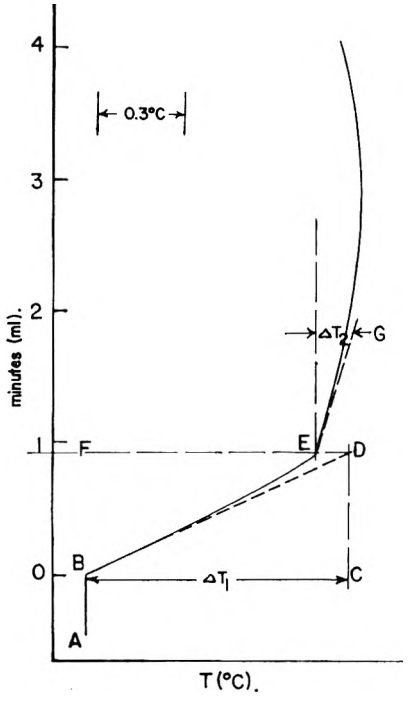

Fig. 1.—Representative thermometric titration curve for reaction of tertiary aliphatic amines with trichloroacetic acid in benzene.

confidence limits for line number 14. From ΔHNP data obtained by Streuli[9,10] in non-aqueous solvents, guanidines, amines containing heteroatoms, and heterocyclic aromatic amines were known to deviate from their respective groups (*i.e.*, 1, 2, or 3°); therefore, these amines were excluded from least squares calculations (Table III). A comparison was made of the pooled residual mean square (r.m.s.) solutions for the three lines with the r.m.s. solution for one line with a greater scatter of points. In both the ΔH *vs.* $pK_b(H_2O)$ and ΔH *vs.* ΔHNP (ethyl acetate) cases statistical

(10) C. A. Streuli, *Anal. Chem.*, **31**, 1652 (1959).

TABLE III

EXPERIMENTAL AND CALCULATED HEATS OF REACTION FOR HETEROCYCLIC AROMATIC AMINES, GUANIDINES, AND AMINES CONTAINING HETEROATOMS

No.	Amine	Exptl. $-\Delta H_1$ (kcal./mole)	Calcd.[a] $-\Delta H_1$ (kcal./mole)	Difference (kcal./mole)
6	*p*-Anisidine	18.8	18.0	+0.8
17	Morpholine	25.0	22.7	+2.3
20	1,3-Diphenylguanidine	23.8	26.4	−2.6
21	Tetramethylguanidine	31.2	35.7	−4.5
24	Isoquinoline	12.7	11.8	+0.9
30	Pyridine	13.6	11.6	+2.0
31	Triethylenediamine	21.6	18.7	+2.9
32	Tetramethylethylenediamine	22.2	19.5	+2.7
33	Triethanolamine	27.8	16.8	+11.0
34	Bis-(cyanomethyl)-amine	0.8	4.0	−3.2

[a] Calculated $-\Delta H_1$ values were obtained by substitution of the corresponding pK_b value in the appropriate least squares equation.

proof was obtained of the existence of 3 lines rather than 1 line with greater scatter. The statistical proof involved an "*F*" test. *F*-values of 54.5 and 11.8 were obtained for ΔH *vs.* $pK_b(H_2O)$ and ΔH *vs.* ΔHNP (ethyl acetate), respectively. In both cases these *F*-values corresponded to $4/(N_1 + N_2 + N_3 - 6)$ degrees of freedom ($N_1 + N_2 + N_3 - 6$ equaled 14), and were well above the 99% point (F equals 5.03 at the 99% level) of the *F* distribution. Table II includes for comparison the least squares lines for the plot of ΔH in benzene *vs.* ΔHNP values in nitromethane.

The linear relationship obtained between ΔH and pK_b within the three groups of amines (1, 2, and 3°) indicated that entropy changes (ΔS) were constant, zero, or proportional to the free energy change (ΔF) for each amine. The latter two proposals are not logical in the light of analogies which may be drawn from other systems.[6] Therefore, if

ΔS were constant for the different groups of amines, solvation and steric effects are constant within the various groups.

In benzene, the order of base strength observed for a group of amines such as 1, 2, and 3° *n*-propyl derivatives as well as the negatively substituted allyl or benzyl derivatives is 1° > 2° > 3° (see Table I). This order was observed in ethyl acetate from spectrophotometric measurements by Pearson and Vogelsong[11] and from potentiometric titrations by Streuli.[9] In nitromethane, the base strength order observed by Streuli was 3° > 2° > 1°, while in water the order is 2° > 3° > 1°.[4] "F" strain is believed responsible for the order observed in benzene and ethyl acetate with slight contributions from solvation. F strain (face-to-face strain) involves all *strains* arising from a frontal attack of two reacting species.[12] Since the reacting entities in benzene are presumably the amine and a trichloroacetic acid ion pair or undissociated molecule, the bulky, trichloroacetate anion possibly could cause F strain in this acid–base reaction in benzene. Pearson and Vogelsong[11] observed (spectrophotometric measurements) secondary amines in benzene to be the strongest bases of the three types toward the reference acid 2,4-dinitrophenol. Varying degrees of F strain and solvation involving the different reference acids are believed responsible for the differences in base strength order. "B" strain (back strain) should be independent of solvents,[13] and since different orders of base strength are observed in the various solvents, B strain probably is not important in this case. Some solvation of the protonated amines by the π-electrons of benzene might occur which would favor the order obtained in benzene.[14]

Primary aliphatic amines should exhibit very limited steric strains and only slight solvation in benzene; therefore, one would expect a good correlation between ΔH values in benzene and $\Sigma\sigma^*$ for 1° aliphatic amines. Taft σ^* values are constants expressing the inductive effects of a substituent.[4] A very low standard deviation was obtained for the least squares solution from the correlation of the ΔH in benzene for 1° amines *vs.* $\Sigma\sigma^*$ values available in the literature (Table II). Insufficient $\Sigma\sigma^*$ values were available for least squares solutions for 2 and 3° amines, but from $\Sigma\sigma^*$ data that are available, greater deviations appeared present in the more sterically hindered 2 and 3° amines.

A greater spread of $-\Delta H$ values (approximately 6.5 kcal./mole) was obtained in the benzene:trichloroacetic acid system than the literature indicated for the acetonitrile:hydrobromic acid (about 2 kcal./mole)[6] or benzene:2,4-dinitrophenol systems (about 1.5 kcal./mole).[15] These differences illustrate the importance of the reference acid in determining base strengths in low dielectric media where the acid anion is intimately associated with the reactant species.

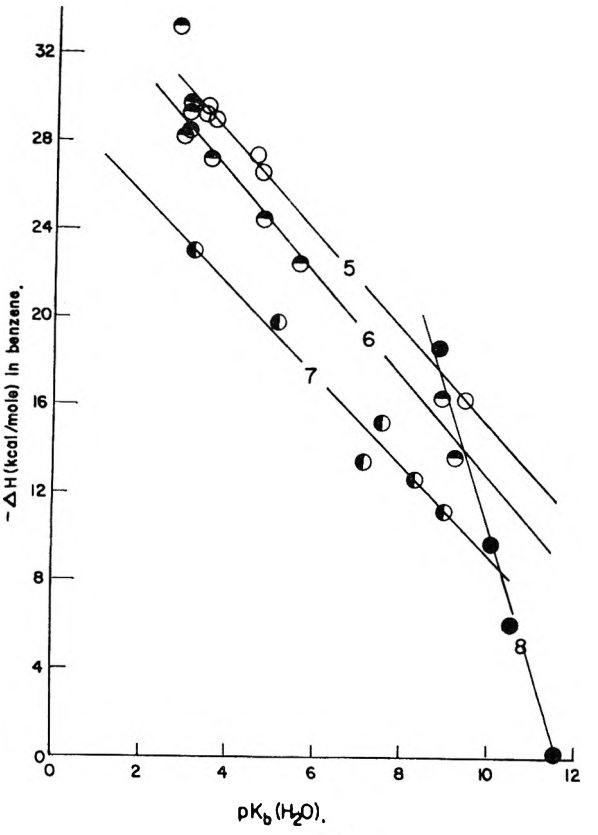

Fig. 2.—ΔH_1 in benzene *vs.* pK_b in water for amines: line 5 = primary aliphatic amines and aniline [⊙]; line 6 = secondary aliphatic amines, N-methylaniline, and N-ethylaniline [◓]; line 7 = tertiary aliphatic and tertiary aromatic amines [◐]; line 8 = primary and secondary aromatic amines (*m*- and *p*-substituted) [●].

Aromatic Amines.—Indistinct end points obtained for aromatic amines indicated that only semiquantitative determinations are possible. A weak base such as *m*-nitroaniline (pK_b = 11.5) represented the limit in detectability (ΔH = −0.3 kcal./mole). Additional heats of association (ΔH_2 and ΔH_3) were indistinguishable due to the rounded end points.

A separate relation of ΔH with pK_b (Fig. 2) obtained for 1 and 2° aromatic amines (*meta* or *para*) indicated a weakening of base strength in benzene relative to the aliphatics and the tertiary aromatics. In nitromethane or ethyl acetate, ΔHNP: pK_a plots are linear over both aliphatic and aromatic amines. Hummelstedt and Hume observed similar phenomena in photometric titrations of acids with aromatic amines in glacial acetic acid and benzene solvents.[16,17] They suggest the formation of a hydrogen-bonded complex between protonated and unprotonated amine species. If this were true, a thermometric titration break should have been obtained at the 1 amine:$^1/_2$ acid concentration. Actually, the titration slopes for all aromatic amines were rounded and could be ascribed to this phenomenon. The 3° aromatics would not be expected to form such a complex, due to steric

(11) R. G. Pearson and D. C. Vogelsong, *J. Am. Chem. Soc.*, **80**, 1038 (1958).
(12) R. Spitzer and K. S. Pitzer, *ibid.*, **70**, 1261 (1948).
(13) R. G. Pearson and F. V. Williams, *ibid.*, **76**, 258 (1954).
(14) Private communication with F. A. Cotton.
(15) J. W. Bayles and A. F. Taylor, *J. Chem. Soc.*, 417 (1961).
(16) L. E. I. Hummelstedt and D. N. Hume, *Anal. Chem.*, **32**, 576 (1960).
(17) L. E. I. Hummelstedt and D. N. Hume, *J. Am. Chem. Soc.*, **83**, 1564 (1961).

considerations. However, the negative inductive effect of the aromatic ring should destabilize any H-bond formed. No explanation was offered as to why the aliphatics would not also form a similar complex.

Guanidines, Heterocyclic Aromatic Amines, and Amines Containing Heteroatoms.—As occurs in other non-aqueous solvents,[3] bases containing O or additional N atoms showed increased basicity in benzene relative to amines of comparable strength in water (Table III). In water the reaction center of a given group of amines (1, 2, or 3°) is solvated to approximately the same extent. These amines in a non-polar solvent are solvated less; therefore, amines containing heteroatoms can solvate intermolecularly and thus enhance their base strength relative to monofunctional compounds. Diamines and guanidines appeared to form a separate line between the 3 and 2° amines from a plot of ΔH in benzene *vs.* $pK_b(H_2O)$ (see Table III), but insufficient data were available to merit calculating a least squares relation.

Amine : Acid Associations Greater Than 1 : 1.—In addition to the 1 : 1 molar reaction observed, 1 : 2 and 1 : 3 amine : acid associations were obtained. The order of ΔH for the second association was the reverse of that for the first, *i.e.*, the ΔH_2 order is $3° > 2° > 1°$ (Table I).

The sum of ΔH_1 and ΔH_2 for each series of 1, 2, or 3° amines is approximately equal. An infrared investigation[18] indicated the point of attack for the second association still occurred at the amine nitrogen rather than the chlorine atom of the acid.

The reaction of trichloroacetic acid with *n*-butylamine and tri-*n*-butylamine was studied by infrared spectroscopy. The prevalent reaction product at the 1 : 1 end point and in the presence of excess acid was a carboxylate anion 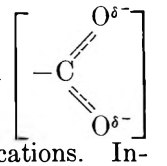 presumably ion-paired to a cation or cations. Infrared measurements also indicated the tri-*n*-butylammonium ion formed a stronger bond with the carboxylate ion than the *n*-butylammonium ion. In the presence of excess acid the carboxylate stretching frequencies of the tributylamine : trichloroacetic acid complex showed a greater shift from the spectrum of potassium trichloroacetate than the *n*-butylamine : acid complex. Recently, Marshall and Steigman[19] reported the presence of triple ions in the reaction of dibutylamine with 2,4-dinitrophenol in benzene. If a triple ion were formed according to

$$[R_3NH^+A^-] + [H^+A^-] \rightleftharpoons [R_3NH^+A^-H^+] + A^- \quad (18)$$

a tertiary amine would form the strongest bonds, for the protonated primary amine probably is more strongly solvated by the benzene π-electrons.

Acknowledgments.—The author is indebted to Dr. Carl A. Streuli for helpful discussions during the course of this work, to Mr. R. P. Davis for performing the infrared analyses, and to Dr. R. B. Hannan for interpreting the infrared spectra.

(18) R. B. Hannan, private communication.

(19) Paper by P. Marshall and J. Steigman presented at the Metropolitan Regional Meeting (New York and North Jersey Sections) of the American Chemical Society.

(20) R. G. Bates and H. B. Hetzer, *J. Phys. Chem.*, **65**, 667 (1961).

(21) A. I. Biggs, *J. Chem. Soc.*, 2572 (1961).

(22) I. M. Kolthoff and N. H. Furman, "Potentiometric Titrations," John Wiley and Sons, Inc., New York, N. Y., 1926, p. 329.

(23) G. W. Stevenson and D. Williamson, *J. Am. Chem. Soc.*, **80**, 5943 (1958).

(24) W. A. Henderson, private communication.

(25) Tables for "Analytical Handbook," by L. Meites, in publication.

ADSORPTION OF ARGON ON GRAPHITIZED CARBON BLACK. SURFACE AREA AND HEATS AND ENTROPIES OF ADSORPTION[1]

BY J. R. SAMS, JR.,[2] G. CONSTABARIS, AND G. D. HALSEY, JR.

Department of Chemistry, University of Washington, Seattle 5, Washington

Received April 6, 1962

Adsorption isotherms of argon on the highly graphitized carbon black P33 (2700°) between 90 and 137°K. are presented. Estimates of the surface area of the adsorbent and heats and entropies of adsorption computed from the data are discussed. The present results are compared with quantities obtained through the virial coefficient treatment of physical adsorption.

Introduction

Our recent studies of the interactions of gases with the highly graphitized carbon black P33 (2700°),[3-6] employing a high precision adsorption apparatus,[7] have yielded considerable information on the nature of these interactions. The data have been analyzed in terms of a virial coefficient treatment analogous to the virial expansion for imperfect gases,[8-10] and the terms in the expansion are

(1) This research was supported in part by the United States Air Force through the AFOSR, and in part by the American Petroleum Institute.

(2) Standard Oil Co. of California Fellow, 1961–1962.

(3) J. R. Sams, Jr., G. Constabaris, and G. D. Halsey, Jr., *J. Phys. Chem.*, **64**, 1089 (1960).

(4) G. Constabaris, J. R. Sams, Jr., and G. D. Halsey, Jr., *ibid.*, **65**, 367 (1961).

(5) J. R. Sams, Jr., G. Constabaris, and G. D. Halsey, Jr., *J. Chem. Phys.*, **36**, 915 (1962).

(6) R. Yaris and J. R. Sams, Jr., *ibid.*, to be published.

(7) G. Constabaris, J. H. Singleton, and G. D. Halsey, Jr., *J. Phys. Chem.*, **63**, 1350 (1959).

(8) W. A. Steele and G. D. Halsey, Jr., *J. Chem. Phys.*, **22**, 979 (1954).

found to be easily separable experimentally. At sufficiently high temperatures or low pressures, one obtains data at surface concentrations so small that effectively the gas atoms are interacting with the surface without interacting with each other. At lower temperatures or higher pressures, the measurements can be extended into the region where interactions between pairs, triplets, etc., of adsorbed atoms become important.

An analysis of the second-order (single gas atom-surface) interaction by the virial coefficient method[3,4,6] yields values for the apparent gas–surface interaction energy, ϵ^*_{1s}, and the capacity factor As_0, where A is the area of the adsorbent and s_0 the separation of the gas atom and the surface at zero net interaction energy. This latter parameter can be evaluated from the observed interaction energy and any one of the several formulas for the constant in the London formulation of dispersion forces (*e.g.*, Kirkwood–Müller, Slater–Kirkwood, etc.).[3-11] Thus one can obtain an estimate of the surface area of the adsorbent.

When the third-order data are analyzed in terms of a two-dimensional gas model,[5] one obtains a virtual two-dimensional gas–gas potential, ϵ^*_{12}, and the quantity A/σ^2. If one assumes that the gas diameter has just the free space value, then another independent estimate of the area is obtained.

From higher coverage data (region of monolayer completion), it is possible to obtain BET estimates of the area from the adsorption isotherms. One also can calculate heats and entropies of adsorption throughout the entire range of coverage. In the present paper such results are presented and are compared with those obtained through the virial coefficient treatments.

Experimental

The gas employed in this investigation was assayed reagent grade argon obtained from Air Reduction Sales Co. The graphitized carbon black P33 (2700°), a well defined, low surface-area solid, has been described by Polley, Schaeffer, and Smith.[12] Details of the apparatus and experimental techniques employed have been published previously.[3,7]

The experiments consist of measurements of the apparent volume of the sample bulb containing the solid

$$V_a = n_b RT/p \qquad (1)$$

where n_b is the number of moles of gas in the bulb, R the gas constant, T the Kelvin temperature, and p the pressure. These data readily can be converted into the usual terms of volume adsorbed at STP

$$V_{STP} = (273.15p)(V_a - V_{DS})/76.000T \qquad (2)$$

or number of moles adsorbed per gram of adsorbent, n_a. The internal dead space volume, V_{DS}, can be estimated from the helium volume at the ice point, corrected for the thermal expansion of the sample bulb and the carbon black. Low temperature adsorption isotherms are presented in Fig. 1, where the gas constant (units: cm.^{3} cm. Hg deg.$^{-1}$ mole^{-1}) times moles adsorbed is plotted against pressure. These units were chosen to correspond with those for higher temperature isotherms for this system which we have previously published.[6] The total temperature range of the data is from 90 to 240°K.

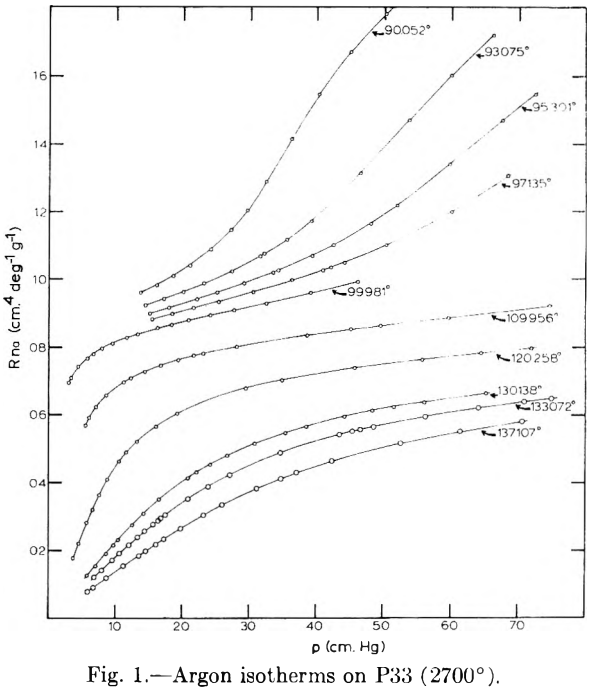

Fig. 1.—Argon isotherms on P33 (2700°).

Discussion

Heats of Adsorption.—From the isotherms shown in Fig. 1 together with those published previously,[5] it is possible to calculate isosteric heats of adsorption, q_{st}, throughout the range of coverage from zero up to about 1.5 layers. The heat *vs.* coverage curve is shown in Fig. 2. Our values (open circles) join quite smoothly with those of Prenzlow and Halsey[13] for higher coverages with the same system (closed circles).

The general shape of the q_{st} curve is as one would expect for adsorption on a very homogeneous surface. There is no apparent initial drop in the heat at very low coverages, but rather a steady increase up to a maximum just prior to the completion of the first layer. If there were any appreciable number of high energy sites in the solid, it would be expected that the gas would be preferentially adsorbed on these sites, and that the heat would decrease fairly rapidly as these sites became unavailable for further adsorption. Beebe and Young[14] have observed that with increasing graphitization of a carbon black, there is a transition from Type II isotherms to the essentially stepwise isotherms which have been predicted on theoretical grounds for adsorption on uniform surfaces.[15] At the same time one observes lower initial heat values as the temperature of graphitization of the black is increased, and the low-coverage drop in heat disappears.

The increase of heat with θ observed on homogeneous surfaces in the region below the monolayer can be attributed to lateral interactions between the adsorbed gas atoms. There are several different ways in which one can predict the slope of the q_{st} *vs.* θ curve, and three such predicted slopes are

(9) W. A. Steele and G. D. Halsey, Jr., *J. Phys. Chem.*, **59**, 57 (1955).

(10) M. P. Freeman and G. D. Halsey, Jr., *ibid.*, **59**, 181 (1955).

(11) R. A. Pierotti and G. D. Halsey, Jr., *ibid.*, **63**, 680 (1959).

(12) M. H. Polley, W. D. Schaeffer, and W. R. Smith, *ibid.*, **57**, 469 (1953).

(13) C. F. Prenzlow and G. D. Halsey, Jr., *ibid.*, **61**, 1158 (1957).

(14) R. A. Beebe and D. M. Young, *ibid.*, **58**, 93 (1954).

(15) G. D. Halsey, Jr., *J. Chem. Phys.*, **16**, 931 (1948); W. M. Champion and G. D. Halsey, Jr., *J. Phys. Chem.*, **57**, 646 (1953).

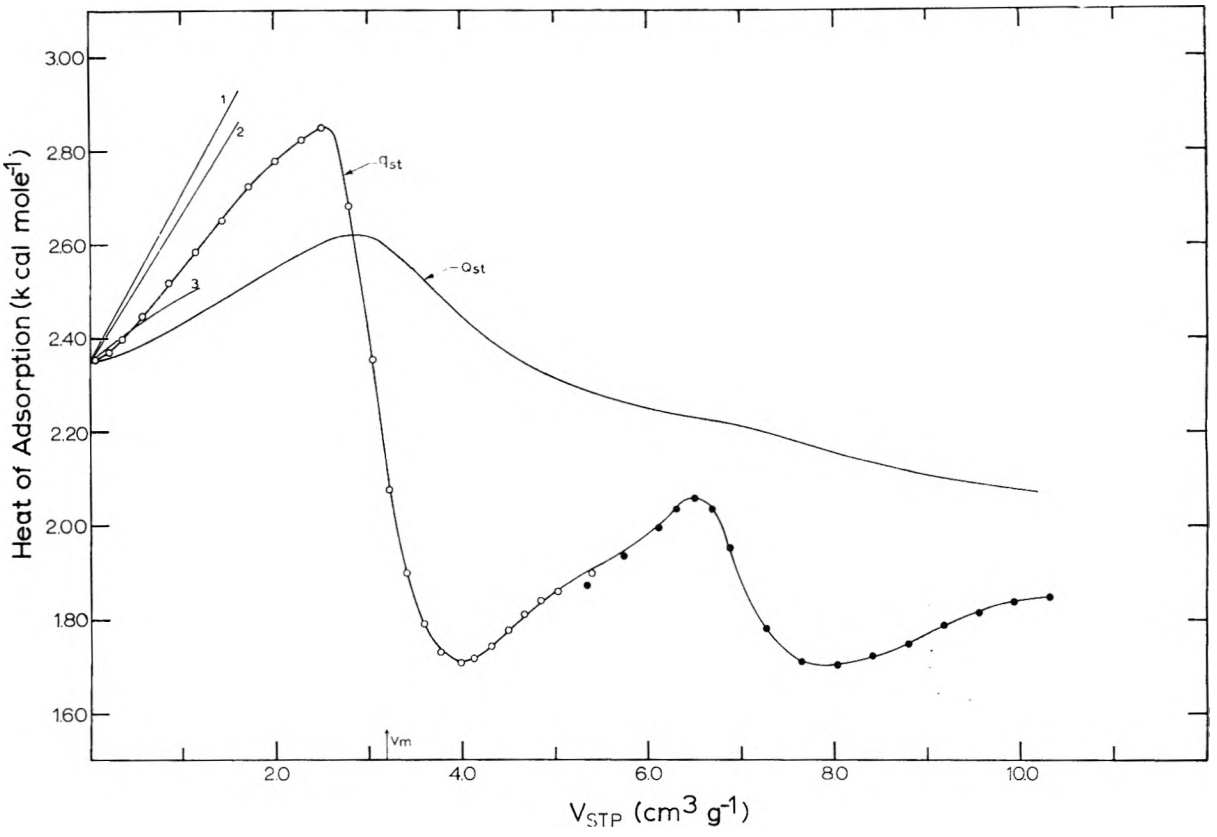

Fig. 2.—Differential and integral heats of adsorption: open circles are new data; full circles are data of Prenzlow and Halsey.

shown in Fig. 2. The first of these (curve 1) is based on a simple "lattice gas" calculation,[16] assuming a hexagonally close-packed monolayer. The value for the pair interaction energy used in this calculation was 191 cal./mole, found through a two-dimensional gas analysis of third-order argon interaction data.[5] As one might anticipate, the agreement between the lattice model and the experimental values is quite poor. The heat of lattice vacancy formation which one calculates by this treatment is about 1150 cal./mole, whereas the experimentally observed difference in heats between the zero coverage value and the maximum is only about 500 cal./mole. Beebe and Young,[14] studying argon adsorption on a series of graphitized blacks, also have observed maxima in the heat-coverage curves which are only about half as much as the values calculated from a lattice treatment, even in the case of the most homogeneous member of their series [Spheron (2700°)]. They suggested that this discrepancy probably was due to some residual heterogeneity in the solid. This does not seem likely in view of the fact that P33 (2700°) appears to have a considerably more homogeneous surface than the corresponding Spheron black.[12] Part of the discrepancy between experimental and calculated values may be due to a coördination number smaller than six, but it does not seem reasonable to postulate a coördination number as small as three. Morrison and co-workers[17] recently have found heats of vacancy formation in solid argon and krypton which are about two-thirds as much as values estimated theoretically, and suggest that this discrepancy is due in large part to the neglect of relaxation around the vacancy. This also may be a significant factor in the present results. Moreover, the lattice treatment really applies only to localized adsorption, which is clearly not the case in the present system.[3]

A second method of predicting the slope of the heat-coverage curve has been used by Aston, *et al.*[18] These authors employ the two-dimensional van der Waals equation as the equation of state of the adsorbed molecules, and find for the differential lateral interaction energy

$$E_L = (a/b)\theta \qquad (3)$$

where a and b are the (three-dimensional) van der Waals constants. Thus, according to this treatment, the slope of the heat-coverage curve should be given by a/b. For argon, a/b = 1005 cal./mole,[18] and curve 2 in Fig. 2 has been constructed using this value in eq. 3. The agreement with the experimental slope is somewhat improved over that obtained with the lattice gas treatment. The maximum slope of the experimental curve is 810 cal./mole, or about 20% lower than the predicted value. This seems entirely reasonable in view of our finding[5] that the virtual two-dimensional interaction energy for argon is about 20% lower than the free space potential minimum.

(16) R. Fowler and E. A. Guggenheim, "Statistical Thermodynamics," Cambridge University Press, Cambridge, 1952, p. 437.

(17) R. H. Beaumont, H. Chihara, and J. A. Morrison, to be published.

(18) J. G. Aston and H. Chon, *J. Phys. Chem.*, **65**, 1015 (1961); J. G. Aston, E. S. J. Tomezsko, and E. Chon, *Adv. Chem. Ser.*, **33**, 325 (1961).

The third method we have employed for predicting the slope is through the temperature derivative of the two-dimensional second virial coefficient (curve 3). For a Lennard-Jones (12–6) potential, this is given by

$$R(\partial B^*_{2D}/\partial T)^{-1} = RT/\sum_{\tau=0}^{\infty} [(3\tau + 1)/36\tau!] (4\epsilon^*_{12}/kT)^{[(3\tau+1)/6]} \Gamma[(3\tau - 1)/6] \quad (4)$$

where

$$B^*_{2D} = B_{2D}/\pi\sigma^2 = -\int_0^{\infty} [\exp(-\epsilon_{12}(r)/kT) - 1]\pi r \, dr \quad (5)$$

and $\epsilon_{12}(r)$ is the intermolecular pair potential. The value of ϵ_{12}/k used in calculating curve 3 was 96° K.[5] The temperature used at each coverage for which the slope was computed was the mean of the temperature range of the isotherms from which the isosteric heat was calculated at that particular coverage. This method can only be expected to predict the initial slope of the heat-coverage curve, since it assumes the occurrence of only pair interactions. At coverages above about 15–20% of the monolayer, one expects that many-body interactions will become significant, and the calculated curve should lie below the experimental one. This is indeed the case; the agreement is quite good up to $\theta \approx 0.2$, but at higher coverages the deviations become rather large.

It should be noted that the virial coefficient treatment is the only one of the three methods which agrees well with the experimental data, even over a relatively short range of coverages. Moreover, the virial treatment also allows one to calculate a value for the isosteric heat at zero coverage. Everett[19] has shown that for mobile adsorption q_{st} ($\theta = 0$) is $RT/2$ greater than ϵ^*_{ls}, the interaction energy of a single gas atom with the solid. This latter quantity can be obtained from measurements of second gas–surface virial coefficients.[3] For a (9–3) potential model, one finds a predicted zero-coverage isosteric heat of 2388 cal./mole, in very close agreement with the experimental value of 2355 cal./mole. Thus, both the zero-coverage heat and the initial slope of the heat-coverage curve are predicted quite well by virial coefficient treatments.

Following the maximum in the heat-coverage curve, there is a steep drop of approximately 1100 cal./mole at about the completion of the monolayer. The rise in heat in the second layer is somewhat smaller than in the first, amounting to about 350 cal./mole, but the second maximum is nevertheless quite pronounced. The drop into the third layer is also about 350 cal./mole and it appears that a third maximum, somewhat lower than the second, would be obtained at about the completion of the third layer. This tendency for subsequent maxima and minima to be less pronounced probably has its explanation in the fact that adsorption into the second and succeeding layers is not as well defined as in the first. As the deposition of layers is continued, of course, the heat of adsorption will approach the heat of vaporization of argon.

(19) D. H. Everett, *Trans. Faraday Soc.*, **46**, 453 (1950).

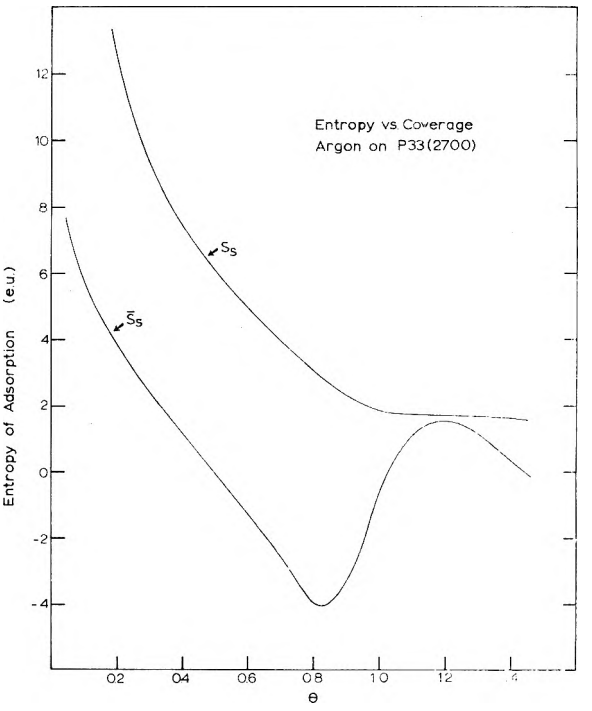

Fig. 3.—Differential and integral entropies of adsorption.

The plot of the integral heat of adsorption, Q_{st}, also shown in Fig. 2, rises slowly to a maximum at the point where it crosses the q_{st} curve, then declines monotonically with θ. The Q_{st} curve shows a general lack of structure, which indicates that the molar heat is roughly constant throughout the range of coverage.

Entropies of Adsorption.—The differential and intergral entropies of adsorption, $\bar{S}_s$ and S_s, respectively, are shown as a function of coverage in Fig. 3, where the θ values are based on a monolayer volume $v_m = 3.20$ cm.^{3}/g. As a convenient standard state, we have chosen the bulk phase (in this case, liquid) of argon at 110°K., so that the differential entropy is given by the equation

$$\bar{S}_s = q_{st}/T - R \ln (p/p_0) - (1/T) \times [\partial \ln p_0/\partial(1/RT)] \quad (6)$$

The vapor pressure p_0 was calculated from data given by Din,[20] which can be fitted by the equation

$$\ln p_0 \text{ (cm.)} = 13.524 - 803.88/T \quad (7)$$

In calculating the integral entropy, we have joined the Langmuir entropy onto the data at coverages below $\theta = 0.04$ by choice of the constant in the Langmuir expression

$$\bar{S}_s = \bar{S}_0 + k \ln [\theta/(1 - \theta)] \quad (8)$$

This of course can be integrated from zero coverage. The integral entropy then is given by the equation

$$S_s = (1/\theta) \int_0^{\theta} \bar{S}_s d\theta \quad (9)$$

As has been pointed out before,[13] it is almost futile to make qualitative remarks about entropy

(20) F. Din, "Thermodynamic Functions of Gases," Vol. 2, Butterworths Scientific Publications, London 1956, p. 150.

curves. However, the present entropy–coverage curves follow roughly the pattern found for similar systems.[13,21,22] We note that the integral and differential curves fail to cross, and that there is no minimum in the integral entropy curve. This same behavior has been observed[13] for the adsorption of argon on preadsorbed layers of argon and xenon. Thus, the statement which has sometimes been made,[22] that the integral entropy curve will exhibit a minimum at the completion of the monolayer, does not have general validity.

Surface Area.—Many different estimates exist for the surface area of this graphitized black. Prenzlow and Halsey[13] have listed 21 different values for the area, assembled from their own and other data.[12,23,24] These estimates fall in the range of 10–15 m.^{2} g.$^{-1}$, and were obtained either from estimates of "Point B" values or from isotherm step heights. In addition to these, independent values have been obtained from both second- and third-order interaction data. These latter estimates depend, of course, on the gas, on the particular choice of potential model, and also on some assumptions external to the model itself. For a Lennard-Jones type potential, second-order interaction data give values for the area of between 8 and 17 m.^{2} g.$^{-1}$, depending on the formula used for the constant in the London expression, and on the exact nature of the potential model.[3] A two-dimensional gas analysis of third-order argon interaction data,[5,25] employing a (12–6) potential function, gives an apparent area of 9 m.^{2} g.$^{-1}$ if one uses the free space value of the molecular diameter.[26]

"Point B" values have been estimated visually from the present isotherms, and the monolayer volumes and areas found are given in the second and third columns, respectively, of Table I. So that the areas reported here for P33 would be on the same basis as those given by Prenzlow and Halsey,[13] we have employed their method for assigning an area to the argon atom. They assigned an absolute area to nitrogen, and the value of 16.2 Å.^{2} used by Polley, Schaeffer, and Smith[12] was selected. To get the relative areas for other gases on a uniform basis, the second virial coefficient molecular diameters based on the Lennard-Jones (12–6) potential and taken from the tabulation of Hirschfelder, *et al.*,[26] were used. The present values for the area (A_1) are in close agreement with those tabulated by Prenzlow and Halsey.[13]

If two-dimensional hexagonal packing of the adsorbate is assumed and the second virial diameter is used to compare the areas, the values listed in the fourth column of Table I (A_2) are obtained. It is perhaps more appropriate to use the gas diameter at the potential minimum rather than the zero-interaction diameter given by Hirschfelder, *et al.*[26] This would increase the A_2 values by a factor of $2^{1/3}$ to yield the areas listed under A_3 in Table I. Also listed for comparison are areas computed from second-order interaction data for argon using the Kirkwood–Müller formula in conjunction with (9–3) and (12-3) gas–surface potentials, and from third-order interaction data employing a (12–6) potential for the two-dimensional gas interactions. It can be seen that the KM areas, the area obtained from third-order data, and the areas computed assuming hexagonal packing all are in quite good agreement.

Table I

Estimates of the Surface Area of P33 (2700°)

T, (°K.)	v_m, (cm.^{3} g.$^{-1}$)	A_1, m.^{2} g.$^{-1}$	A_2, m.^{2} g.$^{-1}$	A_3, m.^{2} g.$^{-1}$
109.956	3.08	11.4	8.4	10.6
99.981	3.16	11.7	8.6	10.8
97.134	3.19	11.8	8.7	11.0
95.301	3.22	11.9	8.8	11.1

(9–3) A_{KM}	(12–3) A_{KM}	(12–6) A_{2D}
8.6	9.3	9.0

It is evident from Table I that the "Point B" estimates diminish fairly rapidly with increasing temperature. On the other hand, as pointed out by Prenzlow and Halsey,[13] area estimates based on step height measurements apparently are independent of temperature, and presumably represent the true monolayer volume. Of course, the uncertainty in assuming a particular type of packing for the adsorbate obviously is more important than these variations in v_m. In light of all the approximations and uncertainties involved in surface area determinations, it is satisfying that the agreement among the various methods is as good as it is. In fact, even though routine BET areas often are reported to three significant figures, we are unable to estimate the absolute area of this very thoroughly investigated powder any more closely than 10 ± 2 m.^{2} g.$^{-1}$.

(21) C. H. Amberg, W. B. Spencer, and R. A. Beebe, *Can. J. Chem.*, **33**, 305 (1955).

(22) T. L. Hill, P. H. Emmett, and L. G. Joyner, *J. Am. Chem. Soc.*, **73**, 5102 (1951).

(23) J. H. Singleton and G. D. Halsey, Jr., *J. Phys. Chem.*, **58**, 330, 1011 (1954).

(24) S. Ross and W. Winkler, *J. Colloid Sci.*, **10**, 319, 330 (1955).

(25) Such a treatment was first proposed by D. H. Everett, *Soc. Chem. Ind. Monograph*, **14**, 98 (1960). See also J. A. Barker and D. H. Everett, *Trans. Faraday Soc.*, to be published.

(26) J. O. Hirschfelder, C. F. Curtiss, and R. B. Bird, "Molecular Theory of Gases and Liquids," John Wiley & Sons, Inc., New York, N. Y., 1954, p. 1110.

THE NEAR INFRARED TRANSITIONS OF THE TRIVALENT LANTHANIDES IN SOLUTION.[1] I. PRASEODYMIUM(III), NEODYMIUM(III), SAMARIUM(III), AND EUROPIUM(III) IONS

BY W. T. CARNALL,[2] D. M. GRUEN, AND R. L. MCBETH

Argonne National Laboratory, Argonne, Illinois

Received April 16, 1962

The solution absorption spectra of Pr^{+3}, Nd^{+3}, Sm^{+3}, and Eu^{+3} were measured in molten $LiNO_3$–KNO_3 eutectic at 150° in the range 0.35–2.6 μ (28,600–3850 cm.$^{-1}$). New observations of a number of absorption bands in solution in the region 1.40–2.6 μ (7140–3850 cm.$^{-1}$) were made by taking advantage of the optical transparency of the $LiNO_3$–KNO_3 eutectic solvent in this region of the spectrum. Theoretical interpretations of the solution spectra are offered based on recent experimental and theoretical analyses of crystalline salts of the lanthanide ions.

Introduction

A great deal of progress has been made within the last five years in understanding the absorption and fluorescence spectra of crystalline salts of the lanthanides. This progress has resulted from a combination of experimental and theoretical analysis. In the present communication we have applied the results of these recent investigations with crystals to an interpretation of the solution spectra of the lanthanides.

With few exceptions, studies of the solution absorption spectra of the trivalent lanthanides have been confined to the region 0.2–1.4 μ, and have emphasized application to chemical analysis and to the characterization of complex ionic species. Previous communications[3-5] in which lanthanide solution absorption bands have been identified with certain excited multiplet components have been limited to a spectral range where in general considerable overlapping of multiplet levels occurs thus restricting the number of unique identifications to only a few of the observed bands.

The conditions for interpretation of lanthanide spectra are much more favorable in the near infrared region where the multiplet levels are fewer in number.

To study this spectral region, we have taken advantage of the wide range of optical transparency of the molten $LiNO_3$–KNO_3 eutectic which extends from ~0.35–2.6 μ. Primary interest in the present paper centers on the 1.4–2.6 μ (7140–3850 cm.$^{-1}$) region; however, since the most recent theoretical and experimental studies have revised many of the assignments appearing in the older literature, certain absorption bands occurring at wave lengths less than 1.4 μ also will be discussed.

In addition to giving a theoretical interpretation of the solution absorption bands of the light lanthanides, it is of interest to contrast the ligand field effects of the anhydrous nitrate media with those observed in aqueous solution. Therefore we also have measured the spectra of the elements concerned in D_2O (dilute $DClO_4$). The use of a deuterated solvent makes it possible to extend spectral investigations beyond the usual H_2O cut-off at 1.4 to ~1.8 μ, giving a wider region of comparison with the spectra obtained in the molten nitrate medium.

The transitions occurring in the near infrared region are associated with upper levels of the ground state multiplets or of the first excited multiplet levels of the lanthanides. Beyond the transparent range of the nitrate eutectic there are a few additional bands which could in principle be observed, but these are located at wave lengths much longer than the infrared cut-off of the nitrate eutectic.

Experimental

The spectral measurements were made using a Cary recording spectrophotometer Model 14. The aqueous solutions were measured at room temperature, 23 ± 2°, while the nitrate eutectic solutions were maintained at 150 ± 1°. Two types of furnaces were used for measurements on the molten salt samples, and have been described in the literature.[6] The eutectic mixture of $LiNO_3$ and KNO_3 employed as a solvent contains 43 mole % $LiNO_3$ and has a melting point of 132°.

Reagent grade chemicals were used without further purification. The lanthanide elements were obtained commercially as oxides and contained <1% impurities. The technique of preparing $DClO_4$ has been described previously.[7] Samples of the dried lanthanide oxides were weighed, then dissolved in the appropriate acid, $DClO_4$ or HNO_3. The HNO_3 solutions were evaporated to dryness in spectrophotometer cells before adding the required weight of solid $LiNO_3$–KNO_3 eutectic.

In some cases, the eutectic solutions remained turbid after essentially all of the dried lanthanide nitrates had dissolved in the melt. This was probably due to the formation of small amounts of lanthanide oxides or oxynitrates produced by partial thermal decomposition of the nitrates. Clear solutions could be obtained by addition of small amounts of solid NH_4NO_3 to the molten system at 150°, followed by bubbling dry N_2 through the solvent. Ammonium nitrate acts as an acid in the nitrate melt, and any excess of this salt can be removed by raising the temperature of the system to 220° for several hours. The existence of H_2O and/or undecomposed NH_4NO_3 in the melt is evidenced by the presence of intense characteristic absorption bands in the 1.9–2.5 μ region. Thus progress in the expulsion of these materials could conveniently be followed spectrophotometrically.

The ability of NH_4NO_3 to dissolve lanthanide oxides directly in the $LiNO_3$–KNO_3 melt already has been described[8] and represents an extention of the work of Audrieth, *et al.*,[9] with pure molten NH_4NO_3. The usefulness of this technique should, however, be emphasized.

(1) This work was performed under the auspices of the U. S. Atomic Energy Commission.

(2) On leave at the University of Munich, Germany.

(3) L. J. F. Broer, C. J. Gorter, and J. Hoogschagen, *Physica*, **11**, 231 (1945).

(4) C. K. Jørgensen, *Dan. Mat. Fys. Medd.*, **29**, No. 11 (1955).

(5) C. K. Jørgensen, *Acta Chem. Scand.*, **11**, 981 (1957).

(6) J. P. Young and J. C. White, *Anal. Chem.*, **31**, 1892 (1959); D. M. Gruen and R. L. McBeth, *J. Phys. Chem.*, **66**, 57 (1962).

(7) J. C. Sullivan, D. Cohen, and J. C. Hindman, *J. Am. Chem. Soc.*, **79**, 3672 (1957).

(8) W. T. Carnall, *Anal. Chem.*, **34**, 786 (1962).

(9) L. F. Audrieth and J. Kleinberg, "Non-aqueous Solvents," John Wiley and Sons, Inc., New York, N. Y., 1953, Chap. 14.

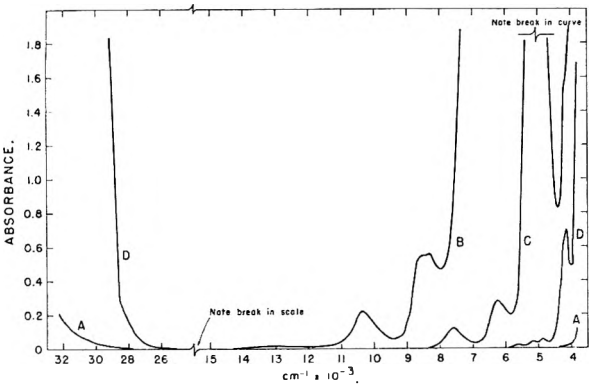

Fig. 1.—Absorption characteristics of (A) borosilicate glass cell with 1-cm. path length; borosilicate glass cell containing (B) H_2O, (C) D_2O, and (D) $LiNO_3$–KNO_3 at 150°.

The techniques used in the preparation and handling of the nitrate eutectic as well as the details concerning the procedure used in obtaining the data and calculating molar absorptivities for the molten salt solutions already have been described.[8]

As can be seen from Fig. 1, the range of optical transparency of the molten $LiNO_3$–KNO_3 eutectic corresponds approximately to that shown by borosilicate glass. Thus satisfactory spectrophotometer cells were fabricated from precision bore square borosilicate tubing. Both H_2O and D_2O absorb strongly in the near infrared, but the latter solvent is seen to have a greater range of transparency.

Results and Discussion

A very useful summary of the theory of lanthanide spectra, together with the necessary parameters required for calculating multiplet energy levels, has been presented by Elliot, *et al.*[10] The interaction of the crystal field with the 4f electrons of a lanthanide ion splits each multiplet level into a group of at most $2J + 1$ components. This splitting is considerably less in magnitude than that due to the Coulomb interaction between the 4f electrons or the spin–orbit coupling interaction. In solution, one would not expect to resolve all of the crystal field components individually, this being accomplished only at low temperature in crystals. The crystal field interaction may, however, shift the maximum of a given absorption band, broaden it and change its shape from one medium to another. Nevertheless, the transition generally can be identified with its analog in a crystal if it is well resolved from other multiplet levels.

For the most part, the absorption bands in the 1.4–2.6 μ region are due to transitions from the ground state to higher components of the ground state multiplet. In some cases the transitions are to levels of the first excited multiplet. It is useful to classify these levels according to the Russell–Saunders coupling scheme even though in many instances it is necessary to allow for deviations from this approximation in order to obtain satisfactory agreement between theory and experiment. Figure 2 shows recent results on multiplet assignments of the *light* lanthanides in the 0–14,000 cm.$^{-1}$ region obtained from studies of the spectra of crystalline salts. Each level is identified by suitable quantum numbers in the R-S system. Data of Pm^{+3} have been omitted since preliminary results obtained to date have not been able to establish the existence of solution absorption bands in the 1.0–2.6 μ region,[8] and crystal studies in this spectral region have not been reported.

The absorption spectra of Ce^{+3} and Gd^{+3} are of little interest from the point of view of the present study. As seen from Fig. 2, Ce^{+3} with one 4f-electron has only one excited level near 4.44 μ[11] which cannot be observed in the $LiNO_3$–KNO_3 eutectic, both because of solvent absorption and because Ce^{+3} is not stable in the nitrate melt. Oxidation to CeO_2 occurs rapidly and the resulting oxide precipitates; an observation which is consistent with studies of the decomposition of hydrated $Ce(NO_3)_3$.[12] Due to the particular stability of the f^7 configuration, the transitions of Gd^{+3} within the 4f shell occur at relatively large energies. The corresponding absorption bands all are found in the ultraviolet region of the spectrum[13] and are masked by intense absorption of the solvent. It remains then to discuss the spectra of Pr^{+3}, Nd^{+3}, Sm^{+3}, and Eu^{+3}.

Pr^{+3}.—The well known spectrum of Pr^{+3} is due to transitions among the 13 multiplet levels arising from the $4f^2$ configuration. Dieke and Sarup[14] have studied the fluorescence spectrum of Pr^{+3} in $LaCl_3$ and were able to fix the centers of gravity of the $^3H_6$, $^3F_2$, $^3F_3$, and $^3F_4$ levels at approximately 4280, 4940, 6330, and 6770 cm.$^{-1}$, respectively. The corresponding absorption bands have now been observed in solution as shown in Fig. 3. Several of the near infrared transitions occur with considerable intensity relative to the bands observed in the visible region. The complex band centered near 2.1 μ can be resolved into two gaussians with maxima at 2.23 μ (4480 cm.$^{-1}$) and 1.93 μ (5180 cm.$^{-1}$). Since the $^3H_5$ level lies 2170 cm.$^{-1}$ above the $^3H_4$ ground state, it is not appreciably populated at 150°; thus there would appear to be little doubt that the two overlapping bands near 2.1 μ are due to the transitions $^3H_4$–$^3H_6$ and $^3H_4$–$^3F_2$. Similarly, the bands observed in the nitrate melt at 1.54 μ (6490 cm.$^{-1}$) and 1.45 μ (6900 cm.$^{-1}$) may be identified with transitions to the $^3F_3$ and $^3F_4$ levels, respectively.

The absorption bands of Pr^{+3} in $DClO_4$ near 1.5 μ show structure not observed in the molten nitrate system. This structure may be interpreted as due to transitions between partially resolved crystal field levels since the components of the bands are separated by ~160 cm.$^{-1}$. The over-all crystal field splitting of the ground term $^3H_4$ in $PrCl_3$ is 131 cm.$^{-1}$,[15] and splittings of similar magnitude occur within the excited $^3F_3$ and $^3F_4$ levels in the same crystal.[12]

As a result of the relative simplicity of the Pr^{+3} spectrum and the large separation between multiplets and multiplet components, other absorption bands shown in Fig. 3 also can be identified. In recent years, general agreement has been reached

(10) J. P. Elliot, B. R. Judd, and W. A. Runciman, *Proc. Roy. Soc.* (London), **A240**, 509 (1957).

(11) R. J. Lang, *Can. J. Res.*, **14**, 127 (1936).

(12) F. Vratny, S. Kern, and F. Gugliotta, *J. Inorg. Nucl. Chem.*, **17**, 281 (1961).

(13) S. P. Cook and G. H. Dieke, *J. Chem. Phys.*, **27**, 1213 (1957).

(14) G. H. Dieke and R. Sarup, *ibid.*, **29**, 741 (1958).

(15) E. V. Sayre, K. M. Sancier, and S. Freed, *ibid.*, **23**, 2060 (1955) (partial revision, *ibid.*, **29**, 242 (1958).

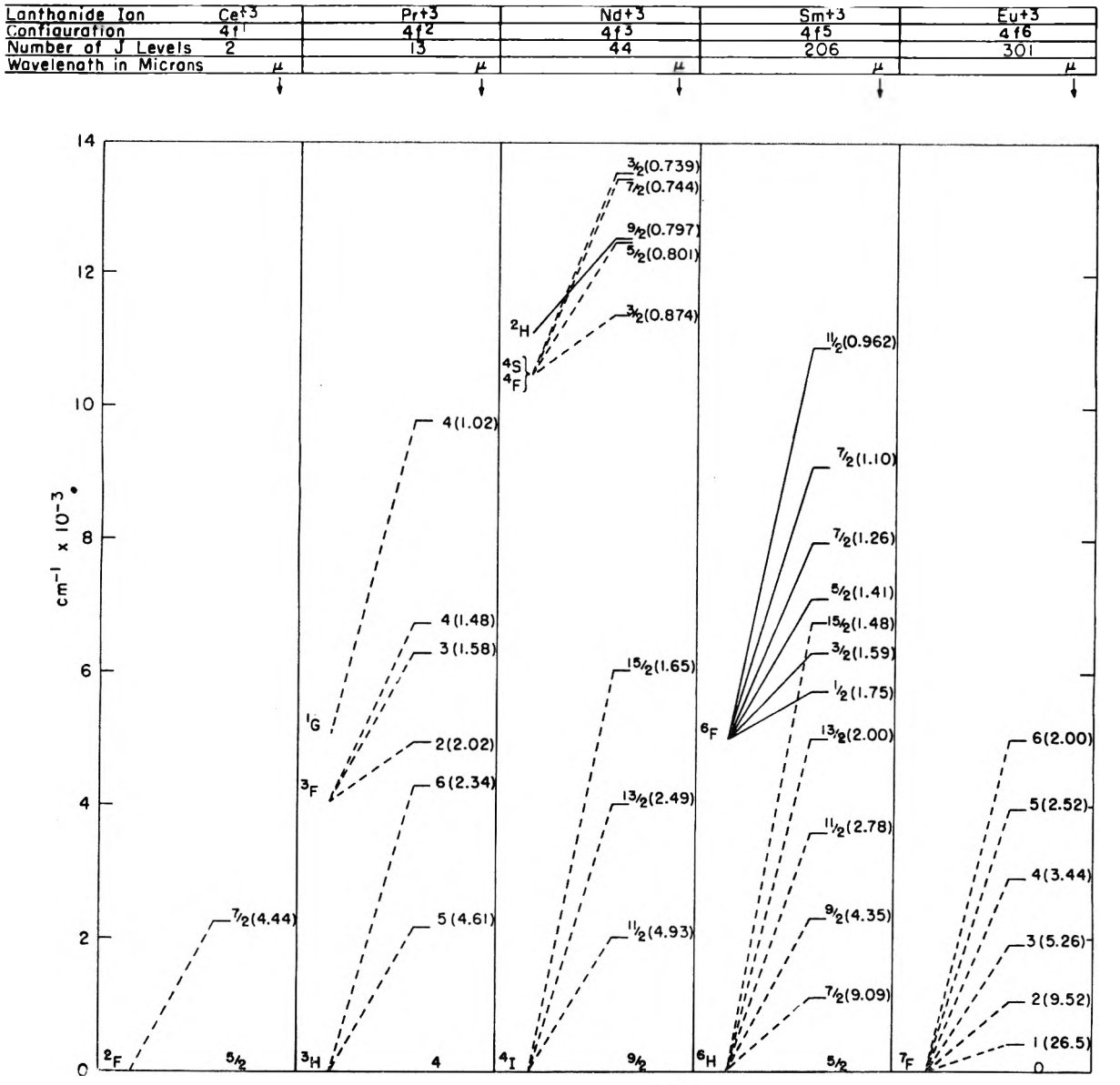

Fig. 2.—Energy levels of the light lanthanide ions from 0–14 000 cm.$^{-1}$. References: Ce^{+3}[11], Pr^{+3}[14,15], Nd^{+3}[18,19], Sm^{+3}[24], Eu^{+3}[30]. Centers of gravity of multiplet levels as given in ref. 10 are: Pr^{+3}....^3F = 4072 cm.$^{-1}$, ^1G = 5106 cm.$^{-1}$; Nd^{+3}....^4S = 10,548 cm.$^{-1}$, ^4F = 10,548 cm.$^{-1}$, ^2H = 11,087 cm.$^{-1}$; Sm^{+3}....^6F = 4958 cm.$^{-1}$.

concerning the assignment of the bands centered at ~1.0 and 0.59 μ and the system centered at ~0.47 μ to transitions from the $^3H_4$ ground state to the excited levels $^1G_4$, $^1D_2$, and $^3P_{0,1,2}$ plus $^1I_6$, respectively.[14] It is of interest to note that with the exception of $^3H_4$–$^3H_5$ and $^3H_4$–$^1S_0$, the transitions from the ground state to all of the excited multiplet components in the $4f^2$ configuration lie in a spectral region that can be studied using the $LiNO_3$–KNO_3 eutectic as a solvent.

It is clear from Fig. 3 that spectra of Pr^{+3} in $DClO_4$ and in the nitrate melt are very similar. The small shifts of the band maxima toward the infrared found in the nitrate melt are paralleled by observations in aqueous solutions where similar shifts are found with increasing NO_3^- concentration[16] and with acetylacetone chelate formation.[17]

Nd^{+3}.—Crystal spectra of Nd^{+3} have absorption bands in the 1.4–2.6 μ region and similar transitions have now been observed in $LiNO_3$–KNO_3 eutectic as shown in Fig. 4. The transitions $^4I_{9/2}$–$^4I_{13/2}$ and $I_{9/2}$–$^4I_{15/2}$ with centers of gravity at ~4010 and ~6060 cm.$^{-1}$ were identified by Varsanyi and Dieke[18] from absorption and fluorescence spectra of Nd^{+3} in solid solution in $LaCl_3$. The crystal field splitting of the ground multiplet components of Nd^{+3} in $LaCl_3$ has been reported to be 249 cm.$^{-1}$ for $^4I_{9/2}$; 85 cm.$^{-1}$ for $^4I_{11/2}$; 151 cm.$^{-1}$ for $^4I_{13/2}$; and 285 cm.$^{-1}$ for $^4I_{15/2}$.[18,19] In the nitrate eutectic, the 2.5 μ (4000 cm.$^{-1}$) band is complex. It can be resolved into two gaussian bands with maxima at 2.35 μ (4260 cm.$^{-1}$) and 2.51 μ (3980 cm.$^{-1}$), respectively. The energy difference of 280 cm.$^{-1}$ is close to the energy separation of the lowest and

(16) P. W. Selwood, *J. Am. Chem. Soc.*, **52**, 4308 (1930).

(17) T. Moeller and W. F. Ullrich, *J. Inorg. Nucl. Chem.*, **2**, 164 (1956).

(18) F. Varsanyi and G. H. Dieke, *J. Chem. Phys.*, **33**, 1616 (1960).

(19) E. Carlson, John Hopkins Spectroscopic Report Number 18 (1960).

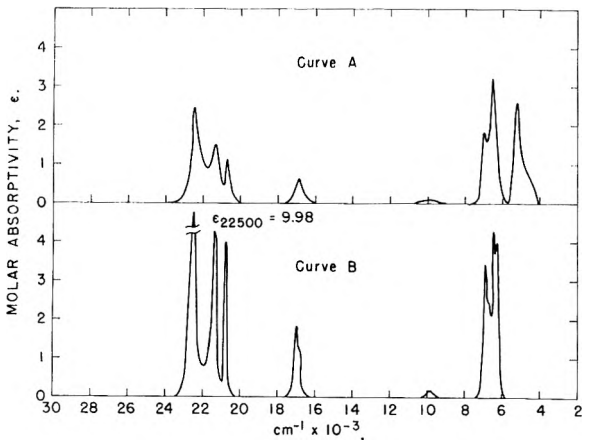

Fig. 3.—The absorption spectrum of Pr^{+3} in (A) molten $LiNO_3$–KNO_3 eutectic at 150°, and (B) in 0.4 *M* $DClO_4$ at 23°.

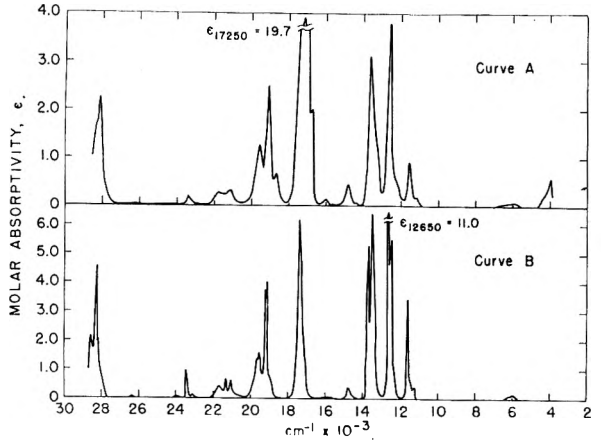

Fig. 4.—The absorption spectrum of Nd^{+3} in (A) molten $LiNO_3$–KNO_3 eutectic at 150°, and (B) in 0.3 *M* $DClO_4$ at 23°.

highest crystal field components of $^4I_{9/2}$ for Nd^{+3} in $LaCl_3$. Assuming that the crystal field splittings are similar in nitrate melts and in $LaCl_3$, one may interpret the structure of the 2.5 μ band in the eutectic as arising from transitions originating from the lowest and highest crystal field levels of $^4I_{9/2}$ and terminating in $^4I_{13/2}$. A temperature study of the intensities of the components of this band would help to indicate the correctness of this assignment.

It should be pointed out that the $^4I_{9/2}$–$^4I_{15/2}$ transition was observed for the first time only recently.[18] In the nitrate melt and in $DClO_4$ solution, this transition appears as a weak, broad band centered at 1.63 μ (6130 cm.$^{-1}$) and could easily have been missed in the absence of information predicting its location.

Transitions to the excited multiplet levels of Nd^{+3} give rise to a much more complicated band structure in the visible region of the spectrum than in the case of Pr^{+3}. All except four of the 44 possible multiplet levels in the $4f^3$ configuration lie at wave lengths < 0.9 μ (11,100 cm.$^{-1}$). Krumholz has shown that under high resolution and at a temperature of 3° the absorption spectrum of Nd^{+3} in dilute $HClO_4$ in the 0.4–0.9 μ range approximates that reported for Nd^{+3} in $Nd(BrO_3)_3 \cdot 9H_2O$ crystals where the symmetry of the crystal field appeared to be trigonal (C_{3v}).[20]

The visible absorption bands of Nd^{+3} show a shift of the band maxima toward the infrared with increasing NO_3^- concentration when comparing the spectra of an aqueous solution of 1.0 *N* $Nd(NO_3)_3$ with that of a crystal of $Nd(NO_3)_3 \cdot 6H_2O$.[16] Similarly, a small red shift is observed in comparing an aqueous to a molten nitrate medium.

Oetjen[21] noted a significant increase in oscillator strength of the band near 0.58 μ (17,250 cm.$^{-1}$) with increasing $Nd(NO_3)_3$ concentration and reported a molar absorptivity $\epsilon_{0.578\mu}$ of 22 for 2.421 *M* $Nd(NO_3)_3$, the highest concentration measured. By comparison, it was found that the concentration of Nd^{+3} in the $LiNO_3$–KNO_3 eutectic can be varied up to ~0.2 *M* Nd^{+3} by using neutral density filters and the band at 0.58 μ was shown to follow Beer's law with ϵ = 19.7. At higher concentrations of Nd^{+3} the band was too intense to permit quantitative measurements to be made. Similar effects with this particular absorption band have been reported in molten LiCl–KCl system[22] and in a study of Nd^{+3} chelate formation,[17] but not in aqueous chloride solutions.[21] In the investigation in which the acetylacetone chelate of Nd^{+3} was dissolved in various organic solvents, it was found that the extinction coefficient of the 0.58 μ band obeyed Beer's law at low concentrations giving an ϵ-value that varied between 21 and 23 depending on the solvent, but in any event close to the value found in the present study.

The remarkable sensitivity of the intensity of the 0.58 μ band to changes in anion environment has recently been justified theoretically by Judd,[23] who found that the oscillator strength *P* corresponding to the transition $\Psi_J \rightarrow \Psi_J'$ is given by

$$P = \Sigma T_\lambda \nu(\Psi_J \| U^{(\lambda)} \| \Psi_J')^2$$

where $U^{(\lambda)}$ is a tensor operator of rank λ, and the sum runs over the three values 2, 4, and 6 of λ. Sets of parameters T_2, T_4, and T_6 can be chosen to fit the experimental data. The parameter T_2 often plays only a minor role in determining the oscillator strengths because of selection rules. However, the matrix elements of $U^{(2)}$ for the transitions $^4I_{9/2} \rightarrow {}^2G_{7/2}$, $^4G_{5/2}$ which give rise to the 0.58 μ band are of the two largest in magnitude and it is the intensities these transitions which are most sensitive to the size of T_2. It is to be hoped that a detailed understanding of the relation between the magnitude of T_2 and the physical model of the rare earth anion complex can ultimately be gained. The interpretation of intensity changes in terms of chemical interactions then will become possible.

Sm^{+3}.—An experimental and theoretical study of many of the 206 possible multiplet levels in the $4f^5$ configuration (Sm^{+3}) has been made by Magno and Dieke,[24] whose experimental results appear to agree with those obtained by Gobrecht.[25] The

(20) P. Krumholz, *Spectrochim. Acta*, **10**, 274 (1958).
(21) G. W. Oetjen, *Z. Naturforsch.*, **4a**, 1 (1949).
(22) C. V. Banks, M. R. Heusinkveld, and J. W. O'Laughlin, *Anal. Chem.*, **33**, 1235 (1961).
(23) B. R. Judd, UCRL-10019, January, 1962.
(24) M. S. Magno and G. H. Dieke, NYO-8098 (June 18, 1959).
(25) H. Gobrecht, *Ann. Physik.*, **31**, 755 (1938).

absorption spectra in the 1.0–2.6 μ range have been interpreted in terms of an overlapping of the terms of the ^6F state with the upper levels of the ^3H ground state multiplet (Fig. 2). The first excited component of the ground state multiplet, $^6H_{7/2}$, lies at an energy which is large compared with kT so that it is not populated at 150°. The crystal field splitting of the ground component, $^6H_{5/2}$, in $Sm(NO_3)_3$ crystals was found to be ~136 cm.$^{-1}$,[26] but neither the bands observed in $DClO_4$ solution nor those in the nitrate melt (Fig. 5) give any evidence of structure traceable to this splitting.

The transitions of Sm^{+3} observed in the near infrared in the nitrate melt are summarized in Table I, and compared to the data reported by Magno and Dieke,[24] and to multiplet levels calculated from theory assuming pure R-S coupling.[10] Judd has shown that intermediate coupling calculations lead to a much better agreement between theory and experiment for the lower levels of the ground term multiplet.[27] The assignment of the level at 6600 cm.$^{-1}$ to $^6H_{15/2}$ is in very good agreement with experimental results of Gobrecht.[25] There is some confusion respecting the order in which $^6H_{15/2}$ and $^6F_{5/2}$ are assigned by Magno and Dieke.[24]

The degree of agreement between theory and experiment for the ^6F multiplet is of particular interest here since the transition to $^6F_{1/2}$ which was reported in crystals near 1.75 μ (5710 cm.$^{-1}$)[24] is not observed in the nitrate melt. We therefore must assume either that this transition is extremely weak or that, as indicated by theory, it occurs at a somewhat higher energy than reported by Magno and Dieke. In this event it would be masked by the relatively intense band at 1.56 μ (6410 cm.$^{-1}$).

TABLE I

A COMPARISON OF THEORY AND EXPERIMENT FOR THE ^6H AND ^6F MULTIPLET LEVELS OF Sm^{+3}

Transition	Exptl. obsd.[24] in crystals (cm.$^{-1}$)	Exptl. obsd. $LiNO_3$–KNO_3 (cm.$^{-1}$)	Calcd.[a] Pure R–S coupling (cm.$^{-1}$)
$^6H_{5/2}$	0	0	0
$^6H_{7/2}$	1100	..	840
$^6H_{9/2}$	2300	..	1920
$^6H_{11/2}$	3600	..	3240
$^6H_{13/2}$	5000	4950	4800
$^6F_{1/2}$	5700	..	6158
$^6F_{3/2}$	6300	6410	6518
$^6H_{15/2}$	6750	6711	6600
$^6F_{5/2}$	7100	7194	7118
$^6F_{7/2}$	7950	8000	7985
$^6F_{9/2}$	9050	9174	9038
$^6F_{11/2}$	10400	10530	10358

[a] Calcd. as shown in ref. 10 using F_2 = 370 cm.$^{-1}$ and ζ = 1200 cm.$^{-1}$.

Although the $^6H_{9/2}$ and $^6H_{11/2}$ transitions lie beyond the experimental limits of the present study, it is of interest to note that absorption bands at ~4.1 μ (2440 cm.$^{-1}$) and 2.62 μ (3820 cm.$^{-1}$) were reported in the absorption spectrum of a glass containing Sm_2O_3.[28]

(26) A. Friedrick, K. H. Hellwege, and H. Lammermann, *Z. Physik*, **158**, 251 (1960).

(27) B. R. Judd, *Proc. Phys. Soc.* (London), **A69**, 157 (1956).

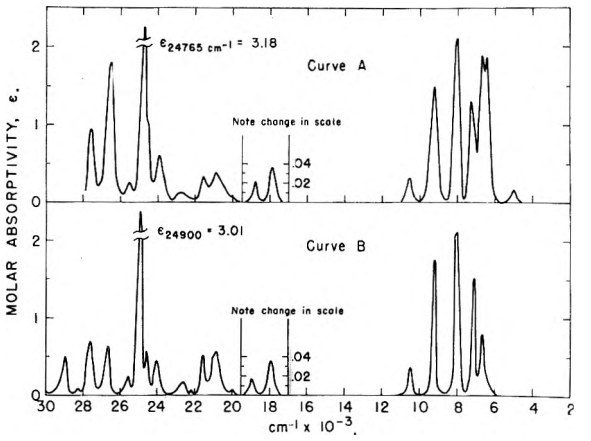

Fig. 5.—The absorption spectrum of Sm^{+3} in (A) molten $LiNO_3$–KNO_3 eutectic at 150°, and (B) in 0.4 M $DClO_4$ at 23°.

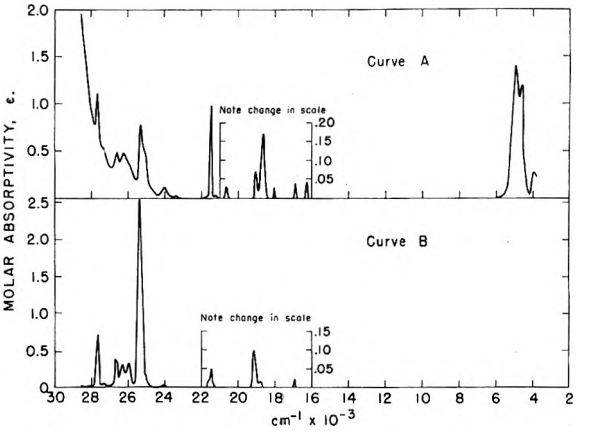

Fig. 6.—The absorption spectrum of Eu^{+3} in (A) molten $LiNO_3$–KNO_3 eutectic at 150°, and (B) in 0.3 M $DClO_4$ at 23°.

Except for the two band structure near 1.5 μ in molten $LiNO_3$–KNO_3, the spectra of Sm^{+3} in $DClO_4$ and in the nitrate eutectic are very similar with no appreciable shift in the energies of the band maxima. Moeller and Ullrich[17] have shown that chelate formation can give rise to modifications of several Sm^{+3} bands in the visible region, but the effects are strongly dependent upon the chelating agent employed.[29]

Eu^{+3}.—A study of the fluorescence spectrum of Eu^{+3} in crystalline $Eu(C_2H_5SO_4)_3 \cdot 9H_2O$ has been made by Sayre and Freed[30] and their results have been interpreted theoretically by Judd.[31] According to an analysis by Gruber and Conway[32] of the energy levels of the f^6 configuration, the highest component of the ^7F ground state multiplet is separated by more than 10,000 cm.$^{-1}$ from the lowest component of the first excited multiplet, $^5D_0$. The centers of gravity of the $^7F_{1,2,3,4,5,6}$ multiplet components occur at approximately

(28) R. Stair and C. A. Faick, *J. Res. Natl. Bur. Standards*, **38**, 95 (1947).

(29) T. Moeller and E. P. Horwitz, *J. Inorg. Nucl. Chem.*, **12**, 49 (1959).

(30) E. V. Sayre and S. Freed, *J. Chem. Phys.*, **24**, 1213 (1956).

(31) B. R. Judd, *Mol. Phys.*, **2**, 407 (1959).

(32) J. B. Gruber and J. G. Conway, *J. Chem. Phys.*, **34**, 632 (1961).

377, 1050, 1900, 2910, 3960, and 4990 cm.$^{-1}$, respectively, as shown in Fig. 2.[30] The magnitude of the crystal field splitting of the ground state multiplet components in $Eu(C_2H_5SO_4)_3 \cdot 9H_2O$ was found to vary from ~40 cm.$^{-1}$ for $^7F_1$ to ~270 cm.$^{-1}$ for $^7F_4$,[30] while the $^7F_0$ ground state is not split in a crystal field. Since the $^7F_1$ level lies very close in energy to the ground state, both levels are populated at room temperature.[33]

The absorption spectrum of Eu^{+3} in molten $LiNO_3$–KNO_3 eutectic (Fig. 6) is clearly in consonance with the results of Sayre and Freed.[30] The bands with centers at ~2.1 and ~2.5 μ thus are to be identified with transitions between ground state multiplet components, while the very weak bands near 0.55 and 0.6 μ are due to transitions to the ^5D state. We propose that the two maxima at 2.17 μ (4610 cm.$^{-1}$) and 2.03 μ (4930 cm.$^{-1}$) arise from the transitions $^7F_0$–$^7F_6$ and $^7F_1$–$^7F_6$, respectively, since the energy difference of 320 cm.$^{-1}$ corresponds reasonably well to that found in $Eu(C_2H_5SO_4)_3 \cdot 9H_2O$. The band with maximum at 2.56 μ (3910 cm.$^{-1}$) thus is to be identified with the $^7F_0$–$^7F_5$ transition. Since the latter occurs so near the experimental limit in the present investigation, it cannot be established whether it too possesses a satellite on the infrared side.

(33) K. H. Hellwege, U. Johnsen, H. G. Kahle, and G. Schaack, *Z. Physik*, **148**, 112 (1957).

The assignment of the absorption bands of Eu^{+3} near 0.579, 0.525, and 0.465 to the ^5D configuration has been discussed by Bayer-Helms.[34] These are all low intensity bands in the solution spectra, (Fig. 6), but sufficiently separated in energy to make possible their characterization. Calculation showed that the oscillator strengths for the $^7F_0$–$^5D_2$ transition (0.465 μ) increased both with increasing temperature and with increasing NO_3^- concentration. This is consistent with the present results since in the nitrate melt, the 0.465 μ band shows a very significant increase in intensity similar to the effect of NO_3^- ion on the 0.58 μ band of Nd^{+3}. Selwood[14] has also noted the sensitivity of the 0.465-μ Eu^{+3} band to NO_3^- concentration.

The correlation between the absorption maxima of the bands found in the present study and those found in crystal spectra suggests that a careful investigation of relatively high concentrations of Pm^{+3} in the $LiNO_3$–KNO_3 eutectic may lead to information on the structure of the ground state multiplet of that system. Such studies are presently being carried out. The applicability of the infrared bands to analytical studies has already been stressed in an earlier publication.[8]

Acknowledgment.—W. T. C. wishes to acknowledge numerous helpful discussions with P. Fields during the early stages of this work.

(34) F. Bayer-Helms, *Z. Naturforsch.*, **13a**, 161 (1958).

A KINETIC STUDY OF TELOMER PRODUCTION FROM CHLOROFORM–ETHYLENE MIXTURES INITIATED BY COBALT-60 γ-RADIATION

BY F. W. MELLOWS AND MILTON BURTON

Department of Chemistry and Radiation Laboratory,[1] University of Notre Dame, Notre Dame, Indiana

Received April 19, 1962

Radiolysis of chloroform–ethylene mixtures in an autoclave produces the addition compounds $C_2H_5CCl_3$, $C_4H_9CCl_3$, and $C_6H_{13}CCl_3$ with G-values as high as 3000 at 100° and 300 at 28°. A study of product distribution as a function of ethylene pressure yields transfer constants for the radicals involved in the chain reaction: at 28° the values for the radicals $C_2H_4CCl_3$, $C_4H_8CCl_3$, and $C_6H_{12}CCl_3$ are 0.21, 1.3, and 1.5, respectively; at 100° they decrease to 0.15, 0.54, and 0.45. A study of the chloroform–carbon tetrachloride–ethylene system using both high energy radiation and thermal decomposition of benzoyl peroxide as initators confirms that the radiation-initiated chain reaction is radical, and not ionic, in nature. The effect of non-polar solvents on the transfer constants suggests that increase in transfer constants with increasing chain length is a result of a decrease in rate of the radical–olefin addition reaction. G-values for pure carbon tetrachloride–ethylene mixtures have not been determined, but indirect evidence indicates G(telomer) of the same order as those obtained with chloroform.

Introduction

In production of telomers (low molecular weight polymers) from radical-initiated chain reactions, the reactants, an olefin M and an adduct AB, usually are sensitized by thermal decomposition of a peroxide to produce high yields of telomers of the type AM_nB. The reaction scheme for production of telomers from these systems usually is given as

$$\dot{R} + AB \longrightarrow RA + \dot{B} \qquad \text{Initiation}$$

$$\left.\begin{aligned} M + \dot{B} &\longrightarrow \dot{M}B \\ M + \dot{M}B &\longrightarrow \dot{M}_2B \text{ etc.} \end{aligned}\right\} \text{ Polymerization}$$

$$\dot{M}_nB + AB \longrightarrow AM_nB + \dot{B} \quad \text{Chain transfer}$$

Kharasch and his co-workers, who performed much of the earlier work, found that many polyhalogen compounds give high yields of telomers with olefins Walling[2] gives an extensive review of this field. For the systems that are pertinent to this work, chloroform–ethylene and carbon tetrachloride–ethylene, the telomers produced have the general formula $H(C_2H_4)_nCCl_3$ and $Cl(C_2H_4)_nCCl_3$, respectively.[3–7]

(1) The Radiation Laboratory is operated under contract with the Atomic Energy Commission.

(2) C. Walling, "Free Radicals in Solutions," John Wiley and Sons, Inc., New York, N. Y., 1957.

(3) I.C.I., British Patent 581,899 (October 29, 1946).

(4) M. S. Kharasch, E. V. Jensen, and W. H. Urry, *J. Am. Chem. Soc.*, **69**, 1100 (1947).

Thermal decomposition, ultraviolet light, and high energy radiation have been used for initiation of telomerization reactions. For a kinetic study, peroxides have several limitations: it is difficult to maintain constant temperature with an exothermic chain reaction; the chain reaction once started cannot easily be controlled and can become hazardous with even moderately scaled preparations; reaction temperatures are limited to decomposition temperatures of the peroxides. Initiation by ultraviolet light would be free from these difficulties but would preclude the use of such olefins as ethylene and propylene at high concentrations where high pressures are encountered. High energy radiation recently has been used as a method of initiating telomerization reactions in carbon tetrachloride–ethylene mixtures[8] and several aldehyde–olefin systems.[9]

In the present work, high energy radiation was employed for a kinetic study of telomerization reactions. Control of the chain reaction permitted by such technique enables the products to be determined as a function of temperature and reactant mixture and thus gives some information on the reactivities of the radicals involved.

Experimental

Materials.—Matheson, Coleman and Bell spectrograde chloroform, Fisher certified-grade carbon tetrachloride, and Matheson C.P. grade ethylene were used without further purification. The ethylene contained less than 1% impurities identified as ethane and a trace of air. Matheson, Coleman and Bell spectrograde *n*-hexane was shaken with concentrated sulfuric acid to remove any traces of unsaturated hydrocarbons.

Dosimetry.—The Ghormley-Hochanadel Co^{60} source used in this work gave a dose rate of 1.26×10^{17} e.v. $g.^{-1}$ $min.^{-1}$. Dose rates were determined with the Fricke dosimeter using $G(Fe^{+3}) = 15.6$. To avoid complications arising from chemical effect of acid solution upon steel, the autoclaves were lined with an inert material. The dose rates in a gold-plated autoclave and in an autoclave coated with a thin film of silicone grease were 5% greater than the dose rate in a closely fitted Pyrex tube inside the autoclave. The higher value was used in this work.

Irradiations.—Stainless steel (316) autoclaves of 10-ml. capacity were charged half full with solvent and degassed by conventional freeze–thaw technique. The amount of ethylene condensed into the autoclave was determined from pressure–volume measurements. Copper–constantan thermocouples introduced into the body of the autoclave recorded the temperature of the reaction to within 1°.

Analysis of Liquid Products.—After irradiation, the autoclave was slowly depressurized and the uncombined ethylene was measured as before. Hand agitation during this procedure reduced solvent loss to a minimum. A Perkin–Elmer fractometer, Model 154B, was used for analysis of liquid products; gram quantities of addition compounds, prepared in 40-and 150-ml. capacity autoclaves, were separated with a Beckman Megachrom and used for calibrating the fractometer.

Chromatographic analysis for addition compounds produced in chloroform–ethylene mixtures initiated either by high energy radiation or by thermal decomposition of 0.5% benzoyl peroxide revealed only three products in both cases.[10] Their retention times on 2-m. columns containing either Apiezon L grease or Carbowax 1500 at 100° showed that the products from the irradiated mixtures are identical with those produced by thermal initiation with benzoyl peroxide; they have the general formula $H(C_2H_4)_nCCl_3$. Densities and refractive indices of the three products produced by irradiation corresponded to the literature values for the compounds $C_2H_5CCl_3$, $C_4H_9CCl_3$, and $C_6H_{13}CCl_3$. Loss of solvent involved in depressurizing and errors involved in analysis and dosimetry lead to uncertainty of ±15% in the reported *G*-values; however, their relative yields are accurate to ±7%.

Determination of Ethylene Solubility.—The fraction of ethylene in the liquid phase was calculated from values of mole fraction of ethylene and molar volume of the chloroform–ethylene system, determined as a function of composition over the temperature range 0 to 100° by Kohn and Shim.[11]

Results

Exploratory Studies.—A number of solvents were irradiated in the presence of ethylene at pressures up to 100 atm. and analyzed for possible addition products. Propionaldehyde, methanol, methyl iodide, and chloroform were irradiated at room temperature; methylene chloride was irradiated at 120°, acetone and acetic acid were irradiated at 200°, and toluene at 300°. Largest yields of addition products from these systems were obtained from the chloroform–ethylene and propionaldehyde–ethylene mixtures, with *G*-values for addition products as high as 300 and 30, respectively. Similar yields were obtained by Stoops and Furrow[4] for the propionaldehyde–ethylene system. Yields from the chloroform–ethylene system were considered adequate for an uncomplicated kinetic study. Other solvents, carbon tetrabromide, bromochloroform, etc., which are known to give high telomer yields with ethylene, were excluded from study because of the problems encountered when analyzing for products with high boiling points and low decomposition temperatures. In the case of the chloroform–ethylene system, the reactants and the addition products are stable at 100° for at least 24 hr. and the vapor pressures of the trichloroalkanes are sufficiently high to allow the first three addition compounds to be analyzed by gas chromatography.

Chloroform–Ethylene Mixtures.—Various chloroform–ethylene mixtures were irradiated at 28 and 100° with doses in the range 5×10^{18} to 90×10^{18} e.v. $ml.^{-1}$. In several runs chloroform was diluted 4:1 and 9:1 with *n*-hexane to obtain high ethylene/chloroform ratios at convenient ethylene pressures.[12] Table I gives yields of the addition products $C_2H_5CCl_3$, $C_4H_9CCl_3$, and $C_6H_{13}CCl_3$. The results show a pronounced effect of ethylene concentration on product distribution. At very low ethylene concentrations, $C_2H_5CCl_3$ is the major product; at concentrations greater than 4 *M*, $C_4H_9CCl_3$ is the most abundant product; only at very high concentrations of ethylene is $C_6H_{13}CCl_3$

(5) R. M. Joyce, W. E. Hanford, and J. Harmon, *J. Am. Chem. Soc.*, **70**, 2529 (1948).

(6) W. E. Hanford and J. Harmon, U. S. Patent 2,440,800 (May 4, 1948).

(7) J. Harmon, T. A. Ford, W. E. Hanford, and R. M. Joyce, *J. Am. Chem. Soc.*, **72**, 2213 (1950).

(8) S. S. Medvedev, in "International Conference on Radioisotopes in Scientific Research, 1st UNESCO Proc.," Vol. I, Pergamon Press, New York, N. Y., 1958.

(9) C. E. Stoops and C. L. Furrow, *J. Org. Chem.*, **26**, 3264 (1961).

(10) Production of higher molecular weight compounds undeterminable by gas chromatography was not followed in this work.

(11) J. P. Kohn and J. Shim, unpublished data.

(12) The solubility of ethylene in these *n*-hexane–chloroform mixtures is assumed to be the same as in chloroform. This assumption is justified from data obtained by W. B. Kay, *Ind. Eng. Chem.*, **40**, 1459 (1948), on the *n*-heptane–ethylene system. The solubility of ethylene in *n*-heptane, which is very similar to that in *n*-hexane, is only some 5–10% less than in chloroform at the pressures and temperatures used here.

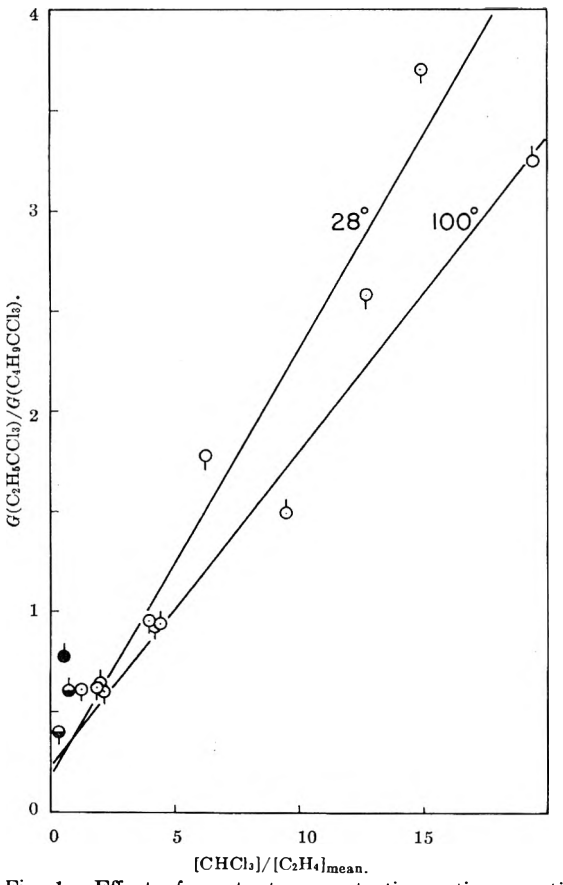

Fig. 1.—Effect of reactant concentration ratio on ratio of products in radiolysis of the chloroform–ethylene system at 28 and 100°: ○, in absence of hexane; ◒, volume ratio n-$C_6H_{14}/CHCl_3$ = 4; ●, volume ratio n-$C_6H_{14}/CHCl_3$ = 9; tail down, 28°; tail up, 100°.

an important product. These results indicate that appreciable yields of the 4:1 addition compound $C_8H_{17}CCl_3$ are possible only at ethylene/chloroform ratios greater than 3. Increase in temperature from 28 to 100° increases rate of telomerization by a factor of 10.

TABLE I

YIELDS OF $C_2H_5CCl_3$, $C_4H_9CCl_3$, AND $C_6H_{13}CCl_3$[a] FROM CHLOROFORM–ETHYLENE MIXTURES, INITIATED BY Co^{60} γ-RADIATION AT 28 AND 100°

Temp., °C.	$\frac{[CHCl_3]}{[C_2H_4]}$[d]	% C_2H_4 consumed	$G(C_2H_5CCl_3)$	$G(C_4H_9CCl_3)$	$G(C_6H_{13}CCl_3)$
28[b]	0.35	20	82	204	138
28	1.22	8	92	150	67
28	1.78	8	223	358	113
28	2.09	2	75	123	33
28	3.86	6	172	181	..
28	4.04	9	248	270	41
28	6.25	3	169	95	..
28	11.8	17	204	79	..
28	12.5	33	219	59	..
100[c]	0.435	24	98	126	85
100[b]	0.800	8	109	181	104
100	1.81	14	1810	2810	1215
100	3.75	30	2910	3080	775
100	7.90	34	2800	1880	328
100	16.3	28	1985	610	..

[a] Values are not given when yields were too small for accurate determination. [b] In 80% n-hexane. [c] In 90% n-hexane. [d] Initial concentration of ethylene.

Chloroform–Carbon Tetrachloride–Ethylene System.—The possibility cannot be eliminated entirely that a chain reaction initiated by high energy radiation is ionic and not radical in nature, although the short lifetime of ions in a condensed system would make this unlikely. A comparative study of yields of reaction products using high energy radiation and thermal decomposition of benzoyl peroxide as initiators would help to differentiate between these two possibilities. However, difficulty in stopping peroxide-initiated chain reactions at low conversions leads to complications in a kinetic study resulting from the large change in reactant composition during the course of the reaction. To avoid such difficulty, we have studied the ratio of rates of competing abstraction reactions of the radical $C_2H_4CCl_3$ with chloroform and carbon tetrachloride to produce $C_2H_5CCl_3$ and $ClC_2H_4CCl_3$, respectively. The ratio of rates should be independent of ethylene concentration.

Yields of $C_2H_5CCl_3$ and $ClC_2H_4CCl_3$ were measured over a wide range of chloroform–carbon tetrachloride mixtures. Doses for the radiation-initiated reactions at 28 and 100° were in the range 6×10^{18} to 50×10^{18} e.v. ml.$^{-1}$. The reactions were carried out in presence of 3 M ethylene with the exception of one run with 1 M ethylene present. The peroxide-initiated reaction was carried out at 90° in the presence of approximately 3.2 mM benzoyl peroxide and 3 M ethylene and the reaction was allowed to go to completion. The results in Table II show that product distribution is greatly affected by solvent composition but not by ethylene concentration. As observed for the chloroform system, G-values at 100° are larger than at 28° by a factor of 10.

TABLE II

YIELDS OF $C_2H_5CCl_3$, AND $ClC_2H_4CCl_3$ FROM CHLOROFORM–CARBON TETRACHLORIDE–ETHYLENE MIXTURES

Ethylene is 3 M except where noted

$\frac{[CCl_4]}{[CHCl_3]}$	$G(C_2H_5CCl_3)$	$G(ClC_2H_4CCl_3)$
	Co^{60} gammas, 28°	
0.547	76	12.5
3.28	138	141
3.28[a]	131	138
8.21	65	156
	Co^{60} gammas, 100°	
1.28	595	555
3.28	130	288
7.39	276	1370
19.7	149	1880
	Peroxide initiated, 90°	
	mMoles $C_2H_5CCl_3$	mMoles $ClC_2H_4CCl_3$
0.821	0.488	0.308
0.821	1.31	0.801
7.39	0.224	1.10
7.39	.485	2.42
15.6	.123	1.09
15.6	.432	3.37

[a] 1 M ethylene.

Discussion

Chloroform–Ethylene System.—The radical chain for the production of the addition compounds $C_2H_5CCl_3$, $C_4H_9CCl_3$, and $C_6H_{13}CCl_3$ is given by the usual reaction scheme

$$CCl_3 \xrightarrow{C_2H_4} C_2H_4CCl_3 \xrightarrow[k_2]{C_2H_4} C_4H_8CCl_3 \xrightarrow[k_4]{C_2H_4} C_6H_{12}CCl_3 \xrightarrow[k_6]{C_2H_4} C_8H_{16}CCl_3$$

$$\downarrow k_1\ CHCl_3 \qquad \downarrow k_3\ CHCl_3 \qquad \downarrow k_5\ CHCl_3$$

$$C_2H_5CCl_3 + CCl_3 \qquad C_4H_9CCl_3 + CCl_3 \qquad C_6H_{13}CCl_3 + CCl_3$$

With r as the rate of production of the radical $C_2H_4CCl_3$, the following rate expressions are obtained

$$\frac{d[C_2H_5CCl_3]}{dt} = r \times \frac{k_1[CHCl_3]}{k_1[CHCl_3] + k_2[C_2H_4]}$$

$$\frac{d[C_4H_9CCl_3]}{dt} = r \times \frac{k_2[C_2H_4]}{k_1[CHCl_3] + k_2[C_2H_4]} \times \frac{k_3[CHCl_3]}{k_3[CHCl_3] + k_4[C_2H_4]}$$

$$\frac{d[C_6H_{13}CCl_3]}{dt} = r \times \frac{k_2[C_2H_4]}{k_1[CHCl_3] + k_2[C_2H_4]} \times \frac{k_4[C_2H_4]}{k_3[CHCl_3] + k_4[C_2H_4]} \times \frac{k_5[CHCl_3]}{k_5[CHCl_3] + k_6[C_2H_4]}$$

From these expressions it follows that

$$\frac{[C_2H_5CCl_3]}{[C_4H_9CCl_3]} = \frac{k_1[CHCl_3]}{k_2[C_2H_4]} + \frac{k_1}{k_2}\Big/\frac{k_3}{k_4}$$

and

$$\frac{[C_4H_9CCl_3]}{[C_6H_{13}CCl_3]} = \frac{k_3[CHCl_3]}{k_4[C_2H_4]} + \frac{k_3}{k_4}\Big/\frac{k_5}{k_6}$$

Figures 1 and 2 show the plots $G(C_2H_5CCl_3)/G(C_4H_9CCl_3)$ and $G(C_4H_9CCl_3)/G(C_6H_{13}CCl_3)$ *vs.* $[CHCl_3]/[C_2H_4]^*$ at 28 and 100°, where $[C_2H_4]^*$ is the mean ethylene concentration. Values of k_1/k_2 and k_3/k_4 are obtained from the slopes in Fig. 1 and 2 and k_5/k_6 derived from the intercepts of the lines in Fig. 2. These relative rate constants are termed transfer constants[2] of the three radicals $C_2H_4CCl_3$, $C_4H_8CCl_3$, and $C_6H_{12}CCl_3$. Values at 28 and 100° are given in Table III.

TABLE III

TRANSFER CONSTANTS FOR THE RADICALS $C_2H_4CCl_3$, $C_4H_8CCl_3$, AND $C_6H_{12}CCl_3$ IN THE CHLOROFORM–ETHYLENE SYSTEM AT 28 AND 100°

Temp., °C.	k_1/k_2	k_3/k_4	k_5/k_6
28	0.205 ± 0.025	1.30 ± 0.15	1.5 ± 0.25
100	0.15 ± 0.02	0.535 ± 0.1	0.45 ± 0.15

From these transfer constants, activation energy differences are obtained: $E_2 - E_1 = 1 \pm 0.2$ kcal., $E_4 - E_3 = 2.6 \pm 0.3$ kcal., and $E_6 - E_5 = 3.5 \pm 1.0$ kcal. Similar variations of transfer constants with chain length have been observed for other systems; *cf.* the carbon tetrachloride–ethylene sytem sensitized by benzoyl peroxide.[2] Such variations were explained in terms of steric hindrance and the donor properties of the radicals. In the case of the radical $C_2H_4CCl_3$, the presence of the electron-attracting group CCl_3 creates an electron deficiency at the radical end of the chain. This electron deficiency will be much less in the radical $C_4H_8CCl_3$ and should be insignificant in the radical $C_6H_{12}CCl_3$. The variation of transfer constants with chain length for these radicals suggests that this polarization of the radicals results in a reduction in their transfer constants.

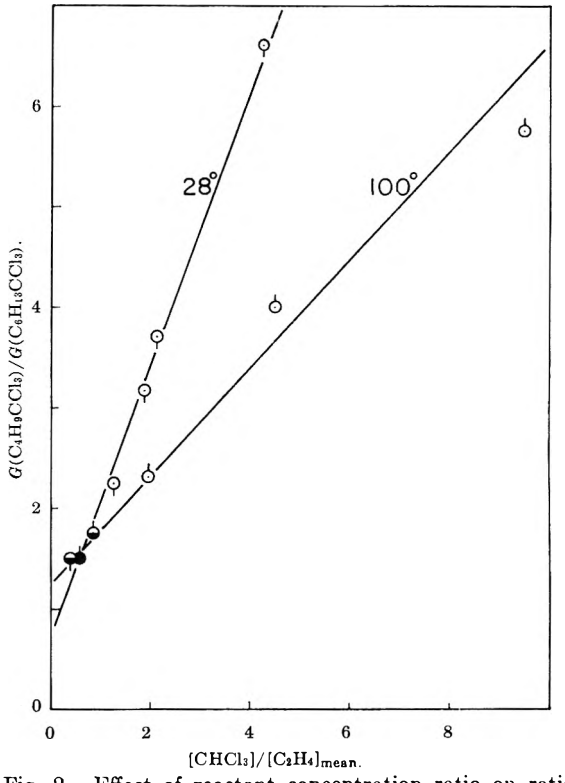

Fig. 2.—Effect of reactant concentration ratio on ratio of telomer products in radiolysis of the chloroform–ethylene system at 28 and 100°: ○, in absence of hexane; ◒, volume ratio n-$C_6H_{14}/CHCl_3$ = 4; ●, volume ratio n-$C_6H_{14}/CHCl_3$ = 9; tail down, 28°; tail up, 100°.

Figure 1 shows deviations from linearity for runs carried out in the presence of n-hexane. At 100°, values of k_1/k_2 in 80 and 90% n-hexane increase from 0.15 to 0.23 and 0.35, respectively. Böttcher[13] has calculated that the induced dipole

(13) C. F. F. Böttcher, "Theory of Electric Polarization," Elsevier Publishing Co., New York, N. Y., 1952.

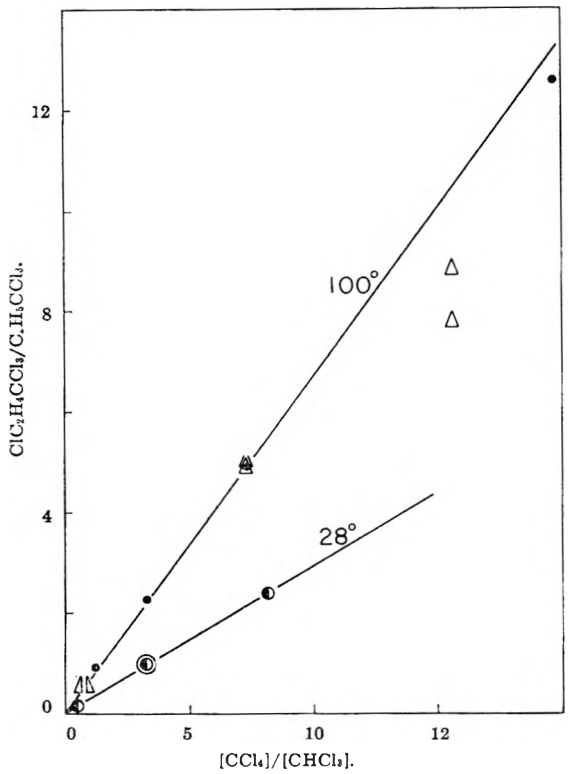

Fig. 3.—Effect of ratio $[CCl_4]/[CHCl_3]$ in the CCl_4–$CHCl_3$–C_2H_4 system on ratio of low molecular weight products in radiolysis and benzoyl peroxide-induced reactions. Unless otherwise indicated, C_2H_4 is ~3 *M*; ○, C_2H_4 ~ 1 *M*; ◐, radiolysis at 28°; ●, radiolysis at 100°; △, 3 m*M* benzoyl peroxide at 90°.

of chloroform in the liquid phase resulting from the reaction field of the surrounding molecules is 24% of the permanent dipole. Thus, the addition of *n*-hexane, a non-polar solvent, to chloroform should result in a reduction in the dipole of chloroform by reducing the reaction field of the surrounding molecules. A reduction in the dipole of the radical $C_2H_4CCl_3$ (*i.e.*, a decrease in the electron deficiency at the radical end of the chain) upon the addition of *n*-hexane to the chloroform–ethylene system would explain the observed increase in value of k_1/k_2. Absence of a similar increase in the transfer constant of the radical $C_4H_8CCl_3$ reflects the reduced influence of the CCl_3 group at this greater distance.

Chloroform–Carbon Tetrachloride–Ethylene System.—Production of the addition compounds $C_2H_5CCl_3$ and $ClC_2H_4CCl_3$ from the chloroform–carbon tetrachloride–ethylene system is described by the reaction scheme

$$C_2H_4 + CCl_3 \longrightarrow \begin{cases} C_2H_4CCl_3 \xrightarrow[CCl_4]{k_1'} ClC_2H_4CCl_3 + CCl_3 \\ C_2H_4CCl_3 \xrightarrow[CHCl_3]{k_1} C_2H_5CCl_3 + CCl_3 \end{cases}$$

$$\frac{[ClC_2H_4CCl_3]}{[C_2H_5CCl_3]} = \frac{k_1'[CCl_4]}{k_1[CHCl_3]}$$

Plots of $[ClC_2H_4CCl_3]/[C_2H_5CCl_3]$ *vs.* $[CCl_4]/[CHCl_3]$ for the radiation-initiated reaction at 28 and 100° and for the peroxide-initiated reaction at 90° are shown in Fig. 3. Values of k_1'/k_1 for the radiation-initiated reaction at 28 and 100° are 0.31 and 0.68, respectively, which correspond to an activation energy difference $E_1' - E_1$ for the abstraction reactions of 2.5 kcal. At 90°, the peroxide-initiated chain reaction has a rate-constant ratio k_1'/k_1 which can be estimated roughly to be ~0.66. In view of the difficulties inherent in such determination, agreement with the calculated value $k_1'/k_1 = 0.62$ for the radiation-initiated reaction at 90° is good and supports the interpretation that the radiation-initiated reaction is radical in nature.

The linear plots in Fig. 3 demonstrate the constancy of k_1'/k_1 over a wide range of chloroform–carbon tetrachloride mixture. Thus, k_1'/k_1 is unaffected by the presence of a non-polar solvent and therefore is insensitive to the polarization of the radical $C_2H_4CCl_3$, unlike the transfer constant k_1/k_2 which increases in the presence of *n*-hexane. Because it is unlikely that k_1' and k_1 would be equally affected by the polarization of the radical $C_2H_4CCl_3$, this result suggests that both k_1' and k_1 are themselves insensitive to the polarization of the radical. It is reasonable, consequently, to assume that k_3 and k_5 also should be unaffected by the polarization of the radicals $C_4H_8CCl_3$ and C_6H_{12}-CCl_3; the suggestion is implicit that the observed increase in transfer constants of the radicals $(C_2H_4)_nCCl_3$ with increasing chain length is a result of a decrease in the rate of addition to ethylene. Such an attack upon an olefin is expected to be favored by an electron deficiency at the radical end of the chain.

Interpolated values of k_1'/k_1 and k_1/k_2 for radiation-initiated reactions at 70° are 0.51 and 0.18, respectively, which lead to the value $k_1'/k_2 = 0.09$. Agreement with the value $k_1'/k_2 = 0.08$ obtained from the carbon tetrachloride–ethylene system initiated by peroxide[2] at 70° is further evidence that the chain reaction initiated by high energy radiation is radical in nature.

Comment on *G*-Values.—The results shown indicate that variation in temperature and control of pressure can be employed not only to give preferred product distribution but also to give absolute *G*-values of product sufficiently large to be of technological importance if the products themselves are useful.

Acknowledgments.—The authors are indebted to Professor J. P. Kohn and Mr. J. Shim for the determination of the phase equilibrium in the chloroform–ethylene system, to Dr. G. F. Koltzenburg for preliminary work carried out in this field, and to Mrs. G. D. Falconer for gas chromatographic analysis.

FUSED SALT SPECTROPHOTOMETRY. III. ISOSBESTIC POINTS GENERATED BY VARIATION IN TEMPERATURE[1]

BY J. R. MORREY

Hanford Laboratories Operation, General Electric Company, Richland, Washington

Received April 23, 1962

A study of the temperature dependence of fused-salt spectra has revealed that several systems produce isosbestic points. As the temperature of a given sample is varied, the corresponding spectra often exhibit several wave lengths at which the absorbance is temperature independent. A phenomenological argument is presented to show that when this happens, one and only one species contributes to the absorbance in the region of an isosbestic point and that this species does not change concentration as a function of temperature because of equilibria involving other non-absorbing species. It also is shown that spectral changes must arise from a linear temperature dependence of the molar absorptivity at a given wave length. These conclusions are in contradistinction to those made by consideration of isosbestic points occurring at constant temperature. In this latter case, their existence proves that two and only two absorbing species are variables.

Introduction

Isosbestic[2] points often are observed in absorption spectra of solutions having a fixed concentration of metal ion but varying concentrations of a given ligand. In such systems, the isothermally measured isosbestic points are ascribed to, and considered proof of, the presence of two, and only two, spectrophotometrically distinguishable species. Isosbestic points also have been observed in spectra of pure molten salts (Fig. 1) and mixtures of molten salts (Fig. 2) measured at different temperatures. Temperature variation is not conducive to the formation of conventional isosbestic points because the concentration of the absorbing species changes as the fluid expands and contracts.

It is the purpose of this paper to establish the conditions which must exist in order for temperature-generated isosbestic points to arise. As a prelude to this undertaking, the isothermal system will be considered, since, to the author's knowledge, its treatment has not been formalized elsewhere.

Discussion

Constant Temperature.—If temperature is not varied, the total absorbance at any wave length due to the concentrations of various species $(C_1, C_2 \ldots C_n)$ is given by

$$A(\lambda,C_i) = L \sum_{i=1}^{n} \epsilon_i(\lambda)C_i \qquad (1)$$

where ϵ_i is the molar absorptivity of the ith species and L is the path length, hereafter assumed to be unity. However, it is important to distinguish the species which are inter-convertible, *i.e.*, related through the law of mass action, from those which are not. To make this distinction, eq. 1 can be rewritten

$$A(\lambda,C_i,D_j) = \sum_{i=1}^{n} \epsilon_i(\lambda)C_i + \sum_{j=1}^{m} \epsilon_j(\lambda)D_j \qquad (2)$$

where the various species C_i are mutually dependent but independent of the various species D_j. If the total concentration of absorbing materials in the system remains invariant, the concentration of the group of dependent species C_i must remain constant and each species D_j remains constant

$$C_0 = \sum_{i=1}^{n} C_i \qquad (3)$$

and

$$D_j = D_{j0}\ ^{3}$$

Substituting $C_0 - \sum_{i=2}^{n} C_i$ for C_1 in (2) produces

$$A(\lambda,C_i,D_j) = \epsilon_1(\lambda)C_0 + \sum_{i=2}^{n} [\epsilon_i(\lambda) - \epsilon_1(\lambda)]C_i + \sum_{j=1}^{m} \epsilon_j(\lambda)D_j$$

At the isosbestic points, λ_c, the total absorbance remains invariant as the relative concentrations of the interdependent species change; thus, with variation of C_1

$$\frac{dA(\lambda_c,C_i,D_j)}{dC_1} = 0 = \sum_{i=2}^{n} [\epsilon_i(\lambda_c) - \epsilon_1(\lambda_c)] \frac{dC_i}{dC_1} + \sum_{j=1}^{m} \epsilon_j(\lambda_c) \frac{dD_j}{dC_1} \qquad (4)$$

By definition, $dD_j/dC_1 = 0$ and $dC_i/dC_1 \neq 0$; thus for the equality (4) to hold, the coefficients $\epsilon_i(\lambda_c) - \epsilon_1(\lambda_c)$ must all be zero; otherwise, the probability of the sum being zero is negligible. The same argument holds for each of the other species.

If, in eq. 4, $n = 2$, then $\epsilon_1 = \epsilon_2$. However, if n exceeds 2, the probability of $(n - 1)$ equations

$$\epsilon_i(\lambda_c) = \epsilon_1(\lambda_c)$$

is remote. This becomes evident through consideration of three spectra of components C_1 = A, C_2 = B, and C_3 = C in Fig. 3. If B and C cross A somewhere between λ_1 and λ_2, the probability of each crossing A in the interval $(\lambda_2 - \lambda_1)$ can be defined as unity. The probability that C will cross

(1) General Electric Co., Richland, Washington. This work was performed under contract no. AT(45-1)-1350 for the U. S. Atomic Energy Commission.

(2) The words "isobestic" and "isosbestic" appear in the literature with about the same frequency. "Isosbestic" is used in this paper because it derives from the Greek ($\sigma\beta\epsilon\sigma\tau\eta\sigma\iota\sigma\varsigma$) meaning "serving to extinguish."

(3) The concentrations D_j could represent a series of interdependent concentrations but have been chosen to be independent since such a choice does not result in a loss of generality.

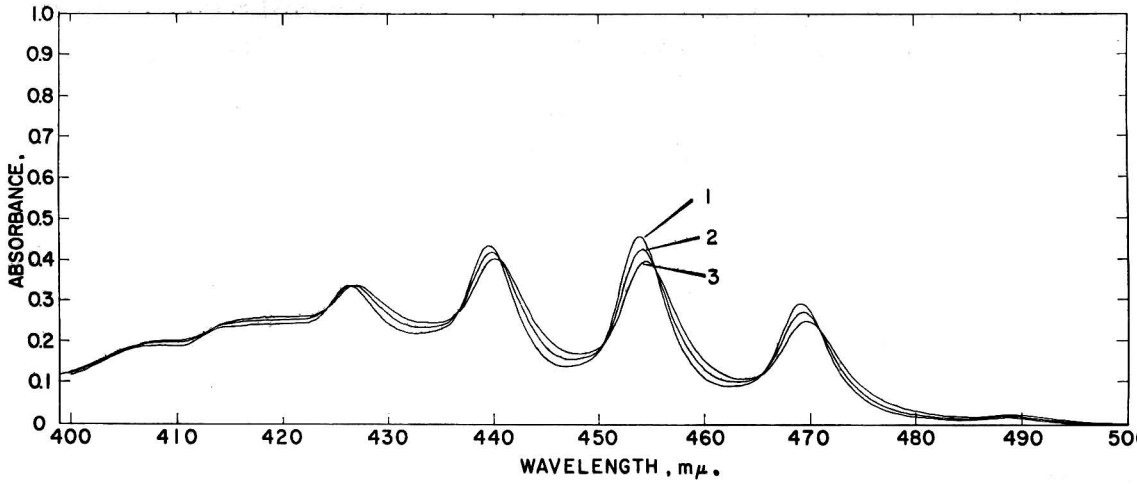

Fig. 1.—Pure molten $(C_2H_5)_4NUO_2(NO_3)_3$ at various temperatures: (1) $T = 110°$; (2) $T = 145°$; (3) $T = 175°$.

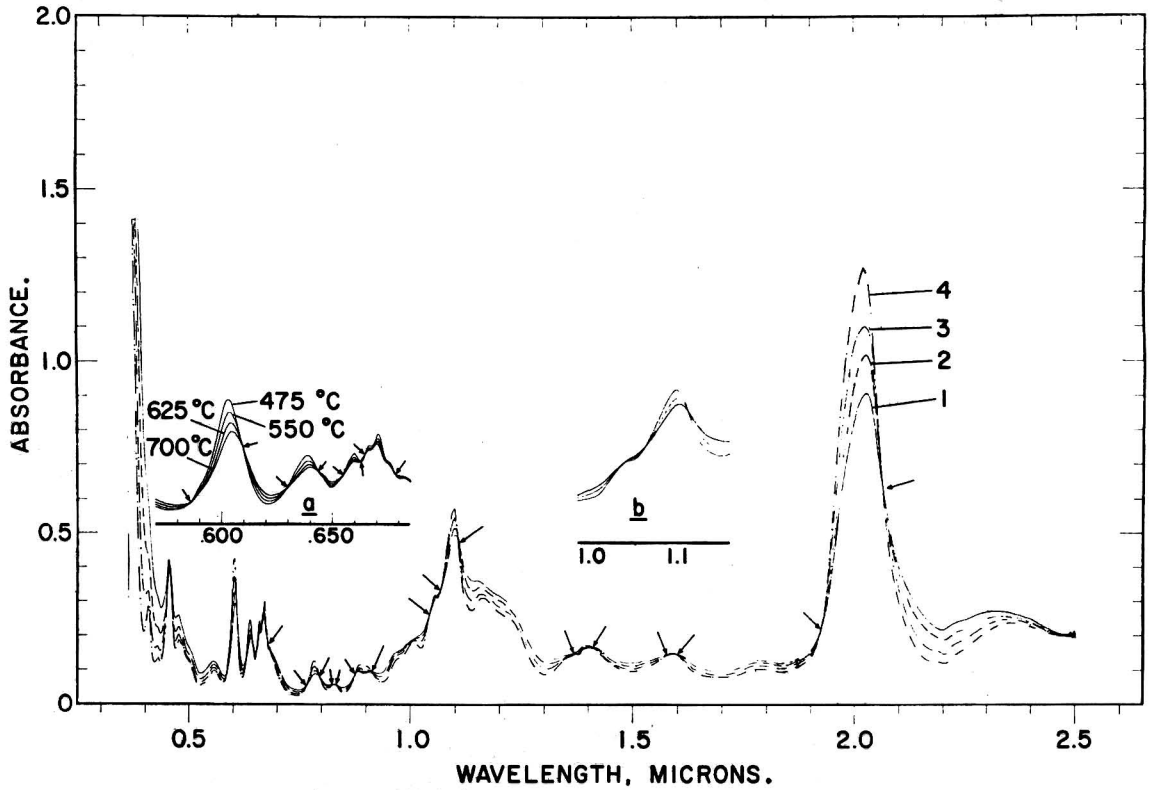

Fig. 2.—UCl_4 in $KAlCl_4$ solvent at various temperatures.

A within the increment $\delta\lambda_i$ from the crossing of A and B then is given by

$$P_i = \frac{\delta\lambda_i}{\sum_{\lambda_1}^{\lambda_2} \delta\lambda_i} = \frac{\delta\lambda_i}{\lambda_2 - \lambda_1}$$

For S such crossings, where S represents the number of isosbestic points on a spectrum, it follows that the probability would be

$$P = \prod^{S} \frac{\delta\lambda_i}{\lambda_n - \lambda_{n-1}}$$

and would become negligible if $\delta\lambda_i \to 0$. Therefore it follows that the existence of isosbestic points is strong evidence of only two *changing* absorbing, species, especially if several such points exist. Furthermore, it is easily shown that *all* intersections of two spectra are isosbestic points if these spectra arise from two solutions, a and b, containing only two absorbing species in different ratios constrained by the condition expressed in eq. 3

$$A^a(\lambda,C_i) = C_0\epsilon_1(\lambda) + [\epsilon_2(\lambda) - \epsilon_1(\lambda)]C_2^a + K$$

and

$$A^b(\lambda,C_i) = C_0\epsilon_1(\lambda) + [\epsilon_2(\lambda) - \epsilon_1(\lambda)]C_2^b + K$$

where

$$K = \sum_{j=1}^{m} \epsilon_j(\lambda)D_j$$

At the points of intersection, $A^a = A^b$, thus

$$[\epsilon_2(\lambda) - \epsilon_1(\lambda)]\, C_2^a = [\epsilon_2(\lambda) - \epsilon_1(\lambda)]C_2^b$$

but since $C_2^a \neq C_2^b$, $\epsilon_2(\lambda) - \epsilon_1(\lambda)$ must equal zero, the condition which uniquely guarantees isosbestic points.

Variable Temperature.—If temperature is also variable, eq. 2 becomes

$$A(\lambda,C_i,D_j,t) = \sum_{i=1}^{n} \epsilon_i(\lambda,t)C_i(t) + \sum_{j=1}^{m} \epsilon_j(\lambda,t)D_j(t) \quad (5)$$

There may be two independent forms of temperature dependence for C_i, one due to volume expansion, $f(t)$, and the other due to the temperature dependence of the equilibrium of C_i with its environment, $g_i(t)$

$$C_i(t) = C_i^0 f(t) g_i(t) \quad (6)$$

The concentrations at a reference temperature are represented by C_i^0 and D_j^0. Since $f(t) = 1/(1 + \alpha t)$ where α is the coefficient of expansion, eq. 5 can be rewritten

$$A(\lambda,C_i,D_j,t) = \left(\frac{1}{1+\alpha t}\right) \times \left[\sum_{i=1}^{n} \epsilon_i(\lambda,t)C_i^0 g_i(t) + \sum_{j=1}^{m} \epsilon_j(\lambda,t)D_j^0\right]$$

At an isosbestic point resulting from a temperature change, the derivative of the absorbance with respect to the temperature is zero

$$\frac{dA(\lambda_c,C_i,D_j,t)}{dt} = 0 = \sum_{i=1}^{n}\left[g_i(t)\frac{d\epsilon_i(\lambda_c,t)}{dt} + \epsilon_i(\lambda_c,t)\frac{dg_i(t)}{dt} - \left(\frac{\alpha}{1+\alpha t}\right)\epsilon_i(\lambda_c,t)g_i(t)\right]C_i^0 + \sum_{j=1}^{m}\left[\frac{d\epsilon_j(\lambda_c,t)}{dt} - \left(\frac{\alpha}{1+\alpha t}\right)\epsilon_j(\lambda_c,t)\right]D_j^0 \quad (7)$$

Again the coefficients of C_i^0 and D_j^0 must be zero in order for eq. 7 to hold with any degree of probability. They therefore give rise to two differential equations, the solutions of which are either trivial, when

$$\frac{d\epsilon_i(\lambda_c,t)}{dt} = \frac{d\epsilon_j(\lambda_c,t)}{dt} = \epsilon_i(\lambda_c,t) = \epsilon_j(\lambda_c,t) = 0 \quad (8)$$

or are

$$\epsilon_i(\lambda_c,t)g_i(t) = \epsilon_i^0(\lambda_c)g_i^0(1+\alpha t) \quad (9)$$

and

$$\epsilon_j(\lambda_c,t) = \epsilon_j^0(\lambda_c)(1+\alpha t) \quad (10)$$

Thus $(n + m)$ equations of the form (8), (9), or (10) must hold at every isosbestic point and $S(n + m)$ such equations must hold for a given spectrum. Since there is no implicit relationship between the absorptivity of a species and its equilibrium with other species, the probability of the existence of $n \times S$ equations 9 and $m \times S$ equations 10 is negligible if n, m, or S is greater than 1 and ϵ_i, ϵ_j, and g_i are functions of t. The only way that two or more species can exist is for eq. 8 to hold for all but one species and eq. 9 or 10 to hold for the remaining species. Furthermore, if this species is an ith species, it is improbable that S relations

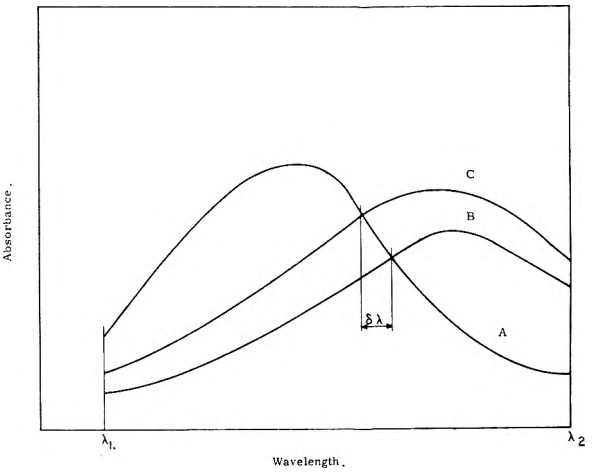

Figure 3.

$$\epsilon_i(\lambda_c,t)g_i(t) = \epsilon_i^0(\lambda_c)g_i^0(1+\alpha t)$$

will exist for one species unless either ϵ_i or g_i is temperature independent. If ϵ_i is temperature independent, then

$$g_i(t) = g_i^0(1+\alpha t)$$

This, however, would result in an unchanged spectrum, *i.e.*, completely independent of temperature, since α is not a function of λ. Moreover, if the temperature dependence of g_i were $1/(1 + \beta t)$ where $\alpha \neq \beta$, then independent spectra would result with no points of intersection. It therefore follows that temperature-induced isosbestic points arise only if $g_i = g_i^0$; *i.e.*, there can be no change in the concentration of the species absorbing at the isosbestic point due to being in chemical equilibrium with a non-absorbing species. In addition, the temperature dependence of ϵ_i must be of the form

$$\epsilon_i(\lambda_c,t) = \epsilon_i^0(1 + h(\lambda)t) \quad (11)$$

Since the ith species must not be in equilibrium with any other species, by definition it becomes a jth species. It therefore is concluded that only a jth species can contribute to the absorbance at an isosbestic point. Isosbestic points thus will occur wherever $h(\lambda) = \alpha$.

Attempts to Correct Spectra for Liquid Expansion.—If one attempts to correct the concentration term of the absorbance for expansion of the fluid, isosbestic points generated by temperature change do not vanish but, as shown by the following argument, they merely shift.

At an isosbestic point made by two spectra obtained at temperatures t_1 and t_2, the relationship

$$\epsilon_i(\lambda_c,t_1)C_i(t_1) = \epsilon_i(\lambda_c,t_2)C_i(t_2)$$

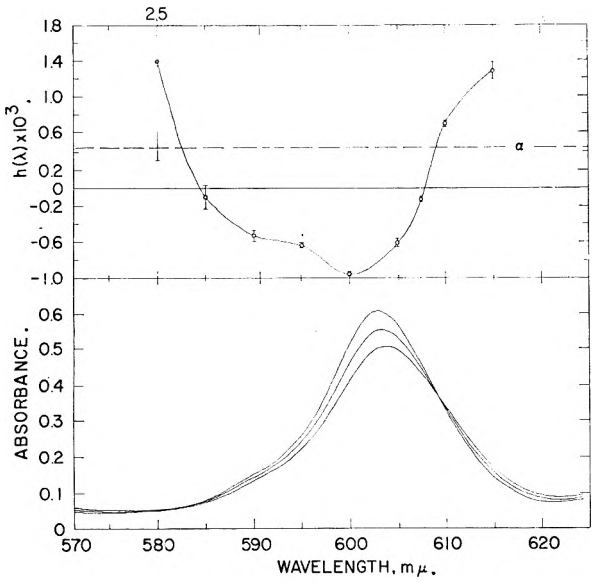

Fig. 4.—An example of the function $h(\lambda)$ for the region 575–625 mμ of Fig. 2.

is valid. An attempt to correct $C_i(t_2)$ to $C_i(t_1)$ by multiplying $C_i(t_2)$ by $(1 + \alpha t_2)/(1 + \alpha t_1)$ results in the inequality

$$\epsilon_i(\lambda_c,t_1)C_i(t_1) \neq \epsilon_i(\lambda_c,t_2)\frac{(1 + \alpha t_2)}{(1 + \alpha t_1)}C_i(t_2) \quad (12)$$

thus destroying the isosbestic point at λ_c. However, to a good approximation, a new isosbestic point λ_c' will occur in the vicinity of λ_c. That the value of $h(\lambda_c')$ at the new isosbestic point is zero can be obtained from eq. 12 after removing the inequality by replacing λ_c by λ_c' and substituting eq. 6 and 11 into it, keeping in mind that $g_i(t)$ is now unity. However, if the expansion coefficient is not known accurately and an assumed value γ is used in the corrective term for concentration, *i.e.*, $C_i(t_2)\cdot((1 + \gamma t_2)/(1 + \gamma t_1))$, eq. 13 results

$$\frac{(1 + h(\lambda_c')t_1)}{(1 + \alpha t_1)} = \frac{(1 + h(\lambda_c')t_2)(1 + \gamma t_2)}{(1 + \alpha t_2)(1 + \gamma t_1)} \quad (13)$$

By solving for $h(\lambda_c')$, expanding, and simplifying terms eq. 14 is obtained

$$h(\lambda_c') = \frac{\alpha - \gamma}{(1 + \gamma t_1) + (1 + \alpha t_1)\gamma t_2} = \frac{K}{1 + K't_2} \cong K \quad (14)$$

As indicated above, when an accurate correction is made then $\alpha = \gamma$ and the new isosbestic point occurs where $h(\lambda_c')$ is not dependent upon t_2 but is zero; even when $\alpha \neq \gamma$, unless γt_2 is very large, $h(\lambda_c')$ is only slightly dependent upon t_2. Thus the temptation to conclude that isosbestic points in spectra corrected to a common concentration prove the existence of two species must be avoided. It is to be noted from eq. 14 and results below that as γ increases, $h(\lambda_c')$ continually decreases. From the nature of the function $h(\lambda)$, it will become obvious that paired isosbestic points will shift closer together as $h(\lambda_c')$ decreases, finally coinciding when $h(\lambda_c')$ is equal to the minimum value of $h(\lambda)$.

Properties of the Temperature Broadening Function.—The function $h(\lambda)$ might be termed the temperature broadening function and generally will be a minimum (a negative value) at or near the absorption peak, depending on whether there is a shift in the peak with temperature. If the transition probability is temperature independent, the area under the absorption peak should remain constant. To ensure this, the function $h(\lambda)$ must become positive on both sides of the wave length of maximum absorbance. Isosbestic points thus will occur whenever $h(\lambda)$ equals α and often will occur in pairs on each side of the peak. This is observed in Fig. 1 and 2.

Figure 4 shows $h(\lambda)$ averaged from three independently obtained values of $h(\lambda)$ according to the equation

$$h(\lambda) = \frac{A(\lambda,t_n)(1 + \alpha t_n) - A(\lambda,t_m)(1 + \alpha t_m)}{A(\lambda,t_m)(1 + \alpha t_m)t_n - A(\lambda,t_n)(1 + \alpha t_n)t_m}$$

obtained by simultaneous solution of the equations

$$A(\lambda,t_n) = C_i^0\epsilon_i^0\left(\frac{1 + h(\lambda)t_n}{1 + \alpha t_n}\right)$$

and

$$A(\lambda,t_m) = C_i^0\epsilon_i^0\left(\frac{1 + h(\lambda)t_m}{1 + \alpha t_m}\right)$$

In each case, the average deviation of $h(\lambda)$ was within the precision of the individual measurements, indicating that $h(\lambda)$ is not in itself a function of t. Using the curve for $h(\lambda)$ and comparing with $h(\lambda_c')$ from eq. 13, one can predict where the new intersections will be if curves 2 and 3 in Fig. 4a are multiplied by factors $(1 + \gamma t_2)/(1 + \gamma t_1)$ and $(1 + \gamma t_3)/(1 + \gamma t_1)$, respectively. It is clear from Table I that, within experimental accuracy, isosbestic points are not destroyed by such operations, unless γ is large enough to separate the curves completely.

TABLE I

THE SHIFT OF ISOSBESTIC POINTS BY LINEAR TEMPERATURE CORRECTION

Assumed temp. coeff. (γ)	Spectral designation M	N	$h(\lambda c')$ $\times 10^3$	Crossing wave length of curves, Å.
10^{-5}	1	2	0 405	6095
	1	3	.405	6095
	2	3	405	6095
10^{-4}	1	2	.287	6091
	1	3	.285	6091
	2	3	.283	6091
10^{-3}	1	2	− .270	6073
	1	3	− .261	6074
	2	3	− .250	6075
10^{-2}	1	2	− .775	6024
	1	3	− .773	6030
	2	3	− .675	6037

Summary.—If an absorbing sample produces several isosbestic points as temperature is varied,

these conclusions can be drawn with considerable confidence: 1. Only one species contributes to the absorbance at a given isosbestic point. 2. The equilibrium of this species is not appreciably affected by temperature changes. 3. The only manner in which isosbestic points can be generated is for the absorptivity of one species at a given wave length to be linearly dependent on temperature, at least to a good approximation.[4] 4. Multiplication of a family of absorption spectra generated at temperatures t_1, t_2, t_3, . . . t_n by the corresponding factor $(1 + \gamma t_n)/(1 + \gamma t_1)$, to a good approximation, only shifts and does not destroy the isosbestic points which have resulted in the original generation.

NOTE ADDED IN PROOF.—Since the foregoing paper was submitted for publication, Cohen and Fischer have concluded in a paper entitled "Isosbestic Points" (*J. Chem. Soc.*, 3044 (1962)) that whenever absorbing components are related linearly, isosbestic points are not confined to two-component systems. It is hoped that the foregoing paper will clearly show that although possible in principle, it is exceedingly unlikely that isosbestic points will arise from multicomponent absorbing systems, even when they are linearly related, especially when more than one isosbestic point occurs.

Cohen and Fischer are correct in stating that systems producing isosbestic points are characterized by only one degree of freedom. At constant temperature two absorbing components are allowed, provided they are linearly related. When temperature is varied, there are no compositional degrees of freedom and only one absorbing component is allowed. Presumably, then, variation of total pressure on a system containing only one absorbing component could give rise to isosbestic points.

Acknowledgments.—The tetraethylammonium dioxotrinitratouranate(VI) of Fig. 2 was kindly supplied by J. L. Ryan of this Laboratory. The author also wishes to acknowledge Drs. G. P. Smith and C. R. Boston for a stimulating discussion on this subject.

(4) It is possible that $\epsilon_i(\lambda) = \epsilon_i^0(\lambda)\exp k(\lambda)t$; in the approximation of $k(\lambda)t << 1$, it would thus assume the form given in eq. 11.

SECONDARY REACTIONS IN CONTROLLED POTENTIAL COULOMETRY. II. SECONDARY ELECTRODE REACTIONS

BY ALLEN J. BARD AND JASPAL S. MAYELL

Department of Chemistry, The University of Texas, Austin 12, Texas

Received April 23, 1962

Controlled potential coulometric experiments in which the product of the primary electrode reaction undergoes secondary chemical reactions involving the formation of an electroactive species are considered. A mathematical treatment of the effect of these secondary reactions upon n_{app}, the apparent number of faradays per mole of electroactive material, and upon current–time behavior, is given. The use of controlled potential coulometric data for the determination of the number of electrons involved in each electrode reaction, for the elucidation of the over-all reaction mechanism, and for the estimation of the rate constants of the intervening chemical reactions, is described, and several examples are given.

Introduction

Controlled potential coulometric electrolysis, a technique for studying electrode reactions, is mainly used for the determination of n, the number of faradays per mole of electroactive substance consumed, and for the production of macro amounts of electrolysis products. When secondary chemical reactions occur, non-integral n-values are sometimes found, and by examination of the variation of n with such variables as concentration and stirring rate, information about the mechanism of the electrode reaction can be obtained. In a previous communication[1] the effects of secondary chemical reactions between the product of the primary electrode reaction and the original electroactive species, or secondary reactions leading to the regeneration of the electroactive species, were discussed. This paper discusses cases in which the product of the primary electrode reaction undergoes reactions leading to the occurrence of additional electrode reactions, and the effect of these secondary electrode reactions upon n, and upon the variation of the electrolysis current with time. The use of controlled potential coulometric data for the determination of the number of electrons involved in the electrode reactions, for the elucidation of the over-all mechanism of the electrode reaction, and for the estimation of the rate constants of the intervening chemical reactions, is described.

(1) D. H. Geske and A. J. Bard, *J. Phys. Chem.*, **63**, 1057 (1959).

Classification.—The four general cases are classified according to the behavior of the reaction intermediate, R. The primary electrode reaction is represented as

$$C \pm ne^- \longrightarrow R$$

where C is the electroactive material and R is the soluble primary product of the electrode reaction. In the reactions below, A, B, P, R_2, Y, and Z represent electrolytically inert materials and the applied potential is such that all electrode reactions occur without activation polarization.

Case I. R′ Undergoes a Single Secondary Pseudo-first Order Reaction and an Electrode Reaction.—

$$R \rightleftarrows R'$$

$$R' + Z \longrightarrow P$$

$$R' \pm ne^- \longrightarrow Y$$

Case II. R′ Undergoes a Single Second-order Reaction and an Electrode Reaction.—

$$R \rightleftarrows R'$$

$$2R' \longrightarrow R_2$$

$$R' \pm ne^- \longrightarrow Y$$

Case III. R Undergoes Parallel Pseudo-first Order Secondary Reactions, One of Which Produces an Electroactive Species.—

$$R + Z \longrightarrow R' + B$$

$$R + A \longrightarrow P$$

$$R' \pm ne^- \longrightarrow Y$$

Case IV. R Undergoes Parallel Secondary Reactions; a Second-order Reaction and a Pseudo-first Order Reaction Which Produces an Electroactive Species.—

$$R + Z \longrightarrow R' + A$$

$$2R \longrightarrow R_2$$

$$R' \pm ne^- \longrightarrow Y$$

Variations of these cases, two of which are discussed later, can be treated by suitable modification of the procedure outlined below.

Mathematical Treatment

General Considerations.—The assumptions and conditions of this treatment are the same as those previously described.[1] The current, i, taken as a positive quantity, is related to the rate of consumption of C and the rate of the production of Y by

$$i = -n_1FV[d(C)/dt] \text{ electrode reaction} + n_2FV[d(Y)/dt] \text{ electrode reaction} \quad (1)$$

where F is the faraday, V is the total volume of the solution, and (C) and (Y) are the concentrations of species C and Y, respectively. The rates of concentration change under limiting current conditions are

$$[d(C)/dt] \text{ elec. rxn.} = -p(C) \quad (2)$$

$$[d(Y)/dt] \text{ elec. rxn.} = p(R') \quad (3)$$

where p is a constant, depending upon the prevailing mass transfer conditions, electrode area, solution volume and cell geometry,[1] and is assumed to be the same for both electrode reactions. Combination of (1), (2), and (3) yields

$$i = n_1FVp(C) + n_2FVp(R') \quad (4)$$

The apparent number of electrons per mole of electroactive materials, n_{app}, is determined experimentally, and is defined as

$$n_{app} = \frac{\int_0^t i\,dt}{FV[(C_i) - (C)]} \quad (5)$$

where (C_i) is the initial concentration of C. The notation n^0_{app} refers to evaluation of n_{app} at the completion of the electrolysis, where (C) approaches zero

$$n^0_{app} = \frac{\int_0^\infty i\,dt}{FV(C_i)} = \frac{Q}{FN} \quad (6)$$

where N is the number of moles of C, and Q is the amount of electricity consumed in coulombs.

Since C is only involved in the primary electrode reaction, the equation

$$(C) = (C_i)e^{-pt} \quad (7)$$

holds in all cases.

Case I.—The intermediate R changes to R′ before undergoing the competing reactions

$$R' + Z \xrightarrow{k_1} P \quad (8)$$

$$R' \pm n_2e^- \longrightarrow Y \quad (9)$$

The production of R′ is assumed to be rapid enough so that the rate of this reaction does not enter into the over-all kinetics of the reaction. When k_1 is either very large or very small, integral values of n^0_{app} are obtained. For $k_1 \approx 0$, the reaction is composed of two succeeding electrode reactions, and $n^0_{app} = n_1 + n_2$, while when k_1 is large, $n^0_{app} \approx n_1$. For the purposes of this discussion Z is assumed present in large excess, so that (8) is a pseudo-first order reaction, with $k_1' = k_1(Z)$. The system is described by the equation

$$d(R')/dt = p(C) - k_1'(R') - p(R') \quad (10)$$

Solving (7) and (10), the value of R′ as a function of time is obtained

$$(R') = \frac{p}{k_1'}(C_i)e^{-pt}(1 - e^{-k_1't}) \quad (11)$$

Combining (4) and (11) the variation of i with time is obtained

$$i = FpV(C_i)e^{-pt}\left[n_1 + n_2\frac{p}{k_1'}(1 - e^{-k_1't})\right] \quad (12)$$

The log current *vs.* time plots in Fig. 1 indicate that the observed deviation from linearity is only slight. Integration of eq. 12 with respect to time, and introduction into (6) yields

$$n^0_{app} = n_1 + n_2[1/(1 + \lambda)] \quad (13)$$

where $\lambda = k_1'/p$. Variation of n^0_{app} with λ, shown in Fig. 2, indicates that non-integral values of n^0_{app} will be obtained for a range of λ of 10^{-2} to 10^2. For this reaction scheme, n^0_{app} is independent of changes in (C_i).

The modification of Case I, where the production of R′ is kinetically controlled

$$R \xrightarrow{k_1} R' \quad (14)$$

with no competitive secondary reaction, may be treated in a similar manner. The equations describing the system are

$$d(R)/dt = p(C) - k_1(R) \quad (15)$$

$$d(R')/dt = k_1(R) - p(R') \quad (16)$$

Solving (7), (15), and (16) yields

$$(R') = \frac{k_1 p(C_i)}{(k_1 - p)^2}\left[(k_1 - p)te^{-pt} - e^{-pt} + e^{-k_1 t}\right] \quad (17)$$

and

$$i = pFV(C_i)\left\{n_1 e^{-pt} + \frac{n_2 k_1 p}{(k_1 - p)^2}\times \left[(k_1 - p)te^{-pt} - e^{-pt} + e^{-k_1 t}\right]\right\} \quad (18)$$

Variations of log i with t for several values of k_1 is shown in Fig. 3. Under all conditions $n^0_{app} = n_1 + n_2$.

Case II.—The intermediate R changes to R′ before undergoing the competing reactions

$$2R' \xrightarrow{k_1} R_2 \quad (19)$$

$$R' \pm n_2 e \longrightarrow Y \quad (20)$$

The limits of n^0_{app} for very large and very small k_1's are the same as in Case I. The production of R′ is given by

$$d(R')/dt = p(C) - p(R') - k_1(R')^2 \quad (21)$$

Combining (21) with (7), a second degree equation in (R') and t which cannot be solved in closed form is obtained. This equation also results as a special case of the reaction scheme in case IV, and results of the numerical solution of this equation will be discussed in that section.

Case III.—R reacts in two parallel chemical reactions, and an electroactive substance is produced in one of these

$$R + Z \xrightarrow{k_1} R' + B \quad (22)$$

$$R + A \xrightarrow{k_2} P \quad (23)$$

$$R' \pm n_2 e^- \longrightarrow Y \quad (24)$$

This treatment assumes Z and A are present in large excess, so that reactions 22 and 23 are pseudo-first order reactions, with $k_1' = k_1(Z)$ and $k_2' = k_2(A)$. When the ratio of k_1'/k_2' is large, n^0_{app} is essentially $n_1 + n_2$, while when k_1'/k_2' is small, $n^0_{app} \approx n_1$. The system is described by the equations

$$d(R)/dt = p(C) - (k_1' + k_2')(R) \quad (25)$$

$$d(R')/dt = k_1'(R) - p(R') \quad (26)$$

Combining (25) and (7) and solving for (R) yields

$$(R) = \frac{p(C_i)}{(k_1' + k_2' - p)}\left[e^{-pt} - e^{-(k_1' + k_2')t}\right] \quad (27)$$

Substituting (27) and (26), and solving for (R'), gives

$$(R') = \frac{k_1' p(C_i)}{(k_1' + k_2' - p)^2}\times e^{-pt}\left[e^{-(k_1' + k_2' - p)t} + (k_1' + k_2' - p)t - 1\right] \quad (28)$$

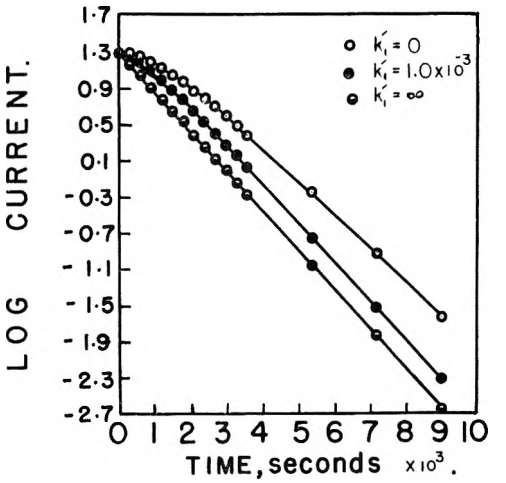

Fig. 1.—Case I: log i *vs.* t at different values of k_1', calculated for $V = 0.2$ l., $p = 10^{-3}$ sec.$^{-1}$, $(C_i) = 1.0$ mM, and $n_1 = n_2 = 1$.

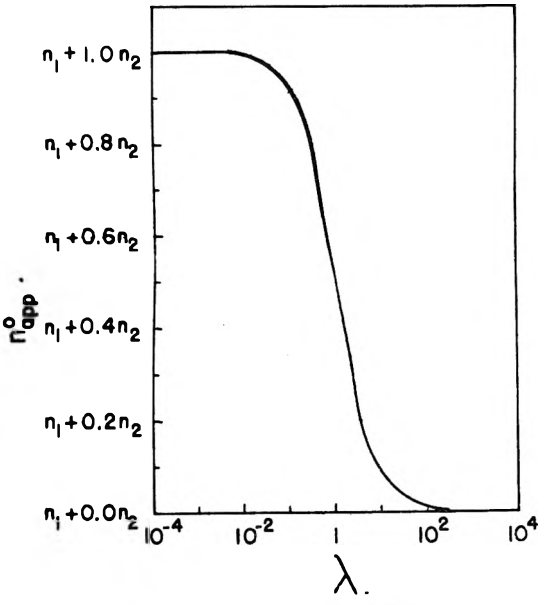

Fig. 2.—Case I: variation of n^0_{app} with λ.

and, from (4)

$$i = pFV(C)e^{-pt}\left[n_1 + \frac{n_2 k_1' p}{(k_1' + k_2' - p)^2}\times \left[e^{-(k_1' + k_2' - p)t} + (k_1' + k_2' - p)t - 1\right]\right] \quad (29)$$

The variation of current with time for several values of k_1' and k_2' is shown in Fig. 4. Combination of (29) and (6) yields

$$n^0_{app} = n_1 + n_2[1/(1 + \lambda')] \quad (30)$$

where $\lambda' = k_2'/k_1'$. Equation 30 is the same form as (13), and variation of n^0_{app} with λ' can be observed from Fig. 2, if λ is replaced by λ'.

Case IV.—R reacts in two parallel chemical reactions, one a second-order reaction and the other a pseudo-first order reaction generating an electroactive species.

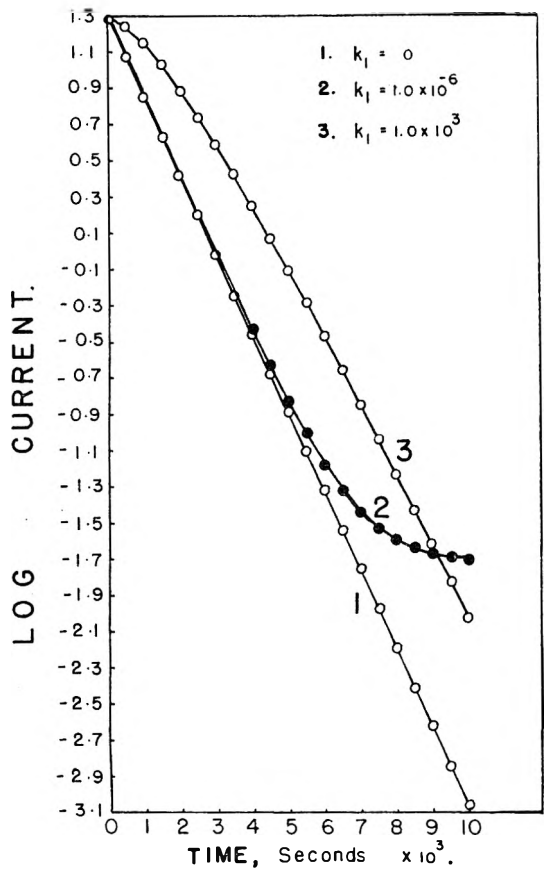

Fig. 3.—Case I: log i *vs.* t at different values of k_1 calculated for V = 0.2 l., $p = 10^{-3}$ sec.$^{-1}$, (C_i) = 1.0 mM, and $n_1 = n_2 = 1$.

$$R + Z \xrightarrow{k_1} R' + B \qquad (31)$$

$$2R \xrightarrow{k_2} R_2 \qquad (32)$$

$$R' \pm n_2e^- \longrightarrow Y \qquad (33)$$

The system is described by the equations

$$d(R)/dt = p(C) - k_1'(R) - k_2(R)^2 \qquad (34)$$

$$d(R')/dt = k_1'(R) - p(R') \qquad (35)$$

where $k_1' = k_1(Z)$, Z being assumed present in large excess. Combination of (24) and (7) yields

$$d(R)/dt = p(C_i)e^{-pt} - k_1'(R) - k_2(R)^2 \qquad (36)$$

It was not possible to obtain a closed-form solution of eq. 36. Numerical solutions were obtained with the aid of a CDC 1604 computer employing a program based on the Adams-Moulton and Runge-Kutta methods. The values of (R) as a function of time for several values of k_1' and k_2 are shown in Fig. 5. Combination of (4), (6), and (7) yields

$$n^0_{app} = n_1 + \frac{n_2 p}{(C_i)} \int_0^\infty (R')dt \qquad (37)$$

and solving (35)

$$\int_0^\infty (R')dt = \frac{k_1'}{p} \int_0^\infty (R)dt \qquad (38)$$

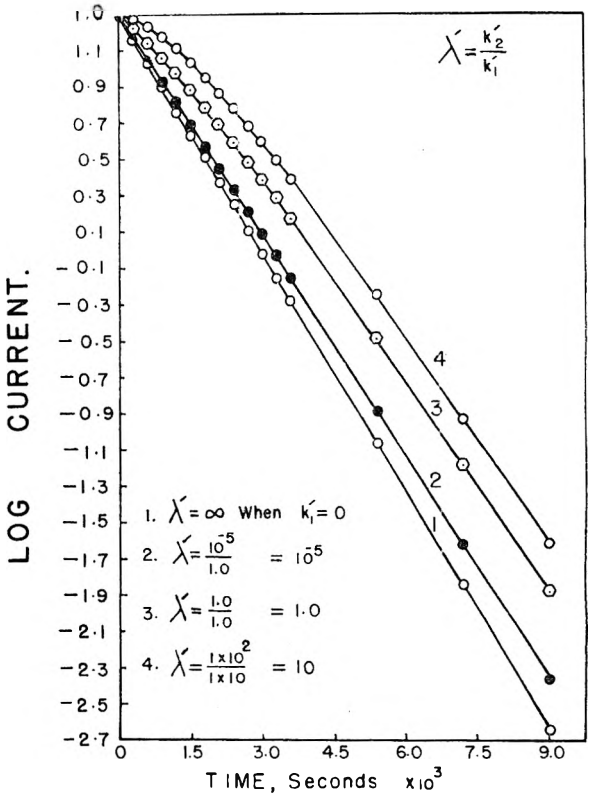

Fig. 4.—Case III: log i *vs.* t at different values of k_2'/k_1' calculated for V = 0.2 l., $p = 10^{-3}$ sec.$^{-1}$, (C_i) = 1.0 mM, and $n_1 = n_2 = 1$.

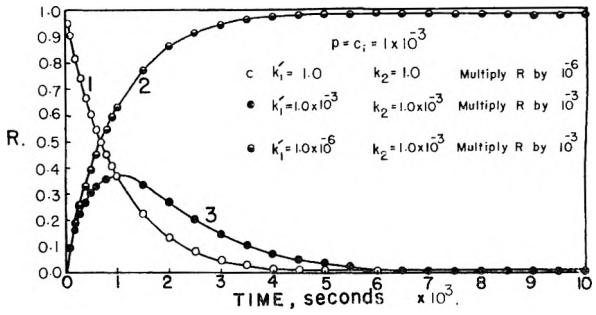

Fig. 5.—Case IV: variation of (R) with t at different values of k_1', k_2, p, and C_i.

The values of $\int_0^\infty (R)dt$ were obtained by graphical integration of (R) *vs.* time plots, and values of n^0_{app} for different values of k_1' and k_2 are shown in Fig. 6. Although the behavior of (R) with time is different for the same value of the ratio k_1'/k_2, for different individual values of k_1' and k_2 (compare curves 1 and 3, Fig. 5), the area under curves of the same k_1'/k_2, when multiplied by $k_1'/(C_i)$, are the same, so that the curves in Fig. 6 depend only upon the ratio of the rate constants.

The variation of the current with time was calculated for several values of k_1' and k_2 by solving eq. 35 for (R'), using values of (R) obtained from the numerical solution of (36), and introducing them into (4). The current–time curves in Fig. 7 depend upon the individual values of k_1' and k_2, rather than their ratio.

Discussion

The rate constants for the secondary chemical reactions in the preceding schemes can be determined from (1) the behavior of the electrolysis current with time, (2) the variation of n^0_{app} with p and (C_i), and (3) the relative quantities of products formed. The current–time behavior in general does not give sufficient information to allow the prediction of reaction mechanisms or the estimation of rate constants. In all cases the current decays to background level, and the slight curvature of log i–t curves, although indicative of kinetic complications, is not significant enough to allow differentiation between the cases. Moreover, curvature of log i–t curves may result in even simple electrode reactions if the potential of the electrode is not maintained at the mass-transfer limiting region. However current–time curves do allow differentiation between these cases and catalytic reactions[1] (reactions involving the regeneration of the original electroactive substance by a chemical reaction following the electrode reaction), in which case the current decays to a constant value larger than the background current.

Differentiation among the four cases under study here can be most easily accomplished by observing the variation of n^0_{app} with (C_i), p, and solvent. In case I, n^0_{app} is independent of (C_i), but varies with p. In case III, n^0_{app} is independent of both (C_i) and p. Cases II and IV are indicated when n^0_{app} is dependent upon both (C_i) and p. Differentiation between these two cases may sometimes be accomplished by changing the solvent or supporting electrolyte (the usual reactants in the secondary chemical reaction), since case IV involves reaction with a second substance while case II does not. Variation of n^0_{app} with temperature will sometimes be a useful diagnostic aid.[2] The analysis of products obtained in controlled potential coulometry is certainly an important aid for deducing reaction mechanisms. Quantitative analysis of these products should lead to reinforcement of the n^0_{app} data. In some cases this data alone may be useful in estimating rate constants, especially when n^0_{app} data is difficult to obtain, (*e.g.*, when an appreciable background current is present).

The range of rate constants accessible for evaluation by these methods depends upon the particular case. Taking p to be adjustable between 10^{-1} and 10^{-4} sec.$^{-1}$, then for case I, k_1' in the range of 1 to 10^{-6} sec.$^{-1}$ will lead to non-integral values of n^0_{app}. For case II, the range of k_1 is between 10^{-1} and 10^{-7} sec.$^{-1}$, for usual concentrations. For cases III and IV only a ratio of rate constants can be obtained. This ratio may be between 10^{-2} and 10^{2} for case III, and between 10^{-4} and 1 (depending upon (C_i)) for case IV. For very large rate constants, the theoretical model may not apply, even if the ratio of rate constants may still appear in the accessible range, since most of the chemical reaction will occur very close to the electrode surface and the homogeneous concentration of intermediate assumed in this treatment will not be obtained. Although qualitatively similar results will be observed in such cases, the calculated numerical value of k_1'/k_2 may be significantly in error.

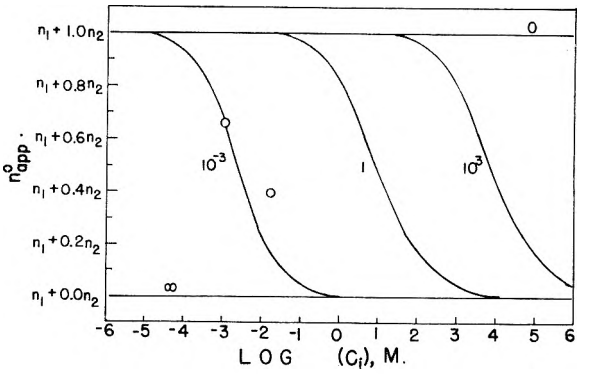

Fig. 6.—Case IV: variation of n^0_{app} with log (C_i) at different values of $\lambda = k_1'/k_2$. O, experimental points obtained for electroreduction of benzyldimethylanilinium bromide at −35° in acetonitrile.

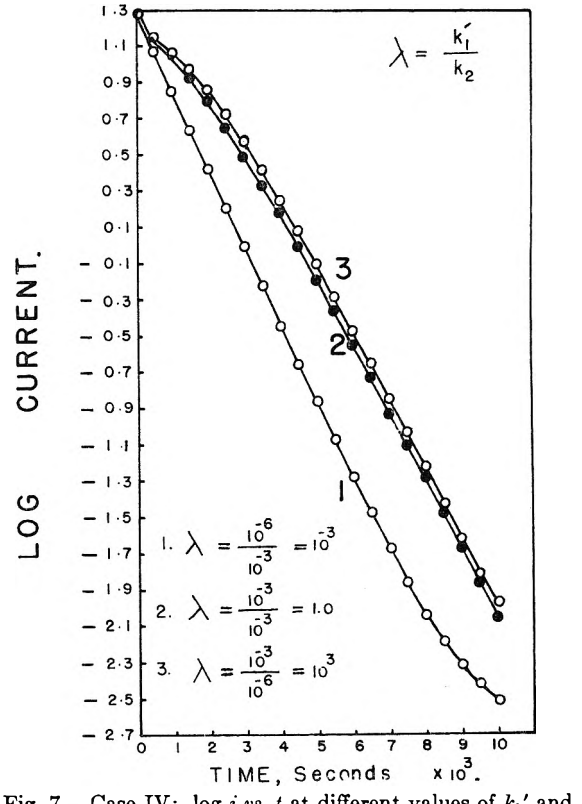

Fig. 7.—Case IV: log i *vs.* t at different values of k_1' and k_2 calculated for V = 0.2 l., $p = 10^{-3}$ sec.$^{-1}$, (C_i) = 1.0 mM, and $n_1 = n_2 = 1$.

Examples of reaction schemes illustrated by the preceding cases will often be found in electrode reactions of organic substances. Frequently the product of the electrode reaction is a free radical which may couple with another radical, react with the solvent, or undergo further electrode reactions. Although the electroreduction of the potassium salt of 2-carboxybenzaldehyde (I) has not been studied by controlled potential coulometry, the products of the electrode reaction are said to be hydrodiphthalyl (II) and phthalide (III).[3,4] A

(2) J. S. Mayell and A. J. Bard, to be submitted for publication.

(3) V. M. Rodionow and V. V. Levchenko, *J. Gen. Chem. U.S.S.R.*, **6**, 1563 (1936).

possible reaction mechanism leading to these products and corresponding to case II involves the reactions

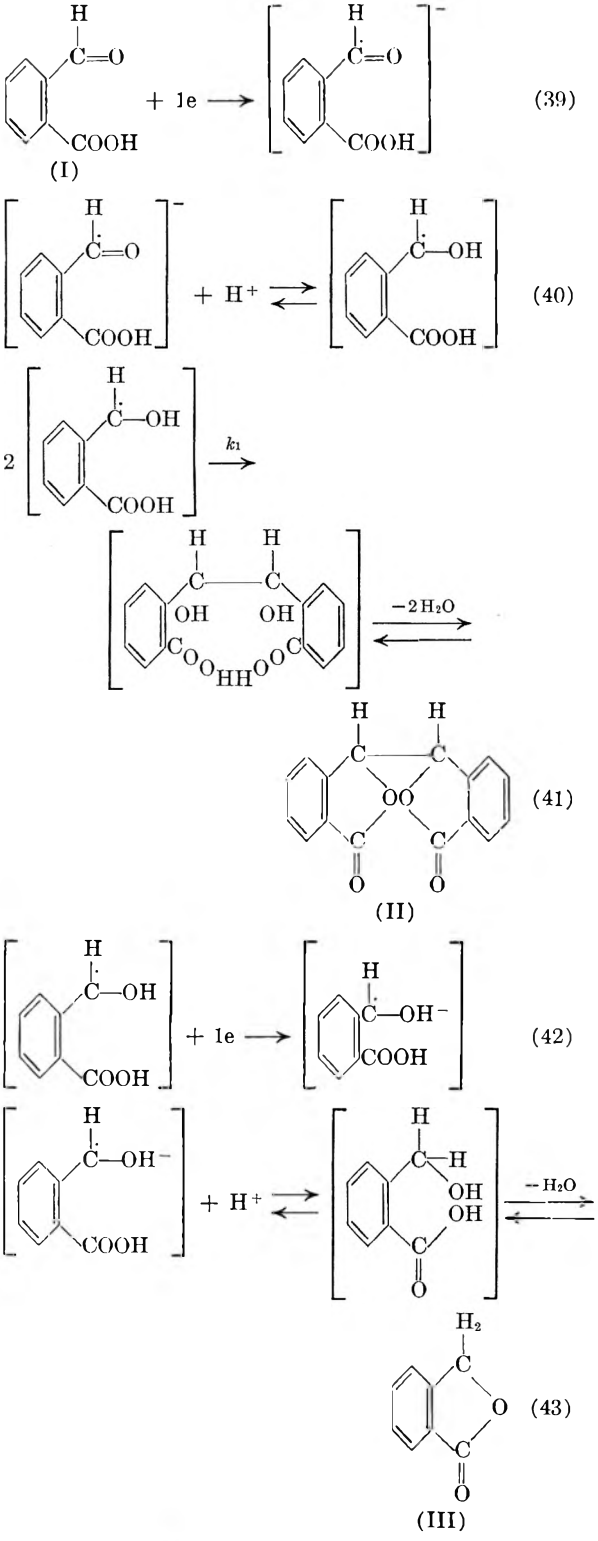

The electroöxidation of hydrazine at a platinum electrode, recently discussed by Karp and Meites,[5,6]

(4) M. J. Allen, "Organic Electrode Processes," Chapman and Hall, London, 1958, p. 71.

(5) S. Karp, M.S. Thesis, Polytechnic Institute of Brooklyn, 1960.

(6) S. Karp and L. Meites, *J. Am. Chem. Soc.*, **84**, 906 (1962).

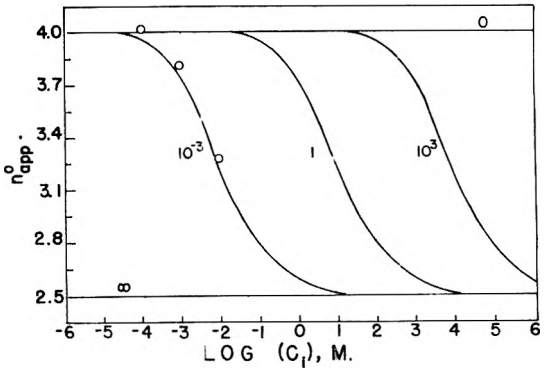

Fig. 8.—Variation of n^0_{app} with log (C_i) for modification of case II for different values of p/k_1: O, experimental points from results of Karp and Meites for electroöxidation of hydrazine, in 0.05 F H_2SO_4.

is related to case II. The mechanism proposed by these authors for dilute sulfuric acid solutions is essentially

$$N_2H_4 - 2e \longrightarrow N_2H_3^+ + H^+ \quad (44)$$

$$N_2H_3^+ \rightleftharpoons N_2H_2 + H^+ \quad (45)$$

$$^1/_2(2N_2H_2 \xrightarrow{k_1} NH_3 + HN_3) \quad (46)$$

$$^1/_2(HN_3 - 1e \longrightarrow H^+ + {}^3/_2N_2) \quad (47)$$

$$N_2H_2 - 2e \longrightarrow N_2 + 2H^+ \quad (48)$$

The previous treatment of case II requires modification before application to this reaction scheme because of reaction 47. The treatment is very similar to that given previously and the result is[7]

$$n^0_{app} = n_1 + n_2 + \frac{p(n_3 - n_2)}{(C_i)} \int_0^\infty (R')\, dt \quad (49)$$

where n_1, n_2, and n_3 are the number of electrons involved in (44), (47), and (48), respectively. The values of the integral in (49) are the same as those determined numerically in case IV. The results for the variation of n^0_{app} with (C_i) for the case of hydrazine ($n_1 = 2$, $n_2 = 1/2$, $n_3 = 2$) is shown in Fig. 8, with the experimental points given by Karp and Meites.[5,6] The proposed mechanism does fit the expected coulometric behavior and yields a value of p/k_1 of about 10^{-3}.

This work was prompted by results obtained in the electroreduction of benzyldimethylanilinium bromide.[2] On the basis of controlled potential coulometry as well as polarographic and other data, the following mechanism, corresponding to case IV, was proposed

$$C_6H_5CH_2{-}\overset{CH_3}{\underset{CH_3}{N}}{-}C_6H_5^+ + 1e \longrightarrow C_6H_5CH_2\cdot + C_6H_5N\overset{CH_3}{\underset{CH_3}{:}} \quad (50)$$

(7) J. S. Mayell, Ph.D. Thesis, The University of Texas, 1962.

$$C_6H_5CH_2\cdot + H_2O \text{ (or } CH_3CN) \xrightarrow{k_1} C_6H_5CH_3 + OH\cdot \text{ (or } CH_2CN\cdot) \quad (51)$$

$$C_6H_5CH_2\cdot + C_6H_5CH_2\cdot \xrightarrow{k_2} C_6H_5CH_2CH_2C_6H_5 \quad (52)$$

$$OH\cdot \text{ (or } CH_2CN\cdot) + 1e \longrightarrow OH^- \text{ (or } CH_2CN^-) \quad (53)$$

Some experimental points obtained during the controlled potential coulometric reduction of benzyldimethylanilinium bromide are plotted in Fig. 6, and indicate a ratio of rate constants for reactions 51 and 52 of about 10^{-3}. Details of this work will be presented elsewhere.[2]

Because controlled potential coulometry allows the unequivocal determination of n^0_{app}, independent of estimations of diffusion coefficients, electrode areas, and transfer coefficients, it is a valuable adjunct to other electrochemical methods in the determination of mechanisms of electrode reactions. Often, to be sure, several possible reaction schemes will lead to the same over-all behavior, and in these cases, actual observation of the reaction intermediates by such techniques as electron paramagnetic resonance spectroscopy and visible or ultraviolet spectrophotometry is necessary.

Acknowledgment.—The authors are grateful to Mr. James L. Raney for his assistance in computer programming and operation. Appreciation is expressed for support of this work to the National Science Foundation (No. G 14478).

VAPOR PRESSURE STUDIES OF SULFUR TRIOXIDE AND THE WATER–SULFUR TRIOXIDE SYSTEM[1]

BY J. H. COLWELL[2] AND G. D. HALSEY, JR.

Department of Chemistry, University of Washington, Seattle 5, Washington

Received April 17, 1962

The vapor pressures of liquid and γ-SO_3 (trimeric form, m.p. 16.86°) have been determined in an all-glass apparatus. The vapor pressure of the so-called β-SO_3, which is only formed in the presence of $>10^{-5}$ mole fraction of water, also is reported. Vapor pressure and melting point studies of the H_2O–SO_3 system are reported in the range of 0.8 mole fraction SO_3 upward. The solutions so formed solidify at constant temperature to form a solid solution of the same composition as the melt. A syneresis upon standing for several weeks was observed in the 0.999 mole fraction SO_3 sample.

Introduction

In the gas[3] and liquid[4] phases, SO_3 has been shown, by spectroscopic studies, to be an equilibrium mixture of monomer and trimer. Liquid SO_3 freezes at 16.8° to an ice-like solid (γ-SO_3) which has been shown by X-ray diffraction studies[5] to be entirely trimeric. There are two other solid modifications of SO_3, α- and β-SO_3, which are high polymers. α-SO_3 is an amorphous appearing solid and β-SO_3 consists of needle-like crystals.

Crystals of β-SO_3 occur only when small quantities of water are present in samples of SO_3. One may assume that these crystals consist of polysulfuric acid molecules and several investigators through the years have proposed that β-SO_3 is a hydrate,[6–8] which amounts to the same thing.

Smits and Schoenmaker[9] found the vapor pressure of mixtures of liquid and β-SO_3 to be the same as that of pure liquid SO_3. Furthermore, they[10] found that by careful distillation, the liquid could be removed from such samples, which left the β-SO_3 apparently unaffected. The vapor pressure of this form was lower than that of liquid SO_3, but above 31° the β-SO_3 slowly melted to a liquid having the same vapor pressure as pure liquid SO_3. From this observation it was concluded that β-SO_3 was a more stable form below 31°, and that water acted only as a catalyst for the transformation from liquid to β-SO_3.

In the present study, the vapor pressures of liquid, β-, and γ-SO_3 were redetermined; the vaporization process of β-SO_3 was studied; and the vapor pressures and melting points of the H_2O–SO_3 system from 80 to 99.9 mole % SO_3 were determined systematically.

Experimental

SO_3 was obtained by degassing 20% fuming H_2SO_4. This was accomplished by bubbling helium through the acid while heating at 120–140° under reduced pressure and condensing the evolved SO_3 in a liquid nitrogen trap. The SO_3 then was distilled under vacuum several times to remove any H_2SO_4 carried over. These distillations were conducted at 23–25° with the vapor being condensed at 20°. Samples obtained in this way consisted entirely of liquid SO_3 with no needles of the β-form appearing upon standing. The samples of SO_3 used by several other investigators were "dried" with P_2O_5. It has been reported,[9] however, that such samples exhibited abnormally high vapor pressures. This phenomenon was reinvestigated[11] and attributed to the

(1) This research was partially supported by the Air Force Office of Scientific Research of the Air Research and Development Command.

(2) Eastman Kodak Company Fellow, 1959–1960. Based in part on a thesis submitted by Jack H. Colwell in partial fulfillment of the requirements for the Ph.D. degree at the University of Washington, 1961.

(3) R. W. Lovejoy, J. H. Colwell, D. F. Eggers, Jr., and G. D. Halsey, Jr., *J. Chem. Phys.*, **36**, 612 (1962).

(4) H. Gerding and W. J. Nijveld, *Rec. trav. chim.*, **59**, 1206 (1940).

(5) R. Westrik and C. H. MacGillavry, *ibid.*, **60**, 794 (1941).

(6) R. Weber, *Pogg. Ann.*, **159**, 313 (1876); *Ber. deut. chem. Ges.*, **19**, 3185 (1886).

(7) A. Berthoud, *Helv. Chim. Acta*, **5**, 513 (1922).

(8) V. R. Grau and W. A. Roth, *Z. anorg. allgem. Chem.*, **188**, 123 (1930).

(9) A. Smits and P. Schoenmaker, *J. Chem. Soc.*, **125**, 2554 (1924).

(10) A. Smits and P. Schoenmaker, *ibid.*, 1108 (1926).

(11) J. H. Colwell, Ph.D. Thesis, University of Washington, 1961.

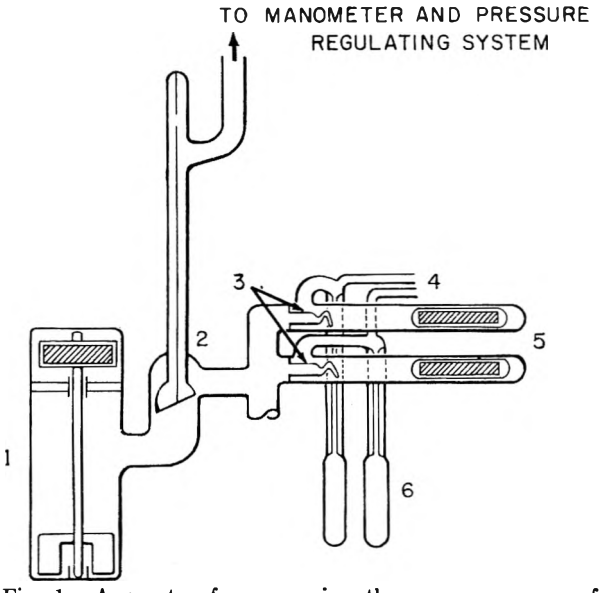

Fig. 1.—Apparatus for measuring the vapor pressure of H_2O–SO_3 samples.

presence of small quantities of SO_2 in the SO_3. Reduction of SO_3 treated with P_2O_5 could result from an oxidation of suboxide contaminants in the P_2O_5. Therefore, in the present work, the liquid SO_3 was used without further treatment, the absence of β-formation serving as the criterion of dryness.

Some idea of the degree of dryness so achieved can be gained from the observation that β-SO_3 is formed in some quantity in a glass vessel that merely has been pumped out carefully but not in one that has been flamed. Even if there were a residual 10 layers of water left on the glass before flaming, the mole fraction of water works out to be of the order 10^{-5}. It is conservative to estimate that by flaming, the dryness is improved by a factor of 100. At this degree of purity, one would expect the chief source of vaporizable contaminant to be poly-sulfuric acids. A reasonable estimate of the amount of water present is less than one part in 10^6 from all causes.

Measurements were made in glass systems free of stopcocks to prevent reduction of the SO_3. Adsorbed water was removed prior to introduction of SO_3 by outgassing under vacuum in a furnace at 400–450°.

Vapor pressures were determined using glass diaphragm gages. These gages consisted of a long glass fiber sealed to the center of a thin glass diaphragm. The fiber was positioned at a considerable angle from the normal to the diaphragm, so that a pressure deformation of the latter resulted in a lateral movement of fiber. A short fiber sealed to the top of the gage acted as a null reference point. Null setting was accomplished by imposing a back pressure of dry nitrogen measured with a manometer. Fiber displacements were observed with a 32× microscope, and pressures could be determined with a precision of ±1 mm.

The apparatus shown in Fig. 1 also was used for measuring vapor pressures in the system H_2O–SO_3. Subsequent to evacuating and degassing the apparatus, SO_3 was distilled into the calibrated sample tubes, 6, through the small connecting tubes, 4, which were then sealed off. The sample tubes had graduated capillary stems to enable determination of liquid SO_3 volume. The molar quantity of SO_3 present was computed using a value for the density at 20° of 1.92 g./cc.[7] Normally, a manifold of six sample tubes was employed in each experiment. The water sample, also measured volumetrically, was contained in one of the tubes. The water and SO_3 samples then could be distilled individually into section 1 by opening the break-seals, 3, by means of a small solenoid slipped over the tubes, 5. In determining the concentrations of the condensed samples in 1, corrections were made for the vapor phase, using the known volume, temperature, and pressure of the system and assuming the vapor phase to be an ideal gas of monomeric SO_3. The samples were mixed in 1 by the magnetically operated stirrer.

A 12-l. water bath, controlled by a variable Hg regulator of 0.002° sensitivity which operated a differential heater, was used as a thermostat. The temperature of the cooling water was controlled to ±0.1° by another thermostat consisting of a refrigerator unit in a large water bath. The primary thermostat could be regulated between 2 and 50° with a temperature fluctuation of less than 0.01°. A temperature of 0° was obtained by filling the thermostat with crushed ice. Thermostat temperatures were measured with a platinum resistance thermometer.

Results

The vapor pressures of liquid and γ-SO_3 were determined between 0 and 45° on a number of samples of pure liquid SO_3 and also samples consisting of mixtures of liquid and β-SO_3. All the samples had identical vapor pressures within experimental error, confirming the observation of Smits and Schoenmaker that the vapor pressures of such samples are independent of the presence of β-SO_3. The measured vapor pressures of liquid SO_3 obey the relation

$$\log P_{mm} = 6.6570 - 0.1549 \times 10^3 T^{-1} - 0.33165 \times 10^6 T^{-2} \quad (1)$$

and those of solid γ-SO_3

$$\log P_{mm} = 12.2346 - 2.9160 \times 10^3 T^{-1} \quad (2)$$

The melting point of γ-SO_3 was observed at 16.86 ± 0.02°. The heat of vaporization of liquid SO_3 calculated from eq. 1 is $\Delta H_v = 11.18$ kcal./mole, and that of solid γ-SO_3 calculated from eq. 2 is $\Delta H_v = 13.45$ kcal./mole; thus the heat of fusion $\Delta H_f = 2.27$ kcal./mole.

By careful distillation of the liquid from systems containing liquid and β-SO_3, samples of β-SO_3 were obtained. The vapor pressures of samples obtained in this way were identical with those observed by Smits and Schoenmaker near 30° but were slightly smaller at lower temperatures. The observed vapor pressures of solid β-SO_3 are represented by the equation

$$\log P_{mm} = 12.5615 - 3.0401 \times 10^{-3} T^{-1} \quad (3)$$

The β-SO_3 curve intersects that of liquid SO_3 at 30.54°. It was observed that the samples of β-SO_3 above this temperature had the same vapor pressure as liquid SO_3 and that liquid began condensing on the walls of the container, but the samples were not maintained at these temperatures long enough to observe whether complete fusion occurred. The heat of vaporization given by eq. 3 is $\Delta H_v = 13.91$ kcal./mole, while that given by eq. 1 for liquid SO_3 at 30.54° is $\Delta H = 10.70$ kcal./mole, so the heat of fusion of β-SO_3 is $\Delta H_f = 3.21$ kcal./mole.

It was found that by slowly condensing the vapor from systems containing only β-SO_3, liquid SO_3 could be obtained which showed no evidence of β-formation upon standing. Although the crystals of β-SO_3 became noticeably smaller, the equilibrium vapor pressure did not change. Upon continuing this process, crystals of β-SO_3 eventually began forming in the distillate, but the equilibrium vapor pressure in the original system did not begin to decrease until the crystals had nearly disappeared.

The investigation of the H_2O–SO_3 system from 80 to 99.9 mole % SO_3 revealed that all samples could be solidified to crystals similar in appearance to those of β-SO_3. Melting points of these crystals increased with SO_3 concentration from 15.5 to 30.5°, but the vapor pressures of the crystals were independent of concentration and identical with that of β-SO_3. The vapor pressures of the liquid samples, on the other hand, increased with increasing SO_3 concentration and approached that of liquid SO_3 asymptotically with the 99.9 mole % sample being indistinguishable from liquid SO_3. Vapor pressures of several liquid samples and all solid samples are plotted in Fig. 2, together with the vapor pressures of liquid, β-, and γ-SO_3. The melting points of the H_2O–SO_3 samples, as given in Table I, were determined by the intercept of the liquid and solid vapor pressure curves.

TABLE I

MELTING POINTS OF H_2O–SO_3 SAMPLES

Concn. (mole % SO_3)	M.p., °C.	Concn. (mole % SO_3)	M.p., °C.
80.1	15.5 ± 1.0	97.3	29.5 ± 0.1
83.1	22.7 ± 0.3	98.2	29.6 ± .1
83.8	24.0 ± .2	98.6	29.8 ± .1
85.9	26.5 ± .2	98.9	29.8 ± .1
88.1	27.5 ± .2	99.1	29.9 ± .1
91.2	28.7 ± .2	99.6	30.1 ± .1
92.9	28.9 ± .1	99.8	30.3 ± .1
93.8	29.0 ± .1	99.9	30.5 ± .1
94.4	29.1 ± .2		

A liquid containing 99.9 mole % SO_3 completely solidified when held at 29° and, upon cooling, its vapor pressure followed that of the solidus curve. However, after standing for several weeks at 20°, the sample underwent syneresis; approximately one-third of the sample was again liquid and the vapor pressure in the system was equal to that of liquid SO_3. Upon further cooling, the liquid froze at 16.8° to form solid SO_3. The stable crystalline phase appeared identical with the crystals of β-SO_3 which grow from the vapor. With approximately one-third of this sample being pure liquid SO_3, the concentration of SO_3 in the crystalline phase is slightly greater than 99.8 mole %. The fact that the over-all concentration of the other samples used was less than the concentration of the stable crystalline phase of this sample explains why no phase separation was observed in any of the other samples, even though several of them also had been allowed to stand for extended periods at 20°.

Vapor pressure measurements in the H_2O–SO_3 system could be reproduced, independent of whether a specified temperature was achieved from higher or lower temperatures, but 20–30 min. normally was required for the solid samples to reach equilibrium after a change of temperature. Upon heating solid samples 2 and 3° above their melting points, a period of several days was required for complete fusion to occur. A similar period was required to recrystallize a sample of the liquid which had been cooled below the melting point by the same amount. Since the melting and crystallization processes were very slow, the vapor pressure could be measured as the transitions were

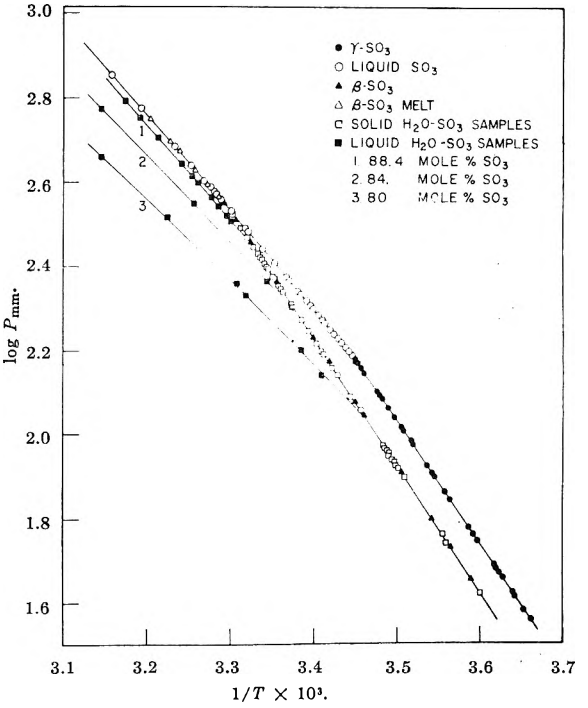

Fig. 2.—Vapor pressure of liquid SO_3, β-SO_3, γ-SO_3, and H_2O–SO_3 samples.

taking place. The vapor pressure of a solid sample heated above its melting point followed the solidus curve. As melting progressed, the vapor pressure decreased, eventually equaling that of the liquid sample as the last of the solid disappeared. The reverse occurred when a liquid sample was cooled below the melting point. The vapor pressure was initially that of the supercooled liquid but slowly dropped to that of the solid as crystallization progressed. The initial change observed upon heating a solid sample above its melting point was the appearance of a considerable amount of liquid, much of this liquid resulting from the condensation of vapor on the walls of the container. The remaining solid slowly disappeared either by decomposing as before or by dissolving in the liquid phase. When a liquid sample was cooled below its melting point, it acquired, initially, a gelatinous appearance, resulting from a network of extremely fine, needle-like crystals throughout the liquid. In stirred samples, these crystals collected on the stirrer, forming an amorphous-appearing solid. The transformation then slowly continued with needle-like crystals growing from this solid, the remaining liquid ultimately being consumed by this latter process.

The crystals of β-SO_3 have been shown by X-ray diffraction studies[12] to consist of linear polymers of SO_3, linked such that a —O—S—O—S— spiral is formed along the needle axis. Open chain polymers of this type would not be expected to form solely from SO_3, for some other molecular species would be required to facilitate chain termination. The linear polymers, therefore, must be polysulfuric acid molecules.

Liquid samples of the H_2O–SO_3 system of 70 mole

(12) R. Westrik and C. H. MacGillavry, *Acta Cryst.*, **7**, 764 (1954).

% SO_3 have been shown[13,14] to consist of H_2SO_4, $H_2S_2O_7$, higher polysulfuric acids, plus a considerable amount of monomeric SO_3. Higher concentrations of SO_3 should produce polysulfuric acids of still higher molecular weight, as well as a larger amount of free SO_3. The asymptotic approach of the vapor pressures of the liquid samples, with increasing SO_3 concentration, to that of pure SO_3 indicates that these samples may be considered solutions of polysulfuric acids in liquid SO_3. From this it may be inferred that the original crystallization observed, as these samples are cooled, is a separation from solution of the higher molecular weight polysulfuric acids. Since the H_2O–SO_3 samples completely solidify at a given temperature, the process must involve not only a separation of the poly-acids from solution but a consumption of the free SO_3 as well. This could occur either by an incorporation of free SO_3 into a gel-like structure of the polymers as they are formed or by an increase in the degree of polymerization of the poly-acids in the crystalline phase.

(13) R. J. Gillespie, *J. Chem. Soc.*, 2516 (1950).
(14) D. J. Millen, *ibid.*, 2589 (1950).

THE PROPERTIES OF α-SULFUR TRIOXIDE[1]

BY J. H. COLWELL[2] AND G. D. HALSEY, JR.

Department of Chemistry, University of Washington, Seattle 5, Washington

Received April 27, 1962

Numerous attempts were made to produce stable samples of α-SO_3, but all samples spontaneously decomposed to liquid SO_3. An irreversible transition was found to occur at $-65°$ upon warming samples formed by depositing SO_3 vapor on cooled surfaces. The heat of this transition, $\Delta H = -2500$ cal., was measured using a specially designed ice calorimeter. A mechanism for the formation of α-SO_3 is proposed.

Introduction

α-SO_3, the amorphous, high polymer form of SO_3, is found only when SO_3 vapor is first condensed on a surface cooled below $-80°$ and then warmed to room temperature. The resulting sample consists of a mixture of liquid and α-SO_3. Smits and Schoenmaker[3] studied the vapor pressures of samples of α-SO_3 formed by repeated condensations of SO_3 vapor with liquid air. After pumping on the samples for some time to remove the remaining liquid SO_3, very low pressures were observed which then increased slowly. The rate of this pressure change was observed at 30, 40, and 50° and was found to decrease steadily with time. The pressure curves were extrapolated to infinite time and the limiting value called the "equilibrium vapor pressure" of α-SO_3. These limiting pressures were much lower than the vapor pressures of liquid or β-SO_3, so that α-SO_3 was considered to be the stable form of SO_3. It was observed, however, that the pressure above these samples was not reversible; when it was increased above the limiting value it showed no tendency to decrease.

In the present study, attempts to reproduce the rates of pressure increase curves as determined by Smits and Schoenmaker were not successful. The results of this work indicate that α-SO_3 is unstable with respect to liquid SO_3 at room temperature. Further, it was discovered that an irreversible transition occurred during the warming of samples of SO_3 vapor condensed on cold surfaces. The heat of this transition was measured, using a specially designed ice calorimeter.

(1) This research was partially supported by the Air Force Office of Scientific Research of the Air Research and Development Command.

(2) Eastman Kodak Co. Fellow, 1959–1960. Based in part on a thesis submitted by Jack H. Colwell in partial fulfillment of the requirements for the Ph.D. degree at the University of Washington, 1961.

(3) A. Smits and P. Schoenmaker, *J. Chem. Soc.*, 1108 (1926).

Experimental

The method used to prepare samples of liquid SO_3 as well as the apparatus used for measuring SO_3 pressures have been described elsewhere.[4] The samples used to determine the rate of pressure increase of α-SO_3 were prepared in a manner similar to that used by Smits and Schoenmaker.

The phase transition of the condensed vapor samples was observed with a simple apparatus consisting of an inner tube of 10 mm. glass tubing, sealed at the upper end to an outer tube of 25 mm. diameter by a dewar seal. The inner tube, which served as a cold finger, was closed at the bottom after having been drawn out to a thin-walled tube of about 4 mm. diameter and 2 cm. length. The bottom of the outer tube was connected to a sample of SO_3. The apparatus was evacuated and outgassed, following which a copper–constantan thermocouple, immersed in sufficient vaseline to obtain thermal contact, was placed in the tip of the cold finger. The cold finger was filled with liquid nitrogen and the SO_3 was distilled onto the tip. After the sample had been distilled completely, the liquid nitrogen in the cold finger was allowed to evaporate and the rate of temperature increase of the sample was determined, using the thermocouple.

To determine the heat of this transition, an ice calorimeter was constructed by which the heat necessary to warm a sample from a lower temperature to the ice point could be measured. In the calorimeter, shown in Fig. 1, the sample is cooled to the desired temperature and transferred into the ice calorimeter entirely within a closed system, thus preventing atmospheric moisture from condensing on the sample. The water jacket, 1, was filled with pure air-free water. The volume increase resulting from the formation of ice in the water jacket displaces mercury from the reservoir, 3, into the calibrated capillary system, 5. The capillary system consists of a 1-m. length of capillary tubing, *ca.* 0.5 mm. i.d., mounted on the upper scale of a horizontal meter bar and three small bulbs of *ca.* 0.075 cc. are connected by short sections of 0.5 mm. i.d. capillary mounted on the lower scale of the meter bar. The volume between any point in these capillary sections on the lower scale and any point in the capillary on the upper scale has been determined accurately. The end of the upper capillary is open to the atmosphere but is covered by a drying tube to prevent moisture from condensing in the capillary system. The sample tube, 11, in the calorimeter is suspended by a thin silk

(4) J. H. Colwell and G. D. Halsey, Jr., *J. Phys. Chem.*, **64**, 2179 (1962).

thread from the iron rod, 7, held in the magnetic field of the solenoid, 8. By moving the solenoid, the sample tube can be transferred between the cooling tube, 16, and the calorimeter.

In operation, the calorimeter is evacuated and then filled with dry nitrogen to a pressure of about 30 mm. After the water jacket reaches thermal equilibrium with the crushed ice–water mixture in 4, an ice mantle, 2, is formed in the calorimeter by transferring the sample tube into the calorimeter from tube 16, where it cooled. This is repeated until sufficient ice forms to force the mercury into the capillary system. The sample is again lowered into the cooling tube. After 15 min. is allowed for establishment of thermal equilibrium between sample and refrigerant and between the newly formed ice mantle and its surroundings, the sample tube is quickly transferred into the calorimeter. The initial and final positions of the mercury in the capillary system indicate the volume of ice formed.

Using liquid oxygen as a coolant, the integral heats of the samples measured were reproducible to ±1 cal. The heat loss of the calorimeter to the surroundings was about 1 cal./hr. All the samples used were found to equilibrate with the calorimeter within 10 min.; thus the heat loss could be neglected. The accuracy of the calorimeter was determined by comparing the experimentally measured integral heats of copper wire samples with values calculated from the known heat capacity of copper.[5] The copper samples were weighed and then sealed in glass tubes, the integral heats of which had been determined previously. The results are shown in Table I.

TABLE I

COMPARISON OF OBSERVED AND CALCULATED INTEGRAL HEATS OF COPPER BETWEEN −183.0 AND 0°

Wt. of Cu sample, g.	Obsd. ΔH(cal.)	Calcd. ΔH(cal.)	% error
7.1158	102.5	104.4	1.8
	103.1		1.2
	102.6		1.7
	103.4		1.0
4.3128	63.0	63.2	0.3
	61.6		2.5
	62.1		1.7

The heat of the irreversible transition in SO_3 was determined as the difference between the measured heats of unreacted sample and the sample after reaction. To form an unreacted sample of SO_3, the sample tube, 11, was lowered into tube 16, after removing the dewar. The lower half of the sample tube was warmed by the heater, 14, distilling the SO_3 into the reservoir, 12, in the top half of the sample tube. The dewar then was replaced so that the level of the coolant was at the lower edge of the heater. The sample tube was lowered so that the nozzle of the tube was just below the level of the coolant. The SO_3 redistilled into the lower half of the tube, condensing on the cold walls and forming an unreacted sample.

Results and Discussion

Although a number of samples of α-SO_3 were prepared during the present study, none was found which had a limiting pressure as observed by Smits and Schoenmaker. In all cases, the samples exhibited a very low initial pressure, which then increased slowly. However, the rate of pressure change, although it originally decreased, eventually began to increase. The pressure of the samples continued to increase until liquid SO_3 began to condense in the system. Upon standing for several months, the samples of α-SO_3 completely decomposed to liquid SO_3. An example of this pressure behavior is given in Fig. 2, together with the results

(5) W. F. Giauque and P. F. Meads, *J. Am. Chem. Soc.*, **63**, 1897 (1941).

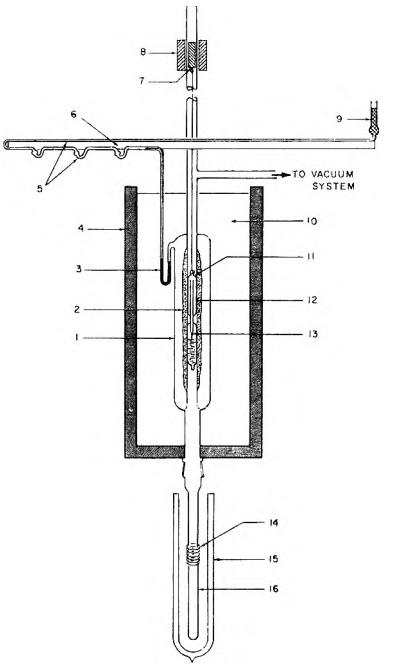

Fig. 1.—Ice calorimeter: 1, water jacket (inner tube, 13 mm., outer tube, 45 mm., length, 35 cm.); 2, ice mantle formed by sample; 3, mercury reservoir; 4, insulated metal can; 5, calibrated capillary system; 6, meter bar; 7, soft iron rod; 8, movable solenoid; 9, Drierite drying tube; 10, crushed ice–water mixture; 11, sample tube; 12, reservoir of sample tube; 13, nozzle of sample tube; 14, 10 turn, 40 ohm/ft. nichrome heater; 15, dewar; 16, cooling tube.

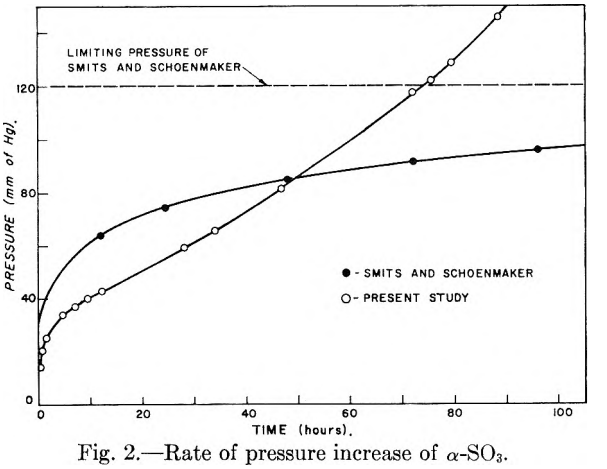

Fig. 2.—Rate of pressure increase of α-SO_3.

of Smits and Schoenmaker, at the same temperature.

Because of the slow rate of the pressure change above these samples, it was found that a sample being observed at 30° could be heated rapidly to 40° and returned to 30° with no observable pressure increase occurring between the initial and final determinations at 30°. However, the amount of vapor in the system, determined from the known volume and the pressures at the two temperatures, was as much as 12% greater at the higher temperature, indicating that there is a condensed phase in reversible equilibrium with the vapor phase. This is believed to be physically adsorbed vapor on the surface of the solid, for, if one considers the α-SO_3 to be undergoing a spon-

taneous decomposition to monomeric SO_3, the adsorption of a large quantity of vapor on the surface of the α-SO_3 would account for the shape of the pressure curves observed in this work.

In measuring the rate of temperature increase of samples of SO_3 formed by condensing the vapor at liquid nitrogen temperatures, a sharp increase in the rate always was observed at $-65 \pm 3°$, indicating the evolution of a large quantity of heat. When the samples were recooled, there was no heat evolved during warming.

The heat of this transition, obtained as the difference in the heat required to warm reacted and unreacted samples from the boiling point of liquid oxygen to the ice point, are given in Table II. The tube used for sample 1 did not have a nozzle on the lower end of the connecting tube (see 13, Fig. 1) and some of the sample condensed on the walls of the tube above the level of the coolant. This portion of the sample probably was warm enough to react so that the subsequent measurements of the heat of reaction gave low values. Samples 2 and 3 gave reasonably constant values, but did vary slightly, depending upon how far the nozzle of the sample tube was below the level of the coolant. The value of 2500 cal./mole of SO_3 can be taken as a lower limit of the heat evolved in this transition.

TABLE II

HEAT OF TRANSITION IN CONDENSED VAPOR SAMPLES OF SO_3

Sample no.	Vol. of sample (cc. at 20°)	Heat of transition at −183° (cal./mole of SO_3)
1	0.910	1797
		2029
		2070
2	0.980	2361
		2251
		2373
		2443
3	0.968	2363
		2407
		2397

It is possible that this is a glass transition as is observed in several solids formed by the deposition of vapor on a cold surface, but the heat of the transition is larger than normally is observed for this type of phenomenon.[6] In the present case, the transition probably is the result of a chemical reaction. SO_3 vapor consists almost entirely of monomeric SO_3, so that the solid formed by condensing the vapor on a cold surface also should be composed of monomeric SO_3. Such a solid would be metastable, for solid γ-SO_3, which forms under equilibrium conditions, is composed entirely of the trimeric ring compound, S_3O_9.[7] Upon warming a low temperature deposit, a spontaneous reaction would take place between adjacent SO_3 molecules. The rapid formation of bonds in the solid could lead to long chain polymers, as well as trimers, and thus account for the high polymer, α-SO_3, always found in samples treated in this manner.

The heat of this reaction should not depend greatly on whether a trimer or a long chain polymer is formed, so that the heat of reaction should be comparable to the heat of trimerization in the gas phase, estimated to be -10 kcal./mole SO_3.[8] The discrepancy between this value and the observed heat of transition could result from the rapid deposition of the samples ($\sim$0.5 g./cm.^{2} hr.), so that the temperature of part of the sample may have exceeded the transition temperature.[9] That this was the case is indicated by the observation that only $\sim$10% of these samples consisted of α-SO_3, whereas, under other conditions, samples have been formed which consisted almost entirely of α-SO_3.

Because of the dynamic equilibrium between monomer and trimer which is known to exist in liquid SO_3 at room temperature,[10] one would expect long linear polymers of SO_3 to undergo random degradation. The identification of α-SO_3 with long chain polymers formed in the solid state reaction thus is consistent with the spontaneous decomposition of α-SO_3 to the liquid, observed in this study.

(6) J. A. Pryde and G. O. Jones, *Nature*, **170**, 685 (1952).

(7) R. Westrik and C. H. MacGillavry, *Rec. trav. chim.*, **59**, 1206 (1940).

(8) R. H. Lovejoy, J. H. Colwell, D. F. Eggers, Jr., and G. D. Halsey, Jr., *J. Chem. Phys.*, in press.

(9) R. H. Beaumont, H. Chihara, and J. A. Morrison, *ibid.*, **34**, 1457 (1961).

(10) H. Gerding and W. J. Nijveld, *Rec. trav. chim.*, **59**, 1206 (1940).

THE ELECTRIC MOMENTS OF ORGANIC PEROXIDES. III. PERESTERS[1]

BY FRANK D. VERDERAME AND JOHN G. MILLER

Department of Chemistry, University of Pennsylvania, Philadelphia 4, Pennsylvania

Received April 28, 1962

The electric moments of the *t*-butyl esters of five different long-chain aliphatic peracids (av. $\mu = 2.94 \pm 0.04$ D.) and *t*-butyl perbenzoate ($\mu = 3.12$) have been measured in non-polar solvents at 30°. Like the values for other peroxides, these moments are in accord with a fixed skew configuration about the peroxy grouping, but a more detailed analysis of the results shows that the acyl group probably is twisted somewhat out of its C–O–O plane.

Introduction

Paper I of this series[2] reported the electric moments of some dialkyl peroxides, alkyl hydroperoxides, and diacyl peroxides. The moments were explained by a fixed spatial arrangement of the C–O–O–C group, the azimuthal angle formed by rotating the C–O bonds about the O–O bond being between 100 and 125°. In paper II on peracids[3] the corresponding C–O–O–H azimuthal angle was found to be much less (70°) due to intramolecular hydrogen bonding for which reliable evidence was cited. These conclusions were in agreement with the widely accepted model for hydrogen peroxide proposed by Penney and Sutherland.[4]

More recently, X-ray studies of single crystals of hydrogen peroxide dihydrate[5] and infrared measurements of hydrogen peroxide[6] and of alkyl hydroperoxides[7] have further confirmed that model. The same type of fixed skew arrangement of the C–S–S–C group in disulfides accounts for their dipole moments.[8–10]

Establishment of the Penney–Sutherland structure for the $\diagdown O\text{–}O \diagup$ part of the organic peroxide molecules permits more certain interpretation of the dipole moments with respect to other parts of those molecules. For example, one may now consider the rotation of an organic group about the bond attaching it to the peroxy grouping. The *t*-butyl peresters reported here are useful reference substances for such purposes because with them one has to consider only the rotation of the acyl group, rotation of the *t*-butyl group having no effect upon the moment. Treatment of the diacyl peroxides[2] was complicated by the simultaneous rotation of two groups and with the peracids[3] the effect of acyl group rotation was submerged by the effect of chelation with the OH hydrogen.

This paper presents the first systematic measurement and analysis of the dipole moments of peresters. The values obtained earlier for diacyl peroxides and peracids are reconsidered in view of the findings for the peresters.

Results and Discussion

The results of the measurements are shown in Table I which gives the dipole moments, μ, calculated by the Halverstadt and Kumler[11] method from the dielectric constant, density, and refractive index data. The symbols used in the table are as defined earlier.[2] For the calculated molar refractions, the atomic refraction of the peroxidic oxygen[12] was taken as 2.19 cc. mole^{-1}.

The mean of the moment values for the five aliphatic peresters is 2.94 D. with a mean deviation of ±0.04 D. Structural interpretation of this result can be based upon the diagram

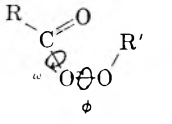

The molecular moment, as a function of the bond moments, bond angles, and azimuthal angles ω and ϕ, will obey the same general formula as developed for the peracids,[3] with H replaced by R′, the *t*-butyl group. In that formula, we assume planarity for the $\overset{O}{\overset{\|}{C}}\text{–}O$ group and measure ω in a clockwise direction looking along the C–O axis from C to O for measurement of rotation of the acyl group out of the plane containing the O–O axis. The other dihedral angle, ϕ, is measured in a clockwise direction looking along the O–O axis from right to left for rotation of the O–O–R′ plane out of the C–O–O plane. The reference diagram shows ω and ϕ both at zero.

If we take the bond angles and bond moments the same as taken earlier for diacyl peroxides,[2] peracids,[3] dialkylperoxides,[2,9] and alkyl hydroperoxides,[2,9] but with the C–O moment equal to 0.73 D. in the acyl group, eq. 1 results.

(1) A report of work done under contract with the U. S. Department of Agriculture and authorized by the Research and Marketing Act of 1946. The contract is supervised by the Eastern Utilization Research Service. This work was presented at the Delaware Valley Regional Meeting of the American Chemical Society, Philadelphia, Pa., January 25, 1962.

(2) W. Lobunez, J. R. Rittenhouse, and J. G. Miller, *J. Am. Chem. Soc*, **80**, 3505 (1958).

(3) J. R. Rittenhouse, W. Lobunez, D. Swern, and J. G. Miller, *ibid.*, **80**, 4850 (1958).

(4) W. G. Penney and G. B. B. M. Sutherland. *Trans. Faraday Soc.*, **30**, 898 (1934); *J. Chem. Phys.*, **2**, 492 (1934).

(5) I. Olovsson and D. H. Templeton, *Acta Chem. Scand.*, **14**, 1325 (1930).

(6) R. L. Redington, W. B. Olson, and P. C. Cross, Office of Naval Research Contract N8 onr-477 (19), Tech. Rept. II (August 31, 1961).

(7) M. A. Kovner, A. V. Karyakin, and A. P. Efimov, *Opt. i Spektroskopiya*, **8** (No. 1), 64 (1960).

(8) C. C. Woodrow, M. Carmack, and J. G. Miller, *J. Chem. Phys.*, **19**, 951 (1951).

(9) M. T. Rogers and T. W. Campbell, *J. Am. Chem. Soc.*, **74**, 4742 (1952).

(10) V. N. Vasil'eva and E. N. Guryanova, *Zh. Fiz. Khim.*, **33**, 1976 (1959).

(11) I. F. Halverstadt and W. D. Kumler, *J. Am. Chem. Soc.*, **64**, 2988 (1942).

(12) N. Milas, D. M. Surgenor, and L. H. Perry, *ibid.*, **68**, 1617 (1946).

TABLE I

SUMMARY OF THE DILUTE SOLUTION VALUES OF THE DIPOLE MOMENTS OF *t*-BUTYL PERESTERS AT 30°

Perester (solvent)	ϵ_{10}	α	V_{10}	β	n^2_{10}	γ	P_{20}	MR_D Obsd.	MR_D Theor.	μ
Perpelargonate (benzene)	2.2626	3.8157	1.1520	−0.0218	2.23405	−0.2165	244.27	56.26	66.45	2.98
Perpelargonate (benzene)	2.2626	3.7318	....	.....	.....	.....	240.57		66.45	2.94
Percaprate (benzene)	2.2624	3.6035	1.1516	− .0113	2.23410	− .1689	249.98	73.33	71.09	2.96
Percaprate (benzene)	2.2630	3.5431	1.1518	− .0145	2.23410	− .1954	246.97	71.80		2.95
Percaprate (benzene)	2.2629	3.5719	1.1521	− .02143	2.23412	− .2050	246.87	70.84		2.96
Perlaurate (benzene)	2.2621	3.0849	1.1520	− .01166	2.23414	− .1967	251.88	80.22	80.30	2.92
Perlaurate (benzene)	2.2640	2.9133	1.1518	− .0158	2.23430	− .2113	242.57	79.12		2.85
Perlaurate (*n*-hexane)	1.8740	2.1237	1.5364	− .4201	1.87690	.1512	246.30	81.42		2.86
Permyristate (benzene)	2.2628	2.6084	1.1516	− .00294	2.23440	− .1909	251.24	89.56	89.54	2.84
Permyristate (benzene)	2.2628	2.679					255.27			2.87
Permyristate (benzene)	2.2627	2.8238	1.1520	− .00125	2.23445	− .1714	263.80	90.87		2.93
Perpalmitate (benzene)	2.2626	2.6843	1.1519	− .00082	2.23411	− .1616	279.72	99.98	98.77	2.99
Perpalmitate (benzene)	2.2633	2.6896	1.1521	− .0074	2.23390	− .2191	279.44	95.72		3.02
Perpalmitate (benzene)	2.2627	2.6067	1.1520	− .008	2.23411	− .1576	274.21	99.56		2.95
Perpalmitate (*n*-hexane)	1.8758	1.9479	1.5365	− .4248	1.8767	.1553	278.95	97.84		3.00
Perbenzoate (benzene)	2.2627	5.3317	1.1516	− .1781	2.23438		252.91	55.12	53.24	3.14
Perbenzoate (*n*-hexane)	1.8716	3.3775	1.5368	− .5764	.....	.....	243.75			3.09

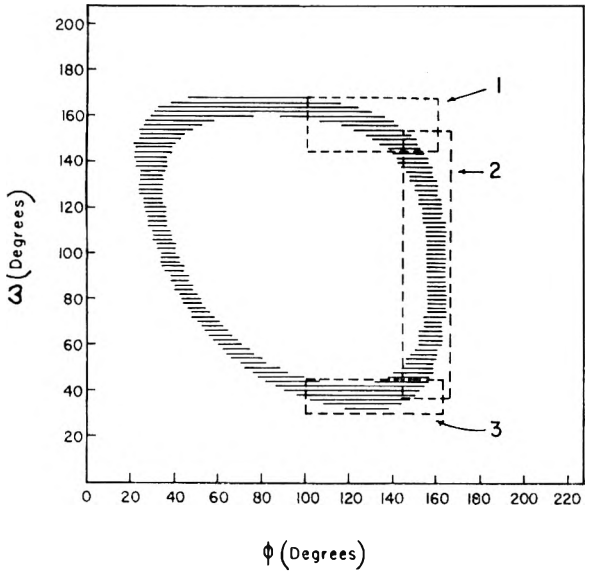

Fig. 1.—Combinations of ω and ϕ for which $\mu = 2.94 \pm 0.04$ D.

$$\mu^2 = (-0.2550 - 0.2550 \cos\phi + 2.2599 \cos\omega)^2 + (2.2599 \sin\omega + 0.9852 \sin\phi)^2 + (0.5208 - 0.9517 \cos\phi)^2 \quad (1)$$

The change from 0.62 to 0.73 for the C–O moment in the acyl group seemed appropriate in view of the experience of others with esters and acids.[13]

Equation 1 gives μ as a function of ϕ and ω and was used to find the simultaneous values of ϕ and ω which correspond to the observed value of μ, *i.e.*, 2.94 ± 0.04. A Univac 90 solid state computer was readily programmed for aid in these calculations. The results are shown in Fig. 1 for 2° ω intervals. Omitted from the figure is the equivalent set of ω–ϕ solutions which would have been obtained by taking the mirror-images of the set shown.

(13) C. P. Smyth, "Dielectric Behavior and Structure," McGraw-Hill Book Co., Inc., New York, N. Y., 1955, p. 306.

For the aliphatic peresters, the Penney–Sutherland model and also steric hindrance, as observed with Fisher–Taylor–Hirschfelder models, eliminate the structures in which ϕ is less than 100°. The remaining structures are put in three groups indicated in Fig. 1 by the areas 1, 2, and 3. Each of these three areas may be regarded as representing a single structure undergoing simultaneous change of ϕ and ω within depicted limits, *i.e.*, a librating molecule. Thus, for area 1, defined by ϕ = 100–160°, ω = 140–165°, we would have the librating molecule of average moment $\bar{\mu}$, given by the following equation which assumes equal probabilities of all the forms encompassed by its limits

$$(\bar{\mu})^2 = \int_{100}^{160}\int_{140}^{165} \mu^2 d\omega d\phi \Big/ \int_{100}^{160}\int_{140}^{165} d\omega d\phi$$

This average moment is found to be 2.97 D., showing the validity of this interpretation. Similarly, area 2, with ϕ = 145–165° and ω = 30–150°, gives $\bar{\mu}$ = 2.93, and area 3, with ϕ = 100–150° and ω = 30–45°, has $\bar{\mu}$ = 2.93.

Of these three structures, we may dismiss the second one on two counts. First, the mean value of ϕ about which the vibrations take place, 155°, seems much too large compared to the values found for other peroxides. Second, the range of ω values, 30–150°, is highly improbable in view of the resonance expected for peresters.

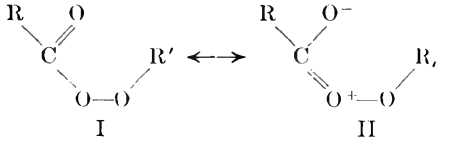

Such resonance would call for ω values near 0 or 180°, due to the double bond character it gives to the C–O link. In ordinary carboxylic acids and their esters this resonance is large, contributions of form II causing a shortening of the C–O bond length[14] from its normal value, 1.46 ± 0.04 Å., to 1.36 ± 0.04 Å. Resonance energies due to

(14) P. W. Allen and L. E. Sutton, *Acta Cryst.*, **3**, 346 (1950).

the same contributions are approximately 30, 15, and 20 kcal. mole^{-1} for anhydrides, acids, and esters, as determined from heats of combustion.[15] The persistence of this resonance in going to the peroxide analogs is shown by the infrared absorption maxima due to the C=O and C–O stretching frequencies. This has been demonstrated for esters and peresters,[16,17] acids and peracids,[18] and anhydrides and diacyl peroxides.[16,19]

Such resonance would involve overlap of the p orbital of the acyl carbon atom with the p orbital of the adjacent peroxy-oxygen atom. Although the resonance energy will be at a maximum when the acyl group is completely coplanar with the C–O–O group, *i.e.*, when ω is 0 or 180°, such perfect coplanarity is not required for the resonance to exist. Dewar[20] has shown that the resonance energy will vary as cos ω or cos^2 ω. While this would eliminate the second structure, it would make the other two plausible. The cause of the twisting of the acyl group out of the C–O–O plane is not evident, although it may be due to electrostatic interaction of the carbonyl and *t*-butoxyl dipoles attended by effects due to the size of the alkyl groups. While librations about higher values of ω (140–165°) would meet lower repulsion between those dipoles, the long alkyl chains (R) would meet steric interference with the *t*-butyl group. For this reason, we favor the structure in which the oscillating twist is centered about values of ω in the neighborhood of 35°. In general, dipole moment values indicate that in ordinary esters the carbonyl and alkoxyl groups are *cis* to each other.[21] It also is interesting that electron diffraction studies[13,14] have shown ω values of 25–40° for methyl formate and methyl acetate.

We may now consider the moment of *t*-butyl perbenzoate. That moment, 3.12 ± 0.04 D., is accounted for by adding to the bond moments of the aliphatic peresters a resonance moment due to contributions from an additional resonance form that exists for *t*-butyl perbenzoate

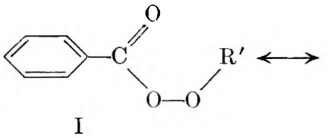

I

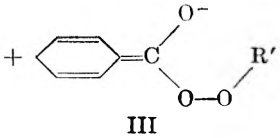

III

When this additional moment is taken equal to 0.4 D. and located along the line of centers of the carbonyl oxygen atom and the benzene ring, with its negative end toward the oxygen atom, then the molecular moment is given by the same combinations of ϕ and ω as shown in Fig. 1. The existence of such a resonance moment also is apparent in ethyl benzoate,[22] which has a dipole moment about 0.15 D. higher than the ethyl esters of the saturated aliphatic carboxylic acids. Furthermore, the molar refractions (Table II) of the pure substances[23] show that optical exaltation in *t*-butyl perbenzoate is markedly higher than in the aliphatic peresters. This also can be explained in terms of enhanced delocalization, indicated by structure III.

TABLE II

THE MOLAR REFRACTION OF *t*-BUTYL PERESTERS MEASURED FOR THE PURE LIQUIDS[23]

Perester	MR_D Obsd.	Calcd.	Exaltation
Perpelargonate	66.70	66.45	0.25
Percaprate	71.37	71.09	.28
Perlaurate	80.65	80.30	.35
Permyristate	89.96	89.54	.42
Perbenzoate	54.86	53.24	1.62
Perbenzoate[12]	54.84	53.24	1.60

In summary, the dipole moment values for all of the *t*-butyl peresters studied here indicate that those esters have the Penney–Sutherland structure with restricted oscillation of the acyl groups out of plane with the peroxy grouping.

Following this analysis of the data for the peresters, the dipole moment values already published[2,3,9] for alkyl peroxides, alkyl hydroperoxides, peracids, and diacyl peroxides were treated in the same detailed manner. No essential change resulted from these analyses. It should be noted, however, that in the peracids and diacyl peroxides oscillations of the acyl groups from strict coplanarity with the peroxy oxygen atoms are indicated. Concerning the diacyl peroxides, the interesting earlier finding[2] of opposition of the carbonyl group directions was confirmed. Bellamy and his coworkers[19] recently have come to the same conclusion from consideration of the relative intensities of the infrared absorption doublets caused by the carbonyl groups of the diacyl peroxides.

Experimental

Preparation of Materials.—The *t*-butyl peresters were prepared by the pyridine acylation method of Silbert and Swern.[23] Important characterizing physical and chemical data of the substances involved are given in Table III. Included are the properties of peresters generously supplied by Dr. Leonard S. Silbert of the Eastern Utilization Research and Development Division, U. S. Department of Agriculture. The acyl halides were obtained from acids prepared by hydrolysis of the purified methyl esters. The methyl esters were analyzed for purity by gas chromatography in which 5-μl. samples were passed through a 6.1-ft. column of 25% silicone oil on Chromosorb maintained at 210° at a flow rate at 120 cc. min.$^{-1}$. There resulted single peaks, indicating the absence of homologs. Of the three different methods of final purification, molecular distillation in a short-path still and passage through a column of activated

(15) G. W. Wheland, "Resonance in Organic Chemistry," John Wiley and Sons, Inc., New York, N. Y., 1955, pp. 99–100.

(16) W. H. T. Davison, *J. Chem. Soc.*, 2456 (1951).

(17) Private communication from Dr. Leonard S. Silbert.

(18) M. Davies and O. Thomas, *Discussions Faraday Soc.*, **9**, 335 (1950).

(19) L. J. Bellamy, B. R. Connelly, A. R. Philpotts, and R. L. Williams, *Z. Elektrochem.*, **64**, 563 (1960).

(20) M. J. S. Dewar, *J. Am. Chem. Soc.*, **74**, 3349 (1952); see also, L. L. Ingraham in "Steric Effects in Organic Chemistry," M. S. Newman, ed., John Wiley and Sons, Inc., New York, N. Y., 1956, pp. 479–522.

(21) G. W. Wheland, ref. 15, p. 235; R. J. B. Marsden and L. E. Sutton, *J. Chem. Soc.*, 1383 (1936).

(22) C. S. Copeland and M. W. Rigg, *J. Am. Chem. Soc.*, **73**, 3584 (1951).

(23) L. S. Silbert and D. Swern, *ibid.*, **81**, 2334 (1959). The first row of data for *t*-butyl perbenzoate in Table II were kindly determined for us by Dr. Silbert.

TABLE III

CHARACTERIZING PROPERTIES OF THE *t*-BUTYL PERESTERS AND INTERMEDIATES IN THEIR PREPARATION

Acyl group	Methyl ester B.p., °C. (mm.)	$n^{25}D$	Acyl chloride B.p., °C. (mm.)	Recrystn. temp., °C.	Final method of purifcn.	*t*-Butyl perester $n^{30}D$	*t*-Butyl perester d^{30}_4	Available oxygen (% of theor.)
Lauric	139–141 (15)	1.4301	145 (18)	−40	Recryst.	1.4333	0.8783	99.7
Lauric[a]	.....	....	.....	..	Recryst.	1.4337	.8784	99.5
Pelargonic[b]	.....	....	.....	30–32[c]	Distill.	1.4273	.8868	99.7
Capric	114 (15)	1.4235	53 (1.5)	−45	Florisil, alumina	1.4297	.8832	99.7
Capric[a]	.....	....	.....	..	Recryst.	1.4293	.8833	100.3
Myristic	153–155 (10)	1.4346	144 (1.5)	−45	Recryst.	1.4373	.8752	100.0
Myristic[a]	.....	....	.....	..	Recryst.	1.4368	.8751	100.0
Palmitic	194 (12)	1.4355 ($n^{35}D$)	137 (0.3)	−45	Recryst.	....	....	99.6
Palmitic	.....	....	.....	..	Florisil, alumina	....	....	99.2
Benzoic[d]	.....	....	39.5 (17)	−45	Recryst.	1.4957	1.00337	99.2

[a] Perester supplied by Dr. L. S. Silbert. [b] Pelargonyl chloride supplied by Dr. L. S. Silbert. [c] Boiling point of perester at 10 μ. [d] N.B.S. benzoic acid was used.

alumina and "Florisil" ensured removal of water which might have occluded during recrystallization. The dipole moments of these samples agreed with the values for those obtained by recrystallization, indicating the absence of water in all the samples. Available oxygen was determined by the improved iodometric method of Silbert and Swern.[24]

Benzene.—Thiophene-free C.P. benzene was dried over phosphorus pentoxide for several days and distilled through a 1.5 × 130 cm. cylindrical column packed with 3/8 in. glass helices, then stored over Drierite until used. All transfers of solvent for weighing and washing were made using drying tubes to avoid contamination by atmospheric moisture.

***n*-Hexane.**—Phillips pure *n*-hexane was treated with concentrated sulfuric acid for 7 days and was then washed with water and 5% sodium carbonate solution. It finally was distilled over phosphorus pentoxide and stored in the same manner as the benzene.

(24) L. S. Silbert and D. Swern, *Anal. Chem.*, **30**, 385 (1958).

Petroleum Ether.—Low boiling, olefin-free petroleum ether, used as solvent in the preparation of the peresters, was prepared in the same manner as was *n*-hexane.

***t*-Butyl Hydroperoxide.**—The *t*-butyl hydroperoxide was prepared as described earlier.[2] The fraction boiling at 42.5° at 18 mm. was used in the preparation of the peresters.

Apparatus and Methods.—Dielectric constants, refractive indices, and densities were measured as described earlier,[2,3] but for most of the capacitance measurements a General Radio Company 716 CS 1 radiofrequency bridge, 1330 A oscillator, and 1212 A null-detector were employed. Solute weight fractions were in the range 0.001 to 0.012. Temperatures were maintained at 30.00 ± 0.005°.

Acknowledgments.—F. D. Verderame expresses his grateful acknowledgment of the encouragement given him by the Research Division of the Frankford Arsenal and of the support of the U. S. Army Research Office. The abundant aid given by Dr. Leonard S. Silbert also is gratefully acknowledged.

IODINE PRODUCTION IN THE γ-RADIOLYSIS OF CYCLOHEXANE–ALKYL IODIDE SOLUTIONS

BY THOMAS S. CROFT AND ROBERT J. HANRAHAN

Department of Chemistry of the University of Florida, Gainesville, Florida

Received April 30, 1962

Iodine production induced by Co^{60} γ-radiolysis has been measured for solutions of methyl iodide in cyclohexane and ethyl iodide in cyclohexane, over the concentration range 0–95% cyclohexane by volume. In each case the addition of cyclohexane caused a smooth decrease in iodine production from the alkyl iodide, but net iodine production persisted until at least 93 electron % cyclohexane was added. These observations are discussed in terms of a previously proposed mechanism.

Introduction

The radiolysis of pure cyclohexane has been studied extensively because of its interest as a model compound, having only two types of chemical bonds. (*Cf.* recent papers by Freeman[1] and by Dyne and Stone[2] for references to earlier work.) It also has been employed repeatedly as one component of the reactant mixture in energy transfer studies.[3–5] Alkyl iodides have given especially interesting results in such studies because they react with both electrons and hydrogen atoms.[3,6,7] Previous studies of the radiolysis of cyclohexane–alkyl iodide mixtures have been concerned with the production of radioactive alkyl iodides[6] or gaseous products.[3,7] Although the production of iodine in the radiolysis of such mixtures has been mentioned briefly,[7] no iodine yields were reported. In the experiments described here, *G*-values were obtained for the production of I_2 in the radiolysis of methyl iodide–cyclohexane and ethyl iodide–

(1) G. R. Freeman, *J. Chem. Phys.*, **33**, 71 (1960).

(2) P. J. Dyne and J. A. Stone, *Can. J. Chem.*, **39**, 2381 (1961).

(3) L. J. Forrestal and W. H. Hamill, *J. Am. Chem. Soc.*, **83**, 1535 (1961).

(4) P. J. Dyne and W. M. Jenkinson, *Can. J. Chem.*, **39**, 2163 (1961).

(5) M. Burton, J. Chang, S. Lipsky, and M. P. Reddy, *Radiation Res.*, **8**, 203 (1958).

(6) R. R. Williams, Jr., and W. H. Hamill, *ibid.*, **1**, 158 (1954).

(7) R. H. Schuler, *J. Phys. Chem.*, **61**, 1472 (1957).

cyclohexane solutions, over the concentration range 0–95% cyclohexane by volume in each case.

Experimental

Phillip's "pure grade" cyclohexane was further purified by stirring with fuming sulfuric acid, washing with water, drying, distilling on a 3-ft. column packed with glass helices (Todd still), and passing through SiO_2 before use. Alkyl iodides (Columbia Organic) were passed through alumina, distilled on the Todd still at a reflux ratio of 25:1, and passed through alumina again before use. Individual 4-ml. samples were prepared volumetrically, dried with P_2O_5, degassed, transferred under vacuum to the irradiation vessels, and sealed off. The irradiation vessels were 13 × 100-mm. test tubes with attached spectrophotometer cells. Irradiations were performed at room temperature using a modified Firestone-Willard type Co^{60} source of 400 c. which is described elsewhere.[8] The dose rate in the Fricke dosimeter was 0.895×10^{18} e.v./ml. min., taking $G(Fe^{+3}) = 15.6$. Analysis of ferric solutions was done with a Beckman DU spectrophotometer at 305 mμ, using an extinction coefficient of 2201 at 25° and a temperature coefficient of 0.7%/deg.[9] Dose rates were corrected for the differing values of μ, the linear absorption coefficient, for the various solutions. For CH_3I and C_2H_5I, values of μ(sample)/μ(dosimeter) were calculated to be 1.950 and 1.679, based on absorption by Compton effect and photoelectric effect. For cyclohexane, the value 0.780 was obtained on the basis of electron density ratios. Relative absorption figures for the intermediate solutions were obtained by assuming an interpolation linear in volume fraction. In order to analyze for I_2 spectrophotometrically, the position of λ_{max} and the corresponding extinction coefficients were determined, using a Beckman DU spectrophotometer with the cell compartment maintained at 25.0 ± 0.2°.

Results

Graphs of λ_{max} for iodine in methyl iodide–cyclohexane and ethyl iodide–cyclohexane solutions are shown in Fig. 1. Extinction coefficients in the pure solvents were found to be 1277 for CH_3I, 1295 for C_2H_5I, and 940 for cyclo-C_6H_{12}, in good agreement with earlier values.[10,11] Several experiments on the mixed solvent systems gave graphs of extinction coefficients *vs.* mole fraction alkyl iodide–cyclohexane which deviated from an assumed linear interpolation by less than experimental error; extinction coefficients used in calculating *G*-values were obtained from the linear relationship.

Initial experiments to determine I_2 production *vs.* dose in methyl iodide–cyclohexane solutions gave very irreproducible results, especially for solutions with compositions in the vicinity of 80% cyclohexane, 20% methyl iodide by volume. However, it appears that this irreproducibility was caused by a little residual moisture, since more careful drying on the vacuum line cleared up the difficulty. It can be seen from Fig. 2 that graphs of iodine concentration *vs.* dose were essentially linear for all of the methyl iodide–cyclohexane solutions studied. The corresponding graph for the ethyl iodide–cyclohexane system looked very similar, and is not shown. Iodine production was linear with dose in that case also. The slopes of the various lines were converted into *G*-values for iodine production, and the resulting values are shown as a function of reactant concentration in Fig. 3.

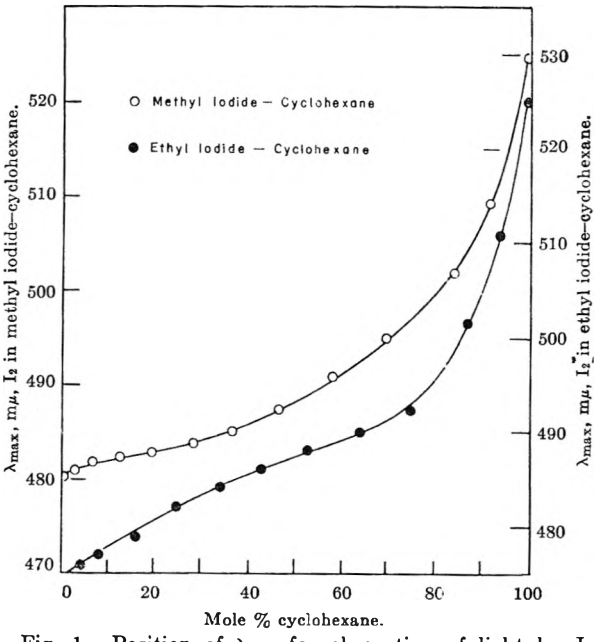

Fig. 1.—Position of λ_{max} for absorption of light by I_2 in various solutions of methyl iodide and ethyl iodide in cyclohexane.

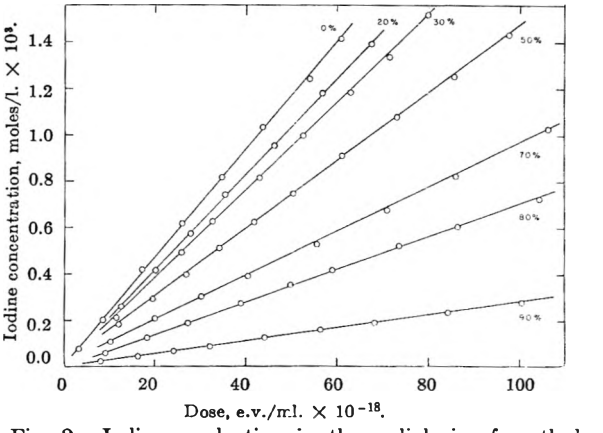

Fig. 2.—Iodine production in the radiolysis of methyl iodide–cyclohexane solutions, measured by light absorption at wave lengths given in Fig. 1. Figures by each line indicate % cyclohexane by volume. Lines for solutions of 5, 10, 40, 60, and 95% were omitted to avoid crowding the diagram.

Discussion

It can be seen from Fig. 3 that $G(I_2)$ is a smooth function of concentration (given in terms of electron % cyclohexane) for both of the alkyl iodide–cyclohexane systems studied, varying from a maximum value for the pure alkyl iodide to zero when the alkyl iodide is diluted with 93 to 100 electron % cyclohexane. Although the curves of Fig. 3 are similar to those which would result if iodine were produced directly from the alkyl iodide in proportion to its concentration, with the cyclohexane acting only as a diluent, such cannot be the case because free radicals from cyclohexane would certainly react with iodine from the alkyl iodide. It then becomes necessary to determine whether

(8) R. J. Hanrahan, *Intern. J. Appl. Radiation Isotopes*, **13**, 254 (1962).

(9) A. O. Allen, "The Radiation Chemistry of Water and Aqueous Solutions," D. Van Nostrand Co., Princeton, New Jersey, 1961, p. 21.

(10) E. O. Hornig and J. E. Willard, *J. Am. Chem. Soc.*, **79**, 2429 (1957).

(11) E. N. Weber, P. F. Forsyth, and R. H. Schuler, *Radiation Res.*, **3**, 68 (1955).

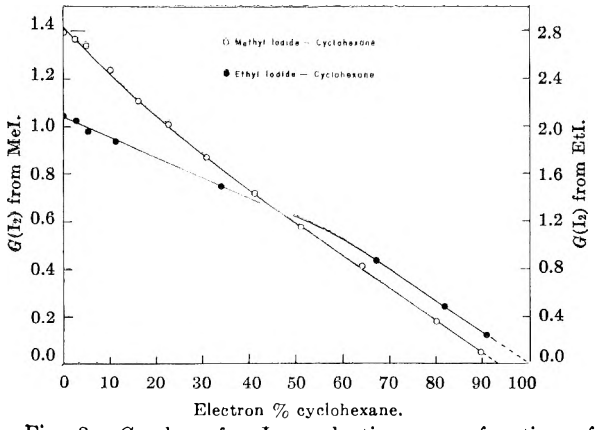

Fig. 3.—G-values for I_2 production as a function of composition for solutions of methyl iodide and ethyl iodide in cyclohexane.

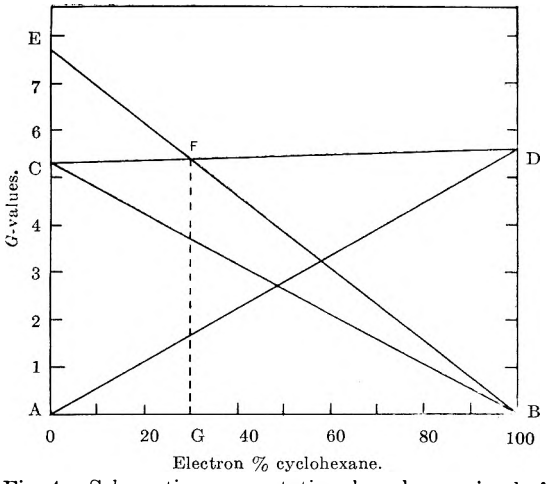

Fig. 4.—Schematic representation, based on a simple free radical mechanism, of the dependence of radical yields (lines BC, AD, and CD) and total iodine yield (BE) for solutions of methyl iodide in cyclohexane. Net iodine production is given by EB minus CD, and falls to zero for solutions richer in cyclohexane than point G. See text.

the situation could be explained by assuming that the primary yields from the alkyl iodide and from cyclohexane are proportional to the fraction of the energy absorbed by each (given presumably by its respective electron fraction), followed by interaction of radicals from both compounds with iodine.

In considering possible mechanisms, the case of methyl iodide–cyclohexane will be discussed in detail because it has been investigated previously by Forrestal and Hamill,[3] and also because of complications arising in the radiolysis mechanism of other iodides. It has been shown previously[12,13] that the observed yield of I_2 in irradiated alkyl iodides represents the excess of I· production over alkyl radical production in spurs (the difference corresponding to the production of stable hydrocarbons), plus an added component due to the reaction of thermal free radicals with HI. In general, the role of HI must be considered in detail, but in the particular case of CH_3I, the HI yield is so low that it may be ignored to a good approximation. Then assuming that the various yields are directly proportional to the electron % of the parent compound (Fig. 4), the total iodine yield (in equivalents) would decrease linearly from its value of 7.7 in pure methyl iodide and the radical yield would decrease from 5.3,[12,14] both going to zero at 0% methyl iodide. At the same time, the free radical yield from cyclohexane would increase from zero to its value of 5.6 for pure cyclohexane,[15] and the total radical yield from the two compounds would follow a linear interpolation between 5.3 and 5.6. In Fig. 4 a graph constructed on this basis is shown, and it can be seen that the total free radical yield should exceed the iodine yield, so that no net iodine could be produced, for all solutions richer in cyclohexane than about 30 electron %. The experimental results in Fig. 3 show that net iodine production persists until methyl iodide is diluted with 93 electron % cyclohexane.

In a recent paper, Forrestal and Hamill[3] presented considerable data on methyl iodide–cyclohexane and related systems, and reviewed earlier work. They measured CH_4 and H_2 yields as a function of CH_3I concentration, both with added HI and I_2, and also measured HI and cyclohexene with I_2 present as a scavenger. Water was used to prevent HI from back-reacting. They concluded that hydrogen arises from cyclohexane in three ways: an ionic mechanism giving molecular H_2, a hot atom abstraction reaction, and a thermal radical abstraction reaction. The latter both are assumed to result from initially excited cyclohexane[17]

$$C_6H_{12} \rightsquigarrow C_6H_{12}^+ + e^- \quad (1)$$

$$C_6H_{12}^+ + e^- \longrightarrow C_6H_{12}^{***} \quad (2)$$

$$C_6H_{12}^{***} \longrightarrow H_2 + \text{olefin} \quad (3)$$

$$C_6H_{12} \rightsquigarrow C_6H_{12}^{**} \quad (4)$$

$$C_6H_{12}^{**} \longrightarrow C_6H_{11}\cdot + \underline{H}\cdot \quad (5)$$

$$\underline{H}\cdot + C_6H_{12} \longrightarrow H_2 + C_6H_{11}\cdot \quad (6a)$$

$$\underline{H}\cdot + M \longrightarrow H\cdot + M \quad (6b)$$

$$H\cdot + C_6H_{12} \longrightarrow H_2 + C_6H_{11}\cdot \quad (7)$$

Reaction 7 has an appreciable activation energy and is subject to competition if other hydrogen atom scavengers are present. With I_2, HI, and CH_3I reactions 8–10 can occur

$$H\cdot + I_2 \longrightarrow HI + I\cdot \quad (8)$$

(12) R. J. Hanrahan and J. E. Willard, *J. Am. Chem. Soc.*, **79**, 2434 (1957).

(13) H. A. Gillis, R. R. Williams, Jr., and W. H. Hamill, *ibid.*, **83**, 17 (1961).

(14) R. J. Hanrahan, Ph.D. Thesis, University of Wisconsin, 1957, available from University Microfilms, Ann Arbor, Michigan.

(15) Based on iodine scavenging work in this Laboratory by W. C. Blasky, and ref. 16.

(16) R. W. Fessenden and R. H. Schuler, *J. Am. Chem. Soc.*, **79**, 273 (1957).

(17) The asterisk designations on excited states are those of Forrestal and Hamill, ref. 3. A further excited state, designated with one asterisk by Forrestal and Hamill, is postulated by them to be produced with $G = 0.75$ and to transfer energy either to HI or CH_3I causing them to dissociate. It is postulated to deactivate with no net effect in pure cyclohexane.

$$H\cdot + HI \longrightarrow H_2 + I\cdot \quad (9)$$

$$H\cdot + CH_3I \longrightarrow HI + CH_3\cdot \quad (10)$$

A portion of reaction 10 may give methane by a diffusion controlled reaction between HI and $CH_3\cdot$.

If CH_3I is the H· atom scavenger present in highest concentration, then reaction 10 is the predominant fate of the H· atoms. The fate of the resulting $CH_3\cdot$ radicals, and of cyclohexyl or other radicals present, depends on what other scavengers are present. If I_2 is the other scavenger, whether added initially or produced by radiolysis, these reactions occur

$$C_6H_{11}\cdot + I_2 \longrightarrow C_6H_{11}I + I\cdot \quad (11a)$$

$$CH_3\cdot + I_2 \longrightarrow CH_3I + I\cdot \quad (11b)$$

and if HI is the other scavenger besides CH_3I

$$C_6H_{11}\cdot + HI \longrightarrow C_6H_{12} + I\cdot \quad (12a)$$

$$CH_3\cdot + HI \longrightarrow CH_4 + I\cdot \quad (12b)$$

In all cases I· atoms combine to form I_2.

Forrestal and Hamill found that their results with 0.1 electron % or less added CH_3I could be explained by competitive hydrogen atom scavenging—reactions 7 and 10. They found that the decrease in $G(H_2)$ is balanced by an increase in G(HI) as would be predicted from the reactions postulated. As the CH_3I concentration is increased into the 1–10% range, however, the H· atom yield remains constant but the molecular H_2 yield drops and is matched by an increase in $G(CH_3\cdot)$—measured by converting it to CH_4 with HI. They postulate that this behavior is due to an interference in the ionic mechanism for production of molecular hydrogen, reaction sequence (1,2,3) above, due to dissociative electron capture by CH_3I

$$e^- + CH_3I \longrightarrow I^- + CH_3\cdot \quad (13)$$

The iodide ion presumably is neutralized without giving any further effect.

The present results concerning I_2 production are not incompatible with the above reaction scheme. However, no combination of reactions 1 through 13 gives a net production of I_2. Most sequences of reactions which can be derived from (1–13) are neutral in I_2 over-all, and the hot atom sequence (5,6a) must consume I_2. The yield of cyclohexyl radicals from this source is given as $2 \times 0.85 = 1.7$ for pure cyclohexane, and if, as argued by Forrestal and Hamill, no energy transfer from the parent excited state occurs, the yield in a solution containing 7 electron % methyl iodide could be taken as $0.93 \times 1.7 = 1.6$. Since this value is nearly 60% of the net iodine atom production rate in pure methyl iodide, it is clear that methyl iodide must be decomposing with high efficiency to give a break even point in iodine concentration at 7 electron % methyl iodide.

The most satisfactory proposal to date for explaining I_2 production in the radiolysis of pure CH_3I is the ion-molecule mechanism proposed on the basis of mass spectroscopic evidence by Gillis, Williams, and Hamill[13]

$$CH_3I^+ + CH_3I \longrightarrow (CH_3)_2I^+ + I\cdot \quad (14)$$

Upon neutralization of the product ion there results a "pocket" containing two methyl radicals and two iodine atoms which can undergo diffusion controlled recombination, giving a net yield of C_2H_6 and I_2. We now postulate that the rather efficient production of I_2 in dilute solutions in cyclohexane is due to this same mechanism, reaction 14 and its consequences, and that it is able to occur under these circumstances with considerable efficiency because of charge transfer from cyclohexane

$$C_6H_{12}^+ + CH_3I \longrightarrow C_6H_{12} + CH_3I^+ \quad (15)$$

Between 10 and 100 electron % methyl iodide, the residual free radical production from cyclohexane would fall to zero, and the efficiency of reaction 14 would approach its value in pure methyl iodide.

Although Forrestal and Hamill considered the charge exchange reaction (15) and found it compatible with their data, they preferred to postulate that the effects observed in the 0.1–10 electron % CH_3I range were to be attributed to the electron capture process, reaction 13. The present results seem to require that the charge exchange process (15) definitely occurs to account for net iodine production, but do not exclude the possibility that electron capture is occurring also. The most likely situation, suggested also by Forrestal and Hamill, is that electron capture and charge exchange both develop in the 0.1–10% concentration range, and tend to promote each other.

The situation regarding the alkyl radical–iodine balance in ethyl iodide must be similar to the methyl iodide case discussed above. However, an examination of the corresponding plot of $G(I_2)$ *vs.* concentration (Fig. 3) shows two regions of markedly different slope. Furthermore, the iodine yield apparently extrapolates to zero only at 0% of ethyl iodide. It is reasonable to assume that these differences are due to differences in the decomposition mechanism of methyl iodide as compared with other alkyl iodides. In the case of methyl iodide, the key step leading to net I_2 production must be a bimolecular step, either hot radical or ion-molecule. Although such processes are possible and presumably also occur for ethyl iodide and the higher iodides, in these cases it is possible to get a unimolecular production of HI (either by a true molecular elimination, or by a caged radical–I· atom reaction) which ultimately can lead to net I_2 formation. Thus the persistence of iodine production to lower concentrations of ethyl than of methyl iodide, observed in the present work, may be correlated with the much higher quantum yields obtained for ethyl than for methyl iodide in various photochemical experiments.

As noted in the Introduction, the measurements of I_2 production reported here are related to some earlier experiments of Schuler,[7] in which it was found that dilute solutions of methyl or ethyl

iodide in cyclohexane produce methane and C_2 hydrocarbons by chain reactions under radiolysis, but that the chains do not develop in the presence of iodine, whether added initially or produced during radiolysis. In the case of methyl iodide at 2 mole %, the chain reaction occurred uninhibited, but it was quenched by 6 mole %. In the case of ethyl iodide, on the other hand, as little as 0.3 mole % dropped the yield of the chain process drastically. Converting from mole % to electron %, these results imply that net iodine production occurs with *ca.* 8 electron % or more methyl iodide, and with as little as 0.4 electron % ethyl iodide in cyclohexane, in good agreement with the present work. It should be noted that all of the experiments reported here were conducted with alkyl iodide concentrations sufficiently high to prevent the chain reaction.

Acknowledgments.—Some preliminary data on the methyl iodide–cyclohexane system were taken by Miss Geraldine Westmoreland. Mr. Wm. C. Blasky aided in several phases of the experimental work. This research was supported by the State of Florida Nuclear Science Program. It was presented in Paper No. 119, Division of Physical Chemistry, 140th National Meeting of the American Chemical Society, Chicago, Illinois, September, 1961.

THE SECONDARY DEUTERIUM ISOTOPE EFFECT IN THE PYROLYSIS OF DIMETHYLMERCURY[1]

BY RALPH E. WESTON, JR., AND STANLEY SELTZER

Chemistry Department, Brookhaven National Laboratory, Upton, New York

Received May 2, 1962

The relative rates of the cyclopentane-inhibited pyrolysis of dimethylmercury and dimethylmercury-d_6 have been measured at 366°. The rate constant ratio is $k_D/k_H = 1.072 \pm 0.009$. This inverse isotope effect is attributed to an increase in C–H stretching frequencies of the transition state compared with the normal molecule, while the C–H bending frequencies remain unchanged. Rate constants for the pyrolysis of dimethylmercury at 303–366° have been determined, and are in good agreement with values obtained previously. This is also true of the C^{13} isotope effect, which at 366° is $k_{12}/k_{13} = 1.0386 \pm 0.0007$. It was found that methyl radicals did not exchange with dimethylmercury under the conditions of these experiments.

Introduction

Within the past few years, several investigations of secondary α-deuterium kinetic isotope effects have been made.[2] Such an effect is defined as the effect of deuterium substitution on the rate of a reaction of the type

$$RR'C(H \text{ or } D)X \longrightarrow RR'C(H \text{ or } D) + X$$

The observed effects have been attributed to a change in the hybridization of the carbon atom (to which the deuterium is bonded) from sp^3 (tetrahedral) to sp^2 (trigonal) in going from the ground state to the transition state.[3] On the basis of the vibrational frequencies of stable molecules (such as aldehydes and alkenes) in which the carbon–hydrogen bond is sp^2 in nature, a large decrease in one of the C–H bending frequencies is expected, and this will produce a normal isotope effect. It was our expectation that a similar isotope effect would be found in a reaction producing methyl radicals, and that the magnitude of this effect might give some information about the vibrational frequencies or configuration of the methyl radical.

The reaction chosen for this study was the pyrolysis of dimethylmercury in the presence of excess cyclopentane. Both the kinetics of this reaction and the C^{13} isotope effect have been previously studied by Russell and Bernstein.[4] The mechanism proposed by these authors on the basis of their kinetic results is

$$Hg(CH_3)_2 \longrightarrow HgCH_3 + CH_3 \quad (1)$$

$$HgCH_3 \longrightarrow Hg + CH_3 \quad (2)$$

$$CH_3 + Hg(CH_3)_2 \longrightarrow CH_4 + CH_3HgCH_2 \quad (3)$$

$$CH_3 + C_5H_{10} \longrightarrow CH_4 + C_5H_9 \quad (4)$$

$$CH_3 + Hg(CH_3)_2 \longrightarrow C_2H_6 + HgCH_3 \quad (5)$$

$$CH_3 + CH_3 \longrightarrow C_2H_6 \quad (6)$$

$$CH_3HgCH_2 \longrightarrow HgCH_3 + CH_2 \quad (7)$$

$$CH_2 + C_5H_{10} \longrightarrow C_6H_{12} \quad (8)$$

$$C_5H_9 \longrightarrow \text{Products} \quad (9)$$

In the presence of a ten- to twentyfold excess of cyclopentane, it can be shown that reactions 3, 5, 6, 7, and 8 are negligible.[4] The rate expression becomes simply

$$-d[Hg(CH_3)_2]/dt = d[CH_4]/2dt = k_2[Hg(CH_3)_2]$$

so that the rate-determining step is the unimolecular decomposition of dimethylmercury. It is not possible to decide, on the basis of the kinetic results, whether step 2 is distinct from step 1, or whether

(1) Research performed under the auspices of the U. S. Atomic Energy Commission.

(2) For a recent review, *cf.* R. E. Weston, Jr., *Ann. Rev. Nuclear Sci.*, **11**, 439 (1961).

(3) Other interpretations of secondary α-deuterium effects have been presented by: (a) M. Wolfsberg, S. Seltzer, and R. S. Freund, private communication; (b) L. S. Bartell, *J. Am. Chem. Soc.*, **83**, 3567 (1961).

(4) M. E. Russell and R. B. Bernstein, *J. Chem. Phys.*, **30**, 607, 613 (1959). These papers contain references to earlier literature on the kinetics.

both carbon–mercury bonds are broken simultaneously.

One can measure the isotope effect in step 1 by allowing a mixture of two isotopic species of dimethylmercury to pyrolyze competitively, and then comparing the isotopic composition of the methane produced with that of the original dimethylmercury.

Experimental

Dimethylmercury was prepared according to the method of Gilman and Brown.[5] After the solvent (ether) was distilled through a 12-in. bubble-plate column, the residue was distilled through a 12-in. platinum-spiral vacuum-jacketed column. The fraction boiling at 92° was collected. Examination of this fraction with the Perkin–Elmer vapor fractometer, Model 154C, disclosed the presence of two impurities: ether (0.4%) and an unknown material with a boiling point at approximately 60° (0.1%). Further purification was necessary; therefore, the dimethylmercury was chromatographed in 4-cc. portions on a 12-ft., 5/8-in. i.d. column composed of 35% Dow Corning 710 silicone oil on Johns-Manville C 22 firebrick (30–70 mesh) at 110° and a helium pressure of 20 p.s.i. Under these conditions, dimethylmercury appeared after 23.5 min. The effluent vapor was condensed in a trap cooled to −78°. Some decomposition occurred on the passage through the hot thermal conductivity cell, as evidenced by the appearance of droplets of mercury. The organic decomposition products are, however, non-condensable gases. A further distillation was performed to free the dimethylmercury of any silicone oil that might have been carried through. An infrared spectrum, after this purification, compared favorably with that reported by Gutowsky.[6]

Dimethylmercury-d_6 was prepared from methyl-d_3 iodide (99.3% D, Merck and Co. Ltd.) and purified in the same manner as described above.

Cyclopentane (Phillips research grade) was chromatographed in 5-cc. portions at 75° on the same macro column as that used for the purification of dimethylmercury. The first 60% of each sample was distilled, so that the cyclopentane was freed of small amounts of impurities, as shown by chromatography in the Perkin–Elmer vapor fractometer.

Reaction Vessel.—The reaction vessel was a 440-cc. Pyrex bulb of roughly cylindrical shape, connected to the vacuum manifold through a section of 1-mm. capillary tubing and a mercury cut-off valve of the type described by Miller, *et al.*[7] The vessel was contained inside a copper cylinder, on which a heating element was wound, and this in turn was inside an insulated box. The temperature-controlling circuit depended on a copper–constantan thermocouple as the sensing element, and has been described elsewhere.[8] Temperature fluctuations at the center of the vessel were ±0.3°, but there was also a spatial inhomogeneity of temperature, with a maximum difference of 3° between the end of the vessel and the center. This should not produce a measurable error in the isotope effect determinations. No correction to the rate constant was made for the volume of the reaction vessel outside the oven, which amounted to <0.5% of the total.

Procedure for Reaction Rate Determinations.—After some initial runs in which dimethylmercury alone was allowed to decompose, in order to condition the surface of the reaction vessel, all experiments were carried out in the presence of a large excess of cyclopentane.

In general, the techniques used were conventional vacuum-line techniques for handling volatile materials. However, it became apparent after a few preliminary experiments that the solubility of both cyclopentane and dimethylmercury in stopcock grease presented a serious problem. This was solved by (1) the use of Cello-grease (Fisher Scientific Co.); (2) use of the mercury cut-off valve on the reaction vessel (see above); (3) allowing only transient contact between the reactant and any of the stopcocks of the vacuum line.

In early runs, dimethylmercury and cyclopentane were introduced into the system separately. Each was contained in a small tube with stopcock and ground joint, and the tube was weighed before it was attached to the vacuum line. Cyclopentane was then allowed to condense at −196° into a small tip on the capillary intake to the reaction vessel. When condensation was complete, the tube was removed and weighed, after the joint had been degreased. The same procedure was used for dimethylmercury, and it was found that this could be introduced into the reaction vessel and quantitatively recovered by the use of this procedure.

In a kinetic run, the frozen mixture of cyclopentane and dimethylmercury was rapidly (15–20 sec.) evaporated into the reaction vessel when the freeze-out was warmed to ~90° with hot water. During the run, the capillary intake and freeze-out were heated electrically to prevent condensation of the reaction mixture.

The reaction was quenched, usually after 10–20% completion, by allowing the reaction mixture to expand through a concentric tube trap and a spiral trap (both at −196°) into a Toepler pump. Preliminary experiments with known mixtures of methane and cyclopentane showed that they were quantitatively separated by this procedure. Mass spectrometric analysis of the non-condensable gas from reaction mixtures did not indicate any constituents other than H_2 and CH_4. The products volatile at −196° were Toepler-pumped into a gas buret, where the pressure was measured by means of a mercury manometer and a Wild cathetometer accurate to 0.01 mm.

In the later kinetic runs, and in all isotope effect experiments, hydrogen in the mixture of non-condensable gases was removed by combustion over activated CuO at 250–300°, and the amount of residual methane was determined.[9]

The possibility of hydrogen exchange during the oxidation process was ruled out by performing the oxidation with a mixture of 9% D_2–91% CH_4. The methane remaining after combustion of the hydrogen was found to contain $\leq$0.05% CH_3D. The analysis by this procedure of a H_2–CH_4 mixture prepared volumetrically gave results which agreed within 1% with the known composition. In addition, mass spectrometric examination of the remaining gas showed that it contained <0.06% hydrogen, and $\leq$0.5% CO_2 from oxidation of CH_4.

Rate constants were calculated on the basis of the amount of methane produced and the original amount of dimethylmercury.

Analysis of the non-volatile product from the kinetic runs was performed with the aid of the Perkin-Elmer vapor fractometer. Standard samples of dimethylmercury and cyclopentane produced peak areas directly proportional to their mole ratios. Samples of the non-volatile products after a predetermined extent of reaction were chromatographed and analyzed in the same way.

Procedure for Determining the Deuterium Isotope Effect.—A solution of approximately 2% $(CD_3)_2Hg$ in $(CH_3)_2Hg$ was prepared gravimetrically, and the isotopic composition was determined by combustion over copper oxide. Baker and Co. copper oxide wire was activated by complete reduction in a stream of hydrogen at about 400° and then oxidation in a stream of oxygen at the same temperature for 2 hr.

Combustion of liquid dimethylmercury was carried out by a modified Wilzbach method.[10] Copper oxide was placed in an 11-mm. o.d. tube of 1720 Corning glass with standard taper joint and break tip. A portion of the tube was pulled out to a fine capillary and the tube was placed on the vacuum line. The tube and contents were degassed at 400–500° for 15 min. Then at the same temperature an atmosphere of oxygen was allowed to remain in contact with the contents for 15 min. The tube and contents were cooled slowly and the system was evacuated. Approximately 50 mg. of the dimethylmercury solution was pipetted into a separate tube. The tube was placed on the vacuum line and the contents degassed. The dimethylmercury then was completely distilled, through a very short distance, into the tube containing the copper oxide. The copper oxide

(5) H. Gilman and R. E. Brown, *J. Am. Chem. Soc.*, **52**, 3314 (1930).

(6) H. S. Gutowsky, *J. Chem. Phys.*, **17**, 128 (1949).

(7) G. H. Miller, G. O. Pritchard, and M. Weston, *Rev. Sci. Instr.*, **30**, 948 (1959).

(8) R. E. Weston, Jr., *J. Chem. Phys.*, **26**, 975 (1957).

(9) A. E. Heron and H. N. Wilson in "Comprehensive Analytical Chemistry," C. L. Wilson and D. W. Wilson, ed., Elsevier Publishing Co., New York, N. Y., 1959, pp. 244–245.

(10) K. E. Wilzbach and W. Y. Sykes, *Science*, **120**, 494 (1954).

tube was sealed off under vacuum and heated at 650° for at least 5 hr.

The products of combustion were condensed into a trap cooled to −196° while the combustion tube and contents were warmed with a hair dryer. Fifteen minutes was allowed for complete transfer. The contents of the trap were then degassed at −78°. The water remaining in the trap was reduced to hydrogen over uranium according to the procedure of Bigeleisen, *et al.*[11] Analyses for HD/H_2 were made with the Consolidated-Nier Model 21-201 mass spectrometer operating as a single collector instrument. Calibration lines were obtained from the concurrent analyses of known HD–H_2 mixtures.

The procedure for a kinetic run with the 2% D mixture was essentially identical with that described previously: One change was introduced because we were concerned about a possible isotopic difference in vapor pressures. This vapor pressure difference was confirmed by analyzing the first and last fractions of the 2% solution for deuterium after simple bulb-to-bulb distillation. For this reason, a solution of dimethylmercury in cyclopentane was made up gravimetrically. An aliquot of this was removed through a serum cap with a hypodermic needle, and introduced into a weighed tube. The tube was rapidly capped, weighed with the solution, and then rapidly attached to the vacuum line. After this, the procedure was similar to that described previously.

After the reaction had been quenched, hydrogen was removed from the non-condensable product by combustion. Methane samples were combusted over activated CuO at 750° for 2 hr. in quartz bulbs fitted with stopcocks and joints. The complete combustion of methane and subsequent reduction of the water was checked by burning a mixture of 2% methane-d_4[12] and methane. The deuterium analysis was, within experimental error, the same as that calculated from the number of moles of each isotopic species in the mixture. The rest of the procedure for determining deuterium content was identical with that used for dimethylmercury.

Procedure for Determining the Carbon-13 Isotope Effect.—The technique in this case was very similar to that used for studying the deuterium isotope effect, except that natural dimethylmercury (containing ~1 atom % C^{13}) was used.

The combustion procedures for dimethylmercury and methane were the same as those described above, except that the carbon dioxide was collected and the water discarded.

The isotopic analyses of carbon dioxide were made with a Consolidated-Nier Model 21-201 mass spectrometer. Analyses of samples were alternated with those of tank carbon dioxide which served as a reference. The ratio C^{13}/C^{12} was calculated from the formula

$$R = (R_{obsd} - \rho - O^{17})F \qquad (1)$$

in which R_{obsd} is the measured mass 45/mass 44 ratio, ρ is the resolution correction (0.00020 in this work), O^{17} is the correction for O^{17} abundance (0.00083 in this work), and F is the amplifier correction (1.020 in this work). It should be noted that ρ and O^{17} corrections do not entirely cancel when two values of R are compared, whereas the F correction does.

Attempted Mass Spectral Investigation of Methyl Exchange in Dimethylmercury.—A sample of a mixture of approximately 58% $(CD_3)_2Hg$ and 42% $(CH_3)_2Hg$ was analyzed by a Consolidated mass spectrometer Model 21-103. In addition, separate determinations were made on natural and fully deuterated dimethylmercury. The ratio of peak heights in the region, m/e 228 to 234 (the parent region) for natural dimethylmercury was essentially identical with the natural abundances of the mercury isotopes as first shown by Dibeler and Mohler[13]; this was essentially the same for the fully deuterated compound except that the peaks were 6 mass units higher. The mass spectrum of the mixture is not just a simple synthesis of the mass spectra for each of the two pure components. Rather, a new group of mercury isotope abundance peaks in the parent region appear which best fit the formula CH_3HgCD_3. If it is assumed that the parent peaks of the three species all have the same sensitivities then the concentrations of the three components produced in the mass spectrometer are: $(CH_3)_2$-Hg, 30%; $(CD_3)_2Hg$, 46%; CH_3HgCD_3, 24%.

Reaction of Azomethane-d_6 with Dimethylmercury.—Dimethyl-d_6-hydrazine was prepared from $LiAlD_4$ and diethylhydrazocarboxylate by the method of Hinman.[14] The oxidation of the hydrazine to azomethane-d_6 was carried out according to the method of Renaud and Leitch.[15] The compound was purified by passing it through a $MgClO_4$ tube.

A mixture of natural dimethylmercury and cyclopentane was made up with Q = 0.0695. Approximately 0.6-g. samples of this mixture were used together with the appropriate amount of azomethane-d_6. The mole ratio of dimethylmercury to azomethane-d_6 varied between 1.59 and 12.5. The reaction was studied from 314 to 348° with a deviation of about ±2° during a run. The reaction time was such that from 75–95% of the azomethane-d_6 decomposed[16] while less than 1.5% of the dimethylmercury decomposed.[4] The reaction was stopped in the usual manner and the material collected in the trap cooled by liquid nitrogen was vapor-chromatographed on a Ucon oil column similar to that used for purification of natural dimethylmercury. The dimethylmercury fraction from each run was converted to hydrogen gas as described above. The atom % D was found to be very small, indicating an upper limit of 7% exchange of methyl radicals into dimethylmercury.

Preparation of CD_3HgCH_3.—Dimethyl-1,1,1-d_3-mercury was prepared from a mixture of 0.64 g. of CD_3I (Merck of Canada), 2.7 g. of CH_3I, and 94 g. of 3.5% cadmium amalgam by the method of Leitch, *et al.*[17] If random labeling is assumed during the synthesis, the mixture should have produced 66% CH_3HgCH_3, 31% CD_3HgCH_3, and 3.5% CD_3HgCD_3. This mixture was used for infrared comparison with a mixture of 80% $(CH_3)_2Hg$ and 20% $(CD_3)_2Hg$ after having undergone 12% reaction to see if there was any methyl exchange.

The antisymmetric methyl–mercury stretching vibration $\nu_7(a_2'')$ is infrared active, and should have a PQR band structure, with a very weak Q band. In the case of $(CH_3)_2$-Hg, the P and R bands are observed at 538 and 553 cm.$^{-1}$, while the P, Q, and R bands of $(CD_3)_2Hg$ are at 490, 497, and 503 cm.$^{-1}$. The mixture of isotopic species containing 31% CH_3HgCD_3 exhibited new bands at 476 and 483 cm.$^{-1}$, and a band at 490 cm.$^{-1}$ much more intense than the $(CD_3)_2$-Hg band at 503 cm.$^{-1}$. Therefore, the P, Q, and R bands of CH_3HgCD_3 are assigned to 476, 483, and 490 cm.$^{-1}$. The spectrum of the dimethylmercury recovered from the $(CH_3)_2Hg$–$(CD_3)_2Hg$ reaction mixture did not show the 476 or 483 cm.$^{-1}$ band, and was identical with that of the original mixture.

These experiments indicate that exchange of methyl groups does not take place under normal experimental conditions. The exchange observed in the mass spectrometer may have been caused by metallic surfaces.

Experimental Results

Observations on the Kinetics and Mechanism of the Cyclopentane-Inhibited Pyrolysis of Dimethylmercury. 1. Reaction Products.—In general, our findings confirm those of Russell and Bernstein,[4] as well as those of McNesby and Gordon[18,19] on the reactions of the cyclopentyl radical.

At the low values of Q (molar ratio of dimethylmercury to cyclopentane) used in this work, the only measurable hydrocarbon product from dimethylmercury is methane. This is formed by the

(11) J. Bigeleisen, M. L. Perlman, and H. C. Prosser, *Anal. Chem.*, **24**, 1256 (1952).

(12) Kindly donated by Dr. D. R. Christman.

(13) V. H. Dibeler and F. L. Mohler, *J. Res. Natl. Bur. Std.*, **47**, 337 (1951).

(14) R. L. Hinman, *J. Am. Chem. Soc.*, **78**, 1645 (1956).

(15) R. Renaud and L. C. Leitch, *Can. J. Chem.*, **32**, 545 (1954).

(16) C. Steel and A. F. Trotman-Dickenson, *J. Chem. Soc.*, 975 (1959).

(17) E. E. Bevege, R. Renaud, and L. C. Leitch, *Can. J. Chem.*, **31**, 1259 (1953).

(18) J. R. McNesby and A. S. Gordon, *J. Am. Chem. Soc.*, **79**, 825, 4593 (1957).

(19) A. S. Gordon, S. R. Smith, and J. R. McNesby, *ibid.*, **81**, 5059 (1959).

abstraction of a hydrogen atom from cyclopentane by a methyl radical produced by rupture of the Hg–C bond in dimethylmercury.

In confirmation of this, a few analyses by vapor phase chromatography were made of the nonvolatile reaction products which remained in the trap when it was warmed to room temperature. From the ratio of dimethylmercury to cyclopentane in the product mixture, together with this ratio for the reactant mixture (Q), one can calculate the amount of methane produced. Within experimental error, this agrees with the amount measured manometrically. Three very small peaks ($\sim$ 0.1%) were observed in the higher molecular weight region, with approximate boiling points 65–80°, but were not identified.

Further confirmation was given by two experiments in which essentially pure $(CD_3)_2Hg$ ($\geq$99 atom % D) was pyrolyzed in the presence of normal cyclopentane (Q = 0.06, 366°). Mass spectra of the hydrogen–methane mixtures from these runs were compared with spectra of pure CD_3H (Volk Radiochemical Co.) by means of a Consolidated Model 21–103 mass spectrometer. Within experimental error, no HD or D_2 was found in the hydrogen. This is in agreement with the experimental results of McNesby and Gordon, who studied the photolysis and pyrolysis of acetone-d_6 mixed with cyclopentane. The hydrogen produced during the pyrolysis of dimethylmercury evidently comes from the cyclopentyl radical by means of a mechanism which does not produce hydrogen atoms. The ratio H_2/CH_4 was found to increase with pyrolysis temperature (*cf.* Table I). This observation and (approximately) the value of the ratio at a given temperature are in agreement with the results of McNesby and Gordon. The ratio also decreased appreciably (Table I), when Q was increased from 0.05 to 0.15, which is to be expected if there is a competition for methyl radicals between cyclopentane and dimethylmercury.

The methane produced in the pyrolysis of $(CD_3)_2$-Hg with cyclo-C_5H_{10} was found to be 97.5% CD_3H, 2.2% CH_4, and $\leq$0.3% CD_4. The amount of CH_4 is greater than that which could be produced from the $(CH_3)_2Hg$ present as an isotopic impurity, and must be a product of the cyclopentyl radical decomposition, although McNesby and Gordon did not report this fact.

The low ratio of CD_4/CD_3H shows that hydrogen abstraction from dimethylmercury is negligible when $Q \simeq 0.05$.

In a few runs (Q = 0.05, 366°) the more volatile reaction products collected in the trap at −196° were examined mass spectrometrically. The trap was warmed to a temperature between −110 and −130°, and the fraction volatile at this temperature was Toepler-pumped off. The amounts of products relative to the amount of CH_4 were: C_2H_4, 0.48–0.95; C_2H_6, 0.080–0.123; C_3H_6, 0.012–0.048; all higher fractions were $\leq$0.001 except C_5H_{10}. The product composition was found to be relatively irreproducible. Ethylene and propylene have been shown to be products of the cyclopentyl radical decomposition according to the scheme

$$CH_3\cdot + C_5H_{10} \longrightarrow CH_4 + C_5H_9\cdot$$

$$C_5H_9\cdot \longrightarrow C_2H_4 + C_3H_5\cdot$$

$$C_3H_5\cdot + C_5H_{10} \longrightarrow C_3H_6 + C_5H_9\cdot$$

$$2C_3H_5\cdot \longrightarrow C_6H_{10}$$

Since this is a chain reaction, and since allyl radicals may react in other ways, it is perhaps not surprising that relative amounts of methane, ethylene, and propylene should fluctuate from run to run. The large amount of ethylene relative to propylene shows that hydrogen abstraction by the allyl radical is a rather unfavorable reaction at 366°.

2. Rate Constants.—In the course of making preliminary runs, as well as during the actual isotope effect experiments, a large number of rate constants for the cyclopentane-inhibited pyrolysis of dimethylmercury were determined. Also, in those experiments with 2% $(CD_3)_2Hg$ present, the gross rate is unchanged, in view of the small isotope effect (see below).

Because the range of Q and total pressure in our work is rather limited, we have corrected the observed rate constants to Q = 0 and P^{-1} = 0 by using the dependence on these parameters found by Russell and Bernstein. The corrected rate constants thus obtained are given in Table I. After roughly ten or so runs, rate constants were extremely reproducible, and did not change over a period of a few months. Hence we feel that any surface effects have been eliminated.

The rate constants we obtained in the temperature range 303–366° are compared with the value obtained by Russell and Bernstein of $k_1 = 5.0 \times 10^{15} \exp(-57{,}900/RT)$ sec.$^{-1}$ in Fig. 1. With the exception of the single experiment at 303°, our data lie on a straight line when log k_1 is plotted against T^{-1}. The agreement with the results of Russell and Bernstein is extremely good at 366°, where most of our runs were made. At lower temperatures, the constants we obtained are somewhat smaller than theirs, and the activation energy we obtain (again disregarding the point at 303°) is 61.2 kcal./mole. The difference of 3.3 kcal./mole is not considered significant, because there appears to have been a drift in the thermocouple calibration during our experiments. An error of 2° at either end of the range would produce the observed discrepancy.

Whether or not the discrepancy in activation energy is real has little effect on considerations of the mechanism, since in either case it is equal to or slightly greater than the bond dissociation energy for both C–Hg bonds. Russell and Bernstein have cited this fact as evidence that there is a simultaneous bond rupture rather than a stepwise one. This is not a necessary conclusion, however. A more serious objection to our higher value of the activation energy is that it leads to an abnormally high pre-exponential factor in k_1 of 7×10^{16} sec.$^{-1}$.

Cattanach and Long[20] recently have criticized

(20) J. Cattanach and L. H. Long, *Trans. Faraday Soc.*, **56**, 1286 (1960).

TABLE I

RATE CONSTANTS FOR PYROLYSIS OF DIMETHYLMERCURY IN THE PRESENCE OF CYCLOPENTANE

T, °C.	10^2Q[a]	Pressure,[b] mm.	% H_2	No. of runs	10^5k_{obsd}, sec.$^{-1}$	10^5k_{corr}[c]
303	9.82	600	4.4	1	0.0787	0.0804
326	9.82	606–630	4.7 ± 0.2	5	0.307 ± 0.001	0.313 ± 0.001
346	5.15–5.75	585–610	5.8[d]	3	1.56 ± 0.02	1.61 ± 0.02
346[e]	6.55	559	5.8[d]	1	1.62	1.67
347	9.82	626–646	5.8 ± 1.1	3	1.70 ± 0.03	1.74 ± 0.03
366	4.56	680	10.0[d]	1	7.55	7.80
	4.86	614	10.0[d]	1	7.43	7.69
	5.00	597	13.9	1	7.80	8.07
	5.32	439–640	10.7 ± 1.1	8	7.62 ± 0.24	7.50 ± 0.24
	5.52	613	10.2	1	7.70	7.95
	5.65	539–655	10.7 ± 1.1	5	7.81 ± 0.21	7.66 ± 0.21
	6.06	636	10.0[d]	1	7.03	7.20
	6.30	604–659	9.4–12.2	2	7.68 ± 0.42	7.45 ± 0.42
	6.34	582	10.0[d]	1	7.80	8.04
	8.91	420–586	8.1 ± 0.5	6	8.10 ± 0.26	7.87 ± 0.26
	15.0	648–677	5.5 ± 0.9	6	8.21 ± 0.12	7.82 ± 0.12
366[e]	5.91	598	10.0[d]	1	7.58	7.80

Mean of 33 runs at 366°, $k = 7.70 \pm 0.24 \times 10^{-5}$ sec.$^{-1}$.
[a] $Q = (CH_3HgCH_3)/(\text{cyclo-}C_5H_{10})$. [b] Total pressure. [c] Rate constant corrected to $Q = 0$ and $P^{-1} = 0$. [d] Assumed. [e] Dimethylmercury-d_6 (≥99 atom % D).

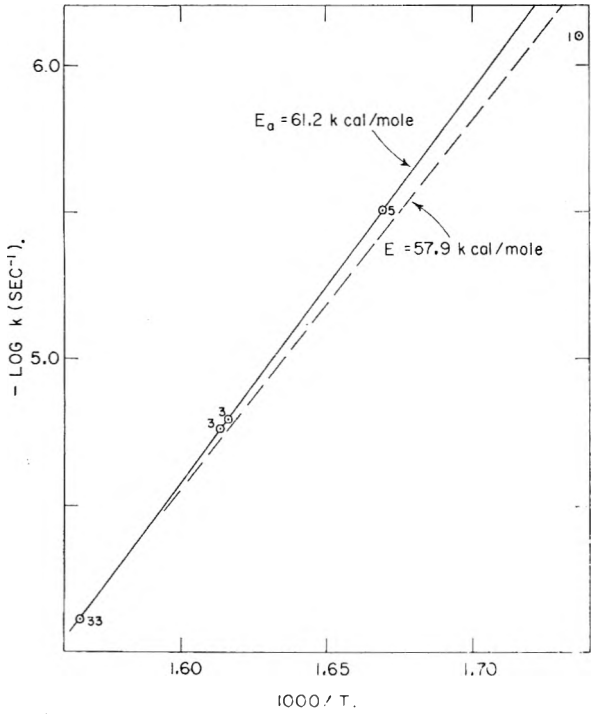

Fig. 1.—Rate constant for the pyrolysis of dimethylmercury: solid line, this work; dashed line, Russell and Bernstein[4]; numbers beside experimental points are the numbers of runs at a given temperature.

the results obtained by Russell and Bernstein, citing the fact that hydrogen has been shown to affect the rate of decomposition of dimethylmercury. This criticism is not well founded. The effect of hydrogen arises from a chain mechanism proceeding by the reactions

$$CH_3 + H_2 \longrightarrow CH_4 + H$$

$$H + (CH_3)_2Hg \longrightarrow CH_4 + Hg + CH_3$$

The rate constant for hydrogen abstraction by methyl radicals from molecular hydrogen is about the same as that for abstraction from cyclopentane,[21] so that the relative rates will be proportional to the relative concentrations. In our experiments and those of Russell and Bernstein, the amount of hydrogen produced from cyclopentane was roughly a thousandfold less than the amount of cyclopentane present, so that the production of hydrogen atoms should be negligible. To test this fact, we carried out pyrolyses at 370° in which the initial reaction mixture contained 10–20 times as much hydrogen as that produced during the normal course of reaction. The rate constants obtained in these runs were at most 7% larger than those for comparable runs with no added hydrogen (this difference is about twice the mean error in rate constants). Therefore, the reaction of methyl radicals with hydrogen is negligible under the usual conditions of our experiments.

Carbon-13 Isotope Effect.—Russell and Bernstein found that the C^{13} isotope effect in this reaction is appreciably lowered if there is a chain mechanism involved. The addition of cyclopentane tends to eliminate this chain mechanism. As a check on the absence of this chain reaction in our work, we redetermined the C^{13} isotope effect in a few experiments. The results are presented in Table II. The ratio of rate constants, k_{12}/k_{13}, is obtained from the formula[22]

$$k_{12}/k_{13} = \log (1 - fR_{xf}/R_{ao})/\log (1 - f) \quad (2)$$

in which R_{ao} is the C^{13}/C^{12} ratio of the original dimethylmercury and R_{xf} is the corresponding ratio for the methane which has been produced at the fraction of reaction f.

The observed value of k_{12}/k_{13} must be corrected to $Q = 0$ and $P^{-1} = 0$. The dependence on these parameters found by Russell and Bernstein gives a corrected value of 1.0412 ± 0.0007, which may be

(21) E. W. R. Steacie, "Atomic and Free Radical Reactions," Reinhold Publ. Corp., New York, N. Y., 1954, pp. 500, 527.

(22) From rearrangement of eq. V. 23, J. Bigeleisen and M. Wolfsberg, *Advan. Chem. Phys.*, **1**, 15 (1958).

TABLE II

C^{13} ISOTOPE EFFECT IN THE CYCLOPENTANE-INHIBITED PYROLYSIS OF DIMETHYLMERCURY AT 366°

10^2Q	P, mm.	f	R_{xf}[a]	k_{12}/k_{13}
5.32	651	0.1209	0.0093778	1.0386
5.32	636	.1267	.0093860	1.0377
5.32	640	.1611	.0093775	1.0395
5.32	640	.1618	.0093788	1.0393
5.32	623	.1722	.0093935	1.0378
				1.0386 ± 0.0007

$(CH_3)_2Hg$: R_{ao} = 0.0097167

[a] Relative to tank CO_2.

compared with their value of 1.0343 at 360°. However, the actual agreement is better than this, since in treating the mass spectrometric results they did not correct for O^{17} abundance and spectrometer resolution. Neglect of these factors would lower our value to about 1.038, which is in good agreement.

The C^{12} enrichment of dimethylmercury relative to tank CO_2 was only about 3%, compared to the 7% found by Russell and Bernstein.

Deuterium Isotope Effect.—The observed relative rates of reaction of dimethylmercury-d_6 and normal dimethylmercury are given in Table III. The rate constants k_H and k_D refer to

$$CH_3HgCH_3 \xrightarrow{k_H} CH_3 + HgCH_3 \text{ or } 2CH_3 + Hg$$

and

$$CD_3HgCD_3 \xrightarrow{k_D} CD_3 + HgCD_3 \text{ or } 2CD_3 + Hg$$

The ratio k_D/k_H is obtained from the equation corresponding to eq. 2. Since each CD_3 radical abstracts a hydrogen atom from cyclopentane to form CD_3H, the value to be used for R_{ao} is three-fourths of the atom per cent of deuterium obtained upon analysis of the original dimethylmercury.

TABLE III

DEUTERIUM ISOTOPE EFFECT IN THE CYCLOPENTANE-INHIBITED PYROLYSIS OF DIMETHYLMERCURY AT 366°

10^2Q	P, mm.	f	R_{xf}	k_D/k_H
5.65	640	0.1170	1.671	1.080
	539	.1276	1.647	1.064
	635	.1402	1.661	1.075
	649	.1435	1.658	1.073
	655	.1735	1.661	1.078
Original dimethylmercury R_{ao} = 1.554				1.074 ± 0.004
8.91	556	0.1224	1.674	1.083
	556	.1362	1.646	1.064
	586	.1609	1.627	1.052
	420	.1636	1.646	1.065
Original dimethylmercury R_{ao} = 1.554				1.066 ± 0.008
15.0	658	0.0629	1.671	1.085
	648	.0688	1.670	1.085
	677	.0696	1.637	1.062
	663	.1129	1.664	1.083
	668	.1141	1.639	1.066
	655	.1554	1.634	1.064
Original dimethylmercury R_{ao} = 1.538				1.074 ± 0.010

Mean of 15 runs = 1.072 ± 0.009.

The small size of this isotope effect, together with the experimental error in R_{xf} and R_{ao} of about 1%, made it seem useless to search for the dependence on Q, P, or T.

Discussion

Deuterium Isotope Effect.—The most striking experimental fact is the *inverse* deuterium isotope effect, which corresponds to a difference in free energy of activation ($\Delta\Delta F^*$) of -15 ± 2 cal./mole/D atom. This effect must somehow be reconciled with a *normal* carbon isotope effect.

One possible way of explaining these results is to postulate a rapid exchange of methyl radicals with dimethylmercury, and a rate of abstraction of hydrogen from cyclopentane which is slower than the exchange but more rapid than the decomposition of dimethylmercury. The observed isotope effect for this kinetic scheme depends on the ratio of rate constants for hydrogen abstraction from cyclopentane and the equilibrium constants for the exchange reaction. However, the results of the experiments with mixtures of azomethane-d_6 and dimethylmercury, and of dimethylmercury-d_6 and dimethylmercury indicate that this exchange is nonexistent under the experimental conditions.

From the arguments given in the next section about the reaction coördinate and its contribution to the temperature-independent factor of the carbon isotope effect, it appears that this term will produce a normal deuterium isotope effect. Therefore, the abnormal contribution must come from an increase of the zero-point energy difference between deuterium and protium compounds in the transition state compared to this difference in the ground state. At the same time, to fit the normal carbon isotope effect, the vibrational frequencies which change must be relatively insensitive to carbon isotope substitution. The type of vibration which most obviously fits this latter criterion is a C–H stretching mode, which would produce the observed deuterium effect if it were increased in frequency in the transition state.

In fact, there is evidence for an increase in the C–H stretching frequency when the bonding to the carbon atom changes from sp^3 to sp^2. The C–H bond in ethylene is about 0.017 Å. shorter than that in ethane,[23] while that of the methyl radical[24] is about 0.013 Å. shorter than the bond in methane.[23] The decrease in bond length will lead to an increase in the stretching force constant, which can be estimated from Badger's rule or one of its variants to be about 0.37×10^5 dynes/cm. This in turn leads to an increase in the vibrational frequency of about 100 cm.$^{-1}$, which is in good agreement with observed values for ethane[25] and ethylene.[26]

The possibility that there is a contribution to secondary isotope effects from this source has been

(23) C. C. Costain and B. P. Stoicheff, *J. Chem. Phys.*, **30**, 777 (1959).

(24) G. Herzberg, *Proc. Roy. Soc.* (London), **A262**, 291 (1961).

(25) G. E. Hansen and D. M. Dennison, *J. Chem. Phys.*, **20**, 313 (1952).

(26) G. Herzberg, "Infrared and Raman Spectra of Polyatomic Molecules," D. Van Nostrand Co., Inc., New York, N. Y., 1945, p. 326.

mentioned by Llewellyn, Robertson, and Scott[27] in connection with solvolysis reactions of methyl-d_3 esters; however, they attributed the inverse isotope effects which they found ($\Delta\Delta F^* = -6$ to -32 cal./mole/D atom) to the increase of a bending force constant in the transition state. The out-of-plane CH_3 vibration is expected to be affected by the presence of the entering and leaving groups, and if these groups are sufficiently close to the central carbon atom, there may actually be an increase in the bending frequency. Robertson and co-workers have calculated the frequencies for a transition state model which is a planar CH_3 group, and have found that the out-of-plane bending frequency would have to be increased to 2565 cm.$^{-1}$ to account for the observed isotope effect. (There appears to be a numerical error on page 232 of ref. 27: the value of ν_2^* should be 2229 cm.$^{-1}$). This estimate is probably high, because the model used for the transition state permits a *decrease* in other frequencies, and because the calculated frequency shift accounts for the sum of the observed effect and a larger estimated "thermodynamic" effect of opposite sign. It is possible that the bending frequency need increase only to about 1400–1900 cm.$^{-1}$ to account for the experimental facts.

There is independent evidence that the original estimate of the bending frequency increase is high. Carbon isotope effects have been determined in a related group of Sn2 reactions of methyl-C^{14} iodide by Bender and Hoeg,[28] who find normal carbon-14 isotope effects of 9–14%. Effects of this magnitude can be predicted for a transition state model in which a C–I stretching vibration has been lost. The contribution to be expected from the increase in bending force constant postulated by Robertson, *et al.*, would be, for carbon-14, about 4% in the inverse direction, which would then make it difficult to account for the magnitude of the observed C^{14} effect. For this reason, it seems very possible that in the methyl-d_3 ester solvolysis reactions the out-of-plane bending mode is influenced by the surrounding groups, but not to the extent originally suggested. Simultaneously, part of the effect may be caused by an increase in the C–H stretching frequencies.

In the pyrolysis of dimethylmercury it is necessary to assume an effect which will prevent the bending frequencies from decreasing appreciably in the transition state, while permitting the change toward sp^2 hybridization to produce an increase in the stretching frequencies. This may simply be caused by the proximity of the departing methyl group to the rest of the molecule in the transition state, or may be somehow related to the size and number of electrons of the mercury atom, which would be expected to lead to large non-bonded interactions.

Frequencies for $(CH_3)_2Hg$, $(CD_3)_2Hg$, and transition state models have been calculated from the F and G matrices given by Gutowsky.[6] The transition state was assumed to differ from the normal molecule in the following way: (1) the C–H bond was 0.02 Å. shorter; (2) the C–H stretching force constants were increased by 0.37×10^5 dynes/cm.; (3) either the symmetric or antisymmetric methyl–mercury stretching frequency was made to become zero by setting the appropriate stretching force constant equal to zero. The methyl–mercury stretch of opposite symmetry was assumed to remain constant.

The results of these calculations for the normal molecules and the transition state with the symmetric stretch set equal to zero are shown in Table IV. Since the reaction coördinate corresponds to a symmetric stretching motion, this is equivalent to the assumption of simultaneous bond rupture. The deuterium compound is symmetrically labeled, so that the relation between the observed rate ratio and the ratio of rate constants for bond rupture is identical for either simultaneous or stepwise bond breaking (unlike the case of the C^{13} effect). For stepwise bond rupture, the pattern of frequency shifts will be comparable to those of Table IV, but it is reasonable to assume that the C–H stretching frequencies of only one methyl group will be affected.

TABLE IV

CALCULATED VIBRATIONAL FREQUENCIES (IN CM.$^{-1}$) OF NORMAL MOLECULES AND TRANSITION STATES[a]

Vibration	DMM	DMM-d_6	T.S.	T.S.-d_6
$\nu_1(a_1')$	2959.7	2178.8	3070.2	2256.4
$\nu_2(a_1')$	1181.4	949.4	1149.5	878.9
$\nu_3(a_1')$	511.8	444.2	0	0
$\nu_4(a_1'')$		Free rotation		
$\nu_5(a_2'')$	2959.8	2179.1	3071.7	2260.9
$\nu_6(a_2'')$	1204.9	969.0	1205.0	969.3
$\nu_7(a_2'')$	549.1	482.3	549.1	482.4
$\nu_8(e')$	2921.2	2171.9	3037.4	2257.9
$\nu_9(e')$	1475.5	1081.0	1475.5	1081.2
$\nu_{10}(e')$	787.2	578.2	786.5	577.4
$\nu_{11}(e')$	156.2	143.6	156.3	143.9
$\nu_{12}(e'')$	2920.5	2170.1	3036.8	2256.2
$\nu_{13}(e'')$	1443.4	1057.7	1443.5	1057.8
$\nu_{14}(e'')$	701.3	512.4	700.8	511.8

[a] Vibrations with e′ and e″ symmetry are doubly degenerate.

It is evident that only the C–H stretching frequencies and the A_1' frequencies are influential, so that the ratio of rate constants is given by[29]

$$\frac{k_D}{k_H} = \frac{\nu_{3D}^*}{\nu_{3H}^*} \prod_{i=1}^{8} \frac{\nu_{iH}\,(1 - e^{-u_{iD}})}{\nu_{iD}\,(1 - e^{-u_{iH}})} \exp\,[(u_{iD} - u_{iH})/2]$$

$$\prod_{j=1}^{7} \frac{\nu_{jD}^*\,(1 - e^{-u_{jH}^*})}{\nu_{jH}^*\,(1 - e^{-u_{jD}^*})} \exp\,[(u_{jH}^* - u_{jD}^*)/2] \quad (3)$$

where the sum over the i's includes the A_1' frequencies and the C–H stretching frequencies of the other symmetry classes, and the sum over the j's includes these same frequencies except for ν_3 (the reaction coördinate). The frequency ratios for the stretching frequencies very nearly cancel out (these vibrations are quite independent of all others), and the

(27) J. A. Llewellyn, R. E. Robertson, and J. M. W. Scott, *Can. J. Chem.*, **38**, 222 (1960)

(28) M. L. Bender and D. F. Hoeg, *J. Am. Chem. Soc.*, **79**, 5649 (1957).

(29) *Cf.*, for example, ref. 22, eq. (II.25).

ratios belonging to class A_1' can be shown to cancel according to the Teller–Redlich product rule. The total contribution from the $1 - e^{-u}$ terms is 0.934, most of which comes from the reaction coördinate. The difference in zero-point energies is larger in the transition state by 77 cm.$^{-1}$, so that at 639°K. the total effect is 1.11 for the ratio k_D/k_H. Hence this model for the transition state gives a predicted isotope effect slightly greater than that observed; this could be adjusted to give better agreement by slight changes in the bending and stretching frequencies.

Carbon-13 Isotope Effect.—The kinetics of the carbon isotope effect are slightly more complicated than those of the deuterium effect because the molecule is not labeled symmetrically. In the case of simultaneous bond rupture, the observed effect is related to the reactions

$$H_3C^{12}HgC^{12}H_3 \longrightarrow Hg + 2C^{12}H_3 \quad k_{1A}$$

$$H_3C^{12}HgC^{13}H_3 \longrightarrow Hg + C^{12}H_3 + C^{13}H_3 \quad k_{1B}$$

$$H_3C^{13}HgC^{13}H_3 \longrightarrow Hg + 2C^{13}H_3 \quad k_{1D}$$

by the expression $k_{12}/k_{13} = k_{1A}/(k_{1B} + k_{1D}) = k_{1A}/k_{1B}$ at the tracer level.[4]

The simplest approach to a theoretical estimate of the rate constant ratio is by use of the equation[30]

$$k_{12}/k_{13} = \sigma_{12}\sigma_{13}^*/\sigma_{12}^*\sigma_{13})(\nu_{12}^*{}_{,L}/\nu_{13}^*{}_{,L}) \left[1 + \sum_{i=1}^{3n-6} G(u_i)\Delta u_i - \sum_{j=1}^{3n-7} G(u_j^*)\Delta u_j^*\right] \quad (4)$$

in which the σ's are symmetry numbers, ν_L^* is the frequency along the reaction coördinate, and the last term has its usual significance. The symmetry number term is only a statistical correction which makes no contribution to the observed ratio. The value of the second term depends on the reaction coördinate, but is not particularly sensitive to its choice. The upper limit is given by the three-mass form of the Slater equation,[31] which is essentially the equation for the symmetric stretching frequency of a linear C–Hg–C system. A more probable reaction coördinate is a symmetrical one in which the methyl groups move as rigid units, corresponding to the "molecular fragment" coördinate.[32] This is very nearly the vibrational mode ν_3 of the normal molecule. The frequency ratio may be estimated by taking the square root of that obtained for the doubly-substituted molecule obtained with the F and G matrices of Gutowsky. The results of these three approaches are

Slater coördinate	1.020
Molecular fragment	1.016
Normal mode ν_3	1.015

The evaluation of the temperature-dependent term requires a more detailed model, and the most consistent approach is to use the same model as that used for the estimate of the deuterium isotope effect. As in the case of the deuterium calculations, only the A_1' vibrations and the C–H stretching vibrations need be considered. The isotopic shifts in these frequencies for a doubly-labeled molecule are given in Table V, and the shifts for a singly-labeled molecule are assumed to be one-half as large. It will be seen that the C–H stretching frequencies make no contribution because of their low sensitivity to the carbon mass. Both ν_2 and ν_3 contribute slightly and the total effect in the temperature-dependent term is 1.0025, which when combined with the temperature-independent term gives a calculated ratio of 1.018 to 1.022 for k_{12}/k_{13}.

TABLE V

FREQUENCY SHIFTS (IN CM.$^{-1}$) FOR $(C^{13}H_3)_2Hg$ RELATIVE TO $(C^{12}H_3)_2Hg$

	Normal molecule		Transition state	
Vibration	$\nu(C^{12})$	$\Delta\nu$	$\nu(C^{12})$	$\Delta\nu$
$\nu_1(a_1')$	2959.7	9.2	3070.2	9.4
$\nu_2(a_1')$	1181.4	12.0	1149.5	7.7
$\nu_3(a_1')$	511.8	14.5	0	0
$\nu_5(a_2'')$	2959.8	9.3	3071.7	9.5
$\nu_8(e')$	2921.2	11.7	3037.4	12.1
$\nu_{12}(e'')$	2920.5	11.5	3036.8	12.1

In the case of stepwise bond rupture, the rate-determining steps are[4]

$$H_3C^{12}HgC^{12}H_3 \longrightarrow HgC^{12}H_3 + C^{12}H_3 \quad k_{1A}$$

$$H_3C^{12}HgC^{13}H_3 \longrightarrow HgC^{12}H_3 + C^{13}H_3 \quad k_{1B}$$

$$H_3C^{12}HgC^{13}H_3 \longrightarrow HgC^{13}H_3 + C^{12}H_3 \quad k_{1C}$$

$$H_3C^{13}HgC^{13}H_3 \longrightarrow HgC^{13}H_3 + C^{13}H_3 \quad k_{1D}$$

At the tracer level, $k_{12}/k_{13} = k_{1A}/(k_{1B} + k_{1C}) = (k_{1A}/k_{1B})/[1 + (k_{1C}/k_{1B})]$, so that the observed isotope effect is a combination of an intramolecular effect (k_{1C}/k_{1B}) and an intermolecular effect (k_{1A}/k_{1B}). Each rate constant ratio is given by an expression analogous to eq. 4. In the expression for k_{1A}/k_{1B} a factor of two is introduced by the symmetry number term: this is just a statistical factor which makes the isotope effect disappear in the classical limit. The ratio of frequencies for the reaction coördinate may be estimated by the methods discussed previously with the following results

	1A/1B	1C/1B	12/13
Slater coördinate	2(1.038)	1.038	1.019
Molecular fragment	2(1.030)	1.030	1.015
Normal mode ν_7	2(1.012)	1.000	1.012

It becomes apparent that as far as the temperature-independent term is concerned, there is no significant difference between the two alternate bond-breaking processes.

In this case, one need only consider the C–H stretching vibrations and the vibrations of class A_2'', which shift in a pattern identical with that of the shifts of the A_1' vibrations in the simultaneous bond-rupture model. The intramolecular effect will reduce the over-all temperature-dependent contribution to one-half the value for the simultaneous bond-breaking model, so that the

(30) Reference 22, eq. (II.21).

(31) J. Bigeleisen and M. Wolfsberg, *J. Chem. Phys.*, **21**, 1972 (1953); **22**, 1264 (1954).

(32) M. Wolfsberg, *ibid.*, **33**, 21 (1960).

total effect will be a ratio of 1.013 to 1.020 for k_{12}/k_{13}. Unfortunately, the carbon isotope effect does not help one decide whether the carbon–mercury bonds are broken simultaneously or not.

DEUTERIUM ISOTOPE EFFECTS IN THE PHOTOCHEMICAL EVOLUTION OF HYDROGEN FROM AQUEOUS FERROUS SOLUTIONS

BY JOSHUA JORTNER AND GABRIEL STEIN

Department of Physical Chemistry, Hebrew University, Jerusalem, Israel

Received May 2, 1962

The dependence of the isotope separation factor in the photochemical evolution of hydrogen from aqueous solutions of ferrous sulfate on the concentration of H^+, ferrous, and ferric ions and on the concentration of an organic scavenger (methanol) was investigated. The results are interpreted in terms of a consecutive mechanism involving isotope separation in each of two steps. The respective separation factors in the first step (leading to H atom formation) and in the second (involving oxidation of Fe^{2+} by H) are derived. Isotope effects in radiation and photochemistry are compared. The isotope separation factors obtained support the intermediate hydride formation mechanism for the oxidation of Fe^{2+} by H atoms.

Introduction

The first investigation of the separation of hydrogen isotopes in the photochemical liberation of hydrogen from aqueous ionic solutions was carried out by Farkas and Farkas.[1] The purpose of their work was the investigation of the isotope separation in a homogeneous system. In the irradiation of 0.05 *M* ferrous sulfate solutions in 0.05 *N* H_2SO_4, isotope separation factors of 3.8–4.8 were obtained depending on the deuterium content of the solutions.[1]

The use of hydrogen isotope effects in photochemistry and radiation chemistry[2] permits the study of primary photochemical radical formation processes by the technique of competitive reactions. In previous work[3,4] on the photochemistry of the ferrous ion in aqueous solution, the mechanism of H atom formation and the oxidation mechanism by atomic hydrogen were investigated. In the present work we attempt to apply the isotope separation technique to obtain further information on the dissociation of the photoexcited ferrous ion in aqueous solution and the reactivity of H atoms.

Experimental

Procedure.—Irradiations were carried out in fused silica vessels using 10 cc. of solution, and a low pressure Hg lamp operated at 1000 v. and 100 ma. was employed as a light source. The light was filtered by 0.5 cm. of 0.1 *M* NaCl solution, eliminating wave lengths below 2000 Å. Approximately 95% of the incident light was at 2537 Å. Irradiations were carried out at 20 ± 1°. The light intensity as determined by the uranyl oxalate actinometer was about 2×10^{-3} einstein $l.^{-1}$ $min.^{-1}$. Evacuation of the solutions was carried out as previously described.[3] After irradiation the gas was transferred by a Toepler pump for isotope analysis.

Materials and Solutions.—Deuterium oxide was purified by triple distillation from alkaline permanganate and $KHSO_4$. Triple-distilled water and A.R. grade sulfuric acid and ferrous ammonium sulfate were used.

Isotope Analysis.—The deuterium content of the liberated gas was determined by using the mass spectrograph built in this Department. The instrument was calibrated using hydrogen–deuterium mixtures prepared by decomposition of standard solutions on Zn at 400°. The analysis was performed on mixtures of relatively low deuterium content so that H_2 and HD only need be considered. The isotopic composition was determined by the mass ratio 2:3 (H_2:HD). Calibration and analysis were carried out at the same gas pressure, which was in the region 10^{-5}–2×10^{-5} mm. The experimental results were reproducible within ±5%.

Results

Ferrous Sulfate–H_2SO_4 Solutions.—The experiments were carried out in solutions of relatively low deuterium content $(D/H)_l \sim 0.2$. We measured the isotope separation factor defined by

$$S = (D/H)_l \times (H/D)_g \qquad (I)$$

where l and g refer to the liquid and the gas, and D and H are in moles.

The dependence of the isotope separation factor on the irradiation time t (at constant light intensity) and sulfuric acid concentration was investigated. The results are presented in Table I.

TABLE I

ISOTOPE SEPARATION IN THE PHOTOCHEMISTRY OF THE FERROUS ION

$[H_2SO_4]$, *N*	$[Fe^{2+}]_0$, mole $l.^{-1}$	t, min.	$10^3[Fe^{3+}]$, mole $l.^{-1}$	S
0.78	0.10	20		4.0
.78	.10	33		4.0
.78	.20	36		3.9
.70	.10	60	4.0	4.2
.031	.10	47		4.0
.0074	.10	60		4.1
.0065	.10	130	1.10	4.0
.0032	.10	140	1.10	3.8
.0009	.10	150	0.35	3.7

These results indicate that within the experimental error the isotope separation factor is independent of the concentration of the ferric ion during irradiation. These results also indicate that the isotope separation factor is independent of the acid concentration in the region 0.8–0.01 *N*. In this region the rate of primary radical formation is pH dependent.[4]

Isotope Separation in KF Solutions.—At low acid concentration (pH > 2) the accuracy of the isotopic analysis was reduced because of the low

(1) A. Farkas and L. Farkas, *Trans. Faraday Soc.*, **34**, 1120 (1938).

(2) J. Jortner and G. Stein, *Intern. J. Appl. Radiation Isotopes*, **7**, 198 (1960).

(3) J. Jortner and G. Stein, *J. Phys. Chem.*, **66**, 1258 (1962).

(4) J. Jortner and G. Stein, *ibid.*, **66**, 1264 (1962).

gas yields obtained under irradiation. Therefore additional experiments were carried out in 0.1 *M* KF solutions. The increase of the photochemical yield in the presence of the fluoride ion is due to two factors.

(a) There is a reduction of the inner filter effect[3] of the ferric ion. The molar extinction coefficient of the ferric ion in 0.8 *N* H_2SO_4 at 2536 Å. is reduced from $\epsilon = 2800$ to 600 l. mole^{-1} cm.$^{-1}$ by the addition of 0.1 *M* KF. The molar absorption coefficient of the ferrous ion is unaffected.

(b) The ferric–fluoride ion pair is stable to reduction by H atoms,[5] compared to the reactivity of $Fe^{3+}OH^-$ ion pairs present in sulfuric acid solution at high pH.[4,5]

The experimental results presented in Table II indicate that the pH effect on the separation factor is rather small. A slight decrease is observed at high pH, within the range of experimental error.

TABLE II

ISOTOPE SEPARATION IN H_2SO_4 SOLUTIONS CONTAINING 0.1 *M* KF; $[Fe^{2+}]_0 = 0.1$ *M*

$[H_2SO_4]$, *N*	pH[a]	*S*
0.78		4.2
.78		3.9
.09	2.8	3.9
.044	3.8	3.7

[a] The pH was measured in identical solutions prepared from ordinary water.

The Effect of Methanol on Isotope Separation.— In an attempt to determine the isotope separation factor in the primary radical formation process, a series of experiments was carried out in solutions containing ferrous sulfate, methanol, and 0.8 *N* sulfuric acid. In this system the atomic hydrogen formed oxidizes ferrous ion[3,4]

$$Fe^{2+} + H + H^+ \longrightarrow Fe^{3+} + H_2 \quad (1)$$

or the organic solute[6,7]

$$CH_3OH + H \longrightarrow CH_2OH + H_2 \quad (2)$$

as in the radiation chemical investigation of this system.[6,7] The radical CH_2OH thus formed may react by dimerization and disproportionation

$$2CH_2OH \longrightarrow CH_2O + CH_3OH \quad (3)$$

$$2CH_2OH \longrightarrow (CH_2OH)_2 \quad (4)$$

In the presence of the ferric ion CH_2OH will act as a reducing agent

$$CH_2OH + Fe^{3+} \longrightarrow Fe^{2+} + CH_2O + H^+ \quad (5)$$

At high $[CH_3OH]/[Fe^{2+}]$ ratio the hydrogen atoms formed will react preferably in reaction 2 and the ferric ion formed will be reduced again according to reaction 5. Table III presents the experimental results.

The formation of formaldehyde was confirmed by determination with chromotropic acid. The decrease of the yield of Fe^{3+} with increasing ratio $[CH_3OH]/[Fe^{2+}]$ is due to the competition between reactions 1 and 2. Under conditions of high $[CH_3OH]/[Fe^{2+}]$ ratio ($\sim$50) the limiting value of 6.2 ± 0.3 was obtained for the isotope separation factor. Under these conditions the yield of Fe^{3+} is only 1% of the yield obtained in the absence of methanol. Hence H atoms react almost entirely by reaction 2, and the oxidation reaction (1) may be neglected. The very low value of Fe^{3+} obtained implies that the value of *S* is a limiting one in view of the nearly total scavenging of H atoms by methanol.

TABLE III

ISOTOPE SEPARATION IN THE PHOTOCHEMISTRY OF Fe^{2+} ION IN THE PRESENCE OF METHANOL

$[H_2SO_4] = 0.78$ *N*

$[Fe^{2+}]_0$, mole l.$^{-1}$	$[CH_4OH]_0$, mole l.$^{-1}$	*t*, min.	$10^3[Fe^{3+}]_t$, mole l.$^{-1}$	$\left(\frac{D}{H}\right)_l$	$\left(\frac{D}{H}\right)_g$	*S*
0.10	0	33	4.0	0.220	0.052	4.2
.10	0.26	52	1.05	.254	.055	4.6
.10	0.55	50	0.75	.240	.050	5.0
.20	1.18	51	.85	.240	.047	5.1
.10	1.25	47	.40	.241	.047	5.2
.05	1.22	49	.11	.241	.045	5.5
.025	1.20	47	.04	.235	.038	6.2

Discussion

The contributions of the following steps to the isotope separation have to be considered: (a) primary radical formation; (b) interaction of H and D atoms with the solvent; (c) oxidation of ferrous ion by H and D atoms; and (d) reduction of the ferric ion by H and D atoms.

The secondary process b probably does not contribute to the isotope separation in our case. The exchange reactions with water and H^+ ions are relatively slow. Farkas and Farkas,[1] using kinetic data from gaseous phase experiments, claimed that for the exchange reaction of deuterium atom and water the activation energy is of the order of 16 kcal./mole. Friedman and Zeltman[8] found for this reaction in aqueous solution at pH 2 a rate constant of 2 sec.$^{-1}$.

Radiation chemical[9] and photochemical[4] evidence indicates that the reduction of Fe^{3+} by H atoms is negligible at low pH, the rate of reduction increasing with increasing pH. No isotope effect was observed in this reaction.[6] Thus reaction d does not contribute to the isotope separations. This conclusion is consistent with the independence of the isotope separation factor of the irradiation time and of the extent of photochemical oxidation. The separation factors presented in Tables I and II include (a) the contribution of the primary H and D atom formation, and (c) a subsequent contribution rising from the oxidation reaction of the ferrous ion by H and D atoms. The experimental results in the presence of methanol allow the separate determination of the two factors.

The rate of introduction into the bulk of the H

(5) T. Rigg, G. Stein, and J. Weiss, *Proc. Roy. Soc.* (London), **A211**, 375 (1952).

(6) J. H. Baxendale and G. Hughes, *Z. physik. Chem.* (Frankfurt), **14**, 306 (1958).

(7) J. H. Baxendale and G. Hughes, *ibid.*, **14**, 323 (1958).

(8) H. L. Friedman and A. H. Zeltman, *J. Chem. Phys.*, **28**, 878 (1958).

(9) A. O. Allen and W. G. Rothschild, *Radiation Res.*, **7**, 591 (1957).

and D atoms, produced from the excited state of the ion, will be represented schematically by the reactions

$$Fe^{2+}{}_{aq}^{*} \begin{cases} \xrightarrow{k_{pD}} D + Fe^{3+} \\ \xrightarrow{k_{pH}} H + Fe^{3+} \end{cases} \quad (p)$$

k_{pH} and k_{pD} represent the rate constants for radical production at constant light intensity. These quantities consist of the quantum yields for atom production (as defined in ref. 3 and 4) multiplied by the light intensity absorbed by the ferrous ion. These constants include a contribution for the preferential solvation of the light absorbing ferrous ion, and of the H^+ ion which acts as a scavenger[4] transferring radicals into the bulk.

The exchange of the atoms thus produced with the solvent is neglected, and only scavenging reactions have to be considered. The oxidation of the ferrous ion will be presented in the form

$$\begin{aligned} H + Fe^{2+} &\begin{cases} \xrightarrow{k_{OXH}} H_2 + Fe^{3+} \\ \xrightarrow{k_{OXD}} HD + Fe^{3+} \end{cases} \\ D + Fe^{2+} &\begin{cases} \xrightarrow{k_{OXH}} HD + Fe^{3+} \\ \xrightarrow{k_{OXD}} D_2 + Fe^{3+} \end{cases} \end{aligned} \quad (1')$$

Assuming that these rate constants are independent of the nature of the attacking atom, k_{OXH} and k_{OXD} represent the rate constants for the oxidation of the ferrous ion depending on whether H or D is detached.

The atoms produced from the excited state of the ion may alternatively react with methanol

$$H + CH_3OH \longrightarrow H_2 + CH_2OH \quad (2')$$
$$D + CH_3OH \longrightarrow HD + CH_2OH$$

As reaction 2′ leads in both cases to a rupture of a C–H bond, the isotope effect in this reaction is negligible.

At high scavenger concentration and at low pH, second-order recombination of H and D atoms may be neglected. From this reaction scheme

$$\frac{d[H_2]}{dt} = k_2[CH_3OH][H] + k_{OXH}(1 - W)[H][Fe^{2+}]$$

$$\frac{d[HD]}{dt} = k_2[CH_3OH][D] + k_{OXD}W[H][Fe^{2+}] + k_{OXH}(1 - W)[D][Fe^{2+}] \quad (II)$$

$$\frac{d[D_2]}{dt} = k_{OXD}W[D][Fe^{2+}]$$

where

$$W = \left(\frac{D}{H + D}\right)_i$$

The steady state concentrations of the H and D radicals are presented by

$$[H] = \frac{(1 - W)k_{pH}}{k_2[CH_3OH] + \{k_{OXH}(1 - W) + k_{OXD}W\}[Fe^{2+}]} \quad (III)$$

$$[D] = \frac{Wk_{pD}}{k_2[CH_3OH] + \{k_{OXH}(1 - W) + k_{OXD}W\}[Fe^{2+}]}$$

The experimentally determined quantity is

$$\left(\frac{H}{D}\right)_g = \frac{2[H_2] + [HD]}{2[D_2] + [HD]} \quad (IV)$$

which at low deuterium content of the solution is reduced to

$$\left(\frac{H}{D}\right)_g = 1 + \frac{2[H_2]}{[HD]} \quad (IV')$$

In the integration of eq. II the contribution of the inner filter effect[3] should be taken into account. However, as the right hand side of eq. IV′ is only dependent on the ratio of amounts of the hydrogen isotopes produced, the contribution of the inner filter effect cancels out.

Using eq. II, III, and IV′, we obtain

$$\left(\frac{H}{D}\right)_g = 1 + \frac{\dfrac{k_2[CH_3OH]}{k_{OXH}[Fe^{2+}]} + (1 - W)}{\dfrac{k_2[CH_3OH]}{2k_{OXH}[Fe^{2+}]}\dfrac{k_{pD}}{k_{pH}}\dfrac{W}{1 - W} + \dfrac{W}{2}\left(\dfrac{k_{OXD}}{k_{OXH}} + \dfrac{k_{pD}}{k_{pH}}\right)} \quad (V)$$

Applying this equation to some limiting cases, the isotope separation factors in the primary radical production process, and in the oxidation reaction, can be obtained. Under limiting conditions when most of the radicals produced react with the organic scavenger, the separation factor observed is solely determined by the isotope separation in the primary process. This condition will be fulfilled when $[CH_3OH]/[Fe^{2+}] >> 1$. Then we get

$$\left(\frac{H}{D}\right)_g = 1 + \left(2\frac{k_{pH}}{k_{pD}} \times \frac{1 - W}{W}\right) \quad (VI)$$

Defining the separation factor S_p in the primary process for the introduction of H and D atoms into the bulk by

$$S_p = \frac{k_{pH}}{k_{pD}} \quad (VII)$$

and using the definition of W we readily get

$$S_p = \frac{\{(H/D)_g - 1\}}{2} \times \left(\frac{D}{H}\right)_i \quad (VIII)$$

Application of the experimental results obtained under these limiting conditions (Table III) leads to the value $S_p = 2.9 \pm 0.3$.

The isotope separation factor for the oxidation of ferrous ion by H and D atoms will be defined by

$$S_{OX} = \frac{k_{OXH}}{k_{OXD}} \qquad (IX)$$

This value can be obtained from the experimental results obtained for ferrous ion–H_2SO_4 solutions in the absence of methanol when sufficient Fe^{2+} is present for total scavenging of the atoms. Setting $[CH_3OH] = 0$, the following expression is obtained for consecutive isotope separation at relatively low deuterium content

$$\left(\frac{H}{D}\right)_g = 1 + \frac{2(1-W)}{W}\frac{1}{\frac{k_{OXD}}{k_{OXH}} + \frac{k_{pD}}{k_{pH}}} = 1 + \frac{2(1-W)}{W}\frac{1}{\frac{1}{S_{OX}} + \frac{1}{S_p}} \qquad (X)$$

Using the experimental results in the absence of methanol and the value of S_p previously obtained from eq. X we get $S_{OX} = 5 \pm 0.5$.

The separation factors presented in Table III depend on the concentration ratio $[CH_3OH]/[Fe^{2+}]$. The gradual increase of the isotope separation factors with the increase of this ratio results from the competition between the scavenging reactions 1 and 2. The dependence of the isotope separation factors on the concentration ratio $[CH_3OH]/[Fe^{2+}]$ could be interpreted adequately by eq. V using the values of S_p and S_{OX} previously obtained and setting $k_2/k_{OXH} = 0.15$. The comparison between the calculated data and the experimental results is presented in Fig. 1. The rate constants ratio which was found to yield best agreement with the experimental results is in good agreement with the value of 0.17 obtained in ordinary water at pH 1[6,7] in acid solutions irradiated with ionizing radiations.

In our previous work[3,4] on the photochemistry of Fe^{2+} ions it was shown that the mechanism of radical introduction into the bulk involves two distinct mechanisms: (a) a pH dependent process involving essentially electron scavenging by the H^+_{aq} ion, and (b) a residual pH independent yield involving dissociative electron capture by a solvent molecule in the solvation layer of the excited ion. The H (or D) atom thus formed diffuses into the bulk.

At pH 0.4, the contributions of these two reaction paths to the total quantum yield are about equal.[3,4] In both these reactions roughly the same intramolecular isotope effect is expected.[2]

The primary photochemical isotope separation factor S_p obtained in the present work is identical within the experimental range of error with the separation factor in the primary production of H and D atoms in the radiolysis of aqueous solutions, $S_A = 2.7 \pm 0.1$ obtained at low D content.[10,11]

(10) F. Fiquet Fayard, *J. chim. phys.*, **57**, 467 (1960).
(11) C. Lifshitz, Ph.D. Thesis, Jerusalem, 1961.

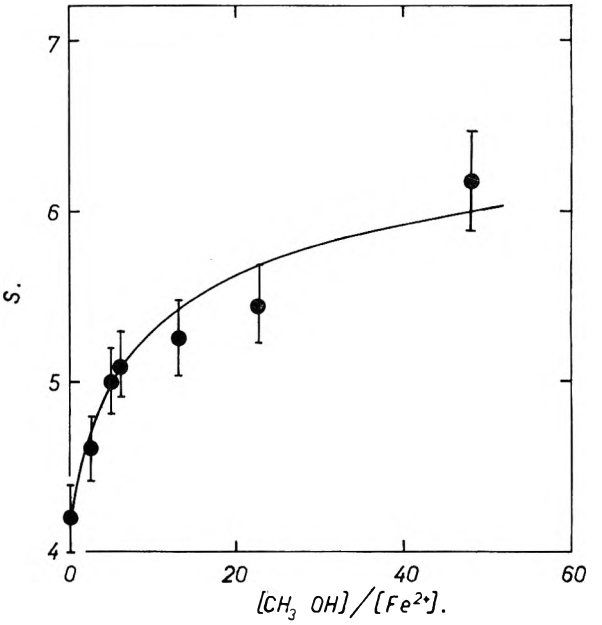

Fig. 1.—The dependence of the isotope separation factor in the presence of methanol on the concentration ratio $[CH_3OH]/[Fe^{2+}]$. $[H_2SO_4] = 0.8\ N$; $(D/H)_l = 0.22$ to 0.25. Solid curve calculated from eq. V with $k_{H+CH_3OH}/k_{H+Fe^{2+}} = 0.15$.

S_p is equal to the separation factor in the radiation chemistry of aqueous solutions[12,13] where H atoms are formed by the interaction of e_{aq} with H^+_{aq}.

For the oxidation of Fe^{2+} ion by H atoms, the separation factor $S_{OX} = 5 \pm 0.5$ at low deuterium content is obtained. Baxendale and Hughes[7] derived a rate constants ratio of 2.4 between the rate constants for the oxidation of the ferrous ion in H_2O and D_2O. They considered this result as evidence against the oxidation mechanism involving the intermediate formation of the H_2^+ molecule ion. The conclusions are not unambiguous,[2] as an isotopic effect may be observed when the rates of an electron transfer reaction are compared in H_2O and D_2O. However, the marked isotope effect observed in the present work at low D content definitely rules out the oxidation mechanism involving H_2^+, since in the present case electron transfer in a medium of constant composition does occur. From the value[10] of

$$S_{H^+} = \frac{(H/D)_{H_3O^+}}{(H/D)_{H_2O}} = 1.66$$

at low deuterium content, the isotope separation factor for the oxidation reaction can be derived, corrected for the preferential solvation of the hydroxonium ion. Denoting this corrected separation factor by S'_{OX} we set $S'_{OX} = S_{OX}/S_{H^+}$. Using the experimental value $S_{OX} = 5 \pm 0.5$ we get $S'_{OX} = 3$, in fair agreement with the results of Baxendale and Hughes. Investigations of the oxidation of Fe^{2+} by H atoms externally generated[14] or produced photochemically[3,4] showed that this oxidation mechanism may involve the formation of a hydride intermediate[14]

(12) J. T. Allan and G. Scholes, *Nature*, **187**, 218 (1960).
(13) G. Czapski and A. O. Allen, *J. Phys. Chem.*, **66**, 262 (1962).
(14) G. Czapski, J. Jortner, and G. Stein, *ibid.*, **65**, 956, 960 (1961).

$$Fe^{2+}_{aq} + H \rightleftharpoons FeH^{2+}_{aq} \quad (6)$$

$$FeH^{2+}_{aq} + H^{+}_{aq} \longrightarrow Fe^{3+}_{aq} + H_2 \quad (7)$$

The isotope effect in the oxidation reactions is consistent with this reaction mechanism, as reaction 7 involves the rupture of an O–H bond in the hydroxonium ion.

Acknowledgment.—We thank Miss T. Feldman for valuable assistance. This work was sponsored by the Israel Atomic Energy Commission.

COULOSTATIC METHOD FOR THE KINETIC STUDY OF FAST ELECTRODE PROCESSES. I. THEORY

BY PAUL DELAHAY

Coates Chemical Laboratory, Louisiana State University, Baton Rouge, Louisiana

Received May 8, 1962

A new method (*charge-step* or *coulostatic*) for the kinetic study of fast electrode processes is discussed. The method involves: (a) charging of the electrode with a known quantity of electricity by means of a *coulostat* to cause a departure from the equilibrium potential, and (b) recording of the overvoltage–time curve during the subsequent discharge of the double layer capacity c_d by the electrode reaction. Overvoltage–time curves are derived for the following cases: constant c_d and linearized current–overvoltage (I–η) characteristic without mass transfer control or with mass transfer controlled by semi-infinite linear diffusion; constant c_d and quadratic and cubic approximations of the I–η characteristic in the absence of mass transfer control; and variable double layer capacity. Conditions for pure control by either diffusion or the charge transfer reaction are derived, and it is shown that conditions can be selected for which diffusion need not be considered when the apparent standard rate constant does not exceed 0.2–0.3 cm. sec.$^{-1}$. The method has about the same potentialities as the potentiostatic and single-pulse galvanostatic methods but has the advantage of somewhat greater simplicity of technique and interpretation of results. The coulostatic method also allows the determination of the differential capacity of the double layer even when a fast charge transfer reaction occurs on the electrode.

A method, which is new to the writer's knowledge, recently was suggested in this Laboratory for the study of fast adsorption processes at a metal–electrolyte interface[1] and for electroanalytical determinations in the 10^{-5}–10^{-7} M concentration range.[2] The method also can be applied to the kinetic study of fast electrode processes. The theory for the latter application is reported here, and experimental results are given in part II.[3] The principle is as follows. The electrode being studied is initially at equilibrium. The charge density on the electrode is changed abruptly (perhaps in 0.1–1 μsec.) in such a way that the electrochemical cell is essentially at open circuit once charging is completed (part II[3]). The potential departs from the equilibrium value as a result of the change of charge density. The increment of charge supplied to the electrode is consumed progressively by the electrode reaction, and the potential drifts back to its initial equilibrium value (unless there is a permanent change of the electrode). The overvoltage–time variations depend on the charge increment, the double layer capacity, and the characteristics of the electrode process. Study of electrode kinetics from overvoltage–time curves therefore should be possible.

The expression "coulostatic method" was coined[1] for this method when it is applied to adsorption kinetics because the charge density on the electrode remains constant during recording of potential–time curves. Further, the instrument supplying a known charge might be called a "coulostat" by analogy with "potentiostat." The charge density varies in the study of electrode processes by this method since the double layer is discharged until the equilibrium potential is reached, and the expression "charge-step method" might be preferable for application to electrode kinetics. However, there hardly seems a need for two expressions.

The theory of the method will be developed for a simple charge transfer reaction, O + ne = R, for which O and R are soluble. Processes without diffusion control will be considered first, and the effect of diffusion will be analyzed afterward. It will be assumed, as usual, that a large excess of supporting electrolyte is present.

Control by the Charge Transfer Reaction

Overvoltage–Time Variations for the Linearized Current–Overvoltage Characteristic.—The increment of charge is

$$\Delta_q = q_m - q_i \quad (1)$$

where q_i is the charge density at the equilibrium potential for the electrode reaction O + ne = R and q_m is the charge density immediately after charging. It is assumed that the charging time is so short that leakage by the charge transfer reaction can be neglected during charging. The overvoltage η($\eta = E - E_e$, E_e equilibrium potential) at time t after charging is

$$\eta = (q - q_i)/c_d \quad (2)$$

where q is the charge density at time t and c_d is the differential capacity of the electrode. It is assumed that variations of E are so small ($|\eta| < 5$ mv. approximately) that c_d is constant. The case of a variable double layer capacity is considered below. The signs in eq. 2 are consistent with the definition, $\eta = E - E_e$, and the dependence of q on E, namely $\eta \gtrless 0$ for $q - q_i \gtrless 0$. The charge density q is

(1) P. Delahay and D. M. Mohilner, *J. Phys. Chem.*, **66**, 959 (1962); *J. Am. Chem. Soc.*, **84**, Nov. 20 (1962).

(2) P. Delahay, *Anal. Chim. Acta*, in press.

(3) P. Delahay and A. Aramata, *J. Phys. Chem.*, **66**, 2208 (1962).

$$q = q_m + \int_0^t I\,dt \qquad (3)$$

where I is the faradaic current density for discharge of the double layer and the integral is equal to the quantity of electricity used by the electrode reaction at time t. The integral is preceded with a plus sign, *i.e.*, $q \gtrless q_m$ for $I \gtrless 0$, in agreement with the convention of regarding a net cathodic current as positive and a net anodic current as negative. It follows from eq. 1 to 3 that

$$\eta = [(q_m - q_i)/c_d] + (1/c_d)\int_0^t I\,dt \qquad (4)$$

$$= \eta_{t=0} + (1/c_d)\int_0^t I\,dt$$

where

$$\eta_{t=0} = \Delta q/c_d \qquad (5)$$

is the overvoltage after charging at $t = 0$.

The derivation of the solution of eq. 4, in which c_d is supposed to be constant, requires the explicit form of I as a function of η. We consider first the linearized I–η characteristic in the absence of mass transfer[4]

$$I = I_a^0(nF/RT)\eta \qquad (6)$$

where I_a^0 is the apparent (*i.e.*, not corrected for the effect of the double layer) exchange current density, and F, R, and T are as usual. Note that $I \gtrless 0$ for $\eta \gtrless 0$ and that eq. 6 holds well for $|\eta| \leqslant 5$ mv., approximately. The combination of eq. 4 and 6 and the solution of the resulting equation yield the equation

$$\eta/\eta_{t=0} = \exp[-(I_a^0/c_d)(nF/RT)t] \qquad (7)$$

which is identical to the relationship for the voltage–time variations for discharge of a capacitor across a constant resistance. The overvoltage decays exponentially with time, and a plot of log $|\eta|$ against t is linear. I_a^0 is readily computed from the slope of this plot, and the transfer coefficient is deduced from the variations of I_a^0 with the concentrations of O and/or R (*cf.* ref. 4). The differential capacity c_d which is needed in the computation of I_a^0 is obtained from independent measurements or, more simply, from[5] eq. 5.

Equation 7, which was derived on the assumption of no mass transfer control, is useful because it is generally possible and advisable, even for rather fast reactions, to avoid correction for mass transfer (see below). Experimental results substantiating the validity of eq. 7 are given in part II.[3]

Overvoltage–Time Variations for the Quadratic and Cubic Approximations for the Current–Overvoltage Characteristic.—The η–t variations can be derived for any value of η exceeding a few mv., but then it may be necessary to take into account the variations of c_d with potential (see below). We shall assume c_d constant and use the quadratic or cubic approximation for the I–η characteristic. Thus

$$I = I_a^0\left\{\begin{matrix}-(nF/RT)\eta + (\alpha - 1/2)(nF/RT)^2\eta^2 \\ -(1/2)(\alpha^2 - \alpha + 1/3)(nF/RT)^3\eta^3\end{matrix}\right\} \qquad (8)$$

The quadratic or cubic approximation generally suffices for $|\eta| < 10$ to 20 mv. and $|\eta| < 20$ to 40 mv., respectively. The solution of eq. 4 for the quadratic approximation is

$$G(\eta,\alpha) - G(\eta_{t=0}, \alpha) = (I_a^0/c_d)t \qquad (9)$$

where

$$G(\eta,\alpha) = (RT/nF)\ln[(1/\eta) - (\alpha - 1/2)(nF/RT)] \qquad (10)$$

It follows from eq. 9 that a plot of $G(\eta,\alpha)$ against t is linear. The parameters c_d, I_a^0, and α can be determined from experimental η–t curves by plotting[6] $G(\eta,\alpha)$ for different values of α until a linear plot is obtained. The intercept of this plot at $t = 0$ yields $\eta_{t=0}$ and c_d (eq. 5), and I_a^0 then is readily computed. All three parameters c_d, I_a^0, and α thus can be obtained from a single η–t curve. Determination of I_a^0 for different concentrations of O and/or R allows further verification of the self-consistency of data.

The same procedure applies to the cubic approximation but $G(\eta,\alpha)$ is now[6]

$$G(\eta,\alpha) = -\frac{RT}{nF}\left\{\begin{matrix}\frac{1}{2}\ln\left[\frac{1}{\eta^2} - \frac{nF}{RT}\left(\alpha - \frac{1}{2}\right)\frac{1}{\eta} + \frac{1}{2}\left(\frac{nF}{RT}\right)^2\left(\alpha^2 - \alpha + \frac{1}{3}\right)\right]^{-1} \\ + \frac{\alpha - \frac{1}{2}}{\left(\alpha^2 - \alpha + \frac{5}{12}\right)^{1/2}}\tan^{-1}\frac{\frac{nF}{RT}\left(\alpha^2 - \alpha + \frac{1}{3}\right)\eta - \left(\alpha - \frac{1}{2}\right)}{\left(\alpha^2 - \alpha + \frac{5}{12}\right)^{1/2}}\end{matrix}\right\} \qquad (11)$$

where the quantity $\alpha^2 - \alpha + 5/12$ is always positive.

Overvoltage–Time Variations for a Double Layer Capacity Varying with Potential.—In this case we write

$$(c_i)_E(E - E_z) - (c_i)_{E_e}(E_e - E_z) = \Delta q + \int_0^t I\,dt \qquad (12)$$

where $(c_i)_E$ and $(c_i)_{E_e}$ are the integral capacities of the double layer at E and E_e, respectively, and E_z

(4) (a) For a detailed treatment see K. J. Vetter, "Elektrochemische Kinetik," Springer-Verlag, Berlin, 1961; (b) for a survey see P. Delahay in "Advances in Electrochemistry and Electrochemical Engineering," Vol. 1, P. Delahay, Editor, Interscience Division, John Wiley and Sons, Inc., New York, N. Y., 1961, pp. 233–318.

(5) Application of the coulostatic method to the determination of c_d when a fast electrode process occurs might be of interest in double layer studies. The conventional bridge method fails under these conditions because of the contribution of the capacitive component of the faradaic impedance to the electrode capacity.

(6) A table of the function G is available upon request.

is the potential at the point of zero charge. It follows from eq. 12 that

$$[(dc_i/dE)(E - E_z) + c_i]\,(dE/dt) = I \quad (13)$$

and

$$t = \int \frac{(dc_i/dE)(E - E_z) + c_i}{I}\,dE + \text{constant} \quad (14)$$

where I is expressed as a function of $\eta = E - E_e$ by[7] eq. 8 or the complete I–η characteristic. The integration constant is determined by noting that $E = E_{t=0}$ at $t = 0$, where $E_{t=0}$ is such that

$$(c_i)_{E_{t=0}}\,(E_{t=0} - E_z) - (c_i)_{E_e}(E_e - E_z) = \Delta q \quad (15)$$

Solution of eq. 14 is obtained most conveniently after introduction of c_i as a series expansion of E. A linear or quadratic approximation for $c_i(E)$ may suffice.

Control by Diffusion and the Charge Transfer Reaction

Current–Time and Overvoltage–Time Variations for Small Overvoltages.—Equation 4 will be solved for the linearized I–η characteristic and mass transfer controlled by semi-infinite linear diffusion. The current density in eq. 4 for overvoltages not exceeding a few mv. is

$$I = I_a^0\,[(C_O/C_O^0) - (C_R/C_R^0) - (nF/RT)\eta] \quad (16)$$

where the C and C^0 terms are the concentrations at the electrode surface and in the bulk of solution, respectively. No correction is made for the double layer structure in the evaluation of the C terms. (See, *e.g.*, ref. 4b for a discussion of this point.) The concentrations C_O and C_R are functions of time since steady state is not reached. It is assumed that $C_O = C_O^0$ and $C_R = C_R^0$ for $x \geq 0$ and $t = 0$. Further, $C_O \to C_O^0$ and $C_R \to C_R^0$ for $x \to \infty$ and ≥ 0. Equation 16 is one of the boundary conditions provided η is introduced from eq. 4 and I is expressed in terms of the flux of O at $x = 0$. Thus

$$nFD_O\left(\frac{\partial C_O}{\partial x}\right)_{x=0} = I_a^0\left\{\frac{C_O}{C_O^0} - \frac{C_R}{C_R^0} - \frac{nF}{RT}\frac{\Delta q}{c_d} - \frac{(nF)^2 D_O}{RT\,c_d}\int_0^t \left(\frac{\partial C_O}{\partial x}\right)_{x=0} dt\right\} \quad (17)$$

where D_0 is the diffusion coefficient of O. The second boundary condition expressed the conservation of flux, *i.e.*

$$D_O(\partial C_O/\partial x)_{x=0} + D_R(\partial C_R/\partial x)_{x=0} = 0 \quad (18)$$

The current density[8] I, as derived by Laplace transformation, is

$$I = -I_a^0\,\frac{nF}{RT}\,\frac{\Delta q}{c_d}\,\frac{1}{a-b}\left\{\begin{matrix} a\exp(a^2t)\,\mathrm{erfc}\,(at^{1/2}) \\ -b\exp(b^2t)\,\mathrm{erfc}\,(bt^{1/2})\end{matrix}\right\} \quad (19)$$

where

$$a = [P + (P^2 - 4NQ)^{1/2}]/2N \quad (20)$$

$$b = [P - (P^2 - 4NQ)^{1/2}]/2N \quad (21)$$

$$M = I_a^0(nF/RT)\,(\Delta q/c_d) \quad (22)$$

$$N = nFD_O$$

$$P = I_a^0\,[(1/C_O^0 D_O^{1/2}) + (1/C_R^0 D_R^{1/2})]D_O \quad (23)$$

$$Q = I_a^0[(nF)^2/RT]\,[D_O/c_d] \quad (24)$$

The function $y = \exp(\lambda^2)\,\mathrm{erfc}\,(\lambda)$ decreases continuously as λ increases. One has $y = 1$ for $\lambda = 0$ and $y \to 0$ for $\lambda \to \infty$. At $t = 0$ one has (*cf.* eq. 2)

$$I_{t=0} = -I_a^0(nF/RT)(\Delta q/c_d) = -I_a^0(nF/RT)\eta_{t=0} \quad (25)$$

as one would expect since transfer polarization has not set in at $t = 0$. One has $I \to 0$ for $t \to \infty$.

The overvoltage is derived by integration of eq. 4 for the value of I given by eq. 19. Thus

$$\eta = \eta_{t=0} - I_a^0\,\frac{nF}{RT}\,\frac{\Delta q}{c_d^2}\,\frac{1}{a-b}\left\{\begin{matrix}(1/b)\,[1 - \exp(b^2t)\mathrm{erfc}(bt)^{1/2})] \\ -(1/a)\,[1 - \exp(a^2t)\mathrm{erfc}(at^{1/2})]\end{matrix}\right\} \quad (26)$$

Since $a > b$ and consequently $\exp(b^2t)\ \mathrm{erfc}(bt^{1/2}) > \exp(a^2t)\mathrm{erfc}(at^{1/2})$, the quantity between braces in eq. 26 is always positive. Hence, $\eta \gtrless \eta_{t=0}$ for $\Delta q \lessgtr 0$, in agreement with the definition of ($\eta = E - E_e$) and the dependence of q on E. One verifies that eq. 26 yields $\eta = \eta_{t=0}$ at $t = 0$ and $\eta = 0$ for $t \to \infty$.

Condition for Pure Control by the Charge Transfer Reaction.—It follows from eq. 19, 20, and 21 that there is essentially no control by diffusion when $4NQ >> P^2$, *i.e.*, when

$$4\,\frac{nF}{RT}\,\frac{1}{c_d\,I_a^0} \gg \left[\frac{1}{nF}\left(\frac{1}{C_O^0\,D_O^{1/2}} + \frac{1}{C_R^0\,D_R^{1/2}}\right)\right]^2 \quad (27)$$

The parameters a and b are imaginary when condition 27 is fulfilled, and eq. 26 reduces to eq. 7, as one can readily ascertain.[9] Condition 27 can be expressed in terms of the apparent standard rate

(7) The capacity correction is hardly necessary when eq. 6 is applied because $|\eta| \lesssim 5$ mv. in that case.

(8) The concentrations are easily derived but are not needed here.

(9) Note that

$$\mathrm{erf}(i\lambda) = \frac{2i}{\pi^{1/2}}\int_0^\lambda \exp(z^2)dz$$

where $i = (-1)^{1/2}$.

constant k_a^0 for the charge transfer reaction which is related to I_a^0 by

$$I_a^0 = nFk_a^0 C_O^{1-\alpha} C_R^{\alpha} \qquad (28)$$

If one assumes, to simplify matters, that $C_O^0 = C_R^0 = C^0$ and $D_O = D_R = D$, one deduces from condition 27, after introduction of k_a^0 from eq. 28, the condition

$$k_a^0 \ll [(nF)^2/RT](D/c_d)C^0 \qquad (29)$$

In principle, it is possible to avoid the complications due to mass transfer by selection of a sufficiently high concentration C^0 to satisfy condition 27 (or 29). This is to be expected since the quantity of electricity Δq available for the charge transfer reaction for a given $\eta_{t=0}$ is fixed and the influence of mass transfer decreases when C^0 increases. Increase in C^0, however, causes η to decrease more rapidly with t (see eq. 7) because I_a^0 is proportional to $C_O^{1-\alpha}C_R^{\alpha}$ according to eq. 28. Because of experimental limitations, one can prescribe the condition, $t \geqslant 10^{-6}$ sec., which requires Δq to be supplied in a time interval[10] $\Delta t \leqslant 10^{-7}$ sec. Therefore, one has the additional condition (*cf.* eq. 7)

$$(RT/nF)(1/I_a^0)c_d > 10^{-6} \text{ sec.} \qquad (30)$$

Combination of conditions 29 and 30 leads for the usual orders of magnitude of c_d (20 μf. cm.$^{-2}$), D (10^{-5} cm.^{2} sec.$^{-1}$), and T (25°) to the condition

$$C^0 \gg 2 \times 10^{-6}\,(1/\eta^2) \qquad (31)$$

If one introduces in condition 30 the value $C^0 = 2 \times 10^{-5}\,(1/n^2)$, which satisfies condition 31, one concludes that *k_a^0 should not exceed 0.2 to 0.3 cm. sec.$^{-1}$ under optimum conditions for $t \leqslant 10^{-6}$ sec., if essentially pure charge transfer control is to prevail.* Equation 7 then can be applied, and the method is very simple. Condition 27, *if it is amply satisfied*, also should suffice when η exceeds a few mv., and eq. 9 can be applied. (Condition 27 was derived only for $|\eta| \leqslant 5$ mv.)

(10) Shorter times might be considered but experimental requirements are very stringent for an actual electrochemical cell.

Correction for mass transfer by means of eq. 26 would allow the study of somewhat faster processes than those corresponding to $k_a^0 < 0.2$ to 0.3 cm. sec.$^{-1}$, but such a correction appears cumbersome. The linearization of the error function by series expansion for arguments which are small in comparison with unity is of little value because it requires values of $at^{1/2}$ and $bt^{1/2}$ corresponding to rather low I_a^0 values for which mass transfer correction, at any rate, is not necessary.

Condition for Pure Control by Diffusion.—One concludes from eq. 19, 20, and 21 that there is pure diffusion control when $P^2 \gg 4NQ$, or

$$\left[\frac{1}{nF}\left(\frac{1}{C_O^0 D_O^{1/2}} + \frac{1}{C_R^0 D_R^{1/2}}\right)\right]^2 \gg \frac{4nF}{RT}\,\frac{1}{c_d I_a^0} \qquad (32)$$

If one sets $C_O^0 = C_R^0 = C^0$, $D_O = D_R = 10^{-5}$ cm. sec.$^{-1}$ and $T = 25°$, condition 32 becomes

$$k_a^0 \gg 2 \times 10^6 \eta^2 C^0 \qquad (33)$$

Conclusion

The coulostatic method has approximately the same potentialities as the potentiostatic and single pulse galvanostatic methods,[11] and it allows the determination of apparent standard rate constants up to 0.2 to 0.3 cm. sec.$^{-1}$. No mass transfer correction is necessary and, as will be shown in part II, technique and interpretation of data compare favorably with those for other relaxation methods for fast electrode processes (*cf.* ref. 4b for review). The method is, in fact, an interrupter technique[12] in which the duration of electrolysis before current interruption approaches zero.

NOTE ADDED IN PROOF.—For Barker's priority of the principle of this method, of which I became aware after preparation of this paper, see a recent letter to the Editor of *Analytical Chemistry*.[13]

Acknowledgment.—This investigation was supported by the Office of Naval Research.

(11) For a review *cf.* ref. 4b.

(12) A. Hickling, *Trans. Faraday Soc.*, **33**, 1540 (1937). See earlier references in this paper. The method has been highly perfected since Hickling's work.

(13) P. Delahay and W. H. Reinmuth, *Anal. Chem.*, in press.

COULOSTATIC METHOD FOR THE KINETIC STUDY OF FAST ELECTRODE PROCESSES. II. EXPERIMENTAL RESULTS

BY PAUL DELAHAY AND AKIKO ARAMATA[1]

Coates Chemical Laboratory, Louisiana State University, Baton Rouge, Louisiana

Received May 3, 1962

Methodology for the coulostatic study of electrode kinetics is discussed, and application is made to the discharge of Zn(II) on a Zn–amalgam hanging drop in 1 *M* KCl. Known quantities of electricity were supplied to the Zn–amalgam electrode by discharge of a small capacitor ($\approx$300 $\mu\mu$f.), initially charged at a known voltage ($\approx$10 v.), across the electrochemical cell. Overvoltage–time curves were recorded by means of a cathode-ray oscilloscope in the interval 0–40 μsec. after charging. The theory of part I was verified experimentally, and essentially pure control by the charge transfer reaction was achieved. The influence of the cell resistance is treated quantitatively. Kinetic parameters at 25 $\pm$ 1°: apparent standard rate constant, 0.004_1 cm. sec.$^{-1}$; transfer coefficient, α = 0.30.

The coulostatic method discussed in the preceding paper[2] is applied to the discharge of Zn(II) on Zn–amalgam, and some points of methodology are taken up.

Experimental

Solutions and Zn–Amalgam.—Solutions were prepared with analytical grade reagents and bidistilled water (over $KMnO_4$). Solutions were treated with purified activated charcoal according to Barker's technique[3] to decrease the concentration level of traces of adsorbable substances. Zn(II) was determined by EDTA titration.[4] Zinc in the amalgam was determined by collecting the amalgam flowing from the dropping electrode in dilute acetic acid containing a slight excess of Hg(I); the resulting Zn(II) solution was analyzed by polarography after calibration of the instrument with a solution of known Zn content. Oxygen was removed by purified nitrogen which was passed over activated charcoal in Dry Ice to remove traces of adsorbable substance.

Cell.—An all-glass cell with dropping amalgam and hanging amalgam (0.034 cm.^{2}) electrodes was used. The platinum electrode on which amalgam drops were hung was prepared according to Shain, *et al.*[5] A 4-cm.^{2} Ag–AgCl cylindric electrode surrounding the hanging drop served as reference and auxiliary electrode. A three-electrode cell (working, reference, auxiliary) similar to that used in the potentiostatic method could be used but was not necessary. However, the rather large transitory charging current may change, momentarily, the potential of the reference electrode in a two-electrode cell, and a three-electrode cell then must be adopted to avoid distortion of the overvoltage–time curve by recovery of the reference electrode potential. (See also discussion of the effect of the cell resistance.) No controlled temperature bath was used to avoid stray capacity, and the temperature was 25 $\pm$ 1°.

Coulostat and Recording of Potential–Time Curves.—Known quantities of electricity were supplied to the cell with the coulostat[6] of Fig. 1. The capacitor c_1 was charged at a known voltage by battery B with the switch in position 1. The cell e.m.f. was compensated by the voltage across the potentiometer. Capacitor c_1 then was discharged across the cell, and the overvoltage–time curve was recorded with a cathode-ray oscilloscope. The sign of the charge supplied to the cell was changed by reversal of the battery connections.

The voltage across B was measured with a student potentiometer and a voltage divider. A "Mylar" capacitor was selected because some other dielectric materials exhibit hysteresis and thus lengthen the time constant for discharge. Capacity c_1 was calibrated with a General Radio bridge, type 1650-A. Transients in switching were minimized by the use of two mercury relays (Clare, type 1010) which opened contact 1 and closed contact 2 with an interval of 5 to 7 msec. A single pole, double throw relay was not satisfactory because the circuit between 1 and 2 was closed by mercury momentarily during switching. Capacitor c_2 shunted the potentiometer to avoid an increase of the circuit time constant by the inductance and resistance of the potentiometer. Connections between c_1 and c_2 and the cell were as short as possible to minimize inductance. CRO was a Tektronix oscilloscope, type 535, with preamplifier D. The frequency characteristic of this preamplifier for 1 mv. cm.$^{-1}$ sensitivity, which is flat up to 350 kc., was adequate in this work.

Description and Discussion of Results

Determination of Kinetic Parameters.—Overvoltage–time curves and plots of log $|\eta|$ against t are given in Fig. 2 and 3, respectively, for cathodic overvoltages, and results are summarized in Table I. The log $|\eta|$ *vs.* t plots are linear, in agreement with eq. 7 of part I, and they intersect at the same $\eta_{t=0}$ within experimental error. The differential capacity of the double layer was calculated from

$$c_d|\eta_{t=0}| = c_1V^0 \qquad (1)$$

where c_1 is the charging capacitor (Fig. 1) and V^0 is the voltage to which this capacity was charged. The resulting capacities (Table I) agree well with the values given by Grahame and Parsons.[7] Values of I_a^0 were deduced from the log $|\eta|$ *vs.* t plots (*cf.* eq. 7, part I), and the apparent standard rate constant k_a^0 was computed from eq. 28, part

TABLE I

DATA ON THE DISCHARGE OF Zn(II) ON Zn(Hg)[a] IN 1 *M* KCl[b] AT 25°

$C_{Zn(II)}$, mM l.$^{-1}$	r_f, ohms cm.^{2}	c_d, μf. cm.$^{-2}$	I_a^0, ma. cm.$^{-2}$	k_a^0, cm. sec.$^{-1}$
0.5	9.35	16.4	1.37	0.0043
1	5.78	17.5	2.22	.0042
5	1.84	17.8	6.96	.0043
10	1.19	17.2	12.0	.0041
50	0.73	16.9	27.6	.0035
				av. 0.0041

[a] C_{Zn} = 8.8 $\times$ 10^{-2} mole l.$^{-1}$. [b] Cell resistance, 13 ohms at 50 and 100 kc.

(1) Predoctoral student since 1960.

(2) P. Delahay, *J. Phys. Chem.*, **66**, 2204 (1962).

(3) G. C. Barker, "Transactions of the Symposium on Electrode Processes, Philadelphia, 1959," E. Yeager, Ed., John Wiley and Sons, Inc., New York, N. Y., 1961, pp. 325–365.

(4) G. Schwarzenbach, "Complexometric Titrations," translation by H. Irving, Methuen and Co., London, 1957, p. 59.

(5) J. D. Ross, P. D. DeMars, and I. Shain, *Anal. Chem.*, **28**, 1768 (1956).

(6) The following arrangement also was tested and now is being investigated: the cell in series with a diode rectifier is connected to a generator of square-wave pulses, and the voltage–time variations are recorded with a cathode-ray oscilloscope. Charges can be supplied to the cell in 0.1 to 1 μsec. with this circuit, and possibly in shorter times. A transistor also can be used: the square-wave pulse is applied between the base and emitter and the cell is in the emitter-collector circuit.

(7) D. C. Grahame and R. Parsons, *J. Am. Chem. Soc.*, **83**, 1291 (1961). Dr. R. Parsons kindly supplied additional data not given in the paper.

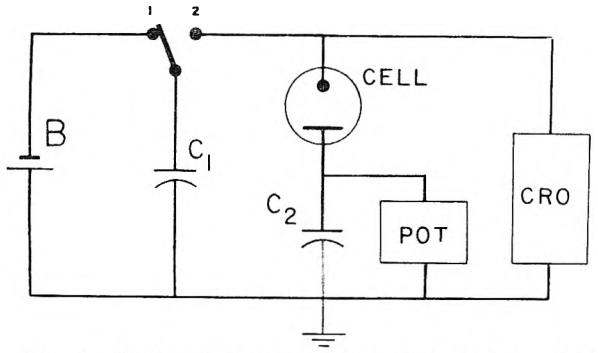

Fig. 1.—Coulostat and recording of overvoltage–time curves: B, 9.30 v. battery; c_1, 286 $\mu\mu$f. "Mylar" capacitor; c_2, 300 μf. electrolytic capacitor; POT, 10-turns, 50-ohm "Helipot" potentiometer connected to 1.5 v. battery; CRO, Tektronix cathode-ray oscilloscope, type 535, with preamplifier D.

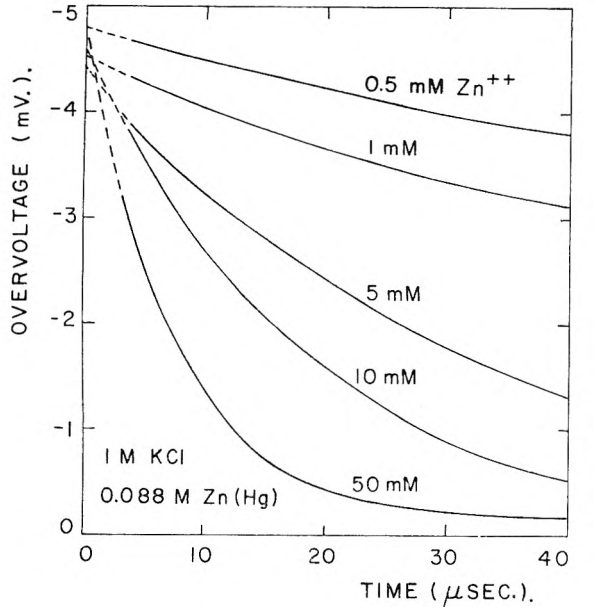

Fig. 2.—Tracings of overvoltage–time curves for Zn^{+2} discharge on Zn–amalgam for different Zn^{+2} concentrations; dashed segments are extrapolated to the overvoltage obtained from Fig. 3 at time zero.

I. The average value, $k_a^0 = 4.1 \times 10^{-3}$ cm. sec.$^{-1}$, agrees with $k_a^0 = 4 \times 10^{-3}$ cm. sec.$^{-1}$ deduced by Randles and Somerton[8] from faradaic impedance measurements. Results of experiments for anodic overvoltages were similar and yielded $k_a^0 = 4.2 \times 10^{-3}$ cm. sec.$^{-1}$. The transfer coefficient, as computed from the slope of the log I_a^0 *vs.* log $C_{Zn^{+2}}$ plot, was $\alpha = 0.30$ both for cathodic and anodic overvoltages.

One readily verifies that condition 27 in part I for pure control by the charge transfer reaction is fulfilled. This condition becomes here $3.4 \times 10^9 \gg 3.3 \times 10^4$ for $D_{Zn} \approx D_{Zn^{+2}} \approx 10^{-5}$ cm.^{2} sec.$^{-1}$ and the lowest $C_{Zn^{+2}}$. This concentration $C_{Zn^{+2}}$ corresponds to the worst possible case, and condition 27 thus is amply satisfied for all concentrations of zinc ions.

Influence of the Cell Resistance.—The influence of the cell resistance was analyzed for the equivalent

(8) J. E. B. Randles and K. W. Somerton, *Trans. Faraday Soc.*, **48**, 951 (1952).

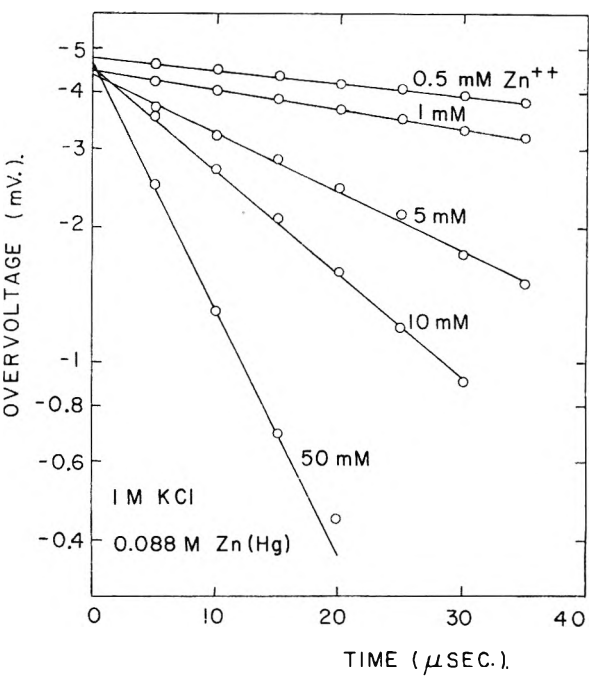

Fig. 3.—Plot of the logarithm of overvoltage *vs.* time for the data of Fig. 2.

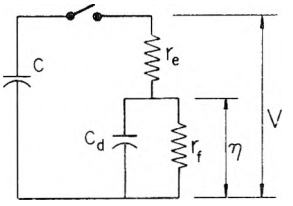

Fig. 4.—Equivalent circuit of coulostat and cell: r_e electrolyte resistance; r_f, charge transfer resistance; c' charging capacity; c_d, differential capacity of double layer.

circuit of Fig. 4. One has at any time for the measured cell voltage[9]

$$V = Ir_e + I_f r_f \qquad (2)$$

where I is the total current for discharge of capacity c, I_f is the faradaic current passing through the charge transfer resistance r_f of the electrode being studied ($r_f = (RT/nF)/I_a^0$) and r_e is the electrolyte resistance. One derives by standard circuit analysis

$$I = (V^0/r_e)\exp(t/\tau) \qquad (3)$$

$$I_f = \frac{V^0}{r_e}\,\frac{1}{1 + \dfrac{r_f c_1}{\tau}}\,[\exp(t/\tau) - \exp(-t/r_f c_1)] \qquad (4)$$

with[10]

$$\tau = -{}^1/_2(r_f c_1 + r_e c + r_f c) + {}^1/_2[(r_f c_1 + r_e c + r_f c)^2 - 4r_e c r_f c_1]^{1/2} \qquad (5)$$

where V^0 is the voltage across c at $t = 0$ before discharge. One has $I_f = 0$ at $t = 0$, and $I_f \to 0$ for $t \to$

(9) We dispense with the convention for current and overvoltage and set $V > 0$, $I > 0$, $I_f > 0$.

(10) Only the + sign before the expression between brackets is retained in eq. 5 because τ must approach zero for $r_e \to 0$. This is not the case when the − sign is kept.

∞ (since $\tau < 0$). Consequently, I_f passes through a maximum at a value of t which is readily derived. The overvoltage V, which is measured, was computed from eq. 2–4 for several values of r_e, and results are listed in Table II. It is seen that the influence of the resistance is negligible when $t >> \tau$. In practice, however, the large ohmic drop across the cell for short times may saturate the amplifiers of the cathode-ray oscilloscope. Recovery of the oscilloscope amplifiers may be relatively sluggish, and the measured overvoltage is too high. This effect can be quite pronounced and may lead to serious error. For instance, the experimental $|\eta|$ values at 10 μsec. for Zn(II) discharge under the same conditions as above, except for insertion of a resistance in series with the cell, were 2.75, 4.5, 6.5, and 20 mv. (*cf.* Table II), respectively, for r_e = 13, 560, 1210, and 2710 ohms. This type of error could be minimized by insertion of a filter network between the cell and the cathode-ray oscilloscope. More simply, a three-electrode cell could be used so that only a fraction of the ohmic drop is applied to the oscilloscope. Further, one should select the smallest possible V^0 and the largest capacity c which are compatible with the desired time constant τ.

TABLE II

CALCULATED OVERVOLTAGE (IN MV.) FOR DIFFERENT TIMES AND CELL RESISTANCES FOR THE DISCHARGE OF 10 m*M* Zn[a]

r_e, ohms	τ, μsec.	t, μsec.					
		1	2.5	5	10	20	40
0	0	4.28	3.96	3.45	2.66	1.56	0.54
13	0.0037	4.28	3.96	3.45	2.66	1.56	0.54
560	.16	22.2	3.96	3.45	2.66	1.56	0.54
1210	.33	43.6	7.5	3.31	2.54	1.49	0.52
2710	.71	227.4	28.3	11.4	2.52	1.48	0.51

[a] Other conditions, except for r_e, are the same as for Table I.

Acknowledgment.—This work was supported by the Office of Naval Research. The authors are indebted to Professor L. W. Morris of the Physics Department, Louisiana State University, for suggesting capacity discharge as a practical means of devising a coulostat.

NON-STOICHIOMETRY IN CADMIUM SELENIDE AND EQUILIBRIA IN THE SYSTEM CADMIUM–SELENIUM[1]

BY A. REISMAN, M. BERKENBLIT, AND M. WITZEN

Thomas J. Watson Research Center of International Business Machines, Yorktown Heights, New York

Received May 5, 1962

Studies of the condensed system Cd–Se have indicated a solubility limit of Cd in CdSe corresponding to a Cd/Se molar ratio of from 1.010–1.015. The system shows the formation of a two-liquid region in the selenium-rich portions, and a tendency toward such formation in the cadmium-rich portions. The melting point of the selenide was determined as 1239 ± 3°. Using precision X-ray fluorescence techniques to study products of vacuum heat treatments of initially stoichiometric CdSe, it has been concluded that this compound vaporizes incongruently and achieves a steady-state vaporization along the three phase line $Cd_{1+\delta}Se$ solid solution–liquid–vapor.

Introduction

The first paper in this series dealing with some aspects of the detailed chemistry of compound semiconductors discussed direct synthesis of II–VI compounds from the elements at temperatures not much in excess of the melting point of the higher melting constituent.[2] The present report is concerned specifically with deviations from stoichiometry in CdSe as a function of temperature, steady state vaporization of this material at a given temperature, phase equilibria in the system Cd–Se under equilibrium pressures, and the solid solubility limits of Cd and Se for a system under its equilibrium pressure.

CdSe always has been observed as an "n" type semiconductor, indicating that it tends to be selenium deficient. Hines and Banks,[3] in studies of CdSe, observed rather large conductivity changes along a given crystal but could not relate these conductivity differences numerically to varying selenium vacancy counts. The only published work on the system Cd–Se dates back to work by Chikashige and Hitosaka[4] in 1917. The proposed diagram appears to be a non-equilibrium one, since the data for all compositions simultaneously show thermal effects attributable to the meltings of Cd and Se. Similar behavior has been described in connection with the studies of the synthesis of CdSe from equimolar mixtures of Cd and Se, and an explanation, believed valid for all compositions, has been presented.[2]

Experimental Procedure

A. Thermal Studies.—Differential thermal analysis (d.t.a.) was used to define the phase diagram for the system Cd–Se. Discussions of equipment and other relevant information are given elsewhere.[2,5]

B. Fluorescence Analysis.—The analysis of CdSe by wet chemical techniques lacks sufficient precision for purposes of studying non-stoichiometry. Of the available instrumental methods, X-ray fluorescence analysis appeared to be the only one with potential for characterizing major

(1) This paper was presented in part at the Symposium on Non-stoichiometric Compounds, 141st National Meeting of the American Chemical Society, Washington, D. C., March 20–29, 1962.

(2) A. Reisman and M. Berkenblit, *J. Phys. Chem.*, in press.

(3) D. Hines and E. Banks, *J. Chem. Phys.*, **24**, 391 (1956).

(4) M. Chikashige and R. Hitosaka, *Mem. Coll. Sci., Univ. Kyoto*, **2**, 239 (1917).

(5) See for example: A. Reisman, Ph.D. Thesis, Univ. Mic. No. 58–2876, Chem. Phys.; A. Reisman, *Anal. Chem.*, **32**, 1566 (1960); A. Reisman and J. Mineo, *J. Phys. Chem.*, **64**, 748 (1960); A. Reisman and J. Karlak, *J. Am. Chem. Soc.*, **80**, 6500 (1958); F. Holtzberg, A. Reisman, M. Berry, and M. Berkenblit, *ibid.*, **79**, 2039 (1957).

element content, and this method was explored as a means for studying non-stoichiometry.

A Philips vacuum spectrograph was employed, and with proper sample preparation and equipment modification, the technique was found suitable for the present studies. It was found that simple manual powder packing on the sample holder resulted in appreciable scatter of data, and that solution techniques presented serious problems because the CdSe required strong acids to achieve solution. A successful method of sample preparation involves pressing of <400 mesh powders (3 g.) at 10,000 p.s.i. into $1^1/_4$ in. diam. pellets without use of binders. Examination of many such pellets using CdSe, whose synthesis is described in ref. 2, revealed that within experimental limits (± 1 part/1000) the materials were homogeneous. These studies involved rotation of the sample holder and inversion of the pellets.

The modifications of the Philips equipment were necessitated by the stringent mechanical and electrical requirements imposed by the experimental approach. The equipment as purchased utilized a friction coupling between the goniometer and single crystal holder shafts. The coupling exhibited slippage beyond that which could be tolerated, and was replaced by a positive drive linkage.

Since full excitation of Cd K3 emission requires greater voltages than the unit is designed to deliver, it was necessary to provide a means for reproducing excitation voltages exactly from run to run to within 100 v. to obtain fine line voltage stabilization. To enable voltage resetting within ± 50 v., a sensitive differential voltmeter and voltage setting control were constructed and used in conjunction with the KV meter supplied with the unit. The constant voltage reactor supplied with the equipment was replaced by one of greater current carrying capacity and stability (Sorensen a.c. voltage regulator Model 5000-2S, 5KVA).

In addition to the above, the spectrograph was bolted to the base and a special alignment tool was incorporated as an integral part of the unit.

Experimental Results

A. The System Cd–Se.—Samples were prepared by inserting Cd and Se pellets, cleaned as described in ref. 2, into the d.t.a. holders described in the same reference. In order that the composition of the condensed phases not be influenced to a great extent by selective volatilization from the melts, attempts were made to restrict the vapor space available over the samples. This space was generally approximately 0.5 cc. above a 3-g. sample. The procedure followed was to heat the reactants at 3°/min. in the d.t.a. apparatus past the reaction exotherm in the 900–1000° temperature range and then through the liquidus.[2,6] The samples then were taken through cooling cycles followed by two or more heating and cooling cycles. In general, these tended to supercool markedly in the first cooling cycle, yielding unreliable liquidus data. An approximate liquidus temperature then was determined from this initial curve simply by noting the peak temperature of the supercooled crystallization. The sample then was reheated to some 10–20° past this approximate temperature and taken through a second cooling cycle which resulted in a smaller supercooling effect. This process was repeated, from 5–10° above the approximate liquidus temperature determined in the preceding cycle. Normally, the second or third cooling curves gave no evidence of supercooling and from this point liquidus points obtained from intersection of the base line with an extrapolated line from the peak slope were reproducible to $\pm 3°$.

During preliminary studies of the freezing point of CdSe, using commercial material, the samples wet the inside of the d.t.a. silica ampoules, indicating a reaction between CdSe and silica. It was found subsequently that CdO contamination was the cause of the wetting, forming cadmium silicates which bonded the selenide to the silica. In a d.t.a. sample preparation starting with clean Cd and Se, it was found that if the container were evacuated only with a mechanical pump, wetting still occurred, but that when a room temperature pressure of 1–3 $\times 10^{-6}$ mm. was attained, wetting could not be detected.

Table I shows the results of the d.t.a. experiments and Fig. 1 presents the proposed equilibrium diagram based on these and other data. In the system CdSe–Cd it is seen that the eutectic temperature, 317°, lies only 3° below the melting point of Cd metal, 320°, and that within experimental limits the liquidus field for Cd is undetectable. The solubility of CdSe in Cd-rich melts is negligible until approximately 900°, at which point the slope of the solubility curve decreases appreciably. It is interesting to note that the liquidus curve exhibits an inflection point indicating

TABLE I

THERMAL DATA FOR THE SYSTEM Cd–Se

Mole % Cd	Mole % Se	Liquidus	Transformation	Solidus	M.p., °C
0.0	100.0				215
0.5	99.5	885		212	
1.0	99.0		991	214	
2.0	98.0		989	213	
3.0	97.0		990	214	
5.0	96.0		989	212	
10.0	90.0		990	214	
15.0	85.0		994	213	
20.0	80.0		992	215	
22.5	77.5		995	215	
25.0	75.0		992	213	
27.5	72.5		987	215	
30.0	70.0		992	213	
32.5	67.5	1053	993	212	
35.0	65.0	1062	993	213	
37.5	62.5	1081	983	212	
38.0	62.0	1094	990	213	
40.0	60.0	1111	992	214	
42.5	57.5	1148	987		
45.0	55.0	1168	992	214	
47.5	52.5	1213	992	212	
50.0	50.0				1239
55.0	45.0	1189		317	
60.0	40.0	1158		317	
65.0	35.0	1151		316	
70.0	30.0	1140		317	
75.0	25.0	1124		319	
80.0	20.0	1095		318	
85.0	15.0	1079		316	
90.0	10.0	1031		317	
95.0	5.0	976		315	
97.5	2.5			313	
100.0	0.0				320

(6) During the major portion of this study, the low temperature synthesis of CdSe described in ref. 2 had not been developed and samples were prepared *via* the technique described above. Toward the completion of the work the low temperature synthesis was employed and duplicate runs on selected compositions were made. These gave data in agreement with that already obtained.

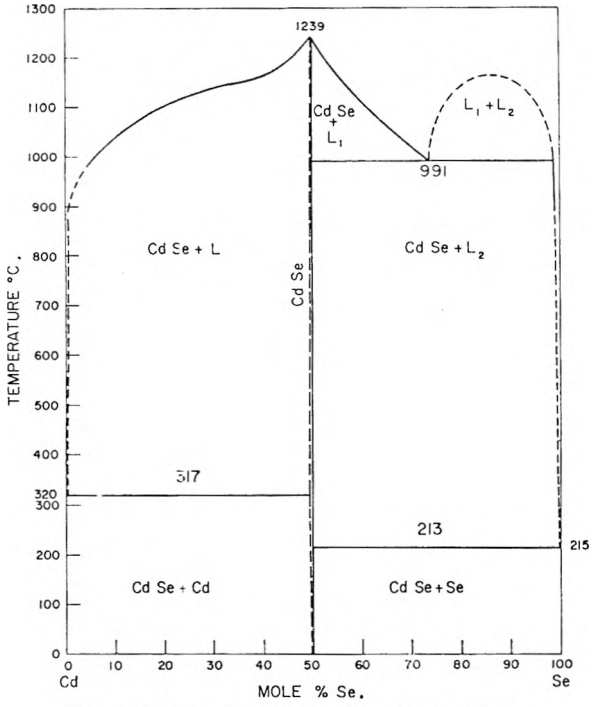

Fig. 1.—Phase diagram for the system Cd–Se.

a tendency toward formation of a two liquid system. Such behavior also was observed in the system Cd–Te described by deNobel.[7] The melting peak of CdSe at 1239° is very sharp, which indicates little dissociation of the material in the liquid phase, an unexpected behavior in view of recent vapor phase data pointing to almost complete dissociation of the selenide in the gas phase to Cd and Se_2 species.[8,9]

Because of this apparently small amount of liquid-phase dissociation of the compound, it would be expected that the solubility of the selenide in Cd-rich melts should be larger than it actually is. The observed low solubility probably is due to an appreciable degree of ordering of liquid phase Cd species (indicated by the tendency toward unmixing) which excludes the selenide.

The solubility of Cd in the CdSe structure was investigated as follows. Samples of CdSe were synthesized with molar Cd/Se ratios of 1.005/1 to 1.05/1 in steps of 0.005/1. These were examined with d.t.a. at a gain of 5 μv./in. Distinct eutectic meltings were observed in all samples having Cd/Se ratios of 1.015/1 and higher. This peak abruptly terminated in the 1.01/1 sample. If we assume that there are no retrograde solubilities along the three phase line CdSe s.s.–liquid–vapor in the system CdSe–Cd which would place the solubility limit higher, then this limit lies between 1.01/1 and 1.015/1. A similar series of samples was prepared containing Se/Cd ratios of 1.002/1–1.005/1 in steps of 0.001/1. When examined, first appearance of a eutectic halt occurred in the 1.002/1 sample. This places the Se solubility limit at between 1.000/1 and 1.002/1, which result was expected in view of the n-type behavior of CdSe.

The liquid immiscibility hinted at in the CdSe–Cd system does occur in fact in the system CdSe–Se. The high pressures developed in the two liquid region, owing to the presence of a liquid phase comprised of almost pure Se, made it impossible to determine its boundary due to shattering of the containers. A d.t.a. sample containing 80 mole % Se was heated to 1025° while being examined telescopically. Its appearance initially was that of an oil in water dispersion and finally showed resolution into two distinct liquid layers.

The eutectic composition for this system approaches the pure component isopleth, and the eutectic temperature is depressed only slightly from the melting point of Se. Because Se tends to solidify in the amorphous state,[2] eutectic halts could not be detected in cooling curves. Upon heating solidified samples, the exotherm for the conversion amorphous to crystalline selenium was observed, followed subsequently by the eutectic melting. It is to be noted that Fig. 1 is not an isobaric section through the system Cd–Se, but a projection on the temperature composition plane. Since the pressures developed cannot be very large, Fig. 1 probably is a good approximation to the constant pressure section at one atmosphere.

B. Non-stoichiometry in CdSe.—Somorjai's equilibrium vapor pressure and dew point data for CdSe indicate, within the limits of his experimental techniques, that CdSe vaporizes congruently. The existence of an appreciable range of solid solubility of Cd in CdSe, on the other hand, leads one to expect that within this range of solid solution the selenium and cadmium each will develop partial pressures, different from one another, leading to incongruent vaporization. If one considers the homogeneous condensed phase equilibria, eq. 1–3, depicting disorder in CdSe followed by development of partial pressures of each of the components, it is evident that thermodynamically the existence of a congruently vaporizing binary compound is improbable unless the equilibrium constant for eq. 1 is zero.

$$CdSe^{\alpha} \rightleftarrows Cd^{\alpha} + Se^{\alpha} \qquad (1)$$

$$Cd^{\alpha} \rightleftarrows Cd^{\beta} \qquad (2)$$

$$2Se^{\alpha} \rightleftarrows Se_2^{\beta} \qquad (3)$$

where the superscript α refers to the solid phase and β to the vapor phase.

G. Mandel, of this Laboratory, considering such phenomena, has developed a theory leading to the conclusion that under certain conditions it is possible for an incongruently vaporizing binary compound to achieve a single phase composition, $A_1 + {}_{\delta}B$, and then continue to vaporize in steady-state fashion with no further change in composition of the condensed phase.[10] Extending these ideas the authors, G. Cheroff, and G. Mandel (by different approaches) have derived an equation of the form

(7) D. deNobel, Ph.D. Thesis, Univ. of Leiden, 1958.

(8) P. Goldfinger, M. Ackerman, and W. Jeunehomme, Tech. Rept., Univ. Libre Bruxelles, January, 1959.

(9) G. A. Somorjai, *J. Phys. Chem.*, **65**, 1059 (1961).

(10) G. Mandel, to be published.

$$\frac{\text{Cd atoms}}{\text{Se atoms}} - 1 = K_{Se}e^{-\Delta H_{Se}/RT} \qquad (4)$$

for the variation of Cd/Se ratio as a function of temperature under steady-state vaporization conditions. It has been assumed in deriving this equation, in which the term ΔH_{Se} is related to forming a mole of Se vacancies in the crystal, that the number of cadmium vacancies is much smaller than the number of selenium vacancies.[10]

In the event that steady-state vaporization is not attained prior to the formation of a second phase, one would not expect, in general, that steady-state vaporization would occur. This can be seen from the following. The inability to develop a steady-state composition in the solid solution will cause the composition of the system to become richer in the component exhibiting the lower evaporation rate. When the three phase boundary is reached, the solid solution will continue to volatilize selectively, analogously to a hydrate decomposition, with continued formation of the second phase and continued composition variation of the condensed portion of the system.

When a commercially purchased sample of CdSe was analyzed, it was found to contain 6% excess Se by weight of the bulk. This material was subjected to a vacuum bakeout at 640° in a long tube and after 6 hr. the cooler portions of the tube were examined. In the coldest portion a dark red deposit of Se was detected, while closer to the furnace a metallic belt of Cd had deposited. In the hottest region a black deposit of CdSe was formed. The sample then was placed in a clean apparatus and the experiment was repeated. This time the quantities of Se and Cd in the outer bands were greatly reduced in size. Subsequent treatments always gave qualitatively similar behavior without any indication that the Se and Cd bands would vanish completely. Examination of the sample by the fluorescence method after each treatment revealed a constant Cd/Se ratio. This experiment indicated either that a steady-state single phase vaporization had been effected, or that a less probable steady state two condensed phase vaporization had occurred.[10,11]

A series of 100-g. samples of CdSe, stoichiometric within the limits of weighing error and the detectability of the fluorescence technique, were synthesized by the process described in ref. 2. These were subjected to vacuum bakeout treatments in the temperature interval 408–950° inclusive and two of the samples were subjected to two different time periods of bakeout to corroborate the less controlled observation of steady-state vaporization discussed above. These samples were analyzed with fluorescence analysis using as standards several of the samples used in the Cd solubility studies. Data for the latter are presented in the first two columns of Table II and in Fig. 2. It is seen that not only is the precision level excellent, but that variation of Cd Kβ/Se Kβ count ratio with Cd/Se

(11) The occurrence of separate bands of Se and Cd is not conclusive proof that vaporization was being effected from a two condensed phase system, since one can postulate such an occurrence based on the known dissociation of CdSe in the vapor phase.

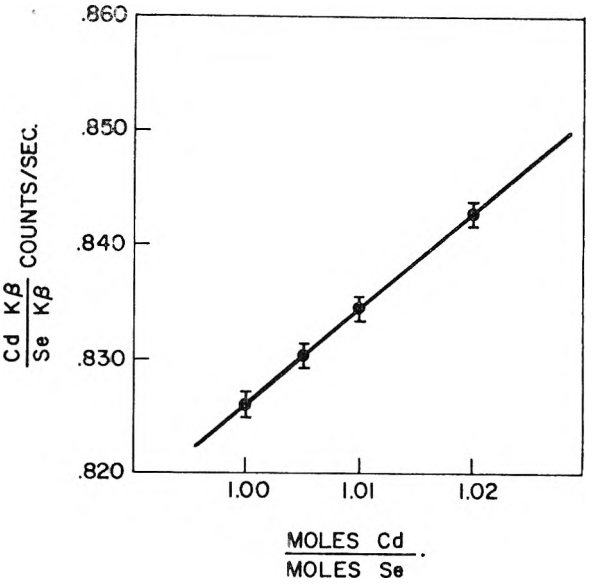

Fig. 2.—Variation of Cd Kβ/Se Kβ count ratio with variation of Cd/Se molar ratio.

molar ratio is linear even in the composition region known to consist of two condensed phases. Fluorescence data for the end products resulting from the vacuum heat treatments of initially stoichiometric CdSe are presented in the remainder of Table II. It is evident from the data at 510–515 and 598–599° that steady-state vaporization had indeed been achieved. It is equally evident, however, that the variation of stoichiometry over a temperature interval of some 540° is not within the range expected from eq. 4. The data can be explained by postulating that the incongruent vaporization of CdSe results in the formation of a liquid phase, composed of almost pure Cd, around the particles of the CdSe solid solution. This second phase having a large surface to volume ratio evaporates rapidly, constraining the composition along the three phase line, yielding what essentially amounts to a steady-state vaporization without great composition–temperature dependence. If the explanation is valid, it follows that the three phase line shows retrograde solubility to the extent of several thousand p.p.m.

The non-stoichiometry of CdSe and other related compounds might be expected to show variations with impurity content, depending upon the major valence state of such impurities in the structure, *e.g.*, monovalent cation substitutions should result in increased Se vacancy count at a given temperature. The non-stoichiometry of other II–VI compounds with and without impurity incorporation presently is being investigated and will be reported on at a later date.

It should be noted, finally, that the results of the above indicate how CdSe, containing unreacted Cd or Se, or both, can be made of constant and predictable composition. Whether such vacuum bakeout procedures for attaining constant composition at a specified temperature are applicable to other binary compound semiconductors is another topic presently being explored.

TABLE II

EFFECT OF VACUUM HEAT TREATMENT ON CdSe STOICHIOMETRY

Initial Cd/Se weighed molar ratio	Initial Cd Kβ/Se Kβ count/sec. ratio[a]	Heat treatment temp., °C.	Heat treatment, time, min. at temp.	Wt. loss, %	Final Cd Kβ/Se Kβ count/sec. ratio	Final Cd/Se molar ratio from smooth curve of Fig. 2
1.00000	0.826 ± 0.001[b]					
1.00500	0.830 ± .001					
1.01000	0.834 ± .001					
1.02000	0.843 ± .002					
1.00000	0.826	408	405	0.64	0.832 ± 0.001	1.007
1.00000	0.826	510	1425	1.05	.830 ± .000	1.005
1.00000	0.826	515	1275	1.11	.831 ± .001	1.006
1.00000	0.826	598	405	5.23	.835 ± .001	1.011
1.00000	0.826	599	105		.835 ± .000	1.011
1.00000	0.826	602	225	3.53	.836 ± .001	1.012
1.00000	0.826	676	15	2.69	.827 ± .000	1.013
1.00000	0.826	694	45	8.00	.835 ± .001	1.011
1.00000	0.826	950	60	~50	.831 ± .001	1.006

[a] Tungsten target, 50 kv. 26 ma. [b] Arithmetic deviation based on 4 or more sets of counts (1.024×10^5 counts).

Acknowledgments.—The authors wish to express their appreciation to R. Rohr for the design and incorporation of mechanical modifications in the vacuum spectrograph and to M. Koblenz and M. Yablon for the design and incorporation of electrical modifications into the same equipment. They also wish to thank G. Mandel for his many stimulating conversations and contributions to the clarification of ideas concerning incongruent vaporization.

COÖRDINATION KINETICS BY ION EXCHANGE

BY D. W. MARGERUM AND B. A. ZABIN[1]

Department of Chemistry, Purdue University, Lafayette, Indiana

Received May 7, 1962

Cation-exchange resin is used as a metal ion buffer to give very low but constant concentrations of metal ions in order to control the rate of fast coördination reactions in the solution phase. The rate of formation of nickel(II)–EDTA is used to test two variations of the system. Particle diffusion rates limit the magnitude of the coördination rate constants which can be measured. The fraction of resin in the hydrogen ion form compared to sodium ion form has an unexpectedly large effect on the diffusion of nickel ion under conditions of low nickel loading where the coupled resin diffusion process should depend largely on the self-diffusion constant of nickel ion.

Introduction

In this work an ion-exchange method designed to permit the study of some fast coördination reactions is tested. A strong acid cation-exchange resin (Dowex 50W) serves as a metal ion buffer giving extremely low but reproducible and constant concentrations of metal ion in the solution phase in equilibrium with the resin phase. The reacting ligand in the solution must be excluded from the resin so that its coördination rate depends on the equilibrium metal ion concentration. The system has the advantage of greatly slowing reactions but giving readily measurable concentrations of product. The reaction of nickel ion with ethylenediaminetetraacetic acid (EDTA) served to calibrate the method because this formation rate can be calculated from its measured dissociation rate[2] and the stability constant for nickel–EDTA.[3] The particle diffusion rate of nickel ion limits the speed of the coördination reaction which can be studied.

The resin in the sodium form is loaded with a few per cent of nickel ion and a low concentration of sodium ion is maintained in the solution. A sufficient quantity of resin is used so that this loading does not change significantly during the reaction. Under these conditions the nickel ion concentration in the solution is expressed by eq. 1 and can be adjusted readily from 10^{-7} to 10^{-5} M and kept constant during a run.

$$[Ni^{+2}] = \frac{K_R[NiR_2][Na^+]^2}{[NaR]^2} \qquad (1)$$

The reaction rate is second order

$$d[NiY_T]/dt = k_{Ni^{Y_T}}[Ni^{+2}][Y_T] \qquad (2)$$

where Y_T and NiY_T refer to the total acid forms of the EDTA anion and the nickel complex, respectively. Combining eq. 1 and 2 gives a pseudo first-order reaction so that a plot of $-\log [Y_T]$ against time gives a slope equal to $k_{Ni^{Y_T}}[Ni^{+2}]/2.303$. The $[Ni^{+2}]$ is determined experimentally for different $[Na^+]$.

(1) Abstracted from the Ph.D. Thesis of B. A. Zabin, Purdue University, 1962.

(2) C. M. Cook, Jr., and F. A. Long, *J. Am. Chem. Soc.*, **80**, 33 (1958).

(3) G. Schwarzenbach, R. Gut, and C. Anderegg, *Helv. Chim. Acta*, **37**, 937 (1954).

In an alternative method the same reaction is studied by loading the resin with low fractions of zinc and nickel and zinc–EDTA is used in place of free EDTA. The rapid equilibrium

$$ZnY_T \rightleftharpoons Zn^{+2} + Y_T \qquad (3)$$

and the Zn^{+2} equilibrium with the resin phase now makes $[Y_T]$ small but constant so that eq. 2 becomes pseudo zero order. The coördination reaction is now so slow that diffusion in the resin phase does not interfere. The reactions in eq. 3 must be much faster than the coördination rate studied for the zero-order system to be applicable.

Experimental

Apparatus and Reagents.—Reactions were run in a 3-necked 1-l. round-bottomed flask fitted with a paddle stirrer and immersed in a constant temperature bath at 25.0°. One of the side necks of the flask contained a test tube which served as a baffle to help mixing, while the other neck contained a dip tube with a 1-cm. diameter sintered glass disk. Samples free of resin could be drawn rapidly into this tube and accurate aliquots could be taken for analysis. Stirring rates were 400–500 r.p.m. (measured with a Strobovac) unless otherwise specified.

Dowex 50W cation-exchange resins purified by Bio-Rad Laboratories were used. The capacity of the air-dried resins in the hydrogen form was determined by potentiometric titration with base in the presence of excess NaCl. The resins were treated with a sequence of HCl, water, EDTA, water, NaOH, water, EDTA, and water rinses to remove all traces of possible interfering metallic impurities. When metal ions were loaded on the resin, the slurry was stirred for 0.5 hr. to assure equal distribution of the metal. All water was first purified on mixed resin beds.

Reagent grade EDTA, recrystallized twice from water and dried, checked satisfactorily as a primary standard when analyzed by dissolving it in base and titrating a standard copper solution using PAN indicator.[4]

Solutions of $NiCl_2$ and $ZnSO_4$ were standardized with EDTA using murexide and Eriochrome Black T indicators, respectively.[4]

Control of pH in the first-order nickel–EDTA reactions without upsetting the concentration of counterion was vital. The sodium ion contribution to the counterion concentration for these experiments was 0.020 *M*, 0.010 *M* in NaCl, and 0.010 *M* from the sodium salt of the buffer. The buffers used were: pH 2.5, sulfate–hydrogen sulfate; pH 3.2, chloroacetate–chloroacetic acid; pH 4.0, formate–formic acid; pH 4.5, acetate–acetic acid. At these concentrations, nickel complexes of the buffer salts are not important.

The analysis for $[Ni^{+2}]$ in equilibrium with the resin and in the rate studies was based on the $Ni(CN)_4^{-2}$ absorption peak at 267 mμ with $\epsilon = 1.16 \times 10^4$. Aliquots were added to NaCN solutions buffered at pH 10 and the absorbance was measured on a Beckman DU spectrophotometer.

Preliminary Studies.—The rates of elution of zinc, cadmium, nickel, and aluminum from 10 g. of Dowex 50–X16, 200–400 mesh, 10% metal loading with 500 ml. of 0.005 *M* EDTA at pH 5 were compared. The zinc and cadmium were eluted rapidly, the nickel rather slowly, and the aluminum very slowly. The nickel rate showed diffusion interference (first-order plots of $-\log [Y_T]$ against time curved upward as the coördination rate slowed with time and the diffusion rate caught up to build the $[Ni^{+2}]$ back up to its equilibrium level).

Steps were taken to minimize both particle and film diffusion. A low cross-linked resin was used to increase particle diffusion after it was shown that EDTA did not enter the resin to react with the metals. A large quantity of resin of small particle size was used to give a large particle area near the surface and a large film area to minimize both diffusion steps. Film thickness was minimized by using rapid stirring. The coördination rate was slowed by lower pH, lower initial EDTA concentrations (10^{-3} to 10^{-4} *M*), and lower loading.

(4) F. J. Welcher, "The Analytical Uses of Ethylenediamine Tetraacetic Acid," D. Van Nostrand Co., Inc., Princeton, New Jersey, 1958.

First-Order Formation of NiY_T (Ni^{+2} in Resin and Y_T in Solution).—Two hundred meq. of resin (about 200 g. of wet Dowex 50W-X2, 200–400 mesh), loaded 2% with nickel, was placed with 500 ml. of solution containing $[Na^+] = 0.020$ *M* and the desired buffer in the 3-necked flask and after 30 min. fractions were taken for analysis of the equilibrium nickel. The resin was filtered, washed with water, and the process repeated to check reproducibility of values obtained for the equilibrium nickel. Then a solution of EDTA containing the same counterion concentration was added and 5-ml. fractions were taken at time intervals for analysis. The $[NiY_T]$ is the nickel found less the equilibrium nickel. Plots of $-\log [Y_T]$ against time were linear and did not show the diffusion interference observed previously.

Zero-Order Formation of NiY_T (Ni^{+2} and Zn^{+2} in Resin and ZnY_T in Solution).—The same resin conditions for the first-order runs were used except that the resin was loaded 4% with zinc as well as 2% with nickel. The solution was 0.10 *M* in sodium ion and was varied in chloride and acetate ion. The resin (100 meq.) was added to 500 ml. of the sodium salt solutions and samples were withdrawn after 30 min. for nickel and zinc analysis. The zinc was determined using Zincon[5] at pH 9 with correction made for the nickel interference. The solution then was made 10^{-3} *M* in ZnY_T and the reaction was followed by the determination of nickel as before. Only a few per cent of ZnY_T reacted during the rate study and the reaction plots of $[NiY_T]$ against time were linear in accordance with a zero-order rate.

Dissociation of NiY_T (Resin in H^+ and Na^+ Form).—The rate of dissociation of NiY_T was measured using 200 g. of the X-2 resin without metal loading to displace the reaction. The reaction volume was 500 ml., the $[Na^+]$ was 0.10 *M*, the initial $[NiY_T]$ was about 5×10^{-5} *M*, and the pH varied between 1 and 2. Plots of log $[NiY_T]$ against time were linear.

Results

The rate constants for the dissociation of nickel–EDTA using the resin to displace the equilibrium are compared in Table I with values calculated from the radionickel exchange[2] at the same ionic strength. In general, the agreement is excellent and where the deviation occurs, the resin experiment gives the constant by a far more direct route. In any case, the resin certainly does not catalyze the reaction despite the fact that the resin phase acidity is greater than 1 *M* and NiY_T dissociation in 1 *M* H^+ is almost instantaneous. Thus, NiY_T does not enter the resin phase in its dissociation and by the principle of microscopic reversibility, the formation of NiY_T should not occur in the resin phase. Further evidence that EDTA reaction in the resin phase is not appreciable is seen in Fig. 1, where increased concentrations of EDTA in the solution phase do not result in increased rate constants.

TABLE I

FIRST-ORDER RATE CONSTANTS FOR THE DISSOCIATION OF NiY_T

$[Na^+] = 0.10$, 25.0°

pH	$[NiY_T]$ initial $\times 10^5$	This work k_d, min.$^{-1}$	Cook and Long[2] k_d, min.$^{-1}$
1.92	4.76	2.8×10^{-2}	4.5×10^{-2}
1.63	5.34	0.19	0.20
1.40	2.72	0.81	0.74

The second-order rate constants calculated from the observed first-order formation of nickel–EDTA are shown in Fig. 1 as a function of the initial EDTA concentration and pH. Despite the fact that the individual rate plots did not show sig-

(5) R. M. Rush and J. H. Yoe, *Anal. Chem.*, **26**, 1345 (1954).

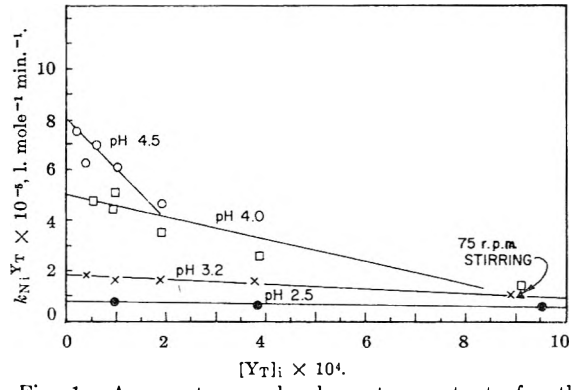

Fig. 1.—Apparent second-order rate constants for the formation of Ni(II)–EDTA from free EDTA and Ni(II) from cation-exchange resin: 200 meq. Dowex 50W-X2, 200–400 mesh; 2% Ni^{+2} loading; $[Na^+] = 0.020$ *M*; total volume, 500 ml.; 25.0°; stirring rate, 400–500 r.p.m.

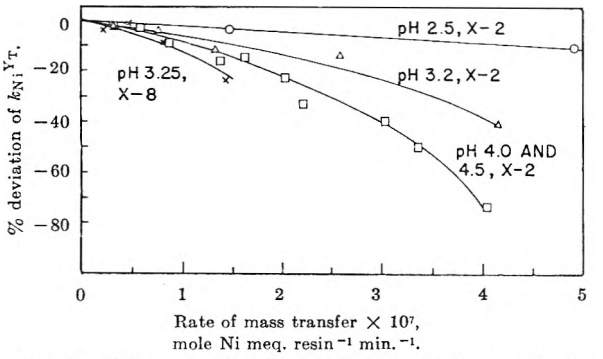

Fig. 2.—Effect of pH and cross-linking on the error in the second-order rate constant due to particle diffusion: 200 meq. Dowex 50W-X2, 200–400 mesh; 2% Ni^{+2} loading; $[Na^+] = 0.020$ *M*; total volume, 500 ml.; 25.0°; stirring rate, 400–500 r.p.m.

nificant diffusion interference, Fig. 1 indicates that the diffusion problem still persists at higher pH and higher initial EDTA concentrations where the diffusion rate cannot quite maintain the equilibrium nickel ion concentration because of the increased coördination rate. The correct value for $k_{Ni}Y_T$ is taken as the extrapolation to zero initial EDTA. Decreasing the quantity of resin also decreased the apparent rate constant. The stirring rate of 400–500 r.p.m. should result in a film of constant thickness surrounding the resin beads and minimize film diffusion.[6] Reducing the stirring rate to only 75 r.p.m. would have increased greatly any contribution of film diffusion, but as seen in Fig. 1, this had no effect. Increasing the resin cross-linking did cause considerable reduction of the apparent rate constants, so particle diffusion appears to be the source of interference in the kinetic studies. It is convenient to define the *initial rate of mass transfer* in terms of the moles of nickel transferred per meq. resin phase per min. to the solution phase. In Fig. 2 the per cent deviation of the apparent rate constant from the extrapolated value is plotted against the *initial rate of mass transfer*. The X8 resin shows much more deviation than the X2 resin at the same pH, illustrating the crosslinking effect on particle diffusion. At pH 4.0 and 4.5, the limitation of particle diffusion in maintaining the desired equilibrium nickel concentration is the same. However, at lower pH, as the fraction of resin in the hydrogen form begins to be appreciable, the particle diffusion rate of nickel appears to increase and causes less deviation in the kinetic study for the same mass transfer rate.

A rate of mass transfer at pH 3 was estimated for copper ion. The copper coördination reaction with EDTA is much faster than the nickel reaction and the rate of transfer from the resin phase probably is not coördination controlled. Using the same resin and solution conditions copper ion reacted with 2×10^{-4} *M* EDTA in 30 sec., giving an average rate of mass transfer of 1×10^{-6} mole Cu^{+2} per meq. resin per min. This is greater than the initial rate of mass transfer for nickel, which is controlled by both diffusion and coördination, but if it represents the limiting rate for nickel diffusion it could cause the deviations observed at low pH.

The extrapolated values for $k_{Ni}Y_T$ are plotted in Fig. 3 as the measured constants and are compared to those calculated from the dissociation rate constants and the stability constant for nickel–EDTA. The agreement is within the accuracy of the calculated constants except at higher pH, where in one case diffusion limits the accuracy of the ion-exchange method and in the other case the contribution of other terms in the radionickel exchange[2] could easily lead to high values for the formation rate constant. The comparison is made for ionic strengths of 0.02 to 0.03 in both cases.

The results of the zero-order ion-exchange system for the same reaction but at a higher ionic strength (0.10) are shown in Fig. 4. In this system, diffusion is not a problem because the coördination rate is much slower and the larger rate constants at higher pH values can be measured accurately. The relative change of the rate constant with pH follows the results found for the first-order exchange system given in the lower curve in Fig. 3. The constants used for the calculations include the values for the stability constant[7] of ZnY^{-2}, the acid dissociation constant[3] for $ZnHY^-$, and the acid dissociation constants[3] of EDTA corrected for temperature.[8] The equilibrium $[Zn^{+2}]$ and $[Ni^{+2}]$ were greater than 10 times that used for the first-order runs and therefore were determined with greater precision. The curve in Fig. 4 can be resolved into the individual rate constants for Ni^{+2} with H_2Y^{-2} and HY^{-3} in the same manner used by Tanaka and Sakuma.[9] Table II compares their data at 0° and their treatment of the data of Cook and Long[2] at 25.0° with our data. The agreement is satisfactory, considering the accuracy of the various stability constants that must be used in the calculations. The curve in Fig. 4 has several points for reactions run in 0.10 *M* NaOAc using the observed equilibrium nickel and correcting for zinc acetate. The $NiOAc^+$ ion appears to react at the same rate as the aquo Ni^{+2} ion. This is in disagreement with the results of Tanaka and

(6) M. Tetelbaum and H. P. Gregor, *J. Phys. Chem.*, **58**, 1156 (1954).

(7) C. N. Reilley, *J. Am. Chem. Soc.*, **78**, 5513 (1956).

(8) M. J. L. Tillotsom and L. A. K. Staveley, *J. Chem. Soc.*, 3613 (1958).

(9) N. Tanaka and Y. Sakuma, *Bull. Chem. Soc. Japan*, **32**, 578 (1959).

Sakuma,[9] who find that the acetate species reacts somewhat faster.

TABLE II

SECOND-ORDER RATE CONSTANTS FOR THE REACTION OF Ni^{+2} WITH EDTA, L. MOLE^{-1} MIN.$^{-1}$

	$k_{Ni}^{H_2Y}$ × 10^{-4}	k_{Ni}^{HY} × 10^{-7}	μ	Temp., °C.
This work	12.	1.1	0.10	25.0
Tanaka and Sakuma	4.8[2]	1.8[2]	.10	25.0
	1.2	0.06	.20	0.0

Discussion

The dissociation study of metal complexes using ion exchange resin should prove to be a valuable approach to the measurement of the dissociation rates of EDTA and other coördination complexes where so frequently the equilibrium cannot be shifted by other means without catalyzing the rate.

The first-order and zero-order ion-exchange formation rate studies of nickel–EDTA are shown to give accurate rate constants within the limitations set by particle diffusion. The first-order ion exchange method can readily measure rate constants about 100 times larger than can be measured by direct conventional mixing techniques. The ion-exchange method is limited to negatively charged complexes of moderate stability. The zero-order ion exchange method should be capable of extending this by another factor of 10 to 100. The greatest source of error in the first-order system is obtaining an accurate and reproducible measurement of the equilibrium metal concentration. In this case 10–20% error was encountered for the very low nickel concentrations. This was reduced to about 5% error in the zero-order system, which had a higher nickel concentration. The main source of error for the absolute values obtained in the latter system is the accuracy of the several stability constants which must be used in the calculations. Cumulative errors of 0.1 pK unit are possible, giving 25% error in the rate constant. The general applicability of the zero-order system is limited by the requirements of the second coördination system relative to the desired reaction rate.

The diffusion interference should be reduced by operating at lower temperatures. The activation energy for the diffusion of small ions through the resin is about the same as that through water.[10] On the other hand, the activation energy for many coördination reactions is much higher. Thus, at lower temperatures the coördination rate would be decreased relative to the diffusion rate.

The effect of the solution pH on the particle diffusion of nickel ion in the resin is seen in Fig. 1 and 2. Table III summarizes this effect in terms of the per cent resin in the hydrogen form and the slight swelling of the resin which can be expected.[11] The dissociation rate data in Table I and the formation rate data in Fig. 3 show no contribution of EDTA reaction within the resin, so this cannot account for the particle diffusion pH dependence.

(10) G. E. Boyd and B. A. Soldano, *J. Am. Chem. Soc.*, **75**, 6091 (1953).

(11) O. D. Bonner, *J. Phys. Chem.*, **59**, 719 (1955).

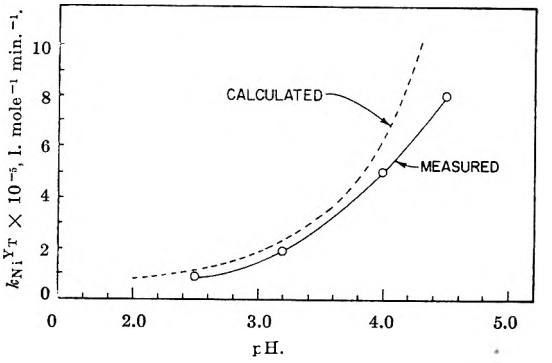

Fig. 3.—Agreement of first-order ion-exchange kinetic method with calculated rate constants for the formation of Ni(II)–EDTA: 25.0°; μ = 0.020. The calculated values are from the dissociation rate constants reported from radionickel exchange[2] and the equilibrium constants.[3]

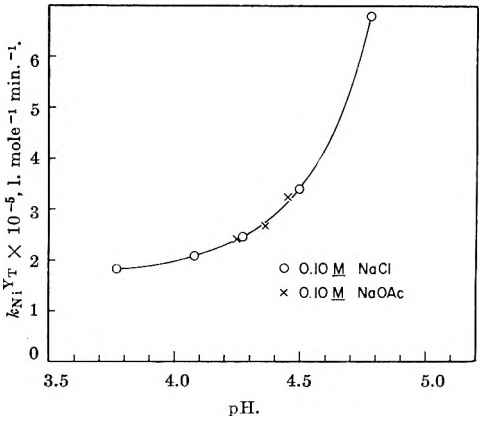

Fig. 4.—Variation of rate constants with pH for the formation of Ni(II)–EDTA using zero-order conditions: 25.0°; μ = 0.10.

TABLE III

THE EFFECT OF pH ON PARTICLE DIFFUSION

Dowex 50W-X2, 0.02 M Na^+

pH	% RH	Swelling, %	Initial rate of mass transfer[a]
4.5	0.1	...	1.1×10^{-7}
3.2	2.6	+0.5	1.8×10^{-7}
2.5	13	+3	4.6×10^{-7}

[a] With 10% or less deviation of coördination rate constant.

Table III indicates that relatively small percentages of hydrogen ion in the resin can double and quadruple the diffusion rate of nickel ion even when there is only 2% nickel loading in the resin. This is given in terms of the *initial rate of mass transfer* which essentially normalizes the differences in coördination rate as the pH changes. The slight swelling of resin cannot account for these large changes. The mobility of hydrogen ion in solution is six times that of sodium ion and this factor may carry over to the resin phase. However, Helfferich's calculations[12] indicate that the rate of particle diffusion in a divalent–monovalent coupled diffusion at low divalent metal ion loading is due largely to the divalent metal ion diffusion rate and is almost independent of the monovalent counterion diffusion. In the present case the

(12) M. S. Plasset, F. Helfferich, and J. N. Franklin, *J. Chem. Phys.* **29**, 1064 (1958).

coupled diffusion constants for Ni^{+2}–Na^+ and Ni^{+2}–H^+ will be essentially identical because of the low nickel concentration in the resin. Thus, there should be little difference between the rates of mass transfer for hydrogen or sodium forms, but a large effect is observed. Hydrolysis of nickel ion is not important in solution at these pH values and the resin phase has a much higher acidity than the solution phase, so this cannot be the cause of the diffusion effect. These data suggest that nickel ion transfer is not a simple diffusion controlled process but that the nickel at the sulfonic acid sites may be activated by hydrogen ion. It has been well established that the transfer of other cations in the sulfonate resin phase is diffusion controlled.[13] However, nickel might be an exception because of its sluggish reaction. For example, nickel ion is slower to react with sulfate ion than many other metals, but this would mean that the hydrated ion must lose coördinated water at some resin sites.[14] If this is the case similar effects might be found with other metal ions which have sluggish coördination reactions and this deserves further investigation.

Coördination control in the elution of metal ions from resins can be an asset in the separation of metal ions in ion exchange processes, giving a kinetic separation factor in addition to an equilibrium factor.

Acknowledgment.—The authors wish to thank the Air Force Office of Scientific Research and the Monsanto Chemical Co. for support of this research.

(13) G. E. Boyd and B. A. Soldano, *J. Am. Chem. Soc.*, **75**, 6107 (1953).

(14) M. Eigen, in S. Kirschner, Ed., "Advances in the Chemistry of Coordination Compounds," The Macmillan Co., New York, N. Y., 1961, pp. 371–378.

TRANSFER FREE ENERGIES FOR SOME UNIVALENT CHLORIDES FROM H_2O TO D_2O FROM MEASUREMENTS OF ION EXCHANGE MEMBRANE POTENTIALS

BY J. GREYSON[1]

International Business Machines Corporation, Thomas J. Watson Research Center, Yorktown Heights, New York

Received May 12, 1962

The cells $Ag|AgCl|\begin{matrix}MCl\ (a_1)\\H_2O\end{matrix}\|\begin{matrix}MCl\ (a_2)\\D_2O\end{matrix}|AgCl|Ag$ with $\|$ representing a cation exchange membrane and M representing the ions Li^+, Na^+, K^+, Cs^+, NH_4^+, and $(CH_3)_4N^+$ have been investigated. The e.m.f. values show a spontaneous transfer of salt from D_2O to H_2O. The measurements, combined with published enthalpy data and with additional measurements of systems of H_2O–D_2O mixtures, yield entropy values which are interpreted according to Frank's "iceberg" theory.

Because of the property of permselectivity which ion exchange membranes possess they may be used as reversible electrodes[2,3] in systems for which no other reversible electrodes can be prepared or in systems in which the reactivity of ordinary electrodes may interfere with the measurement. They are therefore suited to investigations of cells of the type

$$Ag|AgCl|\begin{matrix}MCl,\ a_1\\solv.\ A\end{matrix}\|\begin{matrix}MCl,\ a_1\\solv.\ B\end{matrix}|AgCl|Ag \quad (I)$$

where $\|$ is a cation exchange membrane, M is any cation of interest and solvents A and B are any solvents of interest. Such membrane cells are similar to the amalgam cells

$$Ag|AgCl|\begin{matrix}MCl\ (a_1)\\solv.\ A\end{matrix}|\begin{matrix}Hg\\M\end{matrix}|\begin{matrix}MCl\ (a_1)\\solv.\ B\end{matrix}|AgCl|Ag \quad (II)$$

which have been studied by Akerlof[4] and others to obtain information about the process of transfer of salt from solvent A to B. In both types of cells the potential is given by

$$E = \Delta E_T + \frac{RT}{F}\int_A^B \sum_i t_i \, d \ln a_i$$

where the leading term is the free energy of transfer of the salt from A to B and the integral, which extends over the composition range from A to B, expresses the contributions of the transport of ionic species and of solvents that are coupled to the flow of current through the cell.[3] For the amalgam all these transport processes certainly are negligible. They also would be negligible in cell I with an ideal ion exchange membrane and may be assumed to be negligible for cell I with a real membrane in certain limiting cases.

Such a limiting case assumption can be made for cell I if A is H_2O and B is D_2O because proton exchange is rapid. The solvation sheath of the diffusing species can exchange within the membrane making the coupled mass transport of solvent negligible. We therefore have undertaken to investigate the potentials of a series of membrane cells in which the half cells were, respectively, H_2O and D_2O solutions of the salts LiCl, NaCl, KCl, CsCl, NH_4Cl, and $(CH_3)_4NCl$. It would be interesting to verify our assumptions or at least determine the extent of error due to them by undertaking a similar series of measurements using

(1) Research Center, Stauffer Chemical Company, Richmond, California.

(2) *Discussions Faraday Soc.*, No. 21 (1956).

(3) G. Scatchard, *J. Am. Chem. Soc.*, **75**, 2883 (1953).

(4) G. Akerlof, *ibid.*, **52**, 2353 (1930).

amalgam membranes. Unfortunately circumstances prevent our doing so. The results and conclusions presented here are of course subject to this criticism.

Experimental

Cell.—The membrane was clamped between two no. 15 "O" ring joints each of which was sealed to the bottom of a short 50 ml. test tube. The volume of each half cell was about 65 cc. but only 25 cc. of solution was used and the liquid levels in the test tubes were maintained equal. An electrode and thermometer were inserted in each half cell through a rubber stopper at the top. During measurements the cell was kept in an air thermostat controlled to 24.8 ± 0.2°.

Potential measurements were made with a Rubicon portable potentiometer and a Keithley 151R null detector. The impedance of the null detector (10 megohms) is such that the current flow through the cell was negligible.

The electrodes were silver chloride crystal electrodes with asymmetry potentials of 0.1 mv. or less. Their preparation and characteristics have been described elsewhere.[5]

Materials.—Membrane material was supplied by the Ionac Chemical Company and designated by them No. 3142 Cation Exchange Membrane. The permselectivity of the membrane, determined by the ratio of measured to theoretical concentration potential using approximately 0.1 *N* KCl solution, was better than 0.99.

All reagents except CsCl and $(CH_3)_4NCl$ were reagent grade and were used without further treatment. The $(CH_3)_4NCl$ was supplied by the Eastman Organic Chemical Company. Volumetric chloride analysis showed it to be at least 99.8% pure. It was used without further treatment. CsCl was prepared from Cs_2CO_3 supplied by the Eastern Chemical Corporation and reported to be 99.9% pure. The carbonate was converted to the chloride with HCl and ignited at the melting temperature of CsCl for several hours and used without further treatment.

The D_2O (99.5%) was obtained from the Isomet Corporation. It was distilled under dry nitrogen at least twice before using. Aqueous solutions were prepared from conductivity water.

All solutions were prepared by weight from salts which were oven-dried to constant weight.

Measurement Procedure.—Before any series of measurements, the membrane was equilibrated with the solute by immersing it for several days in either saturated or normal aqueous solutions of the salt to be used. (The measured potential was insensitive to the equilibration procedure.) It then was washed thoroughly in water and clamped in the cell. After clamping the membrane, each half cell was rinsed several times with small portions of the solutions which were to be used. The cell then was filled, the electrodes inserted, and measurements started.

Because of solvent permeability of the membrane, the time dependence of the cell potential required that readings be made at regular intervals for each measurement for at least 2 hr. At the end of a measurement period the electrodes were interchanged and allowed to re-equilibrate for 15–30 min. A time-corrected average was calculated and extrapolated back to the time of cell assembly. The time-corrected average never deviated more than 0.1 mv. from the extremes. The entire extrapolation correction never exceeded 0.5 mv. Therefore the error in measurement should be less than 0.2 mv.

No attempt was made to prepare exactly equal concentrations of the aqueous and D_2O solutions. Instead, concentrations varying ±10% around 0.1 *N* were prepared and matched against one another to yield a range of measurements. The use of volume concentration units for H_2O and D_2O solutions is equivalent to using units of moles of salt per 55.5 moles of solvent as was done by LaMer and Noonan[6] in a similar investigation and places the solutions in thermodynamically comparable states. The measured potential was plotted *vs.* the logarithm of the mean activity ratio. The activity ratios were estimated from the compositions with the aid of the expression

$$\ln \nu_{\pm} = -Am^{1/2}/(1 + m^{1/2}) + Bm$$

due to Guggenheim and Turgeon[7] assuming that expression valid for the concentration units used and assuming the tabulated "*B*" values given by those authors applicable to heavy water solutions. Within the limits of those assumptions, the intercept (at unit ratios) is the cell potential with equal activities in each half cell and the slope is a measure of the permselective efficiency of the membrane. For a perfect membrane at 25° in this cell, a tenfold change in activity ratio yields an e.m.f. change of 118 mv. Each concentration ratio was measured at least twice and reproduced to better than 0.3 mv. The reported values are the averages of the repeated measurements. For three salts, KCl, LiCl, and $(CH_3)_4NCl$, new solutions were prepared and the measurements repeated. The new measurements agreed with the old within 0.3 mv.

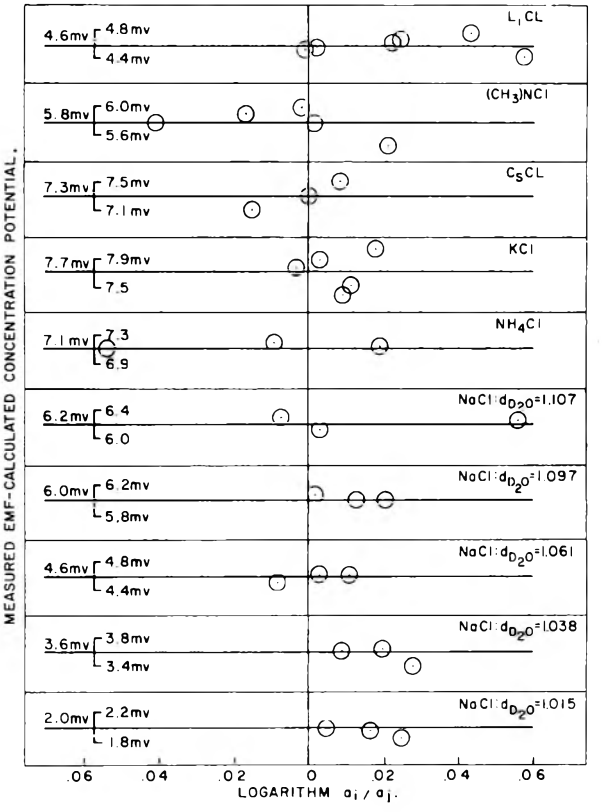

Fig. 1.—Deviation plot of the quantity $[E_{meas} - 118 \log (a_i/a_j)]$ *vs.* $[\log (a_i/a_j)]$ for all salts.

Results

Results are shown graphically in Fig. 1, which is a summary of all the data plotted to show the deviations from the best intercept on the e.m.f. axis.

Since the cell was not stirred, the effect of diffusion films at the membrane solution interfaces were a source of concern. Relatively concentrated (0.1 *N*) solutions were used to minimize these effects.[8] The slopes of the curves for all salts were theoretical within the over-all precision of the measurements, about 5%, and the reproducibility of concentration cell potentials indicated that film effects were not significant.

Equal activity cell potentials obtained as described are shown as straight lines in Fig. 1 and are listed in Table I. Positive values indicate that the

(5) J. Greyson, *J. Electrochem. Soc.*, **109**, 745 (1962).

(6) V. K. LaMer and E. Noonan, *J. Am. Chem. Soc.*, **61**, 1487 (1939).

(7) E. A. Guggenheim and J. Turgeon, *Trans. Faraday Soc.*, **51**, 747 (1955).

(8) F. Helfferich, *Discussions Faraday Soc.*, **21**, 83 (1956).

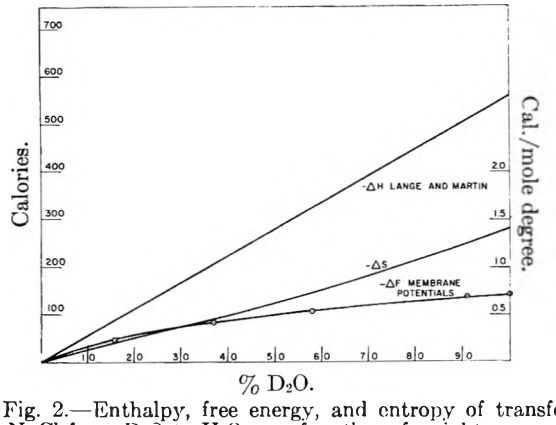

Fig. 2.—Enthalpy, free energy, and entropy of transfer of NaCl from D_2O to H_2O as a function of weight per cent D_2O in D_2O–H_2O mixtures.

salt is passing spontaneously from D_2O to H_2O. All the e.m.f. values are positive and in the range of 4 to 8 mv.

In Fig. 2 the free energies of transfer obtained from the e.m.f's. of the cells

$$\mathrm{Ag}\left|\mathrm{AgCl}\right|\begin{matrix}\mathrm{NaCl}\ (a_1)\\ \mathrm{H_2O}\end{matrix}\Big\|\begin{matrix}\mathrm{NaCl}\ (a_1)\\ \mathrm{H_2O}:n\mathrm{D_2O}\end{matrix}\Big|\mathrm{AgCl}\left|\mathrm{Ag}\right.$$

are shown as a function of the weight per cent of D_2O in the right half cell. These values were obtained in a manner identical with those given in Table I and measurement precision is indicated in Fig. 1.

TABLE I

E.M.F., FREE ENERGY, MOLAL ENTHALPY, AND ENTROPY OF TRANSFER FROM D_2O TO H_2O

Salt	Cell e.m.f., mv.	$-\Delta F$, cal./ mole	$-\Delta H$,[8] cal./ mole	$-\Delta S$, cal./ mole deg.	Bingham[14]
LiCl	4.6	110	420	1.03	−14.0
NaCl	6.2	140	510	1.23	− 9.60
KCl	7.7	180	560	1.27	+ 0.28
CsCl	7.3	170	660	1.63	+ 2.59
NH_4Cl	7.1	..	..	..	+ 0.44
$(CH_3)_4NCl$	5.8	..	..	..	−14.0

Discussion

The e.m.f. for the KCl cell can be compared to that obtained by LaMer and Noonan[6] for a cell in which a liquid junction served as a membrane. The net reaction for that cell can be expressed

$$t_c\mathrm{KCl}(m \text{ in } \mathrm{D_2O}) = t_c\mathrm{KCl}(m \text{ in } \mathrm{H_2O})$$

where t_c is the cation transport number and E = 4.75 mv. For the cation membrane cell, the reaction is

$$\mathrm{KCl}(m \text{ in } \mathrm{D_2O}) = \mathrm{KCl}(m \text{ in } \mathrm{H_2O})$$

with E = 7.7 mv. (Since t_c for KCl solutions at a liquid junction is of the order of 0.5, the value of 7.7 obtained for a system in which t_c is near unity is quite reasonable.) LaMer and Noonan, in addition, measured the temperature dependence of their KCl cell potential and from it calculated the enthalpy and entropy of transfer of KCl from D_2O to H_2O. Their results indicate that the salt experiences a decrease in entropy in the transfer process.

Lange and Martin[9] have measured integral heats of solution of the alkali chlorides in D_2O and H_2O up to end concentrations of about 0.5 N. For these concentrations, the integral heats per mole and molal enthalpies are approximately the same and the enthalpies of transfer from D_2O to H_2O can be compared to the free energies of transfer calculated from the cell potentials.[10] In Table I this is done and approximate values for transfer entropies are calculated and listed. It is seen that in every case, the salt experiences a decrease in entropy in the transfer process in agreement with the measurements of LaMer and Noonan.

The thermodynamic and transport properties of D_2O, compiled by Whalley,[11] show that D_2O is more structured than water. A salt dissolved in D_2O can have a proportionately greater disruptive effect on it than on the less structured H_2O, *i.e.*, one expects the entropy of solution in D_2O to be greater than in H_2O. The salt then, in passing from D_2O to H_2O, experiences a decrease in entropy. The entropy decrease apparently is not a linear function of the amount of D_2O mixed with water, as can be inferred from Fig. 2. In measuring heats of solution of NaCl in water and H_2O–D_2O mixtures, Lange and Martin[12] reported a linear relationship between integral heat and per cent D_2O. Since ΔF is concave to the abscissa and if it can be assumed that the molal enthalpies are essentially the same as the integral heats, the entropy variation is convex to the abscissa. That is, the largest entropy changes occur as the solvent structure approaches that of pure D_2O.

The order of entropy change from one ionic species to another is less clear. We might attempt an explanation from the point of view of the "iceberg" theory of Frank and Evans.[13] These authors in developing that concept and the effects of ionic size and character on icebergs showed that fluidity elevation properties, among other things, correlated with disorder-promoting ions. For example, lithium ion with a negative fluidity elevation value tends to promote structure while cesium ion, with a positive value, disorders. The variations in transfer entropies from ion to ion shown in Table I and compared with fluidity elevation values[14] imply that the disorder-producing ions are more effective in doing so in D_2O than in H_2O. That is, cesium ion, being very order-destroying in water, attacks the more structured D_2O iceberg still more vigorously, while lithium ion, although order-producing, disrupts the D_2O structure but with lesser effect.

Acknowledgment.—The author would like to thank W. R. Heller for a suggestion which originally stimulated this work and H. L. Friedman for his

(9) H. E. Lange and W. Martin, *Z. Elektrochem.*, **42**, 662 (1936).

(10) The extent to which these free energies reflect the values of the standard free energy of transfer is limited to the extent to which the assumptions made in the section on measurement procedure are valid.

(11) E. Whalley, Proceedings of the Joint Conference on the Thermodynamic and Transport Properties of Fluids, Inst. of Mech. Eng., London, 1958, p. 15.

(12) H. E. Lange and W. Martin, *Z. physik. Chem.*, **A178**, 214 (1937).

(13) H. S. Frank and E. W. Evans, *J. Chem. Phys.*, **13**, 507 (1945).

(14) E. C. Bingham, *J. Phys. Chem.*, **45**, 885 (1941).

many helpful, interesting, and provoking conversations and suggestions. Thanks are due also to P. R. Mackey for invaluable assistance in the experimental work.

THE CHARGE TRANSFER COMPLEX BETWEEN β-CAROTENE AND IODINE. I. SYNTHESIS AND OPTICAL SPECTRA

BY J. H. LUPINSKI AND C. M. HUGGINS

General Electric Research Laboratory, Schenectady, New York

Received May 15, 1962

Experimental evidence confirms a previous assumption that β-carotene triiodide is a charge transfer complex. Results of the synthesis are discussed and a method for the preparation of a relatively pure, solid complex is described. In dilute solution the complex is unstable. It appears to decompose, at least partly, into its components, resulting in a chemical equilibrium. Spectra of this system under various conditions are given. The equilibrium probably constitutes the first step in the interaction between β-carotene and iodine which ultimately leads to isomerization and iodination of β-carotene.

Introduction

Charge transfer complexes have become a subject of increased study, particularly because of the electrical and magnetic properties of the solids. Most of the complexes described in the literature are derived from aromatic donor molecules and various acceptors; little is known about complexes made from linear polyenes, R(C=C—)$_n$R, and iodine. Recently, Huggins and LeBlanc[1] reported on the electrical conductivity and paramagnetism of β-carotene triiodide. Our interest in the physical properties of this compound[2] has led to a further investigation of its chemical characteristics.

On several occasions, carotene–iodine compounds have been described in the literature, resulting in a rather complicated over-all picture. Isomerization as well as iodination can take place and, as will be shown, a charge transfer complex also can be formed. β-Carotene–iodine compounds can be made by adding solid iodine to a solution of β-carotene or by mixing solutions of the components. Details are given in a number of publications describing these experiments.[3–6]

In the earlier papers, two different compounds were mentioned, diiodide, $C_{40}H_{56}I_2$,[4,5] and a triiodide, $C_{40}H_{56}I_3$.[3,5] Later, a tetraiodide[6] was described. Savinov and Tretyakova[6] claim that in general two compounds are formed in the reaction of iodine with β-carotene; namely, $C_{40}H_{56}I_2$ and $C_{40}H_{56}I_4$; the reaction product consists of a mixture of these two compounds. Support for this conclusion also can be found in the work of Willstätter,[4,5] who reported that the iodine content of $C_{40}H_{56}I_2$ and of $C_{40}H_{56}I_3$ is not constant; however, it is close to the values expected for the diiodide and the triiodide. It should be emphasized that the experiments of Savinov and Tretyakova do not exclude the existence of a compound with composition $C_{40}H_{56}I_3$. They studied the reaction products when an excess of iodine was used while Arnaud and Willstätter used an excess of β-carotene in the preparation of $C_{40}H_{56}I_3$. Our work confirms the results of Arnaud and Willstätter; it can be shown that the compound $C_{40}H_{56}I_3$ is a charge transfer complex and not a mixture of equal amounts of $C_{40}H_{56}I_2$ and $C_{40}H_{56}I_4$.

In addition to the formation of these compounds, it appears that β-carotene and its compounds with iodine can absorb iodine almost continuously. This we could demonstrate by exposing a known amount of β-carotene to iodine vapor under reduced pressure. After 2 hr. about 8.5 moles of iodine were taken up per mole of β-carotene. Even more iodine is absorbed on continued exposure. In solution, however, products that contain more than about 2 moles of iodine per mole of β-carotene[6] rarely are formed. Thus, depending on the initial circumstances, different products can be obtained.

For a better understanding of the physical properties of β-carotene triiodide, a more definite description of this compound is highly desirable. Considerable support is achieved for the original suggestion that β-carotene triiodide is a charge transfer complex.

Experimental

According to Arnaud[3] and Willstätter,[5] β-carotene triiodide can be made by adding solid iodine to solutions of β-carotene. Repeating this procedure, it was found that in addition to the desired product, a black tarry material also is formed. Furthermore, it appeared that the main reaction product, although its composition is close to that of $C_{40}H_{56}I_3$, consisted of at least two components. The following details may serve as an illustration. Four grams of all-*trans*, 100% β-carotene (Eastman Kodak) was dissolved in 900 ml. of benzene and 1.33 g. of iodine crystals was added while stirring. A dark, colored solution was obtained containing very small crystals and a black tar. The solution with the suspended crystals was decanted from the tarry material and the crystals (sample I) were filtered, washed with benzene and petroleum ether (boiling range 30–60°, and henceforth it will be referred to as petroleum ether), and dried *in vacuo*; yield about 40%.

Sample I (1.4 g.) was treated with benzonitrile resulting in a dark green solution and a residue. This residue (fraction IA) was washed with benzonitrile and petroleum ether and dried. The part of sample I that dissolved in benzonitrile was precipitated by adding petroleum ether. After dissolving the precipitate in chloroform, it was reprecipitated by addition of petroleum ether. The resulting nearly-

(1) C. M. Huggins and O. H. LeBlanc, *Nature*, **186**, 552 (1960).

(2) C. M. Huggins and J. H. Lupinski, to be published.

(3) M. A. Arnaud, *Compt. rend.*, **102**, 147 (1886). Originally Arnaud gave $C_{26}H_{38}I_2$ as composition for the compound which was later shown to be $C_{40}H_{56}I_3$.[5]

(4) R. Willstätter and W. Mieg, *Ann. Chem.*, **355**, 1 (1907).

(5) R. Willstätter and H. H. Escher, *Z. physik. Chem.*, **67**, 47 (1910).

(6) B. G. Savinov and G. S. Tretyakova, *Vitaminy Akad. Nauk Ukr. SSR*, **1**, 137 (1953).

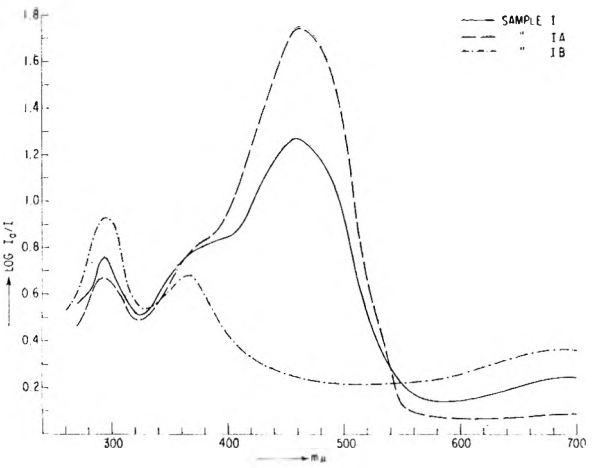

Fig. 1.—Ultraviolet and visible spectra of samples I, IA, and IB; concentrations are approximately 3×10^{-5} *M* in chloroform and a cell of 1 cm. was used.

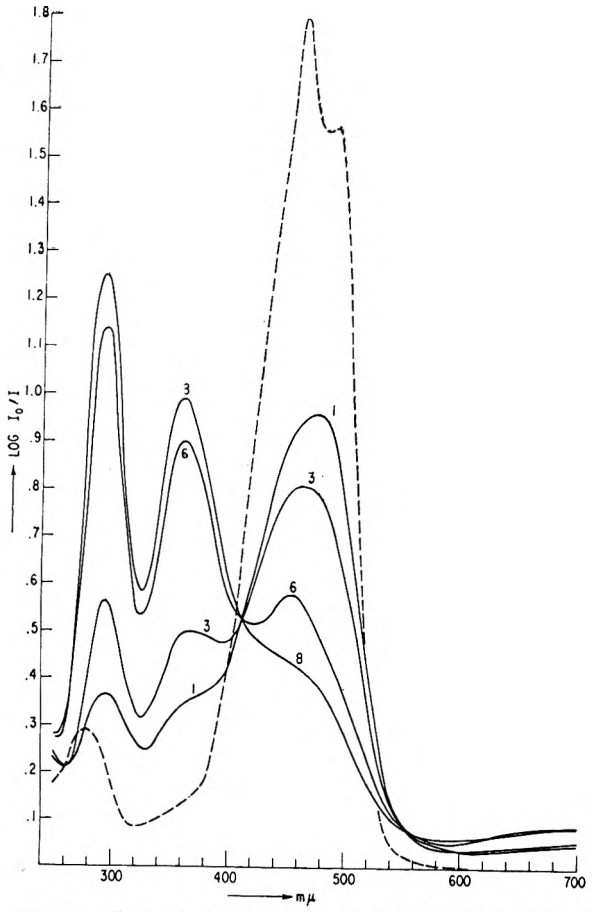

Fig. 2.—Spectra of solutions 1, 3, 6, and 8 from Table I immediately after preparation; ———, 1.5×10^{-5} *M* all-*trans* β-carotene in chloroform. All measurements were made at room temperature in a cell of 1 cm.

black solid (fraction IB) was washed with petroleum ether and dried.

Iodine analysis of the original sample (I) and of the fractions IA and IB gave these results:

Calcd. for	$C_{40}H_{56}I_3$	41.5% I_2
Found:	Sample I	38.8%
	Sample IA	40.4%
	Sample IB	39.4%

These values suggest that some unreacted carotene was present in sample I. Furthermore, the treatment with benzonitrile has effected a separation of the compounds present in sample I. There is no reason to believe that the separation is complete; in fact, fraction IA is somewhat soluble in benzonitrile. Optical spectra of the fractions dissolved in chloroform show clearly the different nature of the compounds.

The spectra of samples I and IA exhibit the characteristics of β-carotene solutions to which catalytic amounts of iodine have been added.[7,8] Apparently, dissociation of the compound takes place in dilute solution. Absorptions of iodine are not found, probably because its band at 5000 Å. has an extinction coefficient of about 1000 compared to that of β-carotene which is between 50,000 and 100,000 at 4600 Å. in these solutions.[7,3] The iodine absorption probably is hidden in the tail of the carotene band. Fraction IB is completely different. The bands at 2920 and 3600 Å. might be due to carotene isomers, the I_3^- ion,[9] or a charge transfer complex. Roughly, the spectra indicate that sample I is a mixture of about 70% of fraction IA and about 30% of fraction IB.

Difficulties with the purity of the sample such as described could be avoided completely by preparing the compound in a slightly different way. This consists of using a solution of iodine and potassium iodide in water rather than using solid iodine.

Potassium iodide (2 g.) and iodine (0.5 g.) were dissolved in 25 ml. of distilled water. All-*trans* β-carotene (1.5 g.) was dissolved in 120 ml. of chloroform. The aqueous iodine solution was added in about 1 min. to the stirred β-carotene solution. After 30 min. at room temperature, another 50 ml. of distilled water was added and the two layers were separated. The chloroform solution, containing the compound in suspension, was filtered and the solid was washed with petroleum ether until the filtrate was colorless. Finally, the sample was dried *in vacuo* over Drierite. During this period the compounds lost a little iodine: yield 0.8 g.

Prepared in this way, the sample (II), in chloroform solution, shows an absorption spectrum identical with that of fraction IA. (Fig. 2, curve 1.) The compound has no sharp melting point; decomposition sets in at about 125°. The iodine content was found to be 41.9%.

In the course of time, the compound decomposes slowly. The originally copper-colored, microcrystalline solid turns black. Treatment of an "aged" sample with a polar solvent gives a green solution and a residue of the original complex. The green extract obtained from an "aged" sample has the characteristics of fraction IB.

Under the conditions of the synthesis, apparently, a weak complex is precipitated from a rather concentrated solution; it dissociates when redissolved. If it is assumed that in solution the following equilibrium exists

$$C_{40}H_{56} + xI_2 \longleftrightarrow C_{40}H_{56} \cdot xI_2$$

then addition of excess iodine will shift the equilibrium to the right.

Spectra taken of sample II to which excess of iodine was added showed a decreasing intensity of the carotene absorption (see Table I). At the same time bands at 2920 and 3600 Å.[1] become more intense (Fig. 2). The spectra are corrected for the absorptions of the excess of iodine. Similar spectra would have been obtained if solutions of iodine of the corresponding concentrations had been used as reference instead of pure chloroform.

Discussion

The spectrum of fraction IB shows no characteristics of carotene but it has the bands at 2920 and 3600 Å. Since these absorptions are rather weak in this fraction, it might be that the fraction still is not pure or that it did not dissolve completely

(7) L. Zechmeister and A. Polgar, *J. Am. Chem. Soc.*, **65**, 1522 (1943).

(8) L. Zechmeister, *Chem. Rev.*, **34**, 267 (1944).

(9) T. L. Gilbert, R. R. Goldstein, and L. M. Lowry, *J. Chem. Soc.*, 1092 (1931); A. I. Popov and R. F. Swensen, *J. Am. Chem. Soc.*, **77**, 3724 (1955).

in chloroform but formed a suspension of very small particles. Finally, fraction IB could be a complex derived from another carotene isomer. As mentioned earlier, the pure complex changes slowly in the course of time, resulting in a product similar to that found in sample I which was prepared by using solid iodine.

Experimental results indicate that the compound (sample II) between β-carotene and iodine is a charge transfer complex rather than a product resulting from iodine addition to the double bonds in the carotene molecule. Such iodinated compounds would not dissociate into their components upon dissolution in chloroform. The absorption maximum of iodinated β-carotene should be found at shorter wave lengths because of shortening of the conjugated chain. This was found indeed by Savinov and Tretyakova.[6] Such a shift is of the order of a few hundred Ångstroms only and the shifted absorptions cannot be correlated to the new bands at 2920 and 3600 Å. These bands cannot be assigned to iodine either, since the absorptions of iodine in this region are of very low intensity and of completely different character. Also a comparison of the infrared spectra of β-carotene triiodide and hexyl iodide showed that there is no absorption in the spectrum of the complex that can be assigned to a carbon–iodine bond.[10]

TABLE I

DETAILS OF SPECTRA TAKEN FROM A 1.5×10^{-5} *M* SOLUTION OF SAMPLE II IN CHLOROFORM USING A 1-CM. CELL

Iodine concentrations are in moles/l.

Soln. no.	Concn. of added iodine	Log I_0/I 4600 Å.	3600 Å.	2920 Å.
1		0.92	0.34	0.36
2	3×10^{-5}	.85	.43	.43
3	6×10^{-5}	.81	.49	.57
4	1.2×10^{-4}	.72	.63	.75
5	2.4×10^{-4}	.60	.78	.93
6	3.6×10^{-4}	.52	.90	1.14
7	4.8×10^{-4}	.45	.95	1.19
8	6.0×10^{-4}	.42	.99	1.25

The fact that there is an isosbestic point at 4125 Å. in the spectra (Fig. 2) clearly indicates that there is an equilibrium between two absorbing species with overlapping absorptions. Apparently, the absorptions of iodine, originating from dissociation of the complex, at this wave length and at these concentrations, are too weak to influence the isosbestic point. Although for simplicity's sake only four of the spectra are given in Fig. 2, it should be mentioned that the four other curves (2, 4, 5, and 7) also go through that same point at 4125 Å.

Probably there is a second isosbestic point at about 5550 Å. arising from overlap between an absorption band of the complex with λ_{max} 8200 Å.[10] and that of β-carotene. However, the point is so little different from the "background" that it could not be determined very accurately.

From the experimental results presented here, one can conclude that treatment of β-carotene with iodine initially leads to a charge transfer complex. In the course of time, isomerization[7,8] as well as iodination of the carotene will take place.[6] Further work on this system will give more information about the equilibrium and also about the species represented as $C_{40}H_{56}I_3$ or, better perhaps, as $(C_{40}H_{56}I_3)_n$. In a later paper we expect to prove or disprove whether the absorption bands at 2920 and 3600 Å. are due to the I_3^- ion.[9]

Acknowledgments.—The authors wish to thank Dr. O. H. LeBlanc for many discussions on the subject and Mr. and Mrs. O. Sovers for their help with the translation of one of the references.

(10) O. Sovers, unpublished work.

AN INFRARED STUDY OF A SILICA–ALUMINA SURFACE

BY MICHAEL R. BASILA

Gulf Research & Development Company, Pittsburgh, Pennsylvania

Received May 21, 1962

In highly dehydrated samples of silica–alumina a single band is observed in the OH stretching region. The results imply that a single surface hydroxyl group type attached to silicon atoms predominates in these samples. The interaction of water with the surface of highly dehydrated silica–alumina is investigated, and it is established that fixedly adsorbed water is held on acidic sites far enough removed from surface hydroxyl groups that hydrogen-bonding to these groups does not occur. The bands in the silica–alumina spectrum from 4000–1000 cm.$^{-1}$ are tentatively assigned, including one which is thought to be due to the AlO linkage in an acidic surface group.

Introduction

In recent years, spectroscopic techniques have been applied to the direct examination of functional groups on the surface of solids. The most studied functional groups have been surface hydroxyl groups. Eischens and Pliskin[1] have given an excellent review of the work done prior to 1957. Recently, surface hydroxyl groups have been studied on a number of solids; *viz.*, silica and porous glass,[2–8] γ-alumina,[9] and titanium dioxide.[10] A

(1) R. P. Eischens and W. A. Pliskin, "Advances in Catalysis," Vol. 10, Academic Press, Inc., New York, N. Y., 1958, pp. 1–56.

(2) R. S. McDonald, *J. Phys. Chem.*, **62**, 1168 (1958).

(3) G. J. Young, *J. Colloid Sci.*, **13**, 67 (1958).

(4) A. Terenin and V. Filimonov, "Hydrogen Bonding," Pergamon Press, Inc., New York, N. Y., 1959, p. 545.

(5) A. N. Sidorv, *Optika i Spektroskopiya*, **8**, 806 (1960).

(6) (a) M. Folman and D. J. C. Yates, *Proc. Roy. Soc.* (London), **A246**, 32 (1958); (b) *J. Phys. Chem.*, **63**, 183 (1959).

(7) M. R. Basila, *J. Chem. Phys.*, **35**, 1151 (1961).

(8) J. A. Hockey and B. A. Pethica, *Trans. Faraday Soc.*, **57**, 2247 (1962).

(9) J. B. Peri and R. B. Hannan, *J. Phys. Chem.*, **64**, 1526 (1960).

(10) D. J. C. Yates, *ibid.*, **65**, 746 (1961).

preliminary observation of the surface hydroxyl groups on silica–alumina was reported by Roev, *et al.*[11] Most of the work has been concerned with the surface hydroxyl groups on silica and it is now well established that they behave very much like molecular hydroxyl groups. In general, however, the hydrogen-bonded shifts of the OH stretching vibration are considerably larger for the surface hydroxyl groups than for molecular hydroxyl groups with the same donor.[2,7] Peri and Hannan[9] have shown that there are three independent surface hydroxyl groups on γ-alumina in contrast to the one type observed on silica. Roev, *et al.*, have indicated that a single band in the OH stretching region occurs at 3750 cm.$^{-1}$ in the silica–alumina spectrum.[11] In the light of the γ-alumina results, it was of interest in this Laboratory to study the surface hydroxyl groups on silica–alumina in greater detail.

The rates of cracking,[12] isomerization,[12] and deuterium exchange[13] for hydrocarbons over a silica–alumina cracking catalyst are markedly affected by the presence of residual bound water in the catalyst. For example, the rate of exchange between isobutane and deuterated silica–alumina is increased by a factor of 13 to 20 by the prior irreversible readsorption of a small amount of D_2O.[13] However, if more than the optimum amount is readsorbed, an abrupt drop in the exchange rate occurs.[13] Similar effects are reported for the cracking and isomerization of a 2-methylpentane over silica–alumina.[12]

In this paper the results of infrared spectroscopic investigations of a commercial silica–alumina cracking catalyst are reported. These studies were primarily concerned with the nature of the surface hydroxyl groups and of the irreversibly readsorbed H_2O. The gradual dehydration from room temperature to 500° also was studied.

Experimental

Materials.—The synthetic silica–alumina (SA) was a sample of American Cyanamid Aerocat Triple A which contained 25% alumina by weight on a dry basis. The surface area of the SA determined by N_2 adsorption was 430 m.^{2}/g. A portion of the SA was base exchanged (KSA) by soaking the uncalcined material in a 1.5 *M* aqueous solution of potassium acetate for approximately 48 hr. Chemical analysis indicated the addition of 0.21 mole of potassium per mole of aluminum. The alumina content relative to silica remained the same. The fraction of the aluminum on the surface of SA was estimated by contacting a sample of uncalcined SA which had particle diameters less than 44 μ with a 1 *N* aqueous HNO_3 solution for 1 hr. followed by thorough washing. The decrease in aluminum content amounted to 0.33 mole per mole of aluminum. The surface area of the uncalcined SA was 430 m.^{2}/g. before and 560 m.^{2}/g. after the treatment with acid. Assuming all of the dissolved aluminum to have been on the surface, one obtains a ratio of 0.63 mole of potassium per mole of surface aluminum. The possibility exists that aluminum other than that on the surface was dissolved.[14] Thus the above ratio is a minimal value and the true value may be considerably higher.

The amorphous silica (S) used was a sample of Cabosil obtained from Godfrey L. Cabot, Inc. The surface area was approximately 215 m.^{2}/g. The *p*-xylene and mesitylene were Eastman White Label materials and were used as received except for drying with P_2O_5 and degassing on the vacuum system.

Sample Preparation.—In order to facilitate handling and reduce the loss of transmission by scattering, the SA samples were pressed into thin wafers 25 mm. in diameter and 0.1 to 0.2 mm. thick. Pressures of the order of 8000 lb./in.^{2} were required. The concentration of SA in these samples was approximately 7 mg./cm.^{2}. The cell design was similar to that of Peri and Hannan[9] and the details need not be given here except to say that it was fitted with sodium chloride windows. The cell was not permanently mounted on the spectrometer, but was transferred back and forth between the spectrometer and the vacuum system for spectroscopic measurements and sample treatment, respectively. In these operations, the sample repositioning was adequately reproducible. For treatment at elevated temperature, the sample was moved to a section of the cell away from the windows around which a furnace was placed. The temperatures were controlled within ±10°.

The vacuum system was conventional, and was capable of evacuating the cell to pressures in the 10^{-6} mm. range.

All samples were calcined in pure oxygen at atmospheric pressure for approximately four hours at 500°. In the initial dehydration the temperature was raised slowly while the sample was continuously pumped. The rate was such that the temperature was raised from ambient to 500° over a period of 3 hr. Following calcination it was evacuated for at least 3 hr. at this temperature to a final pressure less than 10^{-5} mm. A sample so treated is called a dehydrated sample in the text.

Deuterated silica–alumina (DSA) was prepared by a cyclic process *in vacuo*. The sample was repeatedly exposed to D_2O vapors and evacuated between exposures. The process was continued until all of the absorption in the OH stretching region had disappeared. The sample then was dehydrated by the standard procedure.

Spectroscopic Technique.—All spectra were measured on a Perkin–Elmer Model 421 grating spectrophotometer. The instrument was continuously flushed with air from which the H_2O and CO_2 were removed. For most of the samples, it was necessary to attenuate the reference beam with screens to compensate for the loss of transmission through the sample by scattering. In all of the determinations the reference beam attenuation was necessary for the initial part of the scan only, in the region 4000–3000 cm.$^{-1}$. The break on the spectra of Fig. 1–6 indicates the point where the attenuating screen was removed from the reference beam. The spectral slit width of the instrument was of the order of 2 cm.$^{-1}$. The scanning rate was adjusted to cover the spectral region 4000–1250 cm.$^{-1}$ in 60 min.

Results and Discussion

Dehydrated SA.—The spectra from 4000–1000 cm.$^{-1}$ of SA and DSA dehydrated at 500° are given in Fig. 1. For comparison purposes the spectrum of dehydrated S is given in Fig. 2. The positions of prominent bands in these spectra are listed in Table I. The spectra of SA and S are seen to be very similar. This is to be expected since the SA sample is predominantly silica. The apparent background in the high frequency region of the SA spectra probably is due to scattering, since it steadily decreases with decreasing frequency. The primary differences between the SA and S spectra other than in relative intensities are the absence of the 3650 cm.$^{-1}$ band in SA and the absence of the 1394 cm.$^{-1}$ band in S. Most of the bands of SA in this frequency range can be assigned by comparison with existing assignments for the S spectrum. The most recent assignments in the regions of interest have been made by Benesi and Jones[15] and by McDonald.[2] The bands at 1638, 1868, and 1975 in the S spectrum have been assigned as

(11) L. M. Roev, V. N. Filimonov, and A. N. Terenin, *Optika i Spektroskopiya*, **4**, 328 (1958).

(12) S. G. Hindin, A. G. Oblad, and G. A. Mills, *J. Am. Chem. Soc.*, **77**, 535 (1955).

(13) R. G. Haldeman and P. H. Emmett, *ibid.*, **78**, 2922 (1956).

(14) L. B. Ryland, M. W. Tamele, and J. N. Wilson, "Catalysis," Vol. 7, Reinhold Publ. Corp., New York, N. Y., 1960, p. 48.

(15) H. A. Benesi and A. C. Jones, *J. Phys. Chem.*, **63**, 179 (1959).

an SiO overtone and two SiO combination bands, respectively.[15] The similarity in frequency and the absence of a deuterium isotope shift of the corresponding bands in the SA spectrum are consistent with this assignment, and it is hereby adopted.

TABLE I

COMPARISON OF BAND POSITIONS IN THE SPECTRA OF SILICA–ALUMINA AND SILICA

ν_{SA} (cm.$^{-1}$)	ν_{DSA} (cm.$^{-1}$)	ν_{S} (cm.$^{-1}$)
3745	2762	3747
..	..	3650
1975	1975	1975
1866	1866	1868
1633	1633	1638
1394	1394	..

McDonald has assigned the 3747 cm.$^{-1}$ band in the spectrum of dehydrated S to the OH stretching vibration of surface hydroxyl groups.[2] A similar band occurs in the SA spectrum at 3745 cm.$^{-1}$ and is undoubtedly an OH stretching vibration. This band also has been observed by Roev, *et al.*[11] Upon deuteration this band shifts to 2762 cm.$^{-1}$, being the only band to exhibit an isotope shift. Since it has been shown[16] that the total hydrogen content of SA or S can be exchanged for deuterium by the technique used in this work, none of the rema ning bands in the SA spectrum can involve a vibration of a hydrogen containing group. The frequency ratio, ν_H/ν_D, of 1.35 is very close to the value of 1.37 calculated for a diatomic molecule, indicating that the normal coördinate of the vibration is strongly localized in the OH group.

The occurrence of a single band in the OH stretching region is rather surprising. Two bands were expected corresponding to the two surface groups AlOH and SiOH. If hydroxyl groups were attached to the same fractions of surface Al and Si atoms, the ratio of surface SiOH to AlOH calculated on the assumption that the distribution of Al is uniform throughout the sample would be approximately 2.5. Thus, if both groups were present, each should give rise to a band of detectable intensity provided that the magnitudes of the absorption coefficients were roughly equal.

Peri and Hannan have shown that the γ-alumina spectrum has three bands in the OH stretching region at 3698, 3737, and 3795 cm.$^{-1}$ corresponding to three independent hydroxyl group types.[9] The factors giving rise to the three bands have not yet been determined so that there is no basis for predicting the frequency of the OH stretching vibration in the AlOH groups of SA. However, the middle frequency is close to the 3745 cm.$^{-1}$ observed in the SA spectrum suggesting the possibility that the OH stretching frequencies in the AlOH and SiOH groups lie close together so that they overlap strongly and give the appearance of a single band.

The estimated half band widths of 12 ± 1 and 10 ± 1 for the corresponding bands in the SA and S spectra, respectively, would require accidental degeneracy and thus tend to rule out this possibility, but not conclusively. These data suggest that one

(16) R. G. Haldeman and P. H. Emmett, *J. Am. Chem. Soc.*, **78**, 2917 (1956).

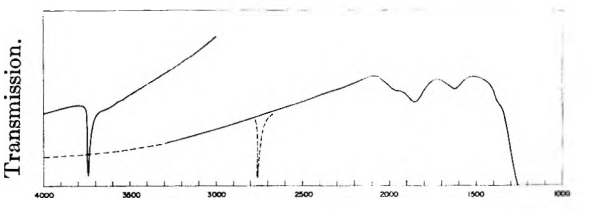

Fig. 1.—Silica–alumina dehydrated at 500°. The dashed lines indicate the spectrum of deuterated silica–alumina.

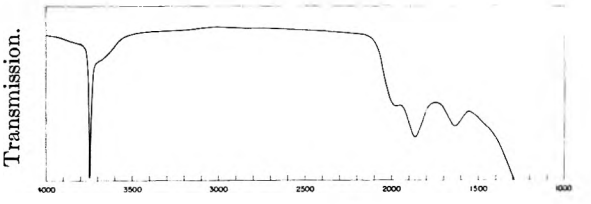

Fig. 2.—Silica dehydrated at 500°.

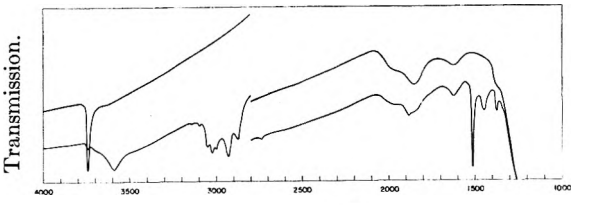

Fig. 3.—The interaction of *p*-xylene with dehydrated silica–alumina.

or the other of these group types is more easily dehydroxylated during the dehydration and that a single group type predominates in high degree of dehydration. On the basis of the frequency and half width of the band in the SA spectrum as compared to that in the S spectrum, the residual hydroxyl groups are tentatively identified as SiOH groups.

Additional supporting evidence is provided by the hydrogen-bonded frequency shifts ($\Delta\nu_{OH}$) of the 3745 cm.$^{-1}$ band which are observed when *p*-xylene and mesitylene are adsorbed on SA and S. In Fig. 3, the spectra of dehydrated SA before and after exposure to *p*-xylene vapor are given. The adsorption of *p*-xylene results in a very large increase in the background intensity. This is accompanied by a large decrease in the intensity of the 3745 cm.$^{-1}$ band and the appearance of a number of new bands. Most of these new bands are due to the physically adsorbed *p*-xylene and their frequencies are in quite good agreement with the corresponding frequencies in the spectrum of the pure liquid. The hydrogen-bonded OH stretching vibration is observed at 3591 cm.$^{-1}$. This band has very broad wings compared with the corresponding band in the S spectrum.[7] Similar results were obtained with mesitylene as the adsorbate, the hydrogen-bonded OH stretching vibration occurring at 3577 cm.$^{-1}$. The $\Delta\nu_{OH}$ values of 154 and 168 cm.$^{-1}$ for bonding with *p*-xylene and mesitylene, respectively, are in good agreement with values of 154 and 166 cm.$^{-1}$ previously obtained for S.[7] It should be mentioned that the $\Delta\nu_{OH}$ obtained for SA are single point

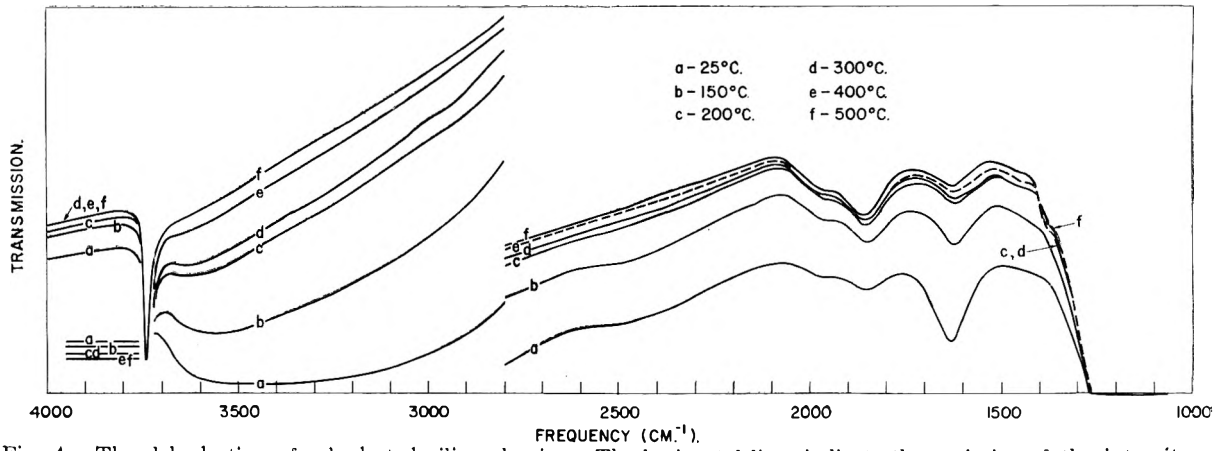

Fig. 4.—The dehydration of rehydrated silica–alumina. The horizontal lines indicate the variation of the intensity of the 3745 cm.$^{-1}$ band with dehydration temperature.

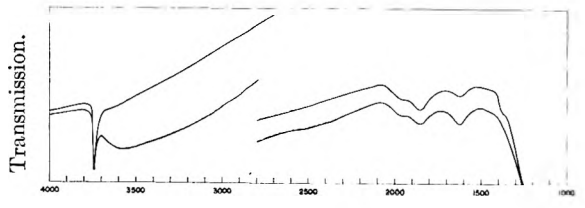

Fig. 5.—The irreversible readsorption of water at 150° on dehydrated silica–alumina.

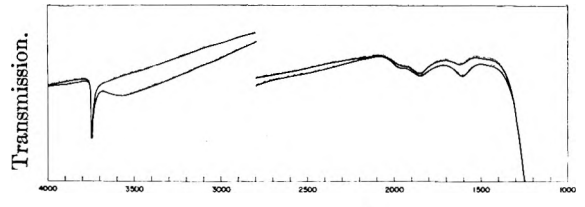

Fig. 6.—The irreversible readsorption of water at 150° on dehydrated potassium base exchanged silica–alumina.

measurements, whereas it has been shown that the magnitude of $\Delta\nu_{OH}$ depends on the fraction (f) of surface hydroxyl groups interacting.[7] The values given for S were obtained by extrapolation of a plot of $\Delta\nu_{OH}$ *vs.* f to $f = 1$.[7] However, in Fig. 3 the intensity of the 3745 cm.$^{-1}$ band is seen to be very small, so that $f \simeq 1$ and the results for SA are thought to be comparable with those for S.

Unfortunately, no $\Delta\nu_{OH}$ data are available for the hydroxyl groups on γ-alumina for comparison. Thus the $\Delta\nu_{OH}$ data are consistent with the assignment of the 3745 cm.$^{-1}$ band to the OH stretching vibration in the SiOH group, but do not provide conclusive evidence.

This assignment is supported by the results of O'Reilley, Leftin, and Hall.[17] These workers studied the proton magnetic resonance spectrum of SA and S. Their data indicate that the majority of protons occur in surface SiOH groups.[17] On the other hand, recent studies by Weiss, Knight, and Shapiro indicate that the ratio of AlOH to SiOH groups on SA increases with increasing dehydration.[18] This result was obtained by measuring the boron exchange of an SA sample which previously had been treated with diborane. It is based on the assumption that the reactions of diborane with the AlOH groups and SiOH groups of SA are the same as in the case of pure alumina and pure silica, respectively. These results would imply that the OH stretching vibrations in AlOH and SiOH are accidently, degenerate giving rise to the single band at 3745 cm.$^{-1}$. Thus, although most of the data appear to support the assignment of the 3745 cm.$^{-1}$ band to a single group type, the possibility of accidental degeneracy cannot be conclusively ruled out. The broad wings on the OH stretching vibration hydrogen-bonded to *p*-xylene or mesitylene may be relevant to these considerations.

The band at 3650 cm.$^{-1}$ in the spectrum of S has been assigned to hydrogen-bonded internal hydroxyl groups.[7] Earlier, it was pointed out that this band was not observed in the spectrum of SA, thus indicating the absence of these groups. This observation is in accord with the recent results of Hall.[19]

While this work was under way, a paper was published by Markova in which he presented a spectrum of a silica–alumina in the OH stretching region.[20] Bands were observed at 3765, 3650, and 3550 cm.$^{-1}$ in his spectrum. with the band at 3650 cm.$^{-1}$ the most intense.[20] In the light of the above discussion, the band at 3765 cm.$^{-1}$ undoubtedly corresponds to the band at 3745 in Fig. 1, while that at 3650 cm.$^{-1}$ is due to internal hydroxyl groups, and finally the band at 3550 cm.$^{-1}$ is due to hydrogen-bonded surface hydroxyl and adsorbed H_2O. Unfortunately, the details of his pretreatment were not given, so that it is difficult to compare his results with those obtained here.

All of the bands on the SA spectrum in the region 4000–1250 cm.$^{-1}$ have been assigned except the 1394 cm.$^{-1}$ band. This assignment will be considered later.

Dehydration.—The spectrum of dehydrated SA which has been rehydrated by exposure to 18 mm. of H_2O vapor for 5 hr. and evacuated for 1 hr.

(17) D. E. O'Reilley, H. P. Leftin, and W. K. Hall, *J. Chem. Phys.*, **29**, 970 (1958).

(18) (a) H. G. Weiss, J. A. Knight, and I. Shapiro, *J. Am. Chem. Soc.*, **81**, 1823 (1959); (b) **82**, 1262 (1960).

(19) W. K. Hall, private communication.

(20) Z. A. Markova, *Kinetika i Kataliz*, **2**, 435 (1961).

at room temperature is given in Fig. 4a. The spectrum of hydrated SA has bands at 3740, 3500 (very broad), 1975, 1866, and 1633 (broad) cm.$^{-1}$. This sample was subsequently dehydrated in stages at 150, 200, 300, 400, and 500°. At each of these temperatures spectra were obtained after 2 hr. evacuation. These spectra are given in Fig. 4b through f. The interpretation of these spectra is difficult because of the breadth of the 3500 cm.$^{-1}$ band and also because of the increase in background absorption over the entire spectral region. A similar large increase in background absorption is observed upon the adsorption of *p*-xylene or mesitylene as can be seen in Fig. 3. This latter phenomenon has been discussed by Roev, who attributes the background increase to extreme broadening of bands of the adsorbate or adsorbent.[21] This broadening is thought to be due to photodesorption which occurs when $h\nu > Q$, where $h\nu$ is the energy of the absorbed photon and Q is the heat of adsorption.[21]

In general, upon dehydration the band at 3745 cm.$^{-1}$ increases in intensity while those at 3500 and 1633 cm.$^{-1}$ decrease in intensity and finally disappear. The largest intensity decreases in the 1633 cm.$^{-1}$ band occur at 150 and 200°. Similar large decreases occur in the 3500 cm.$^{-1}$ band. This band is due to hydrogen-bonded OH stretching vibrations. The 1633 cm.$^{-1}$ band undoubtedly is due to the hydrogen-bonded HOH bending mode in H_2O, indicating that most of the changes in the 150 and 200° spectra are due to the desorption of strongly held physically adsorbed H_2O. The accompanying increase in the 3745 cm.$^{-1}$ band indicates at least part of the desorbed H_2O had been hydrogen-bonded to surface OH groups. The 200 and 300° spectra are essentially identical, except for small decreases in the 3500 and 1633 cm.$^{-1}$ regions which probably indicate removal of the final traces of physically adsorbed H_2O. Dehydration at 400° produces a relatively large decrease in the 3500 cm.$^{-1}$ band. This is accompanied by an increase in the intensity of the 3745 cm.$^{-1}$ band and a small general decrease in background in the rest of the spectrum. Dehydration at 500° produces a further small decrease in the 3500 cm.$^{-1}$ band and over the rest of the spectrum, but no detectable change in the 3745 cm.$^{-1}$ band. The changes in the spectra after dehydration at 400 and 500° may be due to the desorption of additional H_2O. This point will be discussed more fully in the next section.

The final point of interest in these spectra is the absence of the 1394 cm.$^{-1}$ band in hydrated SA. This band can be seen to redevelop in the 400 and 500° spectra.

Fixedly Adsorbed Water.—A sample of dehydrated SA was exposed to 12 mm. of H_2O vapor for 1 hr. and then evacuated for 1 hr., both at 150°. The H_2O retained by the sample has been called "fixedly adsorbed" by Haldeman and Emmett.[16] The influence of fixedly adsorbed H_2O on catalytic activity has been demonstrated.[12,13] The spectrum of SA before and after the addition of fixedly adsorbed H_2O is given in Fig. 5. It strongly resembles the spectrum in Fig. 4 of hydrated SA dehydrated at 150°. One important difference is observed, that being the absence of a significant change in the intensity of the 3745 cm.$^{-1}$ band. This fact implies that the H_2O is essentially immobile and that it is located on sites far enough removed from the SiOH groups to prevent hydrogen-bonding.

The same experiment was performed with a KSA sample. These spectra are shown in Fig. 6. The new bands which are observed in the spectrum of KSA upon the addition of fixedly adsorbed H_2O are the same as those observed in the SA spectrum, but their intensities are greatly diminished.

The appearance of bands at 3500 (very broad) and 1633 cm.$^{-1}$ (hydrogen-bonded OH stretching and HOH bending vibrations, respectively) upon the addition of fixedly adsorbed H_2O indicates that the adsorbed species has not undergone drastic chemical alteration. The large decrease in intensity of the bands in the KSA as compared to the S spectra suggests that the H_2O is held on catalytically active sites which can be deactivated by the addition of K. This result differs somewhat from the findings of Haldeman and Emmett, who found no change in the amount of H_2O fixedly adsorbed at 110° on SA or KSA.[16] On the other hand, the observed increase in the deuterium exchange rate upon the addition of fixedly adsorbed H_2O to KSA at 150° amounted to only a small fraction of that observed on regular SA,[13] which is consistent with the above observation.

It is noteworthy that the 1394 cm.$^{-1}$ band disappears upon the addition of fixedly adsorbed H_2O to SA and that it is absent in the spectrum of dehydrated KSA.

The absence of an intensity decrease in the 3745 cm.$^{-1}$ band upon the addition of fixedly adsorbed H_2O suggests an alternate interpretation of the spectral changes in the final stages of dehydration at 400 and 500° in Fig. 4 which are accompanied by an intensity decrease in this band. These data imply that surface hydroxyl groups which had been hydrogen-bonded to surface SiOH groups are being removed. If this were the case, then the rehydration of SA must result in some regeneration of OH groups. The identity of these groups is unknown. McDonald has observed similar changes in the dehydration and rehydration of S.[2]

At this point it is of interest to consider the assignment of the 1394 cm.$^{-1}$ band. The following observations summarize the behavior of the 1394 cm.$^{-1}$ band: it is absent in the spectra of dehydrated S and KSA; it occurs in the spectrum of dehydrated SA; it is absent in the spectrum of hydrated SA, but appears upon dehydration between 300 and 500°; it disappears upon addition of fixedly adsorbed H_2O; it does not exhibit an isotope shift upon deuteration of SA. The behavior of this band upon the addition of mesitylene or *p*-xylene cannot be determined because of the overlapping bands of these adsorbates; however, it is known that the band disappears upon the chemisorption of pyridine.[22] The sensitivity of this band to presence of an adsorbate indicates

(21) L. M. Roev, *Doklady Akad. Nauk SSSR*, **133**, 561 (1960).

(22) M. R. Basila, unpublished results.

that it is associated with a surface group. The absence of a deuterium isotope shift indicates that it is not a hydrogen containing group. The frequency of the band is in a range which could be assigned to an AlO vibration, possibly an overtone or combination band. The disappearance upon the addition of an adsorbate suggests a shift to lower frequency where it cannot be observed due to overlapping with the strong SiO fundamental.

The absence of the band in dehydrated KSA implies that it is associated with acidic sites on SA which can be poisoned by K. On the basis of these observations, this band is tentatively assigned to a vibration of a surface AlO group, probably an overtone or combination band. If this interpretation were correct, it would be consistent with the suggestion that the acidic surface Al atom changes coördination number from four to five upon interaction with an H_2O adsorbate molecule, since the AlO force constant would be smaller for the higher coördination number.[23]

TABLE II

ASSIGNMENT OF THE BANDS IN THE DEHYDRATED SILICA–ALUMINA SPECTRUM

ν (cm.$^{-1}$)	Assignment
3745	OH stretch in surface SiOH groups
1975	SiO combination
1866	SiO combination
1633	SiO overtone
1394	Surface AlO overtone or combination (?)

The assignments of the bands in the region 4000–1250 cm.$^{-1}$ in the spectrum of dehydrated SA are reviewed in Table II.

Conclusions

The foregoing discussion of the spectroscopic data has led to the following tentative conclusions:

1. In highly dehydrated samples, the surface hydroxyl groups are predominantly attached to silicon atoms.
2. The fixedly adsorbed water added at 150° is held on acidic surface sites which can be poisoned by K.
3. The fixedly adsorbed water added at 150° retains its molecularity and is located on sites far enough removed from the surface hydroxyl groups that essentially no hydrogen-bonding to these groups occurs.
4. A weak band located at 1394 cm.$^{-1}$ may be due to a vibration of the AlO linkage, possibly an overtone or combination, in acidic surface groups.

Acknowledgments.—The author is grateful to Mr. T. R. Kantner for assistance with the experimental work, and to Dr. D. S. MacIver for several informative discussions.

(23) Reference 14, p. 45.

EQUILIBRIA IN ETHYLENEDIAMINE. II. HYDROGEN ELECTRODE STUDIES OF SOME ACIDS AND SODIUM SALTS[1]

BY STANLEY BRUCKENSTEIN AND L. M. MUKHERJEE[2]

School of Chemistry, University of Minnesota, Minneapolis, Minn.

Received May 21, 1962

Hydrogen electrode studies of a series of pure acid solutions have yielded the dissociation constants of four phenols relative to hydrochloric acid. The behavior of these phenols indicates that the reaction $HX + X^- = HX_2^-$($K_{HX_2^-}$) occurs. Values of $K_{HX_2^-}$ found were 15 (phenol), 7 (thymol), 40 (*o*-phenylphenol), and 46 (*p*-phenylphenol). Studies of the acid–sodium salt mixtures permitted the determination of the relative dissociation constants of these salts. The pH of various sodium salts has been found to be independent of concentration and has yielded another means of determining the relative dissociation constants for various acids. The results obtained for $pK_{MX} - pK_{HCl}$ are 5.40 (thymol), 4.35 (*o*-phenylphenol), 4.30 (phenol), 4.20 (*p*-phenylphenol), 2.05 (sodium thymolate), 2.10 (sodium *o*-phenylphenolate), 0.10 (phenylacetic acid), −0.35 (3-methyl-4-phenylazophenol), −0.60 (hydrobromic acid), and ∼ −1.4 (hydriodic acid). The value of K_{NaX}/K_{HX} for thymol is 2.1×10^3 and 2.1×10^2 for *o*-phenylphenol. The difference between the negative logarithm of the autoprotolysis constant of EDA and that of the sodium salt of EDA is 7.0.

Introduction

A large number of compounds have been determined by titration as acids in ethylenediamine (EDA) as solvent using potentiometric methods to detect the equivalence point.[3] However, only one quantitative potentiometric equilibrium study of an acid and its conjugate base in EDA has been reported in the literature,[4] despite the fact that such studies are necessary to assess the limitations and advantages of EDA as a solvent for acid–base titrations. In this study, Schaap and coworkers titrated hydrogen bromide with sodium ethanolamine in the presence and absence of excess sodium bromide and were able to explain their results satisfactorily in terms of the ion-pair dissociation constants of hydrobromic acid, sodium bromide, and sodium ethanolamine using 5×10^{-16} as the autoprotolysis constant (K_S) of EDA. Earlier potentiometric[5] and conductometric[6] stud-

(1) This work was supported by the Office of Ordnance Research, U. S. Army.

(2) From a thesis submitted by L. M. Mukherjee to the Graduate School of the University of Minnesota in partial fulfillment of the requirements for the degree of Doctor of Philosophy, August, 1961.

(3) (a) M. L. Moss, J. H. Elliot, and R. T. Hall, *Anal. Chem.*, **20**, 784 (1948); (b) M. Katz and R. A. Glenn, *ibid.*, **24**, 1157 (1952); (c) V. Z. Deal and G. E. A. Wyld, *ibid.*, **27**, 47 (1955); (d) A. J. Martin, *ibid.*, **29**, 79 (1957); (e) H. Brockman and E. Meyer, *Naturwissenschaften*, **40**, 242 (1953); (f) H. Brockman and E. Meyer, *Chem. Ber.*, **87**, 81 (1954).

(4) W. B. Schaap, R. E. Bayer, J. R. Siefker, J. L. Kim P. W. Brewster, and F. C. Schmidt, *Rec. Chem. Progr.*, **22**, 197 (1961).

ies in EDA have shown that ion-pair formation is extensive, as would be expected for a solvent with a dielectric constant of 12.9. In this work, classical potentiometric methods employing the cell

Reference electrode (S.C.S.E. [2,5])	HX(C_{HX}) and/or NaX(C_{NaX}) in EDA	H_2 (1 atm.), Pt	(I) (1)

have been used to study solutions of acids, acids and their sodium salts, and sodium salts. These data permit the calculation of the pK values of a number of acids and sodium salts relative to that of hydrochloric acid and demonstrate that a simple ion-pair approach cannot explain the behavior of phenols.

Theory

Equilibria in HX Solutions.—From the previous[2,5] potentiometric study of silver salts in EDA it was anticipated that the equilibrium (2a) would describe

$$HX \rightleftarrows H^+ + X^- \qquad (2a)$$

the behavior obtained with acids using cell I. This proved to be the case for hydrochloric acid and for four different phenols in dilute solution, but in more concentrated phenol solutions the additional reaction (2b) must be considered to interpret the experimental results adequately.

$$HX + X^- \rightleftarrows HX_2^- \qquad (2b)$$

The thermodynamic equilibrium constants for reactions 2a and 2b are

$$K_{HX} = a_{H^+}a_{X^-}/a_{HX} \qquad (3a)$$

and

$$K_{HX_2^-} = a_{HX_2^-}/a_{HX}a_{X^-} \qquad (3b)$$

where H^+ is used to represent the solvated proton in EDA. At 25°, the e.m.f. of cell I is given by

$$E = E_{SCSE} + 0.05916 \log a_{H^+} \qquad (4a)$$

where[7]

$$E_{SCSE} = E_{l.j.} + E_{Ref.\ Electrode} \qquad (4b)$$

and the standard potential of the hydrogen electrode is assumed to be zero. Assuming that $E_{l.j.}$ is constant and that the activity coefficients of all univalent ions are the same, while that of HX is one, substitution of eq. 3a and 3b into the rule of electroneutrality for pure acid solutions (4c) yields an expression for a_{H^+} which may be substituted into eq. 4a to yield eq. 5a at 25°.

$$[H^+] = [X^-] + [HX_2^-] \qquad (4c)$$

$$E_{HX} = E_{SCSE} + 0.0296 \log K_{HX} + 0.0296 \log [C_{HX}(1 + K_{HX_2^-}C_{HX})] \qquad (5a)$$

C_{HX} is the equilibrium concentration of undissociated HX. Three limiting cases of eq. 5a are considered below.

1. K_{HX} Very Small.—If K_{HX} is very small, the analytical concentration of HX, $(C_{HX})_t$, differs negligibly from the equilibrium concentration, C_{HX}, and the former may be substituted for the latter in eq. 5a.

At low acid concentrations $1 >> K_{HX_2^-}C_{HX}$, and 5a becomes

$$E_{HX} = E_{SCSE} + 0.0296 \log K_{HX}(C_{HX})_t \qquad (5b)$$

and a plot of E_{HX} *vs.* log $(C_{HX})_t$ has a slope of 0.0296. Eq. 5b also is applicable at all concentrations for those acids which have no tendency to form HX_2^- ions, such as hydrochloric acid.

At high concentrations of acid, if $K_{HX}C_{HX} >> 1$, eq. 5a becomes

$$E_{HX} = E_{SCSE} + 0.05916 \log (K_{HX}K_{HX_2^-})^{1/3}(C_{HX})_t \qquad (5c)$$

A plot of E_{HX} *vs.* log $(C_{HX})_t$ has a slope of 0.05916. This result corresponds to the dissociation $2HX \rightleftarrows H^+ + HX_2^-$ and is similar to that found previously[5] with silver cyanide in EDA. In the concentration range where $K_{HX_2^-} \simeq (C_{HX})_t$, the slope of the plot of E_{HX} *vs.* log $(C_{HX})_t$ is intermediate between 0.0296 and 0.05916.

Evaluation of $K_{HX_2^-}$.—From eq. 5a, 5b, and 5c, it follows that the intersection of the two limiting slopes occurs at $(C_{HX})_t = 1/K_{HX_2^-}$. Behavior of this sort has been observed with four phenols.

A more rigorous procedure for evaluating $K_{HX_2^-}$ uses the method of least squares by transforming eq. 5a to eq. 5d

$$\frac{10^{E_{HX}/0.0296}}{C_{HX}} = K_{HX}\,10^{E_{SCSE}/0.0296} + 10^{E_{SCSE}/0.0296}K_{HX}K_{HX_2^-}C_{HX} \qquad (5d)$$

Thus a plot of $10^{E_{HX}/0.0296}/C_{HX}$ *vs.* C_{HX} is a straight line. $K_{HX_2^-}$ is the ratio of the slope to the intercept for eq. 5d.

2. K_{HX} Very Large.—If K_{HX} becomes very large, $a_{H^+} \approx (C_{HX})_t$ and a plot of E *vs.* log $(C_{HX})_t$ would approach a limiting slope of 0.05916 v.; thus the observed e.m.f.'s would exceed those found with all other acids. This behavior has not been observed in EDA and would not be expected in a solvent with a dielectric constant of 12.9, except in very dilute solution. True strong acid behavior is to be distinguished from pseudo strong acid behavior arising from HX_2^- formation on the basis of the magnitude of the observed e.m.f. values.

3. K_{HX} Intermediate in Value, $K_{HX_2^-}$ Very Small.—EDA is a very basic solvent and levels acids with a $(pK_{HX})_{H_2O} \lesssim 5.00$. One criterion used for leveling is the inability to distinguish a difference of acid strength on the basis of potentiometric measurements. In a solvent such as EDA,

(5) S. Bruckenstein and L. M. Mukherjee, *J. Phys. Chem.*, **64**, 1601 (1960).

(6) (a) W. H. Bromley and W. F. Luder, *J. Am. Chem. Soc.*, **66**, 107 (1944); (b) B. B. Hibbard with F. C. Schmidt, *ibid.*, **77**, 225 (1955).

(7) The notation used is analogous to that used previously.[5]

leveling corresponds to the virtually complete conversion of the non-ionized acid to the ion-pair according to

$$HS + HX \rightleftarrows HSH^+X^- \qquad (6a)$$

while the hydrogen ion concentration is determined by the dissociation reaction

$$HSH^+X^- \rightleftarrows HSH^+ + X^- \qquad (6b)$$

where HS = EDA. Defining the equilibrium constants for reactions 6a and 6b as K_i^{HX} and K_d^{HX}, respectively, it has been shown[8] that

$$K_{HX} = K_d^{HX}K_i^{HX}/(1 + K_i^{HX}) \qquad (6c)$$

The value of K_d^{HX} depends upon steric factors but would not be expected to vary widely for different acids. K_d^{HX} is estimated to be between 10^{-3} and 10^{-4} using the Bjerrum ion-pair relations. Thus, for leveled acids, $K_i^{HX} >> 1$, $K_{HX} \approx K_d^{HX}$, and it is not a good approximation to assume that $(C_{HX})_t = C_{HX}$ when $K_d^{HX} \approx 10^{-3}$ because appreciable dissociation will occur. If $1 >> (C_{HX} \cdot K_{HX_2^-})$, the slope of a plot of E *vs.* log C_{HX} will be between the limiting slope of 0.0296 for a very weak electrolyte and 0.05916 for a strong electrolyte. In addition, E_{HX} for leveled acids will be more positive than for non-leveled acids. Three acids, hydrochloric, acetic, and phenylacetic, were studied anticipating behavior of the type outlined above. The results obtained with these acids indicate the model used probably is an oversimplification in EDA and every acid must be considered individually.

For those acids whose behavior is described by eq. 5d, $pK_{HX} - pK_{HX'}$ is obtained from the difference of the logarithm of the intercepts obtained with the two acids HX and HX'.

Equilibria in HX–NaX Solutions.—E.m.f. measurements obtained with cell I using solutions containing NaX and HX (thymol and *o*-phenylphenol) have been interpreted in terms of reactions 2a and 2b, and the equilibria

$$NaX \rightleftarrows Na^+ + X^- \qquad (7a)$$

$$HS \rightleftarrows H^+ + S^- \qquad (7b)$$

$$NaS \rightleftarrows Na^+ + S^- \qquad (7c)$$

The corresponding equilibrium constants are

$$K_{NaX} = \frac{a_{Na^+}a_{X^-}}{a_{NaX}} \qquad (8a)$$

$$K_S = a_{H^+}a_{S^-} \qquad (8b)$$

and

$$K_{NaS} = \frac{a_{Na^+}a_{S^-}}{a_{NaS}} \qquad (8c)$$

The rule of electroneutrality in a mixture of an acid and its sodium salt is

$$[H^+] + [Na^+] = [S^-] + [X^-] + [HX_2^-] \qquad (9)$$

Using eq. 9 and assuming the activity coefficients of all univalent ions to be the same and those of the undissociated species to be unity, it follows from eq. 2a, 2b, 8a, and 8b that

$$a_{H^+} = \sqrt{\frac{K_S + K_{HX}C_{HX}(1 + K_{HX_2^-}C_{HX})}{1 + \frac{K_{NaX}C_{NaX}}{K_{HX}C_{HX}}}} \qquad (10a)$$

For any EDA solution of an acid which can be titrated successfully with base, in the absence of excess NaS, K_S is negligibly small as compared to the second term in the numerator of eq. 10a. In the experiments reported below with thymol and *o*-phenylphenol, $K_{NaX} >> K_{HX}$ and $1 \ll K_{NaX}C_{NaX}/K_{HX}C_{HX}$; therefore

$$a_{H^+} = K_{HX}C_{HX}\sqrt{\frac{1 + K_{HX_2^-}C_{HX}}{K_{NaX}C_{NaX}}} \qquad (10b)$$

and the e.m.f. of cell I containing acid–salt mixtures is

$$E_{HX,NaX} = E_{SCSE} + 0.0296 \log \frac{K^2_{HX}}{K_{NaX}} + 0.0296 \log C^2_{HX}\left[\frac{1 + K_{HX_2^-}C_{HX}}{C_{NaX}}\right] \qquad (11a)$$

Under the experimental conditions used, analytical concentrations, C_t, may be used in place of equilibrium concentrations, and eq. 11a describes the behavior of mixtures of thymol and *o*-phenylphenol with their sodium salts.

For the purpose of treating the experimental data by the method of least squares, it is convenient to transform eq. 11a to 11b

$$\left\{\frac{C_{NaX}}{C^2_{HX}}\right\} 10^{E_{HX,NaX}/0.0296} = 10^{E_{SCSE}/0.0296}\left\{\frac{K^2_{HX}}{K_{NaX}}\right\} + 10^{E_{SCSE}/0.0296}\left\{\frac{K_{HX_2^-}K^2_{HX}C_{HX}}{K_{NaX}}\right\} \qquad (11b)$$

Thus, a plot of $(C_{NaX}/C^2_{HX})10^{E_{HX,NaX}/0.0296}$ *vs.* C_{HX} is a straight line. As in the case of eq. 5d, $K_{HX_2^-}$ is the ratio of the slope to the intercept, while the ratio of the intercept (or slope) of eq. 5d to the intercept (or slope) of eq. 11b yields K_{NaX}/K_{HX}.

Equilibria in NaX Solutions.—In EDA solutions of pure sodium salts, the principal reaction between NaX and solvent is

$$NaX + HS \rightleftarrows NaS + HX \qquad (12a)$$

The equilibrium constant for reaction 12a is the reciprocal of the formation constant, K_f^{NaX}, of the salt where

$$K_f^{NaX} = \frac{K_{HX}K_{NaS}}{K_{NaX}K_S} = \frac{a_{NaX}}{a_{NaS}a_{HX}} \qquad (12b)$$

The magnitude of K_f^{NaX} is such that the equilibrium

(8) I. M. Kolthoff and S. Bruckenstein, *J. Am. Chem. Soc.*, **78**, 1 (1956).

concentration of C_{HX} is very small, and $1 >> (K_{HX_2^-} \cdot C_{HX})$ in eq. 10b, *i.e.*, the formation of HX_2^- species is negligibly small. Also, the dissociation of NaS and HX is repressed by the dissociation of NaX and $C_{HX} = C_{NaS}$. Thus eq. 10b and 12b yield

$$a_{H^+} = \sqrt{\frac{K_{HX}K_S}{K_{NaS}}} \qquad (13a)$$

and

$$E_{NaX} = E_{SCSE} + 0.0296 \log \frac{K_{HX}K_S}{K_{NaS}} \qquad (13b)$$

This result, that the e.m.f. (or pH) of pure salt solutions is independent of the salt concentration, also was found in anhydrous acetic acid.[9]

The difference in pK of two acids, HX and HX′, whose sodium salts obey eq. 13b is given by

$$pK_{HX'} - pK_{HX} = \frac{E_{NaX} - E_{NaX'}}{0.0296} \qquad (13c)$$

Equation 13c yields results in good agreement with those found using eq. 5d. Using the relationships developed above, it is possible to determine the pK values of acids and their salts relative to one reference acid. In a subsequent paper, a potentiometric procedure for relating the relative equilibrium constants obtained with the hydrogen electrode to those obtained with the silver electrode[5] will be described. In addition, absolute values of dissociation constants based upon a spectrophotometric method will be reported.

The value of $pK_{NaS} - pK_S$ can be obtained by combining data obtained in pure acid solutions with those obtained in solutions of the sodium salt of the acid, *i.e.*, from eq. 13b

$$pK_S - pK_{NaS} = \log [\text{intercept eq. 5d}] - \frac{E_{NaX}}{0.0296} \qquad (14)$$

Experimental

Reagents.—Commercial 98% EDA was shaken with Linde Molecular Sieves (70 g./l.) of type 5A and then with a mixture of 50 g. of calcium oxide and 15 g. of potassiun hydroxide per liter of the solvent, followed by subsequent distillation of the supernatant liquid over a similar batch of molecular sieve in a current of dry and CO_2-free nitrogen. Although there was no improvement in the ultraviolet spectra, as compared to the previously reported procedure,[5] the water content of the fraction boiling at 117.2° was about 0.015 M after this treatment.

Ethylenediammonium Chloride.—EDA·2HCl was prepared by treating pure EDA with a slight excess of concentrated hydrochloric acid; the colorless crystals were repeatedly washed with hot absolute ethanol, air-dried, and, finally, dried *in vacuo* at 50°. Titration against a standard silver nitrate indicated the product to be 99.99% pure.

Acetic Acid.—Glacial acetic acid was fractionated over CrO_3 (10 g./l.); the fraction, b.p. 118.1°, having a water content of less than 0.01% w./v. was used.

Hydrogen.—National Cylinder Gas Co., Inc., hydrogen was passed through a Baker and Co. "Deoxo" purifier, a column of Ascarite, and then a column of Drierite before use.

Phenylacetic Acid.—A commercial product was recrystallized from ethanol–water mixture; m.p. 76–77°.

Phenols.—The compounds are listed below with their source, methods of purification, and melting (or boiling) points. Phenol (twice distilled, b.p. 181.4°), thymol (Mallinckrodt, m.p. 51–52°—dried at 30° *in vacuo*), *o*-phenylphenol (Eastman Kodak White Label, m.p. 56–57°—dried at 40° *in vacuo*), and *p*-phenylphenol (Eastman Kodak White Label—recrystallized from ethanol, m.p. 166–167°—dried at 110° *in vacuo*).

Sodium Phenolates.—The sodium salt of *o*-phenylphenol was purified by double recrystallization of the Eastman Kodak practical grade sample from acetone and then dried *in vacuo* at room temperature. The purity of the sample was found to be 100.35% by titration with standard sulfuric acid in aqueous solution using brom cresol green as the indicator.

The sodium salt of thymol was prepared by treating a solution of thymol in ether (which was pre-treated with sodium hydride) with sodium hydride at room temperature. The sodium hydride was added in several portions while stirring in a dry carbon dioxide-free nitrogen atmosphere; the salt-containing ether solution was filtered, evaporated *in vacuo* at room temperature, and finally dried at ~80° *in vacuo* to a constant weight. The purity of the sample used was estimated to be 97–98% by titration with standard sulfuric acid as above. A batch of the sodium salt of *o*-phenylphenol also was prepared by this method.

Sodium Phenylacetate.—The K and K commercial product—a solution—was evaporated to crystallization on a steam bath; the crystals were washed with absolute ethanol and dried *in vacuo* at 80°. Titration of the sample in glacial acetic acid against standard perchloric acid using crystal violet as indicator showed the product to be 100% pure.

3-Methyl-4-phenylazophenol and its Sodium Salt.—The indicator 3-methyl-4-phenylazophenol was an Eastman highest purity product, m.p. 107–109°; a known amount was treated with a slight excess of sodium hydroxide solution. The solution was evaporated nearly to dryness and taken up with ether. The ether solution was filtered, concentrated by evaporation, and allowed to crystallize. The dark reddish brown crystals were finally dried *in vacuo* at 80°.

Preparation of Solutions.—All glassware was heated *in vacuo* at 180° for about 10 hr., cooled, and stored in a desiccator until used. Solutions generally were prepared immediately before use in a dried volumetric flask using a technique similar to that described earlier.[5] If solutions were not used immediately, they were stored in dry, carbon dioxide-free atmosphere in a tightly stoppered volumetric flask. All manipulations had to be carried out in a dry-box free of carbon dioxide in order to obtain reproducible results. All concentrations were referred to the molar scale (M) and no temperature correction was made.

Potentiometric Methods. Reference Electrode.—The saturated corrosive sublimate electrode (S.C.S.E.) described earlier[5] was used.

H^+ Ion Indicator Electrodes.—A 1-in. long, 16 gage Pt wire sealed into a glass tube was coated with platinum black using a 2% chloroplatinic acid solution by electrolyzing at 5 ma. for 7 to 10 min. Electrodes then were cathodized in sulfuric acid solution and stored in this solution for at least 10 to 12 hr. Electrodes were checked in an aqueous buffer of pH 4.0 before use. All electrodes agreed to within ±0.2 mv. Immediately before use in EDA, the Pt electrodes were washed thoroughly with conductivity water, rinsed with acetone, and air-dried. Electrodes were used only once.

Hydrogen Electrode Half-Cell.—The half cell used was similar to that used earlier[5] except that a coarse, fritted glass, gas dispersion tube was sealed through the outer 34/45 standard taper joint and was used to saturate the EDA solution with H_2. A small capillary sealed to the outer joint served as a vent.

E.m.f. Determination.—The potentiometer and null detector have been described previously.[5]

The hydrogen electrode half-cell was filled and assembled in a drybox under a CO_2-free dry nitrogen atmosphere. The solutions were saturated immediately with hydrogen and the half-cell was placed in an air thermostat at 25 ± 0.1° until temperature equilibrium was attained. Then, the platinum electrode was introduced and the liquid junction formed. The hydrogen electrode half-cell contents were used as the bridge liquid to minimize errors due to diffusion. A current of hydrogen was allowed to stream through the solution for about 5 min. before taking the first e.m.f.

(9) S. Bruckenstein and I. M. Kolthoff, *J. Am. Chem. Soc.*, **78**, 2974 (1956).

TABLE I

SUMMARY OF HYDROGEN ELECTRODE RESULTS OBTAINED IN SOLUTIONS OF FOUR PHENOLS

Acid, HX	Eq. 5d least squares constants[a] Intercept × 10^{24}	Slope × 10^{24}	K_{HX_2}[a]	$pK_{thymol} - pK_{ArOH}$ EDA	Water[b]
p-Phenylphenol	0.155 (0.0280)	7.11 (1.39)	45.9 (15.7)	1.21	0.98
o-Phenylphenol	0.115 (0.0505)	7.51 (3.95)	65.1 (59.8)	1.08	0.52
Phenol	0.117 (0.0458)	1.77 (0.806)	15.1 (11.6)	1.09	0.54
Thymol	0.00935 (0.00211)	0.109 (0.0380)	11.7 (6.1)	0.00	0.00

[a] The standard deviation of the tabulated value follows in parentheses. [b] EDA data at 25.0°, water data at 22.5°.[10]

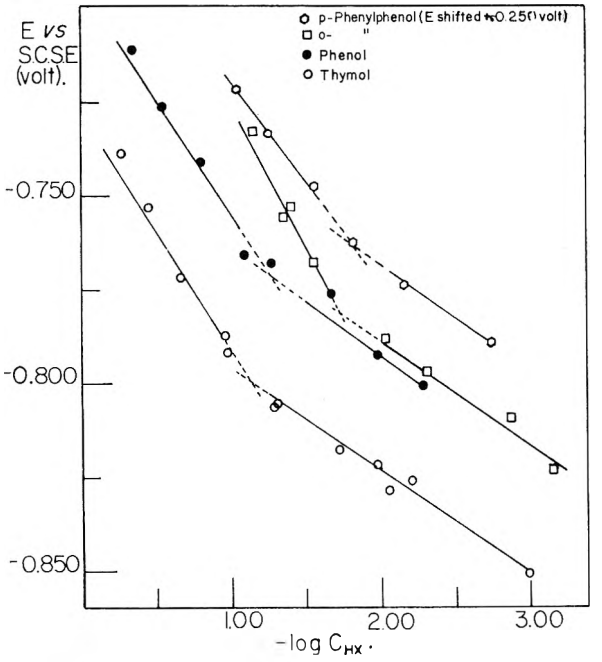

Fig. 1.—E.m.f. of the cell S.C.S.E.//HX in EDA/H_2 (1 atm.), Pt as a function of log $(C_{HX})_t$. The data for four phenols are shown, and the straight lines corresponding to the limiting low and high concentration slopes are drawn. The limiting slopes are 0.064 and 0.027 for thymol, 0.060 and 0.030 for phenol, 0.074 and 0.029 for *o*-phenylphenol, and 0.056 and 0.028 for *p*-phenylphenol. In the latter case, the original data are displaced by +0.025 v. Four *o*-phenylphenol experimental points were omitted for clarity of presentation. If the highest concentration datum is omitted, a line of slope 0.063 rather than 0.074 may be drawn.

reading. E.m.f. values then were recorded every 5 to 10 min.; the reported e.m.f. values are the mean of the first four readings and have an average deviation of ±0.5 mv. The atmospheric pressure normally was about 740 mm., while the vapor pressure of EDA is approximately 10 mm. at 25°. Therefore, the hydrogen partial pressure correction to the observed e.m.f. values is about 0.5 mv. Since this correction is within the experimental error, it has been ignored in the present set of measurements.

Results

The results obtained with phenol, thymol, *o*-phenylphenol, and *p*-phenylphenol using cell I are shown in Fig. 1. In all cases, two limiting slopes of ~ 0.059 and ~ 0.030 are observed. These data were fitted to eq. 5d, using a weighted least squares procedure which assigned all the error to E_{HX}. A summary of the least squares results is given in Table I, along with the values of K_{HX_2} calculated from the ratio of the slope and intercept.

(10) H. C. Brown, D. H. McDanell, and O. Haflinger, "Determination of Organic Structures by Physical Methods," ed. by E. A. Braude and F. C. Nachod, Academic Press, Inc., New York, N. Y., 1955, p. 567.

In addition to these four phenols, hydrochloric, acetic, and phenylacetic acids and 3-methyl-4-phenylazophenol also were studied with the hydrogen electrode. The results obtained are shown in Fig. 2. The hydrochloric acid data may be fitted by the method of least squares to the equation $E = -0.6095\ (\pm\ 0.0031) + 0.03119\ (\pm\ 0.00181) \log(C_{HCl})_t$, where the numbers in parentheses correspond to the standard deviation of the preceding quantity. The acetic and phenylacetic acid results are practically superimposable and yield slopes of 0.038 and 0.039, respectively. The 3-methyl-4-phenylazophenol data indicate that a limiting slope of 0.090 is approached at high concentrations, while a limiting slope of 0.060 is approached at the lowest concentrations studied.

The results obtained studying mixtures of thymol and sodium thymolate, and *o*-phenylphenol and sodium *o*-phenylphenolate are given in Table II. These data were fitted to eq. 11b and the least squares constants are given in Table II.

TABLE II

SUMMARY OF HYDROGEN ELECTRODE RESULTS OBTAINED IN SOLUTIONS OF HX AND NaX FOR *o*-PHENYLPHENOL AND THYMOL

	Compound *o*-Phenylphenol[a]	Thymol[b]
Eq. 11b Intercept[c]	7.39 (0.858) × 10^{-28}	5.31 (0.636) × 10^{-30}
Eq. 11b Slope[c]	2.65 (0.205) × 10^{-26}	3.39 (0.901) × 10^{-29}
K_{HX_2}[c]	35.9 (6.4)	6.4 (2.4)
K_{NaX}/K_{HX} (slope ratios)	2.83 × 10^2	3.21 × 10^3
K_{NaX}/K_{HX} (intercept ratios)	1.56 × 10^2	1.76 × 10^3
K_{NaX}/K_{HX} (wtd. mean)	2.1 × 10^2	2.1 × 10^3

[a] Results of 19 experiments. Concentration ranges used: C_{HX}—0.002 to 0.3 *M*; C_{NaX}—0.001 to 0.25 *M*. [b] Results of 12 experiments. Concentration ranges used: C_{HX}—0.005 to 0.11 *M*; C_{NaX}—0.004 to 0.16 *M*. [c] The standard deviation of the tabulated value follows in parentheses.

Hydrogen electrode data obtained with the sodium salts of thymol, *o*-phenylphenol, 3-methyl-4-phenylazophenol, phenylacetic acid, and sodium bromide and iodide, are given in Table III. The e.m.f. values are constant and independent of concentration as predicted by eq. 13b. Using equation 13c, the pK values of these compounds relative to thymol are: *o*-phenylphenol, −0.99; phenylacetic acid, −5.30; 3-methyl-4-phenylazophenol, −5.75; hydrobromic acid, −6.02; and hydriodic acid −6.81.

Discussion

The behavior of hydrochloric acid (Fig. 2) is described adequately in the concentration range 0.003 to 0.12 *M* by an ion-pair dissociation equilibrium in which the fraction dissociated may be

TABLE III

SUMMARY OF HYDROGEN ELECTRODE RESULTS OBTAINED IN EDA SOLUTIONS OF NaX

Parent acid, HX	$(C_{NaX})_t$, M	E.m.f. (v.)	Av. e.m.f. dev. (mv.)
HI[a]	0.517	−0.7745	−0.2
	.230	− .7771	+2.4
	.119	− .7723	−2.4
		Mean −0.7747 ± 0.0017	
HBr	.1460	−0.7981	+0.1
	.0484	− .7970	−1.0
	.0205	− .7985	−0.5
		Mean −0.7980 ± 0.0005	
3-Methyl-4-phenylazophenol	0.0874	−0.8064	+0.2
	.0552	− .8066	+0.4
	.0212	− .8078	+1.6
	.0063	− .8053	−0.9
	.0025	− .8048	−1.4
		Mean −0.8062 ± 0.0009	
Phenylacetic	0.2250	−0.8190	−0.4
	.0734	− .8203	+1.0
	.0253	− .8188	−0.6
	.0043	− .8195	+0.1
		Mean −0.8194 ± 0.0005	
o-Phenylphenol	0.2042	−0.9502	+2.7
	.1355	− .9485	+1.0
	.1108	− .9474	−0.1
	.0687	− .9476	+0.1
	.0413	− .9467	−0.8
	.0284	− .9450	−2.5
	.0217	− .9430	−4.5
	.0149	− .9455	−2.0
	.0111	− .9459	−1.6
	$.0053_4$	− .9461	−1.4
	$.0044_2$	− .9477	+0.2
	$.0019_2$	− .9504	+2.9
	.0019	− .9466	−0.9
		Mean −0.9475 ± 0.0016	
Thymol	0.1085	−0.9750	−1.1
	.0120	− .9786	+2.6
	.0047	− .9743	−1.8
	.0028	− .9764	+0.3
		Mean −0.9761 ± 0.0015	

[a] Experiment performed by M. M. K. Gracias.

neglected (equation 6b). This result indicates that $K_{HCl} \lesssim \sim 10^{-4}$, since in a previous potentiometric study of silver salts, deviations from the limiting slope of 0.0296 were observed for silver nitrate. K_{AgNO_3} has been estimated to be $\sim 6 \times 10^{-4}$,[11] 4×10^{-4},[6b] and 5.7×10^{-4}.[5] Using the Fuoss–Kraus conductance method, Schaap and coworkers[4] report $K_{HCl} = 1.05 \times 10^{-4}$, in agreement with the above conclusions.

The e.m.f. data obtained with phenol, thymol,

(11) L. D. Pettit and S. Bruckenstein, *J. Inorg. Nucl. Chem.*, in press.

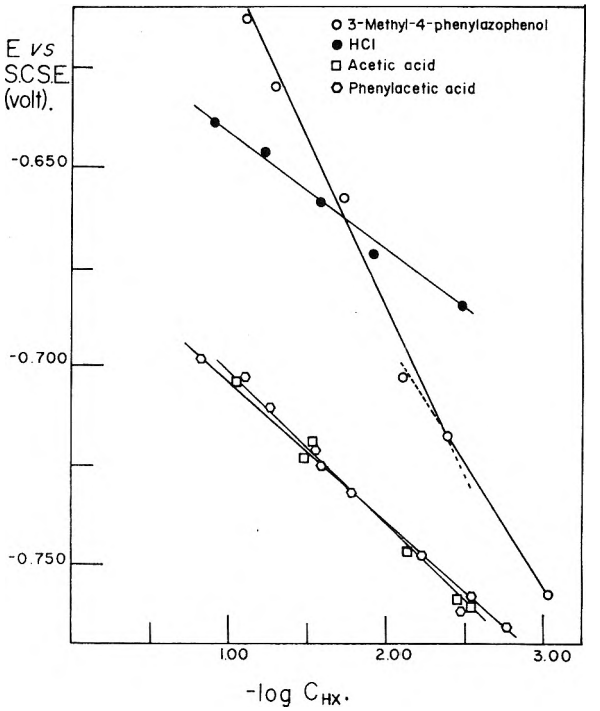

Fig. 2.—E.m.f. of the cell S.C.S.E.//HX in EDA/H_2 (1 atm.), Pt as a function of log $(C_{HX})_t$. The data for hydrochloric, acetic, and phenylacetic acids were fitted to an equation of the form $E = A + B \log (C_{HX})_t$. The results obtained are summarized below in the form—HX, $A(\sigma_A)$, $B(\sigma_B)$. HCl, −0.6095 (0.0031), 0.03119 (0.00181); HAc, −0.6649 (0.0025), 0.0375 (0.0013); phenylacetic acid, −0.6620 (0.0020), 0.0390 (0.0011).

and *o*- and *p*-phenylphenols is satisfactorily explained by postulating an anionic species containing one phenolate ion per parent phenol (HX_2^-). The order of acid strength (Table I) is qualitatively the same as found in water, but is sufficiently different to emphasize the danger in the common practice of assuming a solvent-independent-pK difference between acids of similar chemical composition.

Phenolic ions of the HX_2^- type have been reported previously on the basis of photometric,[12] potentiometric,[13,14] and conductometric[15] evidence. The stability of these conjugate ions (HX_2^-)[16] in the strongly basic and hydrogen bonding solvent EDA is somewhat surprising, since it would appear likely that the solvent would hydrogen bond completely to the undissociated phenols in preference to the phenolate ion and *vice versa*. Probably, these conjugate phenolate ions should not be classified with those of similar stoichiometry arising in the poorly solvating solvents, acetonitrile[17–19] and nitrobenzene.[20] Also, it is unlikely that triple

(12) L. Hummelstedt and D. N. Hume, *Anal. Chem.*, **32**, 1792 (1960).

(13) H. B. van der Heijde, *Anal. Chim. Acta*, **16**, 392 (1957).

(14) G. A. Harlow and D. B. Bruss, *Anal. Chem.*, **30**, 1833 (1958).

(15) D. B. Bruss and G. A. Harlow, *ibid.*, **30**, 1836 (1958).

(16) A term coined by I. M. Kolthoff to describe an ion which contains both partners of a conjugate acid–base couple.

(17) I. M. Kolthoff, S. Bruckenstein, and M. K. Chantooni, Jr., *J. Am. Chem. Soc.*, **83**, 3927 (1961).

(18) C. M. French and I. G. Roe, *Trans. Faraday Soc.*, **49**, 314 (1953).

(19) E. Romberg and K. Cruz, *Z. Elektrochem.*, **63**, 404 (1959).

ion formation arising from simple coulombic forces plays an appreciable role in stabilizing these conjugate ions in EDA since its dielectric constant, 12.9, is too high for equilibrium constants of the stability reported in Table I. No obvious relationship between structure or K_{HX} and $K_{HX_2^-}$ exists.

In the case of 3-methyl-4-phenylazophenol, limiting slopes of 0.060 and 0.090 have been drawn through the experimental e.m.f. values in Fig. 2. These slopes would arise if the principal anionic species in dilute solution was HX_2^- and was $(HX)_2X^-$ in more concentrated solution.

The behavior of acetic and phenylacetic acids is anomalous. While the slope shown in Fig. 2 suggests appreciable dissociation of the parent acids, the magnitude of the observed e.m.f. values indicates a lower activity of hydrogen ion than for hydrochloric acid, whose e.m.f. behavior indicates it is very slightly dissociated. Cryoscopic data indicate that these acids are not significantly associated, thus eliminating any scheme based upon the dimerization of carboxylic acids. Further work on the behavior of carboxylic acids in EDA is currently being undertaken.

The e.m.f. data obtained with the mixtures of thymol and sodium thymolate and *o*-phenylphenol and sodium *o*-phenylphenolate rarely differ from the values calculated using eq. 11b and the least squares constants given in Table II by more than 2 mv. $K_{HX_2^-}$ values calculated from the slope and intercept of eq. 11b are 6.4 and 35.9 for thymol and *o*-phenylphenol, respectively, as compared to 11.7 and 65.1 obtained using eq. 5d. The difference between these results is not significant because of the large relative standard deviations of the individual values, and the weighted mean values of $K_{HX_2^-}$ for thymol and *o*-phenylphenol are 7.1 and 40.0, respectively. The ratio K_{NaX}/K_{HX} is given by the ratio of the slopes (or intercepts) of eq. 5d and 11b. For thymol, the slope ratios yield 3.21×10^3, while the intercept ratios yield 1.76×10^3, with a weighted mean value of 2.13×10^3. For *o*-phenylphenol the slope ratios yield 283 while the intercept ratios yield 156, with a weighted mean of 209. These results are in agreement with the assumption, $K_{NaX}C_{NaX}/K_{HX}C_{HX} >> 1$, used in obtaining eq. 11b.

The values of $pK_{thymol} - pK_{HX}$ for a series of sodium salts as calculated from the e.m.f. values of pure salt solutions using eq. 13c (Table III) have been mentioned earlier. The value of this difference for *o*-phenylphenol is 0.99, as compared to 1.08 (Table I) found from solutions of pure acids. This agreement is within the experimental error.

(20) N. van Looy and L. P. Hammett, *J. Am. Chem. Soc.*, **81**, 3872 (1959).

As pointed out above, in the case of the three phenols listed in Table III, no concentration dependence of the e.m.f. is noted because the equilibrium concentration of the parent acid arising from reaction 12a is so small that significant concentrations of the possible conjugate ions do not form. The sodium phenylacetate data also are concentration independent, even though the behavior of the pure acid solutions is anomalous.

The tabulation of $pK_{MX^-} - pK_{HCl}$ given in Table IV was obtained by combination of all the data obtained in pure acid, some salt, and acid–salt mixture solutions. In combining these data, thymol has been taken as the common reference point for the pure acid solution and the pure salt solutions and the result rounded to the nearest 0.05 pK unit.

The difference $pK_{HBr} - pK_{HCl}$ as calculated from the conductance values listed by Schaap and co-workers,[4] -0.36, is in fair agreement with the value -0.60 given in Table IV.

TABLE IV

pK VALUES OF SOME ACIDS AND SODIUM SALTS RELATIVE TO HYDROCHLORIC ACID

Compound	$pK_{MX} - pK_{HCl}$[a]
Thymol	5.40[b]
	5.40[c]
o-Phenylphenol	4.30[b]
	4.40[c]
Phenol	4.30[b]
p-Phenylphenol	4.20[b]
Sodium thymolate	2.05[d]
Sodium *o*-phenylphenolate	2.10[d,e]
Phenylacetic acid	+0.10[c]
3-Methyl-4-phenylazophenol	−0.35[c]
Hydrobromic acid	−0.60[c]
Hydriodic acid	∼−1.40[c]

[a] Calculated using $E_{SCE} + 0.0296 \log K_{HCl} = -0.6095$ v., $E_{SCE} + 0.0296 \log K_{thymol} = -0.7698$ v., and thymol as common reference in pure salt and pure acid solutions. [b] Based on pure acid solution data. [c] Based on pure salt solution data. [d] Based on acid–salt mixture data. [e] Using $pK_{HX} - pK_{HCl} = 4.40$.

The value of $pK_S - pK_{NaS}$ was evaluated from the data in Tables I and III using eq. 14, and found to be 6.97 from thymol data and 7.00 from *o*-phenylphenol data. Using Schaap's value of $pK_S = 15.3$,[4] yields $pK_{NaS} = 8.35$. On the basis of these data, the monosodium salt of EDA appears to be a very weak electrolyte, and, if it could be prepared, would be a poor choice as a basic titrant. Attempts to prepare this compound by reaction of sodium metal, sodium amide, and sodium hydride with EDA have proved unsuccessful, the ultimate products in all cases being black, tarry residues.

MOLECULAR DIMENSIONS AND INTERACTIONS OF LITHIUM POLYPHOSPHATE IN AQUEOUS LITHIUM BROMIDE SOLUTIONS[1]

BY U. P. STRAUSS AND P. ANDER

School of Chemistry, Rutgers, the State University, New Brunswick, New Jersey

Received May 24, 1962

The behavior of two lithium polyphosphate samples, having molecular weights of 4.3×10^5 and 5.5×10^5, in aqueous lithium bromide solutions was investigated by means of light scattering and viscosity measurements at 25° in order to obtain a quantitative comparison with the previously studied corresponding sodium polyphosphate–sodium bromide system. The theta solvent, in which the second virial coefficient extrapolated to zero, was 1.80 *M* LiBr, in contrast to 0.415 *M* NaBr found previously for the sodium case. The ratio of the theta solvent molecular dimensions to those calculated assuming free rotation about each P–O bond averaged 1.73, in close agreement with 1.68 found in the sodium system. The relationship between the molecular dimensions and the second virial coefficient also was the same for both systems. The dependence of molecular dimensions on ionic strength could be described by Flory's equation: an effective degree of ionization of 0.13 was necessary to reach agreement between theory and experiment. The corresponding value for the sodium system was 0.10. Extrapolation of these data to infinite ionic strength indicates that the sodium polyphosphate has much less solvent affinity than the lithium polymer, a result in agreement with the different theta solvent compositions and previously observed phase separation behavior. It is of interest that at the high LiBr concentrations, selective adsorption of water was so large that correction factors greater than two were needed to obtain the light scattering molecular weights.

For advancing the understanding of polyelectrolytes, it has proved useful to determine how their properties are affected by different counterions. Especially with long chain polyphosphates, this type of study has been fruitful in distinguishing between those effects which are general and those which are specific for each counterion. This paper reports light scattering and viscosity results obtained at 25° with lithium polyphosphate (LiPP) in aqueous LiBr solutions, the main objective being a comparison with results obtained previously in a similar study of sodium polyphosphate (NaPP) in aqueous NaBr.[2]

Such a comparison is of special interest because electrical measurements have shown that at corresponding concentrations of simple electrolyte, lithium and sodium ions are bound by polyphosphates to about the same extent,[3] while membrane equilibrium studies have indicated approximately equal thermodynamic interactions of LiBr and NaBr with the polyphosphate.[4] Yet, in contrast to these similarities, it was found in preliminary studies that the concentration of NaBr (0.47 *M*) needed to cause phase separation was much lower than that of LiBr (2.3 *M*) needed to accomplish the same purpose (with the same polyphosphate sample), and that the intrinsic viscosity of a polyphosphate sample was much lower in NaBr than in LiBr solutions.[5] The present study therefore was aimed at furnishing data which would allow more quantitative interpretations than were obtainable with these preliminary results.

Experimental

Materials.—Two samples of lithium polyphosphate of different molecular weight, LiPP-1 and LiPP-2, were prepared from potassium Kurrol salts by an ion-exchange procedure described by Strauss and Wineman.[2] A flame test indicated no residual K^+. The samples were stored at −15° until used so as to prevent degradation. Viscosity determinations in 0.35 *M* NaBr during each run indicated that no degradation took place during storage. The per cent water in LiPP-1 and LiPP-2, determined by weight loss upon fusion, was found to be 14.41 ± 0.06 and 10.66 ± 0.02, respectively.

Light Scattering.—Light scattering measurements were performed at 25° in a Brice–Phoenix light-scattering photometer,[6] using incident unpolarized monochromatic blue light (λ 4360 Å.). The instrument was modified,[7] following the design of Boedtker and Doty,[8] to include a thermostating housing for the cylindrical light-scattering cells and a collimator attached to the housing to prevent stray reflections. The cells had flat faces at 0 and 180°. The optical uniformity and correct positioning of the cells were checked with the angular envelope obtained from a fluorescein solution. The linearity of the instrument was checked with aqueous fluorescein solutions ranging in concentrations from 2 to 50×10^{-3} g./l. All solvents and solutions were clarified with sintered glass filters of "ultrafine" porosity. The instrument was calibrated with two different standard polystyrene samples, Du Pont B4837 and Bakelite BMS-9-Al, dissolved in purified toluene to give concentrations of 0.5000 g./dl.

Refractive index increments between solutions and solvents were measured in a Brice–Phoenix differential refractometer which was calibrated by means of sucrose solutions.[9]

Viscosity.—Viscosities were measured at 25° in a Bingham viscometer as described previously.[2]

Results and Discussion

Determination of Molecular Weight and Second Virial Coefficient.—Light scattering results for two lithium polyphosphate samples, LiPP-1 and LiPP-2, were obtained by the dissymmetry and Zimm methods,[10] respectively. Plots of Kc_2/R_{90} *vs.* c_2 for LiPP-1 are shown in Fig. 1 and a typical Zimm plot for LiPP-2 is shown in Fig. 2, the various parameters being defined below.

For the three-component system, water (component 1), LiPP (component 2), and LiBr (com-

(1) This work was supported by a grant from the Atomic Energy Commission under Contract AT(30-1)1018. The paper is based on a thesis presented by P. Ander in 1961 to Rutgers, The State University, in partial fulfillment of the requirements for the Ph.D. degree.

(2) U. P. Strauss and P. L. Wineman, *J. Am. Chem. Soc.*, **80**, 2366 (1958).

(3) U. P. Strauss and S. Bluestone, *ibid.*, **81**, 5292 (1959).

(4) U. P. Strauss and P. Ander, *ibid.*, **80**, 6494 (1958).

(5) U. P. Strauss, D. Woodside, and P. Wineman, *J. Phys. Chem.*, **61**, 1353 (1957).

(6) B. A. Brice, M. Halwer, and R. Speiser, *J. Opt. Soc. Am.*, **40**, 708 (1950).

(7) B. L. Williams, Ph.D. Thesis, Rutgers, The State University, New Brunswick, New Jersey, 1959.

(8) H. Boedtker and P. Doty, *J. Phys. Chem.*, **58**, 968 (1954).

(9) C. A. Brown and F. W. Zerban, "Physical and Chemical Methods of Sugar Analysis," 3rd Ed., John Wiley and Sons, Inc., New York, N. Y., 1941, p. 1206.

(10) P. Doty and J. T. Edsall, *Adv. in Protein Chem.*, **6**, 35 (1951).

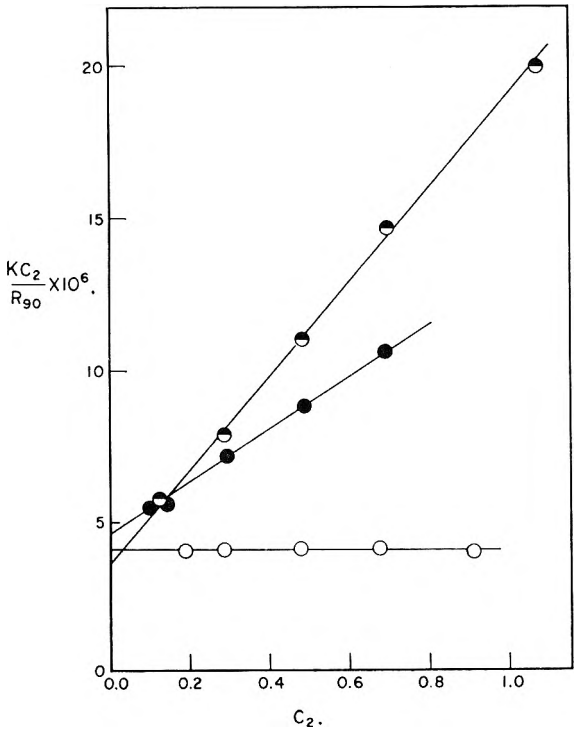

Fig. 1.—Light scattering reduced intensity as a function of polymer concentration for LiPP-1 in: ◓, 0.90 *M* LiBr; ●, 1.35 *M* LiBr; ○, 1.80 *M* LiBr.

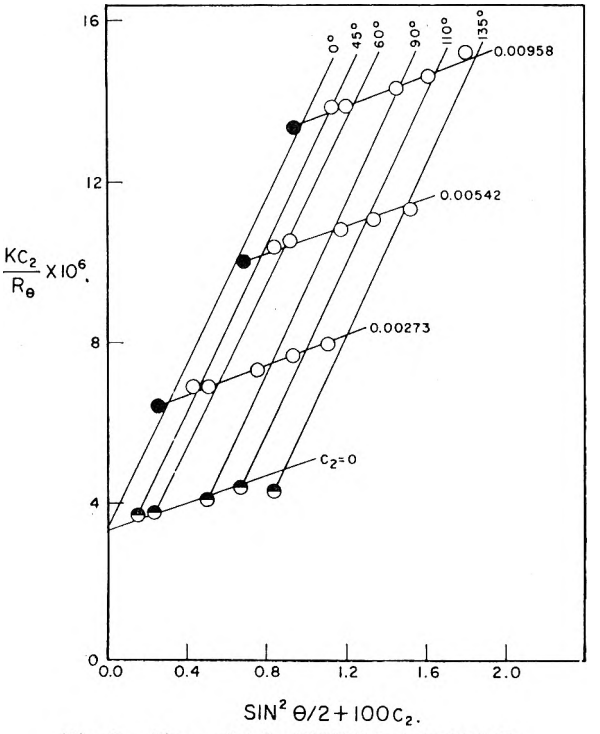

Fig. 2.—Zimm plot for LiPP-2 in 1.15 *M* LiBr.

ponent 3), the light scattering results can be interpreted by the equations[11,12]

$$\frac{Kc_2}{R_0} = \frac{1}{(1 - D)^2}(A + 2Bc_2) \qquad (1)$$

(11) J. G. Kirkwood and R. J. Goldberg, *J. Chem. Phys.*, **18**, 54 (1950).

(12) W. H. Stockmayer, *ibid.*, **18**, 58 (1950).

$$K = 2\pi^2 V_0 n^2 (\partial n/\partial c_2)^2 / N_A \lambda^4 \qquad (2)$$

$$D = \frac{(\partial n/\partial c_3)}{(\partial n/\partial c_2)} \times \frac{M_3}{M_2} \times \frac{a_{23}}{a_{33}} \qquad (3)$$

$$M_2 = \frac{1}{A} \times \frac{6 - 7\rho_u}{6 + 6\rho_u} \qquad (4)$$

In these equations R_0 is the excess Rayleigh ratio of the solution over that of the solvent extrapolated to zero angle, M_j is the molecular weight and c_j is the concentration of component j, in g./g. of water, λ is the wave length of light *in vacuo*, V_0 is the volume of solution containing 1 g. of water, n is the refractive index of the solution, ρ_u is the depolarization, and $a_{jk} = (1/RT)(\partial\mu_j/\partial m_k)$ where μ_j and m_j are the chemical potential and molality of component j. For the dissymmetry method[10] R_0 in eq. 1 is replaced by R_{90}, the excess Rayleigh ratio at 90°, and eq. 4 is replaced by

$$M_2 = \frac{1}{A} \times \frac{1}{P(90)} \times \frac{6 - 7\rho_u}{6 + 6\rho_u} \qquad (5)$$

where $1/P(90)$ is the dissymmetry correction obtained from the intrinsic dissymmetry, $[Z]$, by using the tables of Doty and Steiner.[13] The values of $[Z]$ were obtained from plots of $1/(Z - 1)$ against c_2, where Z is the dissymmetry due to the polymer measured at finite polymer concentrations at 45 and 135°.

In order to calculate D, the term a_{23}/M_2a_{33} was determined from membrane equilibrium data,[4,14] the quantity $(\partial n/\partial c_2)$ was measured, and $(\partial n/\partial c_3)$ was found to be 0.143 from interpolation of literature values.[15,16] The refractive index increments of the polyelectrolyte are given in Table I, as are the values of $1/(1 - D)^2$. The depolarization corrections in eq. 4 and 5 were neglected in the calculations since, based on previous experience,[2] they were not expected to affect the molecular weight significantly.

The light scattering data for LiPP-1 and LiPP-2 are summarized in Table I. The consistency of the molecular weights obtained here with those obtained in the previous light-scattering study of the corresponding sodium system[2] was tested through the intrinsic viscosity of the LiPP samples in 0.35 *M* NaBr. From the Mark–Houwink relation established in the previous study, the molecular weights of LiPP-1 and LiPP-2 were calculated to be 5.5×10^5 and 4.3×10^5, respectively.[17] These values are seen to fall within the range of the directly determined molecular weights. The constancy of the intrinsic viscosity of each sample determined throughout the course of the experimentation period indicated that the small amounts of residual water caused no degradation of the solid polymers at the temperature of storage (−15°).

(13) P. Doty and R. F. Steiner, *ibid.*, **18**, 1211 (1950).

(14) P. Ander, Ph.D. Thesis, Rutgers, The State University, New Brunswick, N. J., 1961.

(15) "International Critical Tables," Vol. 7. McGraw-Hill Book Co., New York, N. Y., 1930, p. 73.

(16) Landolt-Bornstein, "Physik Chem. Tabellen," Auflage 5, Supplement 1, 1927, p. 534.

(17) The difference between the atomic weights of Na^+ and Li^+ was, of course, taken into account.

TABLE I

LIGHT SCATTERING AND VISCOSITY RESULTS OF LiPP-1 AND LiPP-2 IN SEVERAL LITHIUM BROMIDE SOLUTIONS

Sample	Molarity	$(1 - D)^{-2}$	$(\partial n/\partial c_2)$	$\frac{(1 - D)^2}{A} \times 10^{-5}$	$[Z]$	$M_2 \times 10^{-5}$ [a]	$B \times 10^4$	$[\eta]$ (dl./g.)	$[(\overline{R^2})_z]^{1/2}$(Å.) From light scattering	$[(\overline{R^2})_z]^{1/2}$(Å.) From $[\eta]$ [b]
LiPP-1	0.90	1.60	0.108	2.78	1.52	6.2	4.8	1.37	885	855
	1.35	1.88	.102	2.18	1.37	5.2	2.3	0.92	762	750
	1.50	..	...	..	..	...	..	.76	...	719
	1.80	2.36	.094	2.44	1.27	6.9	0	.53	637	624
LiPP-2	1.15	1.73	.105	2.86	..	4.9	2.9	.80	663	673
	1.35	1.88	.102	2.13	..	4.0	1.9	.70	572	644
	1.50	2.04	.098	1.87	..	3.9	1.0	.59	...	608
	1.70	2.25	.094	2.27	..	5.1	0.3	.51	570	580

[a] The molecular weights of LiPP-1 and LiPP-2, determined from intrinsic viscosity measurements in 0.350 M NaBr, were found to be 5.5×10^5 and 4.3×10^5, respectively; see text. [b] Calculated by means of eq. 8 using $M_2 = 5.5 \times 10^5$ for LiPP-1, $M_2 = 4.3 \times 10^5$ for LiPP-2, $\phi = 2.2 \times 10^{21}$, and $q = 1.95$.

It is evident from Table I that the values of the molecular weights obtained at different LiBr concentrations show considerable variations for each sample. We attribute this to two causes. First, in each case $(1 - D)^2/A$, the reciprocal intercept of the light scattering curve seems to be higher at the largest LiBr concentration than would be expected from the trend of the other values. This is believed to be due to complexities in the light scattering curves which may be expected near the theta point[18] when more than one solvent component is used and the dilutions are carried out at constant solvent composition.[19] Second, the values of $(1 - D)^{-2}$ are far from unity and therefore quite sensitive to the experimental uncertainty of the membrane equilibrium data. In view of these difficulties, the observed agreement between the values of M_2 obtained at the intermediate LiBr concentrations (where the attainable precision of the light scattering molecular weight is at an optimum) and the values obtained from the intrinsic viscosity in 0.35 M NaBr is better than might be anticipated.

By extrapolating a plot of B against LiBr molarity, one finds that $B = 0$ when the molarity is 1.80. Thus the 1.80 M solution is a theta solvent for LiPP at 25°.[20] This is in line with the previous observation that a LiBr molarity of 2.3 was necessary to cause phase separation in an aqueous solution of a long-chain polyphosphate.[5]

Molecular Dimensions and Second Virial Coefficient.—The z-average r.m.s. end-to-end distance $(\overline{R^2})_z^{1/2}$ for LiPP-1 obtained from light scattering was determined from the value of $[Z]$ using the "monodisperse coils" tables of Doty and Steiner.[13] For LiPP-2, the z-average radius of gyration, $(\overline{S^2})_z^{1/2}$, was calculated from the relation

$$(\overline{S^2})_z = \frac{3}{16\pi^2}\left(\frac{\lambda}{n}\right)^2\left(\frac{s}{I}\right) \qquad (6)$$

where I and s are the intercept and slope, respectively, of the Zimm plot $c_2 = 0$ line.[21,22]

For a random coil, $(\overline{R^2})_z$ is related to $(\overline{S^2})_z$ by

$$(\overline{R^2})_z = 6(\overline{S^2})_z \qquad (7)$$

Flory, *et al.*,[23] have shown that to obtain comparable z-average values from the intrinsic viscosity, one may use the relation

$$(\overline{R^2})_z = \left(\frac{[\eta]M_w}{\phi/q}\right)^{2/3} \qquad (8)$$

The quantity q was estimated by assuming the molecular weight distribution given by Zimm[21] with the parameter characterizing the heterogeneity equal to unity. This gives $M_w/M_n = 2$ and $q = 1.95$.[24] Using the value of 2.2×10^{21} for ϕ and the value of M_w obtained from viscosity measurements in 0.350 M NaBr, values of $(\overline{R^2})_z^{1/2}$ were calculated using eq. 8. These values are in good agreement with those obtained from light scattering. The results are presented in Table I.

Krigbaum has shown that several first-order approximation theories concerning the excluded volume give the following relation between the intrinsic viscosity and the second virial coefficient

$$[\eta] = [\eta]_\theta + kM_wB \qquad (9)$$

where the subscript θ refers to the theta solvent and k is a dimensionless constant. This equation, which is predicted[25] to apply to ordinary polymers in poor solvents, also holds for LiPP-1 and LiPP-2, as shown in Fig. 3. For comparison, the results obtained with a sample of sodium polyphosphate[2] are included in the figure. From these lines we find that k in eq. 9 is 3.2×10^{-3}, 2.6×10^{-3}, and 2.9×10^{-3} for LiPP-1, LiPP-2, and NaPP-7,[2] respectively. The agreement between the LiPP and NaPP results indicates that the counterion does not affect the relation between the effects of the excluded volume on the *intra*- and *inter*molecu-

(18) The theta solvent is 1.80 M; see below.

(19) U. P. Strauss, unpublished results.

(20) Saini and Trossarelli [*J. Polymer Sci.*, **23**, 563 (1957)] reported that for the system LiPP–LiCl–H_2O the theta solvent composition was 0.4 M LiCl at 20°. Neither the different by-ion nor the slightly different temperature employed by them can account for the large discrepancy between their results and ours. In addition, their reported molecular dimensions per unit of polymer in 0.4 M LiCl are about twice as large as the ones observed by us in our theta solvent, and also much larger than usually is observed for flexible polymers of this type. Their results therefore should be regarded with caution.

(21) B. H. Zimm, *J. Chem. Phys.*, **16**, 1093, 1099 (1948).

(22) K. A. Stacy, "Light Scattering in Physical Chemistry," Academic Press, Inc., New York, N. Y., 1956, p. 33.

(23) S. Newman, W. R. Krigbaum, C. Langier, and P. J. Flory, *J. Polymer Sci.*, **14**, 451 (1954).

(24) The hydrolytic degradation of the polyphosphate during the preparation of its lithium salt is assumed to lead to polydispersity characteristic of unfractionated polymers.

(25) W. R. Krigbaum, *J. Polymer Sci.*, **18**, 315 (1955).

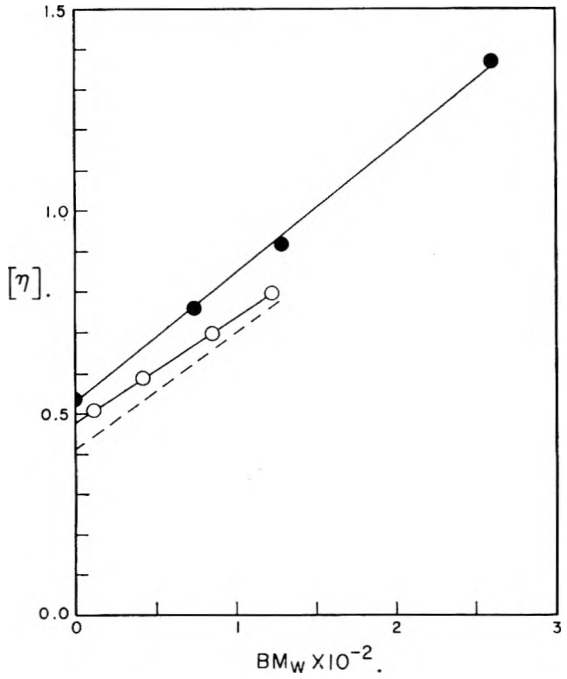

Fig. 3.—Test plot of eq. 9: ●, LiPP-1, $M_w = 5.5 \times 10^5$ (the value of B for 1.50 M LiBr is the one obtained with LiPP-2); ○, LiPP-2, $M_w = 4.3 \times 10^5$; ---, NaPP-7, $M_w = 6.9 \times 10^5$, taken from ref. 2.

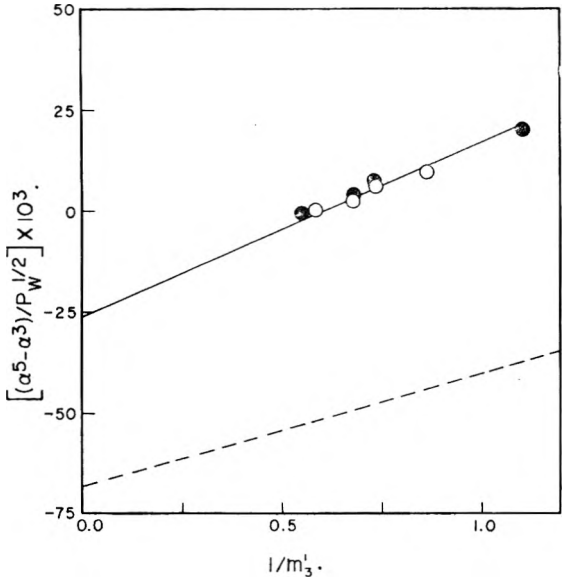

Fig. 4.—Dependence of the molecular expansion coefficient, α, on the simple electrolyte molarity, m_3', for: ●, LiPP-1 in LiBr; ○, LiPP-2 in LiBr; —, NaPP-7 in NaBr, taken from ref. 2.

lar interactions of the segments. The theoretical value for k is 4.4×10^{-3}. In view of the fact that some of the assumptions underlying the theory are still uncertain and that the values of k determined for ordinary polymers also deviate more or less from the theoretical value, it seems premature to ascribe any special meaning to the deviation found here for polyelectrolytes.[26]

(26) One such meaning could be that the value of ϕ, to which k is proportional, is lower than 2.1×10^{21} as assumed by Krigbaum.[25] Such a conclusion, however, would not be in accord with the value of $\phi = 2.2 \times 10^{21}$ which gave good agreement between the light scattering and viscosity molecular dimensions. It is of interest that the opposite was found by Flory and Orofino for polyacrylic acid in NaCl. [T. A. Orofino and P. J. Flory, *J. Phys. Chem.*, **63**, 283 (1959)]. They needed a low value of ϕ to have agreement between the light scattering and viscosity molecular dimensions, while the high value would have given them agreement with their somewhat different theoretical relationship between $[\eta]$ and B.

The values of $[\eta]_\theta$, determined from the intercepts of the lines of Fig. 3, are 0.53 and 0.48 dl./g. for LiPP-1 and LiPP-2, respectively. From these values one then can calculate $(\overline{R^2_0}/P)^{1/2}$, the root-mean-square end-to-end distance per monomer unit of the polymer chain in the absence of long range interactions, where $(\overline{R^2_0})^{1/2}$ is the unperturbed r.m.s. end-to-end distance and P is the degree of polymerization. This quantity, which is characteristic of the intrinsic flexibility of the polymer chain, is obtained by the application of eq. 8 and by dividing the resulting values of $(\overline{R_0^2})_z^{1/2}$ by $P_z^{1/2}$, where P_z is taken to be $1.5P_w$, in line with the assumed molecular weight distribution. The resulting values for LiPP-1 and LiPP-2 are 6.5 and 6.4 Å., respectively, in close agreement with the value of 6.2 Å., determined previously for NaPP.[2] The corresponding values of $(\overline{R^2_0}/\overline{R^2_{0f}})^{1/2}$ are 1.74, 1.72, and 1.68, respectively. Here, $(\overline{R^2_{0f}})^{1/2}$, the hypothetical unperturbed mean square end-to-end distance which the polymer would have if all its bonds were freely rotating, is calculated by the same method and with the same assumption as used previously.[2] This result seems to indicate that at the high electrolyte concentrations employed in these studies, the short-range interactions between polymer segments are neither affected by the nature of the counterion nor by the ionic strength. However, the possibility of a fortuitous cancellation of finite effects of these two properties cannot be completely excluded.

Molecular Dimensions and Electrolyte Concentration.—In view of the equivalence of molecular dimensions and second virial coefficient, as shown in the previous paragraph, only one of these quantities need be considered as a function of electrolyte concentration. The molecular dimensions are chosen since they can be determined more accurately. The difficulties encountered in applying several theories relating molecular dimensions and ionic strength[27-30] to the experimental results obtained with NaPP were discussed by Strauss and Wineman.[2] For the same reasons, only Flory's theory[31] can be tested with the results obtained from this study. Flory's equation relating molecular dimensions to electrolyte concentration can be put into the form

$$(\alpha^5 - \alpha^3)/P^{1/2} = J + 2C_I' i^2/m_3' \quad (10)$$

where

$$C_I' = (3^3 \times 10^3/2^{9/2}\pi^{3/2})N_A^{-1}(R_0^2/P)^{-3/2} \quad (11)$$

(27) J. J. Hermans and J. T. G. Overbeek, *Rec. trav. chim.*, **67**, 761 (1948).

(28) W. Kuhn, O. Künzle, and A. Katchalsky, *Helv. Chim. Acta*, **31**, 1994 (1948).

(29) A. Katchalsky and S. Lifson, *J. Polymer Sci.*, **11**, 409 (1953).

(30) S. A. Rice and F. E. Harris, *J. Phys. Chem.*, **58**, 653 (1954).

(31) P. J. Flory, *J. Chem. Phys.*, **21**, 162 (1953).

and i is an effective degree of ionization of the polyelectrolyte, while m_3' is the molarity of simple electrolyte. The test plots of $(\alpha^5 - \alpha^3)/P^{1/2}$ against $1/m_3'$ for LiPP-1, LiPP-2, and NaPP[2] are shown in Fig. 4. In accordance with the theory, the points for the two LiPP samples fall on the same line. The slopes of these plots are 0.043 and 0.028 for LiPP and NaPP, respectively. Substituting 6.3 and 6.5 Å. for $(R_0^2/P)^{1/2}$ in eq. 11 for NaPP and LiPP, respectively, gives 1.29 and 1.42 for their respective C_I' values. To reach agreement with eq. 10, the values of i would have to be 0.13 for LiPP and 0.10 for NaPP. These i values are slightly lower than their respective values, 0.17 for LiPP and 0.14 for NaPP, obtained from membrane equilibrium experiments by extrapolation to zero ionic strength, but the differences are not large considering that i is really the result of electrostatic interactions which may affect the two types of polyelectrolyte properties differently.

The intercept J of eq. 10, which can be considered a measure of the excluded volume of the hypothetical uncharged polymer, is -0.026 for LiPP and -0.068 for NaPP. Two conclusions may be drawn from this result. First, the fact that these values are negative indicates that the solvent is incompatible with the uncharged polymers. Only when the contribution of the electrical charges, represented by the positive last term in eq. 10, approaches (or exceeds) J, will the polymer go into solution. Second, the difference between the two values of J indicates that the uncharged sodium polymer has a much higher solvent incompatibility than the uncharged lithium polymer. This difference has been postulated previously to account for the differences in both intrinsic viscosities and phase-separation behavior of these polymers, and has been ascribed to the greater ability of the bigger unhydrated sodium ion to cross-link two phosphate groups.[32]

Acknowledgment.—The authors wish to thank Mrs. Jean W. Day for performing many of the viscosity measurements.

(32) U. P. Strauss and P. D. Ross, *J. Am. Chem. Soc.*, **81**, 5295 (1959).

EFFECTS OF MICELLIZATION ON THE KINETICS OF THE HYDROLYSIS OF MONOALKYL SULFATES

BY JOSEPH L. KURZ

Central Basic Research Laboratory of Esso Research and Engineering Company, Linden, New Jersey

Received June 7, 1962

Data are given for the kinetics of the hydrolysis of primary straight chain sodium alkyl sulfates to the corresponding alcohols in acidic, basic, and neutral aqueous solution. Both micellar and non-micellar esters are included. The hydrogen ion-catalyzed rate of hydrolysis is strongly accelerated by the aggregation of the ester anions into micelles, which lowers the enthalpy of activation but has little effect on the entropy. The corresponding hydroxide ion-catalyzed rate is strongly suppressed and the uncatalyzed rate appears to be unchanged. Both the lack of an effect on the uncatalyzed rate and the magnitude of the electrostatic potential of the micelles (calculated from the acid-catalyzed rates) are in agreement with the rough model for micelles. Salt effects on the hydrolysis rate are larger for the micellar esters. They appear to be due to an increase in double layer shielding with increasing salt concentration rather than to any specific competition among counterions for sites on the micelle. The variation in the rate of hydrolysis of sodium decyl sulfate with concentration is used to calculate the critical micelle concentration, and values from conductance measurements are given to provide an independent standard for comparison.

The presence of micellar electrolytes recently has been reported[1-3] to give rise to changes in the rates of various ionic reactions which are far in excess of and far more specific than those expected from an ordinary kinetic salt effect. Duynstee and Grunwald[1] have studied the changes in the rates of the alkaline fading of dyes of various charge types which accompany the partition of the dye molecules into micelles, and have emphasized the dominant role of electrostatic interactions in those effects. The rate of the proton-catalyzed hydrolysis of N-benzylideneaniline has been shown to be strongly retarded in the presence of the cationic detergent, *n*-hexadecyltrimethylammonium bromide, by van Senden and Koningsberger.[2] Large rate factors arising from the presence of ionic micelles also have been reported by Lowe and Phillips[3] for the incorporation of cupric ion into the porphyrin ring.

Since these rate effects were assumed by their investigators to arise from incorporation of the reactants into (or onto) the micelles, it appeared to be of interest to examine a reaction in which the micellar salt itself is directly involved. The hydrolysis of straight chain alkyl sulfate salts to the corresponding alcohols

$$ROSO_3^- + H_2O \longrightarrow ROH + HSO_4^- \quad (1)$$

was chosen for investigation. A single homologous series contains both micellar and non-micellar esters, and since the micelles are constructed directly from the reactant ions, their structure is unperturbed by the presence of foreign molecules during the initial few per cent of reaction. The hydrolysis is known to proceed by three kinetically distinct paths—hydrogen ion catalysis, hydroxide ion catalysis, and uncatalyzed solvolysis—whose

(1) E. F. J. Duynstee and E. Grunwald, *J. Am. Chem. Soc.*, **81**, 4540, 4542 (1959).

(2) K. G. van Senden and C. Koningsberger, *Tetrahedron Letters*, **1**, 7 (1960).

(3) M. B. Lowe and J. N. Phillips, *Nature*, **190**, 262 (1961).

mechanisms have been elucidated,[4-8] thus providing three closely related reactions of different charge types. Since only univalent ions are involved in these reactions, the interpretation of kinetic effects should be simplified. The observation that long chain alkyl sulfates appear to undergo more rapid acid-catalyzed hydrolysis than do the short chain esters has been reported,[9,10] but no discussion of the factors which might have given rise to such an effect was presented.

Both the spontaneous[5] and the hydroxide ion catalyzed[8] routes proceed with carbon–oxygen cleavage, while the acid-catalyzed[5,7,8] path yields sulfur–oxygen cleavage. Calhoun and Burwell[4] have presented evidence supporting the contention that the hydroxide ion-catalyzed reaction proceeds by direct nucleophilic displacement, while the uncatalyzed path is intermediate in character between SN1 and SN2. The existence of appreciable binding of water to carbon in the transition state for the uncatalyzed hydrolysis is shown to be probable by the observation that the uncatalyzed hydrolysis of *sec*-butyl sulfate proceeds with inversion.[5] The acid-catalyzed hydrolysis presumably proceeds through equilibrium protonation of the sulfate moiety followed by attack of water on sulfur.[5]

$$RSO_4^- + H^+ \rightleftharpoons RSO_4H \qquad (2)$$

$$RSO_4H + H_2O \longrightarrow ROH + HSO_4^- + H^+ \qquad (3)$$

Since an ionic micelle in aqueous solution may be regarded as a region of the solution composed of oriented molecules and possessing both a low polarity and a high electrostatic potential with respect to the bulk solution,[11] the study of the effects of micellar electrolytes on the rates of chemical reactions is of interest from several viewpoints. It should be possible to exploit the structure of the micelle to change the rate and course of reactions, and the observed rate effects should be useful in exploring the details of this structure. In addition, the similarity of a micellar solution to systems of biological importance renders such kinetic data of potential biochemical interest.

Experimental

Materials.—Sodium methyl sulfate and sodium ethyl sulfate were prepared by partial hydrolysis of the corresponding dialkyl esters (Matheson, Coleman & Bell) with aqueous sodium hydroxide. The longer chain salts were prepared by reaction of the normal alcohol (Eastman Kodak, dodecanol; Matheson, Coleman & Bell, others) with chlorosulfonic acid. This sulfation was carried out in ethereal solution and, after neutralization with sodium hydroxide, the product was isolated either by evaporation to dryness and extraction with hot methanol or by direct extraction from the aqueous solution into 1-butanol according to the method of Dreger.[12] Each salt was recrystallized at least three times from methanol–isopropyl alcohol mixtures, and was dried over phosphorus pentoxide. Immediately before weighing, each sample of salt was redried over P_2O_5 at 80° under vacuum. The salts were analyzed[13] by potentiometric titration of the acid liberated when a sample was passed through a column of Amberlite IR 120 (H^+). Titrant was compared to potassium acid phthalate as the primary standard. It was necessary to run the ion-exchange column at an elevated temperature in the analysis of the three longest chain salts, since their Krafft points lie above room temperature. It is likely that the high assays obtained for the octadecyl ester arose from partial hydrolysis on the column due to the particularly high temperature (55–60°) necessary to keep this compound in solution. The analytical results are expressed below as percentages of the theoretical titer.

Salt	Assay (%)
Sodium methyl sulfate	100.0; 100.2
Sodium ethyl sulfate	99.7; 99.9
Sodium amyl sulfate	100.0; 99.8
Sodium decyl sulfate	100.1; 100.0
Sodium dodecyl sulfate	100.0; 100.3
Sodium tetradecyl sulfate	100.0; 100.3
Sodium hexadecyl sulfate	100.2; 100.2
Sodium octadecyl sulfate	100.7; 100.9

Carbonate-free sodium hydroxide solutions were prepared by dilution of a filtered 50% solution. Stock solutions of perchloric acid, acetic acid, and sodium tetraborate were assayed by potentiometric titration. Sodium perchlorate solutions were prepared from the reagent grade salt and assayed as described for the sodium alkyl sulfates. All water used was ordinary distilled water which had been passed through an ion-exchange demineralizer.

Measurements.—Determinations of pH were made using a Radiometer PHM4 pH meter which was standardized against borax and phthalate buffers. Measurements were made on solutions which were within 1° of the specified temperature. This same instrument was used to determine the end point (taken to be the inflection point) in all acid–base titrations. Temperatures for the kinetic runs were estimated to the nearest 0.01° using an NBS calibrated thermometer, and the baths showed no fluctuation of temperature within this precision of measurement.

The conductance measurements used in determining the critical micelle concentration (c.m.c.) were made using a conventional a.c. bridge supplied with current at 1000 c.p.s., the null point being detected with an oscilloscope. The conductivity cell was of Jones type[14] with lightly platinized electrodes, but was connected to an Erlenmeyer flask to facilitate mixing of the contents. The oil bath maintained a temperature constant to within ±0.003° over the time period necessary for a sequence of measurements. In order to release the pressure developed within the cell at the temperature used for the measurements (90°), the flask communicated with the air by means of a 12-cm. length of 0.25 mm. capillary tubing which terminated above the oil level. There was no evidence for any significant loss of solvent through this vent. The cell was charged initially with 50 ml. of solvent (either deionized water or sodium perchlorate solution) and additions of a solution of sodium decyl sulfate in the same solvent were made from a weight buret. The equivalent conductivity of the sodium decyl sulfate (corrected for solvent conductivity) was plotted either against its molality (for sodium perchlorate solutions) or against the square root of its molality (for water as solvent), and the c.m.c. was taken from the intersection of the two curves drawn through experimental points taken at molalities above and below that value.

Kinetic Procedures.—Samples of the alkyl sulfate salts were weighed directly into volumetric flasks, stock solutions of the other components were added volumetrically, and the solutions were diluted to the mark. Basic solutions were

(4) G. M. Calhoun and R. L. Burwell, Jr., *J. Am. Chem. Soc.*, **77**, 6441 (1955).

(5) R. L. Burwell, Jr., *ibid.*, **74**, 1462 (1952).

(6) G. H. Green and J. Kenyon, *J. Chem. Soc.*, 1389 (1950).

(7) S. Lieberman, L. B. Hariton, and D. K. Fukushima, *J. Am. Chem. Soc.*, **70**, 1427 (1948).

(8) E. T. Kaiser, Thesis, Harvard University, Cambridge, Mass., 1959.

(9) K. H. Bauer and W. Poethke, *J. prakt. Chem.*, **126**, 296 (1930).

(10) G. Desseigne, *Industries corps gras*, **1**, 136 (1945).

(11) See, for example, P. A. Winsor, "Solvent Properties of Amphiphilic Compounds," Butterworths, London, 1954, Chap. 1 & 2.

(12) E. E. Dreger, *Ind. Eng. Chem.*, **36**, 610 (1944).

(13) E. Lederer and M. Lederer, "Chromatography," 2nd Ed., Elsevier, New York, N. Y., 1957, p. 471.

(14) G. Jones and G. M. Bollinger, *J. Am. Chem. Soc.*, **53**, 411 (1931).

transferred to Teflon containers before placing in the constant temperature bath, while acidic solutions were left in the Pyrex flasks. After thermal equilibrium of the solution with the bath had been attained, aliquots were withdrawn at appropriate intervals and the acid produced was determined by titration. Acidic solutions were analyzed by direct titration with sodium hydroxide solution, strongly basic solutions were added to excess hydrochloric acid and back titrated, borax solutions were added to *ca.* 0.9 of the anticipated titer of hydrochloric acid, and the titration then was completed.

To avoid confusion due to changes in density of the solutions at temperatures above ambient, the solutions for the kinetic runs were weighed after preparation and all "concentrations" were calculated on a molality basis. The maximum difference between the magnitude of a rate constant when calculated on a molality basis and when calculated on a molarity basis corrected for solution expansion would be less than 2%.

The rate constants were calculated from data taken in the first 20% of reaction, using the calculated value of the infinity titer. Within this initial interval no gross physical change in the solution was observed, although later in the reaction gelation and phase separation occurred in runs involving the long chain esters. Also, no drift in rate could be observed during this period even though the micelle structure might have been expected to undergo some change. Actual determination of the infinity titer for the perchloric acid-catalyzed hydrolysis gave values within 2% of the calculated. All rate constants reported are averages of two or more runs, and the indicated precision is the average deviation of a single determination from the mean. The rate constant for each run was taken from the line of visual best fit through the observed points plotted as for a first-order reaction. Since bisulfate ion is sufficiently weak to have its ionization suppressed by the perchloric acid, first-order kinetics were observed in the acid-catalyzed runs as well as in the uncatalyzed buffered runs.[15] The pseudo first-order rate constant observed in acid was corrected for the uncatalyzed rate by subtracting the uncatalyzed rate constant measured in acetate buffers before computing the catalytic rate constant. The complementary correction of the acetate buffer rate was made when required, using the pH of the buffer measured at 90° and the rate constant for hydrogen ion catalysis. No correction of the borax buffer rate for contributions from hydrogen ion or hydroxide ion catalysis was necessary. The rate observed in sodium hydroxide solution was a combination of uncatalyzed (first-order) and hydroxide ion-catalyzed (second-order) rates. The specific rate for hydroxide catalysis was calculated from this by graphically estimating the average value of the pseudo first-order rate constant, subtracting the rate constant for the uncatalyzed reaction as measured in borax buffers, and dividing by the mean value of the sodium hydroxide concentration for the interval during which aliquots were taken. The results of this simple procedure were compared to those from the application of the method of Hughes, Ingold, and Shapiro for predominantly second-order reactions.[16] Runs using sodium methyl sulfate under conditions giving 97% second-order reaction yielded second-order rate constants from the two methods which agreed within 2%. Since runs with other esters had higher ratios of first to second-order reactions, the simple procedure should be an even better approximation for these compounds than for the methyl ester.

Products.—It has been reported[4] that no olefin formation accompanies the hydrolysis of non-micellar primary alkyl sulfates by either the hydroxide ion-catalyzed or the uncatalyzed route. Similarly, it is known[5] that the hydronium ion-catalyzed hydrolysis of *sec*-butyl sulfate is accompanied by butene formation to the extent of only about 10%. This strongly suggests that olefin formation would be negligible during the acid-catalyzed hydrolysis of primary alkyl sulfates. This conclusion was tested for the micellar ester, sodium dodecyl sulfate. A 1.442-g. (5.00 mmole) sample of this salt was sealed into a Pyrex tube with 5 mmoles of perchloric acid and water to make 50 ml. After heating at 90° for a time calculated to exceed 10 half times for the hydrolysis, the tube was opened and the contents were extracted with ether. Upon drying the extracts over potassium carbonate and removing the ether under reduced pressure, 0.925 g. (99.3%) of 1-dodecanol was obtained. The infrared spectrum of this material showed no absorbtion at 6.20 μ (position of the terminal olefin absorbtion in 1-dodecene), and was superimposable upon the spectrum of a sample of pure 1-dodecanol.

Results

The pseudo first-order rate constant for the hydrolysis of the alkyl sulfate salts may be expressed in terms of the three constants measured in this work as

$$k = k_0 + k_H[H^+] + k_{OH}[OH^-] \qquad (4)$$

Values of the first-order rate constant, k_0, for the uncatalyzed hydrolysis were measured at 90° in borax and acetate buffers, and are summarized in Table I. These specific rates appear to decrease smoothly as chain length increases and show no sign of a discontinuity between the rates for micellar and for non-micellar esters. Any change in rate due to micellization must be too small to show clearly. The observation that changing the acetate buffer concentration by a factor of two does not alter the rate within experimental error shows that catalysis by the buffer species is not important in those systems. A similar conclusion for the borax buffer follows from the observation that the rates in that buffer do not exceed those in the acetate.

TABLE I

RATE CONSTANTS FOR UNCATALYZED HYDROLYSIS AT 90° AND μ = 0.51[a]

Ester	$10^7 k_0$ (sec.$^{-1}$) Borax buffer[b]	Acetate buffer[c]	Acetate buffer[d]
Sodium methyl sulfate	2.42 ± 0.02	2.37 ± 0.03	2.47 ± 0.03
Sodium ethyl sulfate	1.32 ± .02	1.32 ± .03	1.38 ± .07
Sodium amyl sulfate	0.63 ± .03	0.87 ± .07	0.78 ± .04
Sodium decyl sulfate	0.37 ± .03	0.47 ± .04[e]	0.50 ± .03[e]
Sodium dodecyl sulfate	0.27 ± .03		

[a] Ionic strength maintained by addition of $NaClO_4$. [b] Initial concentrations: ester, 0.10 *m*; borax, 0.025 *m*; pH 8.63. [c] Initial concentrations: ester, 0.10 *m*; acetic acid, 0.055 *m*; sodium acetate, 0.01 *m*; pH 4.92. [d] Initial concentrations: ester, 0.10 *m*; acetic acid, 0.028 *m*; sodium acetate, 0.050 *m*. [e] Corrected for a *ca.* 12% contribution from the hydronium ion catalyzed reaction.

The picture is quite different in the case of the second-order rate constant, k_H, for the hydrogen ion-catalyzed hydrolysis as measured in perchloric acid solutions (Table II). Here a sharp increase in rate accompanies micelle formation. For each value of the ionic strength, the rate varies little with increasing chain length up to the point at which the ester ions aggregate into micelles. At the lower ionic strength, the rate increase accompanying micellization is near a factor of 40 for sodium dodecyl sulfate and rises to near a factor of 80 for sodium octadecyl sulfate. All of the esters show the negative salt effect expected for a reaction which occurs formally between ions of opposite charge. The salt effect at first decreases

(15) M. H. Lietzke, R. W. Stoughton, and T. F. Young, *J. Phys. Chem.*, **65**, 2247 (1961). This reference gives $pK_a(HSO_4^-) = 2.9$ at 90°, which, together with reasonable estimates of activity coefficients, implies that catalysis by H^+ contributed by the ionization of HSO_4^- is unimportant for $HClO_4$ concentrations above 0.01 *m*.

(16) E. D. Hughes, C. K. Ingold, and W. Shapiro, *J. Chem. Soc.*, 225 (1936).

with increasing chain length, but then increases sharply for the micellar esters. For each salt concentration, the longest chain ester for which a rate constant is listed is the highest member of the series which is sufficiently soluble to permit such data to be taken at 90°. The low value of k_H for sodium decyl sulfate at the lower ionic strength reflects the fact that only a small fraction of this material is aggregated into micelles (c.m.c. = 0.036 *m*, see Discussion).

For the non-micellar esters, specific salt effects at constant ionic strength for k_H are seen to decrease with increasing chain length, thus paralleling the ionic strength effect. For the micellar ester, sodium decyl sulfate, the data show that specific salt effects on k_H arising from the interchange of sodium ion and hydrogen ion are small, although perhaps somewhat larger than expected for a non-micellar ester of the same chain length.

TABLE II

RATE CONSTANTS FOR H^+ CATALYZED HYDROLYSIS AT 90°

Ester	Initial ester concn.[a] (*m*)	$HClO_4$ concn.[a] (*m*)	μ[a,b]	$10^5 k_H$[c] (mole^{-1} sec.$^{-1}$)
Sodium methyl sulfate	0.0409	0.0103	0.51	5.02
	.0409	.0411		5.00
	.0411	.103		5.47
	.103	.103		4.90
	.206	.207		5.18
	.103	.310		6.43
	.0402	.0405	.081	7.48
Sodium ethyl sulfate	.0409	.103	.51	5.68
	.103	.103		5.40
	.207	.208		5.33
	.103	.310		5.92
	.0402	.0406	.081	7.47
Sodium amyl sulfate	0.0409	.103	.51	5.27
	.104	.105		5.25
	.103	.312		5.50
	.0404	.0405	.081	6.38
Sodium decyl sulfate	.0413	.104	.51	41.3
	.104	.105		50.7
	.214	.215		48.3
	.104	.315		48.5
	.104	.420		44.5
	.0405	.0407	.081	33.7
Sodium dodecyl sulfate	.0414	.104	.51	81.7
	.0405	.0407	.081	198
Sodium tetradecyl sulfate	.0414	.104	.51	89.2
	.0406	.0407	.081	280
Sodium hexadecyl sulfate	.0407	.0409	.081	347
Sodium octadecyl sulfate	.0410	.0412	.081	505

[a] Duplicate runs had concentrations identical to within ±1 in the last significant figure shown. [b] Ionic strength was maintained by addition of sodium perchlorate to those runs requiring it. [c] For these rate constants, the average deviation of a single determination from the mean usually is near 1% and in no case exceeds 2% of the reported mean.

The complementary case of a reaction which is retarded by micellization is illustrated in Table III, which lists values of the second-order rate constant, k_{OH}, for hydroxide ion-catalyzed hydrolysis. Here the situation is complicated somewhat by the existence of a decrease in rate accompanying a simple increase in chain length. The discontinuity in rate upon the transition to micellar esters is none the less noticeable, however, since a rate decrease of about a factor of four upon proceeding from the ethyl to the amyl ester is followed by a decrease of at least a factor of 60 upon going from the amyl to the decyl ester.

TABLE III

RATE CONSTANTS FOR OH^- CATALYZED HYDROLYSIS AT 90° AND μ = 0.51

Ester	$10^5 k_{OH}$ (mole^{-1} sec.$^{-1}$)
Sodium methyl sulfate[a]	2.73 ± 0.02
Sodium methyl sulfate[b]	2.63 ± .02
Sodium ethyl sulfate[a]	0.250 ± .005
Sodium amyl sulfate[a]	.060 ± .003
Sodium decyl sulfate[a]	.000 ± .001
Sodium dodecyl sulfate[a]	.000 ± .001

[a] Initial concentrations: ester, 0.21 *m*; sodium hydroxide, 0.30 *m*. [b] Initial concentrations: ester, 0.053 *m*; sodium hydroxide, 0.081 *m*; sodium perchlorate, 0.38 *m*.

As the concentration of micellar ester is decreased toward the c.m.c., the observed rate constant approaches that characteristic of the free non-micellar ions. This behavior is illustrated in Fig. 1, which shows k_H for sodium decyl sulfate as a function of the reciprocal of the ester concentration. In an attempt to minimize the influence of specific salt effects on that curve, the perchloric acid concentration and the total sodium ion concentration (maintained by sodium perchlorate) to which the experimental points refer are constant at 0.02 and 0.49 *m*, respectively. Some variation in the ionic strength of the bulk solution is unavoidable in such a series, since the contribution of the micellar ester is uncertain.

Attempts to measure the c.m.c. conductimetrically at ionic strengths near 0.5 were found to be unfeasible. For this reason, its value was determined at four lower salt concentrations to enable extrapolation to the higher value. It is well established[17,18] that the logarithm of the c.m.c. of a micellar electrolyte is a linear function of the logarithm of the total gegenion concentration. The values determined for the c.m.c. of sodium decyl sulfate at 90° for sodium perchlorate molalities of 0, 0.0498, 0.0989, and 0.2002 were, respectively, 0.0439, 0.0366, 0.0294, and 0.0234 *m*. The least squares linear equation of best fit for these data is

$$\log (\text{c.m.c.}) = -1.878 - 0.392 \log (c + \text{c.m.c.}) \quad (5)$$

where *c* represents the molality of sodium perchlorate. The average deviation of a single point from the line is 0.012 log unit or *ca.* 3% of the measured c.m.c. The slope of this line is significantly lower than the slope reported[19] for sodium decyl sulfate in sodium chloride solutions at 25°.

(17) E. Heymann and I. M. O'Donnell, *J. Colloid Sci.*, **4**, 395 (1949).

(18) R. J. Williams, J. B. Phillips, and K. J. Mysels, *Trans. Faraday Soc.*, **51**, 728 (1955).

(19) K. J. Mysels and P. Kapaunan, *J. Colloid Sci.*, **16**, 481 (1961).

Using the same concentrations as those indicated for the 90° rate data in Table I, the values of k_H were measured at 65 and 75° for sodium ethyl sulfate and sodium dodecyl sulfate. The activation parameters for the acid-catalyzed hydrolysis of these esters were calculated from the rate data for these three temperatures by least squares, and their values and probable errors (expressed to the nearest full tenth of a kcal./mole or e.u.) are given in Table IV. It was necessary to correct the pseudo first-order rate constants measured for

TABLE IV

ACTIVATION PARAMETERS FOR THE H^+ CATALYZED HYDROLYSIS OF SODIUM ALKYL SULFATES

Ester[a]	μ[b]	ΔH^* (kcal./mole)	ΔS^* (e.u.)
Sodium ethyl sulfate	0.081	30.7 ± 0.1	6.6 ± 0.1
	.51	30.0 ± .3	4.2 ± .5
Sodium dodecyl sulfate	.081	28.0 ± .2	5.7 ± .4
	.51	28.3 ± .1	4.8 ± .1

[a] Initial concentrations are those given for Table I. [b] Calculated as if no micelles were formed. (*i.e.*, μ = total uni-univalent salt concentration.)

sodium ethyl sulfate for small contributions from the spontaneous hydrolysis rate before calculating the value of k_H. These corrections ranged from 1 to 10% of the observed rate constant. The corrections for the 90° rates were taken from the observed values of k_0 and those for the lower temperatures were calculated from the 90° rate constant and the value of ΔH^* reported[4] for the neutral hydrolysis. No such corrections were necessary for the sodium dodecyl sulfate data.

Discussion

Uncatalyzed Reaction.—The rate of attack of water at the α-carbon is seen (Table I) to be little affected by the aggregation of the ester anions into micelles. This implies that the micelle is very "wet" at least as far in as the α-carbon. More precisely stated, the water activity and the solvating power of the medium are essentially unchanged at this depth into the micelle. Such a conclusion is consistent with the rough surface proposed by Stigter and Mysels[20] for sodium dodecyl sulfate micelles. In this model, the sulfate groups protrude from the hydrophobic body of the micelle into the solution, thus allowing both counterions and solvent to penetrate between them. This type of structure also has been postulated for alkyl sulfate micelles by Veis and Hoerr[21] on the basis of the electrostatic free energy of micelle formation.

That this wetness is a property only of the outer layers of the micelle and not of its entire volume is suggested by the observation[22] that the uncatalyzed rate of hydrolysis of ethyl trichloroacetate is strongly suppressed by sodium dodecyl sulfate. Since this ester is far more soluble in non-polar solvents (and in aqueous sodium dodecyl sulfate solutions) than it is in water, it would be expected to avoid the wet outer layers of the micelle in favor of the hydrophobic interior where it is protected from solvolysis.

Hydrogen Ion Catalyzed Reaction.—The sharp increase in k_H which accompanies micellization suggests that some factor is operative which does not affect k_0. All of the data are in agreement with the hypothesis that this factor is the electrostatic potential of the micelle with respect to the bulk solution. The effect of micellization on the hydrogen ion catalyzed rate presumably takes place through a shift in the prior protonation equilibrium (eq. 2). The sulfate moieties become stronger bases due to the presence of a negative potential on the micelle in a manner analogous to the change in strength of an acidic group arising from the presence of a charged center in the same molecule.[23] It is known that the acidities of micellized alkyl ammonium ions[21] and of various indicators in the presence of micelles[24] are shifted in the manner expected from a consideration of charge, so that a similar effect for the alkyl sulfuric acids is not unexpected. The rate-determining reaction of the protonated ester molecules (eq. 3) then occurs with a specific rate essentially unchanged from its value in the bulk solution. The increase in the micellar rate effect upon proceeding to still longer chains presumably reflects the increase in size and "tightness" of the micelle expected to accompany the increase in chain length.

The potential may be considered either to act directly on the prior equilibrium constant or to shift that equilibrium by changing the distribution of hydrogen ion in the double layer. These viewpoints are equivalent and differ only in their implied definitions of K. That this electrostatic effect is the only important contributor to the observed rate enhancement is suggested by the following considerations. Since k_0 is free from medium effects arising from the hydrocarbon character of the micelle, k_H (which involves participation of water at a position two atoms further from the micellar interior) also should be free from such influences. Further, the lack of chain-length effects for non-micellar esters suggests that k_H is unaffected by steric hindrance on the hydrocarbon side of the sulfate moiety.

The assumption that the electrostatic effect is the sole important contributor to the rate ratio allows the micellar potential to be calculated from that ratio. The ΔF^* for formation of the transition state from the alkyl sulfate and hydrogen ions may be split into two parts: an electrostatic term ($N\epsilon\psi$) representing the electrical work done in bringing one mole of protons, each with charge, ϵ, from the bulk of the solution up to the sulfate moiety which has a potential, ψ, and a non-electrostatic term including all other contributions and assumed to be constant. Using subscripts m and f to denote functions for micellar and free alkyl sulfate ions, respectively, one can then write

$$\Delta F_m^* - \Delta F_f^* = N\epsilon(\psi_m - \psi_f) = N\epsilon\Delta\psi \quad (6)$$

(20) D. Stigter and K. J. Mysels, *J. Phys. Chem.*, **59**, 45 (1955).
(21) A. Veis and C. W. Hoerr, *J. Colloid Sci.*, **15**, 427 (1960).
(22) E. J. Fuller and J. L. Kurz, unpublished observations.
(23) J. G. Kirkwood and F. H. Westheimer, *J. Chem. Phys.*, **6**, 506. 513 (1938).
(24) G. S. Hartley, *Trans. Faraday Soc.*, **30**, 444 (1934).

Since $\Delta F_m^* - \Delta F_f^*$ also is equal to $-RT \ln (k_m/k_f)$, then

$$\Delta\psi = -\frac{RT}{N\epsilon} \ln \frac{k_m}{k_f} \qquad (7)$$

The quantity, $\Delta\psi$, may be interpreted as the average potential at the surface of the micelle less the contribution to this potential made by the particular sulfate group under consideration. Since the number of anions forming the micelle is of the order of 50 or more,[25] the error made in identifying $\Delta\psi$ with the surface potential of the micelle should be small. This is particularly true for the assumed model of a spherical micelle with the charged groups free to move into the most stable position on the surface. It should be pointed out, however, that the magnitude of both ψ_f and ψ_m would be expected to be much larger than their difference, since the majority of the potential is due to the single negative charge on the ion in question. ($\psi_f = 3$ v., assuming an effective radius of 2.5 Å. and a dielectric constant of 2.)

The values of $\Delta\psi$ calculated for the micelles formed from sodium alkyl sulfates with even numbers of carbon atoms from C_{10} to C_{18} are given in Table V for the two ionic strengths at which measurements were made. The value taken for k_f is that measured for the amyl ester at the same ionic strength. The value of $\Delta\psi$ for the decyl ester is calculated from the value of k_m obtained by extrapolation to infinite ester concentration

TABLE V

$\Delta\psi$ (MV.) FOR SODIUM ALKYL SULFATES

Ester	$\mu = 0.46$[a]	$\mu = 0.04$[a]
Sodium decyl sulfate	−80.1	
Sodium dodecyl sulfate	−85.4	−106.4
Sodium tetradecyl sulfate	−88.3	−117.4
Sodium hexadecyl sulfate		−123.9
Sodium octadecyl sulfate		−135.8

[a] Listed ionic strength does not include contributions from the micellar electrolyte.

at constant ionic strength by the procedure described below for estimation of the c.m.c. from kinetic data. No such correction has been made for the higher esters. Assuming that the c.m.c. at 90° is the same as that measured at 25° and the same ionic strength,[18,26] lack of such a correction would cause the $\Delta\psi$ for the C_{12} ester to be in error by only 1.8 mv. at the lower ionic strength and 0.4 mv. at the higher ionic strength. Errors would be even smaller for the higher esters.

Two features in Table V are immediately evident. The micellar potential increases in magnitude as the chain length increases, reflecting the expected enlarging and tightening of the micelle, and its magnitude is greater at the lower ionic strength where shielding by the double layer would be expected to be reduced. The zeta potential of sodium dodecyl sulfate micelles at 25° has been measured as a function of sodium chloride concentration by Stigter and Mysels.[20] These same authors also have calculated the surface potential (ψ^0) expected for a smooth spherical Gouy micelle having the degree of association observed for sodium dodecyl sulfate micelles. The values of the ionic strength listed in Table V do not include contributions from the micellar electrolyte and hence are directly comparable to the sodium chloride concentrations for which ζ and ψ^0 are listed by these authors.

The value of $\Delta\psi$ at $\mu = 0.04$ (−106 mv.) falls between the values of ζ (−78 mv.) and of ψ^0 (−155 mv.) corresponding to that ionic strength. Stigter and Mysels considered the difference between ψ^0 and ζ to be too large to be accounted for by the 1.5 Å. separation of the two layers to which these potentials refer, and thus were led to their proposal that the micelle has a "rough" surface with sulfate groups projecting and binding counterions between them. Such a model would lead to a magnitude of ψ^0 lower than that calculated for the smooth micelle but still higher than the zeta potential. The quantity ψ_m refers to a potential which is averaged over the various levels in the double layer at which the sulfate moiety undergoes reaction. The fact that $\Delta\psi$ falls in the range expected for ψ^0 thus implies that this reaction occurs predominantly at the inner boundary of the double layer. This is reasonable, since the protonated ester is a neutral species.

Critical Micelle Concentration.—The variation of k_H with ester concentration which is observed for a long chain ester may be related to the c.m.c. if two simplifying assumptions are made. The acid-catalyzed hydrolysis is assumed to take place by two distinct and independent paths, one involving micellar ester and the other involving free, unaggregated ester. The concentration of non-micellar ester (E_f) is further assumed to be independent of the total ester concentration (E_t) so long as the latter exceeds the c.m.c. This would give for k_H

$$k_H = k_m + \frac{E_f}{E_t}(k_f - k_m) \text{ for } E_t \geq \text{c.m.c.}$$

$$k_H = k_f \text{ for } E_t \leq \text{c.m.c.} \qquad (8)$$

A plot of k_H *vs.* $1/E_t$ thus should give two straight lines intersecting at $1/E_t = 1/\text{c.m.c.}$ In practice, some rounding of the intersection (as shown in Fig. 1) is expected due to the somewhat diffuse nature of the c.m.c. The value obtained for the c.m.c. of sodium decyl sulfate at 90° and a total ionic strength of 0.51 was 0.0190 *m*.

This value may be compared to that obtained from the conductivity measurements. Setting $c +$ c.m.c. = 0.51 in eq. 5 yields a value of 0.0172 *m*, which is about 10% lower than the kinetically measured value. The c.m.c. values implied by eq. 5 for the conditions of the kinetic runs in Table II are 0.036 *m* for the lower ionic strength (total $\mu = 0.081$, $c +$ c.m.c. = 0.077 *m*) and 0.018 *m* for the higher ionic strength (total $\mu = 0.51$, $c +$ c.m.c. = 0.49 *m*). These figures support the previous assumption that under the experimental conditions referred to in Table II all of the esters

(25) See, for example, K. J. Mysels and L. H. Princen, *J. Phys. Chem.*, **63**, 1696 (1959).

(26) This assumption is reasonable since the ΔH of micellization is near zero as commented on later in this paper.

with carbon chain lengths of 10 or greater were predominantly aggregated into micelles except for the decyl ester at the lower ionic strength.

Hydroxide Ion Catalyzed Reaction.—The effect of the micellar potential on the rate of attack by hydroxide ion should be formally the same as for the acid-catalyzed reaction. Here the electrostatic free energy for bringing a charge from the bulk solution up to the micelle is added directly to the free energy of activation for the rate-determining step rather than to the free energy change in a prior equilibrium. The concentrations of both hydroxide ion and doubly negative transition state thus are decreased relative to their values in the bulk solution. The situation is not quite so clean cut as in the acid-catalyzed reaction, however, due to the existence of a steric chain length effect on the rate which apparently still is increasing when the micellar esters are reached. The expected result of the summation of this effect and the electrostatic term is consistent with the minimum rate factor of 60 obtained by experiment.

Salt Effects.—The negative ionic strength effect (Table II) observed for the hydrogen ion catalyzed reaction is consistent with its charge type. The increase in the magnitude of this effect from the range 20–40% to *ca.* 300% which accompanies the micellization of the ester is qualitatively consistent with the greater effective charge on the ester in the micellar systems. There is, however, some question of the particular mechanism giving rise to this increased effect. Such a result could arise either from the simple increase in the screening effect of the double layer as the counterion concentration increases, or from a specific replacement of the kinetically active hydrogen ions on the micelle through competition with other cations. This latter site-binding mechanism is the one proposed by Kolthoff and Johnson[27] in order to explain their observation of a decreased catalytic efficiency of hydrogen ion for the iodine–acetone reaction in the presence of alkyl sulfate micelles when potassium chloride was added.

The data indicate that no large change in the value of k_H for sodium decyl sulfate occurs when the sodium ion–hydrogen ion ratio is varied by a factor of 16 from 4 to $^1/_4$ while maintaining a constant ionic strength. This rules out the site-binding mechanism as a major contributor to the salt effect. Apparently, the increase in double layer shielding, which is the colloidal analog of the ion atmosphere shielding of simple ions, is responsible for the observed decrease in rate with increasing salt concentration.

Activation Parameters.—When the over-all rate effect for k_H is separated into its temperature dependent and temperature independent components, it is found that the rate increase accompanying micellization is due to a change in the enthalpy of activation. This is shown in Table IV. Such a finding would not have been expected on the basis of analogy with the usual kinetic effects of simple small charges. Such electrostatic effects commonly manifest themselves in the entropy of activation and not in the enthalpy.[28]

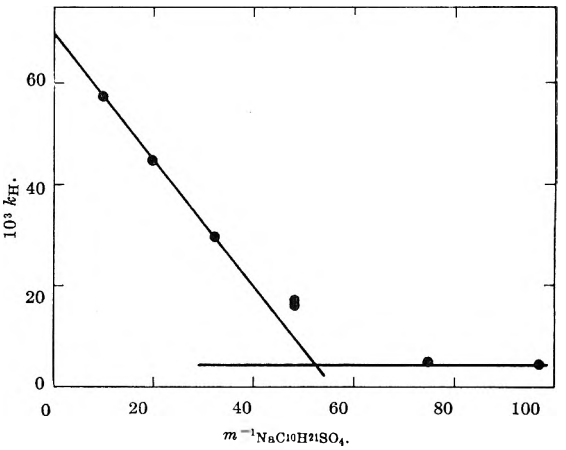

Fig. 1.—k_H at 90° for sodium decyl sulfate as a function of its reciprocal concentration; the horizontal line is defined by the value for k_H for sodium amyl sulfate under the same conditions (μ = 0.51, [$HClO_4$] = 0.02 m).

This apparently contradictory state of affairs is closely related to the anomalous values of the thermodynamic functions found for the micellization process itself. The heat of micellization for alkyl sulfate salts is very near zero,[29–31] which in turn requires that the equilibrium entropy change be zero. These values of the thermodynamic parameters for micellization appear inexplicable on the basis of a naïve model for micelle formation in which large numbers of long chain negative ions together with some smaller positive ions are brought together to form the micelle, since a large decrease in entropy would be expected. A qualitative explanation has been provided by Goddard, Hoeve, and Benson[30] in terms of the breakup of the water structure around the individual hydrocarbon chains when they aggregate into micelles.

The difference between the heats of activation for the micellar and non-micellar esters, $\Delta H_m^* - \Delta H_f^*$, may be shown to be identical with the difference between the enthalpies for the incorporation of the transition and ground states into micelles. The kinetic results thus imply that the enthalpy of incorporation of the transition state into a micelle is *ca.* 2 kcal./mole less than that for the incorporation of a dodecyl sulfate ion. Similarly, the entropies for micellization of the ground and transition states must be nearly equal. In view of the present non-quantitative state of attempts to rationalize the thermodynamic functions for micellization of stable species, these parameters for the micellization of transition states perhaps can best be described as not necessarily unreasonable, even though the transition and ground states are of dif-

(27) I. M. Kolthoff and W. F. Johnson, *J. Am. Chem. Soc.*, **73**, 4563 (1951).

(28) See, for example, A. A. Frost and R. G. Pearson, "Kinetics and Mechanism," 2nd Ed., John Wiley and Sons, New York, N. Y., 1961, Chap. 7.

(29) B. D. Flockhart, *J. Colloid Sci.*, **16**, 484 (1961).

(30) E. D. Goddard, C. A. Hoeve, and G. C. Benson, *J. Phys. Chem.*, **61**, 593 (1957).

(31) E. Hutchinson, K. E. Manchester, and L. Winslow, *ibid.*, **58**, 1124 (1954).

ferent charge types. At least, the failure of the rate effects to appear in the entropy term cannot be cited as evidence against the electrostatic origin of those rate effects.

THE REACTIVITY OF HYDROGEN ATOMS IN THE LIQUID PHASE. IV. THE REACTION WITH SOME HALOGENATED COMPOUNDS

BY T. J. HARDWICK

Gulf Research & Development Company, Pittsburgh 30, Pennsylvania

Received June 11, 1962

Studies have been made on the reactivity of hydrogen atoms with a variety of halogenated alkanes (RX) in liquid *n*-hexane at 23°. With such compounds, hydrogen atoms abstract halogen atoms to form HX, and in many cases, hydrogen to form H_2. For halocarbons of analogous structure, the rate for halogen abstraction is invariably greatest for iodides, least for chlorides. Successive substitution of halogen atoms in an alkane molecule increases the rate of halogen removal. The rates of iodine abstraction from iodoalkanes are among the highest which have been observed in non-ionic solution chemistry ($0.6–2 \times 10^{13}$ cc. mole^{-1} sec.$^{-1}$).

Introduction

The reaction of hydrogen atoms with halogenated hydrocarbons heretofore has been studied only in the gas phase. With only one or two exceptions this has been limited to the halogenated methanes. The most thorough work is that of Cremer, Curry, and Polanyi[1] in which hydrogen atoms, produced by electrical discharge, reacted with methyl chloride, methylene chloride, chloroform, and carbon tetrachloride. In all cases chlorine was abstracted to form hydrogen chloride. In addition, evidence was obtained for hydrogen abstraction from the first three compounds.

With the advent of a method of measuring the reactivity of hydrogen atoms in solution, it became possible to study the reactions of hydrogen atoms with a variety of halogenated hydrocarbons. It is the purpose of this paper to report such experiments.

$$\mathrm{RH} \xrightarrow{G_1} \mathrm{H_2} + \text{Products} \qquad (1)$$

The method of measuring hydrogen atom reactivity in solution has been described in detail previously.[2] Briefly, hydrogen atoms are produced *in situ* during the radiolysis of a saturated hydrocarbon (*n*-hexane in our experiments).

$$\mathrm{RH} \xrightarrow{G_2} \mathrm{H} + \mathrm{R} \qquad (2)$$

The hydrogen atoms diffuse at thermal energies, reacting competitively with solvent by hydrogen abstraction or added solute (<2%) by addition, hydrogen abstraction, and, in the case of halogenated hydrocarbons, by halogen removal.

$$\mathrm{H} + \mathrm{RH} \xrightarrow{k_3} \mathrm{H_2} + \mathrm{R} \qquad (3)$$

$$\mathrm{H} + \mathrm{RX} \xrightarrow{k_4} \mathrm{R} + \mathrm{HX} \qquad (4)$$

$$\xrightarrow{k_5} \mathrm{H_2} + \mathrm{R'X} \qquad (5)$$

In addition, hydrogen gas will be produced directly from the solvent, by some process unaffected by added solutes (eq. 1).

From steady-state kinetics the following relation is derived

$$\frac{1}{G_{\mathrm{H_2(0)}} - G_{\mathrm{H_2(S)}}} = \frac{1}{\Delta G_{\mathrm{H_2}}} = \frac{1}{G_2}\frac{[\mathrm{RH}]}{[\mathrm{RX}]}\frac{k_3}{k_4} + \frac{1}{G_2}\left(\frac{k_5}{k_4} + 1\right)$$

where

$G_{\mathrm{H_{2(0)}}}$ is the radiolytic hydrogen gas yield in pure solvent ($= G_1 + G_2$)

$G_{\mathrm{H_2(S)}}$ is the radiolytic hydrogen gas yield in the presence of solute RX

For *n*-hexane $G_{\mathrm{H_{2(0)}}} = 5.28$, $G_2 = 3.16$.

A plot of $1/\Delta G_{\mathrm{H_2}}$ *vs.* [RH]/[RX] gives a straight line of slope $(k_3/k_4)(1/G_2)$ and intercept $1/G_2$ $(k_5/k_4 + 1)$, from which relative values of k_3, k_4, and k_5 may be found. An intercept equal to $1/G_2$ (0.316) indicates that reaction 5 does not occur to a measurable extent.

Ratios of rate constants have been put on an absolute basis by taking $k_3(\mathrm{H} + n\text{-hexane}) = 4.9 \times 10^9$ cc. mole^{-1} sec.$^{-1}$. Justification for this has been given previously.[2]

Experimental

Materials.—All materials were the best grade available, and, if water white, were used without further purification. Off-color bromides and iodides were washed with sodium carbonate and sodium sulfite, dried, and redistilled. Iodoform and carbon tetraiodide were used as received. Normal hexane was Phillips pure grade, and was purified further by prolonged stirring with sulfuric acid and was stored over anhydrous sodium carbonate. The unsaturation, as measured by bromination, was less than 0.1 m*M*/l.

Radiolytic Hydrogen Yields.—The method of determining hydrogen yields has been described in detail previously.[2] Briefly, 100 ml. of deaerated solution was irradiated with X-rays to about 20 krads and the hydrogen gas was removed, isolated, and measured on a McLeod gage. The energy absorbed by the samples was concurrently monitored using the Fricke dosimeter. All irradiations were made at 23°.

(1) E. Cremer, J. Curry, and M. Polanyi, *Z. physik. Chem.*, **B23**, 445 (1933).

(2) T. J. Hardwick, *J. Phys. Chem.*, **64**, 1623 (1960); **65**, 101 (1961); **66**, 117 (1962); **66**, 291 (1962).

Irradiations.—Samples for irradiation were prepared by diluting a stock solution, or in cases of limited solubility, by direct addition of solute. All solute concentrations used (except for some experiments with alkyl chlorides) were present in less than 1% by volume. Corrections were applied to the results to account for the energy absorbed directly by the solute.

Results

For all systems studied, a kinetic plot of the data ($1/\Delta G_{H_2}$ *vs.* [RH]/[RX]) invariably gave a straight line. The values of the intercepts were 0.316 or more, never less. Kinetic plots of the data for the series—alkyl bromide, methylene bromide, bromoform, carbon tetrabromide are given in Fig. 1, as an example of the precision of the data and the range of concentrations over which experiments were performed.

The rate constants obtained are reported in Tables I–IV. In the first three tables, k_4 is the rate of halogen abstraction. In Table IV, k_4 is the sum of the rates of halogen abstraction and of hydrogen atom addition to the carboxyl group; with the present technique the individual rates in this case cannot be determined. The rate constant k_5 in all cases is the rate of hydrogen abstraction.

Discussion

The reactivity of hydrogen atoms with various halocarbons obviously is related to structure and to the identity of the halogen atoms in the molecule.

Alkyl Halides.—The rates of reaction of hydrogen atoms with alkyl halides are given in Table I. Both halogen and hydrogen abstraction occur. For both types of reaction the reactivity decreases iodide > bromide > chloride. Within each halogen group the rates of both types of abstraction are remarkably similar; where collective brackets are drawn, the same straight line on the kinetic plot can be drawn for all members of the group.

The abstraction of hydrogen can be accounted for only by assuming that the presence of the halogen has weakened the C–H bond considerably. The source of this abstracted hydrogen atom cannot definitely be assigned; most likely it derived from the same carbon atom as the halide. The absence of hydrogen abstraction from *t*-butyl halides would seem to confirm this. However, from other results to be discussed later, this rule apparently is limited to alkyl monohalides.

By and large, the reactivity of each type of alkyl halide is essentially the same. This reaffirms our previous postulate that collision of the hydrogen atom and the halogen atom is required for abstraction, and that the effective collision diameter of each halogen atom will be constant. As in former work[2] it appears that the alkyl portion of the molecule has relatively little influence on the rate of reaction.

Halogenated Methanes. (Table II).—In general, the reactivity of hydrogen atoms toward these compounds increases with increasing halogenation. Again the reactivity of iodides > bromides > chlorides. In the case of chlorides and bromides, it is interesting to note that hydrogen is abstracted at a faster rate from the dihalide than from the mono- or trihalide. It may be that increasing the extent of halogen substitution decreases the

TABLE I

REACTIVITY OF HYDROGEN ATOMS WITH ALKYL HALIDES (RX)

T = 23°

	k_4 (X abstraction) × 10^{11} cc. mole^{-1} sec.$^{-1}$	k_5 (H abstraction) × 10^{11} cc. mole^{-1} sec.$^{-1}$	k_5/k_4
n-Propyl chloride	1.42	0.96	0.68
n-Butyl chloride			
sec-Butyl chloride			
n-Propyl bromide	12.4	3.3	0.27
n-Butyl bromide			
sec-Butyl bromide	16.5	6.4	0.39
t-Butyl bromide	15.1	..	<0.03
Cyclohexyl bromide	17.7	5.5	0.31
Methyl iodide	60	7.2	0.12
n-Propyl iodide	58	3.5	0.06
n-Butyl iodide	76	9.0	0.12
sec-Butyl iodide			
Cyclohexyl iodide			
t-Butyl iodide	67	..	<0.03

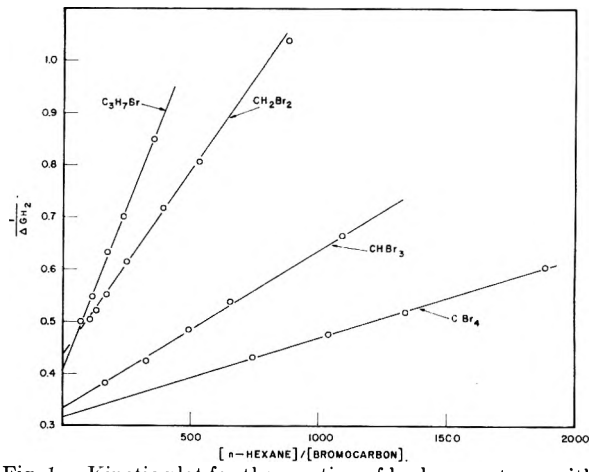

Fig. 1.—Kinetic plot for the reaction of hydrogen atoms with successively brominated methanes.

TABLE II

REACTIVITY OF HYDROGEN ATOMS WITH HALOGENATED METHANES

T = 23°

	k_4 (X abstraction) × 10^{11} cc. mole^{-1} sec.$^{-1}$	k_5 (H abstraction) × 10^{11} cc. mole^{-1} sec.$^{-1}$
RCl	1.4	0.96
CH_2Cl_2	14.9	4.0
$CHCl_3$	16.1	2.2
CCl_4	17.5	..
RBr	12.4	3.3
CH_2Br_2	22.7	8.6
$CHBr_3$	51	2.6
CBr_4	100	..
CF_2Br_2	14.0	..
CH_3I	60	7.0
CH_2I_2	138	..
CHI_3	187	..
CI_4	210	..

TABLE III

REACTIVITY OF HYDROGEN ATOMS WITH POLYHALOGENATED ALKANES

$T = 23°$

	k_4 (X abstraction) $\times 10^{11}$ cc. mole^{-1} sec.$^{-1}$	k_5 (H abstraction) $\times 10^{11}$ cc. mole^{-1} sec.$^{-1}$
1,1-Dichloroethane	8.6	1.7
1,1-Dichlorobutane	8.5	1.7
2,2-Dichlorobutane	11.4	2.3
1,2-Dichloroethane	15.4	7.4
1,1,2-Trichloroethane	13.6	1.5
1,1,1-Trichloroethane	14.2	2.2
1,1,2,2-Tetrachloroethane	33.0	1.4
Pentachloroethane	36.0	...
Hexachloroethane	18.0	...
1,2-Dibromoethane	25	4.5
1,1,2-Tribromoethane	25	1.7
1,1,2,2-Tetrabromoethane	34	0.5
Pentabromoethane	49	...
Hexabromoethane	Insoluble	
1,2-Dibromopropane	21	4.1
1,3-Dibromopropane	21	4.4
1,4-Dibromobutane	19.5	1.2
1,5-Dibromopentane	17.5	3.7
1,1-Dibromobutane	16	2.1
2,2-Dibromobutane	21	4.3
2,3-Dibromobutane	32.3	10.6
1,2,3-Tribromopropane	30	3.9

TABLE IV

REACTIVITY OF HYDROGEN ATOMS WITH HALOGENATED ESTERS

$T = 23°$

	k_4 X abstraction and/or H addition $\times 10^{-11}$ cc. mole^{-1} sec.$^{-1}$	k_5 (H abstraction) $\times 10^{-11}$ cc. mole^{-1} sec.$^{-1}$
Methyl acetate	0.7	<0.05
Methyl chloroacetate	22	1.9
Methyl α-chloropropionate	14.6	2.4
Methyl bromoacetate	39	6.4
Methyl iodoacetate	92	10

energy of activation of the hydrogen abstraction reaction, but that in the haloforms the size of the halogen atoms shields the smaller hydrogen atom from collision.

Replacing the hydrogen by fluorine, as in the case of difluorodibromomethane, apparently strengthens the C–Br bond, for the reactivity of this compound toward hydrogen atoms is less than that of methylene bromide.

It is interesting to compare our results with those obtained in the gas phase reaction of hydrogen atoms on chloromethanes. Chadwell and Titani[3] studied the reaction with methyl and ethyl chlorides, and observed only chlorine abstraction, $k_4 = 5 \times 10^7$ cc. mole^{-1} sec.$^{-1}$, giving $E = 8$–9 kcal. Cremer, *et al.*,[1] found evidence for both chlorine and hydrogen abstraction. For chlorine abstraction $k_4 = 2.2 \times 10^7$ cc. mole^{-1} sec.$^{-1}$, $E = 7.2$ kcal.

(3) H. M. Chadwell and T. Titani, *J. Am. Chem. Soc.*, **55**, 1363 (1933).

Later, Lee and Leroy[4] confirmed the Cremer mechanism, but were not convinced of the presence of hydrogen abstraction.

Cremer, *et al.*,[1] also investigated hydrogen atom reactivity with methylene chloride and chloroform. In both cases evidence was found for hydrogen abstraction as well as for chlorine abstraction. For $H + CH_2Cl_2 \rightarrow HCl + CH_2Cl$, $k_1 = 6.2 \times 10^9$ cc. mole^{-1} sec.$^{-1}$, $E = 5.8$ kcal.; for $H + CHCl_3 \rightarrow HCl + CHCl_2$, $k_1 > 8 \times 10^{10}$ cc. mole^{-1} sec.$^{-1}$, $E = <4.3$ kcal.

The reactivity of hydrogen atoms with carbon tetrachloride has been studied by several workers.[1,5,6] The rate constants at room temperature varied from 2×10^9 to $>4 \times 10^{11}$ cc. mole^{-1} sec.$^{-1}$, while the activation energy is quoted as 3.5 kcal. or <3.3. kcal.

Qualitatively, the gas phase results agree with ours, in that the rate of chlorine abstraction increases with increased chlorine substitution. The rate constants measured, however, are unaccountably low when compared with the present work, even if due consideration is given to the difficulties in measuring hydrogen atom concentrations in a discharge tube.

Halogenated Ethanes. (Table III).—In general, the rate of halogen abstraction from these compounds increases with a greater degree of halogenation. The exception appears to be hexachloroethane, but it may be that the C–Cl bonds are stronger in the symmetrical molecule. Unfortunately, hexabromoethane is too insoluble in *n*-hexane to permit kinetic measurements.

In a previous paragraph we had suggested that the abstracted hydrogen most likely comes from the halogenated carbon atom. In the case of polyhalogenated alkanes this rule does not appear to hold rigorously, for hydrogen abstraction is observed in 1,1,1-trichloroethane.

For the sequence of dibromoalkanes, where in successive compounds a methylene group is inserted between the end CH_2Br groups (*e.g.*, 1,2-dibromoethane, 1,3-dibromopropane, etc.), it is found that the rates of bromine abstraction decrease as the bromine atoms are located farther apart. Such a result, presumably due to decreasing interaction of the bromine atoms, is not unexpected. With the exception of 1,4-dibromobutane, a similar phenomenon is observed for hydrogen removal.

On comparing the results for 1,1-dichloro-ethane and -butane, one finds identical rates both for the halogen and for the hydrogen abstraction. In this type of compound the length of the alkyl chain has negligible effect on rates, and the reasons for such consistency probably are the same as for alkyl chlorides and bromides.

When comparing the isomeric dichloroethanes, it is found that both chlorine and hydrogen are abstracted more rapidly when the chlorines are on different carbon atoms. A similar result is observed in comparing the reactivities of 1,1-dibromobutane and 1,2-dibromopropane.

(4) G. L. Lee and P. J. Leroy, *Can. J. Research*, **28B**, 500 (1950).

(5) H. F. Smyser and H. M. Smallwood, *J. Am. Chem. Soc.*, **55**, 3499 (1933).

(6) J. E. Vance and W. C. Baumann, *J. Chem. Phys.*, **6**, 811 (1938).

Reactivity is highest when the halogens are not on a terminal carbon atom. The rate of both chlorine and hydrogen removal is faster from 2,2-dichlorobutane than from the 1,1-isomer. Similarly both rates are faster for 2,3-dibromobutane than for the 1,4-isomer.

Halogenated Esters.—The increase of reactivity with halogenation of methyl aliphatic esters (Table IV) again is in the order iodides > bromides > chlorides. Significantly, the rates are higher than for the aliphatic halides; obviously, the carboxyl group and the halide are augmenting one another in weakening both the C–X and C–H bonds.

The activation energies (E) for the abstraction of a halogen from alkyl halides by a hydrogen atom generally are quoted as 3–6 kcal., with E decreasing: chloride → bromide → iodide.[7] Except perhaps in the case of alkyl chlorides, these values are too high to correspond to the rate data presented in the present paper.

The rates of reaction with iodides are among the highest ever found for non-ionic reactions in the liquid phase. Further detailed comment on this will be made in a subsequent paper.

(7) E. W. R. Steacie, "Atomic and Free Radical Reactions," 2nd Edition, Reinhold Publ. Corp., New York, N. Y., 1954, p. 733.

MECHANISM OF THE DECOMPOSITION OF INORGANIC NITRATES[1]

BY TUNG-HO CHEN AND EVERETT R. JOHNSON

Chemistry Department, Stevens Institute of Technology, Hoboken, New Jersey

Received June 18, 1962

The radiation induced decomposition of several inorganic nitrates has been studied at room temperature. It has been found that the experimental results are compatible with a simple kinetic scheme, *viz.*, $MNO_3 \rightarrow MNO_2 + O$; $O + MNO_3 \rightarrow O_2 + MNO_2$; $O + MNO_2 \rightarrow MNO_3$, for all the nitrates studied except silver nitrate.

The inorganic nitrates appear to decompose when exposed to ionizing radiation to yield nitrite ion and oxygen,[2-7] *viz.*

$$MNO_3 \xrightarrow{\sim} MNO_2 + {}^1/_2O_2$$

The decomposition has been shown to be complex with a dependence on lattice parameters as yet not clarified. Initial G-values (molecules decomposed per 100 e.v. absorbed) have been shown to be independent of intensity[8] but dependent on the linear energy transfer (l.e.t.)[9] and temperature.[10] Studies of the oxygen isotope effect[10] and heats of solution measurements[6] have indicated the importance of lattice changes which occur during the irradiation of some of these salts.

Kinetic studies have revealed that the decomposition, at least in the case of $NaNO_3$, follows a fairly simple mechanism.[6] It is the intention of this paper to investigate the application of this mechanism to the decomposition of other nitrates.

Experimental

The radiation source was a fixed cylinder of cobalt-60 of approximately 1000 c. The source was located at the base of an 8-ft. shaft ("hole in the ground" type of installation) and shielded by a toroid filled with sand. Access to the source was obtained through five aluminum tubes welded together. Samples were placed in aluminum holders and then lowered into the radiation area. Positioning in the source was completely reproducible. The dose rate varied slightly from the base of the source to the top. Dosimetry was determined using the Fricke dosimeter. Each position was carefully calibrated and dose rate was determined with an over-all precision of better than ±2%. (In previous communications[6,11] a mobile Co-60 source was used and the experimental results using this source were less reproducible.)

A G-value of 15.45 molecules of ferrous ion oxidized per 100 e.v. absorbed was used in all calculations. Absorbed doses were calculated using the true mass absorption coefficients reported in the literature.[4] The value of 0.025 was used for the mass absorption coefficient of 0.8 N H_2SO_4 solution.

Nitrite ion was determined by the method of Shinn.[12] The molar extinction coefficient at 546 mμ was 53,200 l. mole^{-1} cm.$^{-1}$. In determining nitrite yield, concentrations of NO_2^- were used such that when the sample was treated with the reagents and read in the spectrometer, optical density readings of about 0.2 to 0.4 were obtained.

All chemicals except $CsNO_3$ were C.P. and used without further purification. The samples were ground to fine powders. $CsNO_3$ was recrystallized twice from triply distilled water.

Gas analysis was determined by the method described previously.[5] The results for oxygen analysis were obtained with over-all precision of better than ±5%.

Results and Discussion

Figures 1 through 10 show the nitrite yield *vs.* dose for the various nitrates. Oxygen analyses are appropriately indicated. In all cases (except $AgNO_3$) the solid line represents a theoretical curve, which was obtained by applying the following kinetic scheme to the decomposition

$$MNO_3 \xrightarrow{\sim} MNO_2 + O \quad k_1\Phi \qquad (1)$$

$$O + NO_2^- \longrightarrow NO_3 \quad k_2 \qquad (2)$$

$$O + NO_3^- \longrightarrow NO_2^- + O_2 \quad k_3 \qquad (3)$$

The kinetic expression for the appearance of NO_2^- therefore is given by eq. 4.

(1) Research supported by AEC contract number AT(30-1-)-1824.

(2) (a) A. O. Allen and J. H. Ghormley, *J. Chem. Phys.*, **15**, 208 (1947); (b) G. Hennig, R. Lees, and M. S. Matheson, *ibid.*, **21**, 664 (1953).

(3) J. Cunningham and H. G. Heal, *Trans. Faraday Soc.*, **54**, 1355 (1958).

(4) C. J. Hochanadel and T. W. Davis, *J. Chem. Phys.*, **27**, 333 (1957).

(5) E. R. Johnson, *J. Am. Chem. Soc.*, **80**, 4460 (1958).

(6) E. R. Johnson and J. Forten, *Discussions Faraday Soc.*, **31**, 238 (1961).

(7) A. G. Maddock and S. R. Mohanty, *ibid.*, **31**, 193 (1961).

(8) E. R. Johnson, *J. Phys. Chem.*, **66**, 755 (1962).

(9) C. J. Hochanadel, *Radiation Res.*, **16**, 286 (1962).

(10) J. Cunningham, *J. Phys. Chem.*, **65**, 628 (1961).

(11) J. Forten and E. R. Johnson, *J. Phys. Chem. Solids*, **15**, 218 (1960).

(12) M. B. Shinn, *Ind. Eng. Chem., Anal. Ed.*, **13**, 33 (1941).

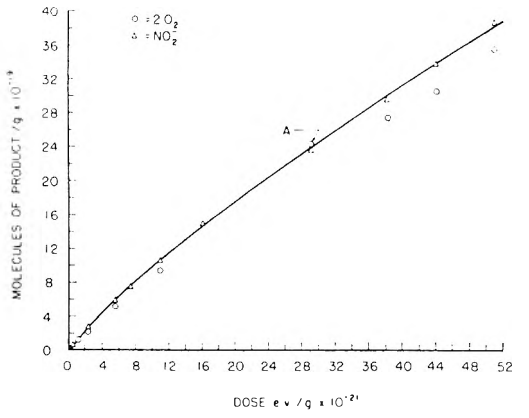

Fig. 1.—Nitrite and oxygen yields in KNO_3.

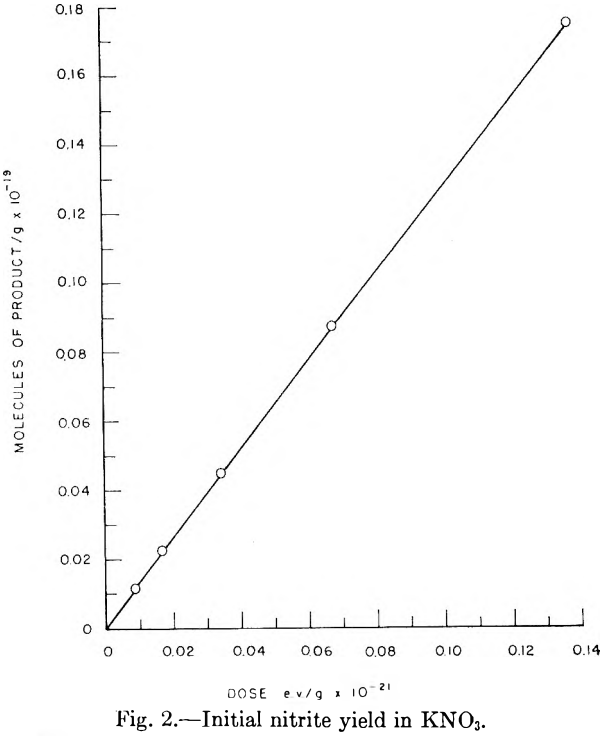

Fig. 2.—Initial nitrite yield in KNO_3.

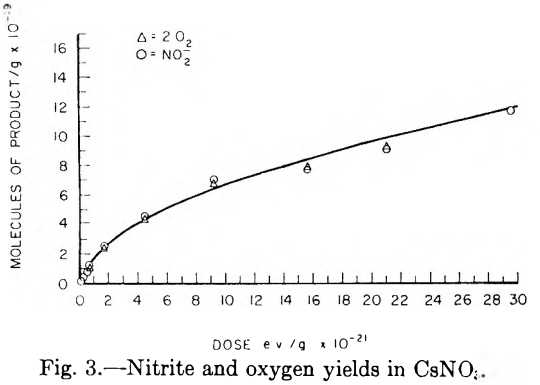

Fig. 3.—Nitrite and oxygen yields in $CsNO_3$.

$$\frac{d(NO_2^-)}{dt} = k_1\Phi(NO_3^-) - k_2(NO_2^-)(O) + k_3(NO_3^-)(O) \quad (4)$$

Substituting for the oxygen atom concentration (using a steady-state approximation), one obtains eq. 5.

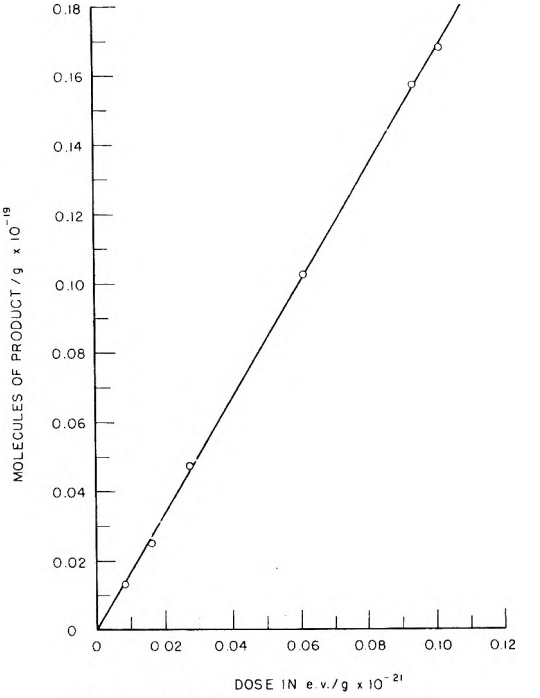

Fig. 4.—Initial nitrite yield in $CsNO_3$.

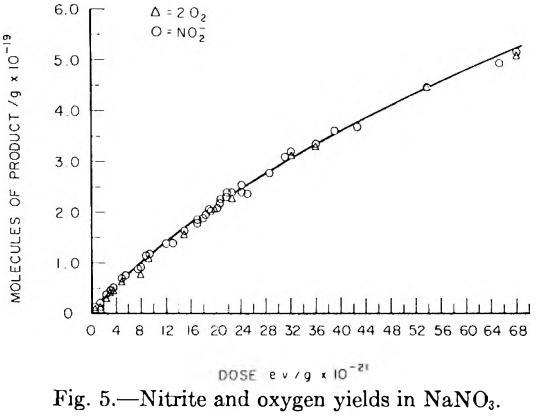

Fig. 5.—Nitrite and oxygen yields in $NaNO_3$.

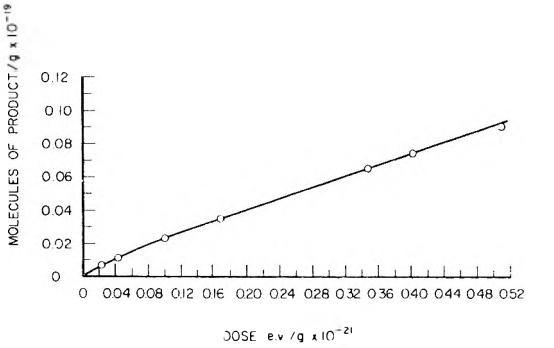

Fig. 6—Initial nitrite yield in $NaNO_3$.

$$\frac{d(NO_2^-)}{dt} = \frac{2k_1K_3\Phi(NO_3^-)^2}{k_2(NO_2^-) + k_3(NO_3^-)} \quad (5)$$

Integrating under the assumption that in the decomposition range studied the NO_3^- concentration is essentially constant, one obtains eq. 6

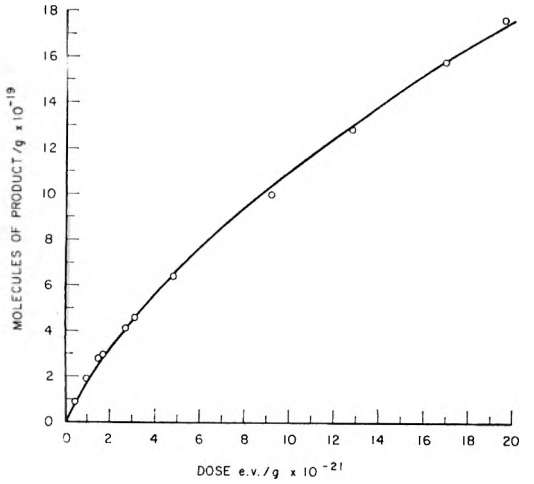

Fig. 7.—Nitrite yield in $Ba(NO_3)_2$.

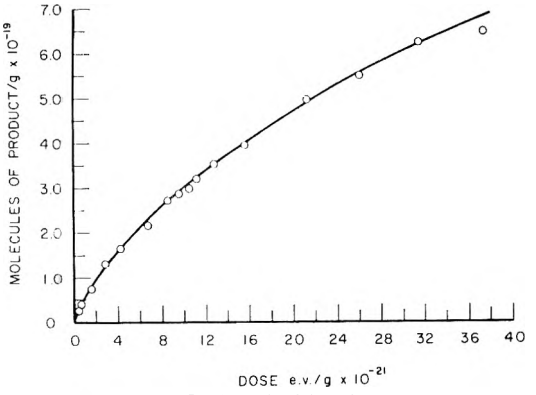

Fig. 8.—Nitrite yield in $Pb(NO_3)_2$.

$$\frac{1}{2}\frac{k_2}{k_3}\frac{1}{(NO_3^-)}(NO_2^-)^2 + (NO_2^-) = 2k_1\Phi(NO_3^-)t \quad (6)$$

or

$$ax^2 + x = bT \quad (7)$$

where x = molecules of NO_2^-/g. $\times 10^{-19}$, and T = dose in e.v./g. $\times 10^{-21}$.

The constants a,b may be evaluated from the appropriate nitrite yield *vs.* dose curves.

Equation 5 may be integrated without assumption of the NO_3^- concentration remaining constant. In this case eq. 5 is rearranged to give

$$\frac{k_2(NO_2^-) + k_3[(NO_3^-)_0 - (NO_2^-)]}{[(NO_3^-)_0 - (NO_2^-)]^2}\,d(NO_2^-) = 2k_1k_3\Phi\,dt \quad (8)$$

where $(NO_3^-)_0$ is the concentration of NO_3^- in molecules/g. $\times 10^{-19}$ at zero dose, which upon integration yields

$$\frac{k_2}{k_3}2.303\log\left[1 - \frac{(NO_2^-)}{(NO_3^-)_0}\right] + \frac{\frac{k_2}{k_3}\frac{(NO_2^-)}{(NO_3^-)_0}}{1 - \frac{(NO_2^-)}{(NO_3^-)_0}} - 2.303\log\left[1 - \frac{(NO_2^-)}{(NO_3^-)_0}\right] = 2k_1\Phi t \quad (9)$$

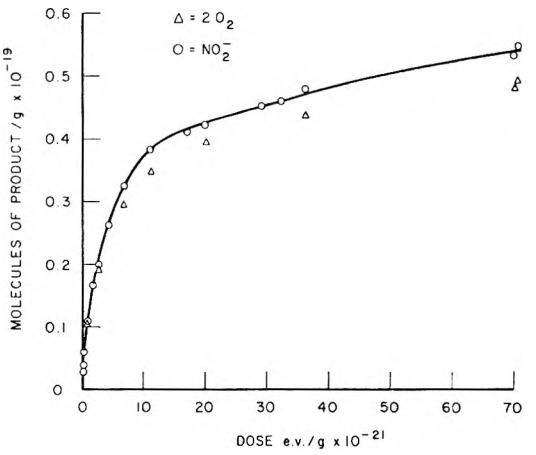

Fig. 9.—Nitrite and oxygen yields in $AgNO_3$.

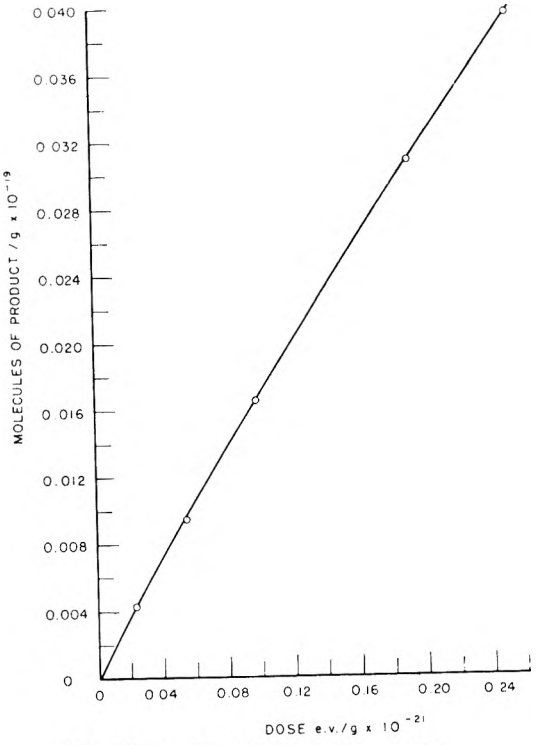

Fig. 10.—Initial nitrite yield in $AgNO_3$.

KNO_3.—Figure 1 shows the nitrite yield *vs.* dose for the decomposition of KNO_3 for the dose range 2×10^{21} to 50×10^{21} e.v./g. The solid curve (theoretical) was calculated from the following expression, which was obtained using eq. 9

$$13.3\left\{2.303\log\left[1 - \frac{(NO_2^-)}{(NO_3^-)_0}\right] + \frac{(NO_2^-)/(NO_3^-)_0}{1 - \frac{(NO_2^-)}{(NO_3^-)_0}}\right\} - 2.303\log\left[1 - \frac{(NO_2^-)}{(NO_3^-)_0}\right] = 0.00181T \quad (10)$$

The dosimetry for these particular results had a precision of $\pm 0.5\%$. The initial G-value for this

decomposition is not constant, but varies as can be seen by reference to Fig. 2.

Cunningham[10] used a first-order plot to summarize his results on the radiolysis of KNO_3 and obtained two straight lines intersecting at a dose of about 80×10^{20} e.v./g. This apparent break in the nitrite yield curve also was observed by Forten and Johnson.[11] Although no such break is apparent in Fig. 1, it is possible, because of the small variation in G-values (small curvature), to redraw Fig. 1 as two or three intersecting straight lines. This would be especially so if the over-all experimental error were of the order of about $\pm 5\%$ (this certainly was true of the results in ref. 11 and 6, except the results on $NaNO_3$).

The fact that Cunningham obtained first-order plots for his results up to a dose of about 20×10^{21} e.v./g. and that a linear plot has been obtained by others may be explained in part as follows.

For the low dose region (up to about 6×10^{21} e.v./g.), eq. 10 can be modified using the assumption that $\ln (1 - x)$ for $x \ll 1 \cong -x$ with a maximum error of 10% to give

$$x = bT \qquad (11)$$

This gives a linear relationship between yield and dose. A first-order plot in the low dose region also will give a linear plot if one applies the condition $\ln (1 + G) = G$ when $G \ll 1$. However, in the high dose region, Cunningham and Heal[3] found that the decomposition of KNO_3 also follows a first-order plot up to about 20 mole % decomposition.

If the data in Fig. 1 in the high dose region are plotted as $-\log M$ *vs.* dose, where M is the fraction of undecomposed nitrate, a straight line also is obtained. This indicates that both the kinetic equation and a log plot fit the data. The apparent "break," therefore, which has been observed in this decomposition, arises primarily out of the method by which the experimental data are treated. However, definite lattice changes do occur in KNO_3 decomposition at a dose of approximately 45×10^{20} e.v./g. This is evidenced by (1) a sudden change in density of about 1%,[11] (2) a low energy transition (lambda type) which occurs just prior to this dose,[11] (3) an anomalous isotope effect,[10] and (4) an effect of pressure on the decomposition yield.[13] The nature of this lattice change which occurs in KNO_3 decomposition has not been clarified; however, effort is in progress in this direction.

Plotted also in Fig. 1 are the oxygen yields for the decomposition of KNO_3. These results show an average departure from stoichiometry of about 10%. The oxygen values were consistently low and the discrepancy is somewhat larger than can be explained by experimental error. The over-all error in gas analysis, as determined by combustion experiments, never exceeded $\pm 5\%$. The disparity in the experimentally determined stoichiometry is believed due primarily to loss of oxygen from the crystal lattice and not to the presence of other decomposition products. Support for this statement comes from the fact that the sample vials from those samples irradiated to high dose indicated the presence of gas pressure when opened. In one sample where good stoichiometry was observed (indicated by A on Fig. 1) the crystals were about 16–32 mesh, whereas all the other samples were powders more than 50% of which passed through 100 mesh. This would appear to indicate that for large crystal sizes the oxygen does not excape from the lattice.

$CsNO_3$.—The experimental points and theoretical curve for $CsNO_3$ decomposition are shown in Fig. 3 for the decomposition range 0.1 to 29.5 $\times 10^{21}$ e.v./g. In the low dose region, *i.e.*, below 0.1×10^{21} e.v./g. (see Fig. 4), the slope within experimental error could be considered a straight line. The G-value found for this slope is 1.65 ± 0.04. Unlike the results obtained for KNO_3, excellent stoichiometry between nitrite ion and oxygen were obtained (mesh size for these crystals was between 24 and 100).

The theoretical curve was determined by using eq. 6 and was calculated from the expression

$$0.66(NO_2^-)^2 + (NO_2^-) = 3.53T \qquad (12)$$

$NaNO_3$.—The experimental points and theoretical curve for $NaNO_3$ are shown in Fig. 5 (this is essentially the same curve shown in ref. 6). The theoretical curve was evaluated from eq. 6 and calculated from the expression

$$0.182(NO_2^-)^2 + (NO_2^-) = 0.149T \qquad (13)$$

The experimental points shown were those obtained in the dose range of 0.6 to 67×10^{21} e.v./g. The results for the dose range of 0.02 to 0.5×10^{21} e.v./g. are shown in Fig. 6. It is apparent that even in this low dose region, the plot is not linear. As with $CsNO_3$, excellent stoichiometry was obtained between NO_2^- and oxygen.

$Ba(NO_3)_2$.—The data on $Ba(NO_3)_2$ are summarized in Fig. 7. The dose range was 0 to 21×10^{21} e.v./g., which corresponds to about 7.6 mole % decomposition. The theoretical curve also was evaluated from eq. 6 and calculated from the expression

$$0.0735(NO_2^-)^2 + (NO_2^-) = 1.99T \qquad (14)$$

No oxygen analyses were done.

$Pb(NO_3)_2$.—In Fig. 8 are summarized the data on $Pb(NO_3)_2$ decomposition. The results shown in ref. 5 are only for the initial portion of this curve (about 2.5×10^{21} e.v./g.). The curve shown in Fig. 8 represents about 3.8 mole % decomposition. The theoretical curve for this decomposition was obtained using eq. 6 and was calculated from the expression

$$0.331(NO_2^-)^2 + (NO_2^-) = 0.599T \qquad (15)$$

As with $Ba(NO_3)_2$, no oxygen analyses were performed on these samples.[14]

$AgNO_3$.—The decomposition curve for $AgNO_3$ is shown in Fig. 9. We were not able to find a theoretical expression corresponding to a reason-

(13) T. H. Chen and E. R. Johnson, *J. Phys. Chem.*, **66**, 2068 (1962).

(14) The nitrite yield data on both $Ba(NO_3)_2$ and $Pb(NO_3)_2$ were obtained by Mr. Chynsons Yeh in this Laboratory, and we are grateful for his permission to use them in this discussion.

able kinetic scheme as was done with the other nitrates. A straight line plot is obtained if one plots log dose *vs.* (NO_2^-). Qualitative tests indicate the presence of a small amount of silver oxide as a product in the decomposition. It could not be ascertained whether the oxide is produced as a primary product or as a product of the decomposition of $AgNO_2$. The initial slope for this decomposition is essentially linear (see Fig. 10), and the initial *G*-value was found to be 0.18.

No other gaseous products other than oxygen were present in any significant amounts.

Conclusion.—It is apparent that the decomposition of the inorganic nitrates may be expressed as the initial formation of a species which corresponds to one which can dissociate to give nitrite ion and an oxygen fragment. The oxygen fragment then may react with a NO_3^- or back-react with NO_2^-.

From the lack of intensity dependence[8] on these decompositions it would appear that O + O recombination reactions are not important in the initial stages of the decomposition. At least with KNO_3, reaction of molecular oxygen with NO_2^- appears insignificant even at high percentages (20%) of decomposition. If eq. 10 is used to determine the yields at 10–20% decomposition, it is found that these yields fit a first-order plot in reasonable agreement with experimental points shown in Fig. 1 in the high dose region. Silver nitrate decomposition does not, apparently, fit this reaction scheme and its decomposition is more complicated.

It would be expected that the relative rates of reactions of the oxygen fragment with NO_3^- or NO_2^- should be affected by lattice parameters; however, exactly how the lattice parameters affect the decomposition is not clear at this time. The concept of "free space" has been used to explain the difference in *G*-values for these decompositions, but there are some discrepancies in the concept, notably in the yield of $CsNO_3$; *i.e.*, $CsNO_3$ has less free space than KNO_3, but the initial yield is appreciably higher.

Investigations are currently in progress in this Laboratory which, it is hoped, will aid in clarifying the role of lattice parameters and lattice changes on the decomposition of these salts.

THE PHOTOLYSIS AND RADIOLYSIS OF $CH_3N_2CH_3$ AND $CH_3N_2CH_3$–$CD_3N_2CD_3$ MIXTURES[1]

BY R. E. REBBERT AND P. AUSLOOS

National Bureau of Standards, Washington 25, D. C.

Received May 21, 1962

Azomethane has been photolyzed in the solid, liquid, and gaseous phases. In the gas phase photolysis, evidence has been obtained for the formation of ethane by a molecular elimination from azomethane. The quantum yield of the formation of nitrogen in the liquid phase is lower than unity and decreases with decrease in temperature. Benzene quenches and 2,3-dimethylbutane enhances the decomposition yield. The effect of collisional deactivation, molecular elimination, and free radical recombination in the cage on the total yield of ethane is discussed. Radiolysis experiments on mixtures of $CH_3N_2CH_3$–$CD_3N_2CD_3$ were performed in the liquid and solid phases. The results indicate that ethane is formed mainly by cage and intercage recombination in the γ-ray spur. A decrease in temperature and addition of solvents has a reducing effect on the relative yield of CH_3CD_3. Evidence for energy transfer from benzene to azomethane was obtained.

Introduction

In recent liquid-phase photochemical studies of fluorinated ketones Bowles, Majer, and Robb[2] obtained evidence for the occurrence of a cage recombination. For instance, in the case of $CF_2ClCOCCl_2F$ (R_1COR_2), it has been shown that

$$\frac{R_1R_2}{[(R_1R_1)(R_2R_2)]^{1/2}} = 2.6$$

as compared to a value of 1.9 in the gas phase photolysis. The percentage of radicals escaping from the cage for this compound was estimated by the authors to be about 90%.

More recently Herk, Feld, and Szwarc[3] undertook an extensive investigation of the liquid phase photolysis of $CH_3N_2CH_3$ and $CF_3N_2CF_3$ in hydrocarbon solution which again provided substantial evidence in favor of a cage recombination for both CH_3 and CF_3 radicals, respectively. These authors succeeded in determining an activation energy for the escape of CH_3 and CF_3 radicals from the cage.

The present work includes a detailed investigation of (a) the photochemistry of azomethane in the liquid phase, and (b) the liquid phase radiolysis of azomethane. The primary purpose of this investigation was to assess the relative importance of energy transfer, cage recombination, and molecular elimination on the over-all yield of ethane. In most experiments mixtures of $CH_3N_2CH_3$–$CD_3N_2CD_3$ have been used in order to distinguish more readily the different processes which may lead to the formation of ethane.

Experimental

Apparatus.—The solid phase photolysis experiments at 4 and 77°K. were performed in a stainless steel low-temperature dewar.[4] This dewar was gold-plated on the inside to reduce heat transfer by radiation. The compound to be photolyzed was deposited on a gold-plated brass plate

(1) This research was supported in part by a grant from the U. S. Atomic Energy Commission. (Presented in part at the 140th National Meeting of the American Chemical Society, Chicago, Ill., Sept., 1961).

(2) R. Bowles, J. R. Majer, and J. C. Robb, *Nature*, **187**, 314 (1960).

(3) L. Herk, M. Feld, and M. Szwarc, *J. Am. Chem. Soc.*, **83**, 2998 (1961).

(4) Research Dewar D-1288, Hofman Laboratories, Inc., Hillside, N. J.

(2.0 × 3.3 cm.) which was attached to a brass block in contact with the refrigerant in the dewar. Directly in front of the brass plate was a quartz-covered porthole, through which unfiltered light passed from a Hanovia S-100 lamp. The inlet tube was at a 45° angle with the brass plate. The flow rate for deposition of the sample on the brass plate was about 1.3 cc. (STP) per min. A micrometer metal needle valve was used to control the flow of gas. The amount of sample deposited was calculated from the pressure drop in a calibrated volume. In most experiments about 11.0 cc. (STP) of gas was deposited.

For the liquid phase photolysis a quartz cell (about 0.05 cm. in depth, 2.8 cm. in diameter, and 0.3 cc. volume) was used. This cell was immersed in a Pyrex dewar flask with double quartz windows. Cold ethanol was the refrigerant for most of the experiments. The light source was an Osram-100 lamp with a Corning 7-39 filter, transmitting mainly 3660 Å.

In the gas phase experiments a cylindrical quartz cell (10 cm. long, 5 cm. diameter, and volume of approximately 200 cc.) was used in conjunction with either an Osram-100 or a Hanovia mercury–xenon lamp. Corning 7-39, 3-75, and 3–74 filters were used to restrict the effective wave length to approximately 3660, 3900, and 4000 Å.

The quantum yield measurements were made by comparing, under comparable experimental conditions, the yields of nitrogen produced in the gas and liquid phases. The assumption was made that $\phi N_2 = 1.0$ for azomethane in the gas phase.[5] A Bausch & Lomb monochrometer, Model No. 33-86-40, was used to measure the extinction coefficient for azomethane at 3660 Å. in the gas phase. This same instrument was used to determine the percentage of light absorption at 3660 Å. for the 10:1 benzene and the 50:1 2,3-dimethylbutane solutions.

Irradiations.—The γ-irradiations were carried out in Pyrex sample tubes about 6 cm. long with an internal diameter of 0.35 to 1.2 cm. The 2000 Curie γ-ray source at the National Bureau of Standards was used. The sample was immersed in a narrow dewar flask containing liquid nitrogen, Dry Ice, or ice. This dewar then was placed inside a sealed cylindrical metal container which then was lowered into the center of the source. Assuming that $G(Fe^{+++}) = 15.45$,[6] the rate of energy absorption was calculated to be 3.4×10^{17} e.v./cc.-min.

Conversions.—In the radiolysis and in the liquid phase photolysis of pure azomethane conversions were kept below 0.1%. In the liquid phase photolysis where a hydrocarbon was added, and in the solid and gaseous phases, conversions usually were kept below 2.0%.

Materials.—Azomethane and azomethane-d_6 were obtained from Merck, Sharp & Dohme of Canada. The azomethane-d_6 was better than 99 atom % deuterium. An equimolar mixture of the two was made and this was degassed before each run at −160° in order to remove any methane or ethane which may have accumulated.

Iodine was Mallinckrodt analytical reagent grade.

Diphenylpicryl hydrazyl (DPPH) was obtained from the Aldrich Chemical Co.

Benzene and cyclohexane were spectro grade from Eastman Organic Chemical Co.

2,3-Dimethylbutane was a standard sample from National Bureau of Standards with 0.11 ± 0.06 mole% impurity.

Analysis.—The analytical system consisted of a series of traps, a modified Ward still, and a Toepler pump-gas buret. Nitrogen, hydrogen, and methane were removed at −196°, while ethane was removed at −175°. These fractions then were analyzed on the mass spectrometer. Standard mixtures of C_2H_6, C_2D_6, and CH_3CD_3 were run on the same mass spectrometer.

Results

Photolysis. Gas Phase.—In the absence of radical scavengers, under the experimental conditions given in Table I, the quantum yield of ethane is close to unity. For equimolar mixtures of $CH_3N_2CH_3$–$CD_3N_2CD_3$, in the presence of oxygen the quantum yield of ethane is reduced to a value less than 0.01, and the ethane does not contain any detectable amount of CH_3CD_3. In the photolysis of $CH_3N_2CH_3$–O_2 mixtures at 3660, 3900, and 4000 Å. the molecular ethane yield was found to increase with increasing wave length. At all wave lengths the quantum yield shows a slight dependence on pressure. It should, however, be noted that the analysis of the relatively small quantities of ethane in a large excess of oxygen has an accuracy of not more than 10%.

TABLE I

GAS PHASE PHOTOLYSIS OF AZOMETHANE

Temp. (°K.)	Ethane $\phi \times 10^2$	Pressure azomethane (mm.)	Pressure oxygen (mm.)	Distribution, % C_2D_6	Distribution, % C_2H_6
		$CH_3N_2CH_3$–$CD_3N_2CD_3$			
		3660 Å.			
302	0.69	221.5	25.0	48.2	51.8
300	.66	113.5	14.0	51.6	48.4[a]
301	.37	57.0	9.5	48.5	51.5
		$CH_3N_2CH_3$			
		3660 Å.			
314	0.82	249.0	47.0		
313	0.57	61.0	10.0		
		3900 Å.			
312	1.09	275.0	47.5		
314	0.83	59.0	10.5		
		4000 Å.			
314	1.23	243.0	45.0		

[a] The ratio of $CH_3N_2CH_3$ to $CD_3N_2CD_3$ was about 0.94 for this run compared to 1.07 for the other two.

Liquid Phase.—The results given in Table II can be summarized as follows

(1) In contrast with the gas phase experiments, in the liquid phase the quantum yield of nitrogen is considerably less than unity.

(2) At 273°K. the quantum yield of nitrogen in the photolysis of $CD_3N_2CD_3$ is less than one-third of that obtained in the photolysis of $CH_3N_2CH_3$.

(3) Values for the ratios C_2H_6/C_2D_6 and $(CH_4 + CH_3D)/(CD_4 + CD_3H)$, which can be calculated from experiments done with mixtures of $CH_3N_2CH_3$–$CD_3N_2CD_3$, are approximately equal to each other. At 273°K. these ratios are comparable to the ratio of the quantum yields of nitrogen for $CH_3N_2CH_3$ and $CD_3N_2CD_3$, respectively.

(4) A drop in temperature from 273 to 194°K. (a) reduces the quantum yield of nitrogen by more than a factor of two, and (b) increases the ratio C_2H_6/C_2D_6.

(5) Benzene has a quenching effect on the yields of nitrogen, ethane, and methane. Saturated hydrocarbons enhance the quantum yields of the measured products.

Radiolysis.—Only nitrogen, hydrogen, methane, and ethane have been determined in these experiments. The rates of formation of these products were, within the experimental error, not affected by a sevenfold change in total dose.

The results are given in Table III and are summarized below.

(5) M. H. Jones and E. W. R. Steacie, *J. Chem. Phys.*, **21**, 1018 (1953).

(6) R. H. Schuler and A. O. Allen, *ibid.*, **24**, 56 (1956).

TABLE II

PHOTOLYSIS OF AZOMETHANE IN THE SOLID AND LIQUID PHASES

Temp. (°K.)	Nitrogen $\phi \times 10^2$	Ethane $\phi \times 10^2$	Methane $\phi \times 10^2$	I_{ab}, quanta cc. sec. $\times 10^{-16}$	Solvent	$\frac{CH_3N_2CH_3}{CD_3N_2CD_3}$	Distribution, % C_2D_6	CH_3CD_3	C_2H_6	$\frac{C_2H_6}{C_2D_6}$	CD_4	CD_3H	CH_3D	CH_4	$\frac{CH_3D + CH_4}{CD_4 + CD_3H}$
4[a]						0.94/1.0	19.4	9.0	71.6	3.69	9.1	23.6	15.4	49.8	1.99
4[a]						.94/1.0	22.0	6.9	71.1	3.23	9.0	25.7	14.3	50.9	1.88
77[a]						.94/1.0	23.4	1.0	75.7	3.24					
77[a]						.94/1.0	15.4	0.5	84.1	5.46					
194	3.0	2.9	0.21	35.0		.99/1.0	15.1	6.2	78.8	5.23	6.0	14.6	15.6	63.8	3.85
194	3.0	2.6	.28	12.0		.94/1.0	15.8	2.1	82.1	5.20	3.5	14.2	13.3	69.0	4.65
194	4.8	4.2	.24	35.0		1.0/0									
232	4.8	3.5	.39	35.0		0.99/1.0	16.6	1.7	81.7	4.92	4.4	13.6	19.1	62.9	4.56
233	7.1	4.9	.82	35.0		1.0/0									
273	6.7	4.1	.58	35.0		0.99/1.0	19.6	1.6	78.8	4.02	4.7	16.0	14.8	64.5	3.83
273	6.7	4.8	.61	12.0		0.94/1.0	20.4	4.9	74.7	3.66					
273	6.7	4.1	.85	3.1		1.07/1.0	18.0	0.7	81.3	4.52	2.6	14.9	9.1	73.4	4.71
273	5.2	3.9	.40	47.0	Benzene (75%)	1.07/1.0	17.8	1.1	81.2	4.56	3.7	13.1	13.9	69.3	4.95
273	4.9	3.9	.30	40.0	Benzene (91%)	1.07/1.0	18.7	0.4	80.9	4.33	3.9	14.0	13.3	68.4	4.56
273	8.0	5.6	2.7	35.0	2,3-Dimethylbutane (86%)	0.99/1.0	21.9	.4	77.7	3.55	0.4	15.0	1.4	83.2	5.49
273	8.7	6.2	2.6	40.0	2,3-Dimethylbutane (91%)	1.07/1.0	23.6	.3	76.1	3.22	0.6	21.9	1.6	75.6	3.43
273	7.9	6.8	3.2	10.0	2,3-Dimethylbutane (98%)	0.99/1.0	21.9	.4	77.7	3.55	0.5	22.9	1.5	75.1	3.27
273	6.2	4.8	0.93	30.0	Cyclohexane (91%)	0.99/1.0	23.1	.7	76.2	3.30	1.2	21.9	3.7	73.2	3.33
273	10.4	6.4	1.5	35.0		1.0/0									
273	10.4	6.8	1.5	47.0		1.0/0									
273	3.0	2.3	0.05	47.0		0/1.0									
273	9.8	...	1.5	36.0	Cyclohexane (91%)	1.0/0									

[a] Solid phase.

(1) An increase in temperature from 77 to 273°K. results in (a) a 30% increase of the nitrogen yield and a somewhat larger increase of the yields of hydrogen and methane; (b) a reduction in the yield of ethane; and (c) an increase in the values for the ratios $CH_3CD_3/[(C_2H_6)(C_2D_6)]^{1/2}$ and CD_3H/CD_4.

(2) Addition of DPPH at 273°K. has, within experimental error, no effect on the nitrogen and hydrogen yields, but does reduce the rates of formation of ethane and methane. The ratio $CH_3CD_3/[(C_2H_6)(C_2D_6)]^{1/2}$ remains the same while the ratio CD_3H/CD_4 undergoes a reduction.

(3) Addition of benzene enhances the yields of nitrogen, methane, and ethane; reduces the ratio $CH_3CD_3/[(C_2H_6)(C_2D_6)]^{1/2}$; and increases the ratio CD_3H/CD_4.

(4) Addition of 4 mole % iodine to the azomethane–benzene mixture slightly reduces the ratio $CH_3CD_3/[(C_2H_6)(C_2D_6)]^{1/2}$.

Discussion

Photolysis. Gas Phase.—It is well established[7] that in the vapor phase at 3660 Å. azomethane decomposes mainly according to process I

$$CH_3N_2CH_3 + h\nu \longrightarrow 2CH_3 + N_2 \quad (I)$$

It is quite possible that this process should be written as a sequence of two steps

$$CH_3N_2CH_3 + h\nu \longrightarrow CH_3N_2 + CH_3$$

$$CH_3N_2 \longrightarrow CH_3 + N_2$$

However the fact that the quantum yield of the nitrogen production is unity from 298 to 473°K. indicates that under these conditions the CH_3N_2 radical, if formed, decomposes before it has a chance to recombine with another radical or to react with an azomethane molecule. The nitrogen quantum yield of unity[8] observed in the photooxidation of azomethane is consistent with the formation of an unstable CH_3N_2 radical. Yet, in this case it is conceivable that a reaction between CH_3N_2 and oxygen may lead to the formation of a nitrogen molecule.

The formation of ethane in the azomethane–oxygen experiments presented in this paper indicates that besides process I, the following rearrangement process has to be considered as well

$$CH_3N_2CH_3 + h\nu \longrightarrow C_2H_6 + N_2 \quad (II)$$

Also, the equal yields of C_2H_6 and C_2D_6 obtained in the equimolar mixture of $CH_3N_2CH_3$–$CD_3N_2CD_3$ show that the quantum yield of this process is the same for the deuterated and non-deuterated azomethane. It can be seen that the quantum yield of process II seems to increase with an increase of pressure (from 60 to 270 mm.) and with an increase in wave length. The values of 0.0082 and 0.0123 obtained for the quantum yield of nitrogen at 3660 and 4000 Å., respectively, are not inconsistent with the value of 0.015 obtained by Herk, Feld, and Szwarc[3] for the ratio C_2H_6/N_2 in the gas phase photolysis of azomethane in the presence of 1,4-cyclohexadiene at wave lengths greater than 3400 Å.

Liquid Phase. A. The Quantum Yield of Nitrogen.—The fact that the quantum yield of nitrogen is lower than 0.1 in the majority of the experiments can be explained either by a cage recombination reaction as

(7) For a review see E. W. R. Steacie, "Atomic and Free Radical Reactions," Reinhold Publishing Corp., New York, N. Y., 1954, p. 376.

(8) G. R. Hoey and K. O. Kutschke, *Can. J. Chem.*, **33**, 496 (1955).

TABLE III

RADIOLYSIS OF AZOMETHANE[a] IN THE SOLID AND LIQUID PHASES

Temp (°K.)	Time (min.)	Cc. (STP)/min. × 10⁴ Nitrogen	Ethane	Methane	Hydrogen	Solvent	Distribution, % C_2D_6	CH_3CD_3	C_2H_6	$\frac{CH_3CD_3}{C_2H_6^{1/2}C_2D_6^{1/2}}$	CD_4	CD_3H	CH_2D_2	CH_3D	CH_4	$\frac{CD_3H}{CD_4}$	D_2	HD	H_2
77[c]	181	N.D.	0.65	N.D.	N.D.		37.1	6.5	56.3	0.143	..	..	..	..	..	..	..	..	..
77[c]	475	0.66	.58	0.14	0.048		35.8	6.6	57.6	.146	16.5	25.7	2.1	14.5	41.2	1.6	16.9	25.5	57.6
194	310	.73	.53	.19	.072		30.6	15.6	53.8	.385	10.6	30.1	0.9	11.8	46.7	2.8	15.0	26.0	59.0
273	1248	.89	.32	.12	.079	DPPH (0.1%)	26.9	27.6	45.4	.790	13.9	29.3	1.3	15.0	40.5	2.1	20.4	26.8	52.8
273	1209	.88	.28	.11	.094	DPPH (0.3%)	26.4	27.5	46.2	.788	17.6	26.8	0.5	18.6	36.5	1.5	20.0	26.6	53.3
273	1230	.88	.36	.22	.080		26.2	27.5	46.4	.784	9.1	33.0	2.2	10.9	44.8	3.6	20.1	26.6	53.3
273	180	.87	.41	.19	.081		25.8	24.9	49.4	.696	13.3	30.3	2.4	12.7	41.2	2.3	20.1	27.7	52.1
273	300	1.29	.55	.25	.096	C_6H_6 (50%)	27.0	21.6	51.4	.580	8.1	32.7	1.2	9.7	48.3	4.0	14.3	21.9	63.8
273	301	1.84	.69	.47	.117	C_6H_6 (75%)	28.9	15.8	55.3	.396	5.8	35.0	0.2	6.8	52.2	6.1	11.0	17.1	71.9
273	300	3.55	.99	.84	.100	C_6H_6 (91%)	30.8	9.4	59.9	.219	3.2	36.7	0.5	3.4	56.3	11.5	9.2	11.7	79.1
273	297	..	..	..	N.D.	C_6H_6 (71%)[b]	26.7	13.7	59.6	.343	11.5	27.7	3.9	12.1	44.7	2.4	..	..	..

[a] In all experiments about 79 cc. (STP) of an equimolar mixture of heavy and light azomethane has been irradiated. [b] 4 mole % iodine added. [c] Solid phase.

$$CH_3N_2 + CH_3 \longrightarrow CH_3N_2CH_3$$

or by a deactivation step

$$CH_3N_2CH_3^* + CH_3N_2CH_3 \longrightarrow 2CH_3N_2CH_3 \quad \text{(III)}$$

The contribution of a cage recombination to the low nitrogen quantum yield will, of course, depend on the stability of CH_3N_2. As mentioned before the evidence available to us at present shows that this radical is unstable in the gas phase above 298° K. The lifetime of this radical may, however, be long enough to undergo a cage recombination with the methyl radical in the liquid phase. A reaction of this type may take place in a short time interval especially if one considers the possibility of a primary recombination.[9]

If a cage recombination is accepted, the increase in quantum yield with an increase in temperature would reflect a higher rate of diffusion of the methyl radical as well as a lower stability of the CH_3N_2 radical at the higher temperature.

Collisional deactivation (process III) can, however, not be excluded as a plausible explanation of the low quantum yield. Collisional deactivation of excited azoethane[10] and azoisopropane[11] molecules has been observed in the vapor phase photolysis of these compounds. Although no collisional quenching has been observed in the gas phase photolysis of azomethane, it may be predicted that such a process will be operative in the liquid phase where the collisional yield is several orders of magnitude higher than in the earlier gas phase studies. From a plot of log N_2 as a function of $1/T$, an apparent activation energy of 1.0 ± 0.1 kcal. can be deduced for the decomposition of $CH_3N_2CH_3$. It is of interest to note that in the case of azoisopropane a value of 2.28 ± 0.35 kcal. was deduced by Riem and Kutschke[11] for the difference in activation energy between decomposition and deactivation.

Although the large difference between the nitrogen quantum yield of $CH_3N_2CH_3$ and $CD_3N_2CD_3$ is rather unpredicted, recent vapor phase studies have shown that at 298°K. the quantum yield of the photochemical decomposition of CD_3COCD_3 is considerably lower than that of CH_3COCH_3.[12]

If we take the ratio C_2H_6/C_2D_6 as a measure of the relative importance of the primary dissociation of $CH_3N_2CH_3$ and $CD_3N_2CD_3$,[13] it can be concluded that $CD_3N_2CD_3$ decomposes with a somewhat higher activation energy than $CH_3N_2CH_3$.

Solvents apparently have some effect on the quantum yield of nitrogen as well as on the ratio C_2H_6/C_2D_6. The nitrogen quantum yield of an

(9) For an extensive discussion see: R. M. Noyes, *J. Am. Chem. Soc.*, **77**, 2042 (1955).

(10) J. L. Weininger and O. K. Rice, *ibid.*, **74**, 6216 (1952); H. Cerfontain and K. O. Kutschke, *Can. J. Chem.*, **36**, 344 (1958).

(11) R. H. Riem and K. O. Kutschke, *ibid.*, **38**, 2332 (1960); R. W. Durham and E. W. R. Steacie, *ibid.*, **31**, 377 (1953).

(12) R. Gordon, Jr., and P. Ausloos, presented at the 140th National Meeting of the American Chemical Society, Chicago, Ill., Sept., 1961.

(13) This is substantiated by the observation that at 273°K. the ratio of the yields of nitrogen for $CH_3N_2CH_3$ and $CD_3N_2CD_3$ is approximately equal to the value for the ratio C_2H_6/C_2D_6 obtained in an equimolar mixture of $CH_3N_2CH_3$–$CD_3N_2CD_3$.

equimolar mixture of $CH_3N_2CH_3$–$CD_3N_2CD_3$ is higher in 2,3-dimethylbutane than it is in the undiluted mixture, while in benzene the quantum yield is lower. Thus, benzene is a more effective deactivating agent than azomethane, while 2,3-dimethylbutane is less effective.

B. The Formation of Ethane.—The fact that in all experiments carried out with liquid phase mixtures of $CH_3N_2CH_3$–$CD_3N_2CD_3$ the ethane fraction consists mainly of C_2H_6 and C_2D_6[14] indicates that ethane is either formed in an intramolecular rearrangement and/or by a cage recombination of methyl radicals originating from the same precursor.

It is rather difficult to assess the importance of a molecular ethane elimination in the liquid phase. The gas-phase results indicate that there is a possibility of a molecular ethane elimination which is both pressure and wave length dependent. In analogy with recent photochemical studies, one may expect that excited azomethane undergoes extensive vibrational deactivation in the liquid phase prior to decomposition.[15] It thus is conceivable that the quantum yield of the molecular elimination process II may be higher than 0.012 and actually comparable to the ethane quantum yield observed in the liquid phase. However, if we assume that both processes I and II are influenced by collisional deactivation, one should rather consider the ethane yield relative to the nitrogen yield instead of the absolute quantum yields. The fact that the ratio ethane/nitrogen approaches unity at low temperatures can be explained in two ways, namely, (a) the cage effect is relatively more important at the lower temperature because of a decrease in the rate of diffusion, or (b) the dissociative process falls off more rapidly with temperature than the molecular elimination process.

In favor of the occurrence of a cage recombination of two methyl radicals is the fact that at constant temperature the ethane/nitrogen ratio is higher in the presence of 2,3-dimethylbutane and benzene than for the undiluted azomethane. This observation is important if one considers that benzene and 2,3-dimethylbutane are stronger and weaker quenching agents, respectively, than azomethane itself. In view of the higher viscosities of benzene and 2,3-dimethylbutane the rate of diffusion of methyl radicals out of the cage will be slower than in pure azomethane. The temperature effect on the relative yield of ethane to nitrogen can of course be accounted for in a similar way. A plot of log [(N_2 − ethane)/ethane] *vs.* $1/T$ gives an activation energy of 2.0 ± 0.2 kcal. If we accept the cage recombination interpretation, this value corresponds to the activation energy of diffusion of the methyl radical in azomethane. It is interesting to note that this value is comparable with the one obtained by Herk, Feld, and Szwarc[3] for the diffusion of methyl radicals in isoöctane.

The fact that for mixtures of $CH_3N_2CH_3$–$CD_3N_2CD_3$ in the absence of solvent

$$\frac{C_2H_6}{C_2D_6} \approx \frac{CH_4 + CH_3D}{CD_3H + CD_4}$$

may be considered as an indication that ethane and methane are formed as a result of the decomposition of the same excited state of azomethane. This observation also favors a cage effect as being mainly responsible for the formation of ethane at 273°K. It would indeed be rather fortuitous that the ratio of the quantum yields of the dissociative and the elimination processes are the same for $CH_3N_2CH_3$ as for $CD_3N_2CD_3$. It should, however, be noted that at temperatures below 273°K. the ratio CH_3/CD_3 becomes considerably lower than C_2H_6/C_2D_6; indicating that at the lower temperatures ethane may be formed by two independent processes.

C. Reaction of Methyl Radicals with Azomethane.—It is known[5] that methyl radicals may react with azomethane to undergo abstraction and addition reactions

$$CH_3 + CH_3N_2CH_3 \longrightarrow CH_4 + CH_2N_2CH_3 \quad (1)$$

$$CH_3 + CH_3N_2CH_3 \longrightarrow (CH_3)_2N_2CH_3 \quad (2)$$

The fact that under these experimental conditions CH_3CD_3 is a very minor product indicates that methyl radicals, because of their low steady state concentration, will not interact with $CH_2N_2CH_3$ or $(CH_3)_2N_2CH_3$. It thus may be concluded that the ratio of the rate of abstraction to addition is given by the equation

$$\frac{k_1}{k_2} = \frac{CH_4}{2(N_2 - C_2H_6 - {}^1/_2CH_4)}$$

As seen below this ratio of rate constants is constant over the temperature range from 194 to 273°K.

Temp. (°K.)	194	233	273
$\frac{CH_4}{2(N_2 - C_2H_6 - {}^1/_2CH_4)}$	0.257	0.229	0.230

Thus, there is no apparent difference in activation energy between the two reactions and consequently the above value is also the ratio of the pre-exponential factors for abstraction compared to addition. However, in mixtures of $CH_3N_2CH_3$–$CD_3N_2CD_3$ not all of the methane seems to be formed in a normal H-atom abstraction process. It can indeed be seen that the ratios CD_3H/CD_4 and CH_4/CH_3D for mixtures of $CH_3N_2CH_3$–$CD_3N_2CD_3$ are consistently lower than expected at all temperatures and actually decrease with a decrease in temperature. There is no obvious explanation for this observation.

Solid Phase.—It was not possible to measure the quantum yields in the solid phase. However, the results indicate that the values for the ratio C_2H_6/C_2D_6 are not greatly different from those obtained in the liquid phase. This may be considered as an indication that the quantum yield for decomposition is not much lower than at 194°K. and does not greatly depend on temperature in the solid phase.

(14) This same observation has been reported in a recent note by R. K. Lyon and D. H. Levy, *J. Am. Chem. Soc.*, **83**, 4290 (1961).

(15) R. Borkowski and P. Ausloos, *ibid.*, **83**, 1053 (1961).

At 4° K. there is an increase in the relative yield of CH_3CD_3. This is accompanied by an increase in the yield of methane.[16] These results could be explained by assuming that at 4°K. the CH_3N_2 and CD_3N_2 radicals are stable enough to undergo secondary photolysis leading to the production of hot methyl radicals, as

$$CH_3N_2 + h\nu \longrightarrow CH_3^* + N_2$$

Radiolysis.—The following initial chemical conversions may be suggested to account for the formation of the products reported in Table III

$$CH_3N_2CH_3 \rightsquigarrow 2CH_3 + N_2 \qquad (I)$$

$$\rightsquigarrow H + CH_3N_2CH_2 \qquad (IV)$$

Several observations show that different electronic states are involved in the radiolysis as compared to the photolysis.

(1) Hydrogen is a product.

(2) The temperature dependence of nitrogen is less pronounced in the radiolysis than in photolysis.

(3) The difference in the yield of decomposition of $CH_3N_2CH_3$ and $CD_3N_2CD_3$ is considerably smaller than in the photolysis. The trends in the results, however, do not exclude the possibility that lowly excited azomethane may contribute to some extent to the formation of the observed products.

The Formation of Ethane.—In contrast with the photolysis results, a considerable fraction of the ethanes consists of CH_3CD_3. The fact that DPPH or I_2 reduces the percentage of CH_3CD_3 by not more than a few per cent clearly indicates that this molecule is mainly formed by a recombination of methyl radicals in the γ-ray spur. The following two observations can be readily explained on the basis of this interpretation.

(1) A decrease in temperature leads to a reduction in the yield of CH_3CD_3 relative to the yield of nitrogen, and an increase in the yields of C_2H_6 and C_2D_6. Diffusion of methyl radicals from one cage to another in the γ-ray spur may be expected to be less important at the lower temperatures, while cage recombination of the original partners should be enhanced.

(2) Addition of benzene reduces the percentage of CH_3CD_3 in the ethane fraction. This effect can be ascribed to a separation of the pairs of methyl radicals in the γ-ray spur by the solvent molecules. Very similar conclusions have been drawn in recent studies of the radiolysis of CH_3COOCD_3 and CH_3COCH_3–CD_3COCD_3 mixtures.[17]

The fact that in all cases $CH_3CD_3/[(C_2H_6)(C_2D_6)]^{1/2}$ is considerably lower than the statistically expected value of 2 indicates that, besides intercage recombination, a cage recombination also may play a role in the radiolysis of azomethane. Considering the wave length trends observed in the gas phase photolysis of azomethane, we may expect that for the apparently highly excited azomethane molecules formed in radiolysis, molecular elimination of ethane is unimportant.

The relative contribution of cage recombination as compared to intercage recombination can be readily calculated[18] from the data given in Table III. In the case of azomethane–DPPH mixtures at 273°K., cage/intercage = 1.24. Similarly for CH_3COCH_3–CD_3COCD_3–DPPH mixtures and CH_3COOCD_3–I_2 mixtures at 289°K., values of 1.12 and 0.82, respectively, can be calculated for this ratio.[17]

The Effect of Benzene.—If we make the reasonable assumption that the yield of nitrogen is a measure of the decomposition of azomethane, it can be seen that energy transfer from benzene to azomethane is an efficient process.

It is interesting to note that although the ratio ethane (total)/N_2 undergoes a decrease with the addition of benzene, the ratio ethane (cage)/N_2 stays approximately constant. Values of 0.237 and 0.246 can be calculated for the uninhibited azomethane and azomethane–benzene (91%) mixture, respectively. The yield of methane also is enhanced by the addition of benzene. The increase in the ratio CD_3H/CD_4 with increase in the relative concentration of benzene can be explained partly by an abstraction of H-atoms from benzene by thermal and hot methyl radicals. Evidence for thermal methyl radical reactions follows from the reduction of this ratio by the addition of DPPH. Part of the methane also may be formed by the recombination of hydrogen atoms with methyl radicals in the γ-ray track.

(16) The ratio of methane to nitrogen at various temperatures is given below.

Temp., °K.	4	77	194
Methane/Nitrogen	0.25	≤ 0.05	0.09

(17) P. Ausloos and C. N. Trumbore, *J. Am. Chem. Soc.*, **81**, 3866 (1959); P. Ausloos, *ibid.*, **83**, 1056 (1961).

(18) These calculations are based on two assumptions:

(1) $\frac{CH_3}{CD_3} = \frac{CH_4 + CH_3D}{CD_4 + CD_3H} = \left(\frac{C_2H_6 \text{ intercage}}{C_2D_6 \text{ intercage}}\right)^{1/2}$ and

(2) Methyl radicals which undergo intercage recombination obey the equation $\frac{CH_3CD_3}{[(C_2H_6)(C_2D_6)]^{1/2}} = 2.0$.

NOTES

THE DIELECTRIC CONSTANT OF EMULSIONS OF THE WATER-IN-OIL TYPE

By Andries Voet

Research Department, J. M. Huber Corp., Borger, Texas

Received March 3, 1962

It has been shown[1] that the dielectric constant E of a dilute dispersion of particles of a high dielectric constant dispersed in a medium of low dielectric constant E_0 can be expressed by the equation

$$E = E_0(1 + 3fV)$$

V is the concentration by volume of the dispersed phase and f is the form factor. For spherical particles $f = 1.00$. For anisometric particles $f > 1$. This factor has been derived theoretically for various rotational ellipsoidical particles.[2]

The above relationship makes it possible to study agglomeration in a number of dispersions by comparing the dielectric constant of these dispersions subjected to shear and at rest.[3] Since agglomerates have a tendency to be more anisometric than the particles from which they are formed, the dielectric constant of a partly agglomerated dispersion will drop sharply upon application of shear or upon chemical deflocculation. In each case less anisometric kinetic units are formed which have a smaller form factor than the agglomerates.

In the case of dispersions of water-in-oil, the same effects are expected to occur. It was, indeed, found that well stabilized dispersions of an aqueous phase in mineral oil showed a high dielectric constant and a high form factor. When subjected to shear, however, an instantaneous decrease of dielectric constant was observed. At rest, a rapid increase occurs, indicating the rebuilding of the agglomerates.[1] These phenomena were confirmed by others[4,5] in older as well as in more recent investigations. The authors concurred with the explanations given above.[6]

It was reported in 1953[7] and only recently brought to the author's attention that the changes in dielectric constant of emulsions of water-in-oil in the quiescent state, upon application of shear as reported,[1] were explained by phase separation occurring at rest, followed by re-emulsification by shear, etc. In view of the observed fact that the dispersions studied by the author and others were stabilized and maintained a stable character over periods of time of many hours, the explanation offered by the Soviet authors cannot be correct. The observed change in dielectric constant is immediate upon discontinuation of shear and essentially complete in less than 5 min., as reported earlier,[1] a period of time far exceeded by the period of perfect stability of the emulsions.

(1) A. Voet, *J. Phys. Chem.*, **51**, 1037 (1947).
(2) A. P. Altshuller, *ibid.*, **58**, 544 (1954).
(3) A. Voet, *ibid.*, **61**, 301 (1957).
(4) E. Collins, Thesis, Univ. of Manitoba, Canada, 1951.
(5) T. Hanai, *Kolloid-Z.*, **177**, 57 (1961).
(6) E. Collins and T. Hanai, private communication.
(7) Yu F. Deinega, A. V. Dumanskii, and O. D. Kurilenko, *Kolloidn. Zh.*, **15**, 361 (1953); *Chem. Abstr.*, **48**, 425a (1954).

THE COMPOSITION OF ANTIMONY VAPOR

By Gerd M. Rosenblatt

Department of Chemistry, and Inorganic Materials Division of the Lawrence Radiation Laboratory, University of California, Berkeley 4, California

Received March 23, 1962

Recent experiments on the vapor density of antimony have been interpreted[1] as demonstrating that unsaturated and saturated antimony vapor consists practically solely of Sb_4 molecules up to 1,000°. This conclusion is in contradiction with the accepted thermodynamic properties of antimony, in particular with the dissociation energy of $Sb_4(g)$.[2] It can be shown that the experimental results of Illarionov and Cherepanova[1] do not contradict the accepted thermodynamic properties of antimony and do not substantiate the conclusions drawn from these results.

Illarionov and Cherepanova carried out experiments of the type diagrammed in Fig. 1. Radioactive antimony liquid in a furnace at temperature T_2 determined the total pressure in the closed system. The vapor density in a furnace at temperature T_1 was determined by radioactive counting. Experiments were performed with T_1 at 1173 and 1223°K. while T_2 was varied from about 930 to 1110°K. Table I shows calculated values of p_{Sb_4} and p_{Sb_2} in the furnace at T_1 at extremes of the measurements using free energy functions from Stull and Sinke,[3] a dissociation energy of $Sb_4(g)$ of 63.40 ± 2.0 kcal./mole,[2] and a heat of sublimation to $Sb_4(g)$ of 49.45 ± 0.1 kcal./mole[4] at 298.15°K. The conclusions presented here do not depend upon the particular literature values chosen. Table I illustrates the discrepancy between the conclusions advanced by Illarionov and Cherepanova and the accepted thermodynamic properties as the table indicates the pressure of Sb_2 to be appreciable.

As the number of disintegrations measured, i, is proportional to the number of Sb atoms in furnace 1, one can write $i \propto 2p_{Sb_4} + p_{Sb_2}$ when T_1 is constant. The slope of the plot of log i *vs.* $1/T_2$ at constant T_1 will then be given by

(1) V. V. Illarionov and A. S. Cherepanova, *Dokl. Akad. Nauk SSSR*, **133**, 1086 (1960); *Proc. Acad. Sci. USSR, Chem. Sect.*, **133**, 901 (1960).
(2) P. Goldfinger and M. Jeunehomme, *Advan. Mass Spectrometry, Proc. Conf., Univ. London, 1958*, 534 (1959).
(3) D. R. Stull and G. C. Sinke, "Thermodynamic Properties of the Elements," American Chemical Society, Washington, D. C., 1956.
(4) G. M. Rosenblatt and C. E. Birchenall, *J. Chem. Phys.*, **35**, 788 (1961).

$$\text{slope} = \frac{\log i_{1100} - \log i_{950}}{(1/1100 - 1/950)}$$

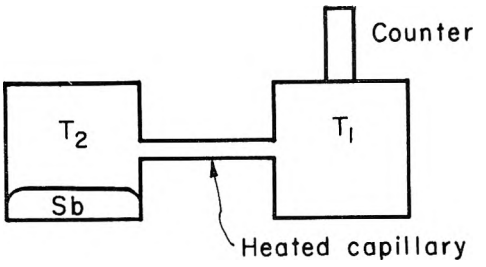

Figure 1.

TABLE I

CALCULATED PRESSURE OF Sb_4 AND Sb_2 IN FURNACE AT T_1

T_1 (°K.)	1173°		1223°	
T_2 (°K.)	950°	1100°	950°	1100°
p_{Sb_4} (atm.)	1.87×10^{-4}	1.87×10^{-3}	1.19×10^{-4}	1.54×10^{-3}
p_{Sb_2} (atm.)	1.84×10^{-4}	0.58×10^{-3}	2.52×10^{-4}	0.91×10^{-3}

Using the pressures listed in Table I, one calculates slopes of 6.19×10^3 and 6.35×10^3 for T_1 equal to 1173 and 1223°K., respectively. These differ by only 2.5%, which is clearly within the range of error of this type of measurement. Illarionov and Cherepanova report a constant slope of 6.40×10^3 for both values of T_1. It was this constant slope which prompted their conclusion concerning the absence of Sb_2. It is clear that this slope is not a measure of the enthalpy of evaporation of Sb_4 molecules at 1,000°K., which other data[3,4] show to be on the order of 25.52 kcal./mole, corresponding to a slope of 5.58×10^3. The agreement between the measured slope and those calculated from Table I indicates that the experiments of Illarionov and Cherepanova are in substantial agreement with the dissociation energy of $Sb_4(g)$ reported by Goldfinger and Jeunehomme.

Acknowledgment.—The author wishes to thank Professor Leo Brewer for his interest and encouragement. This work was supported by the U. S. Atomic Energy Commission.

ADSORPTION OF WATER VAPOR ON POTASSIUM CHLORIDE FILMS

BY P. G. HALL AND F. C. TOMPKINS

Department of Chemistry, Imperial College, London, S.W. 7, England

Received March 30, 1962

Recently,[1] the isosteric heats of adsorption, and their variation with amount adsorbed, of water vapor on several insoluble metal halides have been determined in the temperature range −45 to −23°. Below about one-tenth of the monolayer, the heats were about 5 kcal./mole and increased to 11–12 kcal./mole with increasing adsorption. With the soluble halide, potassium chloride, Papée and Laidler[2] report a calorimetric heat of 36 kcal./mole at 25° at low coverages θ ($\theta < 0.1$). It therefore was of interest to determine the variation of the isosteric heats with increasing adsorption for water vapor on this chloride in the lower temperature range −45 to 0°, particularly since it is possible to obtain microcrystals with a surface area as high as 15 m.²/g. using the evaporation technique of Young and Morrison.[3] These large surfaces allowed the accurate determination of isotherms, and because the film can be deposited on the walls of the adsorption cell, corrections for adsorption on the glass container virtually can be eliminated.

Experimental

Films (~ 0.3 g.) were deposited in a residual gas pressure of 10^{-6} mm. by passing a current of 3 amp. for 30 min. through a conical basket constructed of molybdenum wire and containing a compressed pellet (~ 0.5 g.) of the A.R. chloride. Films thicker than 0.3–0.4 mm. could not be used due to flaking of the deposit from the walls subsequent to water vapor adsorption, and because of the cracking of the film when it was cooled to liquid nitrogen temperatures for a B.E.T. surface area determination. The films were sintered thermally at room temperature with some loss of area, but further sintering occurred on water vapor adsorption; thus, after adsorption at −23° and a relative v.p. of 0.09, the area of a typical film was reduced from 2.6 to 2.1 m.². Subsequent outgassing at 110° for 16 hr. gave reproducible isotherms at and above −23°, but a subsequent adsorption at −45° effected a further small loss of area, although reproducible but different isotherms at −23° and above still could be obtained. Consequently, all films were first stabilized by exposure to a relative v.p. of 0.3 at −45° followed by outgassing as above when reproducibility even at −45° was obtained. Full details of the apparatus and procedure to obtain isotherms by the temperature variation method already have been given.[1]

Results and Discussion

A typical series of results on one film is summarized in the form of the log p plots as a function of the reciprocal of the temperature (°K.) for various amounts adsorbed v (Fig. 1), and Fig. 2 shows the isosteric heats for three different films calculated by application of the Clausius–Clapeyron equation, as a function of the coverage $\theta = v/v_m$, where v_m (the monolayer coverage) was obtained from a B.E.T. analysis of the water isotherms at −23° (see below). Measurement of the adsorption on the glass walls of the cell, without the film, showed that the *maximum* error in the heats could not exceed 0.5 kcal./mole due to this effect.

Above −25°, heats of 12.5 kcal./mole, largely independent of coverage, were obtained for three different films; the isotherms were B.E.T. type II plots from which v_m values (ml. STP) could be evaluated. Using a cross-sectional area[4] of 10.5 Å.² for the water molecule, a "surface area" of 0.65 m.² compared with a B.E.T. krypton area of 2.1 m.² was obtained for a typical film—an explanation of this difference in terms of clustering of water molecules in the monolayer already has been advanced.[1] The B.E.T. c value for water adsorption was 7.0, corresponding to an average adsorption heat of 12.0 kcal./mole, using an extrapolated latent heat value of 10.9_5 kcal./mole for liquid water at −25°.

Below −25°, heats ($-\Delta H$) of 3 kcal./mole for $\theta < 0.1$ were recorded; these increased with coverage to 11.5 kcal./mole at the "water monolayer." This low heat value should be compared with a theoretical one of 3.5 kcal./mole, calculated using

(1) P. G. Hall and F. C. Tompkins, *Trans. Faraday Soc.*, **58**, 1734 (1962).

(2) H. M. Papée and K. J. Laidler, *Can. J. Chem.*, **36**, 1338 (1958).

(3) D. M. Young and J. A. Morrison, *J. Sci. Instr.*, **31**, 90 (1954).

(4) H. K. Livingston, *J. Am. Chem. Soc.*, **66**, 569 (1944).

Orr's method[5] for a water molecule adsorbed above the mid-point of the surface lattice square with the hydrogen atoms oriented[6] toward the chloride ions and the resultant dipole coinciding with the perpendicular bisector of the lattice square. Details of the similar calculation for AgBr as adsorbent already have been given.[1]

The subsequent increase of heat with coverage is due to lateral interactions between the adsorbed water molecules and the calculations follow those that have been given for AgI.[1] The theoretical values for KCl are in good agreement with the experimental points, except that the inflection which is expected theoretically (and found experimentally with the insoluble halides[1]) is absent.

It is evident that there is disagreement with Papée and Laidler's value (36 kcal./mole) at low coverage at 25°; in their work[2] they found the adsorption to be accompanied, in the first stage of the process, by a decrease in area and they suggested penetration of the lattice by water molecules. However, any increase in the heat of adsorption due to sintering and simultaneous incorporation of adsorbed molecules is unlikely as an explanation of our value of 12.5 kcal./mole (at low coverages and above −25°) in view of the reproducibility of our surfaces in the subsequent adsorptions.

It is more likely that there are two different types of adsorption. Thus, the low-temperature adsorption is non-activated, with a $-\Delta H$ value of 3 kcal./mole, comprising single (probably mobile) molecules adsorbed at the mid-point of the lattice square, whereas the high-temperature adsorption is activated with $-\Delta H$ = 12 kcal./mole, and since the coverage is low, probably also is associated with isolated adsorbed water molecules. The time taken to attain adsorption equilibrium at the higher temperatures (30–40 min.) is consistent with an activation energy of about 7.5 kcal./mole, although the presence of the activated process should have been noted experimentally at the lower temperatures. However, since the "equilibrium" state apparently was attained more quickly at the lower temperatures, it is evident that the determinations were not extended to sufficiently long periods to detect this slower process. With the assumptions above, for the same coverage ($\theta < 0.1$), the ratio of the equilibrium pressures of the high- and low-temperature adsorption should be 0.1–0.2, which indeed is found experimentally, as can be seen by reference to Fig. 2.

In order to characterize the nature of the bonding giving a heat of 12.5 kcal./mole, it probably is significant that this high-temperature adsorption is not found with the insoluble halide adsorbents and therefore may well be associated with the water solubility of potassium chloride, or with the high ionic character of its surface ions. The first alternative would involve a water molecule highly coördinated with the lattice ions, *e.g.*, the oxygen atom of the water molecule can penetrate the surface ions from geometric considerations, but calculations show that the high repulsive forces which arise in this position are such as to reduce, and not

(5) W. J. C. Orr, *Trans. Faraday Soc.*, **35**, 1247 (1939).

(6) W. C. Price, W. F. Sherman, and G. R. Wilkinson, *Proc. Roy. Soc.* (London), **A247**, 467 (1958).

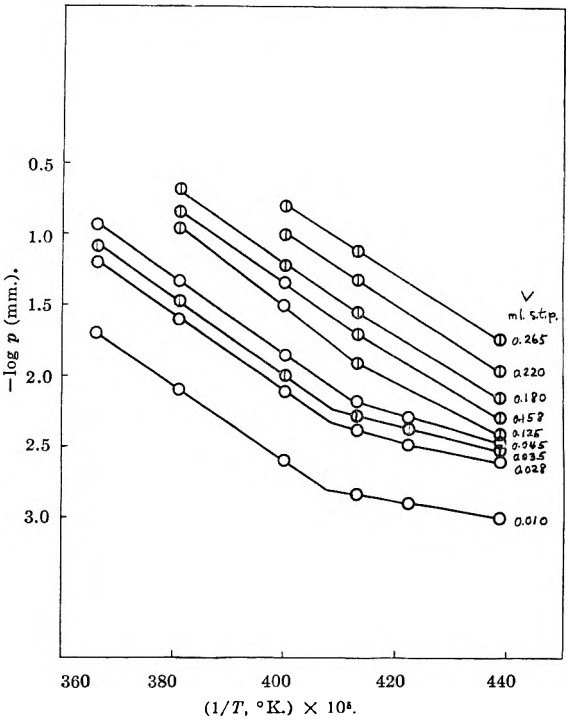

Fig. 1.—Plot of $-\log p$ (p = equilibrium pressure in mm.) as function of $1/T$ (T = temperature in °K.), for various values of amount adsorbed v (in ml. STP) from which typical isotherms may be constructed.

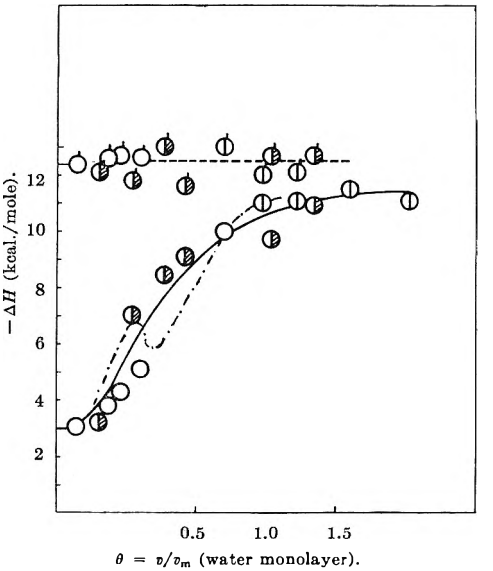

Fig. 2.—Variation of isosteric heat of adsorption $-\Delta H$ (in kcal./mole) as a function of coverage $\theta = v/v_m$, where v_m, in ml. STP, is the water monolayer coverage derived from a B.E.T. analysis, in the temperature range above and below −25°. Different symbols represent determination on separate films: ---------, above −25°; ———, below −25°; —·—·—, calculated heats.

increase, the heat of adsorption of 3 kcal./mole. One might assume the existence of a highly dislocated, yet stable, surface structure into which the water molecule penetrates (having acquired the necessary activation energy) so that it is "engulfed" in an array of ions, but the reproducibility of isotherms renders this improbable.

The second alternative depends on the ionic

character of the surface ions—thus, if the water molecule is adsorbed with its hydrogen atoms oriented toward a positive and negative ion, respectively, it becomes highly polarized and a charge-transfer process is encouraged; in the extreme case, the surface complex has the form

$$\begin{array}{cccc} & & H^- & \\ & & O & H^+ \\ \ldots Cl^- & K^+ & Cl^- & K^+ \ldots \end{array}$$

Such a transformation would require an activation energy (*cf.* $H_2O \rightarrow H^+ + OH^- - 13.6$ kcal./mole) and would become increasingly difficult with increasing covalent character of the surface ions (as, for example, would be the case with the insoluble silver halides). It may be noted that, in general, surface "ions" have a greater covalency than ions in the lattice. This type of adsorption may well lead to a substantially immobile layer, and accords with our estimated values of the entropy of adsorption which are consistent with mobility at the low temperatures ($<-25°$) and an increasing immobility above this temperature. The heat of 12.5 kcal./mole at high coverages decreases to 11.5 kcal./mole since clustering can still be envisaged.

Other explanations of this variation of heat with temperature at the low coverages, *e.g.*, a phase transition in the adsorbed layer, is unlikely in view of the entropy values and the fact that, at $-45°$ at $\theta < 0.1$, only isolated water molecules are present by reason of the low heat of 3 kcal./mole. Similarly, clustering of adsorbed water molecules, which could provide an explanation for the high heats for temperatures above $-25°$, would require, at $\theta < 0.1$, mobility of isolated water molecules at $-25°$ and considerable immobility at $-45°$; this latter requirement is unlikely, even at $-45°$, in view of the low value of the heat (3 kcal./mole).

It may be significant that recent dielectric relaxation measurements[7] by the authors, although referring to high coverages, show no dielectric loss (0.6–1.4 Mc./sec.) at $-45°$, whereas tan δ increases with amount adsorbed above $-25°$.

(7) P. G. Hall and F. C. Tompkins, unpublished observations.

A SECONDARY INTERACTION OF TRI-*n*-OCTYLAMINE WITH HYDROCHLORIC ACID AND THENOYLTRIFLUOROACETONE[1]

BY LEONARD NEWMAN AND PAUL KLOTZ

Brookhaven National Laboratory, Upton, New York

Received April 26, 1962

Introduction

In a previous publication,[2] it was observed by a spectrophotometric approach that thenoyltrifluoroacetone (TTA) interacted with tri-*n*-octylamine (TNOA) in benzene solutions to form an acid salt. The formation constant, K_T, for the reaction

$$R_3N + HT \overset{K_T}{=} R_3NHT \qquad (1)$$

where R_3N represents TNOA and HT represents TTA, was found to be $(1.4 \pm 0.1) \times 10^3$. Acid equilibrium measurements of aqueous phases with benzene solutions permitted the determination of the formation constant of the amine hydrochloride salt

$$R_3N + H^+ + Cl^- \overset{K_{Cl}}{=} R_3NHCl \qquad (2)$$

In this equation and subsequent ones, the uncharged species are present in benzene solutions and the charged species in the aqueous phase. It recently has been brought to our attention that Bizot and Tremillon[3] conducted a similar study in which they found the value of the formation constant to be 1.1×10^4. The value that we obtained for K_{Cl} was $(1.3 \pm 0.3) \times 10^4$ and is in extremely good agreement with their result.

In recent experiments where benzene solutions of TTA and TNOA were equilibrated with hydrochloric acid solutions, it was observed that the amount of acid remaining in the aqueous phase was less than predicted by the above equilibrium constants. However, in these experiments the concentration of TTA was much greater than previously employed. Under these conditions, an interaction must occur in the organic phase which causes a greater withdrawal of acid from the aqueous phase than predicted by the known reactions. The nature of this compound is the subject of this investigation.

Experimental

All reagents and their concomitant purification have been described.[2] A 0.08 *M* solution of amine in benzene was converted to the hydrochloride form by contacting it twice with 2 *M* and once with 0.2 *M* hydrochloric acid. A series of dilutions of this amine hydrochloride was made with benzene to cover the range down to 0.002 *M*. To each of the dilutions, a benzene solution of TTA was added. The amount of the TTA added was adjusted so that the analytical concentration was one tenth molar greater than the concentration of the amine hydrochloride. By employing the formation constants found for the compounds involving TTA, it can be calculated that, after equilibrium, the free TTA concentration never exceeds 0.1 *M* by more than 10% in this, or any of the subsequent experiments.

Aliquots of each of these solutions were shaken for 2 hr. with an equal volume of water and then centrifuged to assure complete separation. A second series of aliquots was shaken with an equal volume of a 2 *M* LiCl solution. The resulting hydrogen ion concentration of each of the aqueous phases was determined from pH measurements utilizing a calibration plot obtained from comparable aqueous solutions of known hydrogen ion concentration *vs.* pH reading. A Radiometer Model 4 pH meter, reproducible to better than 0.005 pH unit, was used for these measurements (Radiometer Corp., 72 Emdrupuej, Copenhagen NV, Denmark). The results appear in the first and second sections of Table I.

Additional data were obtained by preparing a benzene solution which nominally contained 0.01 *M* amine and 0.11 *M* TTA. In this case, the amine was not put into the hydrochloride form. Aliquots of this solution were shaken for 2 hr. with equal volumes of aqueous solutions containing 0.01 to 0.07 *M* hydrochloric acid. After separation of the two phases, the acid concentration of the aqueous phase was measured. To assure the best accuracy, the pH meter was standardized with each of the uncontacted hydrochloric

(1) Research performed under the auspices of The U. S. Atomic Energy Commission.

(2) L. Newman and P. Klotz, *J. Phys. Chem.*, **65**, 796 (1961).

(3) J. Bizot and B. Tremillon, *Bull. soc. chim. France*, 122 (1953).

TABLE I

EXTRACTION OF HYDROCHLORIC ACID AS A FUNCTION OF CHANGES IN COMPOSITION OF AQUEOUS AND ORGANIC PHASES

Initial conditions	Concn. (moles/l.) × 10^2 $(H^+)_t$	(H^+)
Aq. phase (H_2O)	4.00	3.27
Org. phase (R_3NHCl, HT)	3.20	2.81
$(R_3N)_t = (H^+)_t$	2.80	2.56
Symbol used in Fig. 1 ○	2.00	1.91
	1.60	1.34
	1.20	1.12
	0.80	0.74
	0.40	0.38
	0.20	0.18
Aq. phase (2 *M* LiCl)	2.80	0.63
Org. phase (R_3NHCl, HT)	2.00	.54
$(R_3N)_t = (H^+)_t$	1.60	.47
Symbol used in Fig. 1 ●	1.20	.41
	0.80	.33
	0.40	.21
	0.20	.15
Aq. phase (HCl)	7.00	6.66
Org. phase (R_3N, HT)	5.00	4.66
$(R_3N)_t$ = 0.01 *M*	4.00	3.87
Symbol used in Fig. 1 □	3.00	2.86
	2.00	1.94
	1.00	0.96
Aq. phase (HCl, 2 *M* LiCl)	3.00	2.10
Org. phase (R_3N, HT)	2.00	1.15
$(R_3N)_t$ = 0.01 *M*	1.00	0.37
Symbol used in Fig. 1 ■		
Aq. phase (HCl)	5.00	4.50
Org. phase (R_3N, HT)	4.00	3.65
$(R_3N)_t$ = 0.02 *M*	3.00	2.81
Symbol used in Fig. 1 △	2.00	1.85
	1.00	0.95
Aq. phase (HCl, 2 *M* LiCl)	4.00	2.20
Org. phase (R_3N, HT)	3.00	1.27
$(R_3N)_t$ = 0.02 *M*	2.00	0.54
Symbol used in Fig. 1 ▲	1.00	0.15
Aq. phase (HCl)	10.00	8.28
Org. phase (R_3N, HT)	7.00	5.92
$(R_3N)_t$ = 0.03 *M*	5.00	4.30
Symbol used in Fig. 1 ▽	4.00	3.52
	3.00	2.67
	2.00	1.80
	1.00	0.92
Aq. phase (HCl, 2 *M* LiCl)	3.00	0.66
Org. phase (R_3N, HT)	2.00	.25
$(R_3N)_t$ = 0.03 *M*	1.00	.08
Symbol used in Fig. 1 ▼		

acid solutions and their counterparts compared directly. The results of these measurements are presented in the third section of Table I. A similar series of measurements was obtained by contacting aliquots of the organic phase with hydrochloric acid solutions prepared in 2 *M* LiCl. These data appear in the fourth section.

Two additional sets of data were obtained with the amine concentration fixed at 0.02 *M*. The results appear in the fifth and sixth sections. Finally, an additional two sets of data were obtained with the amine concentration fixed at 0.03 *M*. The results are tabulated in the final two sections in the Table.

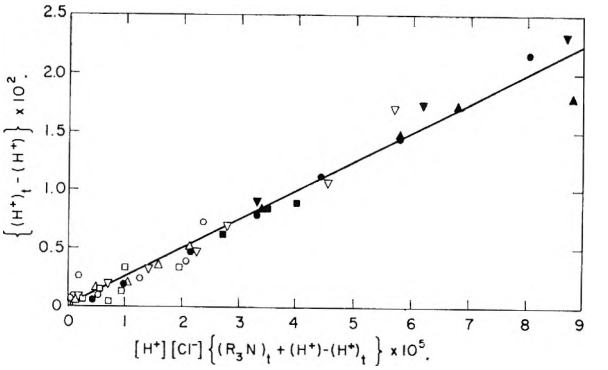

Fig. 1.—Summary plot utilized for determining the formation constant of $R_3NHClHT$. The symbols are explained in Table I.

Results and Discussion

A careful analysis of the data in Table I indicates that the amount of acid found at equilibrium in the aqueous phase cannot be accounted for by the formation constants obtained for reactions 1 and 2. Since the amount of acid found in the aqueous phases is less than would be predicted, an additional compound must be formed in the organic phase which can consume acid. The three simplest compounds which can be suggested as an explanation for this behavior are $(R_3NHCl)_2$, $R_3N(HCl)_2$, and $R_3NHClHT$. The first two should give rise to a second power dependency on hydrogen ion concentration. Since this was not observed, they could be immediately eliminated. An attempt was made to attribute the enhanced extraction of the acid to the formation of $R_3NHClHT$.

The reaction leading to the formation of this species can be written as

$$R_3N + H^+ + Cl^- + HT \overset{K_{Cl,T}}{=} R_3NHClHT \quad (3)$$

where $K_{Cl,T}$ is the formation constant. Therefore, the analytical concentration of the amine, $(R_3N)_t$, is

$$(R_3N)_t = (R_3NHCl) + (R_3NHClHT) + (R_3NHT) \quad (4)$$

Under the conditions of these experiments, the concentration of free amine, (R_3N), is small enough to be neglected. The analytical concentration of acid, $(H^+)_t$, in both phases is

$$(H^+)_t = (H^+) + (R_3NHCl) + (R_3NHClHT) \quad (5)$$

Substituting eq. 1, 2, and 3 into (4) and (2) and (3) into (5), then dividing (4) by (5) and rearranging we obtain

$$(H^+)_t - (H^+) = \left\{\frac{K_{Cl} + K_{Cl,T}[HT]}{K_T[HT]}\right\} \times [H^+][Cl^-]\{(R_3N)_t + (H^+) - (H^+)_t\} \quad (6)$$

The brackets around the aqueous hydrogen ion, aqueous chloride ion, and the organic TTA terms indicate that activities should be used. Concentrations are used for the organic species R_3NHCl, R_3NHT, and $R_3NHClHT$ on the assumption that

their activity coefficients are equal or remain constant. Consequently, a "mixed" formation constant (terms in both activity and concentration) is obtained.

The series of experiments were so designed that data could be obtained from the equilibrations of aqueous phases with benzene solutions containing TNOA and TTA which would test the relationships predicted by eq. 6. In all cases, conditions were selected so that at equilibrium the free TTA concentration was maintained constant at 0.1 *M*. Consequently, from a plot of $(H^+)_t - (H^+)$ *vs.* $[H^+][Cl^-]\{(R_3N)_t + (H^+) - (H^+)_t\}$ a straight line relationship with a zero intercept should be obtained if the postulated product $R_3NHClHT$ is of significance. If such is the case, then utilizing the known formation constants for R_3NHT and R_3NHCl and the activity of the unassociated TTA, the formation constant, $K_{Cl,T}$, can be calculated from the slope of the line. The appropriate terms for the plot were calculated from the known composition of the solutions, $(R_3N)_t$ and $(H^+)_t$, and from the measured aqueous hydrogen ion concentration, (H^+), after equilibration.

The indicated terms were calculated from the data presented in Table I. Activities were calculated for the aqueous hydrochloric acid concentrations from the known activity coefficients.[4] Utilizing the expression of King and Reas[5] the activity of a 0.1 *M* TTA solution was calculated as 0.092. For the systems where aqueous phases contained 2 *M* LiCl, the activity coefficient for hydrochloric acid was taken as unity.[4] The resulting plot is shown in Fig. 1. In accordance with theory, a straight line relationship is obtained with a zero intercept. From the slope of the straight line and the known formation constants, a value of $(2.1 \pm 0.4) \times 10^5$ was calculated for $K_{Cl,T}$. The formation constant for the organic phase reaction

$$R_3NHCl + HT = R_3NHClHT \qquad (7)$$

was calculated by dividing $K_{Cl,T}$ by K_{Cl}. The value that was obtained is 16 ± 5.

The experiments which were performed permitted a test of the suggested reaction under a wide variety of conditions. The analytical amine concentration was varied between 0.002 and 0.04 *M*, the free acid concentration from 0.0008 to 0.08 *M*, and the chloride concentration from 0.0008 to 2 *M*. The TTA concentration was maintained at 0.1 *M*. The formation constant was measured under conditions when each of the amine species participated as either a minor or major component of the solution. Consequently, it has been demonstrated that the extraction of hydrochloric acid by benzene solutions of TTA and TNOA can be completely accounted for by the presence of three species, R_3NHCl, R_3NHT, and $R_3NHClHT$.

This knowledge of the nature and the extent of formation of these species has been applied for an elucidation of the synergistic effect exerted by TNOA on the solvent extraction of thorium by TTA.[6]

(4) H. S. Harned and B. B. Owen, "The Physical Chemistry of Electrolytic Solutions," Second Ed., Reinhold Publ. Corp., New York, N. Y., 1950.

(5) E. L. King and W. H. Reas, *J. Am. Chem. Soc.*, **73**, 1806 (1951).

(6) L. Newman and P. Klotz, *J. Phys. Chem.*, in press.

THE THERMODYNAMICS OF AQUEOUS ELECTROLYTE MIXTURES AT ELEVATED TEMPERATURES. THE SOLUBILITY OF SILVER SULFATE IN KNO_3–K_2SO_4, K_2SO_4–$MgSO_4$, AND K_2SO_4–H_2SO_4 MIXTURES

BY M. H. LIETZKE AND R. W. STOUGHTON

Chemistry Division, Oak Ridge National Laboratory,[1] Oak Ridge, Tennessee

Received April 13, 1962

In a series of previous papers[2] the solubility of Ag_2SO_4 in a variety of electrolyte solutions has been investigated. It was shown that single parameter empirical expressions of the type

$$\ln S = \ln 4s_0^3 + s_T\left[\frac{\sqrt{I}}{1 + A\sqrt{I}} - \frac{\sqrt{I_0}}{1 + A\sqrt{I_0}}\right] \qquad (1)$$

could be used to describe the variation of the solubility product of Ag_2SO_4 over a wide range of temperature and ionic strength. In eq. 1 s_0 is the solubility of Ag_2SO_4 in pure water, s_T is the appropriate Debye–Hückel slope, I the ionic strength of the solution, and A the adjustable parameter. In all cases best agreement between calculated and observed solubilities was obtained when each single parameter A_i was assumed to be temperature independent and to be either ionic strength independent or to decrease slowly with increasing ionic strength. The justification for using eq. 1 without a linear term has been discussed previously.[2]

In the present paper the treatment of the solubility of Ag_2SO_4 in single electrolyte systems has been extended to the solubility in three electrolyte mixtures: (1) KNO_3–K_2SO_4, (2) K_2SO_4–$MgSO_4$, and (3) K_2SO_4–H_2SO_4. In each of the three systems the total ionic strength of the solubility medium was held constant at two different values, while the ratio of the two components was varied. Weight concentrations were used in reporting the data, and the Debye–Hückel limiting slope at any temperature was made density dependent by multiplying its value on the molal scale by the square root of the density of water at that temperature.

Experimental

All solubility measurements were performed with the same techniques described previously[3] and were carried out in the temperature range 90 to 175°.

Results and Discussion

The values for the solubility of Ag_2SO_4 in each system as a function of temperature were fitted by the method of least squares to an equation

(1) Operated by Union Carbide Corporation for the United States Atomic Energy Commission.

(2) M. H. Lietzke and R. W. Stoughton, *J. Phys. Chem.*, **63**, 1183, 1186, 1188, 1190, 1984 (1959); **64**, 133, 816 (1960).

(3) M. H. Lietzke and R. W. Stoughton, *J. Am. Chem. Soc.*, **78**, 3023 (1956).

TABLE I

COEFFICIENTS OF EQUATION 2 FOR THE SOLUBILITY OF Ag_2SO_4 IN THE ELECTROLYTE MIXTURES STUDIED

I of the mixture	m_{KNO_3}	$m_{K_2SO_4}$	$a_0 \times 10^3$	$a_1 \times 10^4$	$a_2 \times 10^6$	σ_{fit}[a] $\times 10^3$
1.0	1.0	0	4.31016	6.41420	−1.57687	2.12
	0.7	.1	3.47859	3.57152	−0.532662	1.37
	.5	.16	2.88124	3.12836	− .284457	2.57
	.28	.24	1.90299	4.43650	− .701309	1.00
	0	.333	1.41304	5.47167	− .875239	0.16
1.416	1.416	0	5.84143	4.86857	− .697144	0.48
	0.3484	.3564	−0.202929	7.32640	−1.45714	1.86
	0	.472	1.59375	5.67500	−0.473332	0.22
	$m_{K_2SO_4}$	m_{MgSO_4}				
1.0	.333	0	1.41304	5.47167	−0.875239	0.16
	.25	.0625	0.642984	5.86084	−1.32865	.92
	.167	.125	0.00169903	6.99906	−1.86183	.43
	.0833	.1875	1.42525	4.68734	−1.06849	1.09
	0	.25	1.27142	5.00573	−1.24572	0.27
1.437	.479	0	1.58357	5.71667	−0.470478	0.15
	.2395	.1796	−1.26804	7.94620	−1.49270	2.20
	0	.3592	1.22750	5.38381	−1.16191	0.30
	$m_{H_2SO_4}$[b]	$m_{K_2SO_4}$				
1.007	.2507	.2500	−0.883321	9.58466	−2.63613	1.39
2.000	.5000	.5000	−3.26708	13.0980	−3.06707	0.68

[a] Standard error of fit. [b] Formal molality based on considering H_2SO_4 as a 1-1 electrolyte.

$$s = a_0 + a_1 t + a_2 t^2 \qquad (2)$$

The resulting equations were solved at 25° intervals from 25 to 200° in the case of the KNO_3–K_2SO_4 system ($I_{KNO_3} + I_{K_2SO_4} = 1.0$), where data were obtained over the entire temperature range, and from 100 to 175° in the other systems. The coefficients and the standard error of fit for eq. 2 describing the solubility of Ag_2SO_4 in each system as a function of temperature are given in Table I, while a typical set of solubility curves for one of the systems ($I_{KNO_3} + I_{K_2SO_4} = 1.0$) is shown in Fig. 1. The other families of curves were similar.

Since in previous work[2] it was demonstrated that temperature independent values of the parameter A in eq. 1 could be calculated such that the difference between observed and calculated solubilities would be minimized for systems in which Ag_2SO_4 was dissolved in solutions of a simple electrolyte, it seemed of interest in the present work to calculate values of the parameter A for the mixtures studied to determine whether a simple combining relationship existed between the values of A in the simple systems and in the mixtures. In carrying out the calculations for the KNO_3–K_2SO_4 and K_2SO_4–$MgSO_4$ mixtures, values of ln S and $\sqrt{I}$ in eq. 1 were computed at 25° intervals for each system using the smoothed values of the solubility of Ag_2SO_4 as obtained from eq. 2 and the appropriate molalities of the components of the mixture. Then the value of A was determined in each case between 100 and 175° by selecting the value which equated the right and left sides of eq. 1. The A parameters so obtained for each system are given in Table II. The values shown are the mean values calculated between 100 and 175°.

Additional calculations were performed in which a linear term was added to eq. 1, *viz.*, BI. In these calculations A was set equal either to 1.0 or to 1.5 and the value of B determined such that the right side of eq. 1 augmented by the linear term was equal to the left side. The values of B so obtained showed a much greater dependence on temperature than did the values of A obtained without the linear term. Since the latter calculation (involving the BI term) offered no advantage over the former, no attempt was made to correlate the B values with temperature and ionic strength fractions.

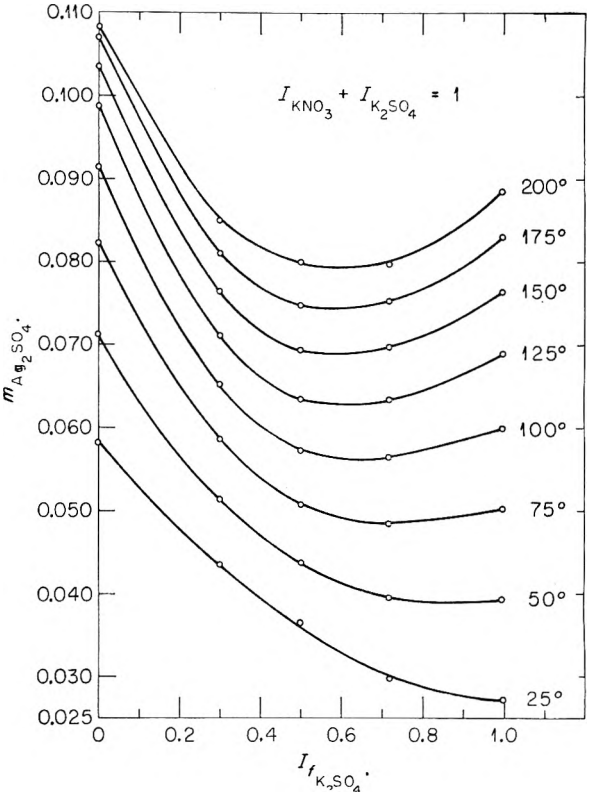

Fig. 1.—The solubility of Ag_2SO_4 in KNO_3–K_2SO_4 mixtures where $I_{KNO_3} + I_{K_2SO_4} = 1.0$.

The observed solubility of Ag_2SO_4 in each system as a function of temperature was compared with values calculated using the average A values given in Table II. In all cases the agreement was very good—within a few tenths of a per cent in most cases and within 2% in the remainder. Hence the behavior of the A values in the electrolyte mixtures was very similar to the behavior of the A values in the individual components.

TABLE II

A PARAMETERS FOR EQUATION 1

Total I	m_{KNO_3}	$m_{K_2SO_4}$	A	Std. dev. from the mean
1.0	1.0	0	0.991	0.004
	0.7	0.1	.994	.018
	.5	.16	.956	.030
	.28	.24	.815	.014
	0	.333	.656	.002
1.416	1.416	0	0.997	0.012
	0.3484	0.3564	.811	.021
	0	0.472	.630	.000
	$m_{K_2SO_4}$	m_{MgSO_4}		
1.0	0.333	0	0.656	0.002
	.25	0.0625	.794	.006
	.167	.125	.834	.006
	.0833	.1875	.892	.003
	0	.25	.940	.006
1.437	0.479	0	0.634	0.000
	.2395	0.1796	.815	.043
	0	.3592	.885	.004
	$m_{K_2SO_4}$	$m_{H_2SO_4}$[a]		
1.007	0.2500	0.2507	0.922	0.036
2.000	0.5000	0.5000	0.832	0.013

[a] Formal molality based on considering H_2SO_4 as a 1–1 electrolyte.

In the case of the solubility of Ag_2SO_4 in K_2SO_4–H_2SO_4 mixtures the calculations were performed essentially as described previously[2] for the solubility of Ag_2SO_4 in H_2SO_4 solutions except that the ionic strength term included the concentration of K_2SO_4. The denominator parameter in the term correcting the bisulfate acid constant for the ionic strength of the solution was taken as 0.4, consistent with previous calculations.[2] At all temperatures from 100 to 175° the observed and calculated solubilities of Ag_2SO_4 agreed to within 1% with a mean A value for I = 1.0 of 0.922 and for I = 2.0 of 0.832.

An attempt was made to relate the A values shown in Table II for each system. In no system was it possible to relate the A value calculated for a mixture with the A values calculated for the corresponding pure systems by taking a linear combination of the latter values weighted according to the ionic strength fractions f_i of the appropriate electrolytes; *i.e.*

$$A_{mixture} = A_1 f_1 + A_2 f_2 \qquad (3)$$

did not hold. However, in the KNO_3–K_2SO_4 systems (I = 1.0) the relationship

$$A_{mixture} = A_1 f_1 + A_2 f_2 + A_1^2 A_2^2 f_1 f_2 \qquad (4)$$

held very well. In the remaining systems the A value for the mixture lay between values computed from the A values of the simple systems by eq. 3 and 4.

Since a simple general combining relationship based on the A values could not be found it seemed of interest to try a direct correlation of the solubility of Ag_2SO_4 in the electrolyte mixtures with the solubilities in the pure component solutions using eq. 5. However, the coefficient s_{12} was not constant but varied quadratically with either f_1 or f_2 and quadratically with temperature. Thus a direct correlation of the solubilities is neither simpler nor more complicated than a correlation through an activity coefficient function.

$$s_M = s_1 f_1 + s_2 f_2 + s_{12} f_1 f_2 \qquad (5)$$

Acknowledgment.—We wish to thank Stanley Anderson and Sarah Ledford for carrying out the experimental solubility measurements and Dr. W. D. Larson for interesting discussions during the early phases of this work.

THE ACTIVATION ENERGY FOR THE DISPROPORTIONATION OF THE HO_2 RADICAL IN ACID SOLUTIONS[1]

BY BENON H. J. BIELSKI AND EIICHI SAITO

Chemistry Department, Brookhaven National Laboratory, Upton, L. I., New York

Received April 16, 1962

The e.p.r. spectrum of the HO_2 radical has been reported independently by several research groups.[2-5] The spectra show good agreement with respect to line shape and line width, although each investigation produced the radical by a different method.

By means of a previously described flow technique,[4] HO_2 was generated by reaction of hydrogen peroxide with ceric sulfate. This method has the advantage of producing the radical in a relatively high concentration in the liquid phase.

Experimental

Chemicals.—The solutions were prepared from triply distilled water and reagent grade chemicals. All solutions were in 0.8 N sulfuric acid. The concentrations of the ceric sulfate solutions were determined spectrophotometrically. The hydrogen peroxide concentrations were determined by the ceric sulfate and iodide method.[6]

Apparatus.—The experimental equipment consisted of a Varian e.p.r. spectrometer, a flow system, and a thermostat. The flow system had a double-jet mixing chamber and a flow tube with an inner diameter of 0.1 cm. The diameter of the flow tube was checked for uniformity with a manganous sulfate solution by sliding it up and down in the microwave cavity of the spectrometer. The maximum deviation from

(1) Research performed under the auspices of the U. S. Atomic Energy Commission.

(2) J. Kroh, B. C. Green, and J. W. T. Spinks, *J. Am. Chem. Soc.*, **83**, 2201 (1961).

(3) L. I. Awramenko and R. W. Kolesnikowa, *Dokl. Akad. Nauk SSSR*, **140**, No. 5 (1961).

(4) E. Saito and B. H. J. Bielski, *J. Am. Chem. Soc.*, **83**, 4467 (1961).

(5) J. Kroh, B. C. Green, and J. W. T. Spinks, *Can. J. Chem.*, **40**, 413 (1962).

(6) I. M. Kolthoff and E. B. Sandell, "Textbook of Quantitative Inorganic Analysis," 1st Ed., The Macmillan Co., New York, N. Y., 1943.

the mean of the signal strength was 3%. The solutions flowed from a thermostat to the mixing chamber and through the flow tube in the cavity. The velocity in the flow tube was 363 ± 5 cm./sec. The tubes leading to the mixing chamber, as well as the flow tube passing through the spectrometer cavity, were fitted with a vacuum jacket. The temperature of the solution was checked with a thermometer at the exit of the flow tube. The distance between mixing chamber and cavity was adjustable.

Calibrations.—The calibration of the e.p.r. spectrometer was carried out with a manganous sulfate solution. It was found that the total area under the absorption curve, which was obtained by graphical integration of the derivative absorption curve, was a linear function of the manganous ion concentration. Further, although there was a change in peak height and line width with temperature, the total area stayed constant. A change in line width with temperature also was observed for the HO_2 radical. This change was 0.26 gauss/deg. at 9.5 kMc.

Results and Discussion

The quantitative oxidation of hydrogen peroxide by ceric sulfate in strong acid media is well known. The over-all reaction can be represented by the equation

$$2Ce^{IV} + H_2O_2 \longrightarrow 2Ce^{III} + 2H^+ + O_2 \quad (I)$$

This reaction takes place in two steps, with the formation of the HO_2 radical as an intermediate[4,7-10]

$$Ce^{IV} + H_2O_2 \rightleftharpoons Ce^{III} + H^+ + HO_2 \quad (1)$$

$$Ce^{IV} + HO_2 \longrightarrow Ce^{III} + H^+ + O_2 \quad (2)$$

The purpose of the present investigation was to determine the activation energy for the reaction

$$HO_2 + HO_2 \longrightarrow H_2O_2 + O_2 \quad (3)$$

It was assumed that if the concentration ratio of hydrogen peroxide to ceric sulfate was high, all the ceric sulfate would react while in the mixing chamber. Under these conditions reaction 2 and the back-reaction in step 1 can be neglected and reaction 3 can be followed in the tube beyond the mixing chamber. This assumption was verified experimentally by changing the ceric sulfate concentration over a tenfold range from 6.12×10^{-3} to 6.72×10^{-4} M. The rate constants which were obtained were identical within experimental error at a hydrogen peroxide concentration of 0.131 M. The signal for the HO_2 radical was detectable for ceric concentrations as low as 7.0×10^{-6} M.

In order to determine the activation energy for reaction 3, e.p.r. spectra of the HO_2 radical were recorded for a number of different flow distances between mixing chamber and cavity at constant flow rate, solute concentrations, and temperature. The concentrations of ceric sulfate and hydrogen peroxide were 1.51×10^{-3} and 0.31 M, respectively.

The area under the absorption curve (which is proportional to the (peak height)(line width)^2 of the derivative absorption curve) is directly proportional to the concentration of the paramagnetic species. Thus a plot of the reciprocal value of (peak height)(line width)^2 of the HO_2 e.p.r. spectrum *vs.* flow time should give a straight line if the reaction follows second-order kinetics. This is indeed the case, as shown by the data plotted in Fig. 1.

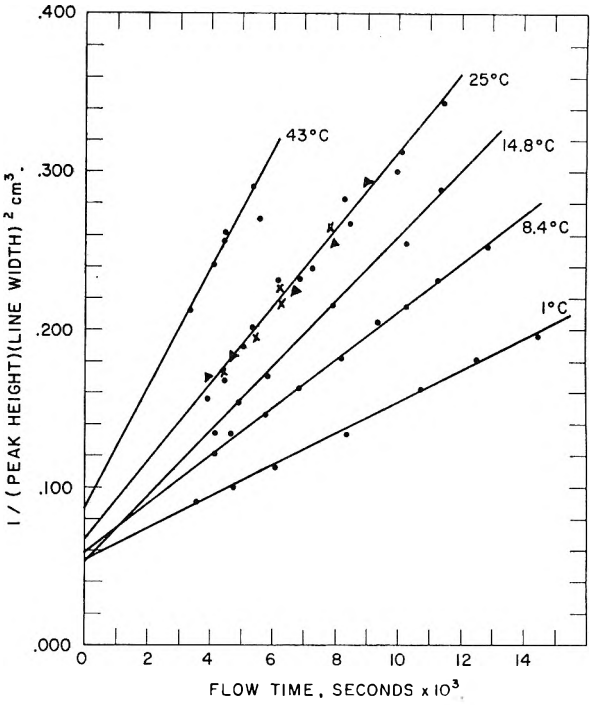

Fig. 1.—Reciprocal (peak height)(line width)^2 cm.^{3} *vs.* flow time of HO_2: ●, pH 0.5, 0.8 N H_2SO_4; ×, pH 1.05; ▲, pH 1.55. The conversion factor is 3.34×10^{18} spins/cm.^{3}.

The relation between the activation energy and the e.p.r. spectra can be represented by the equation

$$\ln(\text{slope}) = -\frac{E_a}{RT} + \text{constant} \quad (4)$$

where the slopes are those of the curves in Fig. 1. As is evident from eq. 4, the activation energy can be computed without the knowledge of the absolute concentrations of the HO_2 radical. The calculations of the activation energy are based on an average intercept of 0.057 cm.$^{-3}$ in Fig. 1. The activation energy computed from a curve of ln (slope) *vs.* reciprocal absolute temperature is 5.9 ± 0.4 kcal./mole.

An attempt also has been made to calculate the absolute rate constants for reaction 3 from the results in Fig. 1. The calculations are based on the graphical integration of the e.p.r. spectra of HO_2 and the calibration spectrum of manganous sulfate. The calibration factor was 3.34×10^{18} spins/cm.^{3}. Using the second-order equation $d(HO_2)/dt = -k_3(HO_2)^2$, the rate constants for this reaction were calculated. The results are given in Table I. Although these values show small relative experimental errors, the absolute values obtained by this technique may have an uncertainty up to 50%.

An investigation of the effect of the H^+ ion concentration upon reaction 3 has been carried out at 25°. The data given in Fig. 1 indicate that the disproportionation reaction of HO_2 is

(7) J. H. Baxendale, *J. Chem. Soc.*, Spec. Publ. No. 1, 40 (1954).
(8) S. Baer and G. Stein, *ibid.*, 3176 (1953).
(9) P. B. Siegeler and B. J. Masters, *J. Am. Chem. Soc.*, **79**, 6353 (1957).
(10) Unpublished work by B. H. J. Bielski and A. O. Allen.

TABLE I

RATE FOR THE DISPROPORTIONATION OF HO_2 IN 0.8 N SULFURIC ACID

Temp., °C.	k_2, l./moles-sec.
1.0	$2.33 \times 10^6 \pm 0.33$
8.4	$2.85 \times 10^6 \pm .35$
14.8	$3.61 \times 10^6 \pm .64$
25.0	$4.74 \times 10^6 \pm .81$
43.0	$7.30 \times 10^6 \pm 1.20$

independent of the hydrogen ion concentration in the pH range from 0.5 to 1.55.

Acknowledgment.—The authors wish to thank Drs. A. O. Allen, H. A. Schwarz, and J. Rush for interesting and helpful discussions of this problem.

PRECISE MEASUREMENTS WITH GLASS ELECTRODES: THE ACTIVITY COEFFICIENTS OF HYDROCHLORIC ACID AT 65°[1]

BY H. LAWRENCE CLEVER AND RALPH M. REEVES

Department of Chemistry, Emory University, Atlanta 22, Georgia

Received April 24, 1962

In 1955 Covington and Prue[2] devised a method of obtaining thermodynamic data from a cell with a glass electrode. In dilute acid the glass electrode potential is assumed to be due to (a) the hydrogen ion activity and (b) a time dependent asymmetry potential characteristic of the glass electrode. If the change in asymmetry potential is linear with time, the potential of a glass electrode–acid anion reversible electrode system can be extrapolated to the time of transferring the electrode system from acid of one concentration to acid of another concentration. The difference in potential of the time of transfer would exactly cancel the asymmetry potential and leave a potential equivalent to that of a reversible concentration cell without transference. A similar technique can be used which is equivalent to a concentration cell with transference.[3]

Covington and Prue have tested their technique using special glass electrodes of large surface area made of low resistance soft glass with a thin hard glass coating. These electrodes are of very low asymmetry potential. They have successfully determined the activity coefficients of HCl, HNO_3, and $HClO_4$ at 0 and 25°[2-4] using a conventional potentiometer circuit. Measurements at 45° or higher were not successful because of deterioration of the hard glass coating of the special glass electrodes which allowed traces of base to leach into the acid solutions.[5]

The present work was undertaken to test the technique at higher temperatures with commercial glass electrodes. A glass–silver–silver chloride electrode system in HCl was used. The potential of the high impedance system was measured as a function of time with a vibrating reed electrometer.

(1) Work performed for the AEC under contract no. AT-(40-1)-2569.

(2) A. K. Covington and J. E. Prue, *J. Chem. Soc.*, 3699 (1955).

(3) A. K. Covington and J. E. Prue, *ibid.*, 3701 (1955).

(4) A. K. Covington and J. E. Prue, *ibid.*, 1567 (1957).

(5) A. K. Covington, *ibid.*, 4441 (1960).

The extrapolated difference in potential at the time of changing the acid concentration from m_1 to m_2 around the electrode system is equivalent to the concentration cell without transference

$$Pt/H_2(1\ atm.)/HCl(m_2)/AgCl/Ag\text{–}Ag/AgCl/HCl(m_1)/H_2(1\ atm.)/Pt$$

The potential is

$$E = E_{m1} - E_{m2} = -k \log \frac{m_1^2\gamma_1^2}{m_2^2\gamma_2^2} \quad (1)$$

where $m_2 > m_1$, E_{m1} and E_{m2} are the experimentally measured potentials extrapolated to the time of changing the acid concentration, and k is $2.303 \times RT/F$.

Since all runs were made with the same initial concentration of HCl, m_1, the potential can be written

$$E = E^0 + 2k \log m_2 + 2k \log \gamma_2 \quad (2)$$

where

$$E^0 = -2k \log m_1\gamma_1$$

Activity coefficients of HCl were calculated from the semi-empirical Debye–Hückel type equation

$$\log \gamma = -\frac{A_m^{1/2}}{1 + B_m^{1/2}} + B'm \quad (3)$$

where A is the Debye–Hückel constant, B is taken as a temperature independent constant, and B' is a constant evaluated from the experimental e.m.f. data.

Substitution of log γ from eq. 3 into eq. 2 and rearrangement gives

$$E - 2k \log m + \frac{2kA_m^{1/2}}{1 + B_m^{1/2}} = E^0 + 2kB'm \quad (4)$$

A plot of the left-hand side against m gives a straight line whose slope is $2kB'$.

Experimental

The glass/HCl (m)/AgCl–Ag cell assembly was completely immersed in a well stirred oil bath controlled to ±0.02°. Oxygen-free, water-saturated nitrogen was kept over the HCl solution at all times.

The e.m.f. was measured with an Applied Physics Corp. Model 32 vibrating reed electrometer as detector.[6] The e.m.f. was fed to the vibrating reed electrometer; all but about 2 mv. was "bucked out" by a Rubicon type B potentiometer standardized against a Bureau of Standards certified Weston standard cell. The final 2 mv. was displayed on a Brown recording potentiometer and followed as a function of time.

Dilute standard acid (about 0.005 m) was placed in the cell and the e.m.f. followed until any change was linear with time. The acid concentration was changed by adding a small amount of concentrated acid to the cell and the e.m.f. again followed until it was linear with time. The linear portions of the e.m.f.–time curves are extrapolated to the time of changing the acid concentration and the e.m.f. difference determined at that time. The acid in the cell at the end of the run was analyzed by titration from weight burets against KHP standardized NaOH solution.

(6) K. A. Kraus, R. W. Holmberg, and C. J. Borkowski, *Anal. Chem.*, **22**, 341 (1950).

The silver–silver chloride electrodes were thermal type prepared by heating to about 550° a 1:8 weight mixture of silver oxide and silver chlorate. The procedure outlined by Greeley, Smith, Stoughton, and Lietzke[7] was followed closely.

The glass electrodes were Beckman commercial glass electrodes. Both the Amber Glass #43509 and the General Purpose #41203 were tried with no detectable difference in results. In most of the runs the Amber Glass electrode was used.

The empirical constant B' was calculated from the slope of a plot of

$$E - 2k \log m + \frac{2kAm^{1/2}}{1 + Bm^{1/2}}$$

against m. Values of the necessary constants at 65° were taken from the tabulation of Manov, Bates, Hamer, and Acree.[8] The Debye–Hückel A is 0.5480 kg.$^{1/2}$ mole$^{-1/2}$ and k was converted to absolute volts and is 67.093 mv. The constant B was treated as an empirical constant. Guggenheim and Prue[9] suggest $B = 1.0$, Scatchard[10] suggests $B = 1.5$ satisfactorily fits most data for 1–1 electrolytes. The data were plotted using $B = 1.0$, 1.5, 2.0, and 3.0.

All four plots were linear; the least squares slopes, the standard error of fit, and the B' values are in Table I. The minimum standard error of fit was found with $B = 1.0$. The calculated activity coefficients are compared with the values determined by Greeley, Smith, Lietzke, and Stoughton[11] in Table II. The calculated activity coefficients agree well with both $B = 1.0$ and $B = 1.5$, with the $B = 1.5$ values giving a slightly closer check.

TABLE I

VALUES OF B' AS A FUNCTION OF B FROM THE LEAST SQUARES SLOPE OF $E - 2k \log m + \frac{2kAm^{1/2}}{1 + Bm^{1/2}}$ AGAINST m

B	Slope	B'	σfit, mv.
1.0	30.4	0.227	0.350
1.5	13.6	.102	.392
2.0	0.844	.0063	.394
3.0	−17.3	− .129	.398

TABLE II

MEAN IONIC ACTIVITY COEFFICIENTS OF HYDROCHLORIC ACID AT 65° CALCULATED FROM $\log \gamma = -\frac{Am^{1/2}}{1 + Bm^{1/2}} + B'm$

Molality	Accepted activity coefficients[a]	Mean ionic activity coefficients calcd. with B equal			
		1.0	1.5	2.0	3.0
0.005	0.923	0.922	0.924	0.925	0.928
.01	.898	.896	.898	.900	.910
.02	.867	.864	.867	.870	.877
.05	.817	.815	.819	.824	.832
.10	.774	.778	.781	.784	.791
.20	.743	.752	.748	.745	.741

[a] Reference 11.

A series of runs at 50° before the experimental technique was refined to rigorously exclude oxygen from the Ag–AgCl electrode and to prevent all evaporation losses gave almost equally good values of activity coefficient but the uncertainty due to the scatter of e.m.f. values was unacceptable. An incomplete set of data at 85° indicated the technique would be equally successful at that temperature with the advantage that the asymmetry potential seemed to become linear in a shorter time at the higher temperature.

Acknowledgment.—We wish to thank Dr. M. H. Lietzke and Dr. R. W. Stoughton of the Oak Ridge National Laboratory for an introduction to this problem.

(7) R. J. Greeley, W. T. Smith, Jr., R. W. Stoughton, and M. H. Lietzke, *J. Phys. Chem.*, **65**, 652 (1960).

(8) G. G. Manov, R. G. Bates, W. J. Hamer, and S. F. Acree, *J. Am. Chem. Soc.*, **65**, 1765 (1943).

(9) E. A. Guggenheim and J. E. Prue, *Trans. Faraday Soc.*, **50**, 231 (1954).

(10) See footnote 9 of M. H. Lietzke and R. W. Stoughton, *J. Am. Chem. Soc.*, **78**, 4520 (1956).

(11) R. S. Greeley, W. T. Smith, Jr., M. H. Lietzke, and R. W. Stoughton, *J. Phys. Chem.*, **64**, 1445 (1960).

THE EFFECT OF SUBSTITUTION ON THE IONIZATION POTENTIALS OF FREE RADICALS AND MOLECULES. IV. δ_K VALUES FOR ALCOHOLS, ETHERS, THIOLS, AND SULFIDES[1a]

BY JOYCE J. KAUFMAN[1b]

RIAS, Baltimore 12, Maryland

Received April 25, 1962

It has been shown previously[2,3] that the effects of substituent groups on ionization potentials of alkylamines (Y_3N) and alkyl free radicals (Y_3C) were almost identical. From measured photoionization potentials of amines a new set of constants, δ_K values, which quantitatively reflect changes in ionization potential with substituent groups, were derived and using these, ionization potentials of alkyl free radicals could be estimated to within the experimental error of their measurements. There is a "saturation" effect and these values are not linearly additive but can be combined following certain set precepts. δ_K values obtained from linear and branched alkyl substituents proved to be extendable to cyclic substituents in which the carbon from whence the unpaired electron was being withdrawn was itself part of the ring.[3]

However, effects of substitution on ionization potentials are not the same for the series of alcohols and ethers as for the amines. δ_K values for these oxygen-containing compounds now will be treated here. This problem has assumed importance recently because of the use of δ_K values as a measure of the magnitude of penetration integrals of neutral substituent groups in quantum chemical calculations. Although these penetration integrals customarily are neglected, they have been shown in several cases to be comparable in magnitude to other terms being calculated.[4]

Since δ_K values derived from nitrogen compounds do not carry over into the oxygen series, a specific set of δ_K values for use with oxygen compounds is presented in Table I. These values are based on photoionization measurements of the molecules.[5] The purpose of these values is twofold: first, to

(1) (a) This work was supported in part by the Office of Naval Research; (b) 1962 Visiting Staff Member, Centre de Mécanique Ondulatoire Appliquée, 23 Rue du Maroc, Paris 19^E, France.

(2) (a) J. J. Kaufman and W. S. Koski, *J. Am Chem. Soc.*, **82**, 3262 (1960); (b) J. J. Kaufman and W. S. Koski, presented before the Section on Physical Chemistry—Structure and Reactivity of Small Molecular Species, 18th International Congress of Pure and Applied Chemistry, Montreal, August, 1961.

(3) J. J. Kaufman, Part III of this series, ONR-TR3. NONR-3471(00), March, 1962; (accepted for publication in *J. Am. Chem. Soc.*).

(4) S. Bratož and S. Besnainou, *J. Chem. Phys.*, **34**, 1142 (1961).

(5) K. Watanabe, T. Nakayama, and J. Mottl, "Final Report on Ionization Potential of Molecules by a Photoionization Method." Dept. of the Army #5B 99-01-004, December, 1959.

TABLE I

δ_K VALUES DERIVED FOR O AND S MOLECULES (IN E.V.)

H_2O and H_2S parent molecules

Oxygen Substituent	$\delta_{K,O}^{(1)}$	$\delta_{K,O}^{(1-0)}$	$\delta_{K,O}^{(2)}$	$\delta_{K,O}^{(2-1)}$	$\delta_{K-Me,O}^{(1)}$	$\delta_{K-Me,O}^{(2)}$
CH_3-	1.74		2.59			
		1.74		0.85		
C_2H_5-	2.11		3.06		0.37	0.47
		2.11		0.95		
n-C_3H_7-	2.39		3.32		0.65	0.73
		2.39		0.93		
i-C_3H_7-	2.43		3.39		0.69	0.80
		2.43		0.96		
n-C_4H_9-	2.55				0.81	

Sulfur Substituent	$\delta_{K,S}^{(1)}$	$\delta_{K,S}^{(1-0)}$	$\delta_{K,S}^{(2)}$	$\delta_{K,S}^{(2-1)}$	$\delta_{K-Me,S}^{(1)}$	$\delta_{K-Me,S}^{(2)}$
CH_3-	1.02		1.77			
		1.02		0.75		
C_2H_5-	1.17		2.03		0.15	0.26
		1.17		0.86		
n-C_3H_7-	1.26		2.16		0.24	0.39
		1.26		0.90		
n-C_4H_9-	1.32				0.30	
		1.32				

enable one to estimate ionization potentials of other oxygen-containing molecules, and second, to permit one to differentiate effects of penetration integrals on different cores, —C· and —N: on one hand and —Ö— on the other hand.

The symbolism and sign convention for δ_K values are the same as those of ref. 2a: δ_K (or $\delta_K^{(1)}$) and $\delta_K^{(2)}$ are the changes in ionization potential caused by substituting one or two identical groups, respectively, for H atoms (on the same central O atom from which the electron is being withdrawn upon ionization). To differentiate these δ_K values from those derived from nitrogen compounds, an extra subscript O will be used:

$$\delta_{K,O} \text{ and } \delta_{K,O}^{(2)}$$

$\delta_{K-Me,O}^{(1)}$ and $\delta_{K-Me,O}^{(2)}$ are the changes in ionization potential caused by substituting one or two groups for methyl groups (under the same conditions as above).

Since there is a saturation effect, another type of δ_K value is the difference in ionization potential found by adding a second identical substituent group when a first substituent group already is present.

$\delta_{K,O}^{(1-0)}$ (or $\delta_{K,O}$ or $\delta_{K,O}^{(1)}$) and $\delta_{K,O}^{(2-1)}$ are the differences in ionization potential between mono- and unsubstituted and between di- and monosubstituted molecules.

The symbols for δ_K values from sulfur compounds are exactly the same with the exception of a subscript S instead of O.

With the δ_K values in Table I, it is possible to: (1) calculate the ionization potentials of mixed ethers or sulfides: As an example one can reproduce by calculation the experimentally measured ionization potential of $CH_3SC_2H_5$.

(a) $I(\text{MeSEt}) = I(H_2S) - \delta_{K,S}^{(1)}(\text{Et}) - \delta_{K,S}^{(2-1)}(\text{Me})$

$= 10.46 \text{ e.v.} - 1.17 \text{ e.v.} - 0.75 \text{ e.v.}$

$= 8.54 \text{ e.v. (calcd.)}$

or

(b) $I(\text{MeSEt}) = I(H_2S) - \delta_{K,S}^{(1)}(\text{Me}) - \delta_{K,S}^{(2-1)}(\text{Et})$

$= 10.46 \text{ e.v.} - 1.02 \text{ e.v.} - 0.86 \text{ e.v.}$

$= 8.58 \text{ e.v. (calcd.)}$

Each of these calculated values is extremely close to the experimentally measured value of 8.55 ± 0.01 e.v. The convention to be adopted for calculation of ionization potentials for S and O compounds is $\delta_{K,S(\text{or }O)}^{(1)}(R_1)$ and $\delta_{K,S(\text{or }O)}^{(2-1)}(R_2)$ where if $R_1 \neq R_2$, then $R_1 > R_2$.

(2) calculate the ionization potential of a cyclic ether or sulfide: In a previous paper[3] it has been demonstrated that it is possible to calculate ionization potentials of cyclic entities by extension of the δ_K values for the corresponding linear groups.

(a) Estimation of the ionization potential of tetrahydrofuran (THF) confirms this conclusion.

$I(\text{THF}) = I(H_2O) - \delta_{K,O}^{(2)}(\text{Et}) = 12.59 \text{ e.v.} - 3.06 \text{ e.v.}$

$= 9.53 \text{ e.v. (calcd.)}$

$I(\text{THF}) = 9.54 \text{ e.v. (expt.)}$

(b) Estimation of the ionization potential of tetrahydropyran (THP) serves as a conclusive

check on the validity of calculation of ionization potentials of cyclic ethers by the δ_K method.

$$I(\text{THP}) = I(H_2O) - \delta_{K,O}^{(1)}(\text{Pr}) - \delta_{K,O}^{(2-1)}(\text{Et})$$

$$= 12.59 \text{ e.v.} - 2.39 \text{ e.v.} - 0.95 \text{ e.v.}$$

$$= 9.25 \text{ e.v. (calcd.)}$$

$$I(\text{THP}) = 9.26 \pm 0.03 \text{ e.v. (expt.)}$$

For cyclic compounds if possible use $R_1 = R_2$; if not, then $R_1 > R_2$.

The much larger effect of the Me group on I(MeS·) radical relative to I(HS·) radical[6] (2.44 e.v. as compared to 1.02 e.v. for MeSH relative to H_2S) indicates an enhanced resonance contribution (due possible to a planarity of the MeS^+ ion). This observation carries with it the subtle implication that one should perhaps use different evaluations of penetration integrals depending upon whether one or two electrons from O or S are contributed to a delocalized system.

Ionization potentials of ethers and sulfides have become of great interest recently in connection with charge-transfer complexes. Formation of various types of complexes is dependent on basicities and therefore on ionization potentials of the donors, and positions of new ultraviolet or visible charge-transfer absorption bands are directly related to ionization potentials of the donors.

Acknowledgment.—The author wishes to thank Dr. F. P. Lossing for graciously sending information on experimentally measured ionization potentials in advance of publication.

(6) F. P. Lossing, private communication.

CONFIRMATION OF THE NATURE OF CATION DEPOPULATION IN SYNTHETIC CRYSTALLINE ZEOLITES

BY GEORGE T. KERR

Socony Mobil Oil Company, Inc., Research Dept., Paulsboro, New Jersey

Received May 16, 1962

Freeman and Stamires[1] studied the electrical conductivity of zeolites A, X, and Y. The two latter zeolites, isostructural with faujasite, differ in composition. These workers defined zeolite X as having molar ratios of silica to alumina between 2.1 and 3.0 and zeolite Y as having ratios between 3.0 and 5.2. Consequently, zeolites of the X group have a higher cation density (number of cations per unit cell) than zeolites of the Y group since zeolites contain one equivalent of cation for each gram-atom of aluminum in the zeolitic framework. The differences in the energies of activation for conduction between zeolites X and Y supported the postulation of Breck and Flanigen[2] that there is more than one type of cation site in zeolites. Freeman and Stamires found that the highest energy-site type (in which the cations are relatively loosely bound to the lattice) is eliminated or depopulated as the cation density decreases; the low energy-site type (tightly bound cations) is retained. They proposed that the loosely bound cations are located in the large cavities or in the eight- or twelve-membered oxygen rings of the zeolite lattices; the tightly bound cations are located in the vicinity of the six-membered rings. In summary, this proposal states that for a given zeolite crystal structure, as the silica to alumina ratio is increased, the cation sites located in the large cavities or rings are depopulated in preference to those located in the smaller cavities or rings. The information to follow supports this proposal.

Sodium zeolite A[3] (2.0 molar ratio of silica to alumina) will not sorb straight chain hydrocarbons. However, replacement of 30 to 40% of the sodium ions by calcium ions renders zeolite A capable of sorbing straight chains.[3b] At this level of exchange the unit cell of zeolite A contains an average of 9.6 to 10.2 cations. Reed and Breck[3c] interpreted this as indicating that sodium ions located in the eight-membered oxygen rings (through which hydrocarbon sorption occurs) are preferentially replaced over the sodium ions located in the six-membered oxygen rings.

On the basis of these findings it would be expected that upon increasing the silica to alumina molar ratio of a zeolite A structure, the cation sites located in the eight-membered oxygen rings would be depopulated in preference to those in the six-membered rings. If the molar ratio of silica to alumina were at least 2.7, the number of sodium ions still located in the eight-membered rings should not be sufficient to preclude the sorption of straight chain hydrocarbons.

Sodium zeolite ZK-4,[4] with a silica to alumina molar ratio of 3.4, fulfills this requirement. This zeolite, containing nine sodium ions per unit cell, has essentially the same sorptive capacity for straight chain hydrocarbons as calcium zeolite A (for example, 12.5 and 12.6 wt. %, respectively, for *n*-hexane on samples purged at 350° with nitrogen). If the nine sodium ions per unit cell in zeolite ZK-4 were distributed among six- and eight-membered oxygen rings in the same proportion as in sodium zeolite A, then each eight-membered oxygen ring would contain one sodium ion thus blocking free passage of a straight chain hydrocarbon through the main crystal cavity, as shown by Reed and Breck.[3c] Hence, the findings of Freeman and Stamires explain our observations. Additional confirmation might be obtained by comparing the energies of activation for conduction of zeolites A and ZK-4 as was done with zeolites X and Y by Freeman and Stamires.

(1) D. C. Freeman and D. N. Stamires, *J. Chem. Phys.*, **35**, 799 (1961).

(2) D. W. Breck and E. M. Flanigen, Abstract 134 of the 134th National Meeting of the American Chemical Society, September, 1958, Chicago, Illinois.

(3) (a) D. W. Breck, W. G. Eversole, and R. M. Milton, *J. Am. Chem. Soc.*, **78**, 2338 (1956); (b) D. W. Breck, W. G. Eversole, R. M. Milton, T. B. Reed, and T. L. Thomas, *ibid.*, **78**, 5963 (1956); (c) T. B. Reed and D. W. Breck, *ibid.*, **78**, 5972 (1956).

(4) G. T. Kerr and G. T. Kokotailo, *ibid.*, **83**, 4675 (1961).

REACTIONS OF TRITIUM ATOMS WITH FROZEN CYCLOPROPANE[1]

BY H. C. MOSER AND R. D. SHORES

Department of Chemistry, Kansas State University, Manhattan, Kansas

Received May 21, 1962

Tritium atoms produced by the atomization of molecular hydrogen containing tritium at a hot tungsten filament have been found to react with frozen hydrocarbons.[2] One of the principal reactions is the exchange of T for H, and this occurs simultaneously with other reactions requiring less activation energy such as hydrogenation of unsaturated compounds. Investigation of tritium atom reactions with cyclopropane was undertaken to help elucidate the energy effects. Hydrogen atoms of different energies have been reported to react differently with cyclopropane.[3-5]

Experimental

Cyclopropane (Matheson Co.) usually was purified by gas chromatography to remove a small amount of propene impurity. A 15-ft. dimethylsulfolane column was used for the separation. Ethane (Matheson C.P.) and propane (Matheson instrument grade) were used without further purification.

Molecular hydrogen containing tritium was produced by the reduction of tritiated water (specific activity 18 mc./mmole) by metallic zinc[6] at 650°.

A 4.3-cm. diameter, thin-walled, Pyrex flask was used as the reaction vessel. Suspended from molybdenum leads at the center of the flask was a 3.1 cm. × 0.008 cm. or 3.1 cm. × 0.005 cm. tungsten filament. The maximum filament to wall distance was 3 cm. An optical pyrometer was used to measure the temperature of the filament at its center. Approximately two thirds of the filament was at the reported temperature, and the remainder was at a lower temperature. A Pirani gage was used to measure the pressure. The gage was frequently calibrated with a McLeod gage.

From 5.7×10^{-5} to 4.2×10^{-2} mmole of cyclopropane was introduced into the system and frozen out as a film on the inside surface of the reaction flask by immersing the vessel in liquid nitrogen. Hydrogen was introduced through a high vacuum needle valve which was used to maintain a pressure of 5 μ during reaction.

Following reaction, products were transferred to a sampler at −195°. The amount of tritium incorporated, exclusive of any present as methane, was measured by counting a known fraction of the gaseous sample with an ionization chamber. Products were separated by gas chromatography with a 15-ft. dimethylsulfolane column operated at room temperature. Methane usually was pumped off with hydrogen remaining after reaction. In a few experiments methane and some hydrogen were adsorbed on silica gel at −195° and separated by gas chromatography using a column packed with Linde Type 5A Molecular Sieve. Following separation the products were passed through a proportional counter placed in the effluent stream.

Results

Table I gives results of reactions run at three different filament temperatures. The hydrogen pressure was maintained at 5 μ during a 5 min. reaction time with 0.042 mmole of purified cyclopropane. The amount of tritium incorporated increased with filament temperature. Exclusive of tritium present in labeled methane, 0.26 μc. was contained in the products from reaction with unpurified cyclopropane at 1750° (0.008 cm. × 3.1 cm. filament).

Table II gives results of reactions with different amounts of purified cyclopropane for a 5 min. reaction time, 1750° filament temperature, and 5 μ hydrogen pressure. Assuming uniform deposition, film thicknesses for these reactions were approximately 6×10^{-8}, 6×10^{-7}, 10^{-5}, and 4×10^{-5} cm.

TABLE I

PRODUCTS OF TRITIUM ATOM REACTIONS WITH FROZEN CYCLOPROPANE

Filament temp., °C.	1180	1520	1750
% Tritium in Products[a]			
Ethane	73	37	12
Propane	27	15	23
Cyclopropane		14	37
Isobutane		8	6
n-Butane		6	5
2-Methylbutane		7	6
n-Pentane		5	4
C_6		7	7

[a] Does not include methane.

TABLE II

EFFECT OF FILM THICKNESS ON PRODUCTS OF TRITIUM ATOM REACTIONS WITH FROZEN CYCLOPROPANE

Amt. of cyclopropane (mmoles)	5.7×10^{-5}	5.7×10^{-4}	1.1×10^{-2}	4.2×10^{-2}
% Tritium in products[a]				
Ethane	25	10	5	12
Propane	26	25	32	23
Cyclopropane	14	28	37	37
Isobutane	13	10	8	6
n-Butane	10	9	7	5
2-Methylbutane	8	7	6	6
n-Pentane	3	5	3	4
C_6	1	5	2	7

[a] Does not include methane.

Methane was found in each sample analyzed for it. In some cases the methane contained more than 30% of the incorporated tritium. The percentage of tritium in methane decreased in reactions run at the higher filament temperatures.

The reactions were not noticeably affected by eliminating thermionic emission from the filament with the use of a negatively charged grid. In a larger reaction vessel (250-cc. volume) the filament was surrounded by an open-structured, wire grid. The negative pole of a 67.5-volt battery was connected to the grid and the positive pole to one end of the filament.

Yields for hydrogen exchange reactions were measured for propane and cyclopropane under the same conditions. Relative yields of 3 and 1 were obtained, respectively, for 3-min. reactions. The yield of the hydrogen exchange reaction on cyclopropane was measured under various experimental conditions. In addition to the effects of filament temperature and film thickness (Tables I and II), the yield was greatly reduced by introduction of 50 μ helium as a moderating gas. Also, when the surface of the cyclopropane was covered with a film of propane or ethane, the yield for the exchange of T for H in cyclopropane was reduced to an undetectable level.

(1) Work performed under Contract AT(11-1)-584 with the U.S. Atomic Energy Commission.

(2) R. D. Shores and H. C. Moser, *J. Phys. Chem.*, **65**, 570 (1961).

(3) H. I. Schiff and E. W. R. Steacie, *Can. J. Chem.*, **29**, 1 (1951).

(4) J. K. Lee, B. Musgrave, and F. S. Rowland, *ibid.*, **38**, 1756 (1960).

(5) D. W. Setser, B. S. Rabinowitch, and E. G. Spittler, *J. Chem. Phys.*, **35**, 1840 (1961).

(6) K. E. Wilzbach, L. Kaplan, and W. G. Brown, *Science*, **118**, 522 (1953).

Discussion

Tritium Atom Production.—New information on the mechanism of atomization of hydrogen on tungsten has been reported by Brennan and Fletcher[7] and Hickmott.[8] Brennan and Fletcher have proposed, for the lower range of temperatures used in the present study, that equilibrium is maintained between adsorbed and gaseous hydrogen and that atomic and molecular hydrogen desorb in their equilibrium ratio as determined by the temperature of the surface and the pressure of the undissociated gas. On this basis a Maxwell–Boltzmann distribution of hydrogen atom energies is considered reasonable.

A large fraction of the hydrogen atoms that leave the filament should have a collision free path to the film of cyclopropane. The mean free path for hydrogen atoms in the reaction vessel is estimated to be about 2 cm. for a pressure of 5 μ measured at the Pirani gage.

Mechanism and Energy Effects.—Atom–radical and radical–radical combinations of hydrogen, methyl, ethyl, propyl, isopropyl, and cyclopropyl free radicals can account for all of the products observed. Hydrogen abstraction to form cyclopropyl and hydrogen atom addition to form propyl are probably the initial reactions of hydrogen atoms and cyclopropane. Subsequent reactions resulting in the formation of other radicals are mentioned later on in the discussion.

Exchange of T for H in cyclopropane can occur only with energetic tritium atoms and therefore must be initiated on the surface of the frozen cyclopropane film. Thermalized D atoms do not exchange for hydrogen in cyclopropane at room temperature,[3] but exchange has been observed[5] in the Hg ($^3P_1$) photosensitization of deuterium–cyclopropane mixtures at 135° and in reactions of recoil tritons with cyclopropane.[4] Our results from reactions with added helium and from reactions when the cyclopropane surface was covered with a frozen film of ethane or propane also indicate that only energetic atoms react by exchange. In our experimental approach, this requirement is met for surface reactions where the pressure in the reaction vessel is low enough to allow a collision free path from the filament to the walls.

There is both a lower activation energy and lower collision efficiency for the formation of propyl radicals than for the formation of cyclopropyl (see Table I) because the relative yield of labeled cyclopropane increases with filament temperature while that for propane decreases. Hydrogen (or tritium) atom addition to cyclopropyl would give excited cyclopropane which could deactivate or could isomerize to form propene. Hydrogen atom addition to a propyl radical would give excited propane which could deactivate or crack to form methyl and ethyl radicals.[9] Isomerization and cracking must occur only on the surface where the probability for collision or deactivation is the lowest. This mechanism is in qualitative agreement with results from the gas phase where at room temperature deuterium atoms and cyclopropane react with low collision efficiency without the formation of deuterated cyclopropane.[3] On the other hand exchange has been observed at 135° presumably through the formation of cyclopropyl radicals.[5]

The relative yield of labeled cyclopropane is diminished when the thickness of cyclopropane is reduced to a few molecular layers (Table II) while yields from cracking and isomerization increase. Deactivation of excited cyclopropane and propane apparently is facilitated by an increase in the thickness of frozen cyclopropane. This behavior is dependent upon the diffusion of cyclopropyl radicals and hydrogen atoms into the frozen film. Rapid diffusion of hydrogen atoms in frozen propene has been proposed[10] and diffusion of cyclopropyl radicals in frozen cyclopropane also is reasonable on the basis of general diffusion behavior.[11]

The excitation energy accompanying addition of a hydrogen atom to cyclopropyl is about 30 kcal. more than the 65 kcal. activation energy required for isomerization.[12] Unless deactivated through collisions, the excited cyclopropane should have a high probability of undergoing isomerization to form propene. In small amounts frozen propene reacts with hydrogen atoms to form principally methane, ethane, and propane.[13]

(7) D. Brennan and P. C. Fletcher, *Proc. Roy. Soc.* (London), **A260**, 389 (1959).

(8) T. W. Hickmott, *J. Chem. Phys.*, **32**, 810 (1960).

(9) C. H. Heller and A. S. Gordon, *J. Phys. Chem.*, **64**, 390 (1960).

(10) R. Klein, M. D. Scheer, and J. G. Waller, *ibid.*, **64**, 1247 (1960).

(11) A. M. Bass and H. P. Broida, "Formation and Trapping of Free Radicals," Academic Press, Inc., New York, N. Y., 1960, p. 77.

(12) H. O. Pritchard, R. G. Sowden, and A. F. Trotman-Dickenson, *Proc. Roy. Soc.* (London), **A217**, 563 (1953).

(13) Han Bo Yun, M.S. Thesis, Kansas State University, 1962.

HIGH TEMPERATURE DISPROPORTIONATION OF LOWER VANADIUM OXIDES REACTING WITH BARIUM OXIDE[1]

BY U. SPITSBERGEN AND P. W. J. JANSEN

Laboratory for Inorganic and Physical Chemistry, University of Leiden, Leiden, The Netherlands

Received December 15, 1961

Products of solid state reactions at temperatures between 1000 and 1450° of mixtures of barium oxide and various vanadium oxides have been studied by X-ray identification. Powder photographs were taken in a Guinier-de Wolff focusing camera, R = 229.2 mm. with CuK$\alpha_{1,2}$ radiation, λ = 1.5418 Å. Samples were mixed with KCl (Analytical Reagent, a_{20} = 6.2919 Å. as given by Hambling[2]) as a reflection standard.

Mixtures of barium oxide freshly dried 20 hr. at 1050° *in vacuo* and a vanadium oxide were thoroughly ground in appropriate ratios, pelletized, and heated *in vacuo*. The mixtures were prefired, reground, and refired to ensure homogeneity. Annealing procedures subsequently were carried out in evacuated silica amopules. Magnesium oxide single crystal was employed as refractory material. Above 1350° two pellets were stacked, the lower one to be discarded after heating. The samples were checked on constancy of weight after each heat treatment. Whole number mole ratio mixtures of BaO and, respectively, $VO_{1.00}$, V_2O_3, VO_2, and V_2O_5 were studied subsequently. Of the BaO,

(1) This work forms a part of the Doctoral Thesis of U. Spitsbergen to be submitted to the University of Leiden, The Netherlands.

(2) P. Hambling, *Acta Cryst.*, **6**, 98 (1953).

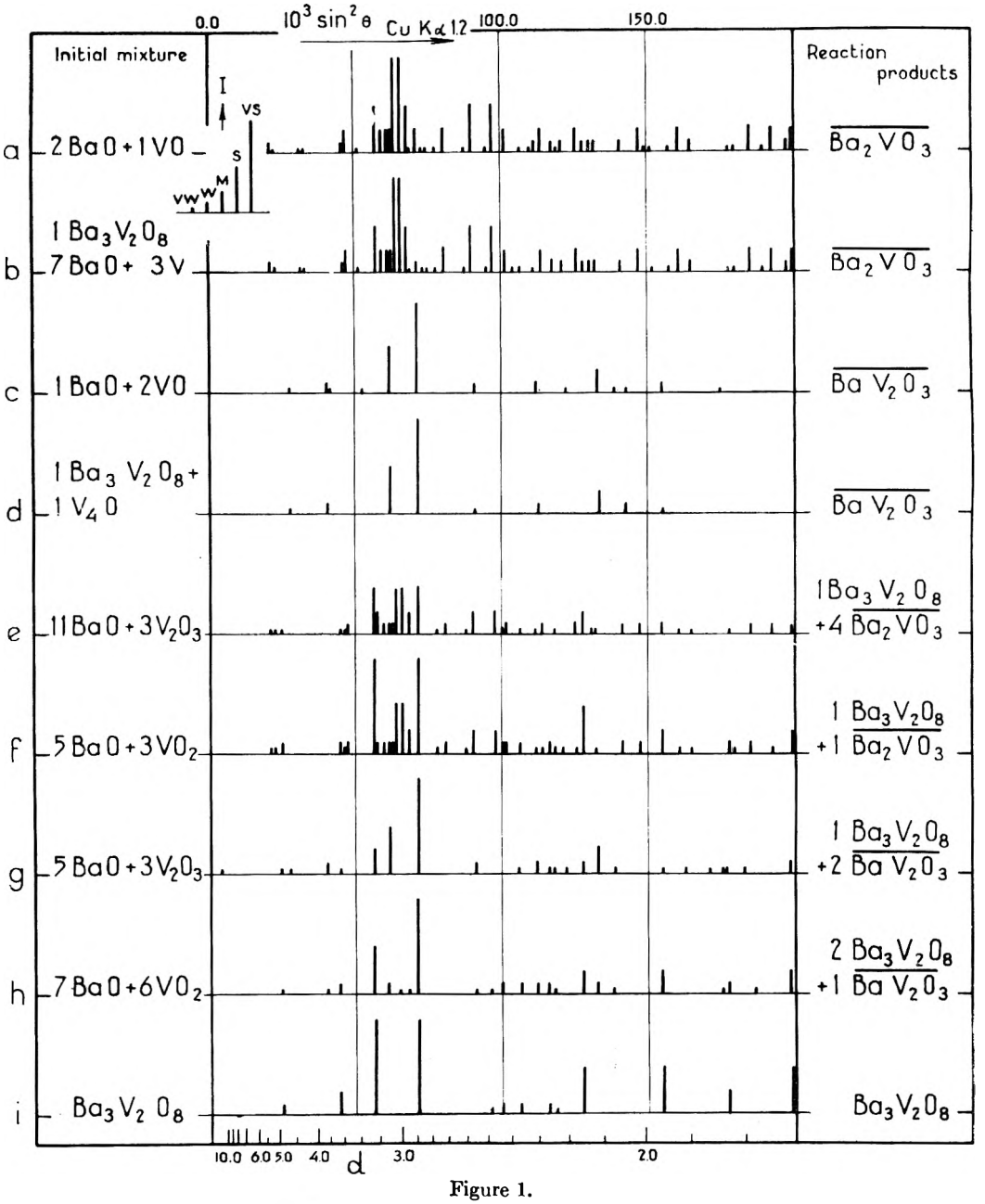

Figure 1.

$VO_{1.00}$ products the compositions $\overline{Ba_2VO_3}$ and $\overline{BaV_2O_3}$[3] appeared to have characteristic powder diagrams. The BaO, V_2O_3, and BaO, VO_2 products showed, without exception, one similar predominant strong reflection pattern. This pattern was found to be identical with that of the compound $Ba_3V_2O_8$. This compound (prepared from $3BaO + 1V_2O_5$ at 800° in an oxygen flow) is one of the isomorphic series $Ba_3(MO_4)_2$ where M = P, As, V, Cr, Mn according to Klemm[4] with the barium orthophosphate structure analyzed by Zachariasen.[5] The hexagonal lattice parameters were found to be $a = 5.777 \pm 0.003$ Å. and $c = 21.31 \pm 0.01$ Å., in agreement with Durif's values[6] of 5.783 and 21.34 Å., respectively. A complete interpretation of the BaO, V_2O_3 and BaO, VO_2 patterns at this stage was hardly feasible, however, because of the fact that the products were multiphased.

The disproportionation of a lower transition metal oxide reacting with an alkaline earth oxide results in a ternary system. The reaction products therefore generally are expected to consist of three co-existing solid phases. A two-phase reaction product or a single phase, *i.e.*, complex forming, must be considered as special cases. In order to force two-phase reaction products from BaO, V_2O_3 and BaO, VO_2 mixtures with the $\overline{Ba_2VO_3}$ and $\overline{BaV_2O_3}$ in mind, ratios were chosen as presented in Table I, e, f, g, and h. Furthermore experiments were done to verify the patterns of $\overline{Ba_2VO_3}$ and $\overline{BaV_2O_8}$ by heating mixtures containing $Ba_3V_2O_8$ as a starting material. Data are listed

(3) $\overline{Ba_2VO_3}$ and $\overline{BaV_2O_3}$ appear to be single phased by X-ray identification. Line displacements, specially those of $\overline{BaV_2O_3}$, suggest a homogeneity range with variable oxygen content. The bars over the formulas indicate the possibility of deviation from stoichiometry.

(4) R. Scholder and W. Klemm, *Angew. Chem.*, **66**, 461 (1954).

(5) W. H. Zachariasen, *Acta Cryst.*, **1**, 263 (1948).

(6) A. Durif, *ibid.*, **12**, 420 (1959).

TABLE I

	Initial mixture	Reaction conditions	Appearance	Products
a	$2BaO + 1VO_{1.00}$	$2 \times 1/6$ hr., 1270° + 72 hr., 1080°	Green	$\overline{Ba_2VO_3}$
b	$1Ba_3V_2O_8 + 7BaO + 3V$	$3 \times 1/4$ hr., 1270° + 150 hr., 1000°	Green	$\overline{Ba_2VO_3}$
c	$1BaO + 2VO_{1.00}$	$2 \times 1/4$ hr., 1450° + 3 1/2 hr., 1340°	Dark gray	$\overline{BaV_2O_3}$
d	$1Ba_3V_2O_8 + 1V_4O$	$3 \times 1/4$ hr., 1220°	Black	$\overline{BaV_2O_3}$
e	$11BaO + 3V_2O_3$	$2 \times 1/2$ hr., 1200° + 150 hr., 1000°	Gray	$1Ba_3V_2O_8 + 4\overline{Ba_2VO_3}$
f	$5BaO + 3VO_2$	$2 \times 1/2$ hr., 1200° + 150 hr., 1000°	Gray	$1Ba_3V_2O_8 + 1\overline{Ba_2VO_3}$
g	$5BaO + 3V_2O_3$	$2 \times 1/4$ hr., 1120° + 50 hr., 1130°	Gray	$1Ba_3V_2O_8 + 2\overline{BaV_2O_3}$
h	$7BaO + 6VO_2$	$2 \times 1/4$ hr., 1230° + 170 hr., 1070°	Gray	$2Ba_3V_2O_8 + 1\overline{BaV_2O_3}$

in Table I while powder diagrams are presented in Fig. 1. For the preparation of the $\overline{BaV_2O_3}$ phase considerably more severe prefiring was shown to be necessary when BaO and $VO_{1.00}$ were employed as starting materials. A difference of the very weak reflections therefore remained even after prolonged annealing at various temperatures. Some very weak lines in patterns Fig. 1g and h do not fit in patterns Fig. 1d or i. The circumstances to obtain both $Ba_3V_2O_8$ and $\overline{BaV_2O_3}$ in a good crystalline state apparently do not coincide: after annealing of a mixture $7BaO + 6VO_2$ at 1200° the $Ba_3V_2O_8$ lines vanished leaving pattern Fig. 1d. (No powder diagram of this sample is presented in Fig. 1.) However, a composition different from $\overline{BaV_2O_3}$ is considered to be possible.

In two respects Ba–V–O products are shown to be remarkable. First the non-existence of M^{III} and M^{IV} complexes at temperatures higher than 1000° has proved to be in contrast with the systems Ba–M–O in which M = Ti, Cr, Mn, Fe. On the other hand no perovskite phases are formed in the Ba–V–O system, contrary to the A–V–O systems in which A = Sr or Ca. Both Sr and Ca form perovskite compounds: Rüdorff and Reuter[7] reported a Sr–V–O phase of this structure which according to Kestigian, *et al.*,[8] forms at 1100° and at compositions between $SrVO_{2.50}$ and $SrVO_{2.75}$, while Rüdorff and Becker[9] observed a Ca–V–O perovskite.

Magnetic measurements and closer X-ray studies on the $\overline{Ba_2VO_3}$ and $\overline{BaV_2O_3}$ phases are being carried out in order to investigate the way in which the 3d electrons of the vanadium metal contribute to chemical bondings. The results will be described elsewhere.[1]

Acknowledgment.—The authors wish to express their gratitude to Professor Dr. A. E. van Arkel for his guidance in many stimulating discussions.

(7) W. Rüdorff and B. Reuter, *Z. anorg. allgem. Chem.*, **253**, 177 (1947).

(8) M. Kestigian, J. G. Dickinson, and R. Ward, *J. Am. Chem. Soc.*, **79**, 5598 (1957).

(9) W. Rüdorff and H. Becker, *Z. Naturforsch.*, **9b**, 613 (1954).

PHOTOCHROMIC SPIROPYRANS

BY ELLIOT BERMAN

Chemistry Laboratory, Itek Corporation, Lexington, Massachusetts

Received May 25, 1962

Previous workers[1-3] in general have proposed a merocyanine-like structure for the colored form II formed photochemically from 1,3,3-trimethylindoline-6′-nitrobenzopyrylospiran (I)[2] by ultraviolet irradiation at room temperature.

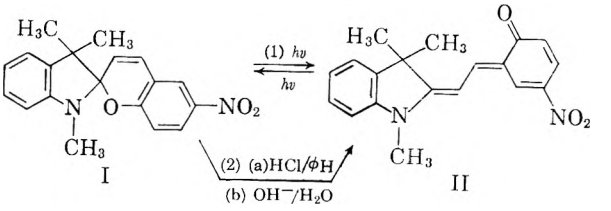

It has recently been reported[4] that electron spin resonance studies of the solid colored form II indicate an unpaired electron suggestive of II being a stable biradical or an ionic free radical.

We have prepared solid II by two different routes: (1) by ultraviolet irradiation of a hexane solution of I, and (2) by treatment of a hydrochloride of I with aqueous alkali. The solid colored material produced by either route gave identical infrared absorption spectra (as Nujol mulls), thermally and photochemically reverted in solution to I, and melted at 172–174° after becoming colorless at about 155°. Electron spin resonance studies[5] showed the absence of unpaired electrons in freshly prepared colored form II. However, a sample of II which had been stored in the dark in air for several months gave a weak absorption ($g = 2.0039 \pm 0.0001$, $\nu = 9405.4$ Mc./sec.) probably due to peroxide formation.

The author agrees with the proposal[3] that the colored forms of spiropyrans are various geometric isomers of the merocyanine type and not biradicals.

(1) Y. Hirshberg, *J. Am. Chem. Soc.*, **78**, 2304 (1956).

(2) E. Berman, R. E. Fox, and F. D. Thomson, *ibid.*, **81**, 5605 (1959).

(3) R. Heiligman-Rim, Y. Hirshberg, and E. Fischer, *J. Phys. Chem.*, in press.

(4) C. A. Heller, D. A. Fine, and R. A. Henry, *ibid.*, **66**, 1908 (1961).

(5) Performed through the courtesy of Dr. Paul Dorain, Brandeis Univ.

EFFECT OF CROSS-LINKING ON THE PROPERTIES OF CARBOXYLIC POLYMERS. II. APPARENT DISSOCIATION CONSTANTS AS A FUNCTION OF THE EXCHANGING MONOVALENT CATION

BY ROBERT KUNIN AND SALLIE FISHER

Rohm & Haas Company, Philadelphia, Pa.

Received June 13, 1962

In a previous paper[1] the authors presented data pertaining to the variation of the apparent dissociation constants of cross-linked polyacrylic and

(1) S. Fisher and R. Kunin, *J. Phys. Chem.*, **60**, 1030 (1956).

polymethacrylic acids with the polymer composition. These measurements, which were made in 1 M KCl solutions, showed that the apparent dissociation constant varied with composition according to the equation

$$pK_a = pK_{a(m=1)}\,[2 - m] \qquad (1)$$

where K_a is the apparent dissociation constant, $K_{a(m=1)}$ is the apparent dissociation constant of the uncross-linked polymer obtained by extrapolation, and m is the mole fraction of acrylate in the polymer.

This study now has been extended to include other members of the alkali metal group. The present work also includes a study of the variation of dissociation constant with ionic strength.

Experimental

As in the previous work, the apparent dissociation constants of polymers cross-linked with varying amounts of divinylbenzene (DVB) were measured under arbitrarily chosen experimental conditions wherein all variables except the polymer composition were held constant. Again the hydrogen form of the polymer was neutralized with the appropriate hydroxide solution in the presence of a constant amount of the corresponding chloride salt. Separate weighed samples of polymer of known equivalency were allowed to equilibrate with known varying amounts of hydroxide solutions until a constant pH was reached. In the case of the more highly cross-linked polymers equilibrated with cesium and rubidium, periods longer than the previously used 48 hr. were required for the establishment of equilibrium.

The design of the experiments reported herein was the same as that used in the previous work.[1] Measurements of the equilibria with lithium, sodium, and potassium hydroxides against a 1.0 M chloride salt background of the same cation were made for both acrylic and methacrylic acid copolymers containing 75–99+ mole % of the respective monomers. Similar measurements using 0.1 M salt background were made for the same cations and for rubidium and cesium as well.

Results and Conclusions

Values of pK_a from the modified Henderson–Hasselbach equation

$$pH = pK_a - n \log \frac{1 - \alpha}{\alpha} \qquad (2)$$

were determined by plotting pH as a function of log $[(1-\alpha)/\alpha]$ (the logarithm of the fraction of polymer neutralized). Values determined in 1 M salt solutions for methacrylic acid and acrylic acid copolymers are given in Tables I and II. When these data are plotted, as in the previous paper,[1] straight-line functions of pK_a (1 M salt) as a function of mole % acrylate are obtained in both systems for all three cations. These lines again are of the form of eq. 1 and for the three cations investigated, are approximately parallel. Deviations from the agreement were minor and of the order of magnitude noted in the plots described previously.[1] Actual values of the constant $pK_{a(m=1)}$ for both the acrylic and methacrylic acid systems are listed in Table IV. As previously noted, this value which is obtained by extrapolation represents the dissociation constant of a linear polymer of infinite chain length or, in our present terms, zero cross-linking. As shown previously, extrapolation of the available data for linear polymers to infinite chain length yields the same numerical value of this constant.

Similar data have been obtained for two copolymers in each series in 0.10 M salt solutions for the neutralization reaction with RbOH and CsOH as well as the LiOH, NaOH, and KOH solutions previously used. Values of the apparent dissociation constants are given in Table III. These data show the general trend in this more dilute concentration range and the slopes (n) indicate that, within the limits of experimental error, here too the data follow the form of eq. 1. Extrapolated values of the constant $pK_{a(m=1)}$ for the 0.1 M salt solutions are listed in Table IV.

Variation of the apparent dissociation constants with ionic strength of the solution can be predicted by expanding the equilibrium expression to include a term for the activity of the cation in the solution phase. The ion exchange reaction is

$$RCOOH + M^+ \rightleftarrows RCOOM + H^+$$

Applying the law of mass-action

$$K = \frac{(RCOOM)(H^+)}{(RCOOH)(M^+)} \qquad (3)$$

Combining the above relationship with the expression for the apparent dissociation constant of the polymer acid and correcting the term of the metal ion concentration in solution with the activity coefficient, the final expression of the dissociation constant of the resin is obtained as

$$K = \frac{K_a}{[M]\gamma M} \qquad (4)$$

or

$$pK = pK_a + \log [M^+]\,\gamma M \qquad (5)$$

When the apparent pK values are substituted in the above equation along with the appropriate activity coefficients, pK values are obtained which are the same for both salt concentrations. The corrected values of pK thus obtained may, therefore, be used for the calculation of approximate dissociation constants for solutions of these cations of known external ionic activity.

With the fuller spectrum of data now available, the behavior of the constant n becomes clearer. It will be noted in Tables I, II, and III that the value of n in a given system increases with increasing ionic size. If, as suggested by Gregor, *et al.*,[2] the magnitude of n is a function of the con-

TABLE I

APPARENT DISSOCIATION CONSTANTS OF METHACRYLIC ACID POLYMERS IN 1.0 M SALT SOLUTIONS

	Mole % acrylate[a]					
	99.3		93.6		77.8	
Exchange reaction	pK_a	n	pK_a	n	pK_a	n
H^+–Li^+	5.25	1.3	5.63	1.4	6.70	1.5
H^+–Na^+	5.36	1.4	5.87	1.6	6.80	1.7
H^+–K^+	5.60	1.5	6.05	1.7	6.90	1.8

[a] All cross-linked with divinylbenzene (DVB).

(2) H. P. Gregor, M. J. Hamilton, J. Becher, and F. Bernstein, *J. Phys. Chem.*, **59**, 874 (1955).

figurational entropy of the chain, this behavior may be predicted from the relative abilities of the ions concerned to stretch the polymer chain. The lowest values of n then would represent the most highly stretched systems. This concept also may be used to explain the variation of n values as the cross-linking agent is changed, with the lowest n values indicating the greatest flexibility of cross-links.

TABLE II

APPARENT DISSOCIATION CONSTANTS OF ACRYLIC ACID POLYMERS IN 1.0 M SALT SOLUTIONS

Mole % acrylate[a]	Apparent pK_a (1 M salt) Li+	Na+	K+	n (1 M salt) L+	Na+	K+
98.4	4.43	4.73	4.90	1.4	1.7	1.8
92.4	4.50	4.93	5.10	1.4	1.7	1.85
75.8	5.47	5.80	6.08	1.85	2.0	2.1

[a] All cross-linked with divinylbenzene (DVB).

TABLE III

APPARENT DISSOCIATION CONSTANTS OF ACRYLIC AND METHACRYLIC ACID POLYMERS IN 0.1 M SALT SOLUTIONS

	Monomer Acrylate				Methacrylate			
	Mole % 92.4		75.8		93.6		77.8	
Reaction	pK_a	n	pK_a	n	pK_a	n	pK_a	n
H+–Li+	5.70	1.5	6.70	1.7	6.60	1.35	7.60	1.8
H+–Na+	5.75	1.8	6.75	2.0	6.70	1.75	7.70	1.85
H+–K+	5.80	1.85	6.90	2.1	6.80	1.95	7.80	1.85
H+–Rb+	5.85	1.85	7.00	2.15	6.85	1.95	7.90	2.25
H+–Cs+	5.95	1.9	7.10	2.35	6.95	2.05	7.95	2.55

TABLE IV

APPARENT DISSOCIATION OF ACRYLIC AND METHACRYLIC ACID POLYMERS AT ZERO CROSS-LINKAGE

	Acrylic acid		Methacrylic acid	
p$K_{a(m=1)}$	1.0 M Salt	0.1 M Salt	1.0 M Salt	0.1 M Salt
Li+	4.30	5.27	5.22	6.27
Na+	4.65	5.30	5.34	6.37
K+	4.83	5.37	5.60	6.44
Rb+		5.40		6.50
Cs+		5.52		6.58

TABLE V

APPARENT DISSOCIATION CONSTANTS OF ACRYLIC AND METHACRYLIC ACID POLYMERS CORRECTED FOR EXTERNAL IONIC STRENGTH

	Li+		Na+		K+	
External ion concn.	0.1 M	1.0 M	0.1 M	1.0 M	0.1 M	1.0 M
$\pm \gamma$ M+Cl[a]	0.792	0.781	0.778	0.658	0.769	0.605
93.6 Mole % MMA						
Apparent pK_a	6.60	5.63	6.70	5.87	6.80	6.05
Corrected pK_a	5.50	5.52	5.59	5.68	5.69	5.83
77.8 Mole % MMA						
Apparent pK_a	7.60	6.70	7.70	6.80	7.80	6.90
Corrected pK_a	4.60	6.59	6.59	6.62	6.69	6.68
92.4 Mole % AA						
Apparent pK_a	5.70	4.50	5.75	4.93	5.80	5.10
Corrected pK_a	4.60	4.40	4.65	4.75	4.69	4.88
75.8 Mole % AA						
Apparent pK_a	6.70	5.47	6.75	5.80	6.90	6.08
Corrected pK_a	5.60	5.36	5.64	5.62	5.89	5.86

[a] H. Harned, and B. Owen, "The Physical Chemistry of Electrolytic Solutions," Second Ed., Reinhold Publ. Corp., New York, N. Y, 1950.

THE RELATIVE BASICITIES OF ETHERS

BY HENRY E. WIRTH AND PAUL I. SLICK

Department of Chemistry, Syracuse University, Syracuse 10, New York

Received May 2, 1962

Measurements of the basicities of cyclic imines toward trimethylboron[1] have shown that the basic strength changes with ring size in the order: 4- > 5- > 6- > 3-membered rings. The same order was observed using hydrogen bond[2] and iodine complex[3,4] formation. Studies of the dissociation constants of ether–boron trifluoride complexes by manometric methods have shown that tetrahydrofuran is a stronger base than tetrahydropyran[5] and that the basic strengths of the acyclic ethers decrease in the order: dimethyl ether > diethyl ether > diisopropyl ether.[6,7] In this work the relative basicities of some ethers and two alcohols were obtained from a study of the equilibrium constants for the distribution of boron trifluoride between two ethers in benzene solution.

Experimental

Procedure.—If a benzene solution of an ether (B_1) is mixed with a benzene solution of either diethyl ether–boron trifluoride or dimethyl ether–boron trifluoride (B_2:BF_3), the equilibrium

$$B_1 + B_2{:}BF_3 \rightleftharpoons B_1{:}BF_3 + B_2$$

is established. The equilibrium constant may be determined from the equilibrium concentration of B_2:BF_3 and a knowledge of the original concentrations. The strong absorption due to the symmetrical B–F stretching frequency in Et_2O:BF_3 at 763 cm.$^{-1}$ or in Me_2O:BF_3 at 816 cm.$^{-1}$ was used to obtain the concentration of the reference ether–boron trifluoride complex. Measurements on standard solutions showed that Beer's law was followed up to a concentration of 0.1 M.

If a is the original molarity of B_2:BF_3, b is the original molarity of B_1, c is the equilibrium molarity of B_2:BF_3, and V is the ratio of the volume of B_2:BF_3 taken to the total volume of mixture, then

aV = concn. of B_2:BF_3 on mixing without reaction
$b(1 - V)$ = concn. of B_1 on mixing without reaction
$(aV - c)$ = equilibrium concn. of B_2 and B_1:BF_3
$b(1 - V) - (aV - c)$ = equilibrium concn. of B_1

The equilibrium constant K is then

$$K = \frac{[aV - c]^2}{[c][b(1 - V) - (aV - c)]}$$

Materials.—Tetrahydrofuran, diethyl ether, di-*n*-propyl ether, diisopropyl ether, tetrahydropyran, diethyl sulfide, and tetrahydrothiophene were first dried over lithium aluminum hydride. A small amount of sodium was added to the methyl alcohol and propylene oxide, and magnesium was added to the ethyl alcohol. Ethyl methyl ether was prepared by the reaction of ethyl iodide and sodium methylate in methanol and the crude product was distilled from lithium aluminum hydride at 0°.

After the initial drying the materials were distilled under vacuum into storage containers to which were added small amounts of boron trifluoride (except for the propylene oxide).

(1) H. C. Brown and M. Gerstein, *J. Am. Chem. Soc.*, **72**, 2926 (1950).
(2) S. Searles, Jr., and M. Tamres, *ibid.*, **73**, 3704 (1951).
(3) M. Brandon, M. Tamres, and S. Searles, Jr., *ibid.*, **82**, 2129 (1960).
(4) M. Tamres and M. Brandon, *ibid.*, **82**, 2134 (1960).
(5) D. E. McLaughlin, M. Tamres, and S. Searles, Jr., *ibid.*, **82**, 5621 (1960).
(6) H. C. Brown and R. M. Adams, *ibid.*, **64**, 2557 (1942).
(7) D. E. McLaughlin and M. Tamres, *ibid.*, **82**, 5618 (1960).

TABLE I

EQUILIBRIUM CONSTANTS FOR THE REACTION

$$B_1 + B_2{:}BF_3 \rightleftharpoons B_1{:}BF_3 + B_2$$

AND STANDARD FREE ENERGY CHANGES FOR THE REACTION

$$B_1 + BF_3 \longrightarrow B_1{:}BF_3 \text{ at } 27°$$

B_1	$B_2{:}BF_3$	K_{27}	No. of detns.	$\Delta F_{27}°$ (cal./mole)	$\Delta F°$ (lit.) (cal./mole)	ν^a (B–F) in $B_1{:}BF$ cm.$^{-1}$
Tetrahydrofuran	$Et_2O{:}BF_3$	~500	2	−6600	−5820[6]	810
Ethanol	$Et_2O{:}BF_3$	75 ± 5	5	−5450		860
Ethanol	$Me_2O{:}BF_3$	24 ± 4	3	−5620		
Tetrahydropyran	$Et_2O{:}BF_3$	37 ± 2	3	−5030	−5040[5]	779
Tetrahydropyran	$Me_2O{:}BF_3$	11 ± 3	5	−5160		
Methanol	$Et_2O{:}BF_3$	34	1	−4970		855
Methanol	$Me_2O{:}BF_3$	10 ± 1	4	−5100		
Dimethyl ether	$Et_2O{:}BF_3$	4.5 ± 0.2	6	−3760	−3730[7]	816
Ethyl methyl ether	$Et_2O{:}BF_3$	3.2 ± .2	3	−3560		783
Ethyl methyl ether	$Me_2O{:}BF_3$	0.43 ± 0.05	5	−3220		
Propylene oxide	$Et_2O{:}BF_3$	1.6 ± .2	5	−3150		846
Diethyl ether	$Me_2O{:}BF_3$	0.24 ± .1	3	−2880	−2870[7]	763
Di-*n*-propyl ether	$Et_2O{:}BF_3$	.20 ± .4	5	−1910		809
Diisopropyl ether	$Et_2O{:}BF_3$	.030 ± 0.004	3	− 780		
Tetrahydrothiophene	$Et_2O{:}BF_3$	.016 ± .006	3	− 400		827
Diethyl sulfide	$Et_2O{:}BF_3$	.0003	2	+2000		822

[a] Based on the assignments made by J. Goubeau and H. Mitschellen, *Z. physik. Chem.* (Frankfurt), **14**, 61 (1958).

Dimethyl ether–boron trifluoride and diethyl ether–boron trifluoride were prepared by reaction of the ethers with an excess of boron trifluoride, and the complexes were purified by fractional distillation in the vacuum system.

Thiophene-free benzene was refluxed over calcium hydride for 3 hr., then distilled in the vacuum system and stored over calcium hydride.

Solutions.—Samples of ether or ether–boron trifluoride complex were transferred by condensation at liquid nitrogen temperatures into a volumetric flask. The weight of ether or complex was determined from the loss in weight of the storage flask. Benzene then was condensed into the volumetric flask at 0° and the volume of the solution determined after warming to room temperature. The concentrations of the stock solutions were 0.1 to 0.2 *M*.

Mixing Apparatus.—The mixing apparatus consisted of the bottom half of a 50-ml. buret to which side arms for the introduction of the solutions were attached. Care was taken that the solutions were not exposed to air or water vapor. The solutions were transferred to the mixing apparatus by use of pressure of dry nitrogen gas. Unlubricated Teflon stopcocks were used wherever stopcocks came into contact with the solutions. A magnetic bar in the buret facilitated mixing. A hypodermic needle fastened to the bottom of the buret was used to introduce the solution into the absorption cell after mixing and determination of the volumes.

Absorption Measurements.—All measurements were made with the same fixed thickness (~0.1 mm.) absorption cell using a Perkin–Elmer infrared spectrometer, Model 137. Absorption bands due to the solvent were compensated for by a variable thickness cell filled with benzene which was placed in the reference beam. Measurements were made at 27 ± 3°.

Precision.—The uncertainty in the equilibrium constants varies from 10% for values near unity to 20% for values between 10 and 100 (or 0.1 to 0.01). Values outside these ranges are rough estimates only.

Results and Discussion

The equilibrium constants are given in Table I. The deviations are the average deviation from the mean. The order of decreasing basicities for the compounds studied is tetrahydrofuran > ethanol > tetrahydropyran > methanol > dimethyl ether > ethyl methyl ether > propylene oxide > diethyl ether > di-*n*-propyl ether > diisopropyl ether > tetrahydrothiophene > diethyl sulfide. These results are in agreement with previous reports[1–5] that the basic strengths of cyclic ethers decrease in the order: 4- > 5- > 6- > 3-membered rings. The results also confirm the order for acyclic ethers found by Brown and Adams[6] and McLaughlin and Tamres[7] by manometric methods, and show that ethyl methyl ether lies between dimethyl and diethyl ethers.

The order for ethanol and methanol shows that in the alcohols the inductive effect[8] is dominant, but as suggested by Brown and Adams[6] steric effects outweigh inductive effects with the ethers. This is especially evident in the propyl ethers. Diisopropyl ether has four β-carbons tending to increase the electron density on the oxygen as compared to two β-carbons in di-*n*-propyl ether. Nevertheless, the added steric hindrance presented by the four β-carbons makes diisopropyl ether the weaker base.

An attempt was made to correlate the symmetric stretching frequency of the B–F bond in the ether–boron trifluoride complex with the basic strength of the ether. No general correlation was possible, although in a limited series of closely related compounds (tetrahydrofuran–tetrahydropyran, dimethyl ether–ethyl methyl ether–diethyl ether) the frequency was observed to decrease as the basic strengths decreased.

The standard free energy change for the reactions

$$(CH_3)_2O + BF_3 \longrightarrow (CH_3)_2O{:}BF_3;\ \Delta F_{27°} = -3730 \text{ cal./mole}$$

$$(C_2H_5)_2O + BF_3 \longrightarrow (C_2H_5)_2O{:}BF_3;\ \Delta F_{27°} = -2870 \text{ cal./mole}$$

(8) C. K. Ingold, *Chem. Rev.*, **15**, 225 (1934).

obtained by extrapolation of the data of McLaughlin and Tamres[7] for the gas phase dissociation of the ether–boron trifluoride complexes at 65–90° were combined with the observed equilibrium constants to give an estimate of the standard free energy changes for the reaction

$$B_1 + BF_3 \longrightarrow B_1:BF_3$$

These estimates are given in Table I. The agreement between values obtained with the same base and two reference boron fluoride complexes (see for example tetrahydropyran and methanol in Table I) indicates the validity of the equilibrium method for the determination of relative basicities.

Acknowledgment.—We wish to thank the Syracuse University Research Institute for its finanical aid to P. I. S. during the summer of 1960.

COMMUNICATION TO THE EDITOR

CONCERNING THE PRIMARY ABSORPTION ACT IN A ONE-ELECTRON PHOTOOXIDATION IN A RIGID MEDIUM[1]

Sir:

Very recently,[2] a quantitative study was reported of a one-electron photoöxidation of N,N,N′,N′-tetramethylparaphenylenediamine (TMPD) in a 3-methylpentane glass at 77°K. A principal discovery was that the wave length dependence of the absolute quantum yield for the photoöxidation shows considerable structure as well as order of magnitude changes over the smooth, completely unstructured near-ultraviolet absorption band of TMPD. In contrast, the wave length dependence of the relative quantum yields of fluorescence and phosphorescence over this same band is constant. The latter observation is not unexpected and can be regarded as reflecting a uniform efficiency at all wave lengths for radiationless conversion to the thermally equilibrated first excited singlet state followed either by emission (fluorescence) or internal conversion to the triplet state with consequent phosphorescence. On the other hand the distinctly different behavior of the wave length dependence of the photochemical quantum yield was much more puzzling.

Attempts to explain the highly structured photochemical quantum yield spectrum were based upon two very different points of view. One explanation posed the possibility of a very weak solute–solvent charge transfer band (not apparent in absorption) coincidentally underlying the near-ultraviolet solute band. The photoöxidation then would arise through an electronic transition directly into this band followed by a very efficient electron ejection. The structure in the photoöxidation quantum yield excitation spectrum then may reflect structure in the charge transfer band; while the observed low quantum yield would be a consequence of its low extinction coefficient. The second point of view assumes that the primary absorption act is the same for both emission and photoöxidation, namely excitation directly into the first excited singlet state of TMPD. This is the excitation responsible for the near-ultraviolet band. Following the excitation, there is competition between electron ejection and thermal equilibration. It was argued that the structure in the photochemical excitation spectrum would, in this case, reflect a dependence of the electron ejecting efficiency on the nature of the vibronically excited normal modes of the upper state. Since this structure was not reflected in an inverse sense in the emission excitation spectrum, it was argued that the absolute quantum yields for emission were much higher than those for the photochemistry. The second mechanism, vibronic photochemistry, was adopted on the basis of a number of arguments, none of them alone conclusive. The purpose of this communication is to present conclusive experimental evidence supporting this choice of mechanism.

By illuminating rigid solutions with polarized (or unpolarized) light, a non-random sample of solute may be selectively excited. The nature of the non-random distribution is fixed by the polarization and orientation of the selecting light and by the orientation of the axis of the primary absorption with respect to the molecular axes. Information regarding the nature of the non-random distribution may be had by observing the polarization of emission from the oriented excited molecules or by observing the orientation of photoproduct molecules (by polarized absorption spectroscopy) which replace the oriented photoselected solute molecules after photochemical change.[3] If the primary absorption act is the same for both luminescence and photochemistry at all wave lengths, then data obtained by the two techniques should reduce to the same non-randomness for each photoselecting wave length. Polarized photochemistry experiments on TMPD in a rigid glass (1-propanol and isopentane) already have been completed.[4] Now the necessary polarized emission studies have been made which permit the crucial comparison, graphically presented here, which establishes that the primary absorption act is the same for both emission and photoöxidation.

The experimental details for the polarized emission studies, especially with regard to photoselection, are similar to those for the polarized photochemistry study[4] and shall not be repeated here. One change involves the use of a double Glan prism for polarized excitation (instead of a stack of quartz

(1) This work has been supported, in part, by a grant from the National Science Foundation.

(2) W. C. Meyer and A. C. Albrecht, *J. Phys. Chem.*, **66**, 1168 (1962).

(3) A. C. Albrecht, *J. Mol. Spectry.*, **6**, 84 (1960).

(4) A. C. Albrecht, *J. Am. Chem. Soc.*, **82**, 3813 (1960).

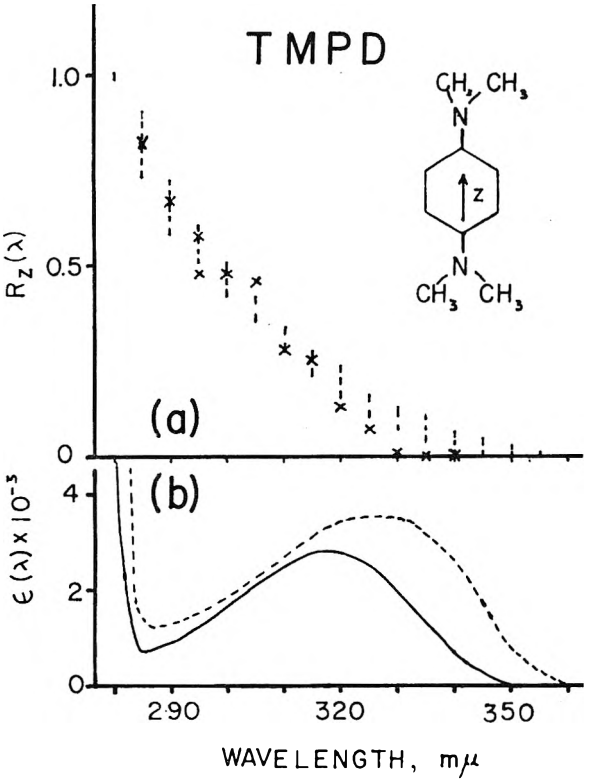

Fig. 1.—(a) Fractional transition probability, $R_Z(\lambda)$: ×, values obtained from polarized photochemistry (1-propanol, isopentane glass); – – –, values obtained from polarized fluorescence (3-methylpentane glass[4]). (b) Molar extinction coefficient, $\epsilon(\lambda)$, at 77°K.: ———, in 1-propanol, isopentane glass[4]; – – –, in 3-methylpentane.[2]

plates[4]). Another difference is the use here of 3-methylpentane as the solvent. The fluorescence component of the emission from the photoselected sample of TMPD was isolated[5] and, for each photoselecting wave length, was analyzed with a second double Glan prism employing a Photovolt multiplier photometer (Series 520-M) with a 1P-21 phototube. The raw data were properly corrected for blank effects and handled by methods, described elsewhere,[3] to convert them to the fractional long-axis component in the primary absorption act as a function of exciting wave length. The results are found plotted in Fig. 1, where the observations reported previously[4] and obtained by polarized photochemistry also are found. It is evident that the two different methods give very similar results. Even were some refinement in the comparison attempted by taking into account in some manner the differences in absorption spectra (which we attribute to solvent differences at low temperatures), the qualitative agreement would not be changed.

We conclude that the primary absorption act leading to one-electron photochemistry and the one leading to fluorescence are one and the same. Furthermore, the primary absorption step must be to the excited state responsible for the near-ultraviolet band of TMPD since the yields for emission are estimated at greater than 0.1 and, in any case, the emission spectrum is a fairly good mirror image of the absorption band. The original proposal[2] of a vibronic photochemical mechanism thus is supported.

More complete details of this and especially of related work on both TMPD and other molecules will appear in the near future.

(5) Corning filters 3850 and 5970 transmitted the higher energy fluorescence (peak at 380 mμ) and none of the partially overlapping phosphorescence (peak about 470 mμ).

DEPARTMENT OF CHEMISTRY A. H. KALANTAR
CORNELL UNIVERSITY A. C. ALBRECHT
ITHACA, NEW YORK

RECEIVED SEPTEMBER 13, 1962

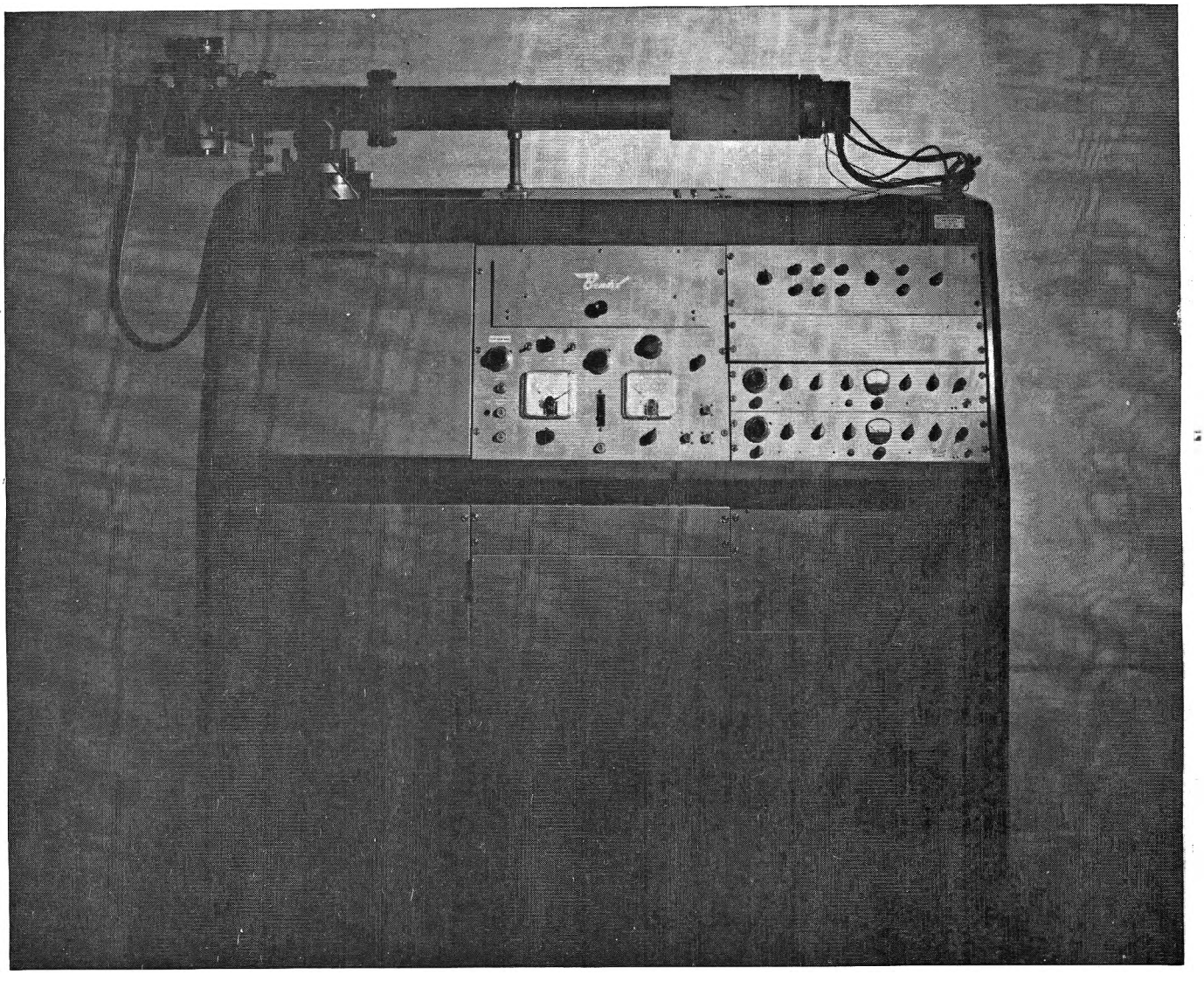

This T.O.F.* analyzes anything

(almost)

There is something the Bendix® Time-of-Flight Mass Spectrometer won't analyze. Diamonds! But hand it any other material and you'll get your quantitative-qualitative analysis fast . . . and accurately. Its versatility is unsurpassed for analytical purposes, research projects or industrial process control.

Depending on project needs and equipment, you can get up to 100,000 spectra per second, unit resolution up to mass 350 and a sensitivity of 1 to 5 ppm. With the analog output system you can record both positive and negative ion spectra and can simultaneously record up to six preselected masses.

The unit is compact and easy to move. Maintenance involves little more than knocking the dust off once a week. And the list of things it can do in the way of analyzing won't even give the dust a chance to collect. Models range from $17,000 to $100,000. What would you like to analyze? Dept. V-11, 3130 Wasson Road, Cincinnati 8, Ohio.

*Time-of-Flight Mass Spectrometer

Cincinnati Division

THE Bendix CORPORATION

60-